

***Arabidopsis thaliana* DNA gyrase:
expression, characterisation and
in vivo insight**

Nidda Farooque Waraich

John Innes Centre
Department of Biological Chemistry
March 2021

This thesis is submitted in partial fulfilment of the requirements of the degree of
Doctor Philosophy at the University of East Anglia

This work was supported by the Biotechnology and Biological Sciences Research
Council

©This copy of the thesis has been supplied on condition that anyone who consults it is understood to recognise that its copyright rests with the author and that use of any information derived there from must be in accordance with current UK Copyright Law. In addition, any quotation or extract must include full attribution.

Statement

The work submitted within this thesis is entirely my own, except where due reference has been paid, and has not been submitted to this or any other university as part of any degree.

Dedication

I dedicate this thesis to:

my mum – the strongest woman I have known. This is for the both of us.

my dad – our pillar of support.

'Somewhere, something incredible is waiting to be known'

— Carl Sagan

Acknowledgements

First and foremost, I'd like to acknowledge the consistent support and encouragement I have received from my supervisor, Prof. Anthony Maxwell – thank you for getting me to the end! I thank each member of my supervisory committee; Ms Lesley Mitchenall for her day-to-day support, guidance and reassurance; Dr Nick Burton for his supervision of my iCASE placement and technical guidance throughout my project, and Dr Janneke Balk for teaching me plant biology, guiding me through that aspect of my project and answering all my naïve plant biology questions.

The Maxwell group has been an incredibly welcoming, friendly and inspiring place to work, for this I am grateful to all current and past members of the group. I am thankful for the immense support, particularly at the start of my project and continued friendship I received from Dr Monica Agarwal. I would like to extend this gratitude to all past and current occupants of office 1.25 - the banter has kept me going!

The Biological Chemistry Department at JIC has been an encouraging and sociable environment to work within. I would like to thank all current and past members of the department for their support, advice and suggestions. I would also like to thank everyone that has worked behind the scenes: the administrative staff, lab managers, lab support staff and horticultural staff (special thanks for keeping my plants alive!).

To all my family – thank you for listening to me moan (again, and again....). A special shout out to Waseem Shahid for sacrificing his weekends to proof-read for me.

Now to thank my pen-pal and confidant, Andy Bates. Thank you for your support, your encouragement, your tolerance, your belief in me, the discussions, guidance and advice (even if you do believe that I just do as I please in the end!). I couldn't have made it to the end without you, thanks for pushing me through. Our friendship is by far my most treasured possession from this journey.

To my siblings, thank you for keeping me entertained, helping me relax and for turning my tears of sorrow into joy. Bilal thanks for recognising that I'm obviously worth the wait. Mum and dad thank you for keeping the fridge stocked whilst I've been writing. More importantly, thank you for putting up with my tantrums, for your unconditional love and for always believing in me more than I could ever dare to do myself. Thank you for helping me through the grim parts of this journey and for paving my path to the light. Finally, to end on a light-hearted note, I thank myself for persevering and resisting the urge to throw in the towel.

Abstract

DNA gyrase is a type II topoisomerase distinguished by its ability to introduce negative supercoils into double-stranded DNA in a reaction linked to ATP hydrolysis. The essentiality of gyrase in bacteria has permitted its exploitation as an antibacterial target. The unanticipated discovery of gyrase within the nuclear genomes of eukaryotes including *Arabidopsis* and *Plasmodia*, was made near to two decades ago. Despite this, our understanding of gyrase within these species remains limited. The work here aimed to heterologously generate eukaryotic gyrases in order to biochemically characterise and better understand their mechanism of actions, gain an insight into their *in vivo* functions and explore their potential for inhibition. The specific inhibition of gyrase within these species would facilitate the generation of novel herbicidal and antimalarial drugs.

In vivo knockdown experiments of *A. thaliana* gyrase have confirmed the embryolethality of GyrA. *Arabidopsis* plants able to propagate with a knockdown of GyrB1 are dwarfed, chlorotic, have reduced numbers and lengths of lateral roots and altered thylakoid ultrastructure. An increase of GyrB1 transcript mediates a stress response within *Arabidopsis*. The functional cooperation to achieve supercoiling of a reconstituted gyrase comprising *A. thaliana* GyrA and *E. coli* GyrB has been shown. The catalysis of *A. thaliana* enzyme (GyrA and GyrB2) is differentially mediated by potassium glutamate levels. The *A. thaliana* DNA gyrase has been determined to be 45-fold more efficient for ATP-independent DNA relaxation than *E. coli* gyrase. A novel sensitive DNA decatenation substrate, 'bis-cat', comprising two singly-linked supercoiled plasmids of disparate sizes has been generated and compared to the current marketed decatenation substrate. The novel substrate determined *A. thaliana* gyrase to be 35-fold more effective for DNA decatenation than the *E. coli* enzyme. The herbicidal and bactericidal specificities of novel fluoroquinolone compounds have also been compared.

Access Condition and Agreement

Each deposit in UEA Digital Repository is protected by copyright and other intellectual property rights, and duplication or sale of all or part of any of the Data Collections is not permitted, except that material may be duplicated by you for your research use or for educational purposes in electronic or print form. You must obtain permission from the copyright holder, usually the author, for any other use. Exceptions only apply where a deposit may be explicitly provided under a stated licence, such as a Creative Commons licence or Open Government licence.

Electronic or print copies may not be offered, whether for sale or otherwise to anyone, unless explicitly stated under a Creative Commons or Open Government license. Unauthorised reproduction, editing or reformatting for resale purposes is explicitly prohibited (except where approved by the copyright holder themselves) and UEA reserves the right to take immediate 'take down' action on behalf of the copyright and/or rights holder if this Access condition of the UEA Digital Repository is breached. Any material in this database has been supplied on the understanding that it is copyright material and that no quotation from the material may be published without proper acknowledgement.

Table of Contents

Dedication	iii
Acknowledgements	v
Abstract	vi
Table of Contents	vii
List of Figures	xiii
List of Tables	xvi
Chapter 1: Introduction	1
1.1. DNA topology	1
1.2. Topoisomerases <i>in vivo</i>	2
1.3. Topoisomerases	2
1.4. Type I topoisomerases	6
1.4.1. Type IA topoisomerases	7
1.4.1.1. Topoisomerase I	8
1.4.1.2. Topoisomerase III	8
1.4.1.3. Reverse gyrase	9
1.4.2. Type IB topoisomerases	10
1.4.2.1. Topoisomerase IB	10
1.4.3. Type IC	11
1.4.3.1. Topoisomerase V	11
1.5. Type II topoisomerases	12
1.5.1. Type IIA topoisomerases	13
1.5.1.1. Topoisomerase II	15
1.5.1.2. Topoisomerase IV	16
1.5.2. Type IIB topoisomerases	18
1.5.2.1. Topoisomerase VI	18
1.5.2.2. Topoisomerase VIII	20
1.5.2.3. Mini-A	20
1.6. Gyrase	21
1.6.1. Structure of gyrase	21
1.6.2. Mechanism of DNA Gyrase	26
1.6.3. Biological role of gyrase	28
1.6.4. Gyrase inhibitors	28
1.6.4.1. Aminocoumarins	29
1.6.4.2. Quinolones	30
1.6.4.3. Simocyclinone D8	32
1.6.4.4. Microcin B17	33
1.7. DNA gyrase in plants	34
1.7.1. Detection of DNA gyrase in plants	34
1.7.2. Topoisomerases in <i>Arabidopsis</i>	35
1.7.2.1. <i>Arabidopsis</i> nuclear genome	35
1.7.2.2. <i>Arabidopsis</i> chloroplast genome	35
1.7.2.3. <i>Arabidopsis</i> mitochondrial genome	36
1.7.3. <i>Arabidopsis</i> topoisomerases	37
1.7.4. <i>Arabidopsis</i> DNA gyrase	38

1.7.4.1. Sub-cellular localisation of <i>A. thaliana</i> DNA gyrase	39
1.7.4.2. <i>A. thaliana</i> gyrase insertional mutagenesis phenotypes	42
1.8. DNA gyrase in plasmodia	42
1.8.1. Apicomplexa	42
1.8.2. Apicomplexan topoisomerases	43
1.8.3. Apicomplexan gyrase	43
1.8.3.1. <i>Plasmodium falciparum</i> gyrase	44
1.8.3.2. <i>Plasmodium vivax</i> gyrase	48
1.8.3.3. <i>Plasmodium berghei</i> gyrase	49
1.8.4. Apicomplexan gyrase inhibition	49
1.9. Project aims	50
Chapter 2: Materials and Methods	51
2.1. Bacteriology	51
2.1.1. Bacterial strains	51
2.1.2. Media	52
2.1.2.1. LB	52
2.1.2.2. SOC	52
2.1.3. Antibiotics	52
2.1.4. Preparation of chemically competent cells	53
2.1.5. DNA transformation of chemically competent cells	53
2.1.5.1. DNA transformation of electrocompetent cells	53
2.2. DNA methods	54
2.2.1. Buffers and solutions	54
2.2.2. Agarose gel electrophoresis	54
2.2.3. DNA gel extractions	55
2.2.4. DNA isolation from reactions	55
2.2.5. DNA precipitation	55
2.2.6. Plasmid DNA production and purification	55
2.2.7. Phenol:chloroform:isoamyl extraction of DNA	55
2.2.8. DNA digestion with restriction endonuclease	56
2.2.9. DNA ligation	56
2.2.10. DNA sequencing	56
2.2.11. DNA concentration determination	56
2.2.12. Polymerase chain reaction	56
2.2.13. In-Fusion cloning	57
2.2.14. DNase treatment of RNA	57
2.2.15. Reverse transcription of RNA	58
2.3. Protein methods	59
2.3.1. Dialysis	59
2.3.2. Protein concentration	59
2.3.3. Protein concentration determination	59
2.3.4. SDS PAGE	59
2.3.5. Western blotting and immunodetection	60
2.4. Insect cell techniques	61
2.4.1. Cell culturing	61
2.4.2. Bacmid DNA isolation	61
2.4.3. pOPIN constructs	61
2.4.4. Codon optimised sequences	61
2.4.5. Generating <i>A. thaliana</i> and <i>Plasmodia</i> expression constructs	61
2.4.5.1. Monocistronic <i>A. thaliana</i> gyrase constructs	61
2.4.5.2. <i>A. thaliana</i> and <i>P. falciparum</i> fusion constructs	62
2.4.5.3. Polycistronic <i>A. thaliana</i> constructs	65

2.4.5.4. <i>Plasmodium</i> pETDuet clones	65
2.4.6. Insect Cell Infections	67
2.4.6.1. pOPIN infections	67
2.4.6.2. pFastBac transfections	67
2.4.7. Virus quantification	68
2.4.7.1. Plaque assay	68
2.4.7.2. qPCR	68
2.5. Insect cell protein production	69
2.5.1. Buffers and solutions	69
2.5.2. Small scale expression and purification	69
2.5.3. Large scale <i>A. thaliana</i> gyrase A & B2 expression	70
2.5.4. <i>A. thaliana</i> gyrase B1 & A fusion	70
2.5.4.1. Expression of gyrase in <i>E. coli</i>	70
2.6. Arabidopsis methods	71
2.6.1. <i>Arabidopsis</i> lines	71
2.6.1. Buffers and solutions	71
2.6.2. Seed sterilisation	71
2.6.3. MS plates	72
2.6.4. <i>Arabidopsis</i> cell culture	73
2.6.5. <i>Arabidopsis</i> genomic DNA extraction	73
2.6.6. <i>Arabidopsis</i> RNA extraction	73
2.6.7. Isolation of intact <i>Arabidopsis</i> mitochondria	74
2.6.8. Isolation of <i>Arabidopsis</i> chloroplasts	74
2.6.9. Organellar DNA extractions	75
2.6.9.1. Mitochondrial DNA extractions	75
2.6.9.2. Plastid DNA extractions	75
2.6.10. Root-length assays	75
2.7. Nicotiana benthamiana transient expression	76
2.7.1. DNA constructs	76
2.7.2. Buffers and solutions	76
2.7.3. Transformation of <i>Agrobacterium tumefaciens</i>	77
2.7.4. Agroinfiltration solution preparation	77
2.7.5. Small scale protein extraction	77
2.7.6. Growth of BY-2 cells	78
2.7.6.1. Cell-pack formation and transient expression	78
2.7.6.2. Protein extraction	78
2.8. Biochemical assays	79
2.8.1. <i>A. thaliana</i> DNA gyrase buffers	79
2.8.2. <i>E. coli</i> DNA gyrase buffers	79
2.8.3. Topoisomerase enzymes	80
2.8.4. DNA supercoiling assay	80
2.8.5. DNA relaxation assay	80
2.8.6. DNA decatenation assay	80
2.8.7. DNA cleavage assay	80
2.8.8. Inhibition assays	81
2.9. Bis-cat substrate development	81
2.9.1. Tn3 resolvase over-expression and purification	81
2.9.2. Plasmids and DNA	81
2.9.3. Tn3 resolvase-mediated <i>In vitro</i> recombination	82
2.9.3.1. Small scale recombination reactions	82
2.9.3.2. Large scale recombination reactions	83
2.10. Microscopy	83
2.10.1. Inverted microscopy for seed assessment	83

2.10.2. Differential Interface contrast microscopy	83
2.10.3. Transmission electron microscopy	84
2.10.4. Chloroplast Imaging	84
2.10.4.1. Quantitative Image analysis	85
2.11. Databases and Software	86
2.11.1. PlasmDB	86
2.11.2. Sequence alignments	86
2.11.3. Densitometric gel analysis	86
Chapter 3: Expression of Eukaryotic gyrases	87
3.1. Introduction	87
3.2. Results and discussion	88
3.2.1. <i>E. coli</i> expression system	88
3.2.1.1. <i>Plasmodium falciparum</i> gyrase	88
3.2.1.2. <i>Plasmodium berghei</i> gyrase	89
3.2.2. Insect cell expression	93
3.2.2.1. OPPF collaboration	95
3.2.2.2. Recombinant pOPIN plasmids	95
3.2.2.3. Recombination rationale pOPIN system	97
3.1.1.1. pOPIN expression trials	100
3.1.1.2. <i>A. thaliana</i> gyrase (GyrA and GyrB2) can supercoil DNA	104
3.1.1.3. Unsuccessful expression of gyrase subunits	105
3.1.2. Bac-to-Bac Baculovirus expression system	105
3.1.2.1. Acquisition of recombinant pFastBac clones	108
3.1.2.2. Recombinant virus generation	109
3.1.2.3. <i>Plasmodium</i> gyrase expression	111
3.1.2.4. <i>A. thaliana</i> GyrB1 is unstable and toxic	111
3.1.2.5. <i>A. thaliana</i> GyrA expression	114
3.1.2.6. Individual GyrA and GyrB2 subunit expression	115
3.1.3. <i>Nicotiana benthamiana</i> expression	116
3.2. Discussion	118
3.3. Conclusions	122
3.4. Future Work	122
Chapter 4: In vitro characterisation of <i>A. thaliana</i> gyrase	123
4.1. Introduction	123
4.2. Results and discussion	124
4.2.1. <i>Arabidopsis thaliana</i> gyrase supercoiling is dependent on high concentrations of potassium glutamate	124
4.2.2. <i>A. thaliana</i> gyrase can supercoil with Mg ²⁺ or Mn ²⁺ as co-factor	129
4.2.3. <i>Arabidopsis thaliana</i> gyrase DNA relaxation is optimum at intermediate potassium glutamate concentrations	131
4.2.4. <i>A. thaliana</i> gyrase decatenation is independent of potassium glutamate	134
4.2.4.1. Relating all activities of <i>A. thaliana</i> gyrase	135
4.2.5. <i>E. coli</i> gyrase supercoiling, relaxation and decatenation activity determination	137
4.2.6. <i>A. thaliana</i> gyrase possesses superior relaxation and decatenation activities relative to <i>E. coli</i> gyrase.	138
	139
4.2.7. Ciprofloxacin is an effective inhibitor of <i>A. thaliana</i> gyrase supercoiling	140
4.2.8. Ciprofloxacin analogues	141
4.2.9. Novel herbicidal compounds inhibit <i>E. coli</i> gyrase with greater potency than <i>A. thaliana</i> gyrase	144
4.2.10. The novel ciprofloxacin inhibitors are cleavage-complex stabilisers	146

4.2.11. Ciprofloxacin is most effective for impeding <i>A. thaliana</i> growth	147
4.2.12. Ciprofloxacin analogue CA09 is >600-fold more selective towards a herbicidal mode of action	149
4.3. Discussion	150
4.4. Future directions	154
Chapter 5: <i>In vivo</i> analysis of <i>Arabidopsis thaliana</i> DNA gyrase	156
5.1. Introduction	156
5.2. Results and Discussion	159
5.2.1. <i>A. thaliana</i> T-DNA lines	159
5.2.1.1. Acquisition of T-DNA lines	159
5.2.1.2. Genotyping to identify homozygous mutants	160
5.2.2. Phenotypes of homozygous mutants	163
5.2.3. The heterozygous GK-10 line	165
5.2.3.1. Aborted GK-10 ^{-/-} seeds do not account for embryo-lethality	165
5.2.3.2. GK-10 ^{-/-} embryos are defective in 'heart stage' to 'torpedo' transition	167
5.2.4. Phenotypes of homozygous mutants	170
5.2.4.1. Plate-based development of GK-06 ^{-/-} plants differed from wild-type	172
5.2.4.2. Homozygous 67 ^{-/-} plants thrived on soil whilst GK-06 ^{-/-} lagged	174
5.2.4.3. GK-06 ^{-/-} plants are dwarfed	174
5.2.5. Phenotype discussion	177
5.2.6. <i>In vivo</i> contribution of GyrB for root development	179
5.2.6.1. The primary root lengths of homozygous GyrB lines are similar to wild-type	179
5.2.6.2. GK-06 ^{-/-} possess altered lateral root morphology	179
5.2.6.3. Discussing the implications of GyrB in root development	181
5.2.7. Probing the <i>in vivo</i> function of GyrB within chloroplasts	185
5.2.7.1. The mutant GyrB lines did not manifest significant differences in live chloroplasts	185
5.2.8. GyrB1 mutant plants have altered thylakoid networks	189
5.2.8.1. The significance of ultrastructural variations in relation to the chloroplast genome	192
5.2.9. Gyrase transcript levels in homozygous lines	194
5.2.10. Genomic DNA analysis	197
5.2.10.1. The function of the chloroplast	197
5.2.10.2. The origin of chloroplasts	197
5.2.10.3. Structure of the chloroplast genome	198
5.2.10.4. Potential role of gyrase in chloroplast genomes	198
5.2.10.5. Attempts to probe the <i>in vivo</i> role of gyrase	199
5.3. Discussion and Conclusions	200
5.3.1. <i>A. thaliana</i> GyrA	200
5.3.2. <i>A. thaliana</i> GyrB1	201
5.3.3. <i>A. thaliana</i> GyrB2	201
5.4. Future directions	203
Chapter 6: Development of a novel decatenation substrate 'bis-cat' DNA	204
6.1. Introduction	204
6.2. Results and Discussion	207
6.2.1. Expression and activity testing of Tn3 resolvase	207
6.2.2. Manipulation of the pMM5 plasmid	207
6.2.3. Development of pMM6	208
6.2.4. Development of pMM7	212
6.2.5. Development of pMM9	214
6.2.6. Generation of bis-cat DNA	214

6.2.7. Comparison of Bis-cat and kDNA for decatenation by type II topoisomerases	218
6.2.7.1. Bis-cat resolves practical implications of kDNA	218
6.2.7.2. Bis-cat assay: enhanced sensitivity and visualisation of multiple DNA topologies	218
6.2.7.3. Bis-cat mediated study of DNA decatenation	219
6.2.7.4. Limitations of bis-cat substrate	220
6.3. Conclusions	222
6.4. Future directions	223
Chapter 7: Discussion	225
7.1. Introduction	225
7.2. Heterologous expression of <i>A. thaliana</i> gyrase	225
7.3. Where are gyrase subunits localised <i>in vivo</i> ?	226
7.4. Why would <i>Arabidopsis</i> chloroplasts and mitochondria require AtGyrB1 and AtGyrB2?	227
7.5. What is the role of GyrB1 <i>in vivo</i> ?	229
7.6. Does <i>A. thaliana</i> gyrase function as a 'dual' topoisomerase?	230
7.7. Can <i>A. thaliana</i> gyrase be exploited as a novel herbicidal target?	231
7.8. Where next for <i>Plasmodia</i> gyrases?	232
7.9. Conclusions	233
Abbreviations	234
References	236
Appendix	278

List of Figures

Figure 1.1: Topological complications arising during DNA replication.	3
Figure 1.2: Typical reactions performed by type I topoisomerases.	4
Figure 1.3: Typical reactions performed by type II topoisomerases.	5
Figure 1.4: Primary domain architecture of type I topoisomerases.	6
Figure 1.5: Reaction schematics for Type I topoisomerases.	7
Figure 1.6: Primary domain architecture of type II topoisomerases.	12
Figure 1.7: Structure and mechanism of type II topoisomerases.	14
Figure 1.8: Structure of topoisomerase IV.	17
Figure 1.9: Cryo-EM structure of <i>Thermus Thermophilus</i> gyrase	22
Figure 1.10: Structure of <i>E. coli</i> gyrase.	25
Figure 1.11. The mechanism of supercoiling by DNA gyrase.	27
Figure 1.12: The structures of selected aminocoumarins.	29
Figure 1.13. Quinolone structures.	31
Figure 1.14: Structure of simocyclinone D8.	32
Figure 1.15: The chemical structure of mature MccB17	33
Figure 1.16. <i>E. coli</i> GyrA and <i>A. thaliana</i> GyrA sequence alignment.	40
Figure 1.17. <i>E. coli</i> GyrB and <i>A. thaliana</i> GyrB1/B2 sequence alignment.	41
Figure 1.18: Primary domain architecture of <i>E. coli</i> and <i>P. falciparum</i> GyrA.	47
Figure 2.1: Schematic of In-Fusion cloning.	57
Figure 3.1: <i>P. falciparum</i> gyrase expression in <i>E. coli</i> .	91
Figure 3.2: <i>Plasmodia</i> gyrase expression in <i>E. coli</i> .	92
Figure 3.3: Schematic of homologous recombination mediated baculovirus transfection of insect cells.	94
Figure 3.4: pOPIN vectors.	96
Figure 3.5: AcMPNV genome engineering.	98
Figure 3.6: Schematic of baculovirus mediated insect cell expression.	99
Figure 3.7: Baculovirus mediated expression trials of <i>A. thaliana</i> gyrase.	101
Figure 3.8: Supercoiling assay of gyrase formed by association of AtGyrB2 and EcGyrA.	102
Figure 3.9: <i>A. thaliana</i> GyrA detection.	103
Figure 3.10: <i>A. thaliana</i> gyrase (GyrA & GyrB2) purification and activity.	104
Figure 3.11: Schematic of the Bac-to-bac expression system	107
Figure 3.12: Recombinant bacmid PCR confirmation.	110
Figure 3.13: <i>A. thaliana</i> GyrB1 expression.	113
Figure 3.14: <i>A. thaliana</i> GyrA infection of sS9-2.	114

Figure 3.15: Individual expression of <i>A. thaliana</i> GyrA and GyrB2.	115
Figure 3.16: Summary of <i>N. benthamiana</i> transient expression.	116
Figure 3.17: Transient <i>N. benthamiana</i> expression.	117
Figure 4.1: <i>A. thaliana</i> gyrase phylogeny.	125
Figure 4.2: Supercoiling assay in different commercial buffers.	126
Figure 4.3: <i>A. thaliana</i> gyrase supercoiling in response to K ₂ Glu titration.	126
Figure 4.4: Response of <i>A. thaliana</i> supercoiling in response to different temperatures.	128
Figure 4.5: Optimum <i>A. thaliana</i> gyrase supercoiling	128
Figure 4.6: <i>A. thaliana</i> DNA supercoiling assay with divalent metal ions.	129
Figure 4.7: <i>A. thaliana</i> gyrase supercoiling titration assay with 4 mM Ca ²⁺ .	130
Figure 4.8: <i>A. thaliana</i> gyrase relaxation activity.	132
Figure 4.9: <i>A. thaliana</i> gyrase DNA cleavage assay.	133
Figure 4.10: Topoisomerase decatenation substrates.	134
Figure 4.11: <i>A. thaliana</i> gyrase mediated reactions.	136
Figure 4.12: <i>E. coli</i> gyrase-mediated reactions	138
Figure 4.13: Determination of <i>A. thaliana</i> and <i>E. coli</i> EC ₅₀ .	139
Figure 4.14: Structures of novel ciprofloxacin analogues.	143
Figure 4.15: Inhibition potential of CA20.	144
Figure 4.16: Ciprofloxacin analogue cleavage assays.	147
Figure 4.17: Screening of ciprofloxacin analogues with <i>A. thaliana</i> .	148
Figure 4.18: GyrA sequence alignments.	152
Figure 5.1: GFP localisation experiments.	158
Figure 5.2: Schematic representation of T-DNA insertions, positions and PCR results.	162
Figure 5.3: Observed phenotypes of GyrA and GyrB2 mutant plants.	164
Figure 5.4: Dissected siliques of the GyrA GK-10 line exposing the next generation of seeds.	166
Figure 5.5. DIC microscopy images of the progeny of GK-10+/+ and GK-10+/- embryos	168
Figure 5.6: Analysis of GyrA transcripts during embryonic development of Columbia-0	169
Figure 5.7: Representative images of assigned growth stages for phenotypic analysis.	170
Figure 5.8: Summarised output of plate-based phenotypic analysis.	173
Figure 5.9: Summarised output of soil-based phenotypic analysis.	175
Figure 5.10: Representative images of wild-type and mutant GyrB lines.	176
Figure 5.11: RNA-based expression profiling of <i>Arabidopsis</i> gyrase subunits.	178
Figure 5.12: Root analysis of wild-type and homozygous lines.	180

Figure 5.13: Expression profiling of GyrB1 and GyrB2 in the Columbia-0 primary roots.	182
Figure 5.14: Expression profiling of GyrB1 and GyrB2 proteins within the concentric cell layers of the Columbia-0 <i>Arabidopsis</i> primary root.	184
Figure 5.15: Two-dimensional determination of chloroplast area.	188
Figure 5.16: Chloroplast transmission electron microscopy images.	190
Figure 5.17: Average chloroplast area determined from TEM images.	191
Figure 5.18: Model for intra-organellar plastid nucleoid organization.	192
Figure 5.20: Homozygous 78 ^{-/-} plants.	194
Figure 5.18: Semi-quantitative RT-PCR analysis of Gyr transcripts.	195
Figure 6.1: Reaction scheme for Tn3-mediated recombination. Schematic diagram of Tn3 resolvase mechanism of action.	206
Figure 6.2: Schematic of Tn3 substrate and product; gel analysis of recombination reaction.	209
Figure 6.3: Tn3 resolvase substrate plasmids.	211
Figure 6.4: Tn3 resolvase recombination with pMM6 and pMM7.	213
Figure 6.5: The generation of bis-cat DNA.	216
Figure 6.6: Analysis of caesium chloride gradient material.	217
Figure 6.7: DNA decatenation mediated by kDNA and bis-cat DNA.	221
Figure 6.8: Inhibition of DNA decatenation.	222
Figure 6.9: Purification of bis-cat DNA from uncatenated DNA using DNA triplex sequences.	224
Figure 7.1: <i>A. thaliana</i> gyrase transcript levels.	228

List of Tables

Table 1.1 <i>Arabidopsis thaliana</i> topoisomerase (topo) genes and predicted targeting according to the Subcellular Localisation Database for Arabidopsis proteins (SUBA)	37
Table 1.2. <i>Arabidopsis</i> DNA gyrase genes adapted from (Wall et al. 2004).	38
Table 1.3. <i>Plasmodium falciparum</i> strain 3D7 topoisomerase genes according to annotations on the PlasmoDB.	44
Table 2.1: <i>E. coli</i> strains and genotypes used in this work.	51
Table 2.2: Antibiotics, their stock and working concentrations used in this work.	52
Table 2.3: Buffers used for DNA analysis in this work.	54
Table 2.4: Polymerases used in this work and their main applications.	57
Table 2.5: RT-PCR primer sequences used in this work.	58
Table 2.6: <i>A. thaliana</i> and <i>P. falciparum</i> gyrase expression constructs. Constructs of codon optimised, and non-codon optimised sequences were sourced commercially.	62
Table 2.7: Monocistronic expression constructs generated for this study.	63
Table 2.9: <i>A. thaliana</i> polycistronic expression clones generated.	63
Table 2.8: Gyrase fusion constructs used in this work.	64
Table 2.10: pETDuet constructs and oligonucleotides for <i>E. coli</i> expression.	66
Table 2.11: Buffers and solutions for insect cell expression and purification.	69
Table 2.12: <i>Arabidopsis thaliana</i> T-DNA lines investigated in this work.	71
Table 2.13: Buffers and solutions used for <i>in vivo Arabidopsis thaliana</i> work.	72
Table 2.14: Percoll gradient preparation.	74
Table 2.15: pHREAC expression constructs used in this work.	76
Table 2.16: Buffers and solutions for transient expression in <i>N. benthamiana</i> .	76
Table 2.17: <i>A. thaliana</i> gyrase assay buffers.	79
Table 2.18: <i>E. coli</i> gyrase assay buffers	79
Table 2.19: Plasmids created for use in Tn3 recombination reactions.	82
Table 2.20: <i>Plasmodium</i> gyrase sequences.	86
Table 3.1: pOPIN expression constructs explored by co-transfection with linearised AcMPNV bacmid DNA.	99
Table 3.2: The clones of <i>P. falciparum</i> , <i>P. vivax</i> , <i>P. berghei</i> and <i>A. thaliana</i> pursued for investigation by the Bac-to-Bac expression system. All clones included a cleavable N-terminal hexa-histidine tag.	109
Table 3.3: Combination of genes from donor plasmids used to form the recombinant bacmid	110
Table 4.1: Relative activities for <i>A. thaliana</i> and <i>E. coli</i> gyrase.	138

Table 4.2: IC50 values determined for inhibition of supercoiling for ciprofloxacin analogues against recombinant <i>E. coli</i> gyrase and <i>A. thaliana</i> gyrase.	145
Table 4.3: Ciprofloxacin analogues of <i>E. coli</i> MIC values <25 mg/L and their respective herbicidal potency for <i>A. thaliana</i> (IC ₅₀). The inhibitory potential <i>in vitro</i> for <i>A. thaliana</i> and <i>E. coli</i> gyrases are also indicated. Error values represent standard error of the mean. Table adapted from (Wallace et al. 2018).	149
Table 5.1: <i>Arabidopsis thaliana</i> T-DNA insertion lines explored in this study.	159
Table 5.2: Primer sequences for T-DNA genotyping PCRs for detection of wild-type genotype or the presence of the T-DNA insertion within the <i>A. thaliana</i> genome.	161
Table 5.3: <i>Arabidopsis</i> growth stages for phenotypic plate-based analysis according to the previous methods of Boyes <i>et al.</i> , 2001.	171
Table 5.4: <i>Arabidopsis</i> growth stages for phenotypic soil-based analysis according to the previous methods of Boyes <i>et al.</i> , 2001.	171
Table 5.5: Average soil-based phenotypic measurements of 10 plants.	176
Table 5.6. Mean chloroplast area and autofluorescence intensities with standard deviations. Number of chloroplasts assessed: wild-type (WT): 250, 67 ^{-/-} : 406, 78 ^{-/-} : 146 and GK-06 ^{-/-} :296.	186
Table 6.1: Plasmids created for use in Tn3 recombination reactions.	210
Table 7.2: Percentage protein sequence identities of <i>E. coli</i> and <i>S. aureus</i> gyrase and topo IV subunits to corresponding <i>A. thaliana</i> gyrase subunits. Percentage identities were determined through the NCBI protein blast feature.	231

Chapter 1: Introduction

1.1. DNA topology

In 1953, Watson and Crick first proposed the double-helix model for DNA. It was promptly evident that the model postulated a possible copying mechanism for genetic material (Watson and Crick 1953a). The problematic implications arising from the double-helix model, in particular, the fact that the two chains of DNA are intertwined, and the need for them to untwist in order to separate and facilitate replication were also quickly realised (Watson and Crick 1953b). Naturally, processes such as replication, transcription and recombination, which require the separation of these intertwined strands of DNA, lead to DNA over-winding and entanglement (Liu and Wang 1987). The topological intermediates formed during these events interfere with vital cell processes such as: gene expression, DNA replication and chromosome segregation. Conversely, DNA supercoiling is a critical step in genome compaction and in promoting DNA unwinding at gene promoter regions and replication origins (Holmes and Cozzarelli 2000; Wang 2002a). Thus, the cell invests energy into both these essential yet contrasting processes, in order to preserve genomic information and to maintain DNA topology in an appropriate topological state.

The topology of DNA is governed by three mathematical concepts, namely; twist (T_w), writhe (W_r) and linking number (L_k). In simple terms, the twist of a segment of DNA is the number of double-helical turns, measured relative to the DNA helix axis (Bates and Maxwell 2005). Conventionally, a right-handed twist of the Watson-Crick structure is assigned a positive value. Writhe, a spatial parameter of DNA, is a measure of the contortion of the helix axis in space, it can be thought of as the number of times the molecule crosses itself when projected in two-dimensions. The two geometric parameters can be summed by a third parameter, linking number ($L_k = T_w + W_r$), which specifies the number of times the two strands of a DNA duplex circle are interwound (Bates and Maxwell 2005). Topoisomerases reorganize the spatial geometry of DNA by altering one of these underlying geometrical properties. In order to do this, it is critical for them to read both the local geometry of DNA segments and the global energetics of the genome (Schoeffler and Berger 2008).

1.2. Topoisomerases *in vivo*

The significance of topoisomerases *in vivo* is evident, for example, if the process of DNA replication, critical for cellular survival, is considered. Replication becomes a topological issue *in vivo*, extending from prokaryotes, which often have closed-circular chromosomal DNA, to eukaryotes, where although the chromosomal DNA is linear, it is often restrained by linkage to biological membranes or scaffolds, essentially creating a topologically constrained domain, not too different to the prokaryotic arrangement (Bates and Maxwell 2005). If the process of replication is considered in more detail, it can be essentially sub-divided into the following stages: initiation, elongation and termination. The DNA found in cells is usually in a negatively supercoiled state, either by the conservation of this topology by topoisomerases (gyrase) or through the action of DNA wrapping around histone proteins. DNA of this topology ensures easier strand separation, due to its physical properties therefore permitting the initiation of replication. The subsequent elongation of replication requires the helix to separate, allowing the active replisome access to nucleotides. The separation of the duplex, comprising effectively of topologically constrained DNA, leads to the accumulation of positive DNA supercoils ahead of the replicating fork and precatenanes behind it (Figure 1.1) (Vos et al. 2011). If allowed to persist, the accumulating positive supercoils would eventually impede the progression of the replication fork resulting in premature termination, whilst the unresolved precatenanes would lead to DNA entanglements, catenation and improper segregation (Vos et al. 2011). The resolution of such DNA complexes and continuation of vital cellular processes is modulated by the topoisomerase enzymes.

1.3. Topoisomerases

Topoisomerases are responsible for catalysing interconversions between different forms of DNA. These enzymes can be distinguished by their ability to create transient DNA strand breaks, either single or double-stranded in nature. The topoisomerases mediate this reaction via nucleophilic attack of a tyrosine residue on the phosphodiester backbone, creating a covalent phosphotyrosyl linkage. The strand-scission mechanism of these enzymes forms the basis for their classification into either type I or type II; the former initiate transient single-stranded breaks and change the DNA linking number in steps of one, whilst the latter introduce transient double-stranded breaks and change the linking number in steps of two. The reactions catalysed by topoisomerases are visually represented in Figure 1.2 for type I enzymes, and Figure 1.3 for the type IIs.

Further classification of topoisomerases is also possible, based on both amino-acid sequence and mechanism of action. The type I topoisomerases comprise the following subgroups: IA, IB, and IC; whilst the type II enzymes comprise only two subgroups: IIA and IIB. All topoisomerase reactions are supported by one of three mechanisms: DNA swivelase, DNA single-strand passage, or DNA double-strand passage (Dean and Cozzarelli 1985; Stewart et al. 1998a; Wang 1998).

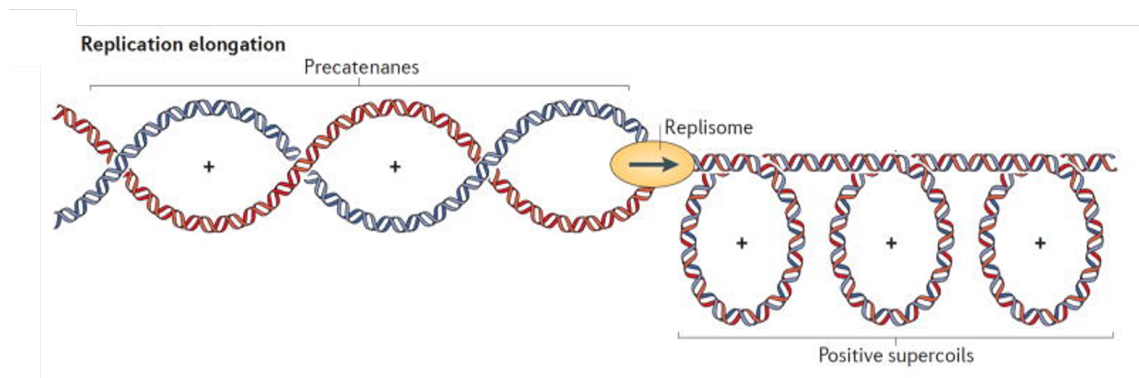


Figure 1.1: Topological complications arising during DNA replication.

The movement of the replisome along the replicating duplex requires its separation. As a consequence, positive supercoils form ahead of the replication fork and precatenanes in the newly replicated DNA behind it. If left unresolved, the build-up of positive supercoils have potential to impede progression of the replisome, therefore leading to premature replication termination. The persistence of precatenanes can lead to tangled DNA through the formation of permanent catenanes and abnormal segregation of DNA into daughter cells. Figure adapted from (Vos et al. 2011) with permission.

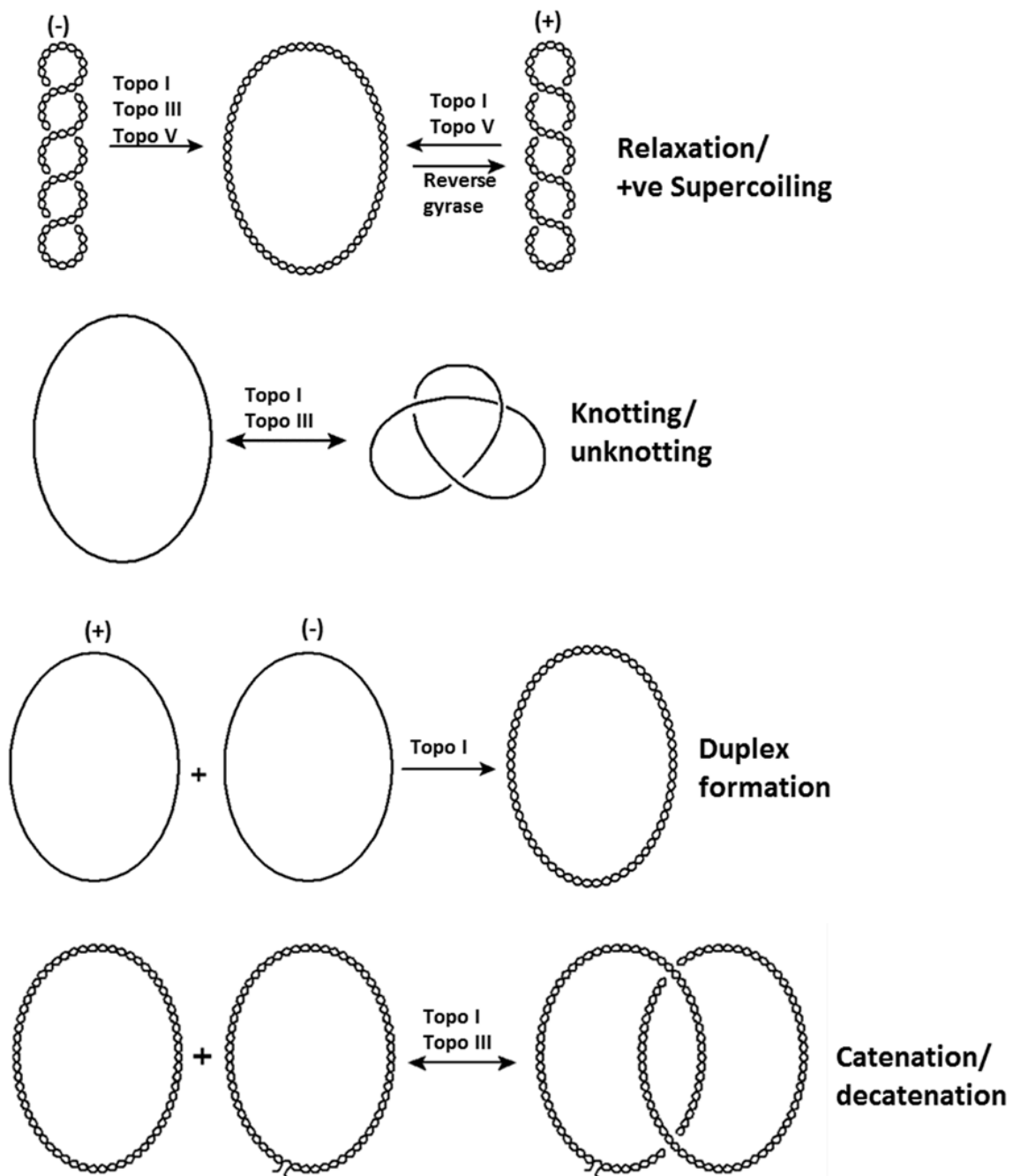


Figure 1.2: Typical reactions performed by type I topoisomerases.

The type I enzymes are able to catalyse the reactions illustrated above, as labelled and according to the directions of the arrows, through the transient introduction of single-stranded breaks in their substrates. The non-nicked plasmids involved in the catenation/decatenation reaction, although illustrated in relaxed form here for demonstrative clarity, may in fact be supercoiled *in vivo*. Figure taken from Bush et al., 2015 with permission (Bush et al. 2015).

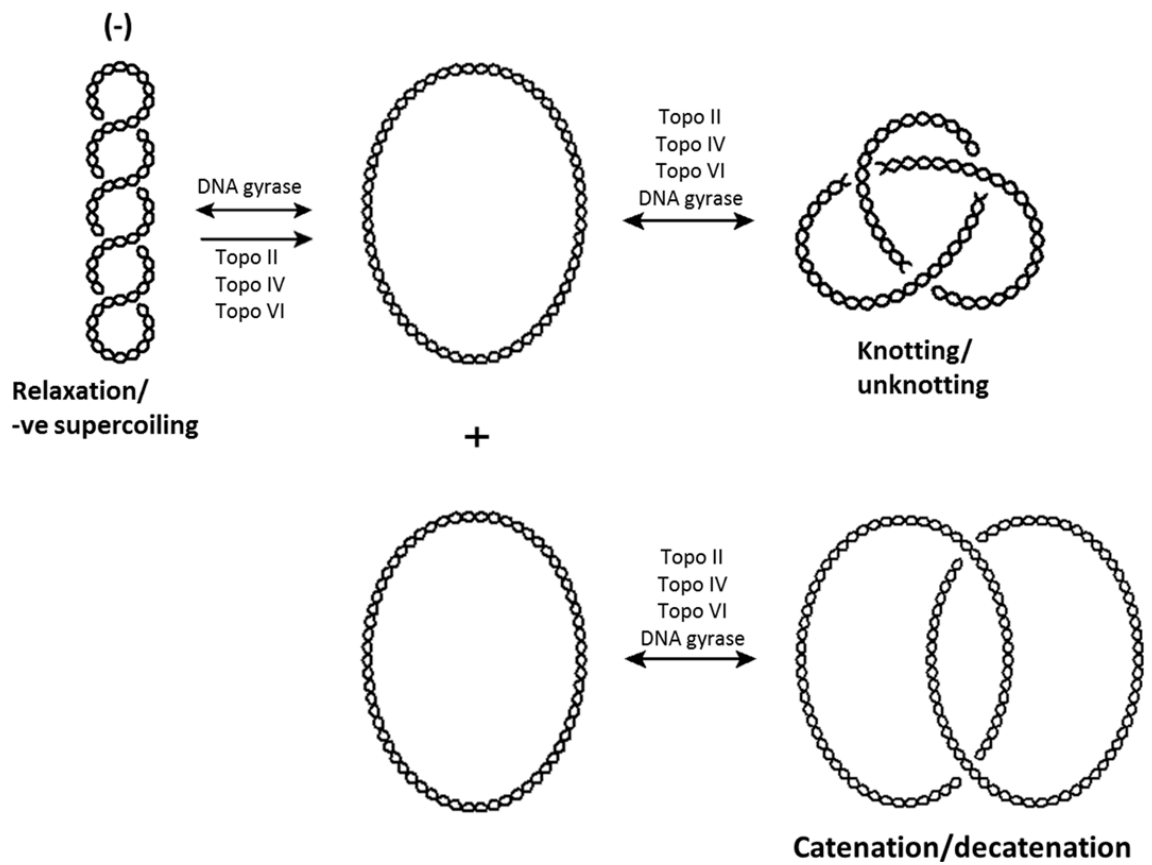


Figure 1.3: Typical reactions performed by type II topoisomerases.

The type II enzymes are able to catalyse the reactions illustrated above, as labelled and according to the directions of the arrows, through the transient introduction of double-stranded breaks in their substrates. The plasmids involved in the catenation/decatenation reaction, although illustrated in relaxed form here for demonstrative clarity, may in fact be supercoiled *in vivo*. Type II enzymes are also able to relax positively supercoiled DNA. Figure taken from Bush et al., 2015 with permission (Bush et al. 2015).

1.4. Type I topoisomerases

The single-stranded type I topoisomerases can be divided based on sequence and mechanistic differences into the sub-types: IA, IB and IC; specific examples for the primary domain architecture of enzymes belonging to each sub-group are given in Figure 1.4

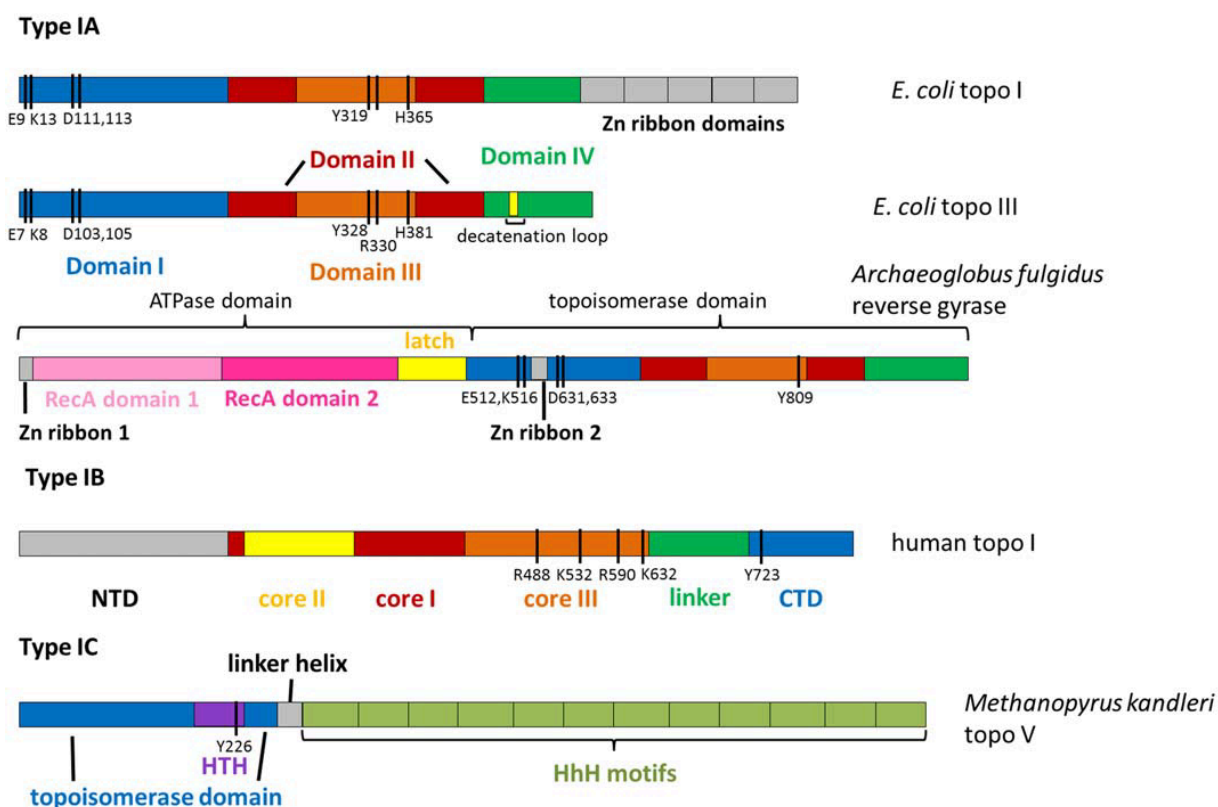


Figure 1.4: Primary domain architecture of type I topoisomerases.

The catalytic residues are given by black bars. The position of the catalytic tyrosine which mediates nucleophilic attack upon the phosphodiester backbone of DNA, prior to covalently attaching to it, is within domain III of type IA topoisomerases but found in the CTD of human topoisomerase I (type IB) and a helix-turn-helix domain in the *Methanopyrus kandleri* topoisomerase V (type IC). The details of other catalytic residues are reviewed in (Schoeffler and Berger 2008). The names of domains are labelled in corresponding colours (HhH: helix-hairpin-helix). Figure taken from (Bush et al. 2015) with permission.

1.4.1. Type IA topoisomerases

The toroidal structured type IA topoisomerases regulate DNA topology using a strand-passage mechanism that involves the formation of a 5' phosphotyrosyl link following DNA cleavage, the physical opening of a single DNA strand, passage of a second DNA strand through the gap and the resealing of the broken strand (Figure 1.5a) (Lima et al. 1994). The arrangement of primary domains of Type IA topoisomerases are well-conserved throughout the three domains of life; bacteria possess two type IA paralogues, topoisomerase I and III, eukaryotes conserve topoisomerase III and archaea maintain reverse gyrase (Forterre et al. 2007). The single-strand passage type IA topoisomerases are individually discussed below.

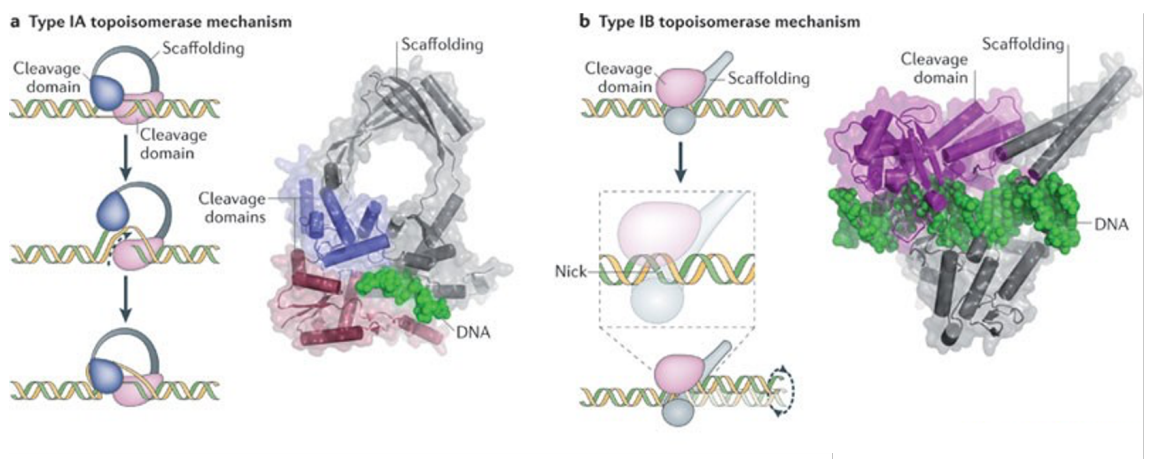


Figure 1.5: Reaction schematics for Type I topoisomerases.

(a) Reaction mechanism of Type IA topoisomerases, these enzymes pass a single strand of DNA (yellow) through a transient single-stranded DNA break (green). To the right is the structure of *E. coli* topoisomerase III bound to DNA (Changela et al. 2001). (b) Reaction mechanism of Type IB topoisomerases, these enzymes nick one strand of the duplex (green) and control its end during the rotation around the intact duplex strand (yellow). The structure of human topoisomerase IB bound to DNA is given to the right (Stewart et al. 1998b). Figure taken from (Vos et al. 2011) with permission.

1.4.1.1. Topoisomerase I

Bacterial topoisomerase IA, the first DNA topoisomerase discovered and originally referred to as 'omega-protein', functions to relax negatively supercoiled DNA in a nucleotide-independent reaction (Wang 1971). Although topoisomerase IA is able to remove supercoils, catenate, decatenate and unknot DNA (Figure 1.2) its principal role within bacterial cells is the removal of negative DNA supercoils, specifically, to prevent the accumulation of transcription-derived negative supercoiling behind the proceeding replication fork (Lima et al. 1994). The loss of topoisomerase I function leads to hypernegative supercoiling of the genome and consequential stabilisation of intracellular R-loops (DNA-RNA hybrids) (Massé and Drolet 1999). The processive removal of negative supercoils has been assigned to the C-terminal region of the *E. coli* topoisomerase IA (Terekhova et al. 2013); specifically, the zinc-ribbon domain of the enzyme from which the removal of bound zinc ions, or mutation of cysteine residues, both resulted in the inability of topoisomerase IA to remove negative supercoils (Tse-Dinh 1991; Zhu et al. 1995). The transcription-related activity of the enzyme is further supported by its direct interaction with RNA polymerase via the zinc-ribbon domains (Cheng et al. 2003). The deletion of topoisomerase IA is particularly severe when RNase H activity is reduced (Stockum et al. 2012). The persistence of R-loops can contribute towards genome instability by the inhibition of transcription and replication (Hamperl and Cimprich 2014; Skourti-Stathaki and Proudfoot 2014). Interestingly, compensatory mutations are often detected in strains in which topoisomerase IA is inactivated, these are often encountered within genes encoding the gyrase enzyme (section 1.6), causing a compensatory reduction in the enzyme's activity to introduce negative supercoils (DiNardo et al. 1982).

1.4.1.2. Topoisomerase III

Topoisomerase III is of the subclass IA, these enzymes are able to relax negative supercoils and decatenate DNA (DiGate and Marians 1989). Uniquely, they also possess the ability to cleave and decatenate RNA molecules (Wang et al. 1996). The two *E. coli* enzymes topoisomerase I and III possess a high level of sequence and structural similarity, however, an exclusive feature of topoisomerase III is the occurrence of an additional loop, termed the decatenation loop, thought to provide the enzyme with its unique decatenation ability (Figure 1.4) (Mondragón and DiGate 1999). The primary function of topoisomerase III is thought to be resolution of precatenanes, chromosome segregation and resolution of recombination intermediates (Perez-Cheeks et al. 2012). The eukaryotic topoisomerase III lacks the decatenation loop but possess two isoforms of the enzyme: topoisomerase

III α and topoisomerase III β . The former isoform plays an important role in DNA-repair complexes, whilst the latter is involved in RNA metabolism.

The *Arabidopsis* genome also possesses the two isoforms of the enzyme, topoisomerase III α and topoisomerase III β , encoded on chromosomes 5 and 2, respectively (Initiative 2000). Although identified as essential in the majority of higher eukaryotes in which topoisomerase III α has been identified, including mammals, *C. elegans*, and *D. melanogaster*, depletion of the *Arabidopsis* protein alone does not result in embryo-lethality (Dorn et al. 2018; Kim et al. 2000; Li and Wang 1998; Plank et al. 2005). Interestingly the protein is involved in the processing of Holliday-junction-like DNA repair intermediates and is targeted to these sites by one of its four zinc-finger domains (Dorn et al. 2018). In contrast, topoisomerase III β mutants only produced phenotypically distinguishable results in mouse mutants, resulting in shortened lifespan, aneuploidy and DNA damage response defects (Kwan et al. 2007; Mohanty et al. 2008). The role of topoisomerase III β , within *Arabidopsis*, remains unexplored. In addition, a putative topoisomerase III of ~710 amino acids, is encoded in the *P. falciparum* genome but its activity thus far remains uncharacterised (Gardner et al. 2002b).

1.4.1.3. Reverse gyrase

Reverse gyrase belongs to the type IA topoisomerase category. It is unique in its ability to introduce positive DNA supercoils and relax negatively supercoiled DNA, by using the energy of ATP hydrolysis (Forterre et al. 1985; Shibata et al. 1987). The enzyme achieves these activities due to its interesting composition. The crystal structure of reverse gyrase has identified two functional domains, the N-terminus, which possesses a helicase-like structure and activity, and the C-terminus, which is remarkably similar to topoisomerase I (Figure 1.4) (Rodríguez and Stock 2002). Indeed, deletion of the N-terminal helicase domain of the enzyme results in ATP-independent relaxation of negative supercoils, that is, typical topoisomerase I function (Déclais et al. 2001). The specific introduction of positive supercoils is thought to be consequential of the enzymes controlled unwinding activity (Rodríguez 2003). Reverse gyrase has been found in thermophilic, hyper-thermophilic archaea and eubacteria (Forterre 2002; Forterre et al. 1985; Shibata et al. 1987). No evidence for its presence is found in eukaryotes, including plants.

1.4.2. Type IB topoisomerases

The type I topoisomerases present in eukaryotes are fundamentally of the type IB, which differ in terms of structure and mechanism from type IA enzymes. Although these enzymes also perform the DNA cleavage reaction mediated by a nucleophilic tyrosine, there are important differences in their mechanism of action. For example, the catalytic tyrosine for a type IB enzyme is provided by a helix-turn-helix fold similar to tyrosine recombinases and integrases (Cheng et al. 1998; Redinbo et al. 1998). In further contrast, the type IB family operate by a swivelase mechanism that involves the nicking of a single strand of DNA and the formation of a covalent 3' phosphotyrosine intermediate (Figure 1.5b) (Champoux 1981; Champoux and Dulbecco 1972). As a result, the 5' end of the cleaved DNA duplex is able to rotate around the intact phosphodiester bond on the opposite strand. The rotation, driven by the free energy stored in DNA supercoils, allows relaxation of both positive and negative supercoils and is controlled by the friction between the enzyme and DNA (Koster et al. 2005). The structure acquisition of human topoisomerase IB interacting with DNA was seminal towards differentiating the mechanism of action of these enzymes from type IA topoisomerases (Redinbo et al. 1998). Type IB topoisomerases are ubiquitous amongst eukaryotes and until relatively recently were thought to be exclusive to eukaryotes and poxvirus. However, orthologues of the enzyme have been identified in certain bacteria, suggesting the possibility of horizontal gene transfer between the kingdoms (Gadelle et al. 2003; Krogh and Shuman 2002).

1.4.2.1. Topoisomerase IB

Topoisomerase IB has been shown to preferentially bind supercoiled DNA over relaxed DNA substrates. Interestingly, some variants of the enzyme have demonstrated proclivity for positively supercoiled DNA, which they can relax at a faster rate (Frohlich et al. 2007; Gadelle et al. 2003). Topoisomerase IB activity has also been identified in plants; the chloroplastic partially purified protein from spinach has been reported to relax negatively supercoiled DNA in a Mg^{2+} -dependent, but ATP-independent manner (Siedlecki et al. 1983); a similar activity has also been identified in wheat mitochondria (Echeverria et al. 1986). The nuclear pea topoisomerase I has been cloned and overexpressed in *E. coli*, the purified protein demonstrates the ability to relax positive and negative supercoils in an ATP- and Mg^{2+} -independent manner; remarkably, it is claimed that in the presence of Mg^{2+} only, the purified protein introduces positive supercoils (Reddy et al. 1998). In a similar fashion, topoisomerase I from *Nicotiana tabacum* has also been cloned and

overexpressed in *E. coli* and the recombinant protein has been shown to relax positive and negative DNA supercoils, in an ATP- and Mg²⁺-independent fashion; the activity of the protein was inhibited by the known topoisomerase I inhibitor, camptothecin (Mudgil et al. 2002).

Topoisomerase IB proteins are also encoded by the *Arabidopsis* genome. Of the three encoded proteins, one possesses a putative N-terminal chloroplast targeting sequence, whilst the remaining two have putative nuclear localisation signals (Singh et al. 2004). The disruption of a nuclear encoded topoisomerase IB protein altered the morphology of *Arabidopsis*; the plants possessed random internode lengths and angles, plausibly thought to be a consequence of an accumulation of torsional tensions in the DNA that essentially prevent cell proliferation (Takahashi et al. 2002).

Topoisomerase IB is also encoded in the genome of *Plasmodium falciparum*, notably recognised as the parasitic cause of human malaria infections. The protein is encoded on chromosome 5, by a gene of 839 amino acids (~104-kDa), and its sequence is 42% similar to the human enzyme (Tosh and Kilbey 1995). The expression of *Plasmodium falciparum* topoisomerase IB was shown to be differentially regulated in the plasmodial life cycle, the gene promoter becomes active during the asexual cycle from its formerly inactive state in the ring form of development, additionally, high transcript levels are found in the trophozoite stage of the life cycle and the enzyme's activity was found to be sensitive to the topoisomerase I inhibitor, camptothecin (Tosh et al. 1999).

1.4.3. Type IC

1.4.3.1. Topoisomerase V

Topoisomerase V is the sole member of the type IC family. The enzyme was initially classed within the type IB category because of its ability to relax positive and negative supercoils independent of both ATP and Mg²⁺ ions, in addition to its attachment to the phosphodiester backbone of DNA via a 3' phosphotyrosine intermediate (Slesarev et al. 1993). However, a combination of biochemical and structural work resulted in the classification of the enzyme, hitherto identified only from *Methanopyrus kandleri*, to form a subfamily of its own (Figure 1.4) (Rajan et al. 2010; Taneja et al. 2006). Interestingly, Topoisomerase V is not only sequentially different, it also adopts a unique fold amongst topoisomerases; an additional unique feature of the enzyme is its role in DNA repair, specifically the repair of abasic DNA damage, through its apurinic/apyrimidic base-excision activity (Belova et al. 2001; Rajan et al. 2013).

1.5. Type II topoisomerases

The double-stranded type II topoisomerases can be subdivided based on sequence and mechanistic differences into the sub-types: IIA and IIB. The primary domain arrangements of specific examples of each sub-class are given in Figure 1.6 for comparison.

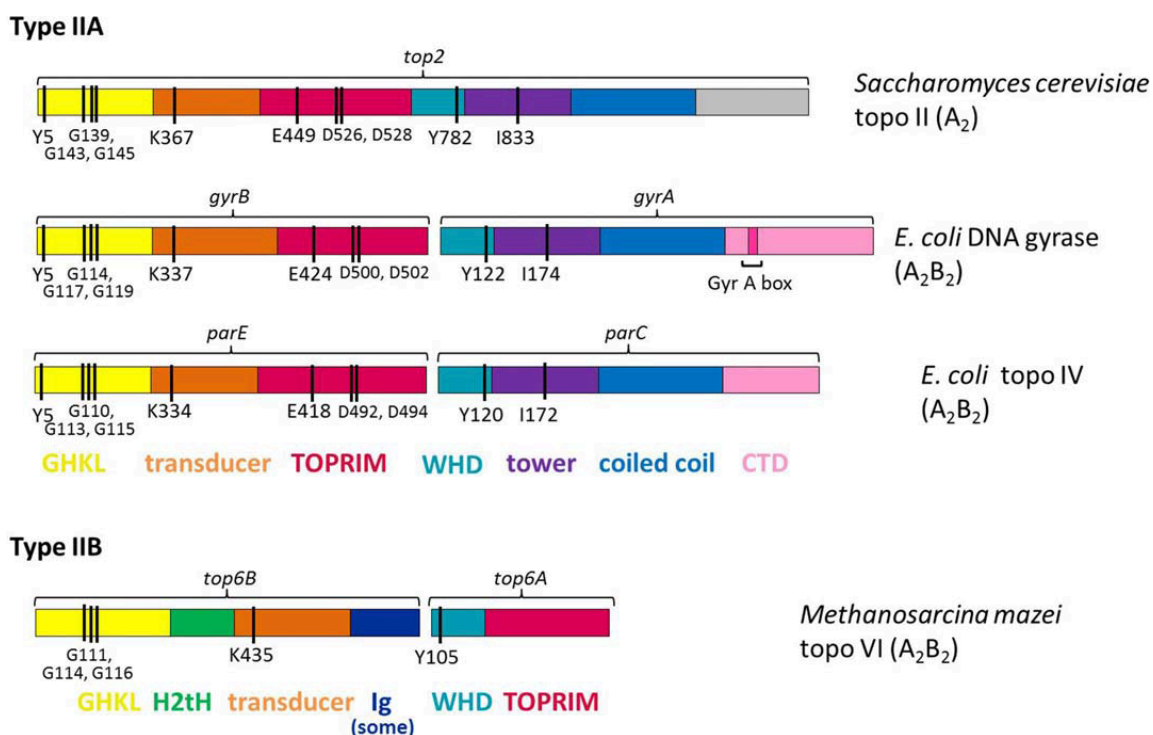


Figure 1.6: Primary domain architecture of type II topoisomerases.

The catalytic residues are given by black bars – the position of the catalytic tyrosine which mediates nucleophilic attack upon the phosphodiester backbone of DNA prior to covalently attaching to it is within the WHD domain of both IIA and IIB topoisomerases. The details of other catalytic residues are reviewed in (Schoeffler and Berger 2008). GHKL domain is the ATPase domain, TOPRIM represents the topoisomerase-primase domain. The two of these in addition to the transducer domain are shared amongst all type IIA topoisomerases. WHD: winged-helix domain; CTD: C-terminal domain; H2tH: helix-helix turn helix; Ig: immunoglobulin type fold. The names of domains are labelled in corresponding colours. Figure taken from (Bush et al. 2015) with permission.

1.5.1. Type IIA topoisomerases

Type IIA topoisomerases function to regulate DNA topology in a similar way to the strand-passage mechanism of type IA enzymes (Brown and Cozzarelli 1981). However, contrary to the action of the type IA enzymes, the type IIA topoisomerases create an enzyme-bridged gap by cleaving both strands of DNA and covalently attaching to the 5' end of each cleaved strand. Subsequently, a second intact DNA segment is passed through the break and the cleaved DNA ends are re-joined (Liu et al. 1980; Mizuuchi et al. 1980; Morrison and Cozzarelli 1979). Therefore, the reactions of type II topoisomerases change the linking number in steps of two, and lead to sign inversion, that is, the conversion of a positive supercoil to a negative supercoil (Brown and Cozzarelli 1979; Mizuuchi et al. 1980). In addition, they use ATP to drive strand passage (Gellert et al. 1976); surprisingly, the majority of type II enzymes consume ATP to support reactions that do not require a net energy input, for example, the relaxation of a supercoiled substrate in an energetic state that already favours relaxation. It has been suggested that the energy released by ATP hydrolysis in such reactions is used to control the separation of protein-protein interfaces during the DNA cleavage step, in an attempt to prevent the accidental formation of lethal double-strand DNA breaks (Bates et al. 2011).

Type IIA topoisomerases are found in all cellular organisms and some viruses. This subgroup can be further divided into three sets, based on differential functions: eukaryotic topoisomerase II, bacterial topoisomerase IV and bacterial and archaeal gyrase (Vos et al. 2011). The type IIA topoisomerases exhibit two-fold symmetry within their three-dimensional structures, despite the fact that the stoichiometry of enzymes may differ; for example, the active enzyme may constitute a homodimer (eukaryotic and viral topoisomerase II), a heterotetramer (gyrase and topoisomerase IV), or a heterohexamer (bacteriophage T4 topoisomerase II). A consequence of this two-fold symmetry, is the formation of subunit interfaces, or gates, that separate two cavities within the protein (Figure 1.7a). Briefly, the type IIA topoisomerases operate through a two-gate mechanism, which involves the binding of two regions of DNA, the gate-segment (G-segment) and transport-segment (T-segment). The mechanism involves binding and bending of the G-segment across the DNA-gate of the enzyme. The binding of ATP at the ATPase domain, results in the capture of a T-segment within the upper cavity. The hydrolysis of ATP is concurrent with double-stranded cleavage of the G-segment, with a 4 bp stagger, and the passing of the T-segment through the double-stranded G-segment break, into the lower cavity of the enzyme, which is formed by the C-terminal domains (CTDs). The G-segment is religated and the T-segment is passed through the final dimer-interface, the C-gate. The

release of bound ADP allows the enzyme to return to its original conformation (Bates et al. 2011; Schmidt et al. 2012). The mechanism of action is described in greater depth for gyrase in 1.6.2.

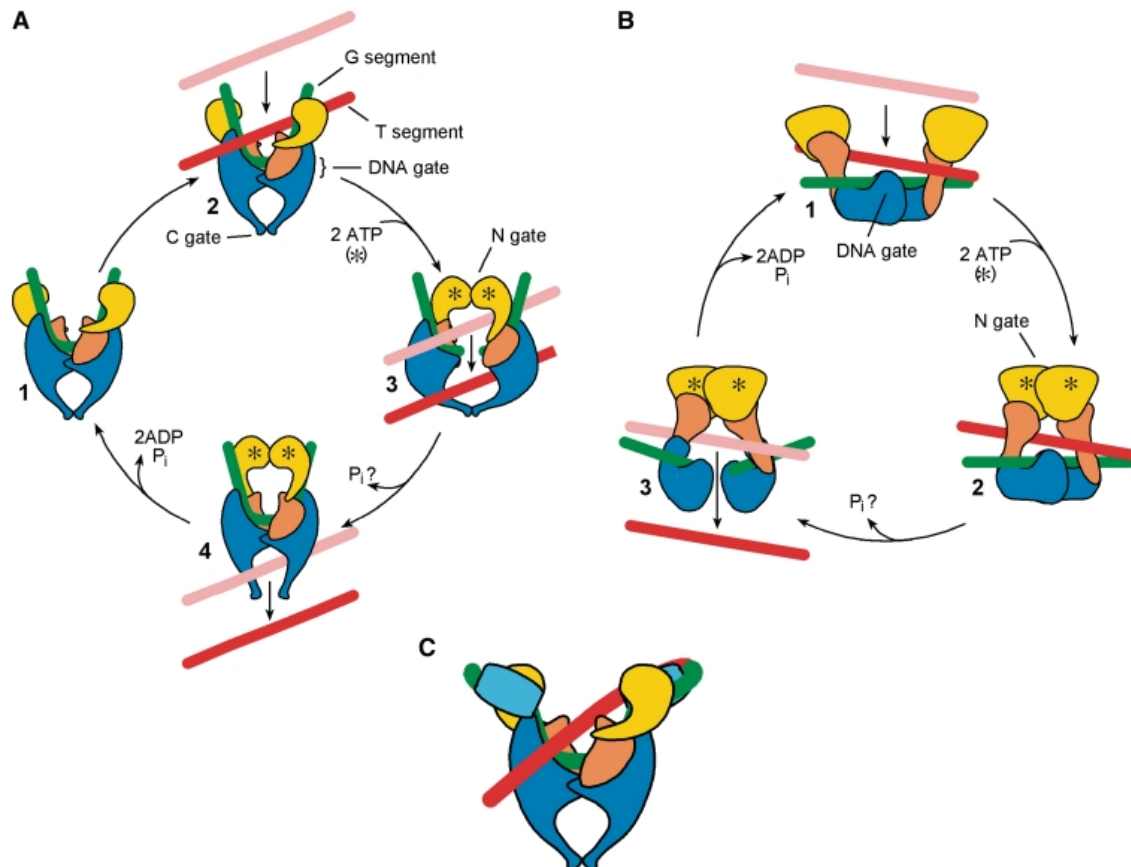


Figure 1.7: Structure and mechanism of type II topoisomerases.

(A) Mechanism of type IIA topoisomerases. These enzymes form three dimer interfaces, the N-gate, the DNA-gate and the C-gate (as labelled). (B) Mechanism of type IIB topoisomerases. These enzymes form two dimer interfaces, the N-gate and DNA-gate (as labelled). Domain colours as follows: yellow: ATPase, orange: TOPRIM, blue: cleavage-religation domain. The G-segment is shown in green and the movement of the T-segment from pink to red. (C) Close-up DNA bound representation of DNA gyrase, with the contiguous segment of DNA to the G-segment wrapped around the C-terminal domain of the enzyme to present an adjoining T-segment to the enzyme as a substrate for strand-passage. Figure taken from (Bates et al. 2011) with permission.

1.5.1.1. Topoisomerase II

Eukaryotic topoisomerase II relaxes positively and negatively supercoiled DNA in an ATP- and Mg^{2+} -dependent manner, in addition to decatenating DNA (Baldi et al. 1980). Thus far, topoisomerase II has been identified in many eukaryotes including humans, *Drosophila* (Hsieh and Brutlag 1980) and yeast (Liu et al. 1980). Higher eukaryotes have two isoforms of topoisomerase II, topoisomerase II α and topoisomerase II β , each of which are expressed during different points of the cell cycle and in different cell types (Drake et al. 1989).

Topoisomerase II α can be identified in proliferating cells and expression of the protein peaks during the G2 and M phases of the cell cycle (Capranico et al. 1992). The isoform demonstrates a higher activity in regions of active genes, demonstrated by its increased association with highly transcribed loci (Yu et al. 2017). Additionally, the specific isoform relaxes positive supercoils more than 10-fold faster than negative supercoils, a reflection of the enzyme's activity in overwound DNA ahead of the replication fork (McClendon et al. 2005). The ability to recognise DNA geometry resides in the CTD of topoisomerase II α (McClendon et al. 2008). Topoisomerase II β , occasionally referred to as the housekeeping topoisomerase, is found in all cell types and its expression is constant throughout the cell cycle (Sandri et al. 1996). Intriguingly, despite their varied expression patterns and roles, the two topoisomerase II isoforms share >70% sequence homology, predominantly in the central body of the enzyme, as the N-terminal domains (NTDs) and CTDs are the regions exhibiting most differences (Bollimpelli et al. 2017). Topoisomerase II is vital for the condensation and segregation of daughter chromosomes following replication (DiNardo et al. 1984).

Topoisomerase II has been identified in various species of plants, including *Arabidopsis*, pea and tobacco (Reddy et al. 1999; Singh et al. 2003; Xie and Lam 1994a). The *Arabidopsis* topoisomerase II protein is nuclear targeted and levels of protein are positively correlated with the proliferative state of the cell (Xie and Lam 1994b). Topoisomerase II plays a role in chromosome segregation and resolution of chromatids during the division of plant cells. Purified *Arabidopsis* topoisomerase II has been shown to possess a processive mode of relaxing negatively supercoiled DNA and the ability to decatenate DNA in an ATP-dependent reaction (Makarevitch and Somers 2005). The *Arabidopsis* topoisomerase II cleavage sites are associated with a weak cleavage efficiency and a unique consensus sequence, when compared to topoisomerase II from other organisms (Makarevitch and Somers 2006). More recently, a direct role of the enzyme has

been detected in the resolution of structural chromosomal interlocks formed during meiosis (Martinez-Garcia et al. 2018).

Topoisomerase II is also encoded on chromosome 14 of the *P. falciparum* genome. The gene encompasses ~1400 amino acids, 47.4% of which are identical and 65.4% similar to the human topoisomerase II (Cheesman et al. 1994); the partially purified protein has been associated with ATP- and Mg²⁺-dependent decatenation activity (Cheesman et al. 1994). Subsequent expression and purification of plasmodial topoisomerase II confirmed its ATP- and Mg²⁺-dependent relaxation activity and indicated selectivity of inhibitors like GSK299423, ciprofloxacin and etoposide for the malarial enzyme over human topoisomerase II (Mudeppa et al. 2015). In addition to the nuclear topoisomerase II activity within *P. falciparum*, partial purification of the mitochondrial DNA topoisomerase II has also been confirmed, interestingly the enzyme was found to be insensitive to fluoroquinolone inhibition (Chavalitsheewinkoon-Petmitr et al. 2001).

1.5.1.2. Topoisomerase IV

Topoisomerase IV primarily functions in bacteria to resolve topologically linked daughter chromosomes that are produced as a consequence of DNA replication (Levine et al. 1998). It is able to relax supercoiled DNA of both handedness in an ATP-dependent fashion (Peng and Marians 1993); though its preferential relaxation of positively supercoiled DNA is obvious (Crisona et al. 2000). Topoisomerase IV is also able to knot and unknot DNA (Deibler et al. 2001). The active topoisomerase IV enzyme forms a heterotetramer constituting two ParC and ParE, homologous to GyrA and GyrB respectively (discussed later in section 1.6), both in terms of primary sequence and structure (Figure 1.6) (Kato et al. 1990). The structure of the core region of bacterial topoisomerase IV, very much like that of gyrase, emphasises the three-dimensional arrangement of the domains (Figure 1.8). Despite similarities to gyrase, there are important functional differences between the two enzymes, the most prominent of which is the inability of topoisomerase IV to negatively supercoil DNA (Kato et al. 1992; Peng and Marians 1993). The origin for this resides in the CTD of ParC, which although similar to the GyrA CTD that consists of a six β -pinwheel structure, the ParC CTD is often described as a 'broken' β -pinwheel with just five blades making up its β -pinwheel, additionally it also lacks a consensus sequence located within the first blade of the β -pinwheel for gyrase (GyrA box), which is essential to mediate gyrase's ability to negatively supercoil DNA (Figure 1.8b) (Corbett et al. 2005). Nevertheless, the small structural differences between gyrase and topoisomerase IV amount to significant functional differences, bestowing

topoisomerase IV with its ability to decatenate 100 times more efficiently than gyrase (Zechiedrich and Cozzarelli 1995). Topoisomerase IV has been shown to recognise left-handed crossings which accounts for the enzyme's ability to decatenate supercoiled right-handed catenanes without also causing their relaxation (Rawdon et al. 2016).

The current understanding is that neither *Arabidopsis* nor *Plasmodia* possess sequences corresponding to topoisomerase IV proteins. Intriguingly, in the case of bacteria that lack topoisomerase IV and possess only one type IIA topoisomerase (gyrase), the enzyme serves as an efficient decatenase (Manjunatha et al. 2002). In the absence of a topoisomerase IV protein, the prospect that *A. thaliana* and *Plasmodia* gyrases may also be similarly adapted remains yet to be explored.

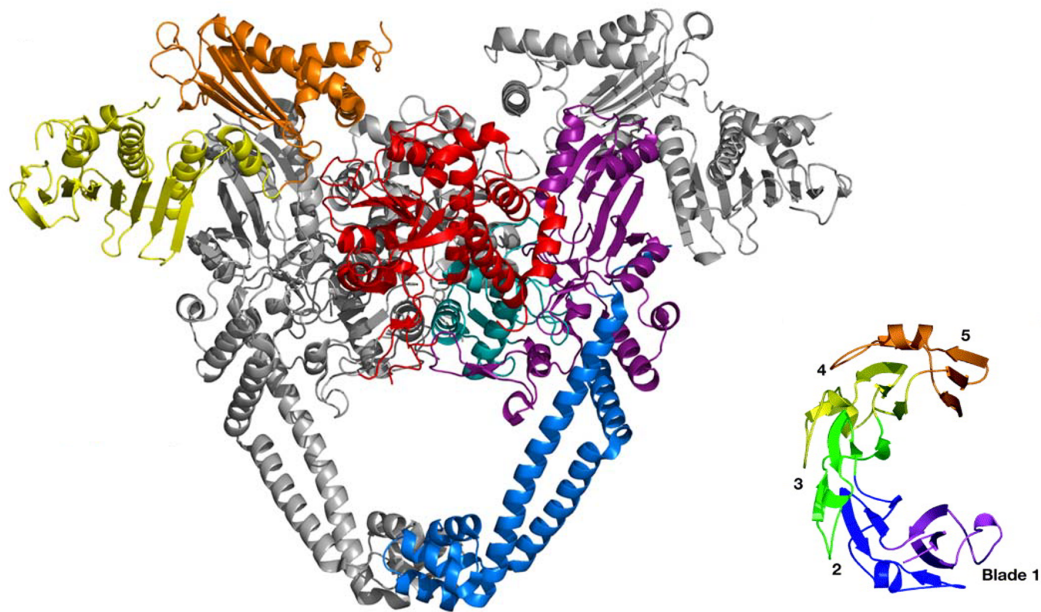


Figure 1.8: Structure of topoisomerase IV.

(a) The structure of *Streptococcus pneumoniae* PacE-ParC55 (Laponogov et al. 2013) (PDB: 4I3H). Domain colours as follows: yellow: GHKL ATPase domain, orange: transducer domain, red: TOPRIM domain, teal: WHD, purple: tower domain, blue: coiled-coil domain. The ParC55 structure is a truncated version of the protein that excludes the CTD domain of topoisomerase IV. (b) The structure of the *E. coli* ParC-CTD displaying the 5-bladed β -pinwheel domain (Corbett et al. 2005). Figure adapted from (Bush et al. 2015) with permission.

1.5.2. Type IIB topoisomerases

The type IIB topoisomerases have been identified in archaeal, plant, protist and algal lineages (Bergerat et al. 1994; Hartung et al. 2002; Malik et al. 2007). Similar to the type IIA topoisomerases, type IIB topoisomerases also employ an ATP- and Mg^{2+} -dependent mechanism for double-stranded DNA cleavage. The family was thought to comprise solely of topoisomerase VI, however, recent *in silico* analysis has identified a novel member, topoisomerase VIII (Gadelle et al. 2014). The type IIB topoisomerases have been categorised separately due to limited sequence similarity to other type II topoisomerases (Aravind et al. 1998). A structural distinction of these enzymes is the formation of only two protein-protein interfaces, in comparison to three interfaces formed by IIA topoisomerases (Figure 1.7b).

1.5.2.1. Topoisomerase VI

Topoisomerase VI comprises two subunits, A and B, the former subunit is homologous to Spo11, a eukaryotic protein involved in the initiation of DNA cleavage during homologous recombination, the latter subunit is involved in the binding and hydrolysis of ATP (Bergerat et al. 1997; Keeney et al. 1997). Similar to type IIA topoisomerases, the active enzyme comprises an A_2B_2 heterotetramer (Bergerat et al. 1994). The limited homology of the topoisomerase VI to the IIA topoisomerases resides in the DNA-binding (TOPRIM), magnesium-chelating (WHD) and ATPase (GHKL) domains of the enzyme, yet the organization of these domains differs by the adjacent placement of the WHD and TOPRIM domain on the same polypeptide (Figure 1.6). Topoisomerase VI can relax positively and negatively supercoiled DNA, as well as decatenate DNA (Bergerat et al. 1997). The sequential revelation of the structures of topoisomerase VIA and topoisomerase VIB subunits, from different species, prior to the complete structure of the protein from *Methanosarcina mazei*, conclusively confirmed key structural differences from the type IIA enzymes, these include: the absence of a post-strand passage cavity, characteristically formed by the A-subunit CTDs of type IIA topoisomerases; and the formation of only two protein-protein interfaces, in contrast to the three interfaces formed by the active type IIA topoisomerases (Corbett and Berger 2003; Corbett et al. 2007; Corbett et al. 2005; Nichols et al. 1999). Furthermore, the *Sulfolobus* enzyme also highlighted a distinct cleavage activity, by introduction of a two base-pair stagger relative to the four base-pair stagger created upon nucleophilic attack in type IIA topoisomerases.

Homologues of topoisomerase VI have been identified in various eukaryotic species, including plants. The *Arabidopsis* genome has been identified to possess homologues of

both A and B subunits of topoisomerase VI. Interestingly, there are three Spo11 homologues within the *Arabidopsis* genome: AtSpo11-1, AtSpo11-2 and AtSpo11-3, but only a single topoisomerase VIB homologue: AtTopo VIB (Grelon et al. 2001; Hartung and Puchta 2000; Sugimoto-Shirasu et al. 2002). Interaction of *Arabidopsis thaliana* topoisomerase VIB with Spo11-2 and Spo11-3 has been confirmed, but no interaction is detected with Spo11-1. The latter protein is essential for production of viable gametes and efficient meiotic recombination (Grelon et al. 2001). The functional topoisomerase VI protein is formed by the Spo11-3 and topoisomerase VIB subunit, disruption to the activity of both or either subunits of this protein provides a dwarfed phenotype in *Arabidopsis* (Hartung et al. 2002; Sugimoto-Shirasu et al. 2002). Specifically, mutant plants have been identified that are defective in the process of endoreduplication, that is, a natural process in which plants undergo successive rounds of DNA replication (an increase in ploidy) in the absence of cellular division; topoisomerase VI is specifically required for endocycles beyond 8C (Sugimoto-Shirasu et al. 2002).

A further intriguing aspect of the *Arabidopsis* topoisomerase VI is the identification of two accessory proteins that interact to form the functional complex and are essential for the process of endoreduplication: BIN4 and RHL1 (Breuer et al. 2007; Sugimoto-Shirasu et al. 2005). Phenotypically, *bin4* and *rhl1* mutants are similar to topoisomerase VI mutants and exhibit dwarfism. The interaction of these accessory proteins is mediated with the topoisomerase VIA subunit (Spo11-3), RHL1 binds only to this subunit of the complex, whilst BIN4 can interact with itself and RHL1, in addition to the topoisomerase VIA subunit (Breuer et al. 2007). These investigations confirm that topoisomerase VI plays a critical role in DNA replication, metabolism and cell growth in *Arabidopsis*.

Topoisomerase VI may potentially be encoded by the *Plasmodium falciparum* genome, although a uniform view with regards to this in the topoisomerase field has not currently been established. *P. falciparum* is believed to encode a topoisomerase VIB subunit, but the existence of the partner subunit remains somewhat disputed, due to difficulties in differentiation of topoisomerase VIA and Spo11, both of which have similar domain architectures. Regardless, heterologous expression of *P. falciparum* topoVIA/Spo11 in combination with topoisomerase VIB from the same species, has been shown to complement a topoisomerase II deficient *Saccharomyces cerevisiae* strain and exhibit sensitivity to an ATPase inhibitor, radicicol (Chalapareddy et al. 2016). Clearly, further in-depth exploration of potential plasmodial topoisomerase VI enzymes is required.

1.5.2.2. Topoisomerase VIII

Topoisomerase VIII was included within the topoisomerase family following its *in silico* identification using the topoisomerase VIB subunit as a bait protein to search databases (Gadelle et al. 2014). Topoisomerase VIII was originally identified in 19 bacterial genomes, three bacterial plasmids and a single archaeon plasmid; where genomically encoded, these are in regions of integrated mobile elements, plausibly ascending from a conjugative plasmid (Gadelle et al. 2014). The topoisomerase VIII enzymes possess domains similar and unique to topoisomerase VI, that is the helix-two-turn-helix (H2tH) and transducer domains, however, these are found encoded on a single polypeptide alongside domains that would classically constitute the topoisomerase VIA subunit, such as, GHKL ATPase and TOPRIM domains; the active enzyme is a homodimer formed by two of such polypeptides (Gadelle et al. 2014). Topoisomerase VIII proteins encoded by bacterial plasmids possess Mg²⁺- and ATP-dependent relaxation and decatenation activities, whilst those encoded by integrated elements possess DNA cleavage activity with ATP-independent relaxation activity or just the latter distinct relaxation activity alone (Gadelle et al. 2014).

1.5.2.3. Mini-A

The most recent addition to the topoisomerase family, specifically of the type IIB is that of Mini-A. These are distant homologs of the type IIB topoisomerases and are encoded by extrachromosomal and integrated bacterial and archaeal viruses (Takahashi et al. 2019). These topoisomerases are aptly named due to their short region of homology to the A-subunit of the type IIB topoisomerases or extreme C-terminus of the single polypeptide of topoisomerase VIII (i.e. region encoding the TOPRIM domain) (Takahashi et al. 2019). Although the Mini-A proteins conserve key residues involved in DNA cleavage, mainly located within the TOPRIM and 5Y-CAP domains, other significant topoisomerase domains, including the ATPase domain have not yet been identified. The function of the Mini-A proteins remains yet to be identified, however, their pairing with other proteins, to constitute a canonical topoisomerase, is yet to be ruled out (Takahashi et al. 2019).

1.6. Gyrase

The type IIA topoisomerase family comprises a third member, DNA gyrase. Gyrase possesses the unique ability to introduce negative supercoils into double-stranded DNA substrates by means of an ATP- and Mg^{2+} -dependent reaction (Gellert et al. 1976). In addition, gyrase is also capable of performing other reactions typical of type IIA topoisomerases when coupled with ATP hydrolysis, such as the relaxation of positive supercoils, decatenation (Kreuzer and Cozzarelli 1980; Marians 1987b) and unknotting (Liu et al. 1980). Notably, the enzyme possesses the ability to relax negative DNA supercoils in the absence of ATP (Gellert et al. 1979; Higgins et al. 1978).

DNA gyrases are ubiquitous in bacteria, the comprehensive study of the *E. coli* protein has led to the enzyme becoming a model for gyrase proteins in other species. *E. coli* gyrase is encoded by the *gyrA* and *gyrB* genes, the gene products for which are 97-kDa and 90-kDa subunits, respectively. The active enzyme is formed by the combination of two of each of the GyrA and GyrB subunits, which combine to form an A_2B_2 heterotetramer (Adachi et al. 1987; Sugino et al. 1980). Limited proteolysis of the gyrase subunits has shown that the GyrB subunit comprises two primary domains (Kampranis and Maxwell 1998; Reece and Maxwell 1989), a 43-kDa N-terminal domain involved in the binding and hydrolysis of ATP and a 47-kDa C-terminal domain that interacts with DNA and GyrA (Brown et al. 1979; Chatterji et al. 2000; Wigley et al. 1991). Similarly, GyrA can be divided into a 59-kDa N-terminal domain involved in DNA cleavage (Horowitz and Wang 1987) and a 35-kDa C-terminal domain that wraps DNA.

1.6.1. Structure of gyrase

The structural information for DNA gyrase was initially limited to individual domains of the protein, subunits, their truncated versions or fusion constructs of core regions determined by X-ray crystallography. However, the latter technique has thus far been unable to provide a structure of full-length gyrase. The structural information was subsequently augmented by low-resolution full-length gyrase structures obtained by small angle X-ray scattering (Baker et al. 2011) or 3D cryo-electron microscopy (cryo-EM) (Costenaro et al. 2007; Papillon et al. 2013). The initial full-length cryo-EM structure was obtained from the *Thermus Thermophilus* fusion of the gyrase B followed by the gyrase A subunit. The active complex was crosslinked by glutaraldehyde, reaction conditions included ADPNP and ciprofloxacin and both the presence and absence of 155 bp DNA (Papillon et al. 2013). Albeit a low-resolution structure at 23 Å, the authors were able to deduce key aspects of the enzyme's structure and dynamics (Figure 1.9). They observed

the intertwined nature of the holoenzyme, inferred the vertical movement of the GyrB ATPase domains upon binding of DNA and observed an asymmetric disposition of the CTDs towards the N-gate (formed by the locked ATPase domains with ADPNP), this was stabilised by DNA (Figure 1.9) (Papillon et al. 2013).

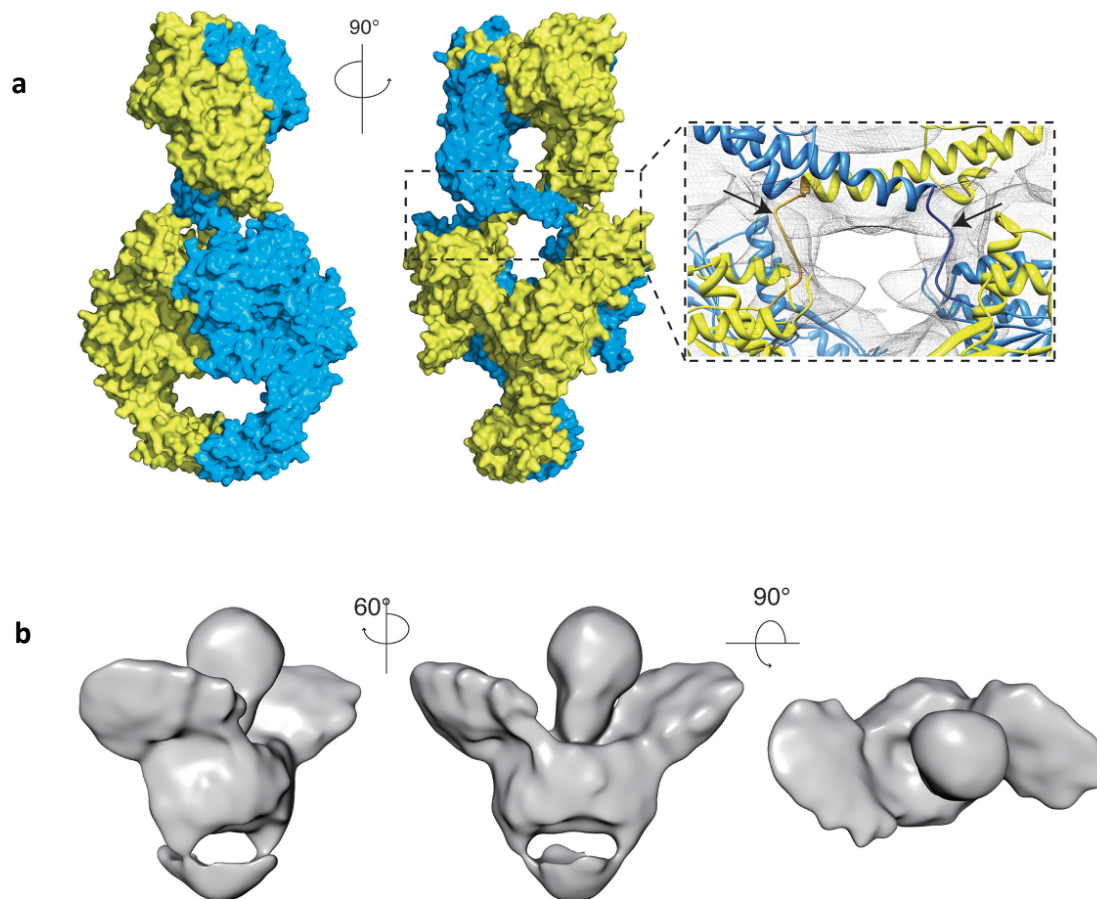


Figure 1.9: Cryo-EM structure of *Thermus Thermophilus* gyrase.

(a) Space-filled model of gyrase full-length BA fusion construct (blue and yellow) complex displaying the intertwining of the subunits. Note the connection of one ATPase domain to the TOPRIM domain on the opposite side via a 10 amino acids linker (arrows on the inset image). (b) Cryo-EM map of DNA bound complex shown in three orientations, the ATPase domain is observed tilted towards the CTD. Figure adapted from (Papillon et al. 2013).

The original low resolution full-length 3D cryo-electron microscopy structure has been superseded by the full-length structure of *E. coli* DNA gyrase, formed by stoichiometric formation of the active complex from individual subunits, at an overall resolution of 6.6 Å (Broeck et al. 2019). The representations of primary domain architecture and its translation into a 3D structure for the *E. coli* gyrase protein is illustrated in Figure 1.10.

The A₂B₂ arrangement of gyrase leads to two-fold symmetry in its three-dimensional structure and the formation of protein-protein interfaces, or gates (Figure 1.10b). The first gate termed N-gate or ATP-gate is formed by two adjacent elements, an ATP binding and hydrolysis domain and a transducer domain (Bellon et al. 2004; Classen et al. 2003; Corbett and Berger 2003; Wigley et al. 1991). The ATPase domain is a member of the GHKL superfamily, which possesses the unconventional Bergerat ATP-binding fold (Dutta and Inouye 2000). The transducer domain functions to transmit signals between the ATP-gate and the DNA-gate (Bjergbaek et al. 2000).

The second protein-protein interface, the DNA-gate, is formed by interactions between the TOPRIM domain of GyrB and the WHD of the GyrA subunit. The TOPRIM domain is responsible for binding the divalent metal ion (Aravind et al. 1998) and the WHD domain encompasses the active site tyrosine (Gajiwala and Burley 2000); contiguous with the latter domain is the tower domain, which is involved in the binding of DNA (Morais Cabral et al. 1997). The combinatorial action of these three domains facilitate the DNA gate in completing its role of binding the DNA and cleaving each strand of the DNA duplex. Notably, the action of DNA cleavage results in the formation of a 5' DNA break, staggered four base pairs apart on each strand of the duplex (Sander and Hsieh 1983).

The final dimerization interface of the protein, the C-gate, is a well-conserved region formed by a coiled-coil extension from the shoulder with a globular protein at the terminus (Berger et al. 1996; Morais Cabral et al. 1997). The C-gate of gyrase is extended by the 35-kDa CTD, which is essential for the ability of gyrase to negatively supercoil DNA (Figure 1.10d) (Kampranis and Maxwell 1996; Reece and Maxwell 1991). Interestingly, deletion of the CTD converts gyrase into a conventional DNA relaxing enzyme, such as topoisomerase II (Kampranis and Maxwell 1996). The CTD adopts a six bladed β-pinwheel structure with a predominant basic outer surface that functions to bind and bend DNA. The domain encompasses a 7 amino-acid motif (QRRGGKG), the GyrA-box, which is essential for the supercoiling activity of gyrase (Kramlinger and Hiasa 2006).

The structure of the DNA binding and cleavage domain of the enzyme was visualised in two orientations by 3D cryo-EM, the first described as the 'closed' conformation and the second as a 'pre-opening' complex (Broeck et al. 2019). Doubly-nicked DNA of 180 bp was used as a substrate for complex formation. Of this 130 bp was mapped in the structure, implying that the remaining DNA may be more flexible. The structure determined by Broeck *et al.* (2019), provided clarity on a speculative function of the GyrA box proposed by Papillon *et al.* (2013). From their 23 Å full-length structure of *Thermus thermophilus*, Papillon *et al.* (2013) proposed an additional function of the GyrA box in stabilising the G-segment/T-segment cross-over structure, in addition to stabilising the circular shape that enforces DNA wrapping. This was confirmed by the latter structure determined by Broeck *et al.* (2019), who observed the DNA to be wrapped around the CTD of the enzyme in an angle close to 200° and determined the GyrA box to be acting as a clamp to compensate for this energetically unfavourable twisting of the DNA (Broeck et al. 2019; Papillon et al. 2013). Additionally, the first point of contact between G-segment DNA and the β-pinwheel of the CTD was determined to be via blade 3, followed by the wrap around blades 4,5 and 6 and the exit of the DNA via the GyrA box on blade 1 (Broeck et al. 2019).

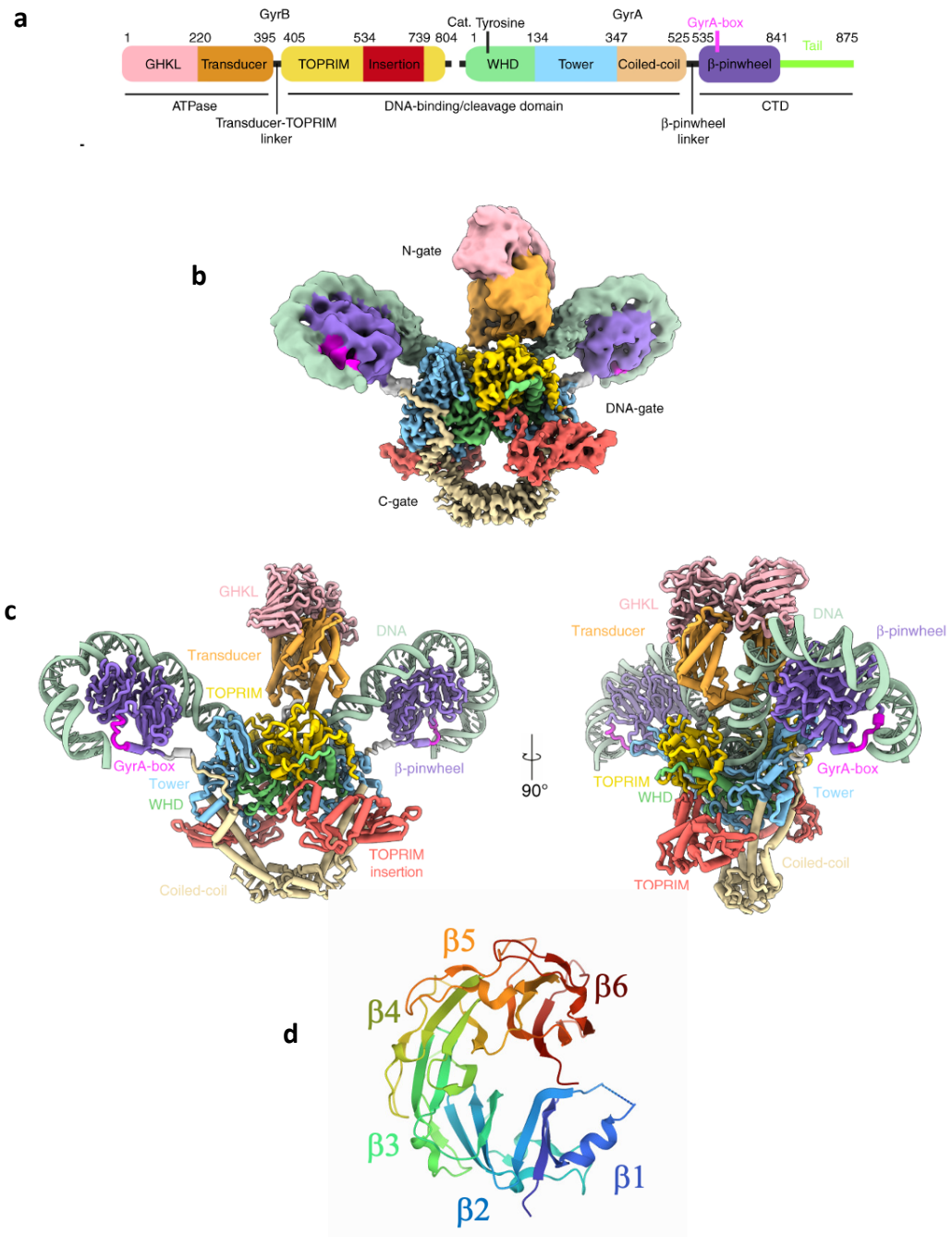


Figure 1.10: Structure of *E. coli* gyrase.

(a) Primary domain arrangement of *E. coli* gyrase. (b) Raw cryo-EM structure of *E. coli* gyrase, highlighting the three protein-protein interfaces. (c) Molecular cryo-EM structure of full-length *E. coli* gyrase complexed with 130 bp DNA (pale green) and a side-on view of the same structure (PDB: 6RKW). Domain colours in b and c as in a. (d) GyrA C-terminal domain highlighting the six bladed β -pinwheel structure (PDB: 1ZI0). Figure adapted from (Broeck et al. 2019) with permission.

1.6.2. Mechanism of DNA Gyrase

Gyrase is able to negatively supercoil DNA using a two-gate mechanism (Figure 1.11) (Mizuuchi et al. 1980). The supercoiling reaction is initiated by the binding of a section of DNA, the gate or G-segment, across the dimer interface of the GyrA N-terminal domains, this interface provides a positively charged saddle to facilitate the binding of DNA; once bound, the DNA is contorted. As a consequence of G-segment binding, the C-terminal domains of GyrA swing upwards allowing an adjacent section of DNA to be wrapped around these domains in a positive supercoil (Heddle et al. 2004; Lanz and Klostermeier 2011; Orphanides and Maxwell 1994). The wrapping of DNA around the C-terminal domains positions a second segment of DNA, the transport or T-segment, across the bound G-segment at an angle of about 60° (Papillon et al. 2013). The binding of DNA and its wrapping activity induces the narrowing of the N-gate, which facilitates capture of the T-segment (Gubaev and Klostermeier 2011). Subsequently, ATP is bound by the N-terminal domains of each GyrB subunit, leading to dimerization of the subunits, trapping of the T-segment and closure of the clamp (Kampranis et al. 1999; Wigley et al. 1991). The steps described thus far, do not require the energy of ATP hydrolysis and are feasible by binding of the non-hydrolysable analogue, 5'-adenylyl β,γ -imidodiphosphate (ADPNP) (Roca and Wang 1992). ADPNP can facilitate a single strand-passage reaction, after which, the enzyme is stranded in an inactive state (Sugino et al. 1978). However, in order for gyrase to carry out further catalytic cycles, the enzyme needs to be reset to its initial conformation, which is achieved by hydrolysis of the bound ATP. Interestingly, an acidic tail at the extreme C-terminus of the GyrA CTD in *E. coli*, has been shown to regulate DNA wrapping and link the activity to ATP turnover, therefore controlling supercoiling (Tretter and Berger 2012). The ATP-independent relaxation of negatively supercoiled DNA can also be supported by DNA gyrase using a similar reaction, albeit in reverse; the T-segment passes through the enzyme in the opposite direction, that is, through the bottom dimer interface or C-gate (Williams and Maxwell 1999). Although energetically favourable, DNA gyrase requires ATP to support relaxation of positively supercoiled DNA; in a reaction analogous to that of supercoiling. Likewise, ATP is also required during catenation-decatenation and knotting-unknotting reactions (Kreuzer and Cozzarelli 1980; Liu et al. 1980).

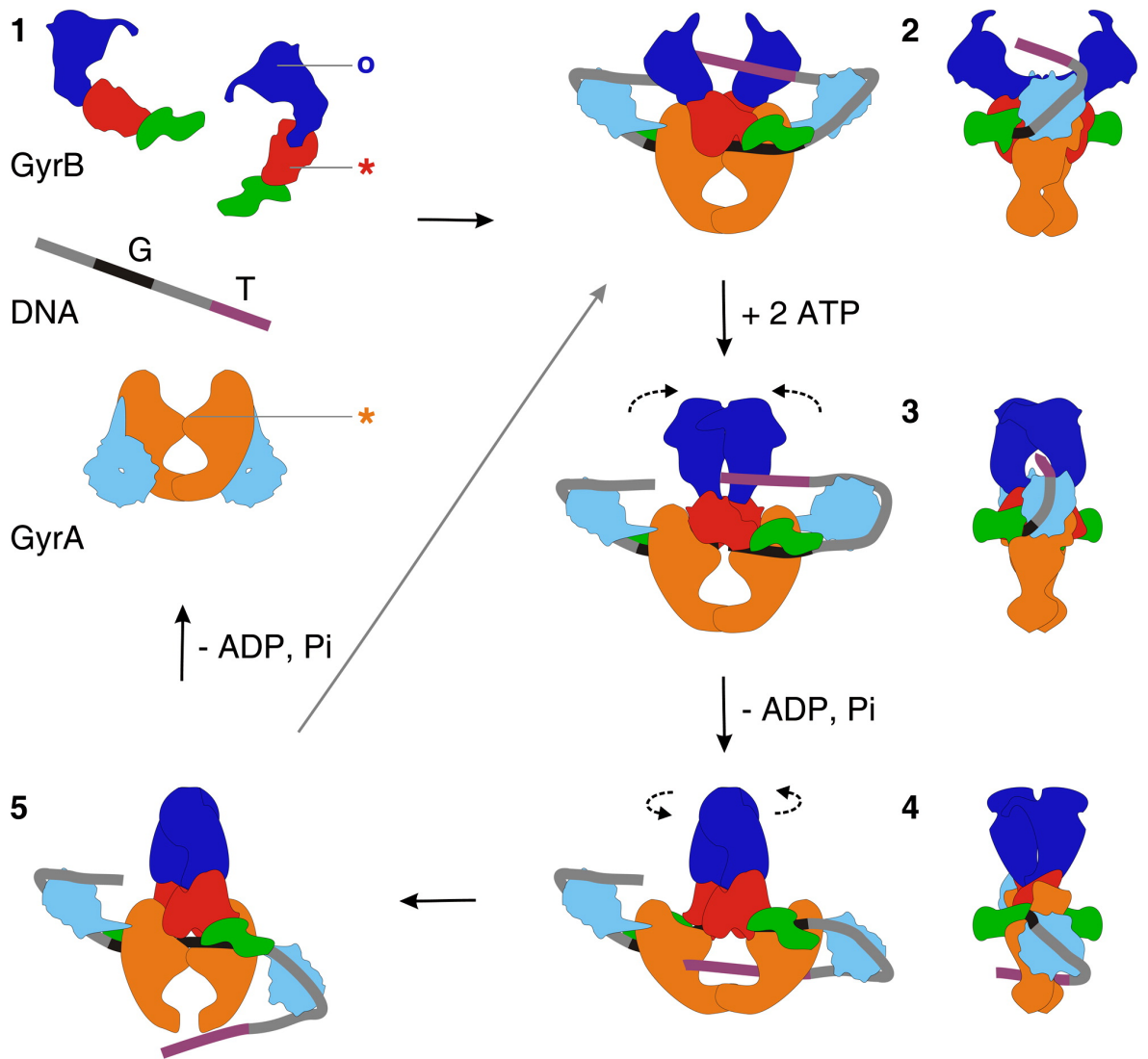


Figure 1.11. The mechanism of supercoiling by DNA gyrase.

1. Gyrase components in solution. 2. The G-segment DNA is bound at the DNA-gate and the contiguous DNA is wrapped (positive crossover) around the GyrA CTD; positioning the T-segment over the G-segment. 3. ATP binds at the GyrB NTDs, leading to dimerization of the domains, capture of the T-segment and transient cleavage of the G-segment. 4. ATP hydrolysis causes the GyrB to rotate, the GyrA dimers to separate, and transport of the T-segment through the cleaved G-segment. 5. The G-segment is re-ligated. The process leads to the introduction of two negative supercoils into the DNA. The T-segment exits the DNA via the last dimer interface, the C-gate. The remaining ATP is hydrolysed to reset the enzyme. The right panel shows steps 2-4 side-on. Symbols are as follows: circle – ATP binding pocket; star – active-site tyrosine. Colour coding of domains: dark blue – GyrB43; red – GyrB TOPRIM; green – GyrB tail; orange – GyrA59; light blue- GyrA CTD. The G- and T- segments are coloured black and purple, respectively. Figure adapted from (Costenaro et al. 2007) with permission.

An alternative and somewhat controversial mechanism, to that of strand passage, for DNA supercoiling by gyrase has been proposed, prompted by apparent negative supercoiling by a version of the enzyme harnessing only a single catalytic tyrosine (Gubaev et al. 2016). The rationale for the proposed mechanism of nicking and closing is initiated by the capture of two positive supercoils in covalently closed DNA and hence the introduction of two compensatory negative supercoils in the substrate, these distinct topological domains of DNA are separated and fixed at opposing ends, the positive supercoils are relaxed by rotation following single-stranded cleavage of one DNA strand, leaving the negative supercoils intact (Gubaev et al. 2016). Intriguingly however, the reactions of ATP-dependent relaxation and decatenation both implicated strand-passage (Gubaev et al. 2016). The nicking-closing mechanism yet remains controversial within the topoisomerase field.

1.6.3. Biological role of gyrase

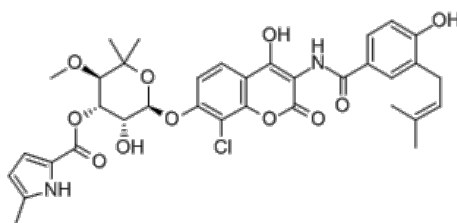
The bacterial gyrase is the sole enzyme responsible for negative supercoiling *in vivo*, be it during the process of chromosome condensation, recombination, or to facilitate replication initiation (Bates and Maxwell 2005; Dorman and Dorman 2016). During the process of DNA replication and the accompanying strand separation, gyrase is implicated in the resolution of positive supercoils that accumulate ahead of the replication fork (Figure 1.1). The *in vivo* supercoiling levels are fundamentally controlled and orchestrated by the antagonistic actions of gyrase and topoisomerase I within bacteria (Drlica 1992). The inability of the cell to remove positive supercoils ahead of the replication fork, a common feature in overwound DNA, induces stalling of the replication machinery and the eventual introduction of lethal double-stranded DNA breaks that are bactericidal (Liu and Wang 1987).

1.6.4. Gyrase inhibitors

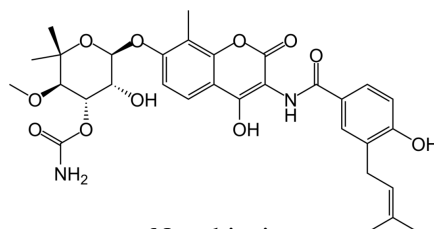
Gyrase conducts an essential function for replication and division within bacterial species explicitly; the combination of this essential role and the lack of gyrase in human cells presents the enzyme as an ideal drug target. DNA gyrase can be inhibited by one of two main mechanisms: direct inhibition of the enzyme's activity, or the enzyme may be poisoned through the stabilisation of the covalent enzyme-DNA complex (Collin et al. 2011).

1.6.4.1. Aminocoumarins

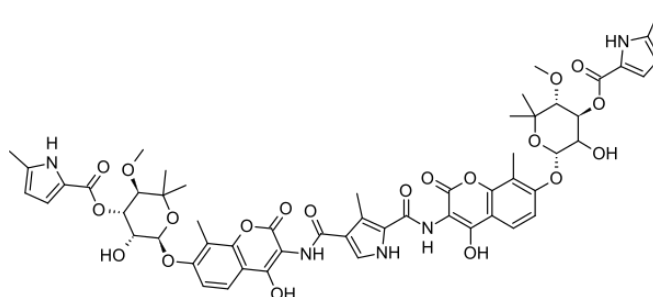
The aminocoumarins are *Streptomyces* products that target gyrase by inhibiting the enzyme's supercoiling reaction (Maxwell 1997). More specifically, these drugs target the ATPase activity of the GyrB subunit, acting as competitive inhibitors of ATP binding (Mizuuchi et al. 1978; Sugino and Cozzarelli 1980; Sugino et al. 1978). Despite topoisomerase IV also possessing ATP-dependent activity, gyrase has been identified as the primary target of these inhibitors (Alt et al. 2011). Aminocoumarins bind gyrase in the 24-kDa N-terminal GyrB domain and overlap the ATP-binding site (Gilbert and Maxwell 1994; Lewis et al. 1996). The aminocoumarins include: novobiocin, chlorobiocin and coumermycin (Figure 1.12). Despite these drugs being potent inhibitors of the ATPase reaction of gyrase, they are not clinically successful due to solubility and toxicity issues (Maxwell 1997).



Clorobiocin



Novobiocin



Coumermycin A1

Figure 1.12: The structures of selected aminocoumarins.

1.6.4.2. Quinolones

The quinolones are the most successful antibacterial compounds targeted to DNA gyrase and have been used to treat a wide range of infections. These synthetic compounds originated from nalidixic acid and now comprise four generations of drugs with improved antimicrobial activity, potency and clinical success: nalidixic acid and oxolinic acid (first generation); ciprofloxacin and norfloxacin (second generation); levofloxacin and sparfloxacin (third generation); moxifloxacin and gemifloxacin (fourth generation) (Figure 1.13) (Collin et al. 2011). The quinolones inhibit the DNA supercoiling and relaxation reactions of gyrase by binding and stabilising the gyrase-DNA cleavage complex (Gellert et al. 1977; Sugino et al. 1977). The bacteriostatic effect of quinolones arises from this stabilised complex impeding movement of the DNA replication fork. Subsequently, double-stranded DNA breaks are formed which is followed by protein synthesis-dependent or -independent chromosome fragmentation and cell death (Drlica et al. 2008).

Interestingly, the quinolones also have a secondary target, topoisomerase IV. Quinolone resistance can be mediated by single point mutations, which frequently map to the N-terminal domains of GyrA (residues 67 to 106 *E. coli* numbering) or ParC (residues 63 to 102); both domains are within close proximity of the active site tyrosine (Tyr122 for GyrA and Tyr120 for ParC) (Hooper and Jacoby 2015; Laponogov et al. 2009; Wohlkonig et al. 2010). These domains have been designated as the 'quinolone-resistance-determining-regions' (Yoshida et al. 1990). Interestingly, resistance can also be mapped to the GyrB and ParE subunits.

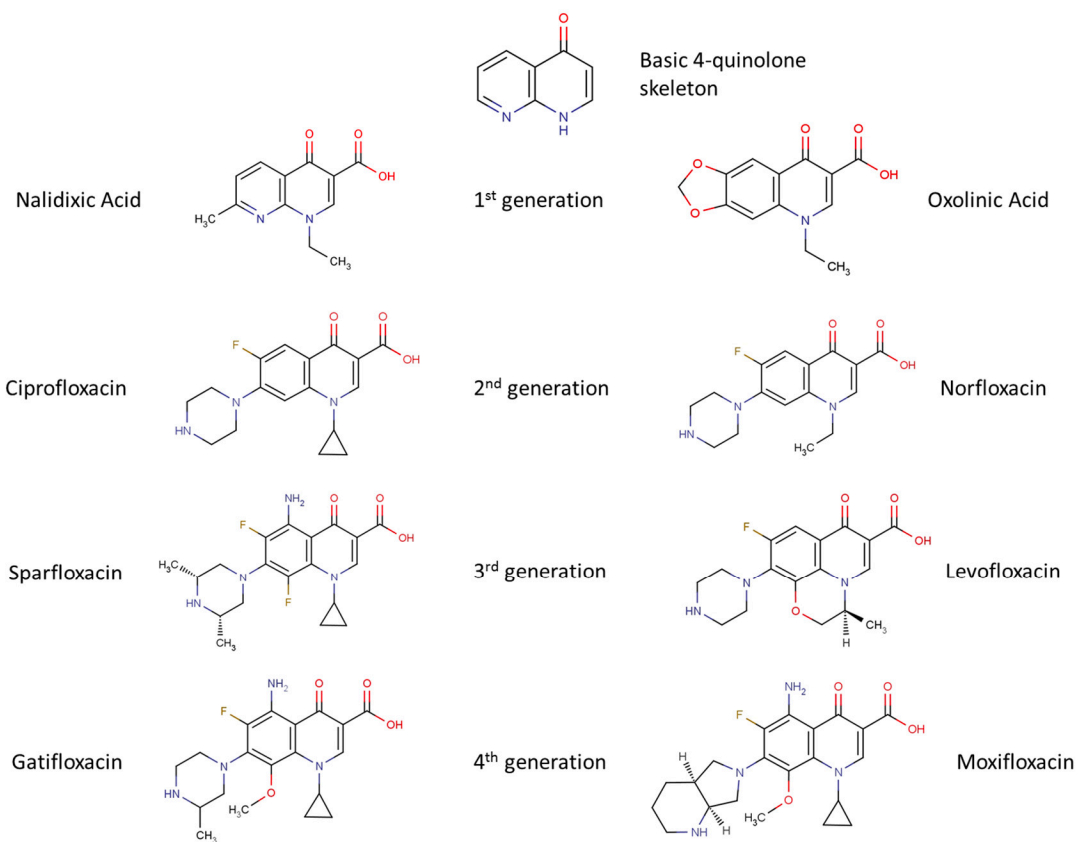


Figure 1.13. Quinolone structures.

Chemical structures of the different quinolone drugs. First generation: nalidixic acid. Second generation: norfloxacin and ciprofloxacin. Third generation: levofloxacin and sparfloxacin. Fourth generation: moxifloxacin and gemifloxacin. The fluoroquinolones are characterised by the addition of a fluoro-group to the scaffold. Figure adapted from (Collin et al. 2011) with permission.

1.6.4.3. Simocyclinone D8

The significance of simocyclinones became apparent upon analysis of its biosynthetic gene cluster, which was found to overlap with the aminocoumarin gene cluster (Galm et al. 2002; Trefzer et al. 2002). Simocyclinone variants, for example simocyclinone D8 (SD8), are produced by *Streptomyces antibioticus* (Holzenkampfer et al. 2002; Schimana et al. 2000). Similar to aminocoumarins and quinolones, SD8 also targets gyrase and specifically inhibits the supercoiling and relaxation reactions of the enzyme. However, SD8 does not inhibit the ATPase reaction of gyrase, neither does it stabilise the gyrase-DNA complex, but the inhibitor functions by a novel mechanism that involves early action in the gyrase catalytic cycle by preventing the binding of DNA to gyrase (Flatman et al. 2005). SD8 is formed by the unity of three subunits: a coumarin moiety, a tetraene linker, and a glycone subunit (Figure 1.14). Observations of the crystal structure of SD8 revealed that the inhibitor interacts with two separate binding pockets of the GyrA domain through each of its ends, thus the molecule was aptly termed as a ‘double-headed antibiotic’ (Edwards et al. 2009). Initially, SD8 was believed to have modest activity against Gram-positive bacteria only; this in combination with its low solubility and high toxicity, rendered it unsuitable as a therapeutic drug (Schimana et al. 2000). However, more recently, the antibiotic has been reported to have strong activity against gram-negative bacteria from clinical isolates (Richter et al. 2010). The latter discovery presents a more optimistic outlook for the development of SD8 as a therapeutic drug.

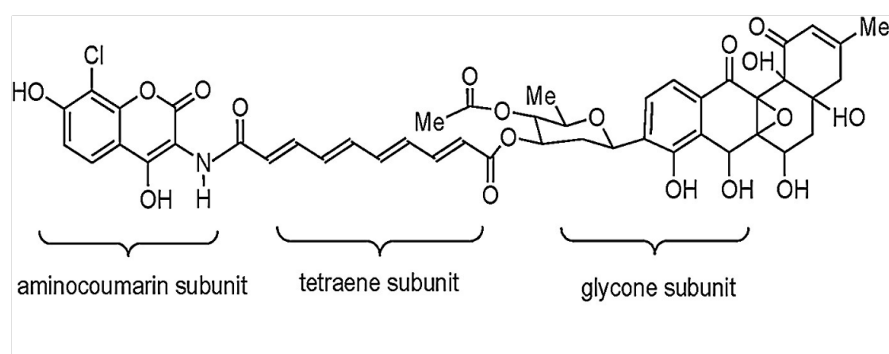


Figure 1.14: Structure of simocyclinone D8. Figure adapted from (Khan et al. 2018) with permission.

1.6.4.4. Microcin B17

Microcin B17 (MccB17) belongs to a class of peptide antibiotics with low molecular masses that are produced and excreted by *Enterobacteriaceae* (Baquero et al. 1978). MccB17 is a 3.1-kDa glycine-rich peptide, with extensive post-translational modifications, produced by *E. coli* harnessing the plasmid-borne MccB17 operon (Figure 1.15) (Davagnino et al. 1986). Similar to quinolones, MccB17 acts by stabilising the covalent gyrase-DNA complex, leading to inhibition of DNA synthesis and formation of double-stranded DNA breaks, ultimately resulting in cell death (Herrero and Moreno 1986; Vizan et al. 1991). However, in comparison to quinolones, MccB17 is a weak inhibitor, it does not completely inhibit gyrase mediated supercoiling and relaxation, but instead slows down these processes around 3-fold. Although the inhibitor functions independently of ATP hydrolysis, the presence of ATP has been shown to enhance its effect by about 10-fold (Bush et al. 2015; Pierrat and Maxwell 2003).

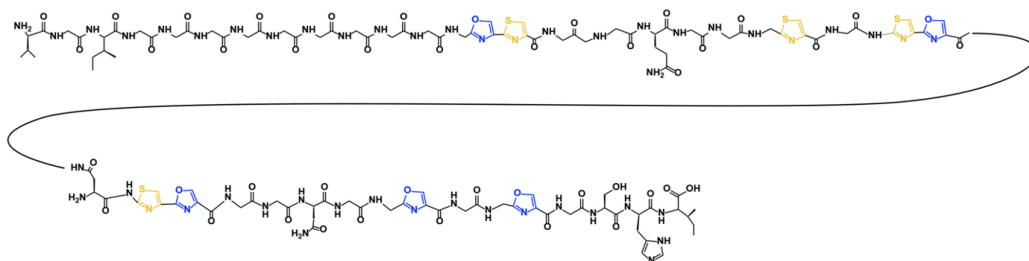


Figure 1.15: The chemical structure of mature MccB17.

The formation of the mature peptide (residues 27-69) involves cleavage of the leader peptide by TldD/E protease (see (Ghilarov et al. 2019)) for more details. Figure adapted from (Ghilarov et al. 2019) with permission.

1.7. DNA gyrase in plants

Conventionally, DNA gyrase has been considered as a bacterial enzyme, but there is now compelling evidence of gyrase in eukaryotes. At a first glance, gyrase may seem surplus to requirement in a eukaryotic cell, due to the chromosomal arrangement of the nuclear DNA, which is responsible for its maintenance in a negatively supercoiled state. However, gyrase is thought to function in the replication of the DNA that resides in the endosymbiotic organelles of these cells, where the condition of DNA is likely to reflect its prokaryotic origin. The discovery of gyrase in plants and plasmodial parasites has generated scientific interest primarily founding upon the success of the bacterial enzyme as a biological target.

1.7.1. Detection of DNA gyrase in plants

Indirect evidence for the existence of DNA gyrase in *planta* was proposed as early as 1987 when researchers discovered a novobiocin-sensitive gyrase-like activity, during investigation of chloroplast gene transcription in peas (Lam and Chua 1987). The simultaneous identification of topoisomerase I led to the conclusion that the topology of organellar DNA impacts transcription of chloroplast genes. Further support was provided upon the inhibition of chloroplast DNA synthesis by typical gyrase inhibitors, nalidixic acid and novobiocin through the recognition of reduced [³H] thymidine incorporation (Mills et al. 1989). The molecular cloning and expression of GyrA from *Pisum sativum* has identified the subunit to be dual targeted to the plastid and mitochondria (Reddy et al. 2018). The PsGyrA shared 42% sequence similarity to its *E. coli* counterpart, but its closest relative based on sequence similarity was found to be the *Medicago truncatula* GyrA.

Investigation of gyrase in *Nicotiana Benthamiana* revealed a role of the protein in governing successful nucleoid partitioning within chloroplasts (Cho et al. 2004). The knockdown of *Nicotiana Benthamiana* GyrA and GyrB through virus-induced gene silencing (VIGS) documented the affected areas of diminished protein expression to possess reduced numbers of chloroplasts, increased DNA content and large abnormal nucleoids with variable DNA sizes and structures (Cho et al. 2004). The same study also identified ultrastructural differences in chloroplasts, specifically, providing evidence of reduced thylakoid membranes as well as the appearance of dumbbell shaped chloroplasts with central constrictions.

1.7.2. Topoisomerases in *Arabidopsis*

Arabidopsis thaliana comprises of three separate genomes: nuclear, plastid and mitochondrial, each served by distinct suite of topoisomerases, according to the individual genomic requirements.

1.7.2.1. *Arabidopsis* nuclear genome

Arabidopsis thaliana serves as a model system for the identification of genes and determination of their functions. The small size, short generation time to produce a significant number of offspring and modest nuclear genome make *Arabidopsis* a tractable system (The Arabidopsis Genome 2000). The nuclear genome of *Arabidopsis* typically resembles that of eukaryotes with its chromosomal arrangement dividing the 135 Mbp genome amongst 5 chromosomes. The nuclear DNA is characteristically arranged by the packaging of the duplex around histones to form nucleosomes that fold into 30 nm fibres, which are further compressed into chromosomes, as in other eukaryotes.

1.7.2.2. *Arabidopsis* chloroplast genome

The *Arabidopsis* chloroplast genome consists of ~160 kbp, the length of DNA contains a pair of inverted repeats of around ~26 kbp that are separated by disproportionate single-copy regions, the larger of which is almost 5 times the length of the other (Sato et al. 1999). The identification of a replicating intact DNA molecule with no identifiable ends, from the *E. coli* K12 strain in 1963, significantly influenced subsequent research on the size and topology of organellar DNA *in planta* including chloroplasts, due to their cyanobacterial origin. The expectation was therefore, to find circular DNA molecules corresponding to the entire genome size, within chloroplasts and mitochondria. Indeed, early investigations of pea chloroplast DNA, concluded the presence of genome-sized closed-circular molecules upon removal of contaminating nuclear DNA (Kolodner and Tewari 1972). Although the circular DNA molecules only accounted for just over one-third of the total DNA, this was interpreted as the natural organellar genomic form, as all linear DNA molecules identified were unable to account for the full genome size (Bendich 2004). Subsequent investigations have however identified DNA molecules of linear and linear-branched forms that possess sizes even exceeding that of the genomic size (Oldenburg and Bendich 2004a; Scharff and Koop 2006; Shaver et al. 2008).

The cyanobacterial origin of the chloroplast organelles is also evidenced by their arrangement of DNA into nucleoid structures. The nucleoids are tethered to the thylakoid membranes by thylakoid membrane anchoring proteins, these include MFP1 and pTAC16. The nucleoid has been proposed to consist of two layers, the first, known as the nucleoid core, is thought to be highly condensed and associated with high transcriptional activity, the second layer, or surrounding DNA, consists of less compact DNA with transient protein interactions (Briat et al. 1982; Hansmann et al. 1985; Krupinska et al. 2013; Sakai et al. 2004a). These findings contradict initial theories that the organellar DNA exists as closed-circular but topologically-constrained molecules, existing freely within the stroma of the chloroplast; in a similar manner to their bacterial ancestors. It is therefore particularly interesting to consider the role of gyrase within organelles encompassing such intricate DNA arrangements.

1.7.2.3. *Arabidopsis* mitochondrial genome

The mitochondrial genomes of plants are notorious for their extensive sizes, often ranging 200-2000 kbp, and complexity compared to those of animal mitochondrial genomes, which are consistently around 16.5 kbp. However, the genome size does not correlate with content; the additional DNA within a plant mitochondrion is accounted by large introns, repeats and non-coding regions (Morley and Nielsen 2017). The *Arabidopsis* genome, 367 kbp in size, encodes for 58 genes, whilst the human mitochondrial genome, more than 22 times smaller in size, encodes for 37 genes (Marienfeld et al. 1999; Taanman 1999) . The encoded genes are often involved in respiration, photosynthesis or other organellar functions. Interestingly, the mitochondrial genome has been found to incorporate alien fragments of both nuclear and chloroplast origin.

The plant mitochondrial genome is often mapped as a single circular molecule, large enough to account for the entire genome size, although this has only been observed in very low levels in liverwort or broad beans (Negruk et al. 1986; Oda et al. 1992) . The alternative and possibly realistic theory is the existence of this genomic DNA as a mixture of linear molecules of varying sizes, sub-genomic closed and open-circular molecules, that may be supercoiled, and other highly complex structures, as has been alluded to by several observations (Backert et al. 1997; Lo et al. 2011) .

The mitochondrial genome is arranged into nucleoids that associate the organellar DNA, RNA transcripts, tethering, scaffolding and compaction proteins together. The DNA stain, DAPI, has been found to be inefficient for mitochondrial DNA staining and identified nucleoids to be unevenly distributed (Sheahan et al. 2005). To avoid the loss of genetic

information, mitochondria frequently divide and fuse, a feature that helps healthy mitochondria to complement defective ones.

1.7.3. *Arabidopsis* topoisomerases

The *Arabidopsis* genome is served by a suite of topoisomerases to manage the array of DNA manipulations required during the process of DNA replication, repair and metabolism. Unsurprisingly, in order to deal with all possible challenges, topoisomerases of both, type I and type II categories are required to deal with instances of single- and double-stranded DNA manipulations, respectively. The *Arabidopsis* genome possesses three topoisomerases of each kind: type I: topoisomerase I α , topoisomerase I β and topoisomerase III α , and type II: topoisomerase II, topoisomerase VI and gyrase. However, there is currently insufficient information to decipher the array of topoisomerases that serves each of the three distinct genomes (nuclear, mitochondrial and plastid) within *Arabidopsis*; regardless, a summary of the sub-cellular localisation of each gene, as predicted by SUBA is provided in Table 1.

Table 1.1 *Arabidopsis thaliana* topoisomerase (topo) genes and predicted targeting according to the Subcellular Localisation Database for Arabidopsis proteins (SUBA).

Name	Locus	Chromosome	No. of amino acids	SUBA prediction [#]			
				N	P	M	O
Topo I α	At5G55300	5	918	8/16	4/16	2/16	2/16
Topo I β	At5G55310	5	917	10/15	0/15	1/15	4/15
Topo III α	At5G63920	5	926	7/15	1/15	6/15	1/15
Topo II	At3G23890	3	1473	7/18	4/18	5/18	0
Topo VIA	At5G02820	5	427	6/11	2/11	2/11	1/11
Topo VIB	At3G20780	3	670	4/12	1/12	3/12	4/12
GyrA	At5G10690	5	950	3/21	14/21	4/21	0
GyrB1	At3G10270	3	772	2/20	9/20	8/20	1/20
GyrB2	At5G04130	5	732	2/21	4/21	14/21	1/21

[#]: The columns of SUBA prediction: N: nucleus, P: plastid, M: mitochondria, O: other (these include cytosol, extracellular, Golgi).

1.7.4. *Arabidopsis* DNA gyrase

The sequencing of the *Arabidopsis* genome revealed four putative gyrase genes, encoding one GyrA and three GyrB subunits: AtGyrA, AtGyrB1 and AtGyrB2 and AtGyrB3 (Initiative 2000; Wall et al. 2004). Phylogenetic analysis of these genes grouped the first three in close association with cyanobacterial species, implying a possible symbiotic origin (Wall et al. 2004). Interestingly, the fourth gyrase gene, AtGyrB3, clustered closer to eukaryotic topoisomerase II. Experimental and bioinformatics analysis of AtGyrB3 revealed that the protein has several differences when compared to other gyrase B subunits; this includes: the shorter length of the protein, the absence of key catalytic domains such as the ATPase domain, the inability of the partially purified AtGyrB3 to support supercoiling in the presence of *E. coli* GyrA, and the inability of AtGyrB3 to complement an *E. coli* temperature-sensitive strain (Evans-Roberts et al. 2010). It was therefore concluded that, contrary to initial belief, AtGyrB3 does not encode a DNA gyrase subunit, but may in fact be a nuclear protein with a role in meiosis (Evans-Roberts et al. 2010).

The three genes encoding DNA gyrase in *A. thaliana* are described in Table 1.2. The *E. coli* GyrA subunit shares 37% sequence identity with its *Arabidopsis* homologue, conserving key catalytic residues; for example the catalytic tyrosine: *E. coli* residue 122 or *A. thaliana* residue 215 (Figure 1.16). Similarly, 33% of residues are conserved between the *E. coli* GyrB and AtGyrB1 and AtGyrB2 subunits, although the two GyrB subunits from *A. thaliana* are 86% identical in terms of their sequence (Figure 1.17).

Table 1.2. *Arabidopsis* DNA gyrase genes adapted from (Wall et al. 2004).

Gene	Locus	Mature Protein Mass (Da)	Transit Peptide Mass (Da)	Mature Protein location
AtGyrA	At3g10690	93,395	8,017 (Chloroplast) 6,513 (Mitochondria)	Chloroplast Mitochondria
AtGyrB1	At3g10270	72,492	8,700	Chloroplast
AtGyrB2	At5g04130	75,803	8,465	Mitochondria

1.7.4.1. Sub-cellular localisation of *A. thaliana* DNA gyrase

The sub-cellular localisation of the gyrase proteins in *Arabidopsis thaliana* has previously been investigated. The experimental approach involved the construction of clones comprising the transit peptide for each gyrase gene fused to a GFP reporter and expressed under the control of the 35S promoter (Wall et al. 2004). Accordingly, AtGyrA was found to be dual targeted to the chloroplasts and mitochondria, AtGyrB1 localised to the chloroplasts, whilst AtGyrB2 was targeted to the mitochondria (Wall et al. 2004). Subsequent to this work, it was realised that due to errors in the online database at the time of publication (the published sequence for AtGyrB1 was in fact AtGyrB2), the AtGyrB2 protein was actually dual targeted to both the mitochondria and chloroplasts, whilst the location of AtGyrB1 is not clear (Evans-Roberts 2007b). Furthermore, exposure of *Arabidopsis* to ciprofloxacin leads to a reduction in the number of chloroplasts and mitochondria, in addition to disrupted chloroplast morphology, although the mitochondria appear normal (Evans-Roberts et al. 2016). These results imply that gyrase may play a role in both of these organelles.

The subcellular localisation of proteins can be determined by using: fluorescent protein tags, mass-spectrometry, or through the identification of conserved protein sequence features as implemented by prediction software. One such useful resource, the subcellular localisation database for *Arabidopsis* proteins (SUBA) combines information from all three sources of data to conclude subcellular localisation of proteins (Hooper et al. 2017). According to the curations of this database, not only are all three gyrase subunits: AtGyrA, AtGyrB1 and AtGyrB2, predicted to be targeted to the chloroplast and mitochondrion, but mass-spectrometry information also supports these predictions (Heard et al. 2015; Heazlewood et al. 2004; Melonek et al. 2016a; Melonek et al. 2016b; Senkler et al. 2017).

```

EcGyrA 1 MSDI-----
AtGyrA 1 MTPVLC HSTASIPNPNLSLSLSTLRLSSSLRRSFFRFPLTDFLCRLRRTEPSA

EcGyrA 5 -----AREITPVNIEEEL
AtGyrA 56 TRFFSSRTPRSGKFVVGAGKRGDEQVQKEESGANNGGLVVSGETESRIVPFEHKEA

EcGyrA 18 KSSYLDYAMSVIVGRALPDVRDGLKPVHRRVLYAMNVLGNDWNKAYKKSARVVGD
AtGyrA 111 TESYNSYALSVLLGRALPDVRDGLKPVHRRILFAMHELGMSSKPKPYKCARVVGE

EcGyrA 73 VIGKHPHPGDSAVYDTIVRMAQPFSLRYMLVDCGNFGSIDGDSAAAMRYTEIRL
AtGyrA 166 VLGKHPHPGDTAVYDSLVRMAQSFSLRCPLIQHGNFGSIDADPPAAMRYTECRL

EcGyrA 128 AKLAHE-LMADLEKETVDFVDNYDGTBKI EDVMPKIPNLLVNGSSGIIVGMATN
AtGyrA 221 DPLAEAVLLSDLDQDQTVDFVANFDNSCKEPAVLEPARLEALLNGASGIIVGMATN

EcGyrA 182 IPPHNLTEVINGCLAYIDDEDISIEGLMEHIPGPDFPTAAIINGRRGEEAYRTG
AtGyrA 276 IPPHNLGELVDVLCALIHNFPEATLQELLEYMPAPDFPTGGIIMGNLGVLDAYRTG

EcGyrA 237 RGVYVIRARAEVE-VDAKTGRETIIVHEIPYQVKNKARLIEKIAELVKEKRVEGIS
AtGyrA 331 RGRVVRGKAEVELLDPKTRNAVITTEIPYQTNKATLVOKIAELVENKTELEGIS

EcGyrA 291 ALRDESDKDGMRIVIEVKRDVAVGEVVLNNLYSOTQLQVSFGINMVALHHGQPKIM
AtGyrA 386 DIRDESDRNGMRVVIELKRCGDPALVLLNNLYRHIALQSSFSGNMVGICDCEPKLM

EcGyrA 346 NLKDIIAAFVRRHREVVTRRTIFELRARDRAHILEALAVAIANIDPIIELIRHA
AtGyrA 441 GLKELLQAFDFRCSVVERRARFKLSAQCRKHIEGIVVGLDNVDEVIELITKA

EcGyrA 401 PTPABAKTALVANPWQLGNVAAMLERAGDDAARPEWLEPEFGVRDGLVYLTEQQA
AtGyrA 496 SSHSSATAALQ-----SEYGLSEKQA

EcGyrA 456 QAILDIRLQKLTGLEHEKLLDEYKELLDQIAELRLIIGSADRLMEVIREBELELVR
AtGyrA 517 EAILEITLRLTALERKKFTDESSSLTEQITKLEQLLSTRTNILKLIQBAIELK

EcGyrA 511 ECFGDKRRTEIT-ANSADINLEDLITCEDVVVTLSHQGYVKYQPLSEYEAORRG
AtGyrA 572 DRFSSPRRSMLEDSDSGDEIDIVIPNEEMLMAVSEKGYVKRMKADTENLOHRT

EcGyrA 565 KGKSAARIKEEDFDRLLVANTHDHILCFSSRGRVYSMKVYOLPEATRGRARCPPI
AtGyrA 627 IGVKGLRVDDAMSDFLVCHADHVLFFSDRCGLVYSTRAYKIPECSRNAAGTPL

EcGyrA 620 VNLPLEEQDERITAILPVTEFEEGVKVFMATANGTVKKTVLTFFENRLRTAGKVAI
AtGyrA 682 VQILSMSEGERVTSIVPVSEFAEDRYLMLTWNGLKPKVSLKLESGIRSTGIITAI

EcGyrA 675 KLVDGDELIGVDLTSGEDEVMLFSAEKVVRFKESSVRAAGONTIGVIRLIGEG
AtGyrA 737 QLNSGDELKWRCCSSDDLVAASONGMVALSTCDGVRTL SRNTKGVITAMRLKNE

EcGyrA 730 DKVVSIIIVPR-----GDC-ALLTATQNGYGKRTAVAEYPTK
AtGyrA 792 DKTIASMDIIPASLRKDMEEKSEDA SLVKQSTGFWLDFVCENGYGKRVPTSSERRS

EcGyrA 765 SRATKGVISIKVTERNGL---VVGAVQVDD---CDQIMMITDAGTVRTRVSEI
AtGyrA 847 RLNRVGLSGYKFAEDDRLA AVFVVGYS LAEDGESDEQVVLVSQSGTVNRKIVRDI
EcGyrA 813 SIVGENTQGVILIRTAEDENVVGLQRVAEPVDEEDLDTIDGSAEEDDEI APEVD
AtGyrA 902 SIQSRRARGVILMRLDHAGKIQSASLISAADDEETEGTILSNBAVEAVSL-----

EcGyrA 868 VDDEPEEE
AtGyrA -----

```

Figure 1.16. *E. coli* GyrA and *A. thaliana* GyrA sequence alignment.

The sequences for GyrA from *E. coli* and *A. thaliana* have been aligned, they share an overall sequence identity of 37%. Conserved residues are shown in black, residues replaced with similar amino acids are in grey. Dashed lines represent gaps in aligned sequences. Figure was produced using T-coffee sequence alignment and boxshade.

EcGyrB	1	M	-----
AtGyrB1	1	MALVQRQHSYLLRYEIRLMA SRPRPRLFSHSLVPSLHRHSSALSSS-----TPRIKQFL	
AtGyrB2	1	MALLQRASYLRLYEIRLMSR--PRLFSSSLSPALHRHSSTLSSPPFSSPSPSFRKIKQFL	
EcGyrB	2	-----SNSYDSSSIKVLKGLDAVRRKRPGMYIGD	
AtGyrB1	54	ANVFSQRLVQRNAVSPKSFMSSTMESLQESSTSKDYSSEHIQVLEGLDPVRRKRPGMYIGS	
AtGyrB2	59	TSVLSQRLLIQRNAISSR-FLST--EASQETTTSKGYSSEQIQVLEGLDPVRRKRPGMYIGS	
EcGyrB	30	TDDGTGLHHMVEVVDNAIDEALAGHCKEIIIVTTHADNSVSVQDDGRGIPTGIHPPEGVS	
AtGyrB1	114	TGS-RGLHHLVYEILDNAIDEAQAGFASKIDVVLHSDDSVSLSDNGRGIPTDLHPATGKS	
AtGyrB2	116	TGS-RGLHHLVYEILDNAIDEAQAGYASKVDVVLHADGSVSVVDNGRGIPTDLHPATKKS	
EcGyrB	90	AAEVIIMTVLHAGGKFDN--SYKVS GGLHGVGVSVVNALSQKLELVIQREGKIHRQIYEH	
AtGyrB1	173	SLETVLTVLHAGGKFGGKSSGYSVSGGLHGVGLSVVNALSEALEVIVRRDGMFQOKYSR	
AtGyrB2	175	SLETVLTVLHAGGKFGGTSSGYSVSGGLHGVGLSVVNALSEALEVSVWRDGMHMQNYSR	
EcGyrB	148	GVFOAPLAV---TGELE-KTGTMRFRWPSLETFNVTFFEYELAKRLRELSFLNSGVSI	
AtGyrB1	233	GKPVTLTCHVLPPEESRGTQGTCLRFWPDKEVFTTALQFDHNTIAGRIRELAFLNPKVTI	
AtGyrB2	235	GKPIITLTCRVLPLESKGTGTSIRFWPDKEVFTTALQFDHNTIAGRIRELAFLNPKVTI	
EcGyrB	204	RLNDKRDGKE---DHFHYEGGKAEVEMLNKNTPIHPNIFYFSTFKDCIGVEVALQW-	
AtGyrB1	293	SLKKEDDDPEKDVYSEYFYAGGLTEYVSWLNTDKNPIH-DVLGFRKEINGSTVDVSLQWC	
AtGyrB2	295	SLKKEDDDPEKTOYSEYSTAGGLTEYVSWLNTDKNPIH-DVLGFRKEINGATVDVALQWC	
EcGyrB	259	NDGFQNTIYCHTNNIPQRGGTHLAGFRAMTRTLNAYMDKEGYSKAKVSATGDDAREG	
AtGyrB1	352	SDAYSDTMLGYANSIRTIIDGGTHIEGVKASLRTLNSLAKKLVKIKKDISLSGEHVREG	
AtGyrB2	354	SDAYSDTMLGYANSIRTIIDGGTHIEGVKASLRTLNLAKKSKTVKEDDISLSGEHVREG	
EcGyrB	319	LIAVSVKVPDPKPFSSOTKDKLVSSEVKSAVEQOMNELLAEYILENPTDAKIVVCKIIDA	
AtGyrB1	412	LTCIVSVKVPNPEFEGQTKTRLGNPEVRKIVDQSVQEYLTEYLELHPDVLSEIISKSLNA	
AtGyrB2	414	LTCIVSVKVPNPEFEGQTKTRLGNPEVRKIVDQSVQEYLTEYLELHPDILESIISKSLNA	
EcGyrB	379	ARAREAAARRAREMTRRKGAIDLGLPGKLADCOERDPALSELYIVEGDSAGGSAKQGRNR	
AtGyrB1	472	YKAALAAKRARELVRSKSVLKSSSLPGKLADCSSTDPAESEIFIVEGDSAGGSAKQGRDR	
AtGyrB2	474	YKAALAAKRARELVRSKSVLKSSSLPGKLADCSSTDPEVSEIFIVEGDSAGGSAKQGRDR	
EcGyrB	439	RNQAAILPLKGIILNVEKARFDKMLSSQEVATLITALEGGIGRDEYNPKLRYHSIIIMTD	
AtGyrB1	532	RFQAAILPLRGKILNIEKDEAAMYKNEEQNLILGLGLGVKGEDFNKENLRYHKI IILTD	
AtGyrB2	534	RFQAAILPLRGKILNIEKDEAAMYKNEEQNLILGLGLGVKGEDFKKENLRYHKI IILTD	
EcGyrB	499	ADVDSGHIRTLTLLTFFRYRQMPETVFRGHVYIAQPLPKVKKGKQEQYIKDDEAMDQYQIS	
AtGyrB1	592	ADVDDGAHIRTLTLLTFFRYQRALFDAGCIYVGVPPFLFKVERGKQAHCYDAAALK----	
AtGyrB2	594	ADVDDGAHIRTLTLLTFFRYQRALFDAGCIYVGVPPFLFKVERGKNAQCYDDADLK----	
EcGyrB	559	IALDGATLHTNASAPALAGEALEKLVSEMNATQKMINRMERRYPKAMLKELIYQPTLTEA	
AtGyrB1	647	-----KITASF-----	
AtGyrB2	649	-----KITSNE-----	
EcGyrB	619	DLSDEQTVTRWVNALVSELNDKEQHGSQWKFDVHTNAEQNLFEPVVRVTHGVDTDYPLD	
AtGyrB1	653	-----PC-----	
AtGyrB2	655	-----PA-----	
EcGyrB	679	HEFITGGEYRRICTLGEKLRGLLEEDAFIERGERRQPVASFEQALDWLVKESRRGLSIQR	
AtGyrB1	655	-----NASYNIQR-----	
AtGyrB2	657	-----NASYNIQR-----	
EcGyrB	739	YKGLGEMNPEQLWETTMDEPSRRMLRVIVKDALAADOHFTTLMGDAVEPRRAFTEENALK	
AtGyrB1	663	FKGLGEMMPAQLWETTMNPDTRILKQLVDDAAETNMVSSLMGARVDVRKELIKSAATR	
AtGyrB2	665	FKGLGEMMPEQLWETTMNPDTRILKQLVDDIAEANMTVSSLMGARVDVRKELIKNAATR	
EcGyrB	799	--AANIIDI	
AtGyrB1	723	MNLENLDI	
AtGyrB2	725	INLQRLDI	

Figure 1.17. *E. coli* GyrB and *A. thaliana* GyrB1/B2 sequence alignment.

Top line: *E. coli* GyrB sequence; middle line: *A. thaliana* GyrB1 sequence; bottom line: *A. thaliana* GyrB2 sequence. Residues conserved between all three GyrB subunits are shown in black, residues replaced with similar amino acids are in grey. Dashed lines represent gaps in aligned sequences. The three GyrB sequences share 33% sequence identity, whilst AtGyrB1 and AtGyrB2 sequences are 86% identical. Figure was produced using T-coffee sequence alignment and boxshade.

1.7.4.2. *A. thaliana* gyrase insertional mutagenesis phenotypes

DNA gyrase plays a significant role in DNA replication, thus in extension of this, it can be anticipated that *Arabidopsis thaliana* gyrase will partake substantially in the process of plant development. This has been investigated using T-DNA insertion mutants, whereby the results indicate that knockout of *Arabidopsis thaliana gyrA* is seedling lethal, whilst those of *gyrB* range from seedling lethality to stunted growth (Wall et al. 2004). Intriguingly, yeast-two hybrid analysis of AtGyrA identified AtGyrB1 as an interacting partner only, whilst no interaction was observed with AtGyrB2 (Evans-Roberts et al. 2010). The lack of interaction with AtGyrB2 is particularly surprising considering the fact that the protein supports supercoiling when partnered with the *E. coli* GyrA subunit (Evans-Roberts et al. 2016; Wall et al. 2004).

Although the toxic effect of quinolones on *A. thaliana* cultures, plants and organelles had been demonstrated relatively early, DNA gyrase had not been identified as the protein target (Wall et al. 2004). Recently, a forward genetics approach identified a point mutation in the AtGyrA subunit that confers resistance to ciprofloxacin; this confirms that the *A. thaliana* gyrase genes encode an active gyrase enzyme, which is targeted by the quinolone class of antibiotics (Evans-Roberts et al. 2016).

1.8. DNA gyrase in plasmodia

1.8.1. Apicomplexa

Apicomplexan parasites comprise many important pathogens linked to disease, including: *Plasmodium* – responsible for malaria, *Toxoplasma* – linked to congenital neurological births, and *Eimeria* – a significant disease of poultry and cattle (Fichera and Roos 1997; Levine 1988). These parasites comprise a non-photosynthetic plastid-like organelle, the apicoplast, thought to be acquired by secondary endosymbiosis of alga (Kohler et al. 1997). The apicoplast contains the third genetic element in *Apicomplexa*, a 35 kbp circular extrachromosomal genome, in addition to the nuclear and mitochondrial genomes (Williamson et al. 1996; Wilson and Williamson 1997). The small apicoplast DNA does not provide any insight into the functions of the apicoplast itself, beyond DNA replication, transcription and translation (Lim and McFadden 2010). Therefore, research efforts focused upon the nuclear-encoded apicoplast proteins instead. These can be identified due to unique N-terminal extensions that are bipartite in nature, comprising a signal peptide and a transit peptide (Foth et al. 2003; Zuegge et al. 2001). Bioinformatics

tools have been used to assemble a predicted apicoplast proteome and putative biosynthesis pathways, based on existing bacterial pathways, for synthesis of fatty acids, isoprenoids, iron-sulphur clusters and haem in the apicoplasts (Ralph et al. 2004). It is believed that at least one of these functions is vital to the host, thus making the apicoplast indispensable.

1.8.2. Apicomplexan topoisomerases

The endosymbiotic relationship of cyanobacteria and an early eukaryote gave rise to chloroplasts and their subsequent diverse forms. The formation of a secondary endosymbiosis event initiated by engulfment of a photosynthetic alga, possibly of the red classification, by an early *Plasmodium* species, resulted in the acquisition of a chloroplast by a non-photosynthetic eukaryote (Oborník et al. 2009). The evolution of this chloroplast into the apicoplast, a remanent chloroplast, was accompanied by loss of its photosynthetic capacity (Howe 1992). As a consequence of their secondary endosymbiotic acquisition, the apicoplast are often surrounded by three to four membranes (Waller and McFadden 2005).

The *Apicomplexa* contain three essential genomes: nuclear, mitochondrial and apicoplast. The vital processes of DNA replication, transcription and recombination all require the unwinding of the DNA duplex, to allow access to DNA or RNA polymerase complexes, this results in topological implications that are resolved by topoisomerase proteins. The apicoplast genome is of particular relevance to the work described here due to its unique association with gyrase amongst the three *Apicomplexan* genomes. The sequencing of genomes of the *Apicomplexa* have identified two putative type I topoisomerases: eukaryotic topoisomerase I and topoisomerase III, and the type II topoisomerases: topoisomerase II, gyrase and topoisomerase VI (Table 1.3).

1.8.3. Apicomplexan gyrase

Typically, *Apicomplexan* gyrases are encoded by two genes, a single GyrA and GyrB, within their nuclear genomes. The gyrase protein biologically functions to support replication of its 35 kbp circular genome, which largely encodes rRNAs and ribosomal proteins (Blackwell et al. 2002; Wilson et al. 1996). The DNA gyrase of *Toxoplasma gondii* is able to negatively supercoil DNA, possesses an efficient decatenation activity as well as sensitivity to classic gyrase inhibitors, such as novobiocin and ciprofloxacin (Lin et al. 2015).

Table 1.3. *Plasmodium falciparum* strain 3D7 topoisomerase genes according to annotations on the PlasmoDB.

Name	Locus	Chromosome	No. of amino acids
Topo I	PF3D7_0510500	5	829
Topo III	PF3D7_1347100	13	710
Topo II	PF3D7_1433500	14	1472
Spo11	PF3D7_1217100	12	327
Spo11-2	PF3D7_1027600	10	336
Topo VIB	PF3D7_1365600	13	561
GyrA	PF3D7_1223300	12	1222
GyrB	PF3D7_1239500	12	1006

1.8.3.1. *Plasmodium falciparum* gyrase

Malaria is a life-threatening parasitic disease that caused 229 million cases in 2019 (World Health 2019). It is transmitted to people through the bite of an infected female *Anopheles* mosquito. The causative agents of malaria are *Plasmodium* parasites; of the five species, two predominantly cause human infections: *P. falciparum* and *P. vivax*.

DNA gyrase genes have been identified in the malarial parasite, *Plasmodium falciparum* (Carucci et al. 1998; Gardner et al. 2002a). The nuclear genome of the parasite comprises 23 Mbp divided amongst 14 chromosomes and is extremely AT rich, averaging 81% overall, 90% for introns and intergenic regions, and about 87% for the apicoplast (Gardner et al. 2002b). In part, as a consequence of the high AT content, the *P. falciparum* genome is also rich in asparagine repeats, which are recognised to enhance intracellular protein aggregation (Aravind et al. 2003; Muralidharan and Goldberg 2013; Nagano et al. 2014). As is the case for the apicoplast in general, most of the proteins in the organelle, gyrase included, are nuclear-encoded, a few exceptions include genes required for apicoplast transcription and translation, 9 duplicated tRNAs, and both subunits of the rRNA genes (Fleige and Soldati-Favre 2008; Wilson et al. 1996).

P. falciparum encodes one GyrA (PfGyrA) subunit and one GyrB (PfGyrB) subunit. An initial indication of the existence of gyrase in the parasite came from the selective sensitivity of the apicoplast to ciprofloxacin, whereas a general topoisomerase II inhibitor, VP-16, also induced cleavage of the nuclear DNA (Fichera and Roos 1997; Weissig et al. 1997). Gyrase from *P. falciparum* has been predicted to have distinct characteristics when compared to the “conventional” *E. coli* protein. This is perhaps unsurprising considering

that the EcGyrA and EcGyrB are encoded by 857 and 804 amino acids respectively, whilst PfGyrA and PfGyrB are encoded by 1067 and 886 amino acids respectively.

The *in vitro* expression of *P. falciparum* gyrase has been attempted on more than one occasion, leading to successful expression of the full-length PfGyrB subunit (Dar et al. 2007; Raghu Ram et al. 2007). Interestingly, the reduction in the ratio of apicoplast to nuclear DNA upon novobiocin treatment suggests that gyrase functions directly in apicoplast DNA replication (Singh et al. 2005). Moreover, the N-terminal sequences of PfGyrA and PfGyrB target GFP to the apicoplast within *T. gondii* and both subunits showed evidence of co-localization with an apicoplast targeted protein in *P. falciparum* itself (Dar et al. 2007). PfGyrB successfully complemented an EcGyrB temperature-sensitive strain, suggesting a somewhat overlapping function of the protein with EcGyrB; interestingly however, PfGyrA was unable to complement an EcGyrA temperature-sensitive strain, unfortunately, the clarity of this result is questionable as no PfGyrA expression was detected within the *E. coli* strain (Dar et al. 2007).

PfGyrB possesses intrinsic ATPase activity, the rates of ATP hydrolysis increase linearly with an increase in PfGyrB concentration; in addition, the ATPase activity is sensitive to the aminocoumarin ATPase inhibitor, novobiocin (Dar et al. 2007; Raghu Ram et al. 2007). This is in contrast to behaviour of the classical *E. coli* gyrase, which exhibits dimerization in the presence of nucleotide and its ATPase activity is stimulated when joined by the EcGyrA subunit and DNA (Ali et al. 1993; Sugino and Cozzarelli 1980). The intrinsic ATPase activity of PfGyrB is stimulated by DNA, even without any corresponding GyrA; this indicates direct DNA binding activity by the PfGyrB protein. Indeed, Dar and co-workers identified PfGyrB to be predominantly dimeric in solution, with the capacity to directly bind DNA (preferably with a high AT content), in accordance with the base-pair bias of the apicoplast, but without any assistance from GyrA (Dar et al. 2009). These distinctive characteristics were found to be attributed to a unique 45 amino acid insertion region, within the TOPRIM domain of PfGyrB (Dar et al. 2009). The deletion of these 45 amino acids, abolished the DNA binding capacity of PfGyrB, in addition to its ability to conduct DNA cleavage and supercoiling when in partnership with EcGyrA, and the ability of PfGyrB to complement an EcGyrB temperature-sensitive strain (Dar et al. 2009). The ATPase activity of PfGyrB is increased in a DNA length-dependent manner, suggesting close communication of the ATPase domain and DNA-binding activity of the enzyme. The dependence of DNA binding upon its passage through the ATP-gate of PfGyrB was confirmed by the inability of the active complex, formed with EcGyrA, to bind or supercoil DNA when preincubated with the non-hydrolysable ATP analogue (AMPNP), which effectively locks the ATP-gate of the enzyme complex; notably DNA cleavage activity was

still detectable (Dar et al. 2009). The treatment of AMPNP preincubation of *E. coli* gyrase reduces its DNA binding activity, but does not abolish it completely, the observations of PfGyrB made by Dar and co-workers resemble that of yeast topoisomerase II (Roca and Wang 1992; Williams et al. 2001).

The heterologous expression of full-length PfGyrA has not yet been possible, but domains of the protein corresponding to the N-terminal region, encompassing the winged-helix, tower and the coiled-coil domains have been expressed and purified (Dar et al. 2007). The unsuccessful expression of the full-length PfGyrA protein is interesting considering its relatively lower expression *in vivo* when compared to PfGyrB, notably expression of both gyrase subunits peak during the trophozoite and schizont stages of parasite development (Dar et al. 2007). The combination of PfGyrA (N-terminal region) with PfGyrB, forms a complex active in the DNA-cleavage reaction only; the resultant enzyme is not expected to supercoil DNA due to the absence of the C-terminal region of the protein, which plays an essential role in the DNA-wrapping activity of gyrase and presentation of a T-segment contiguous to the bound G-segment of DNA. Contradictorily, in later investigations, Dar and co-workers showed that PfGyrB alone was able to cleave DNA, therefore leaving the activity contribution of PfGyrA-NTD questionable (Dar et al. 2009).

In silico analysis of the *P. falciparum* gene has highlighted the lack of a GyrA box, which is essential for supercoiling activity (Nagano et al. 2014). Therefore, plausibly *P. falciparum* gyrase may be inefficient in DNA supercoiling, as has been reported for other gyrases lacking this essential domain (Kramlinger and Hiasa 2006). Sequence alignments of the *E. coli* gyrase protein and its *Plasmodia* counterpart highlighted the core domains to be similar, for example the ATPase binding and hydrolysis site and cleavage-reunion regions of the two enzymes. However, overall, the sequence identity was ~26% for the GyrA of the two species, but this identity was not homogeneously distributed along the entire sequence; the NTD of the GyrAs were up to 34% identical, whilst the CTD was found to be most divergent, with only 18% identical residues between the two species (EGyrA and PfGyrA). The GyrB sequences were more conserved (~39% overall), which were uniformly distributed within the sequence (Nagano et al. 2014). The binding site for fluoroquinolone inhibitors (cleavage-reunion region of GyrA) is conserved between the two species.

Interestingly, domain prediction software only identified PfGyrA to possess three of the typical six β -blades of the β -pinwheel to be conserved in the GyrA CTD (Nagano et al. 2014). Following unsuccessful attempts to express meaningful quantities of soluble full-length PfGyrA, the boundaries of the PfGyrA C-terminal domain (PfGyrA-CTD) were

determined bioinformatically prior to its expression and purification (Nagano et al. 2015). Nagano and co-workers were able to manually identify a further two regions likely to give rise to β -blades within the newly determined PfGyrA-CTD region, therefore accounting for blades 1 and 2 of the β -pinwheel analogous to the *E. coli* gyrase CTD, in addition to blades 3,4 and 5 that were identified by domain analysis software (Figure 1.18) (Nagano et al. 2015). Limited proteolysis of PfGyrA-CTD confirmed the region consisting of a potential sixth β -blade to be well folded, therefore, its existence cannot be ruled out (Nagano et al. 2015). The purified PfGyrA-CTD domain possesses DNA-binding and -wrapping activity (Nagano et al. 2015). Nagano and co-workers identified an asparagine rich plasmodium-specific insert region within the putative blade 1 of the PfGyrA-CTD, which within the prokaryotic blades corresponds to a loop region; however, deletion of the asparagine region did not obviously affect the activity of PfGyrA-CTD (Nagano et al. 2015).

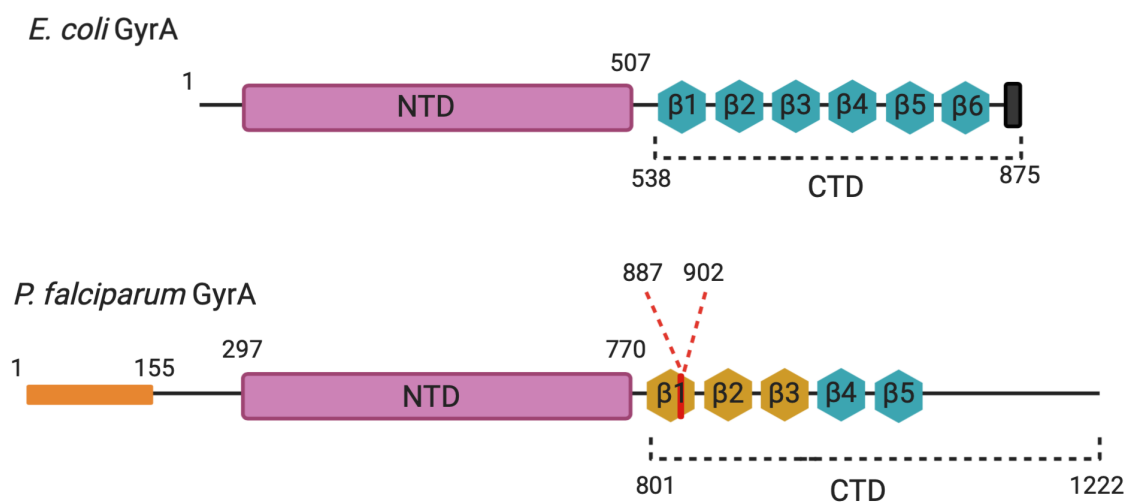


Figure 1.18: Primary domain architecture of *E. coli* and *P. falciparum* GyrA.

The domain architecture of *E. coli* (top) and *P. falciparum* (bottom) GyrA sequences is compared. The domain colours: orange: signal/transit peptide, pink: NTD, blue: β -pinwheel domains as predicted by Pfam server, yellow: β -pinwheel domains manually annotated by (Nagano et al. 2015), red line: unique asparagine repeat within annotated $\beta 1$ -blade, black: acidic C-terminal tail. Numbers refer to amino acid positions for each sequence. Figure redrawn from (Nagano et al. 2015).

The variabilities of gyrase sequences of *P. falciparum* from *E. coli*, including its larger size and plasmodium-specific insertion regions could equate to potential significant structural and functional differences for the enzyme. The situation of gyrase in the *Plasmodia* apicoplast is comparable to *Mycobacterium tuberculosis* where the enzyme is the sole type IIA topoisomerase, due to the absence of topoisomerase IV. The *M. tuberculosis* gyrase was identified to possess a greater ability to decatenate DNA relative to the *E. coli* gyrase, whilst retaining a similar supercoiling activity; albeit, when compared to topoisomerase IV from *Streptococcus pneumoniae*, the *M. tuberculosis* enzyme's activity was still 25-fold lower (Aubry et al. 2006). The unique activity of *M. tuberculosis* gyrase is modulated by Ca²⁺, binding of the divalent ion to a linker region between the NTD and CTD of MtGyrA favours the supercoiling reaction, whilst decatenation and relaxation are favoured in its absence (Karkare et al. 2012). An intriguing prospect is that the *P. falciparum* gyrase may also possess activities akin to a hybrid enzyme of gyrase and topoisomerase IV; this is yet to be explored.

1.8.3.2. *Plasmodium vivax* gyrase

Although *P. falciparum* is the causative agent for almost more than 99% of malaria cases globally, the case contribution of *P. vivax* can be up to 75% in specific regions (World Health 2019). Unfortunately, research efforts of the *P. vivax* gyrase enzyme have also been limited due to considerable hurdles in the heterologous expression of the protein. In a similar manner to the genes of *P. falciparum*, the gyrase genes of the *P. vivax* are also considerably larger than the *E. coli* protein, although the AT base-pair bias of the genome is not as extreme as its *P. falciparum* relative. Thus far, successful attempts of expressing *P. vivax* gyrase have been limited to its B subunit (PvGyrB) only (Khor et al. 2005). The full-length polypeptide of PvGyrB is ~992 residues, harbouring ~35% identical residues to the EcGyrB protein and ~65% identify to *P. falciparum*. However, expression attempts thus far have resulted in predominantly insoluble protein, which upon refolding produced a low but detectable level of DNA-independent ATP activity; critically, the overall globular structure and refolded state of this protein was questionable (Khor et al. 2005). Therefore, Khor and colleagues focussed instead on the 43-kDa ATP-binding and hydrolysis domain of PvGyrB, homologous to the *E. coli* enzyme domain that can independently fold into an active domain (Ali et al. 1993). Indeed, their efforts produced soluble protein of the 43-kDa PvGyrB, they were able to associate the domain to be potentially dimeric in solution and possess a DNA-independent ATPase activity, contrary to the ATPase activity of *E. coli* gyrase (Ali et al. 1993; Khor et al. 2005).

1.8.3.3. *Plasmodium berghei* gyrase

Plasmodium berghei is one of four species causing malaria in rodents. However, the parasite can potentially serve as a model disease case for comparison to human malaria cases due to its similar mechanism of transmission to its host through the female *Anopheles* mosquito, comparable symptoms to those caused in human malaria cases and the additional benefit of the relative ease of genetic engineering within infected rodents (Franke-Fayard et al. 2010). Interestingly, the first purification and description of topoisomerase I β was from the murine parasite *P. berghei*. The enzyme was purified and confirmed to possess ATP- and Mg²⁺-independent relaxation activity, although its activity was stimulated by the divalent metal ion (Riou et al. 1986). At the same time, topoisomerase II activity was also purified from infected red blood cells, and the resultant enzyme was shown to possess ATP- and Mg²⁺-dependent relaxation, unknotting and decatenation activities (Riou et al. 1986). The genes of DNA gyrase have been identified by genome sequencing of *P. berhgei*, however these are yet uncharacterised.

1.8.4. Apicomplexan gyrase inhibition

The cyanobacterial origin of the apicoplast makes it a target for antibacterials that are effective as antimalarials including doxycycline and ciprofloxacin (Wang 2002a). Often, the treatment with drug does not distress the parasite itself but has a profound effect on proliferation of their progeny that exhibit 'delayed cell death', due to the progressive loss of apicoplast function (Dahl and Rosenthal 2007). The response of plasmodial parasites to fluroquinolone drugs is distinct from the bactericidal effect of the inhibitor within *E. coli* (Tang Girdwood et al. 2015). In Plasmodia, the activity of ciprofloxacin correlated with antiparasitic activity. Interestingly, the inhibition activity was found to be stronger than can be accounted by a sole effect against apicomplexan gyrase; suggesting that ciprofloxacin may also have off-target effects in *Plasmodium falciparum* (Tang Girdwood et al. 2015).

1.9. Project aims

Investigation into the basic biochemical properties, structure, reactions and features of the bacterial gyrase proteins have not only been hugely fascinating due to the unravelling of their intricate reaction mechanism but also an immensely rewarding and gratifying field of study, principally due to the subsequent practical exploitation of the protein as an effective target for the development of successful antibiotics. This project has sought to research the gyrase proteins, specifically within the eukaryotic species *Arabidopsis thaliana* and *Plasmodium*, with the ultimate aspiration that any biochemical insight gained could lead to the discovery of, or form the initiation of, the development of inhibitors that have potential as favourable herbicides or antimalarial drugs.

The research here reports efforts for the initiation of biochemical characterisation of eukaryotic gyrase proteins. The endeavour has been to build-upon the preceding challenges of heterologous protein expression and determine the fundamental enzymological reactions conducted by these gyrases. Potentially, the latter characterisation may signify valuable functional differences of these proteins to manipulate for the development of species-specific enzyme inhibitors. Nevertheless, the genesis of such inhibitors is preceded by the work here through determination of *Arabidopsis thaliana* gyrase inhibition by established fluoroquinolone inhibitors and novel variants of it. However, any *in vitro* determination of enzyme characterisation would be incomplete without clues from the functional role of gyrase within its native biological environment. Efforts to initiate exploration of this role for *Arabidopsis thaliana* gyrase, will also be described.

Chapter 2: Materials and Methods

2.1. Bacteriology

2.1.1. Bacterial strains

Bacterial strains typically used for *Escherichia coli* cloning and expression are listed in Table 2.1. Plant transformations were mediated by *Agrobacterium tumefaciens* strain LBA4404.

Table 2.1: *E. coli* strains and genotypes used in this work.

Strain	Genotype
DH5 α (NEB)	F- ϕ 80lacZ Δ M15 Δ (lacZYA-argF) U169 deoR recA1 endA1 hsdR17 (rk -, mk +) phoA supE44 λ - thi-1 gyrA96 relA1
Stellar™ (Cloantech)	F-, endA1, supE44, thi-1, recA1, relA1, gyrA96, phoA, Φ 80d lacZ Δ M15, Δ (lacZYA - argF) U169, Δ (mrr - hsdRMS - mcrBC), Δ mcrA, λ -
BL21 (DE3) (NEB)	fhuA2 [lon] ompT gal (λ DE3) [dcm] Δ hsdS λ DE3 = λ sBamHIo Δ EcoRI-B int::(lacI::PlacUV5::T7 gene1) i21 Δ nin5
Rosetta™ 2 (pLysS) (Novagen)	F- ompT hsdSB(rB- mB-) gal dcm (DE3) pLysSRARE2 (CamR)
α -Select Gold (Bioline)	F- deoR endA1 recA1 relA1 gyrA96 hsdR17(rk-, mk+) supE44 thi-1 phoA Δ (lacZYA-argF)U169 Φ 80lacZ Δ M15 λ -
LE392	sdR514(rk-, mk+), glnV(supE44), tryT (supF58), lacY1 or Δ (lacIZY)6, galK2, galT22, metB1, trpR55
ER2925	ara-14 leuB6 fhuA31 lacY1 tsx78 glnV44 galK2 galT22 mcrA dcm-6 hisG4 rfbD1 R(zgb210::Tn10)TetS endA1 rpsL136 dam13::Tn9 xylA-5 mtl-1 thi-1 mcrB1 hsdR2
Max Efficiency™	F-mcrA Δ (mrr-hsdRMS-mcrBC) Φ 80lacZ Δ M15
DH10Bac™ (ThermoFisher)	Δ lacX74 recA1 endA1 araD139 Δ (ara, leu)7697 galU galK λ - rpsL nupG/pMON14272/pMON7124

2.1.2. Media

The strains listed in Table 2.1 were grown in Luria–Bertani medium or agar (Formedium). For plates, the agar included addition of 1.5% (w/v) agarose to the media, prior to autoclaving.

2.1.2.1. LB

The composition of Luria–Bertani (LB) medium: Tryptone 1% (w/v), Yeast extract 0.5% (w/v), Sodium Chloride 1% (w/v).

2.1.2.2. SOC

Super Optimal Broth with catabolite repression (SOC) medium: 2% tryptone (w/v), 0.5% yeast extract, 10 mM NaCl, 2.5 mM KCl, 10 mM MgCl₂, 10 mM MgSO₄, and 20 mM glucose.

2.1.3. Antibiotics

Antibiotic selection was necessary in bacterial media for isolation of *E. coli* harnessing the desired transformed plasmids. Antibiotics used in this work were prepared according to Table 2.3, filter sterilized through a 0.2 µm filter (where applicable) and stored in aliquots at -20°C or 4°C, as necessary.

Table 2.2: Antibiotics, their stock and working concentrations used in this work.

Antibiotic	Solvent	Stock concentration	Final concentration
Ampicillin	Water	100 mg/mL	100 µg/mL
Chloramphenicol	70% Ethanol	34 mg/mL	34 µg/mL
Tetracycline	70% Ethanol	15 mg/mL	15 µg/mL
Gentamycin	Water	50 mg/mL	7 µg/mL
Rifampicin	DMSO	50 mg/mL	50 µg/mL
Kanamycin	Water	30 mg/mL	30 µg/mL
Ciprofloxacin	Water/DMSO	30 mM	Various
Penicillin-streptomycin	Water	5 mg/mL	100 µg/mL

2.1.4. Preparation of chemically competent cells

Glycerol stocks of the desired *E. coli* cells were streaked onto fresh LB agar plates and grown overnight at 37°C. A single colony was then isolated and inoculated into 5 mL of LB containing the respective antibiotic and incubated overnight. 1 mL of the overnight culture was then used to further inoculate a fresh 100 mL LB. The cell culture was grown at 37°C until OD₆₀₀ 0.4-0.6 was reached. The culture was cooled on ice and cells were harvested by centrifugation at 3,000 rpm for 10 mins. 100 mM calcium chloride was used to resuspend pelleted cells, after which cells were incubated a further 20 mins on ice. Cells were pelleted again by gentle centrifugation and resuspended in 2.4 mL of 100 mM calcium chloride, 20% (v/v) glycerol. Finally, the resuspended cells were aliquoted into 50 µL aliquots and flash frozen using liquid nitrogen. The cell aliquots were stored at -80°C until later use.

2.1.5. DNA transformation of chemically competent cells

Aliquots of chemically competent cells were removed from -80°C and allowed to thaw on ice for ~15-20 mins. Once thawed, ~0.5-2µl of plasmid DNA (2-25 µg/ml) was gently injected into the cell aliquots. The resulting cell aliquots were incubated on ice for a further 20 mins. To initiate plasmid transformation, the cell/DNA mixtures were then heat shocked at 42°C for 30-45s. The cells were immediately transferred back to ice for one minute before 200 – 800 µL of SOC media was added. The cells were incubated at 37°C for a further 1 hr (in shaking incubators), then were plated onto LB agar containing the relevant antibiotic and were subsequently incubated overnight at 37°C for colony selection.

2.1.5.1. DNA transformation of electrocompetent cells

Aliquots of electrocompetent cells were thawed on ice prior to the addition of 2 µL of DNA. After brief incubation of the mixture, it was transferred to a chilled electroporation cuvette. An Eppendorf Electroporator 2510 was used at a voltage of 2000 V to shock cells. Cells were recovered in 800 µL SOC media and incubated at 37°C (shaking, 220 rpm) for 60 mins. The cells were spread onto LB agar plates with appropriate antibiotics.

2.2. DNA methods

2.2.1. Buffers and solutions

Table 2.3: Buffers used for DNA analysis in this work.

Buffer	Composition/Details
STEB (2x)	100 mM Tris.HCl pH 8, 40% sucrose (w/v), 100 mM EDTA and 0.5 µg/mL bromophenol blue
TAE	40 mM Tris.acetate pH 8, 1 mM EDTA
Sample application buffer (SAB)	50 mM Tris.HCl pH 6.8, 2% (v/v) SDS, 100 mM DTT, 10% (v/v) glycerol and 0.05% (w/v) bromophenol blue
Elution Buffer (EB)	10 mM Tris.HCl, pH 8.5
DNA loading dye	100 mM Tris.HCl pH 8, 1mM EDTA, 40% (w/v) sucrose and 0.002% (w/v) bromophenol blue

2.2.2. Agarose gel electrophoresis

Agarose gel electrophoresis is used to separate DNA based on molecular weight or topology. For topology assays, 1% (w/v) agarose gels were prepared by melting agarose (Sigma) in TAE prior to pouring hot agarose into gel casks with appropriate well separators and allowing the gel to set at room temperature for 20-30 mins. Once set, gels were submerged in a gel tank with TAE buffer and DNA samples were injected into the wells of the gel. An electric current ~80 V was applied, to allow separation of the DNA molecules until the dye front had reached 2/3 of the length of the gel. The gel was then stained in TAE buffer containing 2 µg/mL ethidium bromide for 10-20 mins, prior to destaining in TAE for a further 10 mins. Occasionally, gels were run with an intercalating agent, such as chloroquine or ethidium bromide. In these cases, 2 µg/mL chloroquine or 5 µg/mL ethidium bromide was introduced directly into pre-cooled molten agarose, prior to casting of the agarose gel. Once cast, these gels were run in TAE buffer with the respective concentration of intercalator. Gels used for analysis of small fragments of DNA (for example in RT-PCR analysis) were typically of 3% (w/v) agarose. The gels were visualised under an ultraviolet transilluminator and photographed using the Syngene Bio-imaging system.

2.2.3. DNA gel extractions

DNA of desired molecular weights were identified subsequent to electrophoresis (typically 0.8% (w/v) agarose gels) and purified using either Gel purification kit or Nucleospin and PCR clean up kit (Qiagen) according to manufacturer guidelines.

2.2.4. DNA isolation from reactions

DNA was purified from enzymatic reactions using a PCR purification kit (QIAGEN) as according to manufacturer's guidelines.

2.2.5. DNA precipitation

DNA precipitation was occasionally carried out for the purification, concentration and storage of DNA samples. Ethanol or isopropanol were used interchangeably; to the DNA sample were added 1/10 the volume of sodium acetate (3 M, pH 5.2) and either ethanol (2.5-3.0x vol) or isopropanol (1x vol). The resulting mixture was incubated on ice for 15 mins to >8 hours (depending on the quantity of the DNA in the sample) to allow precipitation. The sample was then centrifuged at 4°C, >14,000 g for 30 mins to pellet the DNA. The supernatant was removed, and the DNA pellet was washed with 70% (v/v) ethanol to remove any remaining sodium acetate. The sample was again centrifuged at >14,000 g for a further 15 mins. The supernatant was once again removed, and the DNA pellet was redissolved into the desired solvent.

2.2.6. Plasmid DNA production and purification

Plasmid DNA was transformed into chemically competent cells, which were used to inoculate 5 mL of LB medium (with appropriate antibiotic selection) and grown overnight to reach stationary growth. The bacteria were then harvested, lysed and the DNA was extracted using the appropriate Qiaprep spin miniprep, midiprep or maxiprep kits (Qiagen), depending on the desired quantity of DNA, by following the manufacturer's recommended protocol.

2.2.7. Phenol:chloroform:isoamyl extraction of DNA

Phenol:chloroform:isoamyl extraction was used as an alternative method to purify DNA. An equal volume of 25:24:1 phenol:chloroform:isoamyl alcohol (Sigma-Aldrich) was added to the DNA, and the mixture vortexed for 30 s. It was then centrifuged at 16,000 g

for 10 mins. The upper, aqueous layer was taken and an equal volume of 24:1 chloroform:isoamyl alcohol was added prior to vortexing for 30 s. The mixture was centrifuged at 16,000 g for 10 mins. The upper layer then contained purified DNA.

2.2.8. DNA digestion with restriction endonuclease

Endonucleases from either New England Biolabs or Roche were used to digest DNA. Between 5 and 50 units of enzyme was used in a 50 μ L reaction, with 1x concentration of the appropriate buffer. The total volume of the enzyme was never more than 10% (v/v) of the total reaction volume. The reactions were carried out for one to two hours (occasionally overnight) at the appropriate temperature. Where appropriate the reaction was then stopped by heat inactivation.

2.2.9. DNA ligation

DNA ligations were conducted with 2 μ L T4 DNA ligase (Invitrogen) in a 30 μ L reaction, as according to manufacturer's guidelines.

2.2.10. DNA sequencing

DNA sequencing was performed by Eurofins Genomics.

2.2.11. DNA concentration determination

DNA concentrations were determined by the use of a Nanodrop (ThermoFisher). Typically, 1-2 μ L of DNA solution was compared to a blank buffer. The absorbance at 260 nm was determined by the machine and converted to concentration through the Beer-Lambert equation.

2.2.12. Polymerase chain reaction

The polymerase chain reaction (PCR) was used to amplify fragments of DNA and for sub-cloning of genes. Several polymerases were used for the purpose of this work (Table 2.4). The PCR reactions were carried out according to the manufacturer's guidelines for each individual enzyme. Reactions were incubated in an Eppendorf Mastercycler® nexus thermocycler.

The PCR of bacterial colonies involved submersion of the bacterial colony in 50 μ L of sterile water and heat treatment for 5 mins at 95°C to lyse cells. The lysed cells were then used to template PCR reactions.

A typical 50 μL PCR reaction was run with 0.5 -1 μM of each primer, 1 ng of template DNA, 1 U of polymerase, 200 μM dNTPs (equimolar deoxynucleotide triphosphates, dGTP, dCTP, dATP and dTTP), 1 x PCR buffer and nuclease free water to the required volume.

Table 2.4: Polymerases used in this work and their main applications.

Polymerase	Supplier	Application
Phusion®	ThermoFisher	Fragment amplification and cloning
GoTaq® green	Promega	Colony PCR
PrimeSTAR® Max	TaKaRa	Fragment amplification and cloning
Phire® Plant Direct	ThermoFisher	<i>A. thaliana</i> genomic DNA analysis

2.2.13. In-Fusion cloning

The majority of cloning in this work was carried out using the In-Fusion cloning system (TaKaRa Bio Inc), as according to manufacturer guidelines. The rationale for In-Fusion cloning is based on the design of oligonucleotides with regions of homology to the target plasmid and insert (Figure 2.1). The process can facilitate the sequential insertion of more than one insert, if required. The target plasmid can be pre-digested with restriction endonucleases, or linearised by PCR.

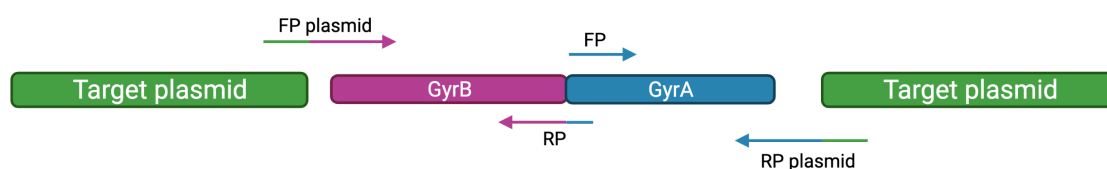


Figure 2.1: Schematic of In-Fusion cloning.

An example for the simultaneous insertion of GyrB and GyrA genes into the target plasmid (note: one gene may also be inserted). The primers designed for In-Fusion cloning are typically 20 bp in length, with regions of homology to the target plasmid at the 5' end and target gene of insertion at the 3' end.

2.2.14. DNase treatment of RNA

Extracted RNA was treated with DNase to remove any contaminating DNA from samples. A TurboDnase kit (ThermoFisher) was used for this purpose and typically 1.5 μg of RNA was treated in a 25 μL reaction as according to manufacturer's guidelines. Treated RNA was stored at -80°C .

2.2.15. Reverse transcription of RNA

Extracted RNA was converted to cDNA by the process of reverse transcription. The reverse transcription for all reactions to be compared were carried out in parallel. The RNA used in reactions had been pre-treated with DNase. Care was taken throughout the procedure to avoid contamination of the reaction with RNase. Reactions were catalysed by SuperScript® III Reverse Transcriptase (ThermoFisher). Primer sequences given in Table 2.5. The components of a typical 20 µL reaction are:

Component	Concentration
Anchored Oligo(dT)20	2.5 µM
RNA	40 ng
dNTP mix (10 mM each)	0.5 mM
Nuclease free water	Up to reaction volume

The mixture of was incubated at 65°C for 5 mins. Following incubation, the following were added:

Component	Concentration
First Strand buffer	1x
DTT	0.5 mM
RNase out	1 U
SuperScript III RT	1 U

Reactions were incubated for 40 mins at 50°C, followed by 15 mins at 70°C (to inactivate enzyme) in an Eppendorf Mastercycler® nexus thermocycler. Typically, 1 µL of synthesised cDNA was used to template downstream PCR.

Table 2.5: RT-PCR primer sequences used in this work.

Gene	Forward Primer	Reverse primer	Expected size (bp)
SAND	AACTCTATGCAGCAT	TGATTGCATATCTTT	~60
GyrA	ACTCCTTGGCTGAGGATGGG	CGGTTACAGTTCGGCTTTG	70
GyrB1	GGTGCTCGGGTCGATGT	GTCTCCCTTTGCATTTACCA	151
GyrB2	CCTCGGTGTGAAGGGAGAAG	ACAGAGGAGGAACACCGACA	179

2.3. Protein methods

2.3.1. Dialysis

Protein samples were dialysed for the removal of salt and solute using SnakeSkin™ tubing (Thermo Scientific) with a 10 kDa molecular weight cut off. The SnakeSkin tubing was secured by clips at each end and dialysed overnight at 4°C with constant stirring.

2.3.2. Protein concentration

Amicon® Ultra centrifugal filters (Merck) with a molecular weight cut off of 10,000 were used for protein concentration. Concentration was typically carried out at between 3000-4500 rpm on a bench top centrifuge (Sorvell Legend RT) or at 14,000 g in a bench top microcentrifuge at 4°C. Concentration analysis was carried out at regular intervals to determine the desired endpoint.

2.3.3. Protein concentration determination

The Bradford method was implemented for determination of protein concentrations in samples (reagents from Sigma). 10 µL of protein solution was diluted into 100 µL of buffer (in which the protein was stored) and mixed with 900 µL of Bradford reagent. Samples were allowed to incubate at RT for 5 mins and their absorbance at 595 nm was subsequently measured using a spectrophotometer. The recorded value corresponded to the background value subtracted by the value recorded from a blank sample consisting of 100 µL of buffer mixed in 900 µL of Bradford reagents. The protein concentration was then derived by a calibration curve obtained from measurements generated from identically treated BSA standards.

2.3.4. SDS PAGE

Analysis of protein samples were carried out by sodium dodecyl sulphate polyacrylamide gel electrophoresis (SDS-PAGE). Samples were heated in a boiling water bath for ~5 mins in 1x SAB buffer. The boiled samples were loaded onto 10% or 12% TruPAGE™ precast gels (Sigma Aldrich) for 60-90 mins at 120-180 V in TruPAGE™ running buffer. All SDS-PAGE gels were stained with InstantBlue™ stain (Expedeon) and imaged in a SynGene gel imager.

2.3.5. Western blotting and immunodetection

Proteins from SDS gels were transferred to a nitrocellulose membrane using the semi-dry blotting process (Trans-Blot® Turbo™ Transfer System, Bio-Rad) using a 10-minute protocol for the transfer of high-molecular weight proteins. A His-tag antibody HRP conjugate (Novagen) antibody kit was used for blotting of proteins by following manufacturer guidelines. For the detection of HRP-conjugated antibodies, Pierce™ ECL Western Blotting substrate (ThermoFisher) was used, as recommended by the manufacturer. Protein bands were visualised with an ImageQuant LAS 500 (GE Healthcare) chemiluminescence detection system with a CCD camera imaging system.

2.4. Insect cell techniques

2.4.1. Cell culturing

Insect cells sf9 (Invitrogen), sf21 (Invitrogen) and sSf9-2 (Oxford Expression Technologies) were commercially obtained; cells were routinely cultured in Sf900II™ II media (Invitrogen). Occasionally, cell cultures were maintained with antibiotic selection (Penicillin-Streptomycin) or inclusion of 1% (v/v) Gibco Fetal Bovine Serum (FBS, Invitrogen).

2.4.2. Bacmid DNA isolation

Bacmid DNA kindly received from Prof. Ian Jones, University of Reading, was grown in LB and chloramphenicol at 37°C overnight. This was isolated using a BacMax DNA purification kit (Epicentre) following manufacturer guidelines and linearized using BSU361 (NEB).

2.4.3. pOPIN constructs

The wild-type sequences, lacking transit peptides, for AtGyrA, AtGyrB2, PfGyrA and PfGyrB were cloned separately into the pOPINF vector by researchers at the OPPF (Table 2.4). All genes included 3C protease cleavable N-terminal hexa-histidine tags.

2.4.4. Codon optimised sequences

Codon optimised sequences of *Arabidopsis thaliana* gyrase for expression in insect cells were obtained from ThermoFisher Scientific, those of *Plasmodium falciparum* and *Plasmodium berghei* gyrase were obtained from Gene Universal (China) (Table 2.6). All genes included 3C protease cleavable N-terminal hexa-histidine tags.

2.4.5. Generating *A. thaliana* and *Plasmodia* expression constructs

2.4.5.1. Monocistronic *A. thaliana* gyrase constructs

The monocistronic expression of codon optimised and non-codon optimised genes was attempted from pOPIN and pFastBac vectors (note: the method of transfections of insect cells differs, described later in 2.4.6). Monocistronic expression vectors, to allow co-transfections, were generated by sub-cloning. The pOPINF vector was digested with NcoI

and KpnI, whilst the pOPINE-3C-eGFP vector was digested by NcoI and PmeI. The details of constructs and primers are given in Table 2.7.

Table 2.6: *A. thaliana*, *P. falciparum* and *P. bergehi* gyrase expression constructs. Constructs of codon optimised, and non-codon optimised sequences were sourced commercially.

Plasmid ID	Gene	Plasmid	Codon#	Source
AtGyrA_pOPF	AtGyrA	pOPINF	×	OPPF
AtGyrB2_pOPF	AtGyrB2	pOPINF	×	OPPF
AtGyrA(CO)_pFBac1	AtGyrA	pFastBac1	✓	ThermoFisher
AtGyrB1(CO)_pFBac1	AtGyrB1	pFastBac1	✓	ThermoFisher
PfGyrA_pOPF	PfGyrA	pOPINF	×	OPPF
PfGyrB_pOPF	PfGyrB	pOPINF	×	OPPF
PfGyrA(CO)_PFDual	PfGyrA	pFastBac dual	✓	Gene Universal
PfGyrB(CO)_PFDual	PfGyrB	pFastBac dual	✓	Gene Universal
PbGyrA(CO)_PFDual	PbGyrA	pFastBac dual	✓	Gene Universal
PbGyrB(CO)_PFDual	PbGyrB	pFastBac dual	✓	Gene Universal

Ticks represent codon optimised sequences for insect cell expression, whilst crosses represent non-codon optimised sequences.

2.4.5.2. *A. thaliana* and *P. falciparum* fusion constructs

A. thaliana gyrase fusion constructs of GyrB and GyrA subunits, using genes before and after codon optimisation, in addition to *P. falciparum* GyrB and GyrA fusion construct prior to codon optimisation, were attempted in different insect cell expression plasmids. The fusions were constructed using the In-Fusion cloning® system (Figure 2.1). The codon optimised fusion genes were subcloned from codon optimised pFastBac1 plasmid encoding AtGyrA (AtGyrA(CO)_pFBac1), and the target plasmid was linearised by PCR. The non-codon optimised *A. thaliana* and *P. falciparum* genes were sub-cloned from AtGyrA_pOPF, AtGyrB2_pOPF, PfGyrA_pOPF and PfGyrB_pOPF into the pOPINE-3C-eGFP plasmid, pre-digested by PmeI and NcoI. All genes included 3C protease cleavable N-terminal hexa-histidine tags. Primer sequences and constructs are given in Table 2.8.

Table 2.7: Monocistronic expression constructs generated for this study.

Plasmid ID	Gene	Plasmid	Codon#	FP	RP
AtGyrA(CO)_pOPF	AtGyrA	pOPINF	✓	AGGAGATATACCATGGGATCCATGGC TCACCACCAC	CCAGTCGGGTTCGACGGTACCAAGCTTTT ACAGGGACACAGCTT
AtGyrB1(CO)_pOPF	AtGyrB1	pOPINF	✓	AGGAGATATACCATGGCTCACCACCA C	CCAGTCGGGTTCGACGTTAGATGTCCAGG TTTTCCAGGTTTCATACG
AtGyrB1_pOPE	AtGyrB1	pOPINE	×	CAAAGGAGATATACCATGGCGCGCCA TATGGCA	AAACAGAACTTCCAGTTTGATATCCAGA TTTTCCAGATTCATACGGGT
AtGyrB2_pFBac1	AtGyrB2	pFBac1	×	CATCGGGCGCGGATCCATGGCACACC ATCACCAC	TACCGCATGCCTCGAGTTATATGTCTAG ACGCTGCAGGTTGATCC

Ticks represent codon optimised sequences for insect cell expression, whilst crosses represent non-codon optimised sequences.

Table 2.9: *A. thaliana* polycistronic expression clones generated.

Gene 1	Gene 2	Plasmid	Codon#	FP	RP
AtGyrA	-	pFBDual	✓	CATGGAGATAATTTAAAATGAT AACC	CTCCCCATCTCCCGGTACCAAGCTTT TAGATGTCCAGGTTTCCAG
AtGyrA	AtGyrB1	pFBDual	✓	GATGCATAGCATGCGGTACCG GATCCATGGCTCACCACC	CTCCCCATCTCCCGGTACCAAGCTTT TAGATGTCCAGGTTTCCAG

Ticks represent codon optimised sequences for insect cell expression, whilst crosses represent non-codon optimised sequences.

Table 2.8: Gyrase fusion constructs used in this work.

Fused Genes	Plasmid	Codon^{&}	SSG linker	FP (plasmid)[¶]	RP (plasmid)[¶]	FP (fusion)[#]	RP (fusion)[#]
AtGyrB2 & AtGyrA	pOPINE	×	×	ATCAAAGGAGATATACCA TGTTGTCTACTGAGGCTT CCCAAGAG	TGAAACAGAACTTCCAGTTTT TACAGGCTAACGGCTTCTACGG C	CGTACTCCTCGGTCCGG CAAA	TTGCCGGACCGAGGAGTAC GTATGTCTAGACGCTGCAG GTTGA
AtGyrB2 & AtGyrA	pFastBac 1	✓*	×	CGTACTCCCGTTCCGG	GCGCCCGATGGTGGG	CCCACCATCGGGCGCAT GGCACACCATCACCACC	GGAACGGGGAGTACGTATG TCTAGACGCTGCAGGTTGA TCCT
AtGyrB2 & AtGyrA	pFastBac 1	✓*	×	TCCTCTGGCCGTA CTCCC CGTTCCGG	GCGCCCGATGGTGGG	CCCACCATCGGGCGCAT GGCACACCATCACCACC	GGAACGGGGAGTACGTATG TCTAGACGCTGCAGGTTGA TCCT
AtGyrB1 & AtGyrA	pFastBac 1	✓	×	CGTACTCCCGTTCCGG	GCGCCCGATGGTGGG	CCCACCATCGGGCGCGG ATCCATGGCT	GGAACGGGGAGTACGGATG TCCAGGTTTTCCAGGTTCA
AtGyrB1 & AtGyrA	pFastBac 1	✓	✓	TCCTCTGGCCGTA CTCCC CGTTCCGG	GCGCCCGATGGTGGG	CCCACCATCGGGCGCGG ATCCATGGCT	AGTACGGCCAGAGGAGATG TCCAGGTTTTCCAGGT
PfGyrA & PfGyrB	pOPINE	×	×	ATCAAAGGAGATATACCA TGATGGCACACCATCACC ACCAT	TGAAACAGAACTTCCAGTTTT TAGATGATATCAA AATACACC AGCTGGT	AACATCAACAACAACAT CAACGAAAG	TTGATGTTGTTGTTGATGT TTTCGCTCAGGCTATTGGT ATTTTCCAGG
AtGyrB1 & AtGyrA	pOPINF	✓	×	AGGAGATATACCATGGAT GGTCACCACCACCAT	CCAGTCGGGTCGACGGTACCTT ACAGGGACACAGCTTCCACAG	CCCACCATCGGGCGCGG ATCCATGGCT	GGAACGGGGAGTACGGATG TCCAGGTTTTCCAGGTTCA
AtGyrB1 & AtGyrA	pOPINF	✓	✓	AGGAGATATACCATGGAT GGTCACCACCACCAT	CCAGTCGGGTCGACGGTACCTT ACAGGGACACAGCTTCCACAG	CCCACCATCGGGCGCGG ATCCATGGCT	AGTACGGCCAGAGGAGATG TCCAGGTTTTCCAGGT

[¶] Forward and reverse primers for cloning of fusion construct into target plasmid

[&]Ticks represent codon optimised sequences for insect cell expression, whilst crosses represent non-codon optimised sequences.

[#]Forward and reverse primers to generate the gyrase fusion.

*AtGyrB2 sequence was non-codon optimised.

2.4.5.3. Polycistronic *A. thaliana* constructs

The *A. thaliana* gyrase genes were subcloned into pFastBac dual plasmid for polycistronic expression. The expression of GyrA genes were mediated from the polyhedrin promoter whilst GyrB genes were mediated from the p10 promoter. AtGyrA was digested from AtGyrA_pFBac1(CO) with BamHI and HindIII. The PbA_pFDual(CO) plasmid was digested with BamHI and HindIII, to free the polyhedrin site of the plasmid, into which the digested AtGyrA DNA was ligated. The resultant AtGyrA(CO)_pFDual plasmid was verified by sequencing and subsequently digested by KpnI, in preparation for cloning of the GyrB gene under the p10 promoter. The non-codon optimised GyrB2 gene was amplified from AtGyrB2_pOPF, whilst the codon optimised GyrB1 gene was amplified from AtGyrB1_pFBac1(CO). Cloning of GyrB2 into a AtGyrA(CO)_pFDual by this technique, or others, did not prove possible, but instead led to large deletions of the plasmid. All genes included 3C protease cleavable N-terminal hexa-histidine tags, details of constructs and primers are given in Table 2.9.

2.4.5.4. *Plasmodium* pETDuet clones

Codon optimised sequences of *P. falciparum* and *P. berghei* gyrase were subcloned from pFastBac constructs with gyrase genes into pETDuet vectors. The GyrA genes were introduced into MCS 2 of pETDuet whilst GyrB genes were introduced into MCS 1. The pETDuet vector was linearised by PCR, all primers given in Table 2.10. All genes included 3C protease cleavable N-terminal hexa-histidine tags.

Table 2.10: pETDuet constructs and oligonucleotides for *E. coli* expression.

Genes	Plasmid	FP (plasmid)[†]	RP (Plasmid)[†]	FP (fusion)[#]	RP (fusion)[#]
PbGyrA	pETDuet	AAAGAAACCGCTGCTGC GA	CATATGTATATCTCCTTCTTA TACTTAACTAATATACTAAG ATGGGGAA	GGAGATATACATATGATGCA TCACCATCATCATCACTCTT	AGCAGCGGTTTCTTTCAA ATATCGAAGTACATCAACT TGTTTCATCTTTGAC
PbGyrB	pETDuet	TCGAACAGAAAGTAATC GTATTGTACACGG	GGTATATCTCCTTCTTAAAGT TAAACAAAATTATTTCTAGA GGG	TTACTTTCTGTTTCGATTAGTT AGATCTACTATTCTTGATGA TGAAATCCTTTCTAGACT	AGAAGGAGATATAACCATGC ACCACCATCACCATCA
PbGyrB	PbGyrA_pE TDuet	TCGAACAGAAAGTAATC GTATTGTACACGG	GGTATATCTCCTTCTTAAAGT TAAACAAAATTATTTCTAGA GGG	TTACTTTCTGTTTCGATTAGTT AGATCTACTATTCTTGATGA TGAAATCCTTTCTAGACT	AGAAGGAGATATAACCATGC ACCACCATCACCATCA
PfGyrB	pETDuet	AAAGAAACCGCTGCTGC GA	CATATGTATATCTCCTTCTTA TACTTAACTAATATACTAAG ATGGGGAA	TTACTTTCTGTTTCGATTACTC TGACAATGAGTTAGTGTCT CAAGGA	AGAAGGAGATATAACCATGC ACCACCACCACCAT

[†] Forward and reverse primers for cloning of fusion construct into target plasmid.

[#]Forward and reverse primers to generate the gyrase fusion.

2.4.6. Insect Cell Infections

2.4.6.1. pOPIN infections

Insect cells 2 mL (0.5×10^5 cells/mL) were transfected with the following mixture: 750 ng linearized bacmid DNA, 4 μ L FuGENE® HD (Promega), 1000-1500 ng of recombinant pOPIN based vectors containing AtGyrA, AtGyrB2, PfGyrA or PfGyrB and 200 μ L Sf900™ II media (Invitrogen). Both single transfections and co-transfections of the pOPIN clones were trialled. A transfer vector encoding GFP, pVSVG™ GFP, was used as a positive control. These transfections were grown in 6-well plates at 27°C for 5-7 days without shaking. Subsequent to the growth, the supernatant was collected and stored, this is the P₀ viral stock. 2 mL of Sf21 cells (1×10^6 cells/mL) were transfected with P₀ viral stock, incubated at 27°C for 5-7 days without shaking; after which the P₁ virus supernatant was collected and stored. Similarly, the P₁ was amplified and P₂ viral stock collected. Protein expression trials have involved transfection of 2-50 mL of Sf21 cells (1×10^6 cells/mL) with 30 - 800 μ L of P₁ or P₂ virus, incubation at 27°C (shaking) for 48-72 h.

2.4.6.2. pFastBac transfections

Insect cell expression using pFastBac1 or pFastBac dual clones were carried out according to the Bac-to-Bac® baculovirus expression system (Invitrogen). The recombinant vectors generated in this study were cloned into chemically competent DH5 α or α -select gold cells, maintained with ampicillin selection and verified by sequencing. The pFastBac constructs were transformed into Max Efficiency® DH10Bac™ *E. coli* (Invitrogen) for transposition into bacmid. Typically, 100 μ L of Max Efficiency® DH10Bac™ *E. coli* cells were transformed with 1 ng of recombinant pFastBac plasmid and selected on kanamycin, gentamycin, tetracycline, 100 μ g/mL X-gal and 40 μ g/mL IPTG plates and incubated at 37°C for 48 h. White colonies were confirmed by re-streaking with the same selection, used to inoculate liquid LB cultures with kanamycin, gentamycin and tetracycline selection.

Recombinant bacmid DNA was isolated using the following adapted method based upon the Qiagen miniprep isolation system. Cells were pelleted from overnight cultures, resuspended in 300 μ L Buffer P1 (50 mM Tris.HCl pH 8, 10 mM EDTA and 100 μ g/mL RNaseA). An equal volume of Buffer P2 (200 mM NaOH, 1% SDS) was added and incubated for 5 mins at room temperature. Subsequently, 300 μ L of 3 M potassium acetate pH 5.5 was added and the mixture was centrifuged at 13,000 rpm for 10 mins. The supernatant

was separated and mixed 1:1 with 100% isopropanol and centrifuged 13,000 rpm, 4°C for 15 mins to pellet the DNA. The recombinant bacmid DNA was resuspended in EB. The recombinant nature of the isolated bacmid DNAs were confirmed by PCR using pUC/M13 FP: CCCAGTCACGACGTTGTAAAACG and pUC/M13 RP: AGCGGATAACAATTTACACACAGG primers, binding sites for which are within the *AcMPNV* bacmid genome.

Typically, insect cell cultures (>95% viable) were sub-divided the day before transfections. The transfections involved seeding 8×10^5 cells in 2 mL of Sf900 media for each transfection, seeded cells were left to attach for 45 mins at 22°C. A 100 μ L transfection mixture was prepared per transfection: 1-2 μ g of recombinant bacmid (note: co-transfections \sim 1 μ g of bacmid each), 4 μ L of FuGENE® HD (room temperature) per 1 μ g of bacmid DNA and Sf900™ II media and incubated at room temperature for 30 mins. The transfection mixture was added dropwise to the attached cells. Infected cells were incubated at 22°C for 3-7 days. Subsequently, virus was separated from cells by brief centrifugation (6,000 g, 5 mins) and the supernatant of virus stock (P_0) stored at 4°C. Viral amplifications of P_0 - P_2 were tried at various MOIs for 5-7 days, as was protein expression (2 – 7 days).

2.4.7. Virus quantification

2.4.7.1. Plaque assay

The plaque assay was performed according to the guidelines of Oxford Expression Technologies (OET) baculoCOMPLETE *flashBAC*™ user guide. Insect cells 4×10^5 cells/well were settled for 60 mins in 6 well-plates. The media of cells was removed and replaced with dilutions of viral stocks of 10^{-1} to 10^{-7} , repeated in triplicate, virus adsorption allowed to proceed for 45-60 mins at room temperature. Low melting point agarose 4% (w/v) (ThermoFisher) was diluted in an equal volume of sterile water, 2 mL of diluted agarose was used to overlay each well of the 6-well plate, set at room temperature, and then the plate was incubated at 28°C for 4 days. Neutral Red (5 mg/mL) was diluted 20x and 500 μ L of the diluted dye was added to each well, incubated for 4 h at 28°C before plaque observation.

2.4.7.2. qPCR

The OET *baculoQUANT*™ ALL-IN-ONE DNA extraction and Quantification kit was used to determine recombinant viral titres according to manufacturer's guidelines.

2.5. Insect cell protein production

2.5.1. Buffers and solutions

The buffer constituents were purchased from Sigma Aldrich or Melford Chemicals. The composition of buffers used for protein purification and analysis are listed in Table 2.11.

Table 2.11: Buffers and solutions for insect cell expression and purification.

Buffers/Solutions	Details
NPI-10	50 mM NaH ₂ PO ₄ , 300 mM NaCl, 10 mM imidazole and 1% Tween-20. Adjusted to pH 8.
NPI-20	50 mM NaH ₂ PO ₄ , 300 mM NaCl, 20 mM imidazole and 0.05% Tween-20 Adjusted to pH 8.
NPI-250	50 mM NaH ₂ PO ₄ , 300 mM NaCl, 250 mM imidazole and 0.05% Tween-20. Adjusted to pH 8.
Buffer A	300 mM NaCl, 20 mM imidazole, 50 mM Tris.HCl pH 8, 10% glycerol.
Buffer B	300 mM NaCl, 1 M imidazole, 50 mM Tris.HCl pH 8, 10% glycerol.
Buffer C	100 mM NaCl, 50 mM Tris.HCl pH8, 10% glycerol, 2 mM EDTA, 2 mM β-mercaptoethanol, protease inhibitor.

2.5.2. Small scale expression and purification

Insect cells (2 mL) were harvested by centrifugation at 6,000 g for 10 mins and cells were then frozen at -80 °C for 30 mins. The transfected cells were thawed and resuspended in 350 μL NPI-10, lysozyme (~750 μg) and 1x concentration of complete EDTA mini-protease inhibitor (Sigma) followed by shaking at 1,000 rpm, 4°C, for 30 mins. The cell lysate was then harvested by centrifugation at 6,500 g for 30 min at 4°C. 200 μL of cell lysate was added to 20 μL of NiNTA magnetic bead (Qiagen) and recombinant protein binding allowed for 30 mins, 4°C, 600 rpm on an Eppendorf ThermoMixer®. Magnetic beads were washed twice with 200 μL NPI-20 (magnetic bead stand), followed by elution of the bound protein, in 50 μL of NPI-250. The volumes of buffers were proportionately adjusted for lysis and purification in accordance with cell densities.

2.5.3. Large scale *A. thaliana* gyrase A & B2 expression

Sf21 insect cells were co-transfected with non-codon optimised monocistronic expression clones of AtGyrA_pOPF and AtGyrB2_pOPF to generate P₀, P₁ and P₂ viruses as described earlier in section 2.4.6.1. Expression involved transfection of a 750 mL culture of Sf21 cells with 5 mL of P₂ virus for 72 hours. Sf21 cells were harvested by centrifugation at 6,500 rpm for 15 minutes. Cells were resuspended in 10 mL buffer A supplemented with protease inhibitor and 2 mM β-mercaptoethanol. Cells were disrupted using an Avestin homogeniser (BioPharma), lysate collected following centrifugation at 18,000 rpm (SS-34 rotor) for 90 minutes. Protein partially purified from the cell lysate using a HisTrap™ FF crude 1mL (Merck) column with a gradient of 0-100% buffer B over 20 minutes. Protein fractions were collected and dialysed with buffer C overnight at 4°C.

2.5.4. *A. thaliana* gyrase B1 & A fusion

The cell viability of sf9 cells was determined as 97%, 8 x 10⁵ cells were seeded into a single well of 6-well plate and allowed to attach at 22°C for 60 mins. Cells were transfected with a transfection mix containing 1.2 µg of AtGyrB1_GyrA bacmid DNA, 4 µL of FuGENE® HD in a total volume of 100 µL Sf900II media (transfection mixture incubated at room temperature for 15 mins). The transfection process was allowed to proceed for 7 days after which P₀ virus was collected and separated from cells by centrifugation at 6,000 g for 5 mins. The collected cells were lysed and processed for protein expression.

2.5.4.1. Expression of gyrase in *E. coli*

Expression plasmids were transformed into expressing *E. coli* Rosetta 2 (DE3) pLysS. The *E. coli* strain carrying the desired expression plasmid was then inoculated into 5 ml of LB broth containing ampicillin, chloramphenicol and 1% glucose and then grown overnight. The following day the OD₆₀₀ of each culture was determined, diluted to 0.5 using LB broth in a final volume of 3 mL. The 3 mL starter culture was used to inoculate 10 mL LB broth with ampicillin, chloramphenicol and 1% glucose. The culture was incubated at 37°C, 200 rpm and induced with IPTG (1 mM final concentration) at OD₆₀₀ 0.4-0.6. Induced cultures incubated at 28°C or 37°C for 1 hour – overnight. To harvest the generated cells, the culture was subjected to centrifugation at 16,000 rpm for 10 mins at 4°C and stored at -20°C. Prior to expression analysis, harvested cells were resuspended in 100 µL buffer (Tris. HCl pH 7, 2% SDS, 10% glycerol), centrifuged at 6,000 g for 15 mins and a proportion of the supernatant mixed with sample application buffer prior to analysis by SDS PAGE.

2.6. *Arabidopsis* methods

2.6.1. *Arabidopsis* lines

The *Arabidopsis thaliana* T-DNA insertion lines used in this study were obtained from the Nottingham Arabidopsis Stock Centre and are listed in Table 2.12.

Table 2.12: *Arabidopsis thaliana* T-DNA lines investigated in this work.

Stock ID	<i>A. thaliana</i> locus
GK-077A10	At3g10690
SAIL_569_G07	At3g10690
SALK_139478	At3g10270
GABI_586A06	At3g10270
SALK_084298.56.00	At3g10270
SALK_002367	At5g04130
SALK_068282	At5g04130

2.6.1. Buffers and solutions

Buffers and solutions used for *in vivo Arabidopsis thaliana* work are listed in Table 2.13 (components sourced from Sigma or Melford).

2.6.2. Seed sterilisation

Arabidopsis seeds were sterilised in tubes within a desiccator containing a mixture of 100 mL bleach and 5 mL 6 M HCl for 90-120 mins. Occasionally, seeds were double-sterilised.

Table 2.13: Buffers and solutions used for *in vivo Arabidopsis thaliana* work.

Buffer/Media	Composition
Sucrose solution	50 mM Tris.HCl pH 7.5, 300 mM NaCl and 300 mM sucrose
Mitochondria extraction buffer (MEB)	0.03 M MOPS-KOH pH 7.5, 0.3 M mannitol, 1 mM EDTA, 0.1% (w/v) BSA, 0.6% (w/v) PVP-40 and 4 mM cysteine (added immediately prior to use)
Mitochondrial wash buffer (MWB)	0.03 M MOPS-KOH pH 7.5, 0.3 M mannitol and 1 mM EDTA
Chloroplast isolation buffer (CIB)	0.3 M D-Sorbitol, 5 mM MgCl ₂ , 5mM EGTA, 5 mM EDTA, 20 mM Hepes.KOH pH 8 and 10 mM NaHCO ₃
HMS buffer	50 mM Hepes. KOH pH 8, 0.3 M D-Sorbitol and 3 mM MgSO ₄
Percoll solution	42 mL (v/v) Percoll solution, 3% (w/v) PEG 6000, 1% (w/v) Ficoll 400 and 1% (w/v) BSA
Gradient solution	25 mM Hepes.KOH pH 8, 10 mM EDTA and 5% (w/v) D-Sorbitol

2.6.3. MS plates

The media consisted of 1x or ½ strength Murashige & Skoog medium without vitamins (Formedium) with 0.8% (w/v) agar (phytagel) and occasionally supplemented with 1% sucrose (Fisher). The pH was adjusted to 5.8 with NaOH prior to sterilisation by autoclaving and pouring of molten agar into appropriately sized petri dishes. Sterilised seeds were transferred to plates containing growth media using a small amount of sterile 0.18% agar in a sterilised laminar flow cabinet. The plates were stored at 4°C for 3 days for seeds to vernalise. After this, plates were transferred to growth cabinets (22°C, 16 h/8 h dark growth photoperiod). Occasionally, plates were incubated in a vertical position.

2.6.4. *Arabidopsis* cell culture

The components of the callus induction medium, per litre were: 3.86 g Gamborg B5 with vitamins (Sigma), 20 g glucose (Sigma), 0.5 g MES (2-(N-morpholino)ethanesulfonic acid), 0.05 mL of 1 mg/mL 2,4-D (auxin analogue) and 50 μ L of 1 mg/mL kinetin. The pH was adjusted to 5.7 with 1 M KOH. For plates, 8 g of agar was added per litre of callus induction medium. Callus was initiated from the roots of plants grown on MS plates vertically in growth cabinets. After 10-14 days, a sharp sterile razor blade was used to slice roots a few mm below the hypocotyl and these were transferred to plates of callus induction medium. Three to four weeks later, small calli could be visualised. These were moved to fresh plates, leaving behind the root tissue. The calli were sub-cultured every three to four weeks in the same way.

2.6.5. *Arabidopsis* genomic DNA extraction

Plant tissue for DNA extractions were collected and placed on ice or frozen in liquid nitrogen. These were ground in 100 μ L sucrose solution using plastic pestles. Once ground, 100 μ L sucrose solution was added and material was immediately heated at 95°C for 10 mins. The material was centrifuged at 6,000 g for 10 s and 50 μ L of the supernatant containing genomic DNA was transferred to a new tube. Typically, 1 μ L of this genomic DNA was used to template PCR reactions.

2.6.6. *Arabidopsis* RNA extraction

RNA was extracted from *Arabidopsis* using Trizol. Frozen plant material was ground using prechilled plastic pestles and 1 mL of Trizol was added to ground material. 200 μ L of chloroform was subsequently added, shaken and left to stand for 2 mins. The mixture was centrifuged at full-speed in a microfuge for 5 mins (4°C). The top aqueous layer ~ 600 μ L was removed, mixed with 500 μ L 100% (v/v) isopropanol and incubated for 3 mins. The solution was centrifuged again for 10 mins to reveal the pellet of RNA. Supernatant was removed and the pellet was washed with 300 μ L 70% (v/v) RNase-free ethanol (made with DEPC water). After centrifugation, the ethanol was removed and discarded, the pellet was air dried and resuspended in RNase free water. The concentration was determined using Nanodrop (as for DNA) and RNA aliquoted and stored at -80°C.

2.6.7. Isolation of intact *Arabidopsis* mitochondria

The mitochondrial isolation procedure was carried out using detergent free equipment and all material and buffers were kept cold during the extraction. Mitochondria were isolated from undifferentiated *Arabidopsis* callus. 5 g of two-week-old callus was ground in 5 mL of MEB with glass beads using a mortar and pestle, until all glass beads were crushed. The ground material was filtered through a double layer of Miracloth (Merk). The filtrate was centrifuged at 1000 g for 20 mins, the supernatant was transferred to a clean tube. The mixture was centrifuged at 12,500 g for 20 mins, after which the supernatant was discarded, and pellet resuspended in 1 mL mitochondrial wash buffer (MWB). The mitochondria were pelleted by centrifugation at 16,000 g for 20 mins and resuspended in MWB. The protein concentration was determined, and aliquots of isolated mitochondria stored at -80°C.

2.6.8. Isolation of *Arabidopsis* chloroplasts

Arabidopsis plants grown on soil for four weeks under 16 h light/8 h dark cycles were used for isolation of chloroplasts. All material and buffers for isolation were kept cold and on ice. *Arabidopsis* leaf material (15-20g) was homogenised in 20-30 mL of chloroplast isolation buffer (CIB) using a Polytron® PT20 (Kinematica) at ~40 % max in bursts of 3-4s (to avoid overheating), in an ice bath. The homogenate was filtered through a double layer of Miracloth (Merck), and the debris was resuspended in 20-30 mL CIB and homogenised again (this step was repeated 5 times). The filtrate was centrifuged at 1000 g for 5 mins and pellet was gently resuspended in 1 mL IB with a Pasteur pipette. A percoll gradient of 10 mL was prepared according to Table 2.14. The resuspended chloroplast material was gently applied to the gradient and centrifuged at 1,500 g for 10 mins. The chloroplast material was extracted, washed in 30 mL HMS buffer by gentle inversion to remove Percoll. The material was centrifuged at 1000 g for 5 mins. The pellet of purified chloroplasts was gently resuspended in HMS buffer and aliquoted. Aliquots were either used immediately or stored at -20°C.

Table 2.14: Percoll gradient preparation.

Gradient layer	Percoll Solution	Gradient Solution
Top layer (7 mL)	2.94 mL	4.06 mL
Bottom layer (3 mL)	2.55 mL	0.45 mL

2.6.9. Organellar DNA extractions

2.6.9.1. Mitochondrial DNA extractions

The mitochondria isolated as according to 2.6.8 were subjected to lysis and DNA purification by two different methods. The first method was as according to (Lang and Burger 2007) with the following modifications: lysis of mitochondrial material was carried out in 1% SDS and 100 µg/mL proteinase K for an extended time of 2 hours, DAPI (5 µg/mL) was used to replace bisbenzimidazole staining of DNA prior to ultracentrifugation. The second method was as according to (Hu et al. 2012).

2.6.9.2. Plastid DNA extractions

The organellar DNA was extracted from chloroplasts isolated in accordance with 2.6.9. The techniques implemented were both based on organelle lysis and nucleic acid precipitation as according to (Hu et al. 2012) (identical to mitochondrial DNA extraction) or an adaptation previously used for isolation of circular chloroplast DNA from a single celled alga as previously published (Manning et al. 1971b).

2.6.10. Root-length assays

Arabidopsis plants of homozygous T-DNA lines were sown on MS agar plates and vernalised to synchronise growth for three days before transfer to a growth cabinet where plates were incubated vertically (16 h light/ 8 h dark). Plates were scanned using a flat-bed scanner and analysed by Adobe Illustrator. Semiquantitative root analysis, including measurement of roots was done with SmartRoot (Lobet et al. 2011).

2.7. *Nicotiana benthamiana* transient expression

2.7.1. DNA constructs

The *A. thaliana* gyrase genes lacking signal and transit peptides were subcloned from the pOPINF and pOPINE plasmids into the pHREAC plasmid (Peyret et al. 2019). The pHREAC plasmid is based upon the pEAQ-*HT* vector but possesses a synthetic UTR to enhance the production of recombinant protein. The pHREAC plasmid was digested by *Bsa*I and N-terminally his-tagged sequences (cleavable by 3C protease) were introduced into the region between the synthetic 5' UTR and 3' CMPV UTR by In-fusion cloning, primers listed in Table 2.15.

Table 2.15: pHREAC expression constructs used in this work.

Gene	Plasmid	FP	RP
GyrA	pHREAC	TAAACGTCTCTAAAAATGGCA CACCATCACCACC	AATGAAACCAGAGCGTTACAGG CTAACGGCTTCTACG
GyrB1	pHREAC	TAAACGTCTCTAAAAATGGCA CACCATCACCACC	AATGAAACCAGAGCGTTAGATA TCCAGATTTTCCAGATTCATACG GGTTGC
GyrB2	pHREAC	TAAACGTCTCTAAAAATGGCA CACCATCACCACC	AATGAAACCAGAGCGTTATATG TCTAGACGCTGCAGGTTGATC

2.7.2. Buffers and solutions

Table 2.16: Buffers and solutions for transient expression in *N. benthamiana*.

Buffer/solution	Composition
YT media	16 g/L tryptone, 10 g/L yeast extract, 5 g/L NaCl. pH adjusted to 7.4 with 5 M NaOH
MMA	10 mM MES pH 5.6, 10 mM MgCl ₂ and 0.1 mM acetosyringone
Extraction buffer	50 mM Tris.HCl pH 8, 300 mM NaCl, 2 mM β-mercaptoethanol, protease inhibitor

2.7.3. Transformation of *Agrobacterium tumefaciens*

Agrobacterium tumefaciens strain LBA4404 electrocompetent cells were transformed by electroporation at 2500 V in an electroporation cuvette. 20 ng of plasmid DNA was used to transform 40 μ L of competent cells, which were immediately recovered in 800 μ L SOC for 60 mins at 28°C. The transformed mixture was plated onto LB agar plates with rifampicin (agrobacterium selection) and kanamycin (transformants selection) and incubated at 28°C for 72 hours.

2.7.4. Agroinfiltration solution preparation

Agrobacteria were grown in 2x YT liquid media with appropriate antibiotic selection. The culture was inoculated in the afternoon with a colony and grown overnight at 28°C, and then subcultured the following day into a larger volume, whilst maintaining antibiotic selection. The culture was centrifuged at 3500 rpm (Sorvall Legend™ T) for 20 mins, room temperature, to pellet cells. The supernatant was discarded, and the pelleted cells were gently resuspended in MMA buffer (Table 2.16) to an OD₆₀₀ of 0.8. The agro-suspension solution corresponding to AtGyrA and AtGyrB1 were combined 1:1, as were AtGyrA and AtGyrB2, to achieve final OD₆₀₀ of 0.4 for bacteria expressing each gene. The combined GyrA&B1 or GyrA&B2 agro-suspension cultures were infiltrated into *N. benthamiana* leaf intracellular spaces using a blunt-ended syringe.

2.7.5. Small scale protein extraction

Protein expression trials and time-courses were conducted on a small scale. Buffers and material all kept cold. Agroinfiltrated plant material was harvested, and a cork-borer was used to take six leaf discs (from different infiltrated leaves), which were weighed in a 2 mL shatterproof screw cap tube with a ceramic bead. 3x volume of extraction buffer, according to the weight of the sample, was added and a Fisherbrand™ Bead Mill 24 homogeniser was used at speed 4 for 30 s to homogenise material. The material was centrifuged at 18,000 g for 20 mins. The supernatant was removed and transferred to a clean tube for analysis by SDS-PAGE. The insoluble pellet material was resuspended in 200 μ L of extraction buffer and also analysed by SDS-PAGE.

2.7.6. Growth of BY-2 cells

BY-2 cells (a gift from Dr Inga Kruse) were grown in Erlenmeyer flasks at 28°C in the darkness whilst shaking at 170-190 rpm. In order to maintain a healthy BY-2 suspension culture every 7 days 1 ml of culture was transferred into 50 ml fresh MS media (Formedium).

2.7.6.1. Cell-pack formation and transient expression

For the purpose of transient expression of recombinant proteins in BY-2 cells, larger suspension cultures had to be set up. MS media was inoculated with 1/10 of its volume of 4-7 days old BY-2 suspension culture. After 72–144 h the cells were harvested using a Büchner funnel lined with filter paper and a vacuum pump to remove the media and form a tight cell pack which was consequently transferred into a petri dish. *A. tumefaciens* were prepared as described in 2.3.2 and dropped onto the cell-pack making sure to fully saturate it. Together with a water container, for stable humidity levels, the cell-packs were incubated in a lightproof box for 8-10 days at 28 °C.

2.7.6.2. Protein extraction

Small-scale extractions were carried out to test expression of recombinant proteins using a cork borer (11 mm in diameter) to sample 4 discs of infiltrated cell-packs. Infiltrated cell-packs were spread out thinly on aluminium foil and dipped in liquid nitrogen until frozen. Extraction buffer was added and the cells were ground to a smooth paste. The crude extract was filtered over 2 layers of Miracloth (Calbiochem) followed by a clarification spin at 9,500 x g for 15 minutes at 4 °C.

2.8. Biochemical assays

2.8.1. *A. thaliana* DNA gyrase buffers

The buffers used to assay the *in vitro* biochemical activity of *A. thaliana* DNA gyrase are given in Table 2.17. The Mg²⁺ is in the form of magnesium acetate.

Table 2.17: *A. thaliana* gyrase assay buffers

Buffer	Composition
Supercoiling assay buffer (SB)	40 mM Tris.HCl (pH 8.5), 10 mM Mg ²⁺ , 10 mM DTT, 2 mM ATP, 800 mM KGlu and 0.05 mg/mL acetylated albumin
Relaxation assay buffer (RB)	40 mM Tris.HCl (pH 8.5), 10 mM Mg ²⁺ , 10 mM DTT and 0.05 mg/mL acetylated albumin
Decatenation assay buffer (supercoiling conditions)	40 mM Tris.HCl (pH 8.5), 10 mM Mg ²⁺ , 10 mM DTT, 2 mM ATP, 800 mM KGlu and 0.05 mg/mL acetylated albumin
Decatenation assay buffer (relaxation conditions)	40 mM Tris.HCl (pH 8.5), 10 mM Mg ²⁺ , 10 mM DTT, 2 mM ATP and 0.05 mg/mL acetylated albumin
Gyrase dilution buffer	100 mM NaCl, 50 mM Tris.HCl pH 8, 10% glycerol, 2 mM EDTA, 2 mM β -mercaptoethanol, protease inhibitor.

2.8.2. *E. coli* DNA gyrase buffers

The buffers used to assay the *in vitro* biochemical activity of *E. coli* DNA gyrase are given in Table 2.18.

Table 2.18: *E. coli* gyrase assay buffers

Buffer	Composition
Supercoiling assay buffer (SB)	35 mM Tris.HCl (pH 7.5), 24 mM KCl, 4 mM MgCl ₂ , 2 mM DTT, 1 mM ATP, 1.8 mM spermidine, 1 mM DTT, 6.5% glycerol (w/v) and 0.1 mg/mL albumin
Relaxation assay buffer (RB)	35 mM Tris.HCl (pH 7.5), 24 mM KCl, 4 mM MgCl ₂ , 2 mM DTT, 1 mM DTT, 6.5% glycerol and 0.1 mg/mL albumin
Decatenation assay buffer	35 mM Tris.HCl (pH 7.5), 24 mM KCl, 4 mM MgCl ₂ , 2 mM DTT, 1mM ATP, 1 mM DTT, 6.5% glycerol (w/v) and 0.1 mg/mL albumin
Gyrase dilution buffer	50 mM Tris.HCl (pH 7.5), 100 mM KCl, 2 mM DTT, 1 mM EDTA, and 50% (w/v) glycerol

2.8.3. Topoisomerase enzymes

Human topoisomerase II α was purchased from Inspiralis (UK). *E. coli* gyrase was either purchased from Inspiralis (UK) or a gift from Ms. Lesley Mitchenall.

2.8.4. DNA supercoiling assay

The DNA supercoiling assays involved incubation of 1 U *A. thaliana* (12 nM) or *E. coli* gyrase (0.3 nM) with 0.5 μ g of relaxed pBR322 DNA plasmid. 1 U of DNA gyrase is defined as the quantity of enzyme required to fully supercoil 0.5 μ g of relaxed pBR322 DNA at 37°C in 30 mins. The supercoiling assay buffer conditions for *A. thaliana* and *E. coli* gyrase are given in Table 2.16 and 2.17, respectively. The assays (30 μ L) were carried out in a temperature-controlled water bath for 30 mins, after which, 30 μ L STEB and 30 μ L chloroform: isoamyl alcohol (24:1) were added. Samples were vortexed, centrifuged at full speed in a microfuge for 2 mins, to separate the organic and aqueous phase, the latter of which was loaded onto a 1% (w/v) agarose gel. The gel was run at 80 V for 2 h, and subsequently stained in ethidium bromide.

2.8.5. DNA relaxation assay

The DNA relaxation assays were conducted in a similar way to supercoiling, with the following exceptions: negatively supercoiled DNA was used as substrate for the enzyme reaction and the reaction was conducted in a relaxation assay buffer (details of *A. thaliana* buffer Table 2.17, and *E. coli* buffer 2.18).

2.8.6. DNA decatenation assay

The decatenation assay was carried out in a similar method to the supercoiling and relaxation assays, details of assay buffers are given in Tables 2.17 for *A. thaliana* and 2.18 for *E. coli* gyrase. The assay involved the use of 200 ng of kDNA or bis-cat DNA (details in chapter 6) as substrate.

2.8.7. DNA cleavage assay

DNA cleavage assays were carried out using negatively supercoiled pBR322 DNA in relaxation assay buffers for 60 mins at 37°C. After this, 3 μ L of 2% SDS (w/v) and 1.5 μ L of 10 mg/mL proteinase K were added to the reaction and incubated at 37°C for a further 30

minutes to denature and digest away the gyrase proteins. The reactions were processed and analysed as for supercoiling assays.

2.8.8. Inhibition assays

Compounds were dissolved in DMSO. Ciprofloxacin and novel analogues were assayed at a final DMSO concentration of 3% (v/v). Human topoisomerase II α was assayed in 1% DMSO. Image J was used to analyse gel images and data were input into GraphPad Prism 7 in order to determine plots and consequently, IC₅₀ values. Alternatively, SynGene GeneTools analysis software was used to quantify gel bands.

2.9. Bis-cat substrate development

2.9.1. Tn3 resolvase over-expression and purification

Overexpression of Tn3 resolvase was achieved by transforming the expression vector pSA1101 (Arnold et al. 1999) into BL21 (DE3) pLysS competent cells. The *E. coli* culture was grown to late log phase, induced with 0.1 mM IPTG and grown for a further 3 h. Resolvase purification was carried out as described previously (Olorunniji et al. 2008).

2.9.2. Plasmids and DNA

Plasmids pMM6 and pMM7 were modified from pMM5 (McIlwraith et al. 1997) by site-directed mutagenesis at res site I. This was achieved using the In-Fusion HD® cloning kit following the manufacturer's guidelines and using the oligonucleotides in Table 1. Reactions involving pMM7 were mediated in ER2925 cells (a dam methylation-deficient background). The conversion of pMM6 into pMM9 involved the removal of three non-res BspHI restriction enzyme sites from the pMM6 plasmid, again by site-directed mutagenesis using the In-Fusion HD® cloning kit; primer sequences given in Table 2.19. The resultant plasmid, pMM9, was transformed into ER2925 cells (a dam methylation-deficient background). Supercoiled pBR322 and kDNA were obtained from Inspiralis Ltd. (Norwich, UK).

Table 2.19: Plasmids created for use in Tn3 recombination reactions.

Plasmid	Res [†]	Res [′]	Uniq ue RE	FP	RP
pMM5	PsiI	PsiI	—		
pMM6	PsiI	BspHI	PsiI	CATGATATTTTCGAACGGA CTAGTGAGC TGTCTGATAATTGATCAT	CATGAATTATCAGACATAG GAATTCGGCTTCG CGTTTCGAAATATGATCAAT
pMM7	PsiI	BclI	BclI PsiI	ATTTTCGAACGGTTGCA 1 [‡] AAGCGCTCATCA GCCCCAAGT	TATCAGACATAGTAAAACG 1 GGCTGATGAGCGCTTGTTT CG
pMM9	PsiI	BspHI	BspHI PsiI	2 GGTAATGAGAT TATCAAAAAGG ATCTTCAC 3 GTCCCATGAGCG GATACATATTTG AATG	2 GATAATCTCATTACCAAAA TCCCTTAACGTG 3 GTATCCGCTCATGGGACAA TAACCCTG

[†]Res and Res[′] denote the restriction enzyme sequence at each site.

[‡]For pMM9, the numbers 1,2 and 3 refer to the forward and reverse primers used to remove all three natural BspHI sites to from the pMM9 plasmid.

2.9.3. Tn3 resolvase-mediated *In vitro* recombination

The optimum concentration of resolvase determined for an efficient recombination reaction was 20 nM per 1 μM of substrate DNA. Resolvase was diluted in resolvase dilution buffer (20 mM Tris.HCl pH 7.5, 1 mM DTT, 0.1 mM EDTA, 1 M NaCl, 50% v/v glycerol) as required. Standard recombination reactions were performed in 50 mM Tris.HCl pH 8.2, 10 mM MgCl₂ and 0.1 mM EDTA (an alternative reaction buffer replaced 10 mM MgCl₂ with 5 mM spermidine). Recombination reactions were carried out at 37°C for 1 h, after which the reaction was stopped by incubation at 70°C for 5 min.

2.9.3.1. Small scale recombination reactions

On a small scale, Tn3 recombination efficiency was routinely estimated by restriction digestion of recombination products. This typically involved the equal division of Tn3 recombined material, adjustment of buffer conditions by addition of appropriate digestion buffer and typically 0.5 – 1.0 μL of restriction enzyme(s) (according to manufacturer guidelines); reactions were stopped by heat treatment, if necessary. Recombination reactions were treated with proteinase K (50 μg/mL, 60 min, 50°C) and either ethanol

precipitated, or reactions were stopped by addition of 30 μ L STEB and 30 μ L chloroform/isoamyl alcohol (v/v, 24:1), vortexed, centrifuged and the upper aqueous phase analysed by agarose gel electrophoresis.

2.9.3.2. Large scale recombination reactions

Large-scale reactions prepared for caesium chloride density ultracentrifugation involved the subjection of approximately 1 mg of Tn3 resolvase-treated DNA to BspHI (200 units, NEB) linearization in a final volume of 20 mL for 1 hour at 37°C, followed by heat inactivation at 80°C for 20 min. The sample was prepared for separation by caesium chloride density gradient by the addition of 1.019 g CsCl and 0.11 mL of 10 mg/mL ethidium bromide solution, per gram of heat-treated solution. Separation was performed using a WX Ultra 1000 centrifuge and a TV860 rotor at 45,000 rpm, at 18°C overnight. The appropriate bands were extracted from the gradient using wide-gauge needles, and ethidium bromide was removed by several washes with water-saturated butanol. The extracted material was then ethanol-precipitated and analysed on agarose gels.

2.10. Microscopy

2.10.1. Inverted microscopy for seed assessment

A Nikon SMZ 1000 stereomicroscope was used to assess siliques of plants. The sample preparation involved detachment and isolation of closed siliques from *Arabidopsis* plants grown on soil for a period of 2-6 weeks (16 h light/8 h dark cycles). The siliques were fixed to the stage of the microscope and sterile needles were used to introduce two incisions on the silique, either side of the dehiscence zone to reveal the septum with attached seeds.

2.10.2. Differential Interface contrast microscopy

Sample preparation for differential interface microscopy (DIC) involved the acquisition of *Arabidopsis* seeds as described in 2.10.1. The isolated seeds were immersed in 30 μ L of Hoyer's solution (9 g gum arabic, 60 g chloral hydrate, 6 g glycerol in 15 mL ultrapure water) on a microscopy slide for ~3 hours, after which a cover slide was placed over the sample and sealed with nail varnish. Samples of siliques from four different *Arabidopsis* plants for each line were compared by this method. A Leica DM6000 microscope connected to a DFC 320 FX monochrome camera was used for imaging.

2.10.3. Transmission electron microscopy

The leaves were cut into 1mm² pieces and immediately placed in a solution of 2.5% (v/v) glutaraldehyde in 0.05 M sodium cacodylate, pH 7.3 for fixation, and left overnight at room temperature. Samples were then placed in baskets and loaded into the Leica EM TP embedding machine (Leica, Milton Keynes) using the following protocol. The fixative was washed out by three successive 15-minute washes in 0.05M sodium cacodylate and post-fixed in 1% (w/v) OsO₄ in 0.05 M sodium cacodylate for two hours at room temperature. The osmium fixation was followed by three, 15-minute washes in distilled water before beginning the ethanol dehydration series (30%, 50%, 70%, 95% and two changes of 100% ethanol, each for an hour). Once dehydrated, the samples were gradually infiltrated with LR White resin (London Resin Company, Reading, Berkshire) by successive changes of resin:ethanol mixes at room temperature (1:1 for 1 hr, 2:1 for 1 hr, 3:1 for 1 hr, 100% resin for 1 hr then 100% resin for 16 hrs and a fresh change again for a further 8 hrs) then the samples were transferred into gelatin capsules full of fresh LR White and placed at 60°C for 16 hrs to polymerize. The material was sectioned with a diamond knife using a Leica UC6 ultramicrotome (Leica, Milton Keynes) and ultrathin sections of approximately 90nm were picked up on 200 mesh copper grids which had been pyroxylin and carbon coated. The sections were stained with 2% (w/v) uranyl acetate for 1 hr and 1% (w/v) lead citrate for 1 minute, washed in distilled water and air dried. The grids were viewed in a FEI Talos 200C transmission electron microscope (FEI UK Ltd, Cambridge, UK) at 200kV and imaged using a Gatan OneView 4K x 4K digital camera (Gatan, Cambridge, UK) to record DM4 files. The work of this subsection was done in collaboration with the JIC Bioimaging facility and specifically with the help of Elaine Barclay.

2.10.4. Chloroplast Imaging

Chloroplasts were isolated immediately prior to quantitative image analysis. Slides were prepared for microscopy by cutting a square frame of 14 mm x 14 mm from a seal adhesive sheet of 0.24 mm thickness (GRACE Bio-labs). 1% agarose was prepared in 1x HMS and 60 µL of this spread evenly within the 14 mm x 14 mm square frame of the adhesive seal to create an agarose bed. Samples of isolated chloroplasts were diluted 1:1 in 100% glycerol and applied carefully to the agarose bed. The adhesive seal was removed, and a cover slide attached. A Zeiss Axio Zoom V16 microscope attached to a monochrome camera was used for image capturing.

2.10.4.1. Quantitative Image analysis

The data analysis was carried out using a custom-made image processing pipeline in Python, a high-level object-oriented programming language which is distributed for free under the GNU public license (Anaconda 2016). The Python libraries used in the image processing pipeline are `czifile` (Gohlke 2019), `NumPy` (Oliphant 2006), `Matplotlib` (Hunter 2007), `scikit-image` (Van der Walt et al. 2014), `tkinter` (Lundh 1999), `tiffio` (Gohlke 2021), `OpenCV` (Bradski 2000), `Pandas` (McKinney and Others 2010), and `Seaborn` (Waskom 2017). The processing pipeline first finds the plane of focus by computing image gradients for each one of the z-slices and then selecting the z-slice with the highest contrast as the plane of focus. The pipeline then generates a binary image by applying Otsu thresholding to the z-slice that was selected as the focus plane. This image is then subjected to closing and binary erosion procedures to eliminate small isolated dark and bright elements, respectively. On a subsequent step, elements with an area of less than 300 pixels are filtered out. Further filtering is then applied using `OpenCV` to only select elements with a circularity of at least 0.01, a convexity of at least 0.95, and an inertia ratio of at least 0.5 (see `OpenCV`'s `SimpleBlobDetector`). Elements that are interconnected below and above the plane of focus are also eliminated. Finally, the area, the total intensity, the mean pixel intensity, the centroid location, the maximum intensity, the minimum intensity, the width, and the length of each element are saved to an Excel spreadsheet. The work of this subsection was done in collaboration with the JIC Bioimaging facility and specifically with the help of Sergio Lopez.

2.11. Databases and Software

2.11.1. PlasmoDB

PlasmoDB database was used to identify sequences of *Plasmodia* gyrase proteins (Bahl et al. 2003). These sequences were blasted using the NCBI sequence blast feature to search for homologous proteins. The sequences were aligned with proteins of high and low homology, in order to determine potential start codons of the gyrase proteins (Table 2.20).

Table 2.20: *Plasmodium* gyrase sequences.

Specie	Gene	PlasmoDB ID	Start codon
<i>Plasmodium falciparum</i>	GyrA	PF3D7_1223300	161
<i>Plasmodium falciparum</i>	GyrB	PF3D7_1239500	114
<i>Plasmodium berghei</i>	GyrA	PBANKA_1438200	146
<i>Plasmodium berghei</i>	GyrB	PBANKA_1454000	101

2.11.2. Sequence alignments

Alignments were performed using ClustalW and coloured using BoxShade or Jalview.

2.11.3. Densitometric gel analysis

Images were analysed using Fiji. Gel bands were quantified using Fiji or SynGene Gene Tools software. Data were plotted using GraphPad prism.

Chapter 3: Expression of Eukaryotic gyrases

3.1. Introduction

The discovery of gyrase from a prokaryotic source and the successive realisation of the enzyme's unique activity to introduce negative supercoils into the closed-circular chromosomal genome of the host, essentially maintaining the genome in a favourable state for efficient duplication, appeared promptly logical. On the contrary, the revolution in DNA sequencing technologies, which allowed sequencing to extend to more genomes and include those of the sizeably challenging eukaryotes, led to the unanticipated discovery of DNA gyrase within particular eukaryotic species. The species initially of interest to this research include *Arabidopsis thaliana* and *Plasmodium falciparum*. The exciting discovery was unforeseen for two reasons: the arrangement of eukaryotic genomes into linear chromosomes that maintain the required negative supercoiled state through their wrapping around the histone DNA compaction proteins; and the non-existence of gyrase in higher eukaryotes including the human genome, which endorsed the gyrase as an awarding antibacterial target.

The revelation of gyrase in *Arabidopsis thaliana* and *Plasmodium falciparum*, from now referred to plainly as eukaryotes, becomes rational when the evolutionary genesis of these species is considered. Specifically, the early endosymbiotic relationship formed upon engulfment of a cyanobacteria or aerobic prokaryote by a eukaryote, which resulted in the formation of the *Arabidopsis* chloroplasts or mitochondria, respectively (Morley et al. 2019; Timmis et al. 2004; Zimorski et al. 2014b). The secondary endosymbiotic relationship between a chloroplast and a photosynthetic alga established the apicoplasts that are found within *Plasmodium falciparum* (Kohler et al. 1997; Oborník et al. 2009). Nevertheless, the eukaryotic gyrases potentially retain unique characteristics, be it the encoding of two GyrB subunits (*Arabidopsis thaliana*) or the outright difference in size of encoding subunits (*Plasmodium falciparum*) as discussed in Chapter 1 of this thesis; the significance of both of which yet remain unexplored.

In this chapter, efforts of recombinant protein expression of eukaryotic gyrases, both successful and unsuccessful, will be discussed as a prelude to the intended biochemical characterisation of the enzymes.

3.2. Results and discussion

3.2.1. *E. coli* expression system

3.2.1.1. *Plasmodium falciparum* gyrase

The challenges of expressing *Plasmodium falciparum* gyrase may originate from the parasite's unusual incorporation of adenine and thymine bases into its genetic code. Nevertheless, the successful expression of gyrase subunits from this species has been achieved to varying degrees of success. As discussed earlier in section 1.8.3.1, Dar and co-workers have reported the expression of full-length PfGyrB and domains of PfGyrA of the enzyme (Dar et al. 2007). Their method of expression involved transformation of the expression constructs carrying individual *P. falciparum* gyrase subunits into BL21 Codon plus strains of *E. coli*, followed by expression of the PfGyrB gene from the lac promoter, upon introduction of IPTG.

Plasmodium falciparum gyrase subunits were chemically transformed into two different *E. coli* strains: BL21 DE3 Codon Plus and Rosetta DE3 2 pLysS; these strains of *E. coli* are equipped with supplemental tRNAs that are rare in *E. coli* but found more frequently in eukaryotic genomes, for the purpose of improving heterologous protein production within the *E. coli* expression system. The published protocol of Dar and co-workers was closely mirrored, albeit the expression was instigated from a shuttle vector, pOPINF, rather than pET28a as implemented in the previous study. Notably, both expression plasmids share a high-copy-number ColE1 origin of replication and drive expression by an inducible T7 promoter (Figure 3.1a). Unfortunately however, the results of Dar and co-workers could not be reproduced; despite multiple attempts we were unable to produce discernible bands of interest of *P. falciparum* GyrA or GyrB, the co-expression of both subunits (GyrA & GyrB; note: co-expressed subunits will be differentiated by incorporation of '&' in this chapter) together was also attempted but no evidence of PfGyrA expression was detected (Figure 3.1c). Interestingly, the GyrB subunit (predicted molecular weight ~101-kDa) provided traces of scarce expression from larger cultures, although the probing of these partially purified fractions using antibodies directed at the hexa-histidine tag fused at the N-terminal of *P. falciparum* GyrB identified several probable degradation products of GyrB; implying the produced *P. falciparum* GyrB to be unstable (Figure 3.1b). However, the potential activity of pooled fractions of partially purified *P. falciparum* GyrB or GyrA&GyrB was determined by a DNA supercoiling assay through complementation of *P. falciparum* subunits with the corresponding *E. coli* gyrase subunit.

No promising supercoiling activity could be detected by the reconstitution of gyrase through any of the combinations tried. At best, reconstitution of gyrase PfGyrB:EcGyrA gave a hint of supercoiling activity above background levels of individual subunits alone (Figure 3d); stronger activity of PfGyrB:EcGyrA was observed with different preparations of PfGyrB protein at the same concentration of EcGyrA (results not shown). However, it cannot be ruled out that the partially purified PfGyrB fraction may also encompass co-purified *E. coli* gyrase and the level of potential activity did not warrant further investigation, by this method. *E. coli* DNA gyrase is capable of conducting the opposing reaction, that is the relaxation of supercoiled DNA, in an ATP-independent reaction. The ATP-independent relaxation activity of PfGyrB:EcGyrA gyrase was investigated, however, the partially purified PfGyrB alone possessed relaxation activity, plausibly due to the co-purification of a topoisomerase I protein (results not shown).

3.2.1.2. *Plasmodium berghei* gyrase

In order to ensure that the inability to express *Plasmodium falciparum* gyrase was not a consequence of its expression from the pOPINF shuttle vector, which has both bacterial and insect cell origins of replication; a bacterial specific vector, pETDuet, was used instead. The pETDuet vector has the additional benefit of coupling two multiple cloning sites that can drive the expression of independent genes, within the same bacterial cell. Plausibly, this may resolve the instability problem of the *Plasmodium* gyrase, if co-expression of its partner subunit is required for the correct folding or stability of the protein.

The objective of cloning *Plasmodium falciparum* GyrA and GyrB into the same pETDuet vector was not possible. Although the sub-cloning of PfGyrB into pETDuet was achieved, the addition of PfGyrA into this vector, or indeed the sub-cloning of PfGyrA into pETDuet alone was not feasible. This is perhaps suggestive of the toxicity of the *P. falciparum* GyrA subunit within bacterial cells. In view of this, the *Plasmodium berghei* gyrase, which remains so far uncharacterised but also encoded by single *gyrA* (PbGyA) and *gyrB* (PbGyrB) genes, was explored. Both *P. berghei* gyrase genes were cloned into a single pETDuet vector, as well as independently into separate vectors. The expression of all possible *Plasmodia* gyrase subunits were evaluated at a range of temperatures and times using the Rosetta 2 (DE3) pLysS strain of *E. coli* (Figure 3.2). The expression of the *P. berghei* GyrA protein, of expected size ~124-kDa, did not prove possible at 18°C, 28°C or 37°C, alone or in combination with PbGyrB, despite the duration of expression (Figure 3a,c). On the contrary, a band of ~96-kDa, corresponding to expression of PbGyrB was seen when expressed alone and in combination with PbGyrA (Figure 3.2 b,c). Interestingly,

when expressed at 37°C an enhancement in the potential degradation products of the protein were observed. However, this issue was circumvented by expression at 28°C; protein expression was increased by overnight expression at this temperature. The efficient expression pattern was also mirrored during the expression of PfGyrB, i.e., expression at a reduced temperature for an extended period of time somewhat reduced the level of degraded protein products (Figure 3.2d).

The difficulty of expressing plasmodial proteins in *E. coli* is commonly associated with toxicity of the plasmodial proteins (Vedadi et al. 2007) and the difference in their amino acid preference, which undoubtedly adds a metabolic burden upon the bacterial cell. This is usually evidenced in the form of ribosome stalling and pausing during the translation process, a repercussion due to the exhaustion of appropriate tRNAs and is output as early termination (Birkholtz et al. 2008). The overexpression of recombinant *Plasmodia* proteins is complicated for a number of reasons: their unusually large size, greater protein disorder, higher pI (>6), occurrence of low complexity regions, plasmodium specific inserts, signal and transit peptides; all of which reduce the level of expressed protein and correlate with insolubility (Birkholtz et al. 2008; Mehlin et al. 2006; Vedadi et al. 2007).

A plausible approach to take is use of a different expression system, potentially more suited to expression of plasmodial proteins. Interestingly, the use of baculovirus-infected insect cells as a recombinant expression system has proved successful for plasmodial proteins aggregating as insoluble bodies upon expression in *E. coli* or other systems (Mehlin et al. 2006; Stack et al. 2007; Teuscher et al. 2007). Moreover, there are instances where an expressed *Plasmodia* protein by means of insect cells and *E. coli* have been directly compared and found the former system of expression to hold superiority (Victor et al. 2010). To our knowledge, the expression of *Plasmodia* gyrase proteins through baculovirus mediated infection of insect cells remains unexplored. Therefore, the expression system was selected for further analysis.

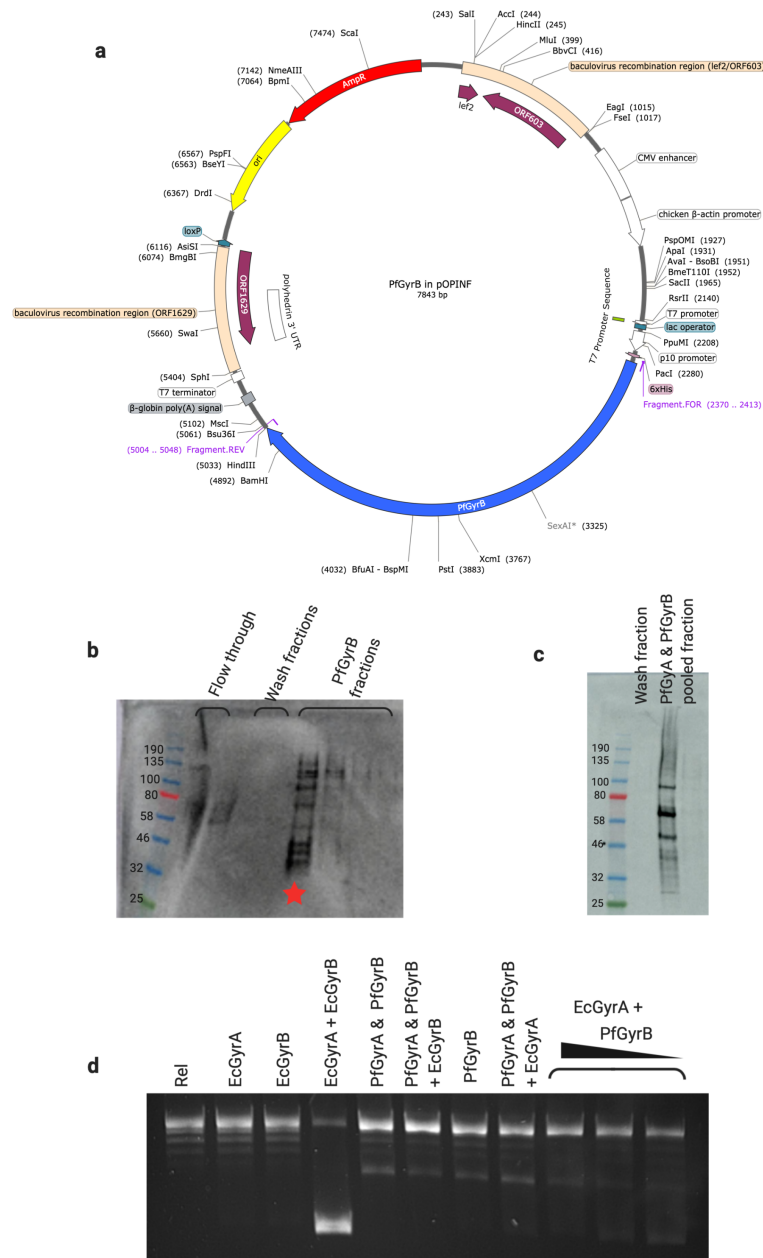


Figure 3.1: *P. falciparum* gyrase expression in *E. coli*.

(a) The shuttle vector pOPINF encoding the PfGyrB gene under the control of a T7 promoter. Western blot using anti-histidine antibody to highlight expression of N-terminal histidine tagged *Plasmodium falciparum* GyrB (~ 101 kDa) (b) or GyrA (~125 kDa)&GyrB co-expressed (c) from 1L of *E. coli*. (d) DNA supercoiling assay using combinations of *E. coli* expressed *P. falciparum* gyrase (PfGyrB and co-expressed PfGyrA&PfGyrB fractions were pooled for assays; note: ‘&’ indicates co-expression, albeit no evidence of PfGyrA expression was detected) and supplemented with appropriate partner subunits of *E. coli* gyrase. The last three lanes: only PfGyrB was titrated from a high to low concentration (EcGyrA: 0.2 μ M, EcGyrB: 40 nM, concentration of partially purified *P. falciparum* were not determined). Lane labels above each lane, Rel: relaxed DNA).

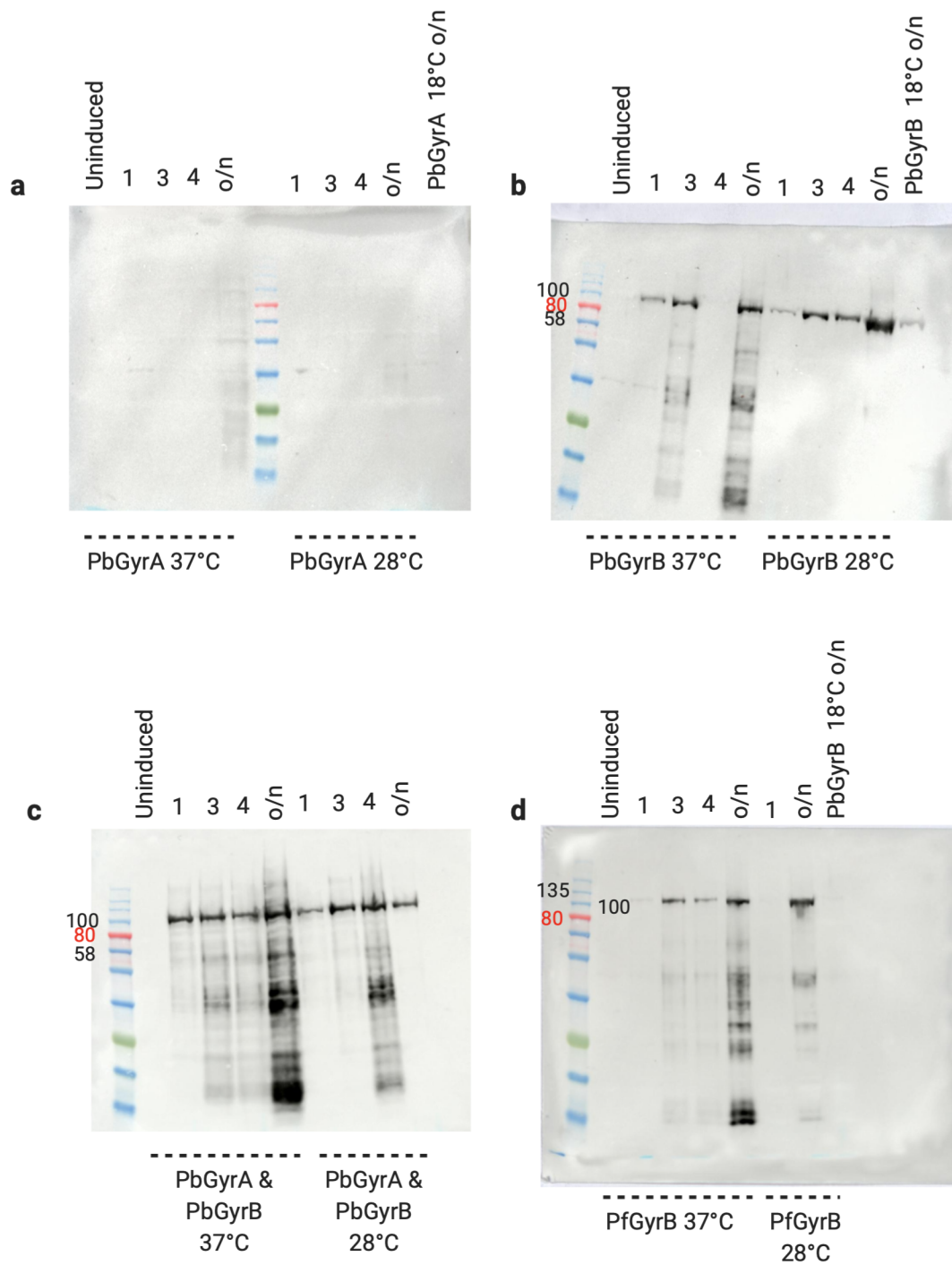


Figure 3.2: *Plasmodia* gyrase expression in *E. coli*.

Western blots using anti-histidine antibodies to detect hexa-histidine tagged expression of *P. berghei*: GyrA (a), GyrB (b), co-expressed GyrA&GyrB (c) and *P. falciparum* GyrB (d) after 1, 3, 4 hours or over-night (o/n) induction at the 28°C, 37°C or 18°C (overnight expression only) in Rosetta 2 (DE3) pLysS cells, as labelled. Expected size: PbGyrA: ~124 kDa, PbGyrB: ~96 kDa.

3.2.2. Insect cell expression

Baculoviruses are insect-pathogenic viruses that were originally tested as pesticides to control *Spodoptera frugiperda* (more commonly known as the fall armyworm) mediated crop damage (Haase et al. 2015; Van Beek and Davis 2016). Subsequently, it was demonstrated that the baculovirus *Autographa californica* multiple nucleohydrovirus (*AcMPNV*) could be exploited for the production of recombinant proteins in a laboratory culture of insect cells: the first of which was IFN- β expression (Smith et al. 1983). This development was founded on the realisation that two proteins, p10 and polyhedrin, were produced in vast quantities by baculoviruses due to their expression from strong promoters, yet the two proteins themselves were nonessential for the propagation of the baculovirus itself within insect cells (van Oers et al. 2015).

The expression system evolved from the engineering of the *AcMPNV* baculoviral genome to allow the creation of a bacterial artificial chromosome (BAC) with sufficient adaptations to promote multicomplex protein production. The modifications of the viral genome included the removal of proteolytic and apoptotic features (Pelosse et al. 2017). The natural infection of a baculovirus upon an insect cell involves the hijacking of host machinery by the virus to manufacture excess baculovirions and ultimately leads to lysis and cell death of the insect host cell. It was realised that the highest level of recombinant protein production correlated with the widespread lysis of cells, to counteract this, the viral genome was altered to delay the induction of cell lysis and allow the production of recombinant protein complexes in intact cells (Berger et al. 2004).

There are several methods of integrating the gene of interest into the engineered *AcMPNV* genome. One such method is to rely on recombination within an insect cell of a linearised engineered *AcMPNV* genome that contains a lethal deletion, with a transfer vector containing the gene of interest under the control of a strong viral promoter, following co-transfection of both DNA entities (Figure 3.3). The lethal deletion within the *AcMPNV* genome can be rescued by the transfer vector, therefore ensuring the propagation of viruses formed by the fusion of the two co-transfecting DNAs; nonetheless, the possibility of forming nonrecombinant viruses is not totally excluded.

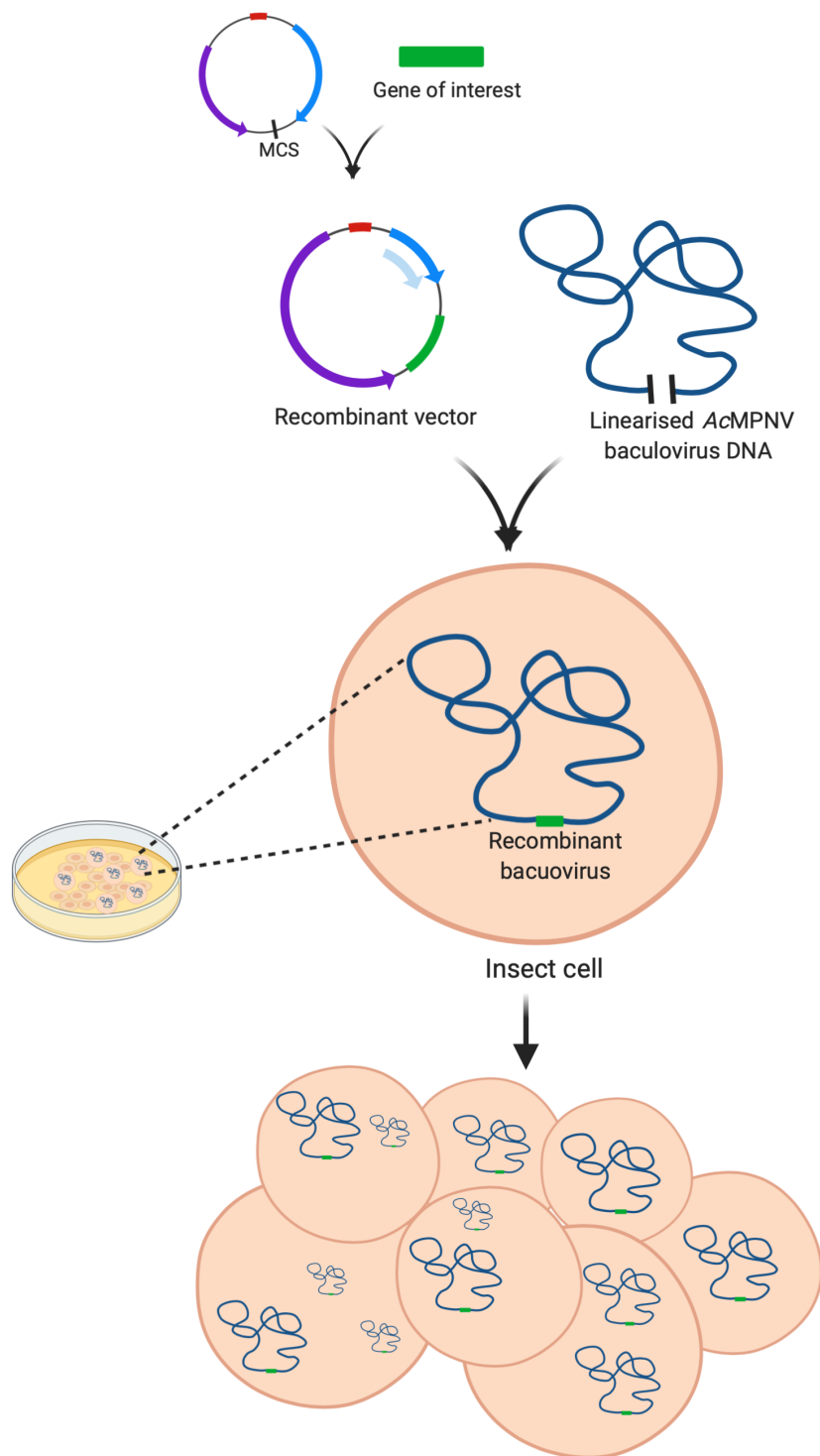


Figure 3.3: Schematic of homologous recombination mediated baculovirus transfection of insect cells.

3.2.2.1. OPPF collaboration

A collaborative project was initiated prior to the start of this work with the Oxford Protein Production Facility (OPPF) based in Oxford, United Kingdom. Researchers at the OPPF developed a versatile ligation-independent method for high-throughput expression screening in bacteria, mammalian and insect cells (Berrow et al. 2007). An outcome of this work was the development of the pOPIN shuttle vectors that offered several benefits, for instance: rapid and reliable high-throughput cloning, the production of a fused purification tag with the protein of interest, and the ability to express in *E. coli*, mammalian cells and insect cells using the same vector (Berrow et al. 2007). The two pOPIN sub-plasmids of interest to this work are pOPINF and pOPINE-3C-eGFP (pOPINE).

The cloning of *Plasmodium falciparum* and *Arabidopsis thaliana* gyrase genes into the pOPINF vector suite was carried out by researchers at the OPPF (sequences were not codon optimised). They also conducted preliminary expression trials that gave promising results for expression of gyrase subunits. The pOPINF clones were obtained from OPPF and further experimental work was carried out in-house at JIC.

3.2.2.2. Recombinant pOPIN plasmids

Gyrase is a multi-subunit protein comprising a heterotetramer formed by two GyrA and two GyrB subunits. There are numerous methods by which expression of such a complex can be investigated within insect cells. For instance, viruses corresponding to each subunit may be generated individually, or a population of insect cells may be co-transfected with viruses corresponding to different subunits; that is, GyrA and GyrB simultaneously (co-transfection). An alternative approach that serves as a mediation of the two involves the assembly of a fusion construct of the gyrase subunits. The fusion constructs follow the order GyrB-GyrA (GyrBA) to reflect the three-dimensional association of the active protein. The GyrBA fusion constructs of *M. tuberculosis*, *M. smegmatis* and *E. coli* retain similar activity to wild-type enzymes formed by stoichiometric arrangement of subunits; this has been confirmed by past and current members of the Maxwell group. The suite of pOPIN expression vectors consist of various tags and fusions to assist downstream protein solubility and purification. The two plasmids incorporated in this work are pOPINF and pOPINE (Figure 3.4a). The peptide products of plasmids constructed at the OPPF are illustrated in Figure 3.4b(i); these were supplemented by the sub-cloning for creation of further peptides, including GyrBA fusion peptides, as depicted in Figure 3.4b(ii).

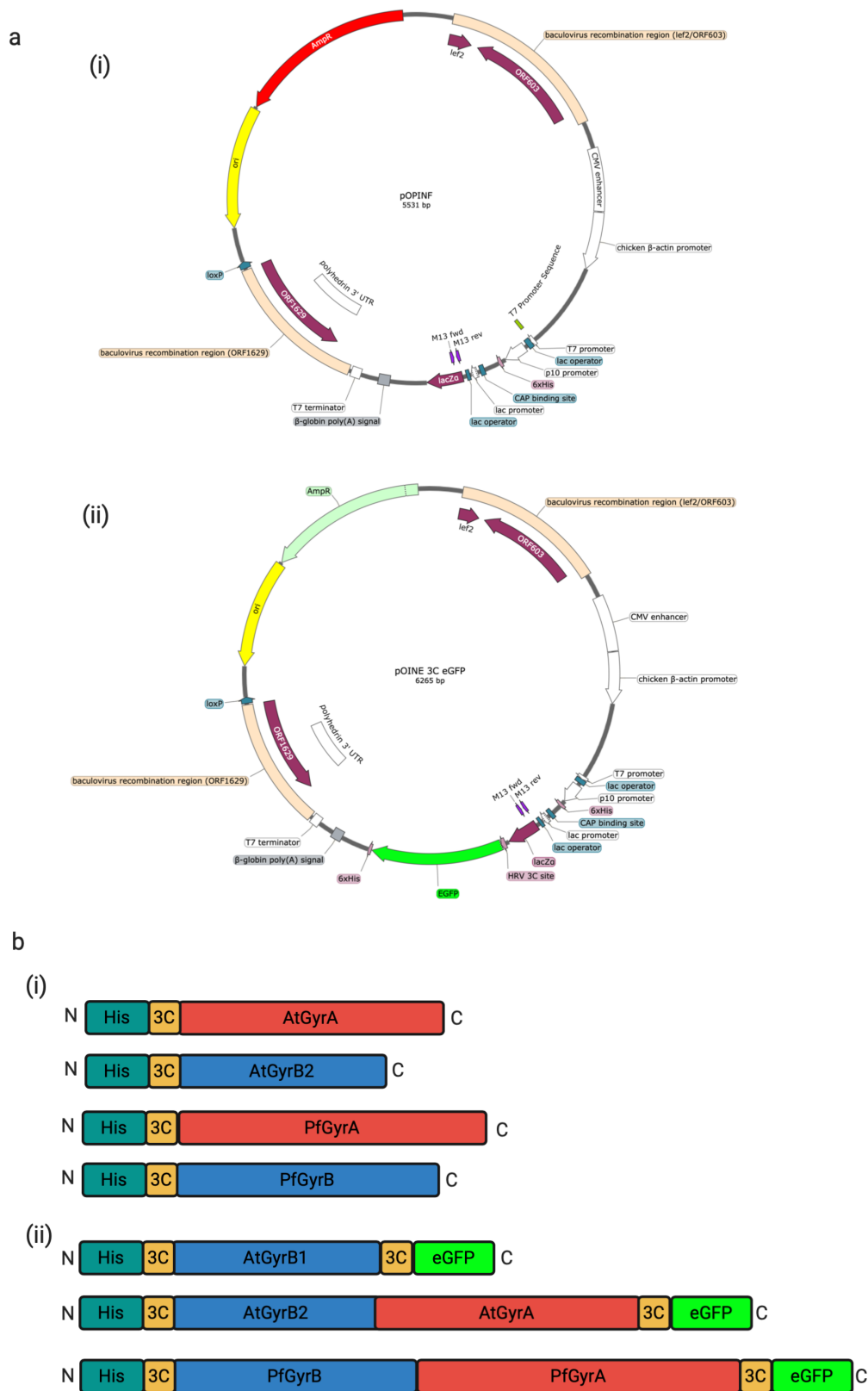


Figure 3.4: pOPIN vectors.

(a) Representation of pOPINF (i) and pOPINE 3C eGFP (ii) vectors. (b) Gyrase peptides as expressed from pOPINF (i) or from pOPINE 3C eGFP (ii) from N to C terminus.

3.2.2.3. Recombination rationale pOPIN system

The rationale of expression involves the co-transfection of viral DNA and a transfer vector (pOPIN) followed by their *in vivo* recombination. The pOPIN transfer vector encodes the gene of interest, flanked by sufficient homologous regions of viral DNA to allow efficient recombination *in vivo*. The first region of homology encompasses the late expression factor-2 gene (*lef-2*) of *AcMNPV*, which is involved in very late gene expression and facilitates efficient amplification of viral DNA immediately after virus entry into the host cell, ORF 603 is encoded directly adjacent to this. The second region of homology contains ORF 1629. The gene of interest is inserted between these two regions on the vector (Figure 3.4a).

The auxiliary component to the pOPIN transfer vector and target for recombination is the *AcMNPV* genome (manipulated to facilitate recombination). Recombination within the *AcMNPV* genome can occur at many sites, yet the most frequently exploited locus is the polyhedrin gene, within the ~134-kbp viral genome (Figure 3.5a). ORF 1629 encodes an essential gene product, the probable function for which is either modification of the virion RNA polymerase or involvement in nucleocapsid packaging (Iorio et al. 1998; Pham et al. 1993; Vialard and Richardson 1993). In principle, inactivation of ORF 1629 would render the *AcMNPV* virus non-viable unless the genome is repaired by recombination with a transfer vector encoding ORF 1629; therefore, propagating the production of recombinant virus. The viral genome inactivation scheme involved manipulation of a bacmid version of the infectious *AcMNPV* genome in *E. coli* from an F-factor based bacmid replicon. ORF 1629 was targeted for insertional inactivation through recombination by introduction of a chloramphenicol acyl transferase gene and a unique *Bsu36I* restriction site (Figure 3.5b) (Zhao et al. 2003). Subsequent linearisation of the bacmid DNA not only renders the virus inactive but the linear nature of the virus is inherently more likely to recombine with the transfer vector (Kitts and Possee 1993); a consequence of which is the transfer of the gene of interest from the recombinant pOPIN plasmid to the viral genome (Figure 3.5c).

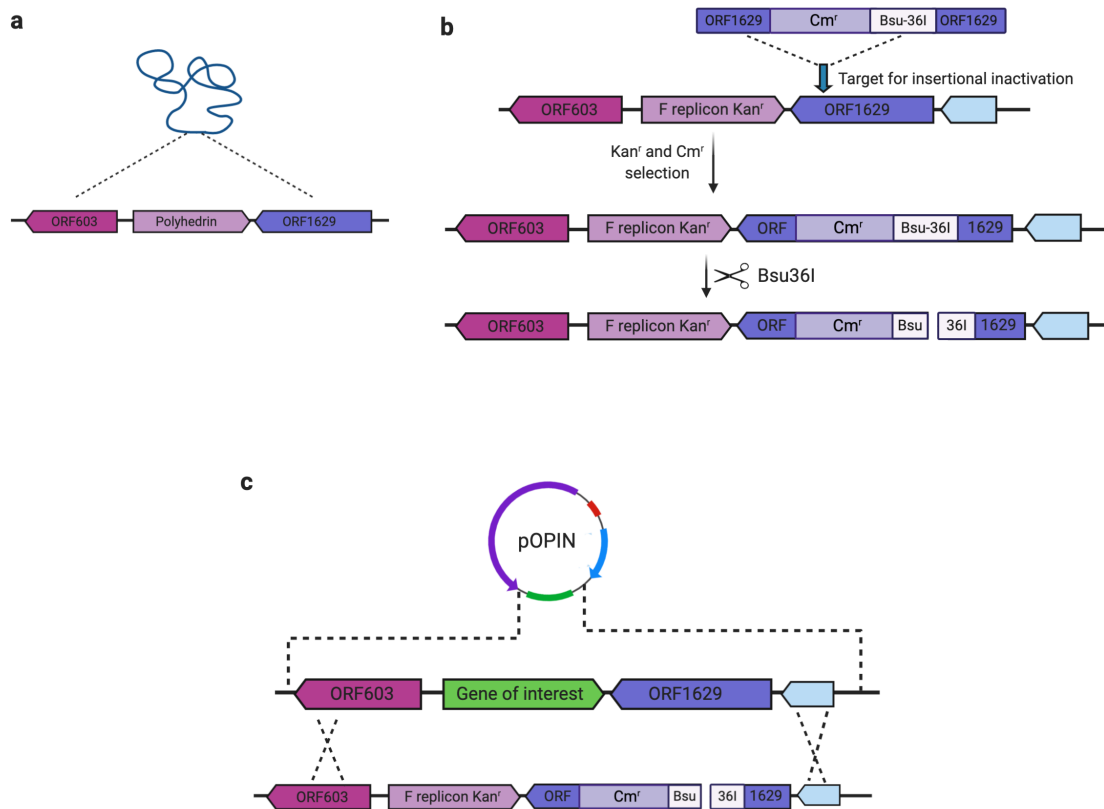


Figure 3.5: *AcMPNV* genome engineering.

(a) *AcMPNV* genome highlighting the region neighbouring a common site of recombination frequently manipulated, the polyhedrin locus. (b) Schematic of insertional inactivation method used to target the essential function of ORF 1629 by introduction of a selection marker and unique Bsu-361 restriction site. The restriction site can be used to linearise and inactivate the *AcMPNV* bacmid DNA. (c) Formation of recombinant virus: recombination between linearised *AcMPNV* bacmid and pOPIN vector to rescue the loss of ORF 1629 and introduce the coding region of the gene of interest into the viral genome. Figure redrawn from (Zhao et al. 2003).

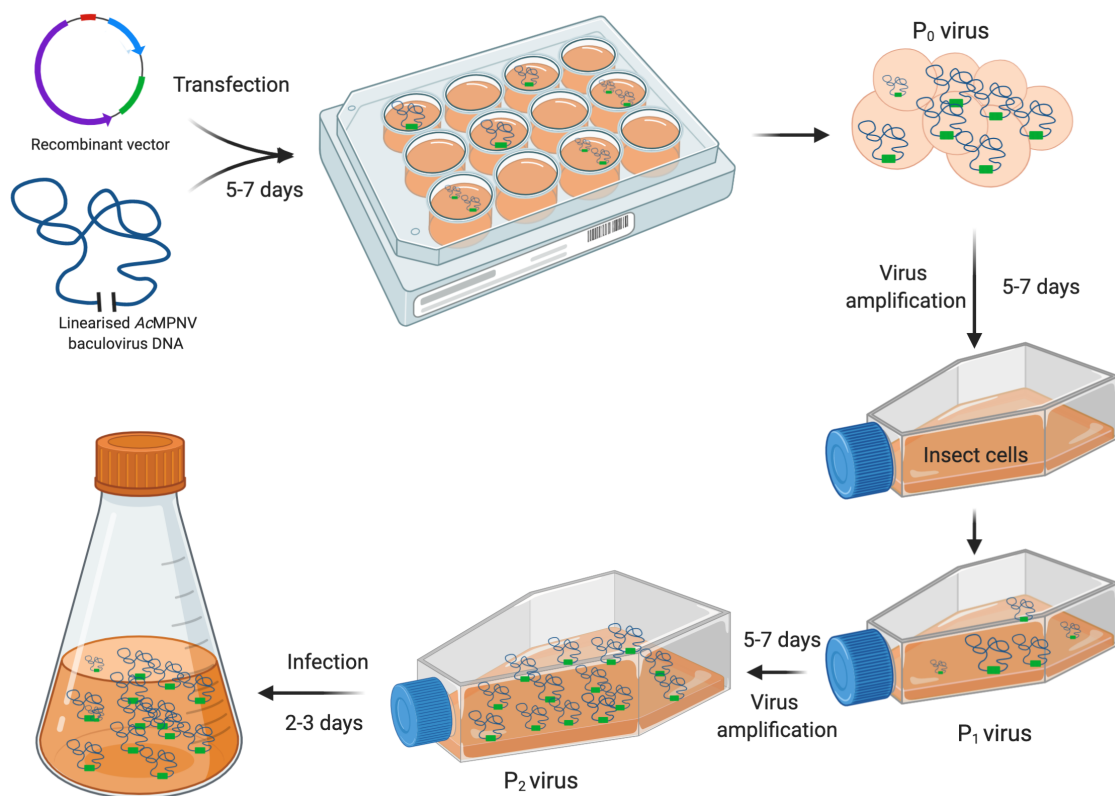


Figure 3.6: Schematic of baculovirus mediated insect cell expression.

Table 3.1: pOPIN expression constructs explored by co-transfection with linearised AcMPNV bacmid DNA.

Plasmid 1		Plasmid 2	
Gene encoded	Plasmid	Gene encoded	Plasmid
AtGyrA	pOPINF	-	-
AtGyrB1	pOPINE	-	-
AtGyrB2	pOPINF	-	-
PfGyrA	pOPINF	-	-
PfGyrB	pOPINF	-	-
AtGyrA	pOPINF	AtGyrB2	pOPINF
AtGyrA	pOPINF	AtGyrB1	pOPINE
PfGyrA	pOPINF	PfGyrB	pOPINF
AtGyrB2A	pOPINE	-	-
PfGyrBA	pOPINE	-	-

3.1.1.1. pOPIN expression trials

The expression of gyrase from *Arabidopsis thaliana* and *Plasmodium falciparum* was explored by baculovirus-mediated insect cell expression. The AcMPNV bacmid DNA was a gift from the laboratory of Professor Ian Jones (University of Reading). The bacmid DNA was purified and linearised by Bsu36I restriction. Insect cells Sf21, which are isolated from the ovaries of the fall army worm and a clonal isolate of these cells, Sf9, were both subjected to expression trials by co-transfection with the pOPIN suite vectors harnessing coding regions for the genes and combinations of genes outlined in Table 3.1.

The baculovirus-mediated expression in insect cells is initiated by co-transfection of the insect cells with linearised bacmid and complementary pOPIN transfer vector (Figure 3.6). The *in-vivo* recombination generates recombinant baculovirus that is functional and able to hijack the inherent replication machinery of the eukaryotic host to produce multiple copies of its own genome, which following *in vivo* recombination; encompasses the gene of interest from the pOPIN vector under the control of a strong viral late expression promoter, p10 or polyhedrin. Albeit manipulations of the viral genome have been incorporated to delay its lytic effect on the eukaryotic host, cell lysis inevitably results and causes the release of the recombinant baculovirus into the surrounding media. The resultant P₀ recombinant virus is collected and cells are separated by brief centrifugation. Subsequent steps of viral amplification involve the transduction of insect cells with recombinant virus to purify P₁ and P₂ virus stocks. Depending on the efficiency of viral amplification, either P₁ or P₂ viruses are applied to cells for the expression of the desired protein; the transfected cells are collected prior to their lysis for downstream protein purification.

The expression testing to verify the competence of viral stocks was routinely conducted on small cultures of Sf21/Sf9 cells prior to potential scale-up. The cell lysates were partially purified by affinity methods that exploited their integrated N-terminal hexa-histidine residues. A positive control of N-terminal tagged green fluorescent protein (GFP) was included for baculovirus expression and downstream protein purification. Gyrase expression of *Arabidopsis thaliana* and *Plasmodium falciparum* was tried according to single-transfection and co-transfection combinations outlined in Table 3.1. Subsequently, small-scale testing and optimisations were carried out for all the proteins by varying the quantity of transfecting virus and testing the optimal length of expression for each gene. Encouraging results were obtained from expression as a result of the co-transfection of monocistronic *Arabidopsis thaliana* GyrA and GyrB2 upon the same collection of recipient insect cells (Figure 3.7).

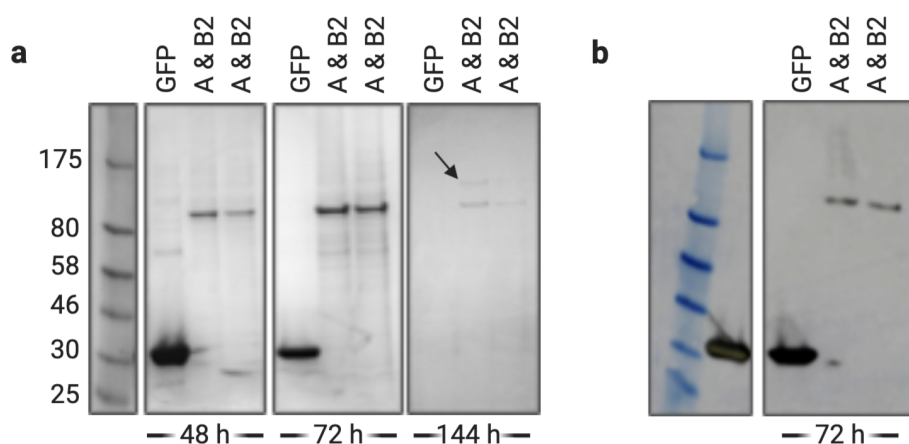


Figure 3.7: Baculovirus mediated expression trials of *A. thaliana* gyrase.

(a) Denaturing protein gel corresponding to co-expression samples of *A. thaliana* GyrA and GyrB2 from insect cells collected 2-, 3- and 6-days post infection, lysed and partially purified using Ni-NTA magnetic beads. The arrow indicates an unconfirmed band of GyrA. (b) Western blot of insect cells co-expressed with *A. thaliana* GyrA and GyrB2 using antibodies targeted to the hexa-histidine purification tag. Note: smear above the distinct GyrB2 band, plausibly corresponding to minute GyrA levels.

Interestingly, although cells were transfected with P₂ virus combining *Arabidopsis thaliana* GyrA and GyrB2 subunits, initially only the production of GyrB2 protein was obviously evident on denaturing protein gels. The optimum length of expression for this subunit was found to be 72 hours post-transfection of cells; this was in contrast to the GFP control protein, which was optimally expressed 48 hours post-transfection. The protein expression after baculovirus transfection is typically monitored up until 3 days post-infection, however, the expression in this case was tracked up to 6 days post-infection. By the 6th day most proteins had been degraded, including the complete degradation of GFP and the majority of GyrB2 protein, as expected. However, at this point, a second protein band became evident, plausibly corresponding to the expression of *Arabidopsis thaliana* GyrA. It is possible that the GyrA expression within the insect cells is delayed or indeed that the subunit is expressed but the corresponding weak expression band is initially lost amidst the high-level background expression of proteins and only becomes evident once the majority of these are degraded

As computed by their sequences, the expected size of GyrB2 is ~72-kDa and that for GyrA is ~100-kDa; yet the bands observed on the protein gels seemed to correspond to slightly higher molecular weights, particularly for the GyrB2 protein. This was

investigated further by western blots using antibodies specific for the hexa-histidine sequence, the protein was confirmed to possess the expected purification tag implying it to correctly correspond to GyrB2 (Figure 3.7b); additionally, this was confirmed by mass spectrometry. However, the unanticipated probable discovery of GyrA remained unconfirmed.

The transfection of insect cells was repeated to comprehensively monitor the expression of *A. thaliana* GyrA and GyrB2 2-, 3-, 4-, 5- and 6-days post transfection. However, on this occasion no clear expression band corresponding to GyrA was detected by a denaturing protein gel, regardless of the period of expression. Nevertheless, the confirmed expression of AtGyrB2 was evident on protein gels on both occasions, partially purified proteins corresponding to these small-scale expressions, specifically 72 hours post-infection, were analysed in DNA supercoiling assays by complementation with *E. coli* GyrA. The active complex formation of EcGyrA:AtGyrB2 is capable of introducing negative DNA supercoils into relaxed substrate DNA as has been previously reported (Evans-Roberts et al. 2016). Insect cell expressed *A. thaliana* gyrase formed by the association of GyrA and GyrB2, after 72 hours of infection did not introduce negative supercoils into DNA (note: no clear GyrA band was detectable on protein gels, only GyrB2). However, when this sample was supplemented with EcGyrA, presumably the EcGyrA:AtGyrB2 protein formed an active complex and introduced supercoils into relaxed DNA, in a EcGyrA concentration dependent manner. However, a supercoiling reaction of AtGyrB2 expressed in *E. coli* with EcGyrA (a gift from Lesley Mitchenall) gave some evidence of supercoiling, but there was also a significant amount of double-stranded cleavage activity detected.

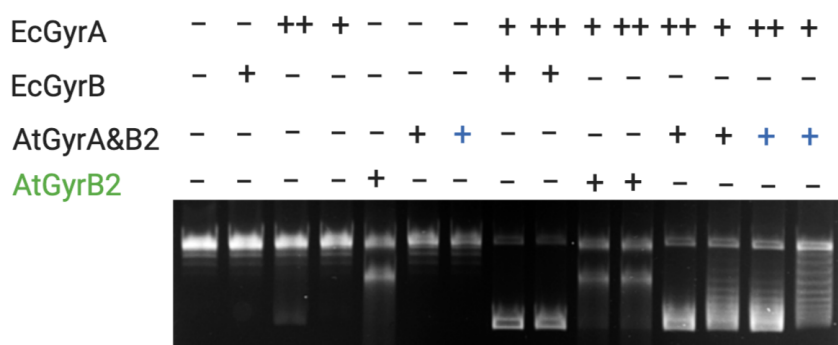


Figure 3.8: Supercoiling assay of gyrase formed by association of AtGyrB2 and EcGyrA.

The formation of a gyrase complex formed by association of EcGyrA and AtGyrB2 (*E. coli* expressed in green, a gift from Lesley Mitchenall; insect cell expressed in black and blue (different expression replicates) using cells co-transfected with AtGyrA (no protein detected). Note – prominent band corresponding to linear DNA by *E. coli* expressed AtGyrB2.

Despite the initial uncertainty of *Arabidopsis thaliana* GyrA expression, the potential miniscule protein expression detected previously by western blot, drove further investigations using a similar approach. Fortunately, these attempts resulted in the recognition of GyrA, again in tiny quantities, barely detectable by western blots. However, impressively, the GyrA protein was detected from cells co-transfected with monocistronic *A. thaliana* GyrA and GyrB2 baculoviruses (Figure 3.9a), in addition to the exposure of insect cells to baculovirus of each subunit individually (Figure 3.9b). The exclusive detection of GyrA alone, previously unreported, was exploited by its partial purification and subjection to a parallel supercoiling assay; as performed previously by members of the Maxwell laboratory after isolation of *A. thaliana* GyrB2. The supercoiling assay confirmed the novel formation of an active gyrase, capable of introducing negative supercoils, by the artificial association of AtGyrA:EcGyrB (Figure 3.9c).

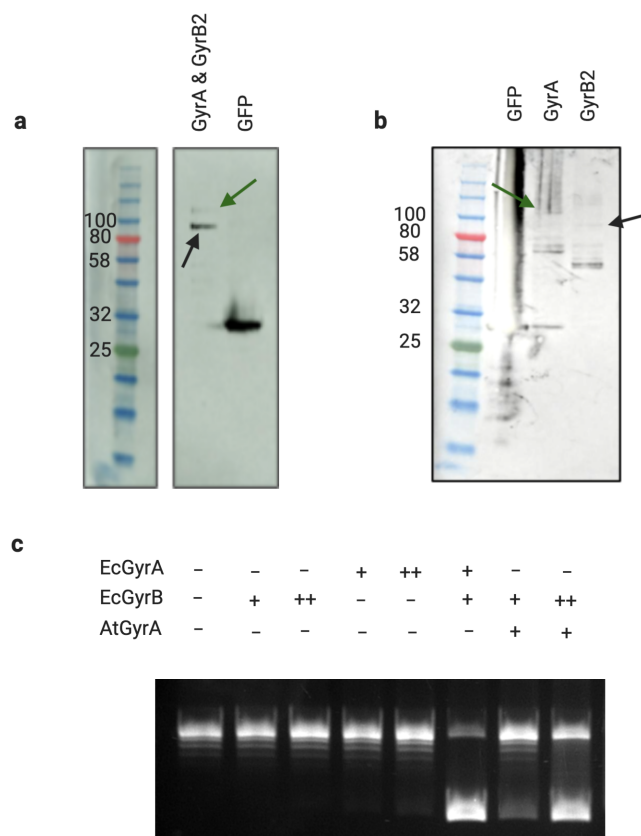


Figure 3.9: *A. thaliana* GyrA detection.

Western blot detection of *A. thaliana* GyrA (green arrow, ~100 kDa) during co-expression with AtGyrB2 (~ 72 kDa) (a) and individual expression (b). (c) DNA supercoiling assay using partially purified AtGyrA partnered with EcGyrB (EcGyrA: +:0.2 μ M, ++:0.4 μ M; EcGyrB: +:0.46 μ M, ++:0.92 μ M).

3.1.1.2. *A. thaliana* gyrase (GyrA and GyrB2) can supercoil DNA

The formation of an active gyrase complex by association of *Arabidopsis thaliana* GyrA and GyrB2, purified from co-transfected Sf21 cells, has been previously reported (Evans-Roberts et al. 2016). The detection of both GyrA and GyrB2 subunits prompted the scale-up process. P₂ baculovirus amplified from cells co-transfected with AtGyrA and AtGyrB2 was used to infect Sf21 cells at a ratio of 1:150. Infected Sf21 cells were harvested 72 hours later, lysed and the protein partially purified. The purified protein consisted of two dominant bands, corresponding to GyrA and GyrB2. However, several bands equivalent to smaller molecular weights were evident. Analysis using an in-gel histidine specific stain identified these bands to possess a histidine tag, implying that they are either a result of protein degradation or premature translation termination (Figure 3.10a). The purified *A. thaliana* gyrase retains DNA supercoiling activity, in a concentration dependent manner (Figure 3.10b). The expressed protein here is directly comparable to *A. thaliana* gyrase expressed by Evans-Roberts et al. 2016.

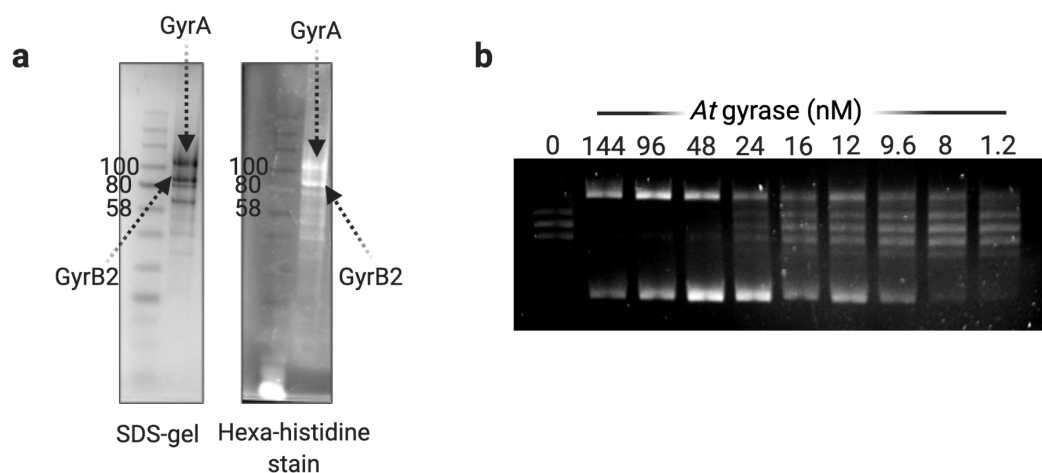


Figure 3.10: *A. thaliana* gyrase (GyrA & GyrB2) purification and activity.

(a) Denatured protein gel analysis of purified *A. thaliana* gyrase (GyrA & GyrB2, expected sizes ~100 kDa and ~72 kDa) and the same fraction after exposure to a histidine specific in-gel stain. (b) DNA supercoiling assay with an enzyme titration of purified *A. thaliana* gyrase (lanes marked with enzyme concentrations in nM).

3.1.1.3. Unsuccessful expression of gyrase subunits

It cannot be overlooked that despite the attempted expression of various *A. thaliana* and *P. falciparum* gyrase subunits, only the expression of the *A. thaliana* GyrA and GyrB2 subunits proved to be successful. Even so, the expression of the latter successful subunits proved unpredictable. Despite numerous attempts, the GyrA and GyrB2 expression using this system could not be reproduced. Notably however, the production of GyrB2 was relatively more reliable than GyrA. The GyrA was routinely produced in minute quantities, often either able to avoid detection by Coomassie staining or remain undetected due to easy submersion amongst the background proteins produced. The use of western blotting, a significantly more sensitive and specific detection technique, often only provided a hint of probable GyrA production.

Plausibly, the inability to detect any *Plasmodium falciparum* subunits and the difficulty of reliably producing *A. thaliana* gyrase may be consequential of the metabolic burden encountered by the insect cells during expression of proteins with a coding bias suited to their native eukaryotic systems. The codon optimization of sequences to reflect the codon usage of the host system in which their expression is being attempted, is an effective trick employed frequently to optimize heterologous expression of target genes and has been applied successfully to a variety of proteins and expression systems.

Nevertheless, it cannot be ruled out that the inefficient and unreliable expression of *A. thaliana* gyrase proteins may be due to failure or low frequency of *in vivo* recombination between linearised AcMPNV and pOPIN transfer vectors. Alternatively, this could be a result of reconstitution of the wild-type AcMPNV virus, which outcompetes the recombinant virus. Therefore, a different transfection system for expression in insect cells was explored. Furthermore, to establish a reproducible system determination of essential factors such as exact multiplicities of infection (MOIs) of the recombinant viruses is crucial.

3.1.2. Bac-to-Bac Baculovirus expression system

The linearization of the AcMPNV genome, harnessing the deletion of an essential region, can increase the proportion of recombinant virus up to > 80%. However, the requirement to perform sequential plaque assays in order to identify and separate recombinant virus from the non-recombinant virus in the progeny can be challenging and easily take several weeks to complete (Davies 1994; Gwatkin 1995; Paterson and Kennedy 1998). In order to investigate whether the unsuccessful and unreliable

expression of the gyrase subunits of *P. falciparum* and *A. thaliana* were a result of the outgrowth of recombinant virus by reconstituted wild-type AcMPNV virus, an altered technique of insect cell expression was exploited.

The alternative expression technique, the Bac-to-Bac system, is reliant upon site-specific transposition of an expression cassette from a donor plasmid into bacmid DNA (bMON14272) propagated in *E. coli*. The bacmid DNA encompasses several manipulations, including a low-copy number mini-F replicon, a mini-*attTn7* attachment site, a kanamycin selection marker and a segment of DNA encoding the *lacZ α* peptide. The specific strain of *E. coli*, DH10bac, in which this modified bacmid is propagated has a chromosomal *lacZ* deletion that can be complemented by the bacmid to allow the formation of blue colonies, when induced by IPTG and provided with appropriate substrate. Additionally, DH10bac cells also incorporate a helper plasmid (pMON7124) that provides transposase function and tetracycline resistance. The donor plasmids, pFastBac, encompass an expression cassette with the following features: a gentamycin resistance gene, a baculovirus specific promoter, a multiple cloning site for insertion of the gene of interest and a SV40 poly(A) signal; all within the left and right regions of the mini-Tn7.

The pFastBac plasmids incorporated in this work were of one of two types: pFastBac1, a monocistronic plasmid that can carry a single foreign gene, or pFastBac Dual, a polycistronic vector that can carry two foreign genes and therefore mediate co-expression. The *in vivo* transposition of the mini-Tn7 from a recombinant pFastBac plasmid containing the gene(s) of interest, to the *attTn7* attachment site on the bacmid DNA, disrupts expression of the *lacZ α* peptide on the bacmid. Consequently, recombinant bacmid can no longer complement the chromosomal *lacZ* deletion of the DH10Bac *E. coli*, so the recombinant colonies can be distinguished from unaltered bacmid by their white colour during blue-white screening. The downstream isolation of recombinant bacmid DNA and subsequent transfection of insect cells with this recombinant bacmid, ensures that the virus is not mixed with non-recombinant virus; eliminating the requirement for multiple rounds of plaque purification. The exemplified work-flow scheme of the Bac-to-Bac system is depicted in Figure 3.11.

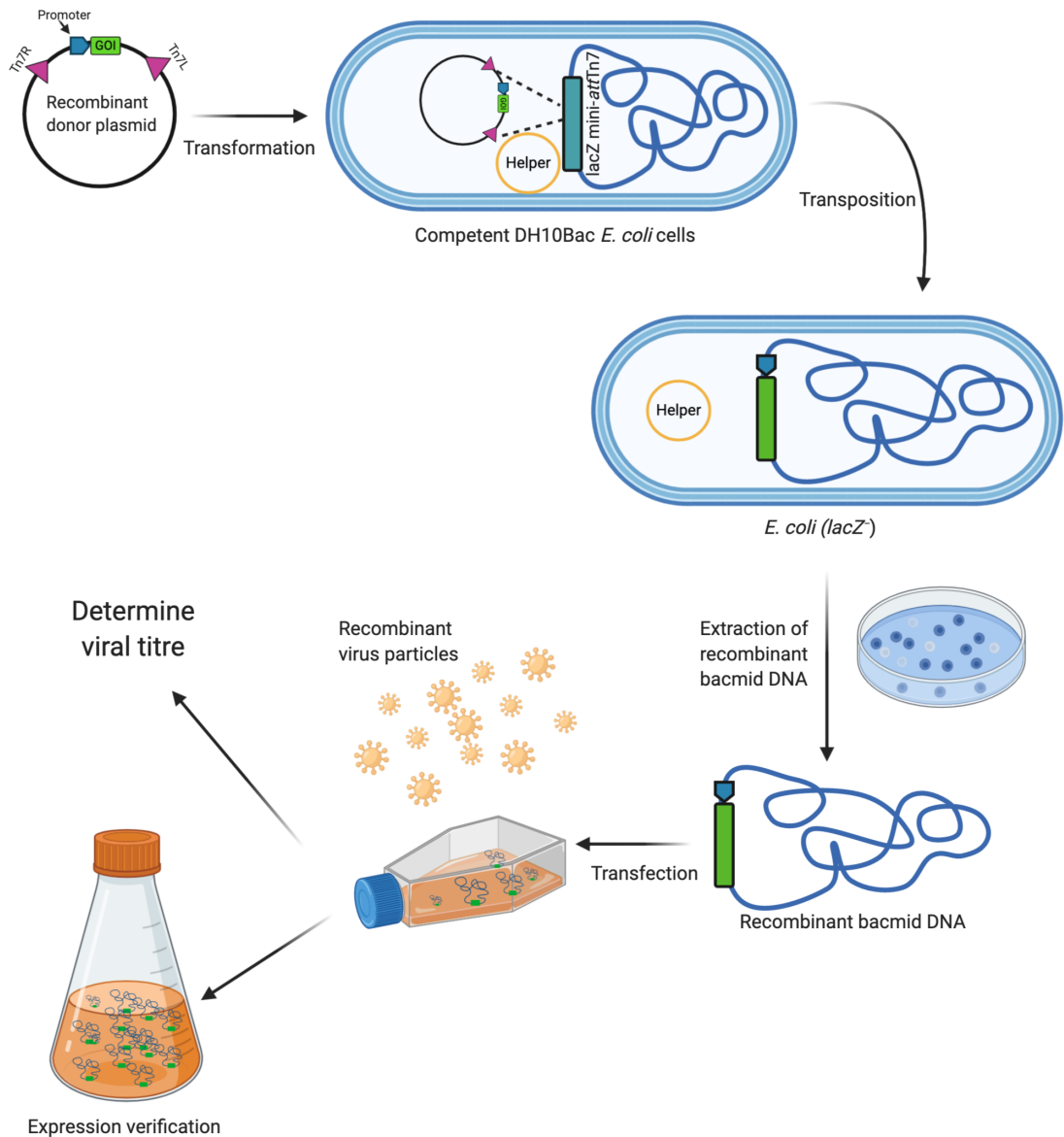


Figure 3.11: Schematic of the Bac-to-bac expression system.

The gene of interest (GOI) is encoded on a recombinant donor plasmid between mini-Tn7R and -Tn7L regions. The *E. coli* DH10Bac cells have a chromosomal *lacZ* deletion, they also harness the *AcMCPNV* bacmid with a mini-Tn7 attachment site and a helper plasmid encoding the Tn7 transposon. Transformation of the donor plasmid to these cells initiates the transposition of the gene of interest from donor plasmid to bacmid DNA, specifically to a region disrupting the production of *lacZ* α peptide. The recombinant bacmid DNA can no longer complement the chromosomal *lacZ* deletion, leading to the identification of these colonies by their white appearance upon blue-white screening. The recombinant bacmid can be purified, confirmed to possess the gene of interest, prior to transfection and downstream expression trials using insect cells.

3.1.2.1. Acquisition of recombinant pFastBac clones

A further adaptation was incorporated in the form of the optimisation of gene sequences to align with the codon bias of insect cells. In addition to the *P. falciparum* gyrase GyrA and GyrB, the codon optimised sequences for both subunits of the genes from *Plasmodium vivax* and *Plasmodium berghei* were sought after. In the interest of time, the task of generating these clones was sub-contracted to a specialist company (Gene Universal, China). The task proved arduous and more time consuming even for the specialist researchers. After a period of significant delay, they were able to produce codon-optimised sequences for *P. falciparum* and *P. berghei*, but despite multiple attempts the same result could not be extended to *P. vivax*. The plasmodial genes were encompassed within the pFastBac dual vector, with GyrA expression under the polyhedrin promoter, whilst GyrB was expressed from the p10 promoter for both species.

The task of codon optimisation for *A. thaliana* gyrase genes, specifically GyrA and GyrB1 was designated to ThermoFisher. The genes were obtained individually cloned into the pFastBac1 plasmid, where expression is driven by a polyhedrin promoter. In addition, the non-codon optimised GyrB2 gene was also cloned into the pFastBac1 plasmid for completeness. Several combinations of clones for *A. thaliana* gyrase within both pFastBac1 and pFastBac dual vectors were attempted, including GyrBA fusion constructs (similar to those described in 3.2.3.2). However, in this case, genes were cloned with and without the addition of a flexible three amino acid linker (serine-serine-glycine, SSG). The clones pursued for expression using the Bac-to-Bac system are listed in Table 3.2. All clones included a hexa-histidine tag cleavable by the action of 3C protease.

The cloning difficulty of *A. thaliana* GyrB2 is particularly notable in circumstances where its insertion is attempted alongside or within a plasmid harnessing a GyrA gene. The complication persists regardless of the expression vector, as it persisted during the use of pOPIN, pFastBac1 and pFastBac dual. Although a GyrB2A fusion construct was obtained within pOPINE, there were two missense mutations within its sequencing region resulting in the replacement of Ile 387 of GyrB2 with valine (within the region corresponding to GyrB2 of the fusion) and Ala 922 with Asp (within the GyrA region of the fusion). The correction of these missense mutations by site directed mutagenesis was attempted but did not prove possible. Therefore, the failed attempts of GyrB2 cloning into pFastBac1 and pFastBac dual in the presence of GyrA implies that the combination of these sequences is particularly toxic to *E. coli*. Furthermore, the introduction of GyrB2 into a pFastBac dual construct containing the GyrA protein resulted in deletions,

rearrangements and insertions of the pFastBac dual vector backbone to compensate the introduction of a truncated GyrB2 protein.

Table 3.2: The clones of *P. falciparum*, *P. vivax*, *P. berghei* and *A. thaliana* pursued for investigation by the Bac-to-Bac expression system. All clones included a cleavable N-terminal hexa-histidine tag.

Gene 1	Gene 2	pFastBac plasmid	Linker	Success
PfGyrA	—	pFastBac dual	—	✓
PfGyrA	PfGyrB	pFastBac dual	—	✓
PvGyrA	—	pFastBac dual	—	X
PvGyrA	PvGyrB	pFastBac dual	—	X
PbGyrA	—	pFastBac dual	—	✓
PbGyrA	PbGyrB	pFastBac dual	—	✓
AtGyrA	—	pFastBac1	—	✓
AtGyrB1	—	pFastBac1	—	✓
AtGyrB2	—	pFastBac1	—	✓
AtGyrA	—	pFastBac dual	—	✓
AtGyrA	AtGyrB2	pFastBac Dual	—	X
AtGyrA	AtGyrB1	pFastBac1	No linker	✓
AtGyrA	AtGyrB1	pFastBac1	SSG	✓
AtGyrA	AtGyrB1	pFastBac dual	—	✓
AtGyrA	AtGyrB2	pFastBac1	No Linker	X
AtGyrA	AtGyrB2	pFastBac1	SSG	X

3.1.2.2. Recombinant virus generation

The recombinant pFastBac plasmids outlined in Table 3.2 were transformed into Max efficiency DH10Bac cells, which hold the complementary bacmid and helper plasmid that are required for transposition of the expression cassette encoded on the donor plasmid into the bacmid DNA. DH10Bac cells no longer able to complement the chromosomal *lacZ* deletion, due to the successful transposition of the expression cassette from recombinant plasmid to the *lacZ* coding region of the bacmid DNA, were identified as white colonies upon blue-white screening. The potential recombinant colonies were re-streaked and recombinant bacmid DNA isolated from positive candidates. The recombinant nature of the isolated bacmid was probed by PCR, to confirm the correct incorporation of the genes using primer binding sites within the bacmid (Figure 3.12).

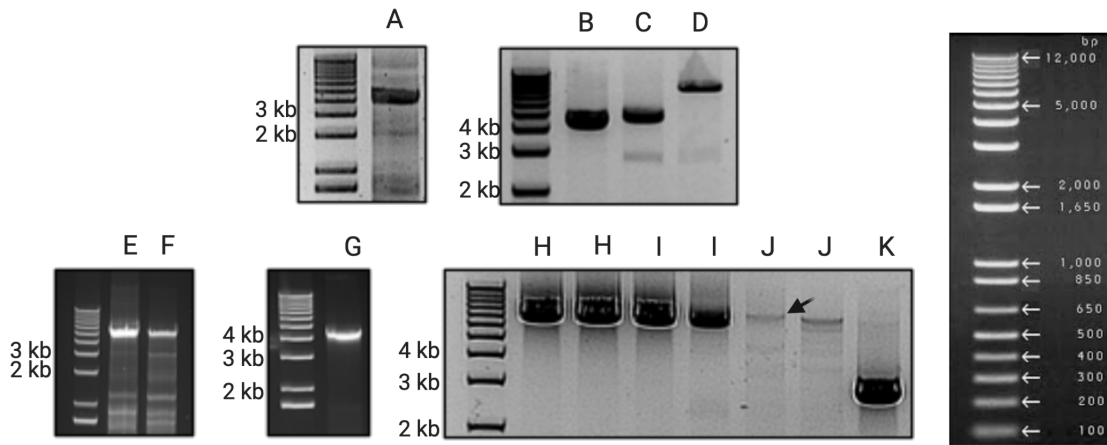


Figure 3.12: Recombinant bacmid PCR confirmation.

Recombinant bacmid DNA formed by transposition of individual or a combination of genes from either pFastBac1 or pFastBac dual donor plasmids to the *AcMPNV* bacmid, transfer of genes of interest confirmed by PCR using binding sites within the recombinant bacmid DNA. Lanes labelled according to recombinant bacmids and approximate band sizes given in Table 3.3. Sizes indicated in kbp on the right and an image of the DNA marker used to the right.

Table 3.3: Combination of genes from donor plasmids used to form the recombinant bacmid

Gene(s)	Plasmid	Label	Approx. size (bp)
PbGyrA	pFastBac dual	A	5700
PbGyrA & PbGyrB	pFastBac dual	B	8500
PfGyrA	pFastBac dual	C	5800
PfGyrA & PfGyrB	pFastBac dual	D	9000
AtGyrA	pFastBac1	E	5000
AtGyrB1	pFastBac1	F	4600
AtGyrB2	pFastBac1	G	4300
AtGyrB1_AtGyrA	pFastBac1	H	7300
AtGyrB1_SSG_AtGyrA	pFastBac1	I	7300
AtGyrA & AtGyrB1	pFastBac dual	J	7900
eGFP	pFastBacHTB	K	3200

The recombinant bacmid DNAs were used to transfect insect cells and generate recombinant virus, which was amplified prior to infection of insect cells for protein expression trials. The titres of recombinant viruses were determined using the baculoQUANT qPCR kit and insect cells of sf9, sf21 and sS9-2 types were infected with recombinant viruses at multiplicities of infections ranging 1-10. The sSf9-2 cell line is specialised for the production of proteins that are toxic or prone to degradation, this is achieved by their adaptation to produce high levels of desired protein shortly after baculovirus infection. The potential degradation of proteins was also addressed by the supplementation of growth medium with protease inhibitors and fetal bovine serum (FBS) as a deterrent. Furthermore, in addition to denaturing protein gels and western blots to identify potential proteins of interest from partially purified insect cell lysates, these fractions were also occasionally tested in topoisomerase activity assays.

Unfortunately, despite a large investment in terms of both time and effort, the expression of codon optimised sequences of gyrases from all three species, *P. falciparum*, *P. berghei* and *A. thaliana* produced extremely limited favourable outcomes.

3.1.2.3. Plasmodium gyrase expression

The expression of *P. falciparum* and *P. berghei* GyrA subunits alone and their co-expression with respective GyrB subunits was tested. Unfortunately, despite varying the length of expression from 24 to 72 hours and infecting cells at multiplicities of infection (MOI) of 1, 2, 5 and 10 no unambiguous expression of any gyrase subunits, considered worth pursuing, were identified by protein gels or western blots. Nevertheless, partially purified cell lysates were tested in topoisomerase activity assays, including supercoiling and relaxation. However, the latter assay was found to be inappropriate due to the cell lysates of insect cells alone possessing relaxation activity in the same conditions, plausibly due to topoisomerase I activity. The lysates corresponding to co-expressed *P. berghei* and *P. falciparum* gyrase did not supercoil DNA.

3.1.2.4. *A. thaliana* GyrB1 is unstable and toxic

The expression of *A. thaliana* GyrB1 was assessed in a variety of ways: expression of the subunit alone through the generation of a monocistronic bacmid, co-transfections of cells with a combination of monocistronic GyrA and monocistronic GyrB1 bacmid, co-expression using a polycistronic bacmid encompassing GyrA and GyrB1 coding regions, and finally monocistronic bacmids corresponding to GyrB1_GyrA fusions as a single

polypeptide with and without an SSG linker between the subunits, GyrB1_GyrA or GyrB1_SSG_GyrA, respectively.

The expression was tested at MOIs ranging 1-10, using insect cells Sf9, Sf21 or sSf9-2 and for various lengths of expression. Despite this, recombinant GyrB1 protein could not be purified. Nevertheless, meaningful observations were made during efforts of expression. Interestingly, when insect cells of all lines, Sf9, Sf21 and sSf9-2 were transfected for the production of GyrB1, the cells manifested the usual characteristics of successful transfection including increased cell size and nuclei, granulated appearance, reduced number of cells in comparison to the negative control of uninfected cells (as virus infection leads to the cessation of cell division) but with the additional appearance of dark cells, plausibly indicating cell death (Figure 3.13a). Additionally, the transfection of cells with GyrB1 fused to a cleavable GFP marker and a C-terminal histidine tag, identified degradation products corresponding to the size of GFP when probed with anti-histidine antibodies, implying that the full-length GyrB1 protein was expressed but N-terminally degraded (Figure 3.13b). Furthermore, transfection of insect cells with GyrB1_GyrA bacmid, to generate the P₀ recombinant virus led to the expression of the fusion polypeptide, this was confirmed by mass spectrometry (Figure 3.13b). Unfortunately, subsequent transfection of insect cells with the generated P₀ virus or succeeding virus amplifications did not reproduce the same result despite varied length of expression or re-transfection of cells. The specific observations outlined for GyrB1 transfected cells imply that the protein is only produced transiently albeit its production is toxic and subject to the action of cellular proteases for degradation. The extrapolation of these reflections upon the *in vivo* production of the protein in its natural plant environment is environment is an intriguing prospect.

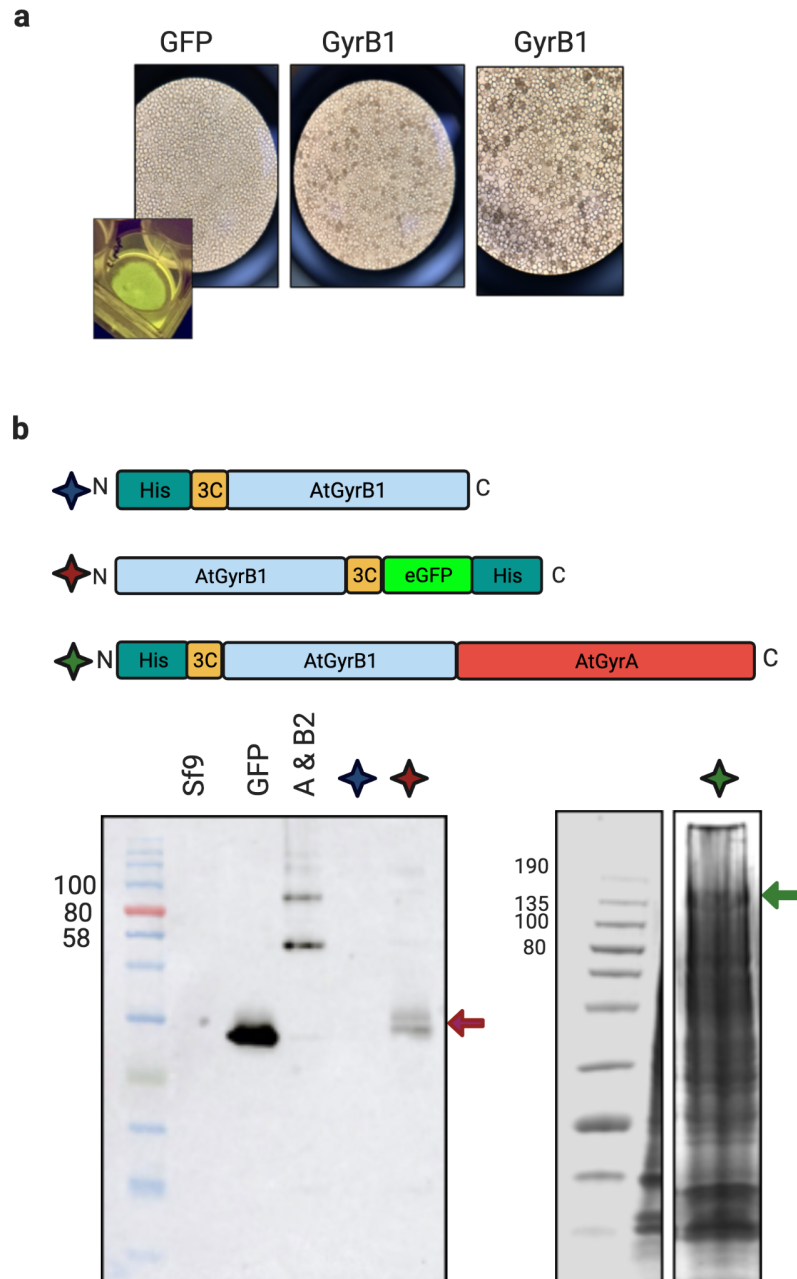


Figure 3.13: *A. thaliana* GyrB1 expression.

(a) Insect cells transfected with GFP (inset shows confirmed expression of GFP protein) retained similar signs of infection to GyrB1 (~72 kDa) cells including enlarged cell size (and nuclei) and reduced number of cells when compared to the negative control of uninfected cells. The GyrB1 uniquely demonstrated the appearance of dark cells, a feasible result of the toxic GyrB1 production and ultimately early cell death. (b) Left: western blot using anti-histidine antibodies to probe cell lysates of GyrB1 expressed clones with N-terminal (blue star) or C-terminal (red star) histidine tags. The red arrow indicates degradation products detected with the C-terminally tagged clone. Right: denaturing protein gel exhibiting GyrB1_GyrA fusion peptide (~175 kDa) confirmed by mass spectrometry (green star and arrow).

3.1.2.5. *A. thaliana* GyrA expression

The sSf9-2 cell line, which has been adapted for the expression of highly toxic and unstable proteins by offering high-level expression over a reduced period of time subsequent to baculovirus infection; exclusively enhanced the expression of *A. thaliana* GyrA but was unable to offer the same result for GyrB1 and *Plasmodium* gyrase genes. The sSf9-2 cells were infected at MOIs of 3,5,7 and 10 for ~60 hours. Expression at a MOI of 3 did not produce any GyrA protein, in contrast to the result obtained at the other MOIs tested (expected GyrA peptide size ~100 kDa) (Figure 3.14). Furthermore, western blot analysis using antibodies probing the histidine tag of the GyrA peptide did not identify any degradation of GyrA, although potential GyrA dimers can be identified.

The sSf9-2 cell line was propagated without supplementation of FBS or addition of antibiotics. Notably, the culturing of this cell line was inherently more difficult than sf9 or sf21. The cells grew comparatively better in adherent layers as compared to suspension cultures but were exceptionally difficult to maintain at high viability and re-establish from glycerol stocks.

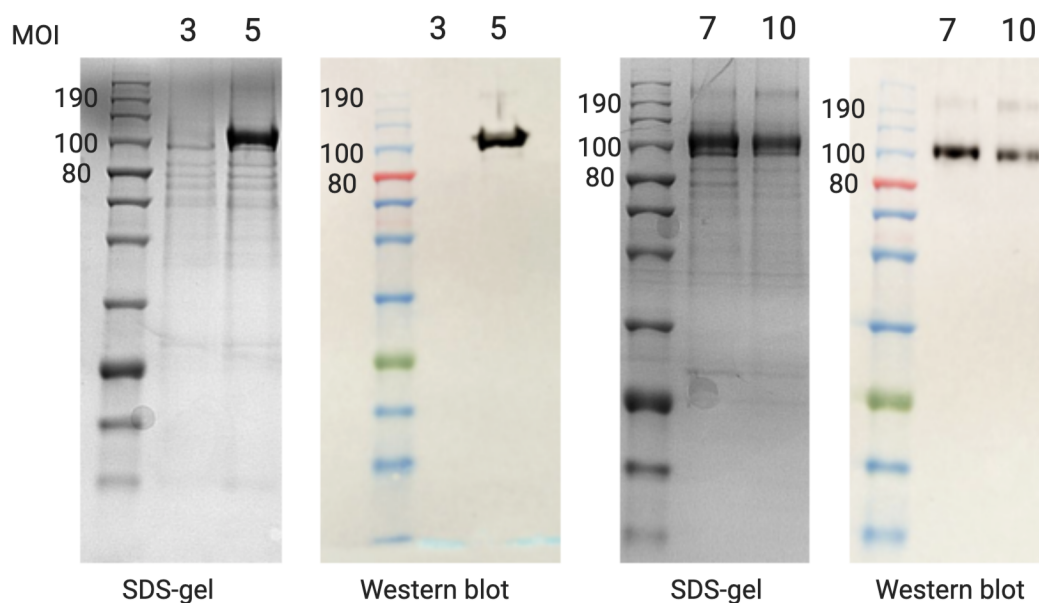


Figure 3.14: *A. thaliana* GyrA infection of sSf9-2.

Expression of GyrA (~ 100 kDa) within the sSf9-2 cell line at MOIs as given above each lane. Western blots were performed using anti-histidine antibodies. Protein marker sizes in kDa.

3.1.2.6. Individual GyrA and GyrB2 subunit expression

The codon optimisation of GyrA significantly increased expression of the protein subunit at a range of MOIs (section 3.2.3.5). The non-codon optimised GyrB2 transfection could not be significantly improved despite testing at various MOIs. In the absence of a viable and healthy sSf9-2 cell line at the time, sf9 cells were infected individually with codon optimised GyrA using a monocistronic bacmid and GyrB2 using the pOPIN system at MOIs of 7. The gyrase A and B2 subunits were separately purified from large scale transfections prior to the reconstitution of the active GyrA₂B₂ heterotetramer. However, no supercoiling activity from the reconstituted gyrase could be detected, despite confirmation of expression and purification of subunits (Figure 3.15).

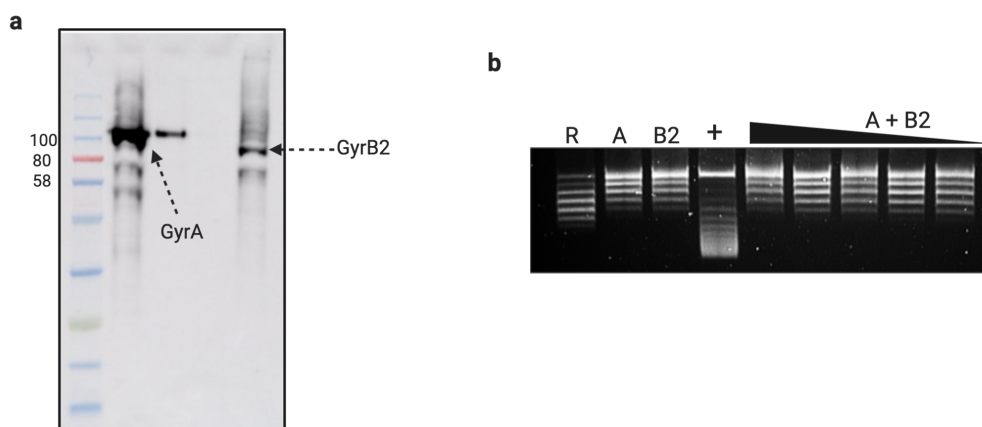


Figure 3.15: Individual expression of *A. thaliana* GyrA and GyrB2.

(a) Western blot analysis using anti-histidine antibodies to probe GyrA transfected cells and GyrB2 transfected cells individually. (b) DNA supercoiling assay using individually expressed and purified GyrA and GyrB2 subunits (A+B2). R: relaxed substrate, A: GyrA only, B2: GyrB2 only, +: positive control of GyrA&GyrB2 co-expressed. Expected sizes: GyrA: ~100 kDa, GyrB2: ~72 kDa.

3.1.3. *Nicotiana benthamiana* expression

In addition to baculovirus-mediated infection of insect cells and somewhat a result of the inability of the system to provide an efficient and reproducible method for *Arabidopsis* gyrase production; an alternative expression system was explored. The alternate system selected was transient expression in *Nicotiana benthamiana*. The selected host system and target protein are both members of the plant kingdom, rationally they may therefore have commonalities in their processes of protein expression and regulation that could promote the heterologous expression of *A. thaliana* gyrase. The gram-negative pathogenic soil bacterium, *Agrobacterium tumefaciens*, is naturally able to mediate the transfer of a fragment of its own genome, T-DNA, to the host plant where the transferred T-DNA segment is incorporated. This feature is exploited to achieve transient expression within *N. benthamiana* (Gelvin 2003; Tzfira and Citovsky 2006). The transient expression system selected for this work is founded on the pEAQ series of expression vectors which utilise a modified, non-replicating version of the Cowpea mosaic virus (CPMV-HT) to drive expression (Sainsbury et al. 2009)

Notably, the transient expression of *A. thaliana* gyrase has formerly been attempted by previous members of the Maxwell group. At the time these attempts were unsuccessful, however subsequently there have been considerable developments in the pEAQ expression system to enhance protein expression. One such adaptation used here, is the implementation of pHREAC, a binary transient expression vector based upon the pEAQ vectors but incorporating a modified synthetic 5' UTR in combination with the 3' UTR of CPMV to enhance the yield of recombinant protein produced (Peyret et al. 2019).

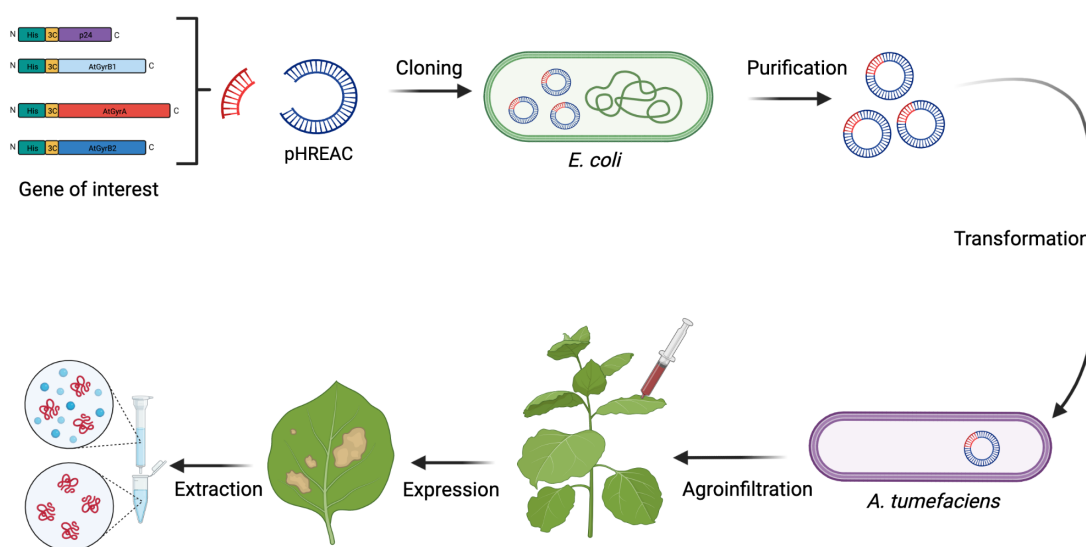


Figure 3.16: Summary of *N. benthamiana* transient expression.

A. thaliana gyrase A, B1 and B2 genes were cloned individually into pHREAC, in a manner that resulted in N-terminal hexa-histidine fusions to the polypeptide of each gene. A positive control construct encoding the p24 protein of the human immunodeficiency virus (HIV), a gift from Dr. Hadrien Peyret, was also included and tested for expression in *N. benthamiana* (Figure 3.16). A further advantage of the pEAQ-derived vectors was drawn upon for the co-expression of gyrase subunits (GyrA&B1 and GyrA&B2), by mixing of the appropriate independent *A. tumefaciens* cultures prior to infiltrating leaves; thus allowing the production of each separate subunit in the infected cells. This is especially significant bearing in mind the importance of subunit co-expression revealed during baculovirus mediated infection. The expression of gyrase subunits was initially propagated in *N. benthamiana* for a period of 8, 9 and 10 days, prior to protein extraction and purification; however, unfortunately, no expression of *A. thaliana* gyrase was detected (Figure 3.17). This was followed up by analysing expression from as early as 3 days post-infiltration, but the result remained unchanged (data not shown).

The pEAQ expression vectors have been implemented in production of proteins in tobacco cell cultures, the production of human serum albumin in transgenic tobacco Bright Yellow-2 (BY-2) suspensions is a specific example of this (Sun et al. 2011). The expression of *A. thaliana* gyrase was assessed in BY-2 suspension cultures; however, preliminary results were unable to detect protein expression of any gyrase subunit.

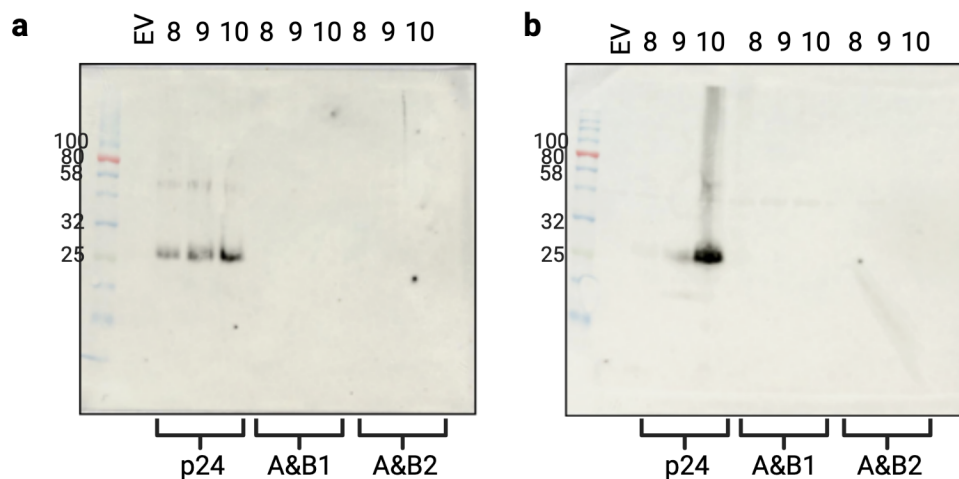


Figure 3.17: Transient *N. benthamiana* expression.

Western blot analysis using histidine targeted antibodies following agroinfiltration of *N. benthamiana* plants with p24, GyrA&B1 or GyrA&B2 (as labelled), followed by protein extraction and purification of soluble protein (a) and corresponding pellets (b). Lane labels: EV: empty vector (pHREAC), the numbers indicate the expression length in days. Expected sizes: p24: 24 kDa, GyrA: ~100 kDa, GyrB2: ~72 kDa. Marker: NEB colour prestained broad range (sizes in kDa).

3.2. Discussion

Three independent host systems have been used to explore the heterologous expression of eukaryotic gyrases. In the case of *Arabidopsis thaliana*, extensive foundation work for the expression of all three of the protein subunits: GyrA, GyrB1 and GyrB2 has been conducted by previous and current members of the Maxwell group. However, despite comprehensive optimisation efforts within *E. coli*, the expression of GyrA and GyrB1 did not prove possible; although GyrB2 purification was possible, the subunit either possessed intrinsic cleavage activity or was accompanied by contaminating nucleases (Figure 3.8). Nevertheless, preliminary expression trials at the start of this project were conducted in *E. coli* but did not generate any justifiable leads worth pursuing (results not shown). Perhaps more interesting is the expression of *Plasmodium falciparum* gyrase in *E. coli*, particularly considering previous reports in the scientific literature of expression of *P. falciparum* GyrB (Dar et al. 2007). In the work of this thesis, the *E. coli* expression of *Plasmodia* gyrase was supplemented by the inclusion of the hitherto unexplored *P. berghei* gyrase. Unfortunately, no GyrA expression from either *Plasmodia* species was detected. In contrast, limited levels of GyrB protein were detected for both species by western blots, but the quantities of overexpressed protein did not warrant further purification.

Prior to the start of this work, the expression of *A. thaliana* gyrase, comprising GyrA and GyrB2 subunits, had been successfully achieved through the use of the baculovirus expression system (Evans-Roberts et al. 2016). Therefore, the baculovirus expression system was selected as an intriguing alternative method for comprehensive expression efforts of not only *A. thaliana* gyrase but also *Plasmodia* gyrases.

The efforts to express plasmodial gyrase proteins of *P. falciparum* and *P. berghei* in insect cells were unsuccessful. The transposition of *Plasmodia* gyrase genes to form recombinant bacmid DNA was confirmed by PCR, as was the generation of virus particles. Unfortunately, however, no full-length subunits of gyrase were identified despite codon-optimization of sequences to alleviate metabolic burden within the host cells. Additionally, no signs of toxicity or premature cell death of the host cells were observed, rather the cells exhibited positive signs of transfection mirroring those observed upon transfection for the production of GFP. Plausibly, despite infection of insect cells with plasmodial constructs, the transcription of the genes may be problematic. Although there are reports of the implementation of baculovirus mediated infection that successfully alleviated expression of *Plasmodia* proteins found to aggregate within inclusion bodies during overexpression in *E. coli*, the same result was not obtained here for expression of gyrase genes (Mehlin et al. 2006). The expression of *Plasmodia* gyrases is no doubt complex. It is difficult to

ascertain whether heterologous expression complications arise due to an inherent feature of the protein or is consequential of its natural targeting to the apicoplast. Plausibly, an essential factor for protein transcription or translation, or the regulation of either process, may not be provided by the foreign expression host; for example, the absence of an apicoplast specific co-chaperonin, *cpn20*, that may be required for the correct folding of the protein (Vitlin Gruber et al. 2013). The high AT content of the *Plasmodia* genome, discussed previously (section 1.8.3.1), formed the rationale for codon optimisation of the *Plasmodia* gyrase proteins prior to heterologous expression. The vast majority of *Plasmodia* species contain insertions within their genes when compared to homologous proteins from other species, *P. falciparum* gyrase included. Often, these insertions correspond to low complexity regions (LCRs), characterised by single amino acid repeat sequences. LCRs have been implicated in immunological responses and co-factor binding, however, an additional function of these regions has been proposed as tRNA sponges that effectively slow down the process of translation to facilitate co-translational folding (Clarke et al. 2003; Frugier et al. 2010; Newbold 1999; Reeder and Brown 1996). Presumably, in the absence of these regions, efficient co-translational folding of *Plasmodia* gyrases is not possible and the misfolded protein is targeted for degradation. A related *Apicomplexa* species to *Plasmodium* is *Toxoplasma gondii* that is responsible for toxoplasmosis. *Toxoplasma gondii* also possesses a nuclear encoded apicoplast targeted gyrase that has been characterised to possess supercoiling activity and a particularly efficient decatenation activity (Lin et al. 2015). This is fascinating when the apicoplast genome arrangement of *T. gondii* and *P. falciparum* are compared. The former maintains more than 90% of the 35-kbp apicoplast DNA as linear concatemers, whilst circular genomic forms only account for ~9% of the total mass of DNA. In contrast, the apicoplast DNA of *P. falciparum* is overwhelmingly circular in topology with only ~3% accounting for linear forms (Sato 2011; Williamson et al. 2001; Williamson et al. 2002). Therefore, considering the predominantly circular form of the *P. falciparum* gyrase, it may be hypothesised that the enzyme would maintain a more efficient supercoiling activity in comparison to *T. gondii* gyrase.

The *Arabidopsis thaliana* DNA gyrase expression was achieved by co-transfection of insect cells with linearised AcMPNV bacmid DNA and independent monocistronic plasmids encoding GyrA and GyrB2. Moreover, the transfection of insect cells with monocistronic bacmid clones of GyrA or GyrB2, followed by the reconstitution of these subunits *in vitro* was unable to form an enzyme active for supercoiling. Furthermore, despite extensive efforts towards the expression of the alternative *A. thaliana* gyrase

enzyme, formed by the association of GyrA and GyrB1, this did not prove possible. Interestingly however, the synthesis of GyrB1 was confirmed within insect cells. Unfortunately, phenotypes of infected cells indicated toxicity upon infection and the resultant peptide was unstable and promptly degraded.

The inability of *in vitro* reconstituted *A. thaliana* gyrase to actively supercoil DNA is an irregular finding. The DNA gyrase enzymes of bacterial species form active heterotetrameric enzymes when the separate subunits are combined *in vitro*. An intriguing possibility is that *A. thaliana* gyrase requires expression of both GyrA and GyrB2 subunits (co-expression) within the same cell. Unfortunately, at the current time there has been little research of the molecular details of multiple baculovirus-infection upon insect cells. The co-transfection of insect cells with monocistronic GyrA and GyrB most likely produces a heterogenous cell culture consisting of individual cells expressing GyrA only, GyrB2 only, or both GyrA and GyrB2. It is not possible to conclude from this evaluation if only cells co-transfected with GyrA and GyrB2 produce active supercoiling enzyme. The co-expression of an individual insect cell with both GyrA and GyrB2 can be insured by use of a polycistronic expression vector, such as pFastBac dual, that expresses both GyrA and GyrB2 from individual promoters. Alternatively, although less ideal, a monocistronic clone of the GyrB2_GyrA fusion could be used. Unfortunately, despite multiple attempts, it did not prove possible to generate the required constructs in *E. coli*. Somewhat contradictorily, the generation of a polycistronic clone of GyrA and GyrB1 was achieved, although the expression of GyrB1 itself has previously been noted to be toxic to *E. coli* and this study confirmed the same to be true of GyrB1 expression within insect cells. Nevertheless, the detection of a GyrB1_GyrA fusion protein is a novel discovery and to date the only successful *in vitro* GyrB1 expression. Indeed, the co-transfection, co-expression or a combination of both can have a significant impact on the production of recombinant protein in the cell.

The generation of active gyrase enzyme although possible through baculovirus mediated transfection, has not proved to be consistently reproducible. The expression of GyrA frequently proved more problematic than GyrB2 and for this reason, the sequence of GyrA was codon optimised. The codon optimisation of GyrA resulted in increased and consistent expression of the protein, an optimum MOI of 7 was identified; notably, an MOI of 3 was ineffective. Additionally, the sSf9-2 background abrogated the degradation of GyrA. The assembly of gyrase by association of monocistronic GyrA and GyrB2, expressed and purified individually, did not form an active supercoiling enzyme. This is an unexpected result particularly considering that the gyrase of bacterial species including *E.*

coli form an active enzyme *in vitro* when expression and purification of the subunits are carried out by a parallel method. There are several possibilities to consider for the lack of supercoiling by the adjoining of the *A. thaliana* gyrase subunits. It is possible that the active *A. thaliana* gyrase requires the co-expression of both GyrA and GyrB2 subunits for the formation of an active enzyme. The requirement for co-expression may be due to the formation of stable GyrA homodimers and GyrB2 homodimers that subsequently are unable to form active heterotetramers upon mixing of individual subunits; similar observations have been made for the formation of protein complexes (Kümmel et al. 2006; Kümmel et al. 2005) . Alternatively, it is also possible that the codon optimised GyrA protein although produced at elevated levels, is incorrectly folded due to improper co-translational folding and hence inactive.

The expression of *A. thaliana* gyrase was also tested by transient expression of *N. benthamiana* using genetically modified agrobacterium carrying expression cassettes for gyrase genes. However, despite varying parameters, including the co-expression of GyrA with GyrB1/GyrB2, no evidence of protein expression was obtained. Preliminary experiments using cultured BY-2 cells did not provide any indication of gyrase expression. The BY-2 cultured cells however are undifferentiated cells that lack biochemical compartments and particular metabolic pathways and may therefore be more suited for the investigation of regulatory elements that are constitutively required, contrary to the requirement/expression of DNA gyrase *in vivo* (discussed later in Chapter 5). The failure of agrobacterium-mediated transient expression of *N. benthamiana* is more perplexing. Plausibly, the expression of foreign gyrase genes overburdens the infected plant host due to their significant size, or the peptides are promptly targeted by intracellular proteases. The transient expression of gyrase was explored with constructs that lacked any signal peptides, however, in view of the organellar targeting of gyrase within *A. thaliana*, the addition of targeting sequences, either those of the natural *A. thaliana* or corresponding sequences of the *N. benthamiana* host, may be a reasonable successive approach to probe the expression of gyrase.

3.3. Conclusions

Although gyrase is targeted to organelles of bacterial ancestry within both eukaryotic species, *Plasmodia* and *A. thaliana*; the expression of the protein has revealed to be much more involved when compared to homologous proteins within bacterial species. The expression of gyrase here has been attempted using three different expression hosts, *E. coli*, *S. frugiperda* and *N. benthamiana*, in addition to optimisation efforts of expression parameters. The gyrase proteins of *Plasmodia* have been more challenging to express, in comparison to *A. thaliana*, albeit proteins of both species have demonstrated instability and host toxicity. Nevertheless, the expression of *A. thaliana* gyrase through baculovirus mediated transfections of insect cells remains unchallenged for the production of active gyrase.

3.4. Future Work

In view of the successful expression of *Arabidopsis* gyrase through baculovirus mediated transfections of insect cells and the production of active gyrase protein, further investment within this system is warranted. However, future work should focus on optimisation parameters that have not been covered in the present study due to time limitations. An unexplored avenue is the time of infection (TOI) of cells. This phenomenon is expressed as the period from inoculation of cells prior to transfection and is a vital determinant for expression as it encompasses several environmental factors of the culture including the conditions of cells, the cell density and availability of nutrients; all of which can affect the reproducibility of expression. To complement this, the co-infection of cells using either monocistronic or polycistronic, or both types of viruses, can be staggered. The complex process of baculovirus infection can be monitored by tracking levels of transcripts through RT-qPCR; this may be particularly useful for obtaining information regarding the expression of *Plasmodia* gyrase proteins and the unstable GyrB1 protein. Otherwise, the use of an alternative eukaryotic expression system such as yeast, may prove to be beneficial for the expression of the specific gyrase proteins attempted here.

Chapter 4: In vitro characterisation of *A. thaliana* gyrase

4.1. Introduction

Topoisomerases possess the ability to perform a plethora of manipulations to modulate and maintain DNA topology in a manner appropriate for the conservation and duplication of genetic information. Often, a single topoisomerase enzyme is capable of performing multiple DNA manipulations. The reactions of DNA gyrase that are characteristically assayed *in vitro* include supercoiling, relaxation and decatenation. Interestingly however, the competence of gyrase to mediate the characteristic reactions is not uniform for all enzymes, but instead differs in a species-specific manner. Critically, even for a gyrase enzyme of a given origin, the propensity to mediate the different topological reactions varies in accordance with assay conditions. Plausibly, this is a reflection of the diverse *in vivo* conditions in which gyrase proteins are required to function in different species.

Thus far, *A. thaliana* gyrase has been reported to successfully supercoil DNA *in vitro* (Evans-Roberts et al. 2016). Beyond this however, the enzymatic reactions and their efficiency remain unexplored. Therefore, after the successful expression of *A. thaliana* gyrase comprising GyrA and GyrB2 (discussed in Chapter 3), comprehensive *in vitro* characterisation of the enzyme activity was carried out. The objective of the work described in this chapter is to explore and confirm the potential of *A. thaliana* gyrase to conduct DNA relaxation and decatenation. The optimum conditions for DNA supercoiling are established and related to conditions for the other gyrase reactions. On a broader scale, the activity of *A. thaliana* gyrase is compared to gyrase enzymes from other species. Finally, in addition to the characterisation of enzyme activity, the potential of *A. thaliana* gyrase for inhibition by quinolone compounds is explored, laying the groundwork for development of potential herbicidal compounds.

4.2. Results and discussion

4.2.1. *Arabidopsis thaliana* gyrase supercoiling is dependent on high concentrations of potassium glutamate

The activity of *A. thaliana* gyrase, formed by the association of GyrA and GyrB2, has previously been reported (Evans-Roberts et al. 2016). The gyrase complex was confirmed to successfully introduce negative supercoils into the relaxed substrate DNA in a ciprofloxacin-sensitive manner (Evans-Roberts et al. 2016). The enzymatic supercoiling activity occurred in an assay buffer comprising 50 mM Hepes.KOH (pH 7.9), 6 mM magnesium acetate, 4 mM DTT, 1 mM ATP, 100 mM potassium glutamate (KGlu), 2 mM spermidine and 0.05 mg/mL albumin. The assay conditions can undoubtedly favourably or unfavourably affect the *in vitro* activity of enzymes. Indeed, the characterisation of gyrase enzymes from different bacterial species have required the adjustment of assay parameters to achieve activity; this is a likely consequence of the evolutionary distances of the enzymes and their adaptation to the physiological conditions in which they are required to function. The evolutionary acquisition of each gyrase gene by *Arabidopsis* has previously been explored by Wall and colleagues (Figure 4.1) (Wall et al. 2004). The environment of *A. thaliana* gyrase, specifically within the chloroplast and mitochondria, is likely distinctive from the surrounding environment of bacterial gyrase proteins. Therefore, this necessitated the systematic optimisation of *A. thaliana* gyrase supercoiling activity *in vitro*.

A typical *in vitro* supercoiling assay involves incubation of gyrase with 0.5 μg (6 nM) of relaxed pBR322 plasmid DNA (substrate) at 37°C, for a duration of 30 minutes in a volume of 30 μL ; after which, the reaction is terminated and the gyrase dissociated from bound substrate DNA by mixing with chloroform:isoamyl alcohol (Germe et al. 2018b). The mixture of treated DNA is then subjected to gel electrophoresis to separate the different topoisomers of DNA, from relaxed to supercoiled. The supercoiled topoisomers are increasingly compacted and therefore travel faster during electrophoresis relative to relaxed topoisomers that have more open conformations. The assay optimisation process requires manipulations of standard enzyme conditions, involving the use of enzyme concentrations achieving only partial supercoiling, time course experiments and temperature manipulations in order to assess the impact of these variables on gyrase supercoiling.

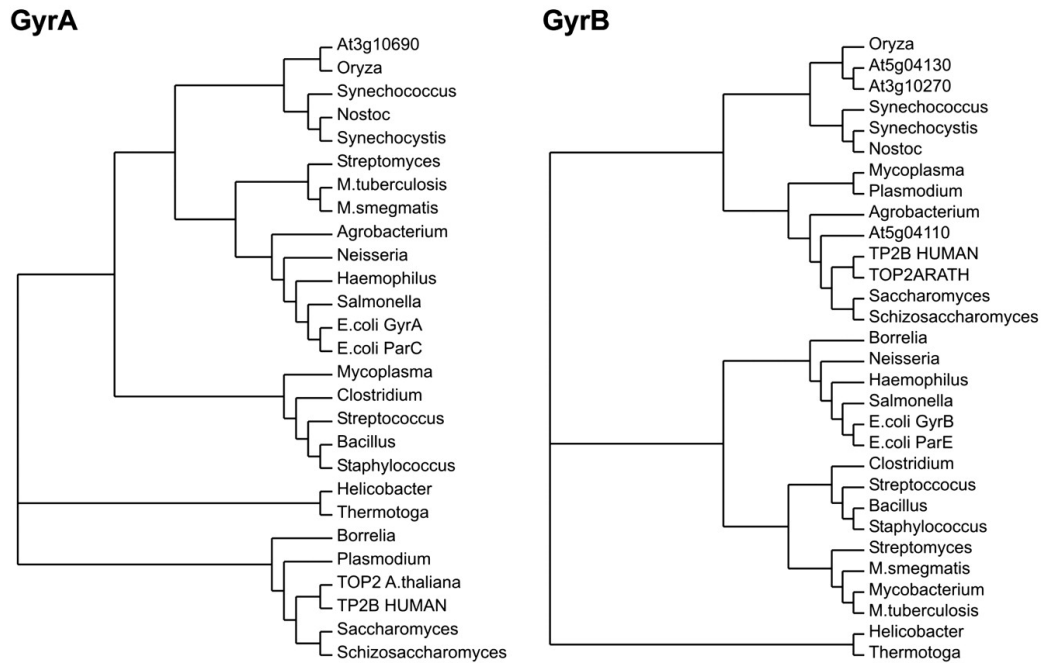


Figure 4.1: *A. thaliana* gyrase phylogeny.

The phylogenetic relationship of *A. thaliana* GyrA (At3g10690), GyrB1 (At3g10270) and GyrB2 (At5g04130) protein sequences to other gyrases and type II topoisomerases. Figure adapted from (Wall et al. 2004).

The optimisation involved assaying of the topoisomerase activity in a variety of commercial assay buffers from Inspiralis (UK), including *E. coli*, *M. tuberculosis* and *Staphylococcus aureus* (*S. aureus*) (Figure 4.2). The *E. coli* gyrase enzyme was assayed in all three commercial buffers in parallel to *A. thaliana* gyrase. The *E. coli* enzyme had strongest activity in *E. coli* assay buffer, followed by *M. tub* and *S. aureus*; in fact, the enzyme was unable to supercoil DNA in *S. aureus* buffer, this signifies the importance of assay optimisation. In contrast to *E. coli*, the activity of *A. thaliana* gyrase was strongest in *S. aureus* buffer, followed by *M. tub* and weakest in *E. coli* assay buffer. Interestingly, upon inspection of the commercial buffers, it became evident that a varying component between the buffers that correlated positively with *A. thaliana* gyrase supercoiling activity was potassium glutamate (KGlu). To directly explore the effect of KGlu concentration on the supercoiling activity of *A. thaliana*, the enzyme activity was assayed in buffers with varying amounts of KGlu. The *A. thaliana* gyrase enzyme was unable to supercoil DNA in the absence of KGlu (Figure 4.3). Indeed, the supercoiling activity of *A. thaliana* gyrase increased linearly with increasing KGlu concentrations up to a concentration of 500 mM KGlu, after which it was difficult to ascertain an increase in supercoiling (Figure 4.3a). However, reducing the concentration of enzyme identified a KGlu concentration of 700-800 mM to be optimum for supercoiling (Figure 4.3b).

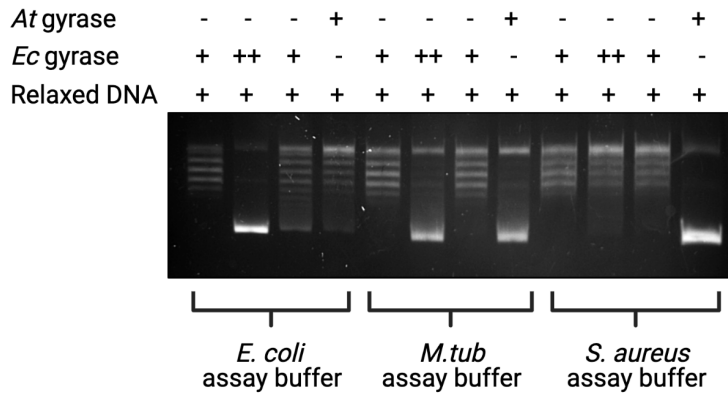


Figure 4.2: Supercoiling assay in different commercial buffers.

Assay carried out at 37°C for 30 mins using relaxed pBR322 (0.5 µg; 6 nM) as substrate, in the commercial buffers indicated. The concentration of *E. coli* gyrase is 4.2 nM (++) or 3.3 nM (+) and *A. thaliana* gyrase (6 nM). The buffer compositions as follows: *E. coli* assay buffer: 35 mM Tris.HCl (pH 7.5), 24 mM KCl, 4 mM MgCl₂, 2 mM DTT, 1.8 mM spermidine, 1 mM DTT, 6.5% glycerol and 0.1 mg/mL albumin; *M. tub* assay buffer: 50 mM Hepes. KOH (pH 7.9), 6 mM magnesium acetate, 4 mM DTT, 1 mM ATP, 100 mM KGlu, 2 mM spermidine, 0.05 mg/mL albumin and *S. aureus* assay buffer: 40 mM Hepes. KOH (pH 7.6), 10 mM magnesium acetate, 10 mM DTT, 2 mM ATP, 500 mM KGlu, 0.05 mg/mL albumin.

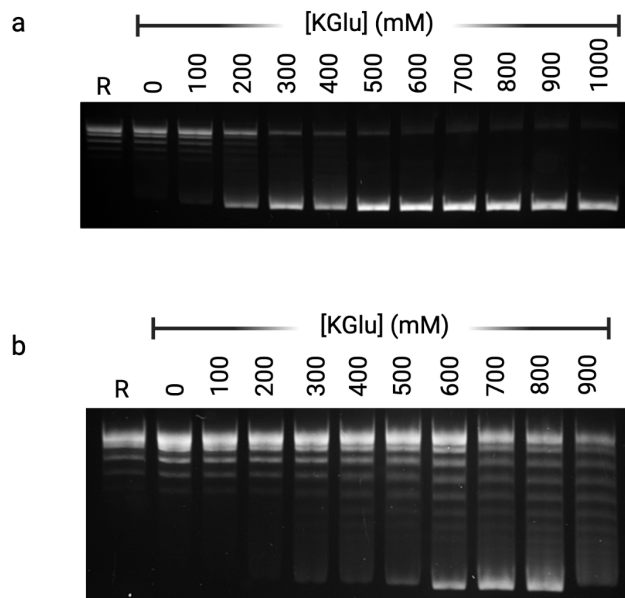


Figure 4.3: *A. thaliana* gyrase supercoiling in response to KGlutration.

The supercoiling assay buffer consisted 40 mM Hepes. KOH (pH 7.6), 10 mM magnesium acetate, 10 mM DTT, 2 mM ATP, 0.05 mg/mL albumin and a titration of 0-1000 mM KGlu. *A. thaliana* gyrase concentration 6 nM (a) and 3 nM (b) R: relaxed pBR322 DNA.

The immobile nature of an *Arabidopsis* plant compels it to adapt efficiently to its environment. Temperature not only acts as a seasonal cue for plants, but it is recognised to effect various biological phenomena, including enzyme activity (Sakamoto and Kimura 2018). Therefore, the supercoiling activity of *A. thaliana* gyrase was investigated at 25°C, 30°C and 37°C and at two concentrations of K₂Glu, in order to determine potential temperature dependence of the enzyme (Figure 4.4). The effect of temperature upon *A. thaliana* gyrase supercoiling activity was determined to be insignificant beyond that due to a natural elevation caused by increased enzyme kinetics (Figure 4.4a); the activity of most enzymes is found to increase more than 50% in accordance with a 10°C rise in temperature. The inclusion of 700 mM K₂Glu favoured supercoiling activity (Figure 4.4b). Therefore, assays were routinely carried out at 37°C to allow direct comparison with gyrase supercoiling of bacterial species.

Another parameter investigated was pH; often the surrounding pH has been demonstrated to impact the shape and activity of enzymes. To investigate the optimum pH range of *A. thaliana* gyrase the enzyme activity was assayed in HEPES and Tris based buffers at a range of pHs; the optimum conditions were confirmed through time course experiments to involve a Tris.HCl buffer of pH 8-8.5. The *E. coli* gyrase supercoiling activity is enhanced by the addition of spermidine within assaying conditions, the polyamine, which is abundant within bacteria, has been identified to increase negative DNA supercoiling specifically within *E. coli* (Gellert et al. 1976). However, the addition of spermidine had no effect upon supercoiling mediated by *A. thaliana* gyrase (data not shown) and it was therefore omitted from the assay. Polyamines are widely distributed in eukaryotic and prokaryotic cells. In higher plants, polyamines mainly comprise putrescine, spermidine and spermine; collectively, these are involved in the regulation of plant physiological responses (from embryogenesis to senescence) and are involved in biotic and abiotic stresses (Chen et al. 2019). Polyamines that are free within plants are found to be protonated and positively charged at physiological pH and can therefore form covalent interaction with acidic proteins and nucleic acids (Igarashi and Kashiwagi 2015). Although the addition of spermidine did not enhance the activity of *A. thaliana* DNA gyrase *in vitro* this may be because the enzyme is sensitive to fluctuations in the levels of one of the other polyamines (i.e., putrescine or spermine). The species-specific polyamine preference for stimulation of gyrase has been demonstrated in the case of *E. coli* and *Salmonella Typhimurium* (Duprey and Groisman 2020).

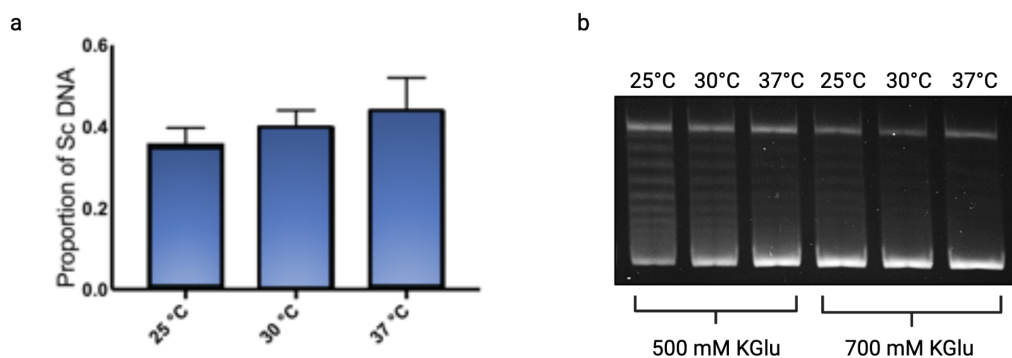


Figure 4.4: Response of *A. thaliana* supercoiling in response to different temperatures.

The supercoiling activity of *A. thaliana* gyrase was assayed at 25°C, 30°C and 37°C (a) in assay buffers with 500 mM KGLu and 700 mM KGLu (b) (remaining assay conditions as for Figure 4.3). Error bars represent standard error of the mean.

The conditions eventually defined for optimal supercoiling activity of *A. thaliana* gyrase were 40 mM Tris.HCl (pH 8.5), 10 mM magnesium acetate, 10 mM DTT, 2 mM ATP, 800 mM KGLu and 0.05 mg/mL acetylated albumin. The optimisation parameters improved the enzyme activity and allowed the definition of a unit of enzyme activity (Figure 4.5). One unit of *A. thaliana* gyrase was defined as the quantity of enzyme required to supercoil 0.5 µg of relaxed pBR322 DNA at 37°C, in 30 mins. In a standard 30 µL assay, this corresponded to 12 nM gyrase. Through this optimisation, the activity of *A. thaliana* gyrase was increased four-fold relative to conditions originally investigated by Evans-Roberts *et al.*, (Evans-Roberts *et al.* 2016).

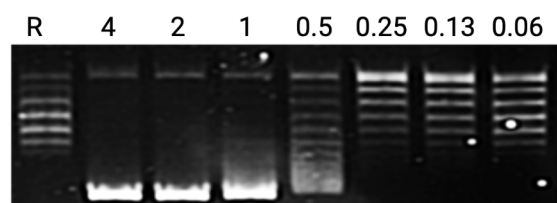


Figure 4.5: Optimum *A. thaliana* gyrase supercoiling.

The supercoiling activity of *A. thaliana* gyrase was assayed under conditions defined as optimum i.e., 40 mM Tris.HCl, 10 mM magnesium acetate, 10 mM DTT, 2 mM ATP, 800 mM KGLu and 0.05 mg/mL acetylated albumin for 30 mins at 37°C. Lanes marked according to units of enzyme activity, where 1 U (12 nM) is defined as the quantity of *A. thaliana* gyrase required to fully supercoil 0.5 µg of relaxed pBR322 DNA at 37°C.

4.2.2. *A. thaliana* gyrase can supercoil with Mg²⁺ or Mn²⁺ as co-factor

The introduction of negative supercoils by gyrase involves transient double-strand DNA breaks. The catalytic cleavage step of a topoisomerase reaction is mediated by nucleophilic attack on the phosphodiester backbone of DNA and requires a divalent metal ion. In the case of bacterial gyrase the *in vivo* metal ion is magnesium; however, other divalent metal ions have been shown to support topoisomerase reactions to varying extents, from full ATP-linked catalytic activity to the cleavage/ligation reactions only (Deweese and Osheroff 2010). *Arabidopsis* chloroplasts and mitochondria incorporate a variety of divalent metal ions, including copper, zinc and manganese (Schmidt et al. 2020; Tan et al. 2010), and thus the ability of these ions to support the supercoiling reaction of *A. thaliana* DNA gyrase was tested.

The optimum supercoiling conditions for *A. thaliana* gyrase include 10 mM magnesium acetate. The supercoiling activity was investigated by substituting the divalent ion in the assay buffer with 10 mM of one of the following: CuCl₂, CoCl₂, CaCl₂, MnCl₂ or ZnCl₂ for a period of 30 min at 37°C. *A. thaliana* gyrase is able to supercoil DNA using either Mg²⁺ or Mn²⁺ as a co-factor to mediate nucleophilic attack upon the phosphotyrosyl-backbone of DNA; no supercoiling is apparent using Cu²⁺, Co²⁺ or Zn²⁺ (Figure 4.6). Furthermore, a titration of either magnesium acetate or manganese chloride revealed no activity with 2 mM of either ion, but similar activity for both in the range 4 mM -14 mM (data not shown).

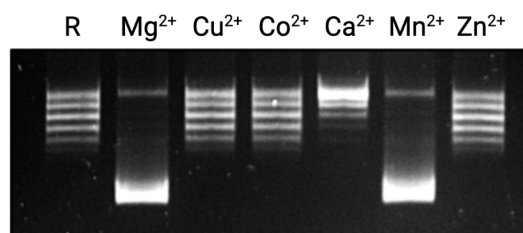


Figure 4.6: *A. thaliana* DNA supercoiling assay with divalent metal ions.

DNA supercoiling assays conducted at 37°C for 30 mins, supported by the chloride salts of the divalent metal ions at 10 mM, as listed above each lane. *A. thaliana* gyrase 1 unit. R: relaxed pBR322.

The use of Ca^{2+} as a co-factor gives a distinct and intriguing result compared to the other metal ions investigated (Figure 4.6). This activity was examined further by reducing the Ca^{2+} concentration to 4 mM and titrating *A. thaliana* gyrase. With 2 units of *A. thaliana* gyrase a shifting of the topoisomerase band pattern from that of the relaxed topoisomers (lane 1) is apparent (Figure 4.7), but the size of this effect appears to decrease with increasing concentrations of enzyme. These results imply that in the presence of 4-10 mM Ca^{2+} , *A. thaliana* gyrase produces a limited amount of negative supercoiling; although, the reaction stoichiometry (2 gyrase per plasmid) suggests that this is less than 2 negative turns per gyrase and therefore likely to be stoichiometric as opposed to catalytic supercoiling. Chloroquine is a DNA intercalator that can insert between the bases of DNA, thereby decreasing the twist (increase the helical repeat) of DNA, the consequence of which is an increase in DNA writhe for covalently closed DNA. The increased DNA writhe is manifested by the conversion of relaxed DNA into positively supercoiled DNA in terms of its behaviour on the gel (as seen in Lane 1 of Figure 4.7b). The sub-stoichiometric negative supercoiling introduced by 2-8 units of *A. thaliana* gyrase is differentiated on the chloroquine gel by its reduced mobility; while from 16-24 U of enzyme, the mobility increases again.

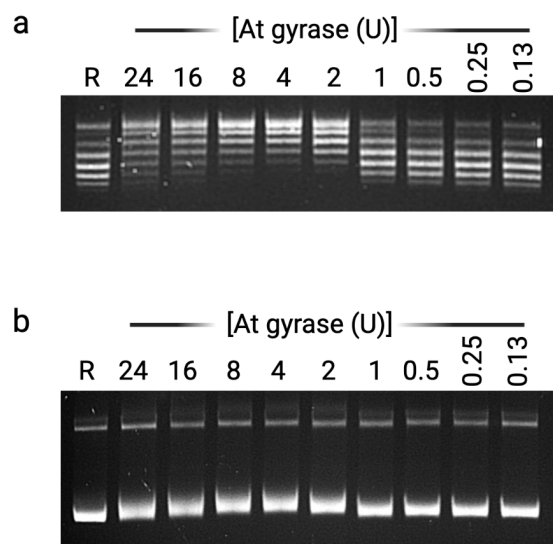


Figure 4.7: *A. thaliana* gyrase supercoiling titration assay with 4 mM Ca^{2+} .

(a) Supercoiling assay with 40 mM Tris.HCl, 4 mM CaCl_2 , 10 mM DTT, 2 mM ATP, 800 mM KGLu and 0.05 mg/mL acetylated albumin for 30 mins at 37°C and quantities of *A. thaliana* gyrase as given above each lane, in units. (b) Assay as in (a) reactions run on a gel with 2 µg/mL chloroquine.

Bates *et al.*, (1996) have reported the stoichiometric supercoiling of DNA in the presence of ADPNP to decrease in efficiency as the substrate DNA becomes more negatively supercoiled (Bates et al. 1996); by extension, the same would be expected of Ca²⁺-mediated stoichiometric supercoiling of *A. thaliana* gyrase. Indeed, the observations at 16-24 units of gyrase (Figure 4.7) are consistent with this, since the addition of an excess of enzyme and subsequent wrapping of DNA will cause a local positive writhe of the DNA, thus making the free DNA more negatively supercoiled. Therefore, Ca²⁺-dependent *A. thaliana* supercoiling becomes counterintuitively less efficient at higher enzyme stoichiometries. Interestingly, the situation of *A. thaliana* gyrase is similar to Ca²⁺-dependent supercoiling of *M. tuberculosis* gyrase observed by Karakare *et al.*, (2012), where an excess of gyrase is required for seemingly non-catalytic supercoiling.

4.2.3. *Arabidopsis thaliana* gyrase DNA relaxation is optimum at intermediate potassium glutamate concentrations

Optimal supercoiling by *A. thaliana* gyrase is dependent on high salt concentrations. The relaxation activity of gyrase is mechanistically distinct from the supercoiling reaction; an important difference is the ATP-independent nature of the reaction. In fact, the reaction can occur in the absence of the ATPase domains of the GyrB subunit. The supercoiling activity of gyrase involves the capture of T-segment DNA by wrapping around the GyrA CTDs, however, the mechanism of T-segment capture for the relaxation reaction does not. In fact, this catalysis is likely to occur by 'bottom-up' transport of the T-segment (Kampranis and Maxwell 1996). Therefore, given the differences in the two activities of the enzyme, this hitherto uncharacterised activity of *A. thaliana* gyrase was explored.

The DNA relaxation assays involved incubation of 0.5 µg supercoiled pBR322 DNA substrate with *A. thaliana* gyrase at 37°C for a period of 30 minutes. An *A. thaliana* gyrase enzyme titration was conducted in a minimal assay buffer lacking ATP and K₂Glu to determine potential relaxation activity; the results confirmed that the DNA relaxation activity of *A. thaliana* DNA gyrase is independent of both and 2-4 units of enzyme were sufficient for complete relaxation (Figure 4.8a). Moreover, to comprehensively investigate the effect of K₂Glu on the *A. thaliana* gyrase relaxation activity, a concentration of enzyme for sub-optimal DNA relaxation was selected to conduct a K₂Glu titration. Interestingly, the relaxation activity of *A. thaliana* gyrase was enhanced in the presence of moderate K₂Glu concentrations of 150-450 mM, however, high concentrations of K₂Glu inhibited the relaxation reaction (Figure 4.8b). Moreover, time-course relaxation experiments confirmed that K₂Glu in the 300-450 mM range was optimum for relaxation (Figure 4.8c).

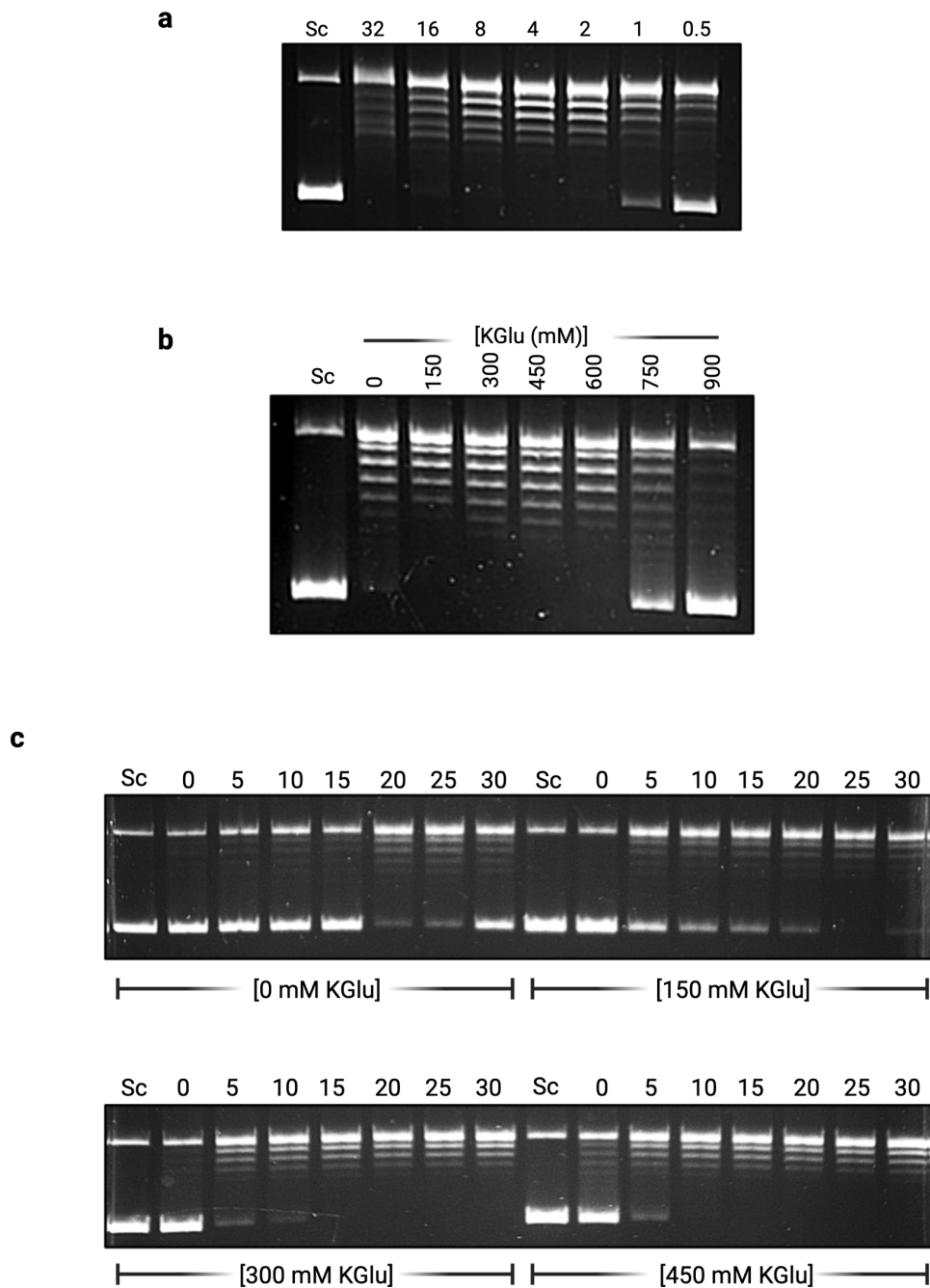


Figure 4.8: *A. thaliana* gyrase relaxation activity.

(a) *A. thaliana* gyrase relaxation of supercoiled pBR322 DNA at varying enzyme concentrations as labelled above each lane in units of enzyme (1 U: 12 nM). (b) *A. thaliana* gyrase (3 nM) relaxation with varying KGlU concentrations, as given above each lane in mM. (c) Time-course relaxation experiments of *A. thaliana* gyrase (1.5 nM) with 0, 150 mM, 300 mM and 450 mM KGlU, lanes labelled according to time of incubation in minutes.

The necessity for strand passage during the DNA relaxation reaction of gyrase involves the generation of transient double-stranded breaks in the G-segment DNA to allow passage of the T-segment DNA, albeit this reaction is conducted “bottom-to-top” for relaxation in contrast to supercoiling (Kampranis and Maxwell 1996). A DNA cleavage assay that allows the determination of enzyme-mediated cleavage in relaxation conditions (i.e., no ATP and supercoiled substrate) involves incubation of gyrase for 60 minutes at 37°C. Following this initial incubation, SDS and proteinase K are added, and the reaction is allowed to proceed for a further 30 minutes to denature and digest away the bound protein from the DNA-protein complex. Subsequent to this, the free DNA is analysed by gel electrophoresis.

The level of DNA cleavage in relaxation conditions incorporating either 800 mM or 350 mM K₂Glu was compared for *A. thaliana* gyrase to assess enzyme mediated cleavage in conditions inhibitory or optimum for relaxation (note: 800 mM is the optimum K₂Glu concentration for supercoiling). *A. thaliana* gyrase possesses enhanced concentration dependent double-stranded DNA cleavage activity at 350 mM K₂Glu as compared to 800 mM (Figure 4.9). Interestingly, at both K₂Glu concentrations single-stranded DNA cleavage is also observed; the latter is likely to be enzyme-mediated, as opposed to nuclease contamination, as it is not observed in supercoiling conditions. These results suggest that intermediate salt concentrations promote double-stranded DNA cleavage of supercoiled DNA.

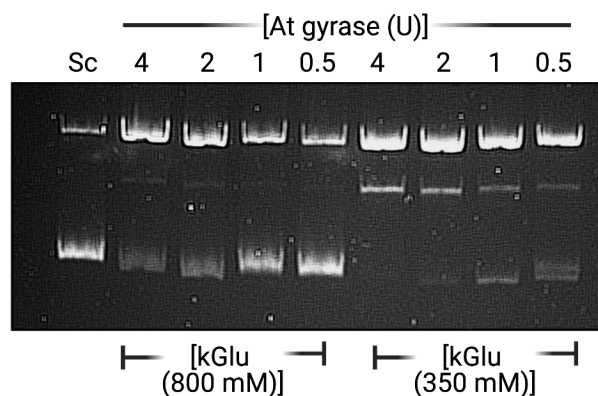


Figure 4.9: *A. thaliana* gyrase DNA cleavage assay.

The intrinsic DNA cleavage activity for *A. thaliana* gyrase was assessed using supercoiled pBR322 DNA in relaxation conditions (i.e., no ATP) with buffers of either 800 mM or 350 mM K₂Glu, at 37°C for 60 mins, prior to addition of SDS and proteinase K. The reaction products were visualised on an agarose gel and stained with 0.5 µg/mL ethidium bromide. Sc: supercoiled DNA; *A. thaliana* gyrase concentrations provided in units of enzyme.

4.2.4. *A. thaliana* gyrase decatenation is independent of potassium glutamate

DNA decatenation is a further reaction catalysed by gyrases and involves the unlinking of catenated DNA circles. The mechanism of action for decatenation differs from supercoiling and relaxation, as the G-segment and T-segment of DNA are located on separate closed-circular DNAs that are juxtaposed, as opposed to the T segment being provided intramolecularly by wrapping of DNA around the CTD in preparation for negative supercoiling; in addition to this, the ATP-dependence of the decatenation reaction, in contrast to relaxation by gyrase, differentiates decatenation from the second reaction of gyrase.

The assessment of gyrase decatenation activity classically involves incubation of 200 ng of kinetoplast DNA (kDNA) for 30 minutes at 37°C, prior to stopping the reaction by a method akin to supercoiling and relaxation, the reaction products are analysed by gel electrophoresis. The standard substrate of the reaction, kDNA, is a large complex network of DNA mini-circles and maxi-circles catenated together and found as the natural DNA form within the mitochondria of trypanosomes, from which it is isolated and purified (Figure 4.10a). An alternative substrate termed bis-cat, which comprises supercoiled singly-linked catenated DNA plasmids of disparate sizes, was also constructed and used to assay the decatenation reaction of *A. thaliana* DNA gyrase (Figure 4.10b) (development of the bis-cat substrate is described in Chapter 6).

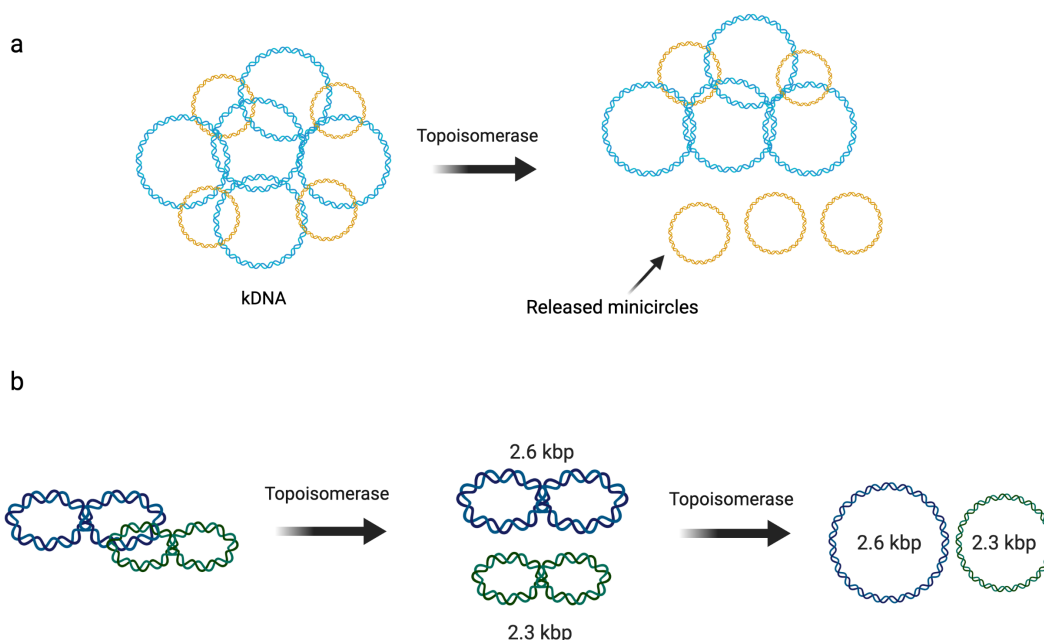


Figure 4.10: Topoisomerase decatenation substrates.

Diagrammatic representations of topoisomerase mediated decatenation using either kDNA (a) or bis-cat DNA (b) as substrate.

4.2.4.1. Relating all activities of *A. thaliana* gyrase

1 unit of *A. thaliana* gyrase was defined as the quantity of enzyme required to fully supercoil 0.5 µg of relaxed pBR322 DNA within 30 mins at 37°C under optimum conditions (Figure 4.11a). The DNA relaxation activity of *A. thaliana* gyrase was investigated in conditions without ATP or KGlu and was found to require 3-fold more enzyme as compared to supercoiling (Figure 4.10b). The hitherto unexplored decatenation activity of *A. thaliana* gyrase was reviewed through the classical kDNA decatenation assay and the novel bis-cat substate mediated assay (Figure 4.11). Decatenation activity of *A. thaliana* gyrase was confirmed, as evidenced by the release of minicircles from the kDNA network in a concentration-dependent manner (Figure 4.11c). In contrast to the relaxation activity of *A. thaliana* gyrase but similar to supercoiling, enzymatic decatenation of kDNA occurred at high concentrations of KGlu (800 mM), albeit four units of *A. thaliana* enzyme were required to completely decatenate kDNA. The bis-cat DNA provides a novel and sensitive alternative substrate to kDNA for assessing the decatenation activity of topoisomerases. The bis-cat-mediated decatenation assay carried out in identical conditions to the kDNA assay, identified 1 unit of enzyme to sufficiently decatenate 200 ng of bis-cat DNA into two decatenated plasmids, supercoiled in topology (Figure 4.11d). The supercoiled nature of the bis-cat DNA substrate, in addition to the specific feature of KGlu-independent relaxation of *A. thaliana* gyrase, allowed the simultaneous observation of *A. thaliana* gyrase decatenation and relaxation within a single experiment (Figure 4.10b). Intriguingly, when the bis-cat mediated decatenation was conducted in conditions also permissive of DNA relaxation by *A. thaliana* gyrase (i.e., no KGlu), the requirement for *A. thaliana* gyrase was reduced to 0.25 units of enzyme, confirming that KGlu is not required for decatenation by *A. thaliana* gyrase, but in fact, the decatenation activity is more efficient in its absence (Figure 4.10e). Notably, *A. thaliana* gyrase is able to relax the decatenated DNA although ATP is present in the reaction.

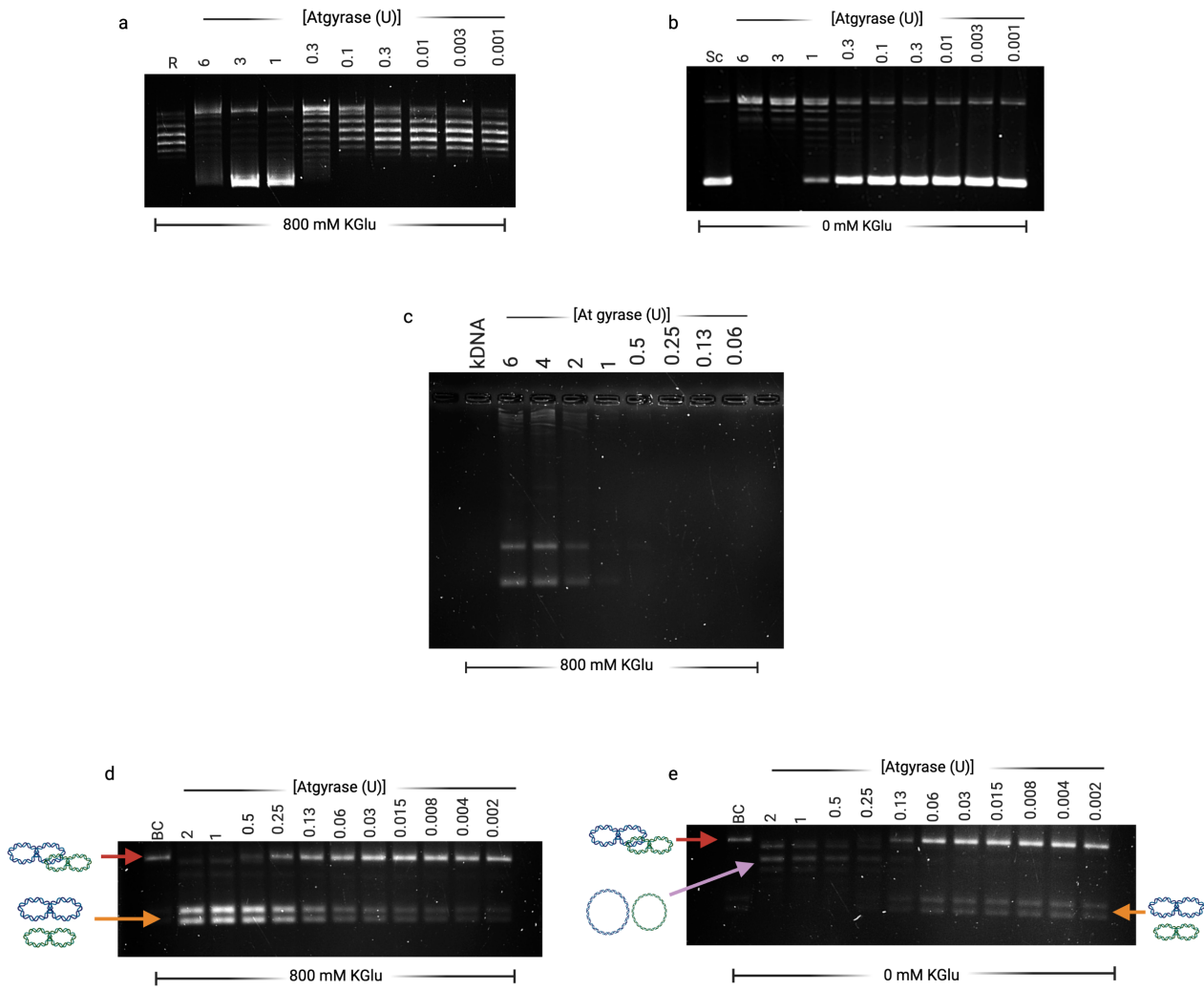


Figure 4.11: *A. thaliana* gyrase mediated reactions.

(a) Supercoiling under conditions of optimum activity to identify 1U of enzyme activity, i.e., quantity of *A. thaliana* gyrase required to supercoil 0.5 μ g of relaxed pBR322 DNA in 30 mins at 37°C. (b) DNA relaxation activity. (c) DNA decatenation using kDNA as substrate. (d) DNA decatenation using bis-cat DNA as substrate in an assay with 800 mM KGlucose (i.e., conditions in which relaxation is inhibited). (e) DNA decatenation with bis-cat DNA and no KGlucose (i.e., decatenation and relaxation permitted). Lanes marked above with quantities of *A. thaliana* gyrase in units of enzyme and concentrations of KGlucose (mM) beneath gels. Arrows as follows: red: bis-cat substrate, orange: supercoiled-decatenated bis-cat, pink: relaxed-decatenated bis-cat. R: relaxed pBR322 DNA, Sc: supercoiled pBR322 DNA, kDNA: kinetoplast DNA, BC: bis-cat DNA.

4.2.5. *E. coli* gyrase supercoiling, relaxation and decatenation activity determination

Arabidopsis includes gyrase as the only type IIA topoisomerase, as in contrast to *E. coli*, the plant probably does not encode a topoisomerase IV equivalent. Interestingly, this situation is not unique to *Arabidopsis*, as certain bacteria, notably *M. tuberculosis* also encompass gyrase as the sole type IIA topoisomerase. Consequently, the gyrase of *M. tuberculosis* has been identified to supercoil DNA at levels similar to the *E. coli* enzyme but also possess enhanced relaxation and decatenation activities (Aubry et al. 2006). Plausibly, as the sole type IIA topoisomerase, *A. thaliana* gyrase may also possess similar functional differences from the canonical *E. coli* gyrase enzyme.

The activities of *E. coli* gyrase were investigated using methods parallel to characterisation of *A. thaliana* gyrase activity. The supercoiling activity of *E. coli* gyrase was examined under optimum conditions and a unit of *E. coli* enzyme was defined as the quantity of enzyme required to supercoil 0.5 µg of relaxed pBR322 in 30 mins at 37°C (Figure 4.12a). Relaxation of the same quantity of supercoiled pBR322 under conditions suited for relaxation, i.e., the omission of spermidine and ATP, required 135 x more *E. coli* gyrase than needed for supercoiling (Figure 4.12b). Additionally, *E. coli* gyrase-mediated DNA decatenation was also assessed, the probing of this activity through kDNA substrate required >80 units of enzyme, relative to supercoiling; notably, at this concentration, catenated kDNA was evident in the wells of the gel, indicating that the reaction was not complete (Figure 4.12c). The sensitive bis-cat DNA mediated assay identified 9 units of *E. coli* gyrase as sufficient to fully decatenate an equal amount of bis-cat substrate into two supercoiled and decatenated plasmids (Figure 4.12d).

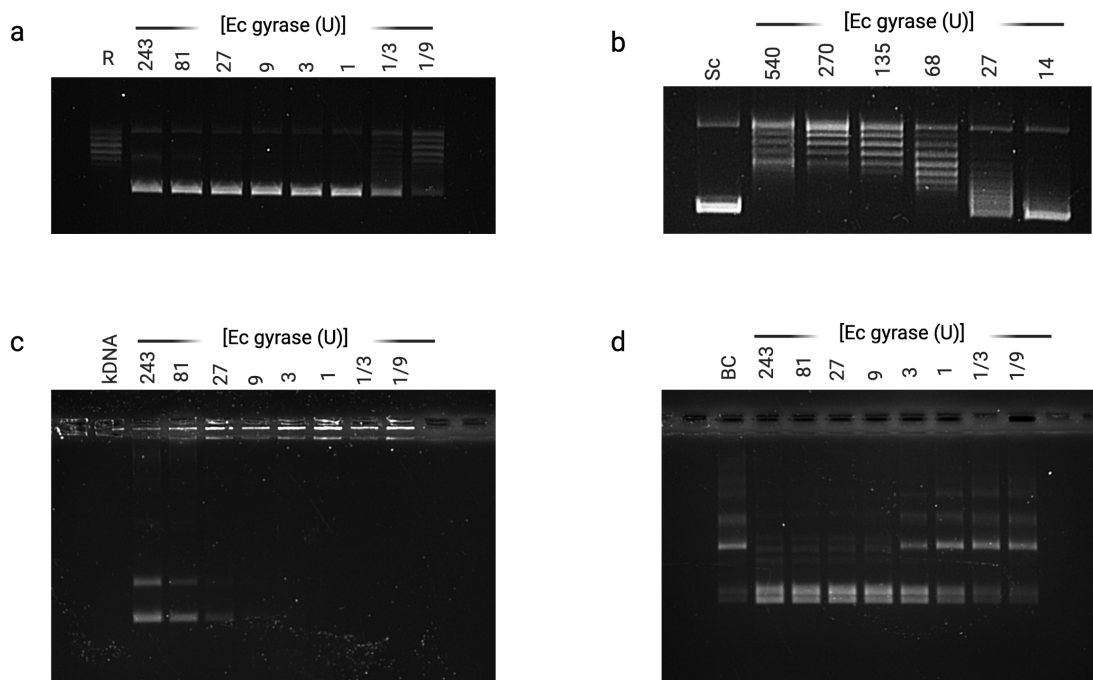


Figure 4.12: *E. coli* gyrase-mediated reactions.

E. coli gyrase enzyme titrations, quantity given above each lane in units of enzyme, for supercoiling (a), relaxation (b) and decatenation with either kDNA substrate (c) or bis-cat substrate (d). R: relaxed pBR322 DNA, Sc: supercoiled pBR322 DNA, kDNA: kinetoplast DNA, BC: bis-cat DNA.

4.2.6. *A. thaliana* gyrase possesses superior relaxation and decatenation activities relative to *E. coli* gyrase.

The activities of *E. coli* and *A. thaliana* gyrase were assessed relative to the supercoiling activity of each enzyme; a unit of enzyme was identified as the quantity of enzyme required to supercoil 0.5 μ g of relaxed pBR322 DNA in 30 mins at 37°C. The results are summarised in Table 4.1.

Table 4.1: Relative activities for *A. thaliana* and *E. coli* gyrase.

Gyrase	Relative activity to supercoiling (units)				
	Supercoiling	Relaxation	kDNA		
			decatenation	0 mM KGlu	800 mM KGlu
<i>E. coli</i>	1	135	>81	n/a	9
<i>A. thaliana</i>	1	3	4	0.25	1

The *A. thaliana* gyrase relaxation activity is 45-fold more proficient for DNA relaxation than that of *E. coli* gyrase. The decatenation activity of the enzyme was identified to be ~20-fold more efficient using kDNA as substrate, although under identical conditions this difference was reduced to 9-fold when the substrate was substituted by bis-cat DNA. However, under conditions optimal for decatenation by *A. thaliana* gyrase, 0.25 supercoiling units of *A. thaliana* enzyme were needed for the decatenation activity; notably, this indicates that the relative proficiency of *A. thaliana* decatenation is >35 fold, compared to *E. coli* decatenation. The comparison of relative activities of *E. coli* and *A. thaliana* gyrase imply the latter enzyme to be superior in terms of DNA relaxation and DNA decatenation activities. These results suggest that the *A. thaliana* gyrase may be a stronger decatenase than the *M. tub* gyrase, as the latter enzyme has previously been identified to possess a 10-fold decatenation advantage over the *E. coli* protein. This enhanced decatenation activity of *A. thaliana* gyrase is likely to be consistent with the *in vivo* role of the enzyme in decatenating replicated mitochondrial and plastid DNA.

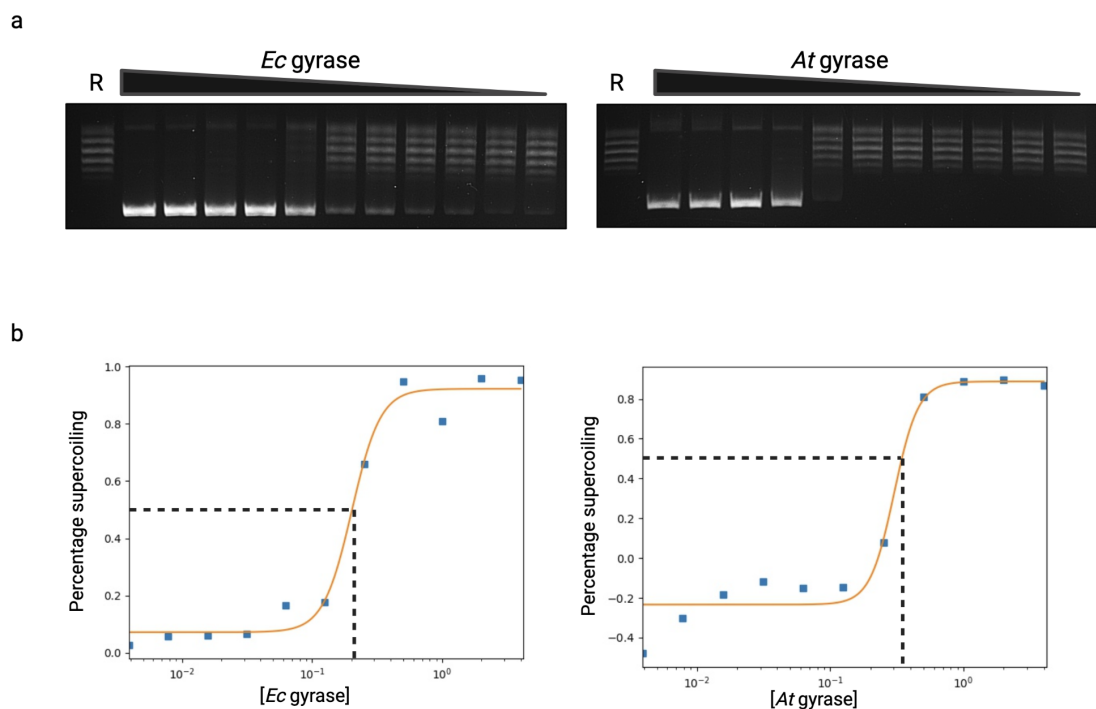


Figure 4.13: Determination of *A. thaliana* and *E. coli* EC_{50} .

(a) *E. coli* and *A. thaliana* gyrase supercoiling titrations (gyrase 50 nM - 50 μ M). (b) Output plots of *E. coli* and *A. thaliana* gyrase plots subsequent to densitometric analysis to determine fraction of supercoiled DNA relative to enzyme concentration. The concentration of enzyme that gives half maximal supercoiling is referred to as EC_{50} .

4.2.7. Ciprofloxacin is an effective inhibitor of *A. thaliana* gyrase supercoiling

The bacterial gyrases are recognised as ideal targets for drug inhibition essentially due to their absence in the genomes of humans. Many gyrase inhibitors have been discovered or developed; these possess the capacity to inhibit different aspects of the gyrase catalytic cycle and are discussed in greater detail in section 1.6.4. Of notable clinical relevance are the quinolone antibiotics that comprise four generations of inhibitors, all of which have a related mechanism of inhibition (discussed in 1.6.4.2). These inhibitors are often referred to as gyrase poisons due to their action of poisoning the enzyme by stabilising the covalent gyrase-DNA complex (cleavage-complex), subsequent to gyrase mediated double-stranded cleavage of the G-segment DNA, thereby converting transient double-stranded breaks into stable double-stranded breaks, which lead eventually to a bactericidal effect.

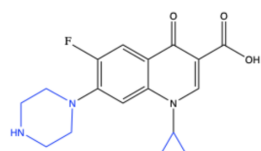
The initial indications of suspected gyrase-encoding genes in plants came from early work identifying novobiocin-sensitive gyrase-like activity during the transcription of pea genes, and later clues of chlorosis of plant cultures upon ciprofloxacin treatment (Lam and Chua 1987; Wall et al. 2004). Direct biochemical evidence of ciprofloxacin activity against *A. thaliana* gyrase, specifically, was provided much later through the identification of ciprofloxacin-resistant *Arabidopsis* plants (Evans-Roberts et al. 2016). However, no comparison of the potency and selectiveness of inhibitors such as ciprofloxacin has been made for *E. coli* gyrase and *A. thaliana* gyrase. Testing the *in vitro* druggability of *A. thaliana* gyrase with effective bacterial gyrase inhibitors, is a vital prerequisite for the development of novel drugs targeting *A. thaliana* gyrase-specific action with the potential to be developed into herbicidal compounds.

Prior to the determination of the inhibitory concentration for a drug, adjusting the enzyme concentration to ensure that the activity of the enzyme is within its linear range is crucial to determine the true inhibition characteristics. DNA supercoiling assays were conducted with varying concentrations of *E. coli* and *A. thaliana* gyrase to determine the concentration of each enzyme required for half-minimal activity in the absence of any inhibitor (EC_{50}) (Figure 4.13a). Densitometric analysis was used to determine the percentage of supercoiled DNA and this was plotted against enzyme concentration to determine the EC_{50} of *E. coli* gyrase, found to be ~ 1.0 nM and that of *A. thaliana* gyrase of ~ 3 nM. DNA supercoiling assays were carried out with gyrase from both *A. thaliana* and *E. coli*, the latter was included as a positive control and for comparison purposes. The concentration of ciprofloxacin required to inhibit the supercoiling of DNA gyrase by 50% (IC_{50}) for *A. thaliana* gyrase was determined to be 0.68 ± 0.060 μ M whilst the IC_{50} for *E. coli*

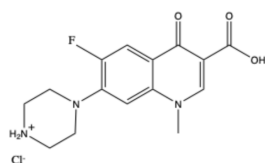
gyrase was determined to be $0.56 \pm 0.070 \mu\text{M}$, under these experimental conditions. Reassuringly, the IC_{50} of ciprofloxacin determined for *E. coli* gyrase is similar to values previously determined of $0.45 \mu\text{M} - 1 \mu\text{M}$ (Cambau et al. 2009; Germe et al. 2018b; Khan et al. 2018).

4.2.8. Ciprofloxacin analogues

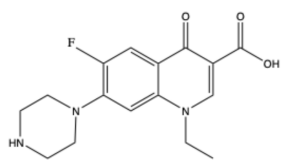
A collaborative project was initiated with the research groups of Dr Joshua Mylne and Dr Keith Stubbs based at the University of Western Australia (UWA). The project was founded upon the prior knowledge that ciprofloxacin is effective against plant DNA gyrase but must lack selectivity relative to bacterial gyrase, therefore hindering the potential of the quinolone as a herbicide. The objective of the project was to enhance the selectivity of fluoroquinolones for plants rather than bacterial targets and thereby improve the activity of fluoroquinolones for a herbicidal mode of action. In an effort to achieve the desired outcome, the chemical preparation of several ciprofloxacin analogues was carried out at UWA, essentially by retaining the fluoroquinolone scaffold whilst manipulating the N-1 and C-7 positions by substitution with chemical moieties of variable size, shape and hydrophobicity (Figure 4.14). The work of this collaborative project is published (Wallace et al. 2018).



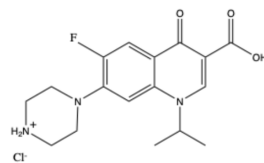
Ciprofloxacin



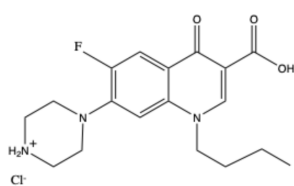
CA01



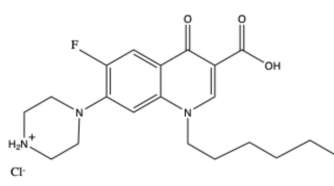
CA02



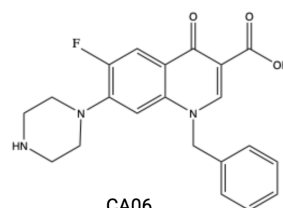
CA03



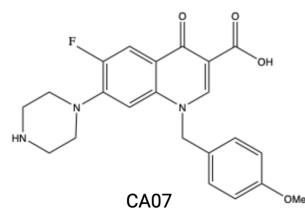
CA04



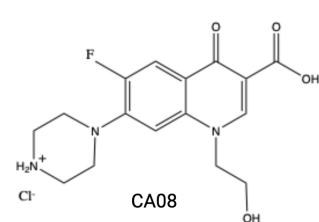
CA05



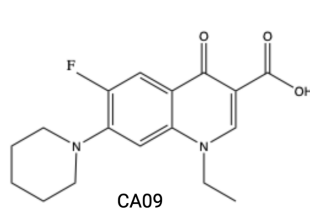
CA06



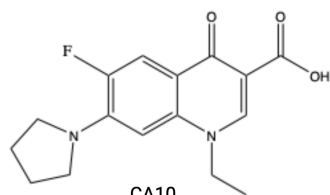
CA07



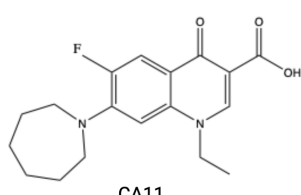
CA08



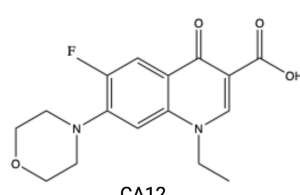
CA09



CA10



CA11



CA12

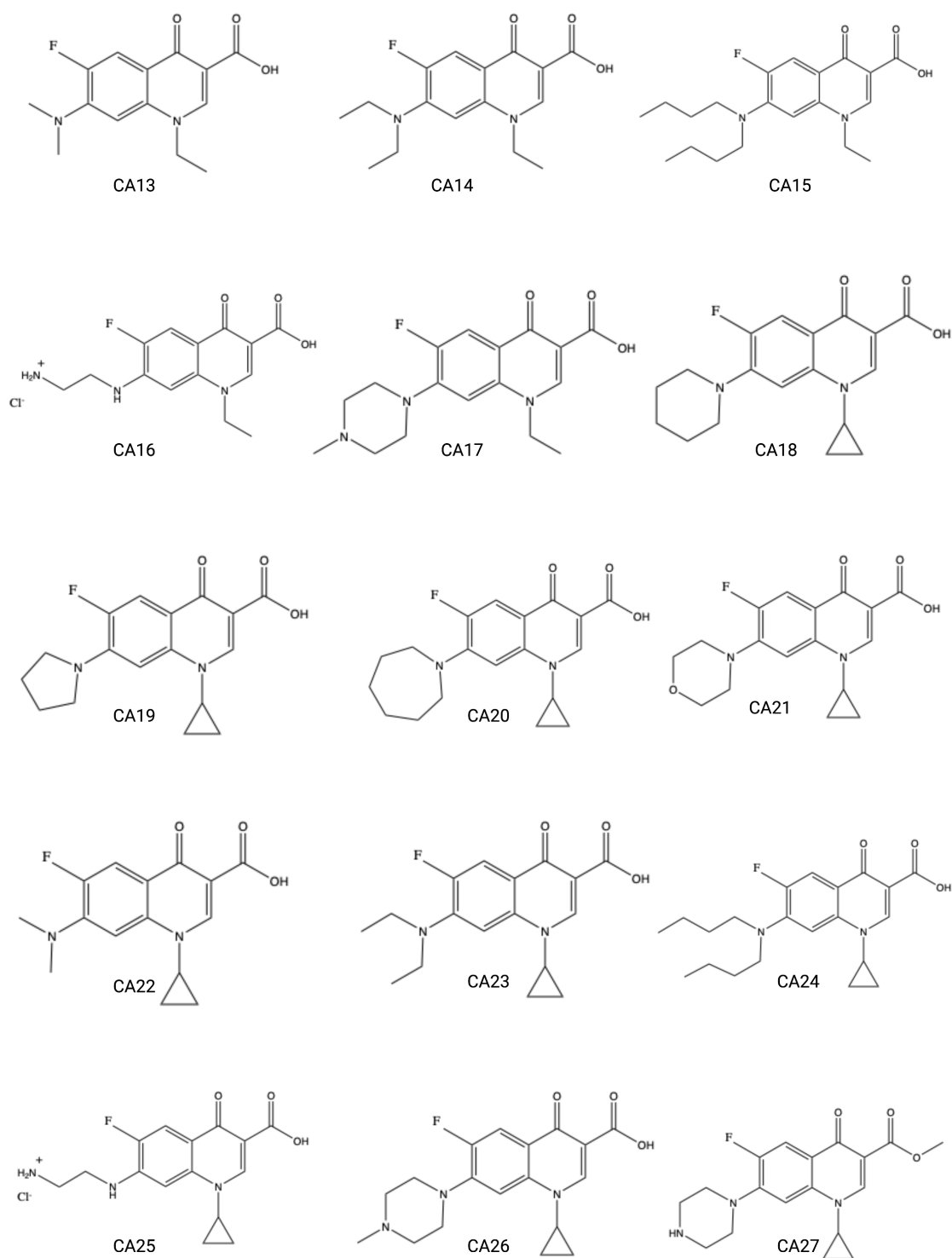


Figure 4.14: Structures of novel ciprofloxacin analogues.

The positions of the ciprofloxacin fluoroquinolone manipulated are highlighted in blue.

4.2.9. Novel herbicidal compounds inhibit *E. coli* gyrase with greater potency than *A. thaliana* gyrase

The novel analogues of ciprofloxacin were tested for inhibition of supercoiling activity for both *A. thaliana* and *E. coli* gyrases *in vitro* to determine their IC₅₀s. Similar to the determination of IC₅₀ values for ciprofloxacin, the analogues were tested at a range of concentrations in gel-based assays and densitometric analysis was used to estimate levels of supercoiling at each concentration from which plots of percentage supercoiling were generated; an example of the data generated with CA20 is illustrated for *A. thaliana* gyrase (Figure 4.15a) and *E. coli* gyrase (Figure 4.15b). The IC₅₀ data for all ciprofloxacin analogues are summarised in Table 4.2.

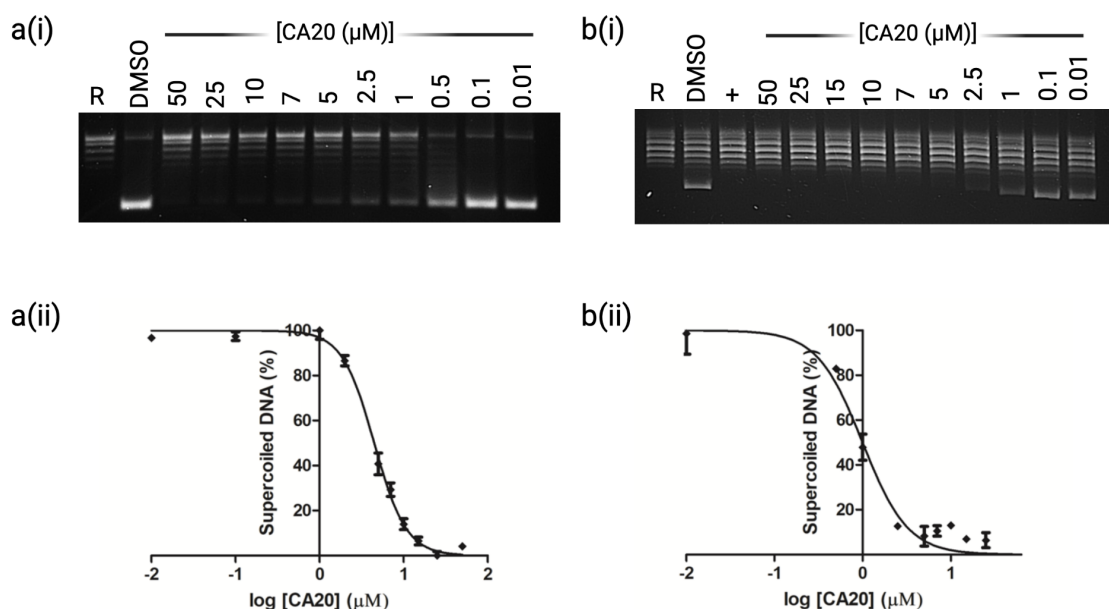


Figure 4.15: Inhibition potential of CA20.

Titration of CA20 against *A. thaliana* gyrase (a) and *E. coli* gyrase (b). Plots of percentage supercoiled DNA and log concentration of inhibitors given in (ii) for each enzyme, respectively. R: relaxed pBR322, DMSO: negative control of gyrase and identical concentration of DMSO as compounds, +: positive control of 50 μM ciprofloxacin.

Table 4.2: IC₅₀ values determined for inhibition of supercoiling for ciprofloxacin analogues against recombinant *E. coli* gyrase and *A. thaliana* gyrase.

Compound	Mean IC ₅₀ ± SEM (µM)	
	<i>E. coli</i> gyrase	<i>A. thaliana</i> gyrase
CFX	0.56 ± 0.070	0.68 ± 0.060
CA01	9.26 ± 1.95	74.7 ± 3.3
CA02	1.35 ± 0.25	3.15 ± 0.15
CA03	2.85 ± 0.25	6.60 ± 0.20
CA04	4.35 ± 0.56	25.9 ± 1.95
CA05	>100	>100
CA06	2.1 ± 0.53	20.6 ± 1.55
CA07	>100	>100
CA08	2.70 ± 0.60	10.6 ± 1.39
CA09	2.65 ± 0.050	26.9 ± 3.3
CA10	1.56 ± 0.088	9.25 ± 1.3
CA11	2.43 ± 0.16	14.9 ± 1.1
CA12	2.45 ± 0.45	28.4 ± 3.6
CA13	16.1 ± 2.6	29.9 ± 5.8
CA14	10.7 ± 1.48	21.8 ± 2.05
CA15	>100	>100
CA16	11.9 ± 0.95	19 ± 2.25
CA17	0.79 ± 0.14	5.80 ± 1.08
CA18	1.90 ± 0.50	4.70 ± 0.70
CA19	0.25 ± 0.040	2.80 ± 0.60
CA20	0.83 ± 0.073	4.6 ± 0.1
CA21	0.77 ± 0.095	5.85 ± 0.65
CA22	1.90 ± 0.40	8.13 ± 1.76
CA23	4.35 ± 0.21	5.1 ± 0.38
CA24	>100	>100
CA25	1.52 ± 0.16	4.75 ± 0.15
CA26	0.55 ± 0.11	3.75 ± 0.15
CA27	>100	>100

The ciprofloxacin analogues were more potent inhibitors of *E. coli* gyrase supercoiling than *A. thaliana* gyrase. Generally, compounds that retained the cyclopropane at the N-1 position were stronger inhibitors, although this inhibition was not supplemented by *A. thaliana* gyrase selectivity over *E. coli* gyrase. Further to cyclopropane conservation at N-1, seemingly, the broad preservation of cyclic hydrocarbon ring at C-7, be it by the substitution of the secondary amine to a methylene group or an oxygen atom, or a change in ring size, preserved the inhibition activity as compared to the opening of the ring to different moieties; the latter observation was also typical for the N-1 ethyl derivatives of ciprofloxacin.

The analogue of strongest potency for *A. thaliana* gyrase, CA19, differs at the C-7 position by substitution of the cyclohexane ring by cyclopentane, this subtle change reduces the potency to *A. thaliana* gyrase four-fold relative to ciprofloxacin. Interestingly, the same chemical modification increased the potency of CA19 ~two-fold for the inhibition of *E. coli* gyrase, as compared to ciprofloxacin. The compound CA13 was least potent amongst those tested, relative to ciprofloxacin, for the inhibition of *E. coli* gyrase. Although CA13 incorporates modifications at both N-1 and C-7 positions, the analogue retained ~2-fold selectivity towards recombinant *E. coli* gyrase over *A. thaliana* gyrase. Indeed, analogue CA23 possessed practically no selective advantage and retained almost equal inhibition to gyrase from either species. Unfortunately, in the absence of structural information for *A. thaliana* gyrase, it is difficult to determine the biochemical nature of these subtle differences between the two recombinant gyrase enzymes *in vitro*. Nevertheless, the subtle inhibition differences imply divergence in the gyrase architecture between the two species.

4.2.10. The novel ciprofloxacin inhibitors are cleavage-complex stabilisers

Although the inhibition potential of all novel ciprofloxacin analogues had been confirmed *in vitro* against plant and bacterial enzymes, the mechanism of action of these compounds remained unexplored. The mechanism of inhibition of ciprofloxacin is through stabilisation of the gyrase-DNA covalent-complex, subsequent to G-segment DNA cleavage by the enzyme. Rationally, as all compounds are derivatives of ciprofloxacin, it was anticipated that they may also be cleavage-complex stabilisers. The mechanism of inhibition was investigated for a representative set of analogues of differential structures, by means of DNA cleavage assays, using supercoiled pBR322 as substrate and assay buffers without ATP (i.e., relaxation conditions). All representative compounds were

confirmed as cleavage-complex stabilisers, at concentrations of 100 μM (Figure 4.16), 50 μM and 10 μM .

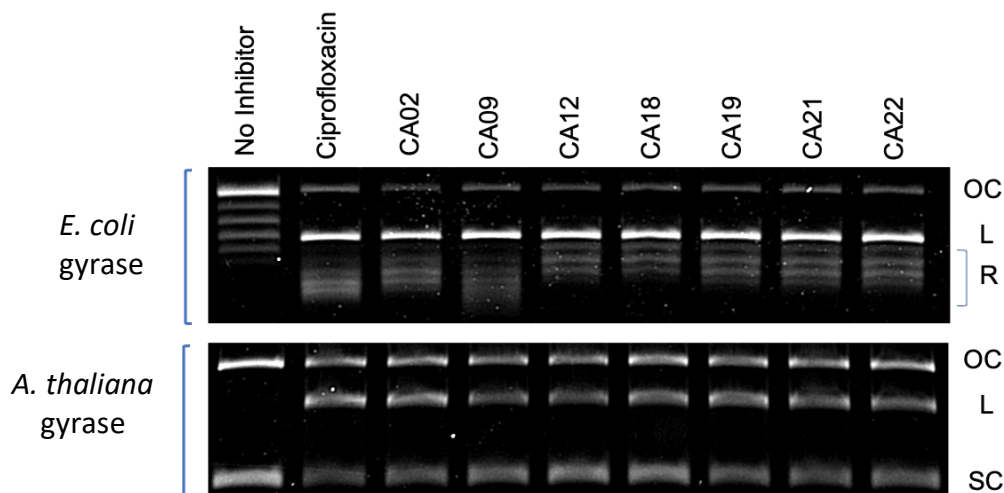


Figure 4.16: Ciprofloxacin analogue cleavage assays.

Gyrase cleavage assays with 100 μM of each indicated compound. Top gel: *E. coli* gyrase (Ec); bottom gels: *A. thaliana* gyrase (At). R: relaxed topoisomers, SC: supercoiled DNA, L: linear DNA, NP: no protein control and +: 50 μM ciprofloxacin (positive control).

4.2.11. Ciprofloxacin is most effective for impeding *A. thaliana* growth

In order to complement the *in vitro* data, it is vital to test the potency of the analogues against the organisms for which specificity is desired; therefore, the inhibitory effect of all analogues was tested against *A. thaliana* and bacterial species including *E. coli*, *P. aeruginosa* and *S. aureus*. The work in this section was carried out in the laboratories of Dr Mylne and Dr Stubbs by Michael D. Wallace.

Assays were conducted against *A. thaliana* plants using a concentration gradient of each compound to identify the phenotypic changes that correspond to the IC_{50} at the organismal level, control compounds ciprofloxacin and HCl:norfloxacin (CA01) were included for comparison (Figure 4.17) (Wallace et al. 2018). The results indicated that a substitution of the secondary amine to a methylene, CA18, or oxygen atom, as in CA21, retained herbicidal activity, with an increase in potency for CA21 (Figure 4.17). A change in ring size as for CA19, CA20, CA10 and CA11 resulted in a reduction of activity compared to the parent compounds ciprofloxacin and CA01 respectively. The open chained moieties CA14-CA15 and CA22-CA24 had differing activity, with the smaller dimethyl moieties

CA22 and CA13 being the most potent; CA22 closely resembled the effect of ciprofloxacin treatment. Compounds CA16 and CA25 bearing a single linear chain had very little herbicidal activity. Lastly, compound CA26 retained herbicidal activity compared to ciprofloxacin and CA17 retained modest herbicidal activity compared to CA01. To test potential differences in the ability of the ciprofloxacin analogues to penetrate bacteria, antibiotic susceptibility tests (MIC) against *E. coli*, *P. aeruginosa* and *S. aureus*. Interestingly, in the specific case of *E. coli*, with the single exception of CA26, all other analogues possessed MICs above that determined for ciprofloxacin, this result was extended to *P. aeruginosa* where no exceptions were highlighted; however, in the case of *S. aureus*, compounds CA18-CA22 were additional exceptions with higher MIC concentrations than ciprofloxacin, plausibly due to the gram-positive nature of the bacterium.

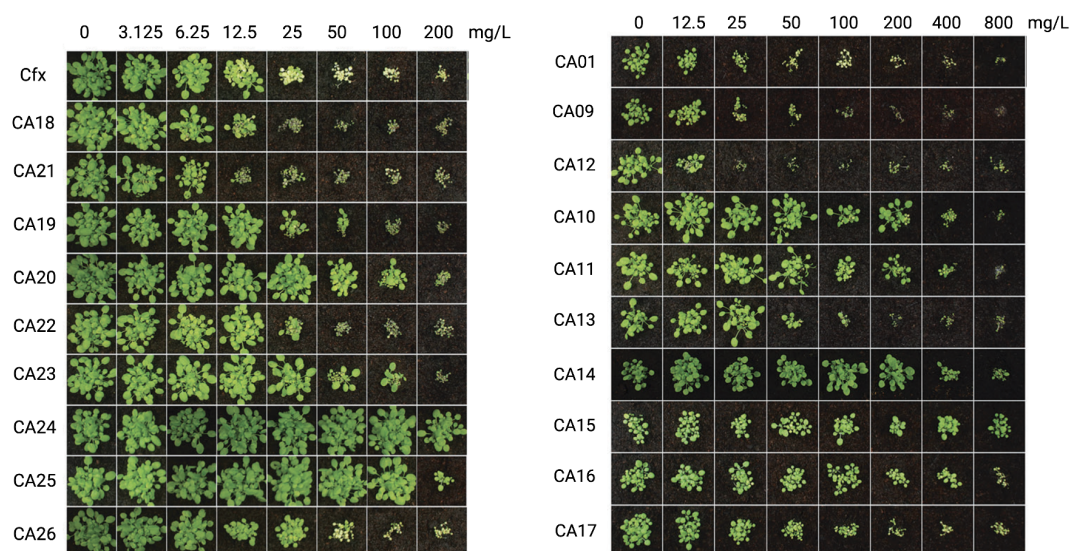


Figure 4.17: Screening of ciprofloxacin analogues with *A. thaliana*.

Representative screening assay of *Arabidopsis* treated with differing concentrations of ciprofloxacin analogue compounds. The rows of analogues are labelled to the left and concentrations specified above each column in mg/L. Figure adapted from (Wallace et al. 2018).

4.2.12. Ciprofloxacin analogue CA09 is >600-fold more selective towards a herbicidal mode of action

The results of *in vitro* enzyme inhibition were combined with *in vivo* organismal level inhibition to determine the selectivity of each analogue and determine whether differences are due to compound availability to the organism (*A. thaliana* or *E. coli*) or a direct manifestation of enzyme inhibition. The results are summarised in Table 4.3 for all compounds with MICs against *E. coli* of less than 25 mg/L.

Table 4.3: Ciprofloxacin analogues of *E. coli* MIC values <25 mg/L and their respective herbicidal potency for *A. thaliana* (IC₅₀). The inhibitory potential *in vitro* for *A. thaliana* and *E. coli* gyrases are also indicated. Error values represent standard error of the mean. Table adapted from (Wallace et al. 2018).

Compound ID	IC ₅₀ <i>A. thaliana</i> (mg/L)	MIC <i>E. coli</i> (mg/L)	Selectivity# (MIC/IC ₅₀)	DNA gyrase IC ₅₀ (μM)	
				<i>A. thaliana</i>	<i>E. coli</i>
Ciprofloxacin	10.2 ± 0.4	0.0078	7 x 10 ⁻⁴	0.68 ± 0.06	0.56 ± 0.07
CA01	19.3 ± 2.8	0.0625	3 x 10 ⁻⁴	3.15 ± 0.15	1.35 ± 0.25
CA18	6.1 ± 1.0	1	0.16	4.70 ± 0.70	1.90 ± 0.50
CA21	4.0 ± 0.3	0.25	0.06	5.85 ± 0.65	0.77 ± 0.095
CA19	21.4 ± 2.6	2	0.09	2.80 ± 0.60	0.25 ± 0.40
CA22	24.0 ± 3.2	0.5	0.02	8.13 ± 1.76	1.90 ± 0.40
CA09	17.8 ± 1.6	8	0.45	26.9 ± 3.3	2.65 ± 0.05
CA12	12.0 ± 1.0	1	0.08	28.4 ± 3.6	2.45 ± 0.45

#Selectivity towards a herbicidal mode of action (defined as MIC/IC₅₀).

The analogue CA19, determined to be most potent for *in vitro* inhibition activity of *A. thaliana* gyrase supercoiling, is approximately two-fold less potent against the *A. thaliana* plant as a whole when compared to ciprofloxacin. However, its selectivity towards a herbicidal mode of action over a bactericidal mode is ~130-fold greater than that of ciprofloxacin. More impressively, CA09 has been identified to favour a herbicidal mode of action with a selective advantage of >600-fold as compared to ciprofloxacin. Intriguingly, the justification for this selectivity is not manifested at the level of gyrase enzyme inhibition, as both CA09 and CA19 are ~10-fold less effective against the plant gyrase enzyme, as compared to the bacterial gyrase enzyme, instead, the selectivity predominantly stems from the reduced availability and uptake of the novel analogues by *E. coli*.

4.3. Discussion

The *in vitro* supercoiling activity of *A. thaliana* gyrase had been confirmed through previous investigations by Evans-Roberts and colleagues (Evans-Roberts et al. 2016). However, despite the confirmation of gyrase supercoiling, no optimisation of the activity, or indeed investigations into other reactions of the enzyme had been conducted. The systematic optimisation of gyrase supercoiling conditions assessed here involved determination of optimal buffer and pH, temperature, addition of spermidine, effect of salt in the form of KGlu and the assessment of different divalent metal ion co-factors. The conditions for optimum supercoiling were determined as 40 mM Tris.HCl (pH 8.5), 10 mM magnesium acetate, 10 mM DTT, 2 mM ATP, 800 mM KGlu and 0.05 mg/mL acetylated albumin. The conditions of assay optimisation increased the activity of *A. thaliana* gyrase four-fold as compared to the conditions implemented by Evans-Roberts and colleagues. The most prominent effect upon supercoiling was mediated by KGlu, the inclusion of which was essential for supercoiling activity. The DNA supercoiling activity was stimulated gradually as KGlu concentration was increased up to a concentration of 700-800 mM; this is in contrast to the supercoiling activity of *E. coli* gyrase, which was diminished by the inclusion of 500 mM KGlu.

A. thaliana gyrase was confirmed to mediate supplemental topoisomerase reactions to supercoiling, i.e., DNA relaxation and decatenation. Following the establishment of KGlu-dependent supercoiling activity for the enzyme, the influence of salt on the DNA relaxation and decatenation activities was explored. This is particularly intriguing considering that the supercoiling reaction is intrinsically different to both relaxation and decatenation, as evidenced by a DNA gyrase enzyme encompassing a GyrA CTD deletion that was able to relax and decatenate DNA but lost only its ability to supercoil DNA (Kampranis and Maxwell 1996). The relaxation and decatenation reactions of gyrase seemingly are dependent upon the recognition of a DNA juxtaposition prior to strand passage, rather than dependent upon the wrapping of DNA around the CTDs of the enzyme. The influence of KGlu is directly opposite on the DNA relaxation reaction of gyrase as compared to supercoiling, i.e., the enzyme is able to relax DNA without KGlu but this activity is abolished at high concentrations of KGlu (>600 mM), in which supercoiling is optimum (~800 mM). Interestingly, intermediate salt concentrations in the range of 300-450 mM were optimum for the relaxation activity of plant gyrase. The DNA decatenation reaction of gyrase was independent of KGlu concentrations, the reaction was effective with 0 mM and 800 mM KGlu; although, permissive at both salt concentrations, decatenation

with the novel bis-cat DNA substrate required 4-fold less enzyme without KGlu relative to inclusion of 800 mM KGlu, implying that decatenation may be more efficient in the absence of KGlu. The novel bis-cat mediated decatenation reaction allowed the simultaneous assessment of *A. thaliana* gyrase decatenation and relaxation. Interestingly, the *A. thaliana* gyrase was able to relax the supercoiled decatenated plasmids, despite the inclusion of ATP; this is an intriguing result and warrants further exploration. Relaxation by *E. coli* gyrase of highly negatively supercoiled DNA in conditions of physiological ATP has previously been reported (Kataoka et al. 1996).

Parallel assays of *E. coli* and *A. thaliana* gyrase were implemented to determine the relative amounts of gyrase required for relaxation and decatenation as compared to supercoiling for each enzyme. *A. thaliana* gyrase was determined to be an efficient relaxation and decatenation enzyme, 45-fold and >35-fold, respectively, when compared to the relative *E. coli* gyrase activities. The situation of increased DNA relaxation and decatenation activity is reminiscent of the *M. tub* gyrase, which in a manner identical to *A. thaliana* gyrase in chloroplasts and mitochondria, is the sole type IIA topoisomerase encoded within the bacterium, due to the absence of a topo IV equivalent (Aubry et al. 2006).

The ability of divalent metal ion co-factors to mediate nucleophilic attack on the phosphodiester backbone of DNA for transient G-segment cleavage has also been explored here. The natural environment in which *A. thaliana* gyrase is found within mitochondria and chloroplasts provides the opportunity for the supercoiling reaction to be mediated by a variety of divalent metal ions, including Mg^{2+} , Mn^{2+} , Co^{2+} , Cu^{2+} , Zn^{2+} and Ca^{2+} , the divalent metal ion preference for *A. thaliana* gyrase was found to be unique (Tan et al. 2010). In the conditions tested, *A. thaliana* gyrase did not convey a strong preference for Mg^{2+} over Mn^{2+} , in fact, either metal ion successfully mediated the supercoiling of DNA with concentrations of 2–14 mM. This is plausibly a consequence of the similar chemical features of the two metal ions, including their boarder-line hard-soft character and similar ionic radius ($\sim 0.82\text{\AA}$) (Blanche et al. 1996; Sissi and Palumbo 2009). Additionally, the substitution of Mg^{2+} with Ca^{2+} largely abolished the negative supercoiling activity of plant DNA gyrase, although the enzyme was seemingly still able to bind and wrap DNA and may carry out sub-stoichiometric supercoiling. The divalent cation preferences of *A. thaliana* gyrase are unique to this enzyme, as the *E. coli* gyrase metal co-factor preference for supercoiling has been established as $Mg^{2+} > Ca^{2+} > Mn^{2+}$ (Noble and Maxwell 2002). However, in this regard, the plant gyrase most closely resembles the activity of *M. tub*

gyrase, for which the supercoiling dependent metal ion preference has been determined as $Mg^{2+} > Mn^{2+} > Ca^{2+}$ (Aubry et al. 2006).

Unique features have been identified for *M. tuberculosis* gyrase, that have often been associated with the lack of a topoisomerase IV enzyme within the bacterium. Amongst these features, is the identification of a second functional GyrA-like-box and a putative Ca^{2+} -binding site in the GyrA subunit; the latter is proposed to have a regulatory role for enzymatic activity (Bouige et al. 2013; Karkare et al. 2012). The sequence alignments of GyrA proteins of *A. thaliana* with bacterial gyrase sequences is given in Figure 4.18.

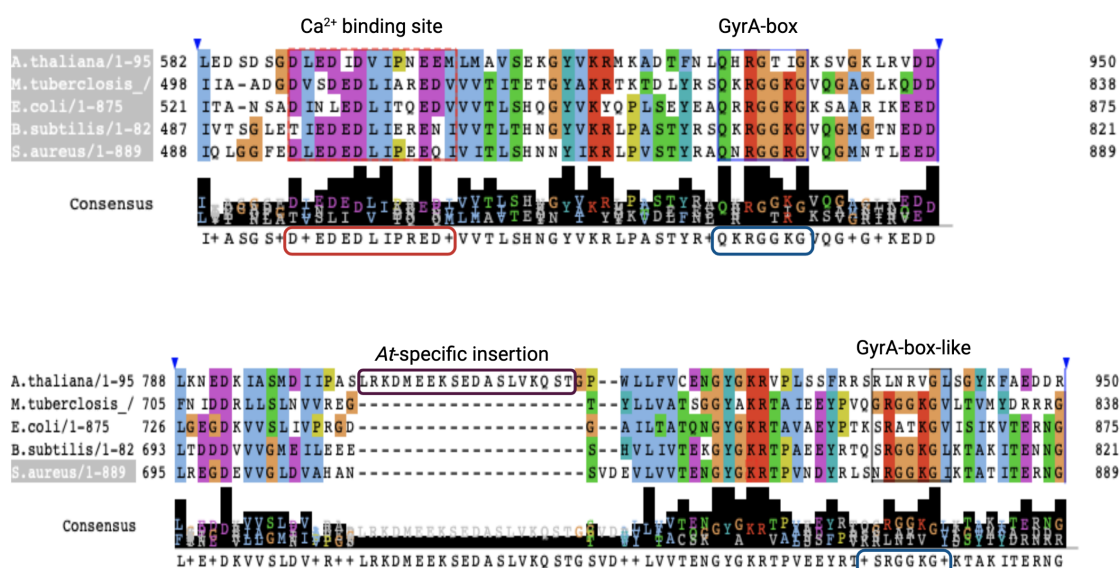


Figure 4.18: GyrA sequence alignments.

The gyrase A sequences of *A. thaliana*, *M. tub*, *E. coli*, *B. subtilis* and *S. aureus* gyrase were aligned and areas corresponding to the putative Ca^{2+} binding site, GyrA box and GyrA-like box highlighted and labelled.

Karkare *et al.*, 2012 observed that the removal of Ca^{2+} ions from assaying conditions of *M. tuberculosis* gyrase, specifically, reduced the ability of the enzyme to relax and decatenate DNA rather than supercoil DNA. Interestingly, through site directed mutagenesis of the putative Ca^{2+} binding site, they identified that a double mutant (E508A, D509A) did not significantly affect the supercoiling activity, whilst a quadruple mutant (D504A, E508A, D509A and E514A) was only able to carry out partial supercoiling; this implies that the conservation of E508 may not be crucial for the supercoiling activity of the enzyme. Intriguingly, *A. thaliana* gyrase conserves all but the equivalent residue of *M. tuberculosis* E509 (replaced by Isoleucine at position 603 of *A. thaliana* sequence) (Figure

4.18). Plausibly, calcium may have a similar regulatory role to modulate the activity of *A. thaliana* gyrase.

A. thaliana gyrase only conserves four of the seven residues of the GyrA box (consensus sequence: Q(R/K)RGG(R/K)G) yet it is still able to negatively supercoil DNA. Perhaps more interestingly, *M. tub* was identified to harness a second GyrA-box-like motif in the fifth blade of its CTD (*M. tub* sequence QGRGGKG). The mutation of conserved glycine residues to alanine in this region, reduced the ability of *M. tub* gyrase to supercoil and decatenate DNA (Bouige et al. 2013). Albeit the GyrA-like-box sequence is conserved to varying degrees in gyrases of different species, only a single glycine residue is conserved in the *A. thaliana* sequence, corresponding to G896, removal of the equivalent *M. tub* G749 abolished the enzymatic supercoiling and decatenation activity (Figure 4.18). Plausibly, the conservation of G896 only, reduces efficiency with which a T-segment is wrapped around the GyrA CTD for the *A. thaliana* gyrase protein, therefore reducing the ability of the plant enzyme to discriminate an intramolecular T-segment from an intermolecular segment, the result of which is efficient decatenation and relaxation activity. It is proposed that the later lack of discrimination is assisted by the *A. thaliana* gyrase specific insertion ahead of the GyrA-box-like sequence (Figure 4.18).

The potassium glutamate dependency of *A. thaliana* gyrase for DNA supercoiling is dissimilar to glutamate requirements by *M. tub* gyrase (routinely assayed from 100 -250 mM) (Aubry et al. 2006) (Bouige et al. 2013). Nevertheless, in this regard, the *A. thaliana* gyrase resembles glutamate dependency of the *S. aureus* enzyme, that requires > 700 mM KGlu for supercoiling but not for the processes of DNA relaxation or decatenation (Blanche et al. 1996; Hiasa et al. 2003). The *in vitro* effect of KGlu to replace KCl has been observed as an increase in protein-DNA association, protein folding and assembly (Cheng et al. 2016; Leirimo et al. 1987). Indeed, the KGlu dependence of *S. aureus* gyrase has been proposed to be due to either increased DNA-binding and wrapping around the CTD or increased stabilisation of the GyrB ATPase domain of the protein by the monovalent K⁺ ion (Hearnshaw et al. 2015; Hiasa et al. 2003; Sissi et al. 2005).

A. thaliana gyrase is seemingly a distinct topoisomerase. The enzyme has evolved to adapt to its intracellular surrounding within the chloroplast and mitochondria of plants. In accordance with the observations thus far, it appears that the ancestral *A. thaliana* gyrase protein was similar to a Gram-positive bacterium, such as *S. aureus*. However, in the absence of the associate type IIA topoisomerase, topo IV, the *A. thaliana* gyrase seemingly evolved and adapted to acquire decatenation functions, most likely via adaptations of its CTD to reduce the efficiency of DNA wrapping and promote the selection

of an intermolecular T-segment and thereby increase DNA relaxation and decatenation activities. Furthermore, it is proposed that the intracellular salt concentrations of the chloroplast and mitochondria modulate the efficiency of the 'dual' *A. thaliana* gyrase to switch from DNA supercoiling to decatenation/relaxation. Plausibly, it is envisaged that fluctuation of intracellular salt during the replication of DNA in chloroplast/mitochondria controls the efficiency of DNA gyrase for either the removal of positive supercoils ahead of the proceeding fork (high K_{Glu}) or resolution and relaxation of catenated DNA at the end of each cycle (low K_{Glu}). Unfortunately, the hypothesis cannot yet be confirmed as research into fluctuations of intracellular K_{Glu} levels within chloroplasts and mitochondria remains limited and largely unexplored. Regardless, it is proposed that the *A. thaliana* gyrase (GyrA and GyrB2) enzyme functions as the mitochondrial and plastid DNA decatenase *in vivo*.

The dual function of *A. thaliana* gyrase presents the enzyme as the sole target of quinolone antibacterials within the plant. The investigations conducted in this work confirmed that *A. thaliana* gyrase has similar sensitivity to ciprofloxacin as *E. coli* gyrase. However, all novel ciprofloxacin analogues revealed *in vitro* selectivity for *E. coli* gyrase, over *A. thaliana* gyrase, additionally, ciprofloxacin remained the most potent inhibitor for *A. thaliana* gyrase. Notably however, the ciprofloxacin analogue CA09 was determined to be >600 fold more selective towards a herbicidal mode of action. The groundwork of *A. thaliana* gyrase inhibition described in this chapter signifies the influence of compound penetration and availability at the organismal level for which its inhibition is intended, in the absence of structural information. The inhibition activity here has been determined for the supercoiling of *A. thaliana* gyrase. However, given the strong decatenation activity of the enzyme (plausibly its predominant activity), perhaps decatenation inhibition should be assessed in future work.

4.4. Future directions

The *A. thaliana* gyrase enzyme has been confirmed to possess enhanced decatenation and relaxation activities. The ATP-dependence of these reactions can be explored. An intriguing avenue of research, given the 'dual' gyrase and topoisomerase IV capabilities of the enzyme, is the determination of a chiral preference for the enzyme. Plausibly, *A. thaliana* gyrase may preferentially interact with DNA of positive superhelicity as compared to negative superhelicity, as has been confirmed for topoisomerase VI (Crisona et al. 2000; Neuman et al. 2009). Another interesting prospect to explore is the strength of

interaction of *A. thaliana* gyrase CTD wrapping of DNA, the comparison of this interaction in conditions of varying K_{Glu} and the effect of directed mutations in the GyrA box, GyrA-like box and upon deletion of the *A. thaliana*-specific insertion ahead of the GyrA-box-like sequence (Figure 4.18).

The exploration of *A. thaliana* gyrase inhibition here has been limited to specific quinolones and analogues. The potential of the other classes of gyrase inhibitors, including aminocoumarins, simocyclinone and MccB17 are as yet unexplored. Furthermore, given the revelation of dual topoisomerase action of *A. thaliana* gyrase, inhibition experiments with topoisomerase IV specific drugs are also warranted. However, ultimately, to examine and understand the specificity of *A. thaliana* gyrase inhibition, structural information of the enzyme, or domains of it, with inhibiting compounds is required.

Chapter 5: In vivo analysis of *Arabidopsis thaliana* DNA gyrase

5.1. Introduction

The sequencing of the *Arabidopsis* genome revealed four putative genes corresponding to DNA gyrase; a single putative GyrA subunit and three putative GyrB subunits (Initiative 2000). The proteins, AtGyrA, AtGyrB1, AtGyrB2 and AtGyrB3 are encoded on either chromosome 3 or 5 of the nuclear genome but organellar targeted, with the exception of AtGyrB3. In fact, a detailed investigation into AtGyrB3 later identified it to be non-essential in *Arabidopsis* whereby its expression pattern differed from the other AtGyr subunits. Additionally, bioinformatic analysis revealed that the shorter amino acid sequence of AtGyrB3 was at the cost of the ATPase domain, a functional domain known to be essential for the enzymatic catalysis of DNA gyrase (Evans-Roberts et al. 2010). The conclusion of this study contested the possibility of AtGyrB3 encoding a GyrB subunit.

Wall *et al.* (2004) identified *gyrA* to be embryo-lethal and the *gyrB* genes to be either seedling-lethal or result in stunted growth. Their work established that *E. coli* GyrA or GyrB temperature-sensitive strains could be complemented with AtGyrA or AtGyrB2 respectively; however, no evidence of complementation by AtGyrB1 was found (Wall et al. 2004). The identification of ATP-dependent supercoiling activity from fractionated organellar extracts was found to be sensitive to the conventional DNA gyrase inhibitors, ciprofloxacin and novobiocin, thereby strongly implying the existence of functional gyrase in *Arabidopsis*. Interestingly, they used putative N-terminal transit peptides fused to GFP to classify the GyrA protein to be dual targeted to both the chloroplast and mitochondria, whilst the GyrB1 and GyrB2 proteins were specifically either chloroplast or mitochondrial targeted, respectively (Figure 5.1) (Wall et al. 2004). This observation at the time, provided a satisfactory explanation for the occurrence of two GyrB subunits in *A. thaliana*. An independent subsequent investigation found AtGyrB1 to be dual targeted to chloroplasts and mitochondria, through the use of an artificial start codon (Christensen et al. 2005). The localisation results of Wall *et al.*, 2004 were disputed by GFP experiments conducted independently, whereby clones comprising the first 100-150 amino acids of each gene, GyrA, GyrB1 and GyrB2 fused to GFP determined the GyrA protein to be only chloroplast targeted, whilst both the GyrB1 and GyrB2 subunits were found to be dual-targeted to the mitochondria and chloroplasts (Monika Murcher, personal communication) (Figure 5.1). Furthermore, recent transcriptomic analysis of *Arabidopsis*

are suggestive of all gyrase genes to be dual targeted to the chloroplasts and mitochondria within *Arabidopsis* (discussed further in chapter 7) (Romanowski et al. 2020).

The contradictory observations have warranted further investigation into the role of *A. thaliana* DNA gyrase. Although the *A. thaliana* gyrase subunits have been identified and shown to be active, the biological function within *Arabidopsis* remains unknown. The work in this chapter set out to examine the *in vivo* role of the three *Arabidopsis* gyrase proteins. As the gyrase enzyme has been deemed essential within *Arabidopsis* (Wall et al. 2004), the *in vivo* role of gyrase was investigated through subtle changes to the encoding genes, through T-DNA insertions. A systematic approach was implemented to characterise intricate phenotypic differences between mutant and wild-type plants that could help elucidate the function of each protein within the organelles.

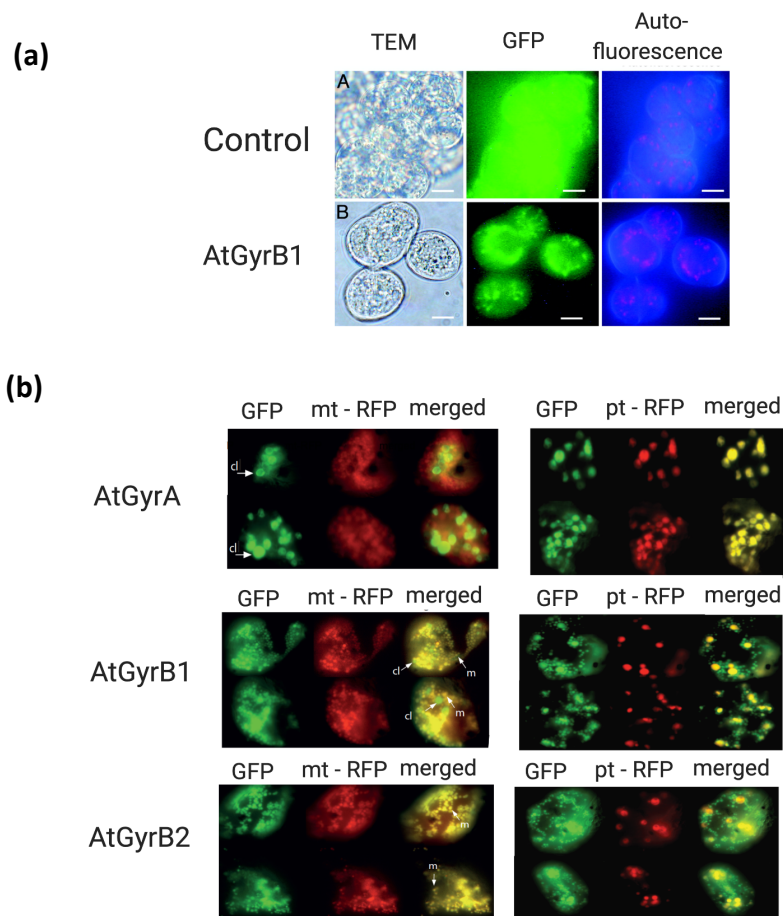


Figure 5.1: GFP localisation experiments.

(a) The transit peptide of AtGyrB1 (bottom panel) and non-targeted empty vector control (top panel) linked to the GFP protein and constitutively expressed by the 35S promoter. The empty vector control GFP signal is dispersed throughout the nucleus and cytosol; whereas the AtGyrB1:GFP signal is chloroplast targeted. Figure adapted from (Wall et al. 2004) with permission.

(b) Expression of the first 100-150 amino acids of AtGyrA, AtGyrB1 or AtGyrB2 fused to GFP and constitutively expressed under the 35S promoter. Lanes as follows: GFP: signal to mark the potential localisation of AtGyrA, AtGyrB1 or AtGyrB2; mt-RFP: mitochondria marked with RFP; pt-RFP: chloroplasts marked with RFP; merged: the signals of GFP and RFP superimposed. The AtGyrA protein is chloroplast targeted, whilst the GyrB1 and GyrB2 proteins are dual targeted to the chloroplasts and mitochondria. Data from Monika Murcher (personal communication).

5.2. Results and Discussion

5.2.1. *A. thaliana* T-DNA lines

The biochemical and developmental contribution of gyrase was analysed *in vivo* by exploiting a library of mutants that involved insertional mutagenesis, by means of *Agrobacterium tumefaciens* t-DNA (T-DNA) within the gyrase genes of the Columbia-0 background of *A. thaliana*. The purpose of mutagenesis is to analyse the underlying genetical, biochemical and developmental contributions of the targeted gene *in vivo*. The generation of the T-DNA library relies on the natural transformation of a section of sequenced DNA from a modified version of the tumour-inducing (Ti) plasmid, flanked either side by 25 bp border sequences, which is randomly incorporated into the genome of the infected plant. The resulting T-DNA mutant library which covers the majority of *A. thaliana* genes, is accessible to researchers through seed repositories.

5.2.1.1. Acquisition of T-DNA lines

Arabidopsis lines were ordered from the Nottingham Arabidopsis Stock Centre (NASC). The relevant lines with T-DNA insertions in the gyrase genes of *A. thaliana* used for the purpose of this work are given in Table 5.1. The gyrase genes have been identified to be crucial for the survival and development of *Arabidopsis* (Wall et al. 2004), therefore the aim was to deliberately select T-DNA lines likely to be non-lethal.

Table 5.1: *Arabidopsis thaliana* T-DNA insertion lines explored in this study.

Gene	Locus	Name	Database reference	Previous reference
GyrA	At3g10690	GK-10	GK-077A10	Wall et al., 2004
GyrA	At3g10690	07	SAIL_569_G07	n/a
GyrB1	At3g10270	78	SALK_139478	n/a
GyrB1	At3g10270	GK-06	GABI_586A06	n/a
GyrB1	At3g10270	98	SALK_084298.56.00	n/a
GyrB2	At5g04130	67	SALK_002367	Wall et al., 2004
GyrB2	At5g04130	82	SALK_068282	n/a

5.2.1.2. Genotyping to identify homozygous mutants

The *Arabidopsis* lines listed in Table 5.1 were sterilised and grown on ½ MS plates. Genomic DNA was extracted from cotyledons and the genotype of each plant was categorised by bifold PCR as homozygous *gyrA*, *gyrB1* and *gyrB2*, where possible. The genotyping involves PCR of the genetic material with primers within the gene of interest and the inserted T-DNA sequence (Figure 5.2). According to the scheme of Figure 5.2 the primer combination LP and RP can be used to confirm a wild-type genotype, whilst BP and either LP or RP can be used to confirm the T-DNA insert within the genome, that is a mutant plant. Subjecting genomic DNA to both combinations of the aforementioned PCR reactions was used to categorise the genotype. Accordingly, the lines used for this work were categorised using primer combinations given in Table 5.2 as either wild-type, heterozygous or homozygous (wild-type: $+/+$, heterozygous: $+/-$ and homozygous: $-/-$) (Figure 5.2c). No bands of wild-type size were observed when homozygous mutants were subjected to LP and RP border combination; a band was only observed for the heterozygous GK-10 $^{+/-}$ line.

Table 5.2: Primer sequences for T-DNA genotyping PCRs for detection of wild-type genotype or the presence of the T-DNA insertion within the *A. thaliana* genome.

Line	Gene		Primer Sequences	Primer Combination	
				WT	TDNA
GK-077A10	GyrA	LP	AACTGGACCATCCTCTTCACTC	RP + LP	RP + BP
		RP	TGAATGCAGACTCGATGTGAG		
		BP	ATATTGACCATCATACTCATTGC		
SAIL_569_G07	GyrA	LP	ACGGGTCCATGGCTATTATTC	RP + LP	LP + BP
		RP	GACAGAAGAAGAGCGACATGG		
		BP	TAGCATCTGAATTCATAACCAATCT CGATACAC		
SALK_139478	Gyr B1	LP	TTGGTGGAGAGGTTAACATGC	RP + LP	RP + BP
		RP	CCCTGAAAGTGACCAAATACG		
		BP	ATTTTGCCGATTTTCGGAAC		
GABI_586A06	Gyr B1	LP	CTGCTGAAACTCCATTCCATC	RP + LP	RP + BP
		RP	ATCCTTGACAACGCAATTGAC		
		BP	ATATTGACCATCATACTCATTGC		
SALK_084298. 56.00	Gyr B1	LP	TTCCCCTTCCAACACACTATG	RP + LP	RP + BP
		RP	CGAAGGTAGAAGCACGTGTTC		
		BP	ATTTTGCCGATTTTCGGAAC		
SALK_002367	Gyr B2	LP	GATAATGACCTGCACCCATTG	RP + LP	LP + BP
		RP	GCCTTTGTTATCTGTCCAACG		
		BP	ATTTTGCCGATTTTCGGAAC		
SALK_068282	Gyr B2	LP	CAGGTTGATCCTAGTTGCAGC	RP + LP	RP + BP
		RP	AGCTTGAAAGGCAATTCTTCC		
		BP	ATTTTGCCGATTTTCGGAAC		

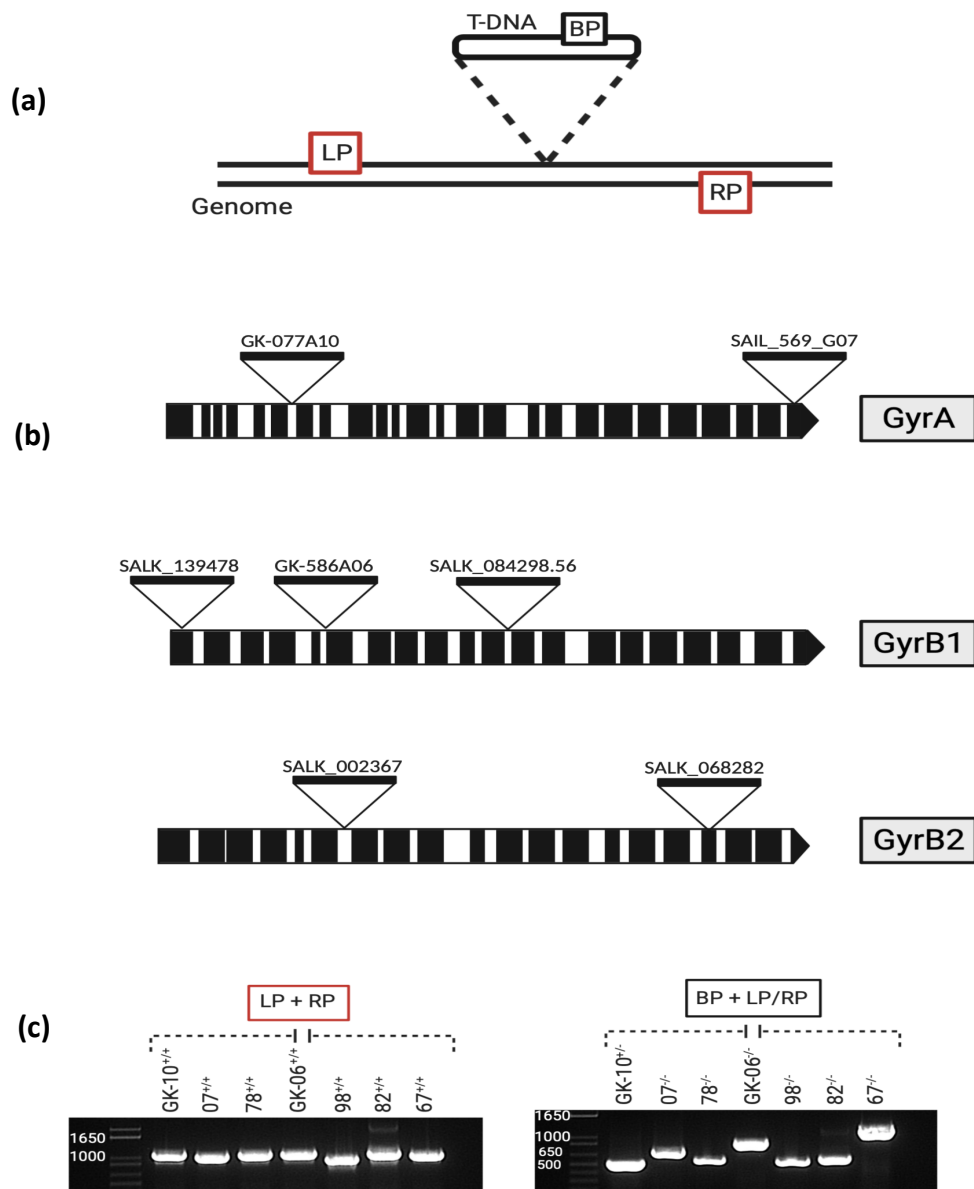


Figure 5.2: Schematic representation of T-DNA insertions, positions and PCR results.

(a) Diagrammatic representation of T-DNA insertion into the *A. thaliana* genome, with positions and orientations of genomic primers (RP or LP) and T-DNA insertion primer (BP) marked. (b) Positional representations of the inserted T-DNA lines explored in this work, with respect to positions within either GyrA, GyrB1 or GyrB2 proteins. The black filled boxes represent exons, whilst white areas represent introns. (c) The results of combinatorial PCR reactions for each line described in Table 5.2 using respective primer combinations for identification of either wild-type (left panel) or T-DNA (right panel) genotype, using primer combinations listed in Table 5.2; description of each line given above the gel (+/+ = wild-type, +/- = heterozygous, -/- = homozygous lines). Note: combinations of the genomic primers (LP + RP) did not give any detectable PCR product for each homozygous line (results not shown).

5.2.2. Phenotypes of homozygous mutants

The T-DNA mutant lines in this study presented various challenges during characterisation. The routine procedure to identify a homozygous recessive plantlet involves germination of the line onto artificial media that complements the nutrient requirement for development. To establish this, mutant lines were germinated in the presence of half-strength Murashige and Skoog (MS) medium, a critical mixture of basal salts, used to encourage the germination of dormant seedlings.

Interestingly, select mutant lines including GyrA homozygous recessive lines SAIL_569_G07 (07^{-/-}) and GyrB2 line SALK_068282 (82^{-/-}), were unable to germinate in basic conditions. The addition of an external carbohydrate source in the form of sucrose, aided germination in these specific cases. Sucrose constitutes the most frequent source of carbohydrate within the phloem sap of plants and its incorporation can be necessary to alleviate the consequential heterotrophy of *in vitro* cells; therefore enabling the cells to carry out the energy consuming developmental process (Yaseen et al. 2013). However, the relief provided by an external carbohydrate source did not support plant growth outside controlled and sterile conditions. The transfer of 07^{-/-} and 82^{-/-} plantlets to soil did not support further development and maturation of the plantlets beyond the rosette leaf stage. Additionally, besides the mutual development in sterile conditions with supplemental energy, both homozygous lines displayed a noteworthy difference in rosette sizes as compared to wild-type (Figure 5.3).

Homozygous plantlets of 07^{-/-} were particularly infrequent but displayed an interesting phenotype. These plantlets were noticeably smaller than their corresponding wild-types and produced leaves that were translucent as well as pointed at the apex (Figure 5.3a). Leaf tissue is particularly high in chloroplast genome content, often with an excess of 10,000 copies of organellar DNA per cell (Morley and Nielsen 2016). Therefore, it is plausible that the observed phenotype of 07^{-/-} is a direct result of the sub-optimal GyrA activity. The GyrB2 mutant 82^{-/-} displayed a relatively subtle phenotypic difference from the wild-type plants; their distinction residing mainly in their relatively smaller size (Figure 5.3b).



Figure 5.3: Observed phenotypes of GyrA and GyrB2 mutant plants.

(a) Representative images of GyrA 07 line; wild-type plant on the left (07^{+/+}) and homozygous GyrA mutant on the right (07^{-/-}). The GyrA mutant plantlet is considerably smaller, retains a pale green colour and its leaves are clearly pointed at the apex. (b) A similar representation of wild-type *Arabidopsis* (82^{+/+}) and mutant plants (82^{-/-}); possessing a clear size difference in comparison to the wild-type. The mutant plants of both lines are only viable in sterile growth conditions, with supplemental carbon sources, yet possessing a significant size difference in comparison to the wild-type.

5.2.3. The heterozygous GK-10 line

The T-DNA insertion line GK-077A10 (GK-10), corresponding to an insertion in intron six of *GyrA* (Figure 5.2b), has been phenotypically assessed and categorised as seedling lethal by Wall *et al.*, 2004. The result suggests that the *GyrA* protein may have a significant contribution in the early embryonic developmental stages of *A. thaliana*.

Investigation of GK-10 line was initiated by seed sterilisation and sowing onto agarose plates supplemented with half-strength Murashige and Skoog (MS) medium for identification of a homozygous seedling (GK-10^{-/-}). A large population of GK-10 plants were screened for the purpose of identifying a single homozygous recessive mutant, but this did not prove possible. This suggests, as suspected by Wall *et al.*, that the GK-10^{-/-} embryos are unable to develop into a mature seed. In order to investigate further, GK-10 plants confirmed by genotyping as either wild-type (GK-10^{+/+}) or heterozygous (GK-10^{+/-}) were germinated in soil. No obvious phenotypic differences were apparent during the development of the two genotypes.

5.2.3.1. Aborted GK-10^{-/-} seeds do not account for embryo-lethality

According to the principles of Mendelian inheritance, the F2 progeny of GK-10^{+/-} should include one-quarter homozygous recessive GK-10^{-/-} seeds, yet vigorous genotyping efforts were unable to identify a single GK-10^{-/-} plant. In order to further investigate this the developing siliques, which harbour seeds of the maturing embryos, were analysed more closely. This involved careful incisions along the dehiscence zones of the siliques, under an inverted microscope, to reveal the septum with attached F2 progeny offspring seeds. A clear observable difference was apparent in mature heterozygous siliques, from wildtype siliques; specifically, the possession of a larger proportion of shrivelled, dried and dark seeds, denoted as aborted, in the former siliques (Figure 5.4). Traditionally, mutant *Arabidopsis* seeds have been identified by changes to their size, shape and colour (Errampalli *et al.* 1991; Meinke 1995; Meinke and Sussex 1979). Feasibly, the observed aborted seeds could account for the seedling-lethal GK-10^{-/-} seeds. The GK-10^{+/-} siliques possessed ~18% more aborted off-spring than equivalent GK-10^{+/+} siliques. To determine the significance of this result, a Chi-Square goodness of fit analysis was applied to establish whether the GK-10^{+/-} line follows the expected Mendelian pattern of inheritance, that is, 25% wild-type (homozygous dominant), 50% heterozygous and 25% homozygous recessive distribution in the F2 progeny. However, only potential homozygous recessive seeds displayed phenotypically distinguishable characteristics. Therefore, the actual distribution tested in this case is 3:1 wild-type: heterozygous and homozygous recessive.

The heterozygous siliques possessed 19% of seeds classified as aborted in comparison to only 6% within wild type siliques. A Chi-Squared test of independence showed that F2 progeny of GK-10^{+/-} yielded an observed frequency of aborted seeds that significantly differed from the expected 3:1 ratio $X^2(1, N= 1018) = 8.371, p= .0038$. Hence, the GK-10^{-/-} off-spring of the defective GyrA line, presumed by Wall *et al.* to result in a seedling-lethal phenotype cannot statistically be accounted for by the appearance of the aborted seeds. Undoubtedly however, the striking difference in the maintenance of seed vitality of GK-10^{+/-} and GK-10^{+/+} siliques is not trivial and most certainly is the observable output of possessing functionally compromised GyrA protein *in vivo*.

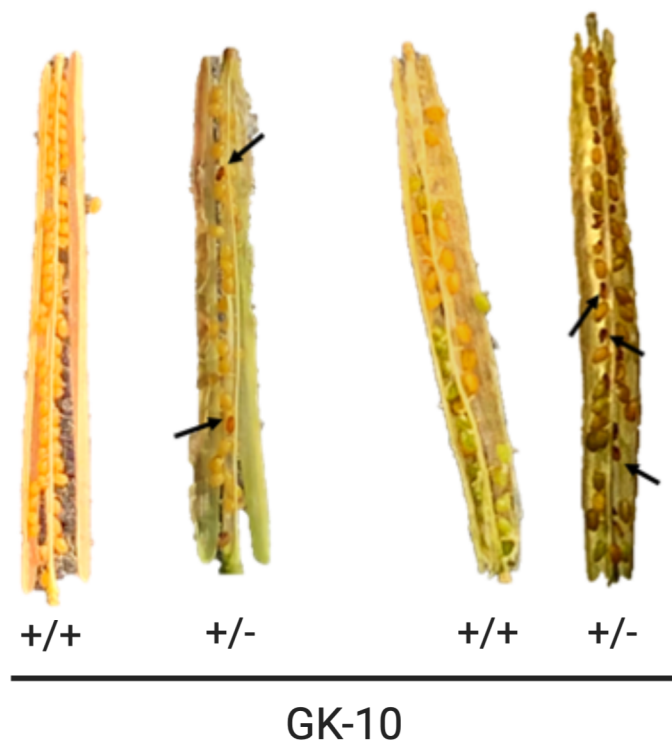


Figure 5.4: Dissected siliques of the GyrA GK-10 line exposing the next generation of seeds. The seeds held within wild-type plants (+/+) and heterozygous GK-10 plants (+/-) are displayed. The black arrows indicate potential aborted seeds, identified by their darker colour and dried and shrivelled phenotype; these seeds may account for the homozygous recessive GK-10 progeny (GK-10^{-/-}).

5.2.3.2. GK-10^{-/-} embryos are defective in ‘heart stage’ to ‘torpedo’ transition

The *in vivo* significance of GyrA during the process of embryogenesis was investigated further. The F2 progeny seeds of GK-10^{+/-} plants were stained with Hoyer’s solution, which clears pigmentation from thin tissue samples and possesses a high refractive index, allowing the penetration of light through the specimen with minimal dispersion. Stained seeds were assessed by differential interface chromatography (DIC). Parallel control experiments with GK-10^{+/+} plants were also conducted.

DIC of wild-type seeds established a benchmark representation of healthy embryos. The aborted seeds, categorised by their dark, dried and shrivelled appearance, became indistinguishable to the naked eye after embryo clearing with Hoyer’s stain. Individual GK-10^{+/+} seed pods revealed mature embryos, characterised by the presence of fully developed cotyledons (Figure 5.5a). Interestingly, the seed pods originating from a GK-10^{+/-} parent line additionally revealed immature embryos. The observations predominantly ranged of embryos identified at the ‘globular stage’ through to the ‘heart stage’ of embryogenesis, though certain embryos could not be clearly categorised (Figure 5.5b).

It is evident that the GK-10^{+/-} line possesses seeds defective in the process of embryogenesis. The embryos are able to develop into an apical and basal cell from the fertilized egg and then proceed through the octant, triangular and heart stages of embryogenesis, although arrest of cell differentiation may be halted before a mature heart shape is formed. The problematic developmental transition for GK-10 was identified to be the advancement from the heart stage into forming the torpedo, where a more apparent root apical meristem is formed and critically, the cotyledons start to mature. The cotyledons serve the essential function as a food source within the seed and are fated to form the first photosynthetic leaves of the plant. Evidently, the results of this investigation suggest an embryo-defective phenotype for the GK-10 line. These results corroborate transcriptome data obtained from the analysis of genes in the Columbia-0 *Arabidopsis* background, where expression of the GyrA protein has been acknowledged as extremely high, particularly from the globular embryo until the late heart embryo, with the level only slightly reduced in the early torpedo (Figure 5.6a) (Hofmann et al. 2019). Furthermore, the GyrA transcript has been recognised as being abundant within the cotyledon segment of the heart embryo (Casson et al. 2005); further providing support for the defective transition from heart stage embryo to torpedo embryos being down to insufficient GyrA in the GK-10^{-/-} line (Figure 5.6b).

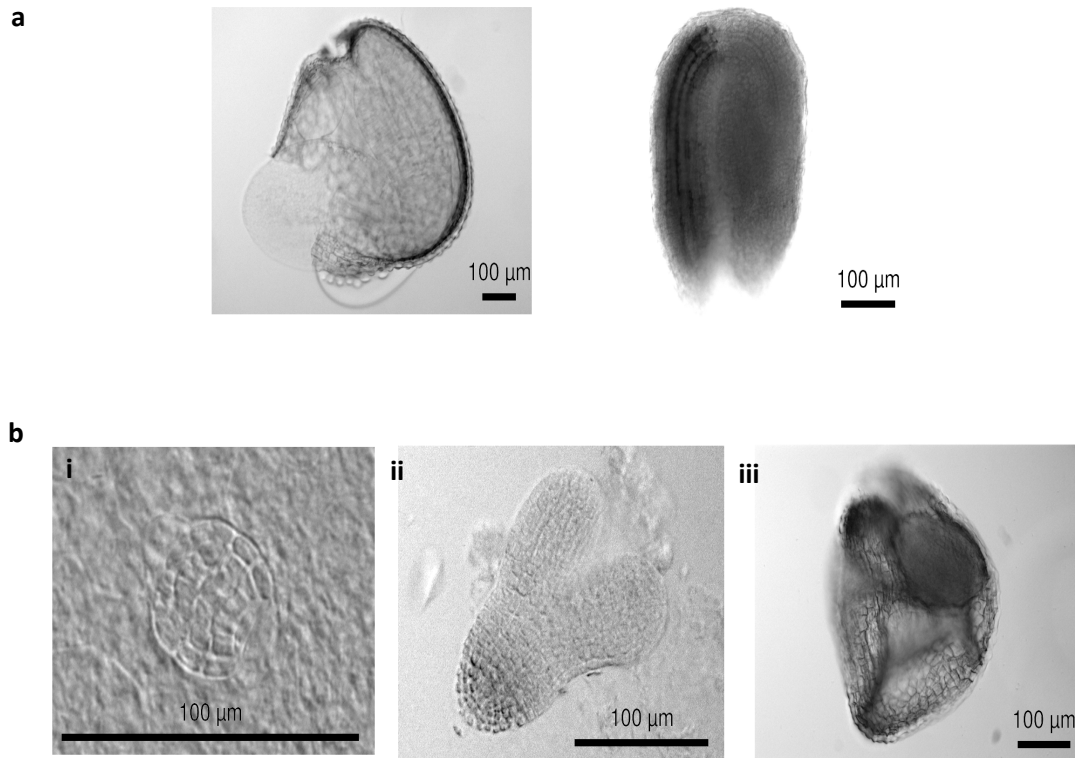


Figure 5.5. DIC microscopy images of the progeny of GK-10^{+/+} and GK-10^{+/-} embryos.

Seeds corresponding to GK-10^{+/+} and GK-10^{+/-} were cleared with Hoyer's solution and visualised by DIC. (a) Representative GK-10^{+/+} seeds displaying a mature embryo where the seed predominantly comprises the embryo and cotyledons. (b) Images of seeds from the GK-10^{+/-} line, at the same time point. i) Embryo development halted at the globular stage. ii) Embryo development halted at the heart stage. iii) A representative dead seed missing any indication of a mature embryo or cotyledons.

The GK-10 line has been an invaluable resource to evaluate the *in vivo* function of GyrA. In-depth analysis, beyond previous work by Wall *et al.*, indicates a vital role for GyrA from the onset of embryogenesis; the GK-10^{+/-} line shows that possession of at most, a single functionally compromised GyrA protein, can severely hinder embryogenesis as is indicated by the discovery of embryos paused during development. Although statistical analysis concluded that the expected one-quarter GK-10^{-/-} seeds from a GK-10^{+/-} progeny, could not be accounted by the aborted seeds, it is plausible that a sub-population of GK-10^{-/-} demonstrated embryo-defectiveness without a characterizable phenotype, the embryos may be in a dormant state of embryogenesis, or the homozygous recessive line may be unable to initiate embryogenesis.

The embryo-lethality of GyrA evidenced by the GK-10 line provides an insight into the *in vivo* role of the subunit. Investigation of large mutant collections of the Columbia-0 accession of *Arabidopsis* have highlighted a strong association of an embryo-lethal outcome to aberrant chloroplast translation (Meinke 2020). Considering the essential role that the gyrase protein plays in the replication of DNA and advancement of the replication fork; the embryo-lethal phenotype of GK-10 is likely a consequence of abnormal DNA replication of the chloroplast encoded ribosomal proteins, which are subsequently required for the translation of essential organelle-encoded genes.

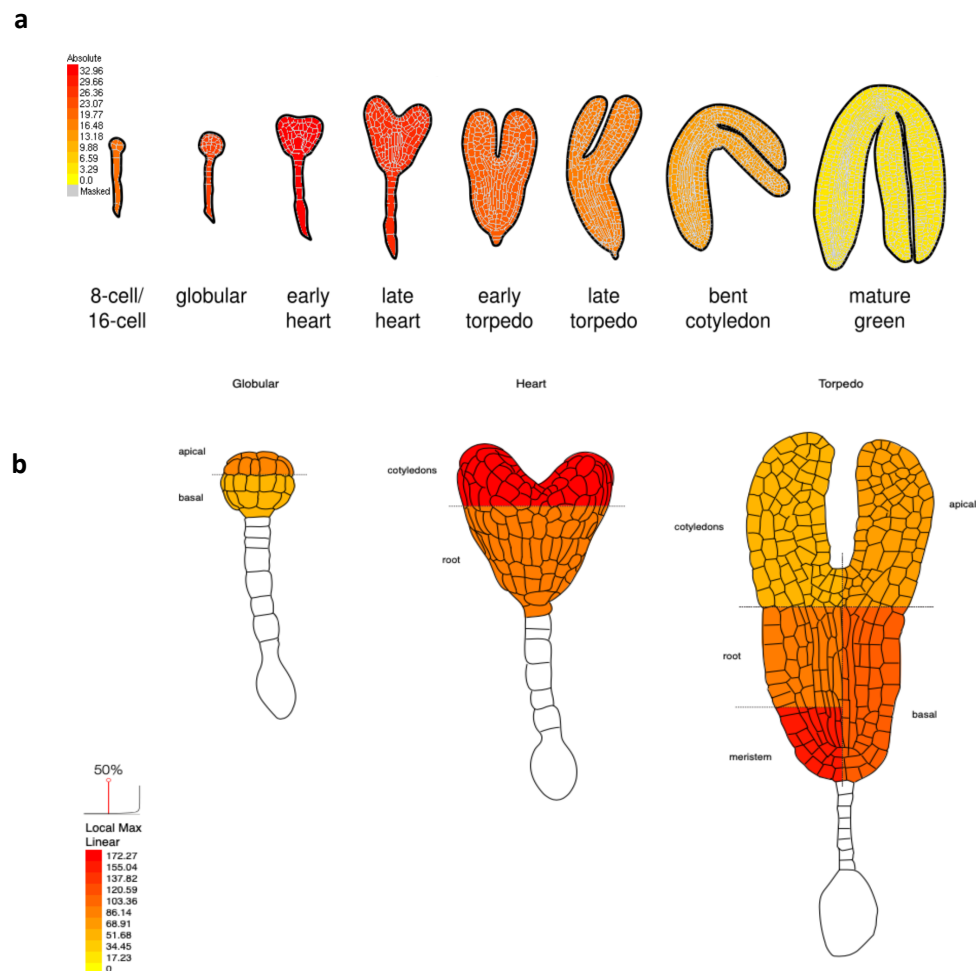


Figure 5.6: Analysis of GyrA transcripts during embryonic development of Columbia-0.

(a) The absolute levels of GyrA mRNA quantification in Columbia-0 seeds grown in 16 hour light/8 hour dark cycles at 20-22°C (Hofmann et al. 2019). (b) GyrA transcript quantification of Columbia-0 plants, RNA was hybridized to ATH1 GeneChip and amplified. Plants grown in 16 hour light/8 hour dark cycles (Casson et al. 2005). This image was generated using Tissue Specific Embryo Development eFP at bar.utoronto.ca/eplant by (Waese et al. 2017).

5.2.4. Phenotypes of homozygous mutants

The remaining lines that were viable on soil were assessed comprehensively to identify phenotypic differences. The assessment was adapted from a model of growth stage-based analysis of *Arabidopsis* previously conducted by Boyes *et al.* (2001). The method involved scoring development of wild-type *Arabidopsis* seedlings against predetermined criterion. The assessment is divided into two stages, the first analysis involves assessment of characteristics during the plate-based phase and the second during the soil-based phase of growth.

The adapted criterion used to score development of wild-type and mutant *Arabidopsis* lines used in this work are given in Table 5.3 for plate-based analysis and Table 5.4 for soil-based. Sterilised seeds were first stratified at 4°C for three days to synchronize germination. The homozygous seedlings of wild-type Colombia-0 lines GyrB1: SALK_139478 (78^{-/-}), GABI_586A06 (GK-06^{-/-}) and GyrB2 line SALK_002367 (67^{-/-}) were scored according to the criterion in Table 5.3 and Table 5.4. The majority of exemplar phenotypic stages are documented in Figure 5.7 (Boyes *et al.* 2001).

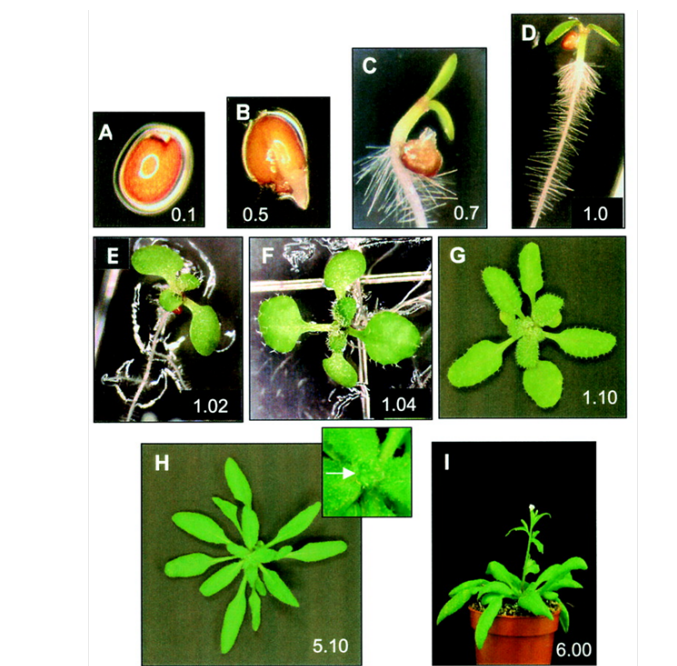


Figure 5.7: Representative images of assigned growth stages for phenotypic analysis.

(A) Stage 0.1 – seed imbibition. (B) Stage 0.5 – emergence of radicle. (C) Stage 0.7 – emergence of hypocotyl and cotyledons. (D) Stage 1.00 – fully opened cotyledons. (E) Stage 1.02 – two rosette leaves > 1 mm. (F) Stage 1.04 – four rosette leaves > 1 mm. (G) Stage 1.10 – ten rosette leaves > 1 mm. (H) Stage 5.10 – appearance of first flower buds (inset). (I) Stage 6.10 – opening of the first flower. Figure taken with permission from (Boyes *et al.* 2001).

Table 5.3: *Arabidopsis* growth stages for phenotypic plate-based analysis according to the previous methods of Boyes *et al.*, 2001.

Stage	Description
Principle growth stage 0	Seed germination
0.10	Seed imbibition
0.50	Radicle emergence
0.70	Hypocotyl and cotyledon emergence
Principle growth stage 1	Leaf development
1.00	Cotyledons fully opened
1.02	2 rosette leaves > 1 mm
1.04	4 rosette leaves > 1 mm

Table 5.4: *Arabidopsis* growth stages for phenotypic soil-based analysis according to the previous methods of Boyes *et al.*, 2001.

Stage	Description
<1.10	Less than 10 rosette leaves > 1 mm
1.10	At least 10 rosette leaves > 1 mm
Principle growth stage 3	Rosette growth
Principle growth stage 5	Inflorescence emergence
5.10	First flower buds visible
Principle growth stage 6	Flower production
6.10	First flower open
Principle growth stage 7	Silique ripening
7.10	First filled silique developed

5.2.4.1. Plate-based development of GK-06^{-/-} plants differed from wild-type

The results of the plate-based analysis are summarised in Figure 5.8. The data represents the percentage of plants at each growth stage (0.10 through to 1.04) for each day of development, subsequent to the three-day stratification at 4°C. Figure 5.8a represents results of wild-type Columbia-0 *Arabidopsis*. Dead seeds were not included in the analysis.

All of the wild-type Columbia-0 seeds progressed either onto radicle or hypocotyl emergence by day three. At the end of analysis at day 15, 80% of seeds had successfully developed a minimum of four rosette leaves, each greater than 1 mm. Although a small proportion of seeds were unable to develop cotyledons or progress further beyond that point. The plate-based development of 67^{-/-} and 78^{-/-} largely coincided with that of wild-type *Arabidopsis*. The seedlings started with either emerged radicles or cotyledons and hypocotyls at day three; with the incidence of first cotyledons fully opening by day four. Two rosette leaves bigger than 1 mm were first identifiable by day nine and four similar rosette leaves apparent by day twelve.

The advantage of this method is its potential to highlight ultrafine differences during development, which are no doubt noticeable between wild-type 67^{-/-} and 78^{-/-}. This is mainly evident in the proportion of seedlings progressing from one growth stage to the next. For example, a larger proportion of wild-type seeds with fully opened cotyledons (growth stage 1.00) then went on to successfully develop two rosette leaves (growth stage 1.02) within a 24-hour period than 67^{-/-} and 78^{-/-}. Additionally, the transition from growth stage 1.00 to 1.02 encompassed days 8-11 in wild-type and 78^{-/-} but continued until day 14 for 67^{-/-}. The two mutant lines also possessed a small proportion of seeds that were extremely slow in development, characterised by the late emergence of a radicles by days 14 and 15.

Interestingly, the plate-based development of GK-06^{-/-} was more distinct. Initially, the rate of development surpassed the wild-type line as the majority of seeds had already emerged hypocotyls and cotyledons by day three. Beyond this however, only approximately 40% of plants were able to develop four rosette leaves. The remaining proportion were unable to develop further once cotyledons had formed and opened.

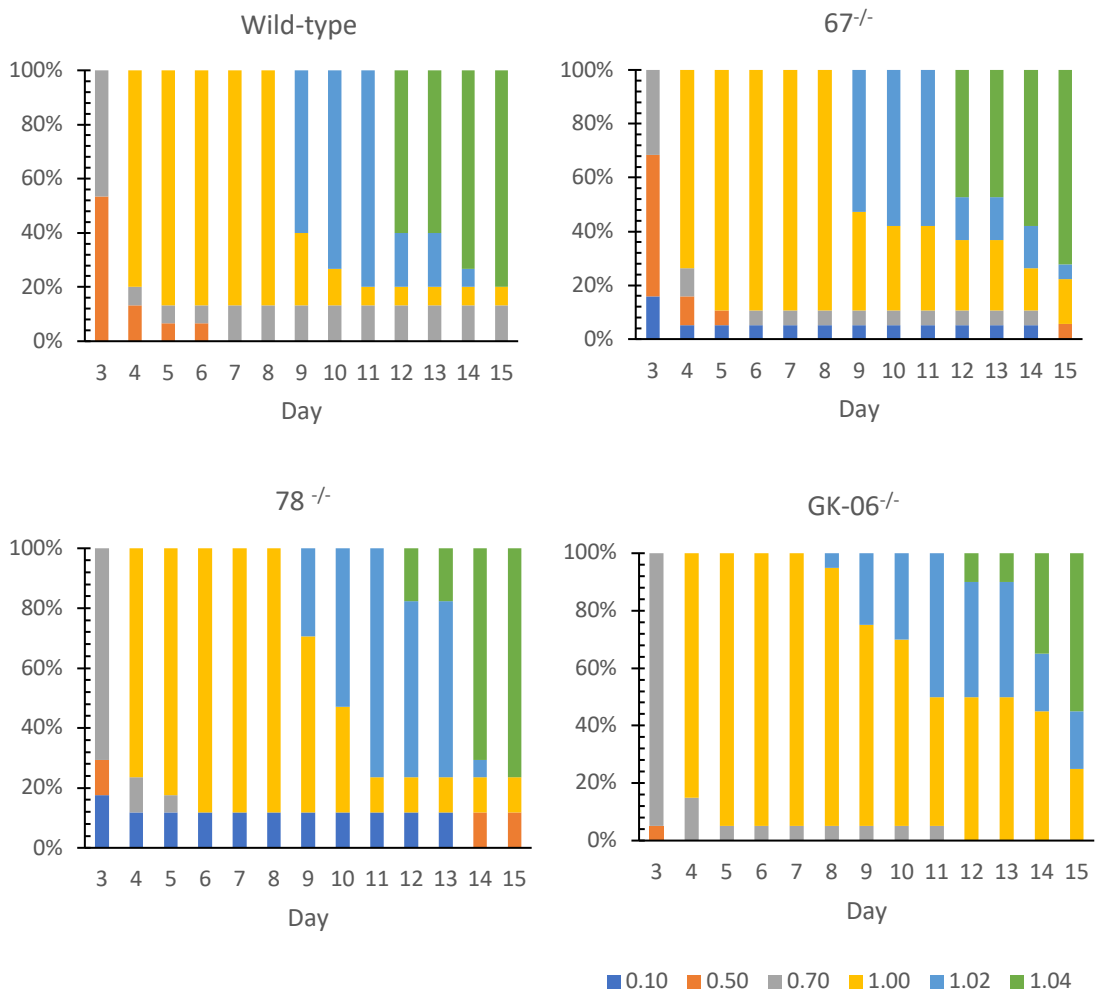


Figure 5.8: Summarised output of plate-based phenotypic analysis.

The plants of Columbia-0 and homozygous 67^{-/-}, 78^{-/-}, GK-06^{-/-} lines were assessed in parallel according to the criterion in Table 5.3. The data is represented as the percentage of total plants assessed for each line at a particular growth stage, for each day of analysis post-sowing of the seeds onto plates. The growth stages are as follows: 0.10 – dark blue, 0.50 – orange, 0.70 – grey, 1.00 – yellow, 1.02 – light blue and 1.04 – green.

5.2.4.2. Homozygous 67^{-/-} plants thrived on soil whilst GK-06^{-/-} lagged

Plantlets corresponding to each line that had successfully reached stage 1.04 of development (marked by four rosette leaves greater than 1 mm), were transferred to soil for further developmental analysis (Table 5.4). The development was scored every two or three days; the summarised results of the percentage of plantlets at each growth stage (Figure 5.9). All lines followed the common trend of development. However, line 67^{-/-} exhibited an accelerated rate of growth compared to wild-type; exemplified by a proportion of its plantlets initiating the process of inflorescence as early as day 9, three days earlier than the wild-type. Line 78^{-/-} largely correlated with the wild-type trend of development; differing once again only by a reduced proportion of plantlets reaching each developmental benchmark. The developmental lag of GK-06^{-/-} during plate-based analysis was also observed after transfer to soil. These mutants were able to initiate the process of inflorescence emergence with identifiable flower buds and at least the production of one flower in coordination with wild-type plants. The process was complete within the seven days for all wild-type seedlings, yet required twice as much time for completion by GK-06^{-/-}.

5.2.4.3. GK-06^{-/-} plants are dwarfed

Various physical characteristics were noted during development, including the average rosette diameters at the point at which flower buds became visible for each line, in addition to the average length of stem and number of filled siliques at the end of analysis (Table 5.5). The data reinforces that the development of all lines largely coincide at face value; notably however, the dwarfed phenotype of GK-06^{-/-} is apparent by its reduced rosette diameter and significantly shorter length of stem. Furthermore, at the time of experimentation further characteristics unique to GK-06^{-/-} were also noted. The GK-06^{-/-} line exhibited notable chlorotic patches in areas of leaves particularly during early development, from which the plant seemingly recovered, as such chlorotic areas were not obvious towards the end of the soil-based analysis. A further atypical feature of the line became apparent during the process of silique development marked by the revelation of a number of underdeveloped siliques, miniature in size and devoid of embryos (Figure 5.10).

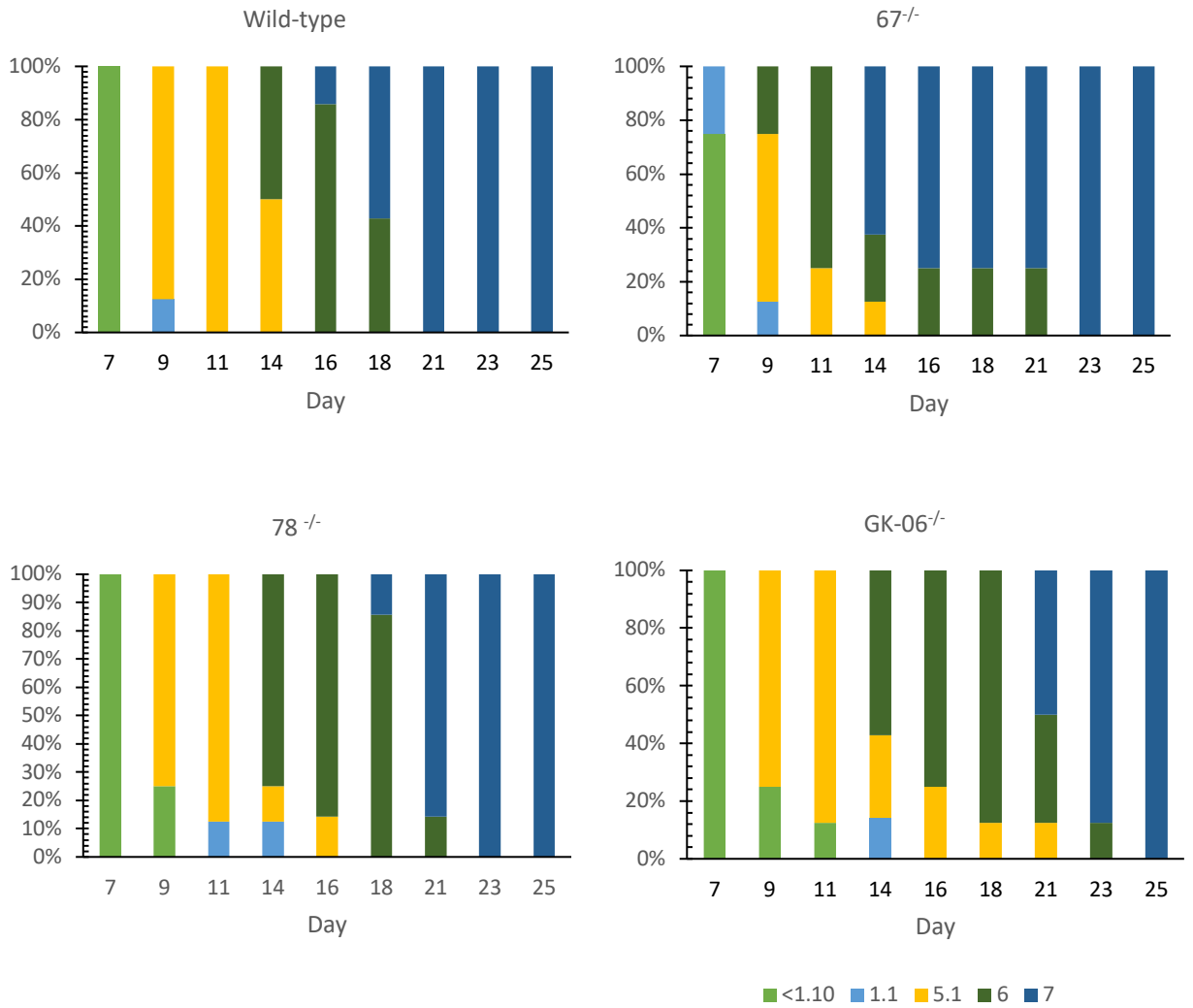


Figure 5.9: Summarised output of soil-based phenotypic analysis.

The plants of Columbia-0 and homozygous 67^{-/-}, 78^{-/-}, GK-06^{-/-} lines were assessed in parallel according to the criterion in Table 5.4. The data is represented as the percentage of total plants assessed for each line at a particular growth stage, for each day of analysis post-transfer of the plants to soil. The growth stages are as follows: <1.10 – light green, 1.10 – light blue, 5.10 – yellow, 6.00 – dark green, 7.00 – dark blue.

Table 5.5: Average soil-based phenotypic measurements of 10 plants.

Line	Rosette diameter at stage 5 (cm)	Length of stem (cm)	Number of filled siliques per plant
WT	47	195	9
67 ^{-/-}	51	265	16
78 ^{-/-}	44	210	6
GK-06 ^{-/-}	37	115	6

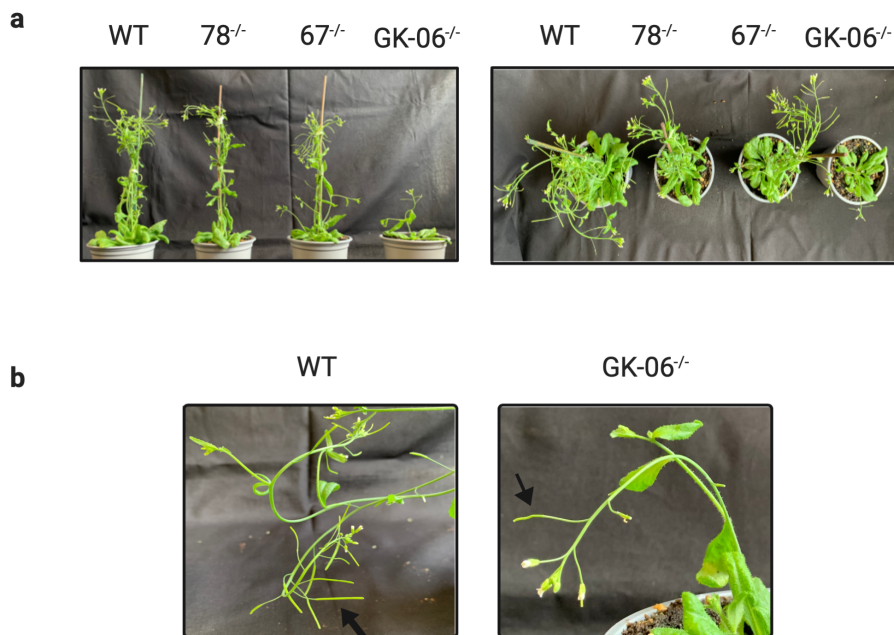


Figure 5.10: Representative images of wild-type and mutant GyrB lines.

(a) Front view (left) and top view (right) of each line assessed at the end of soil-based analysis. (b) Close-up view of wild-type (left) and GK-06^{-/-} siliques (black arrows) at the end of analysis. The siliques of GK-06 frequently appeared under-developed.

5.2.5. Phenotype discussion

The developmental analysis of GyrB mutant plants from the process of germination until development into a mature plant can be used to understand the role of GyrB proteins in *Arabidopsis*. The plants of 67^{-/-} did not deviate strongly from development of wild-type plants during the early plate-based analysis, yet these plants seemingly flourished to a greater extent when transferred to the nutrient dense soil conditions; evident by their accelerated transition through the assigned developmental targets, their increased average rosette diameter, stem length and number of filled siliques at the end of analysis.

The phenotypes of the two GyrB1 lines assessed here, 78^{-/-} and GK-06^{-/-}, did not show an overall unity. Plants of line 78^{-/-} predominantly followed wild-type Columbia-0 development, with the exception of a small proportion of seedlings retaining extremely slow growth on plates. In contrast to the GyrB2 line 67^{-/-}, these plants also largely harmonized with wild-type developmental patterns when transferred to soil, apparent by the similar average rosette diameter, stem length and number of filled siliques.

Klepikova *et al.*, (2016) conducted transcriptome-based RNA-sequence profiling during development of wild-type *A. thaliana*; according to the fluorescent pictographs generated using their data the GyrB1 and GyrB2 proteins are expressed to different degrees within the cotyledons, hypocotyl and roots of young seedlings (Klepikova *et al.* 2016) (Figure 5.11). According to their analysis, the scales of absolute expression for each GyrB gene varied somewhat. Both genes are expressed strongest in the cotyledon, however the expression of GyrB1 is slightly reduced but consistent within the hypocotyl and root; whilst that of GyrB2 is reduced more in the hypocotyl than in the root of the seed.

The observations by Klepikova *et al.*, confirm the requirement of GyrB proteins during early development in wild-type *Arabidopsis*. Two of the mutant lines, 78^{-/-} (GyrB1) and 67^{-/-} (GyrB2) do not differ significantly from wild-type development; plausibly, this may be a consequence of functional redundancy of the GyrB proteins, which would reinforce the observation of dual targeting of both GyrB1 and GyrB2 subunits to the chloroplasts and mitochondria (Monika Murcher, personal communication, Figure 5.1). Alternatively, the insertional mutagenesis within these genes may not affect the level of GyrB transcripts, thus the level of functional protein remains stable.

The second GyrB1 line phenotypically assessed, GK-06^{-/-}, exhibited hastened hypocotyl and cotyledon emergence. Interestingly, the majority of these plants were unable to proceed beyond the point of cotyledon development during plate-based growth analysis. This is particularly noteworthy considering the relatively higher energy investment of the GyrB1 subunit required for hypocotyl development, as determined by

data from Klepikova *et al.*, (2016), in wild-type plants when compared to levels of GyrB2. Conceivably, the substantial investment of GyrB1 required for hypocotyl and cotyledon production in this line exhausts the pool of available protein, thus limiting development beyond this point. Nevertheless, a fraction of GK-06^{-/-} plants were able to match wild-type development during plate-based analysis, but in the long-term these plants displayed further characteristic phenotypic differences from wild-type including: leaf chlorosis, underdeveloped siliques and somewhat stunted overall growth (Figure 5.10). It is interesting to consider the rationale for the progression of a fraction of GK-06^{-/-} plants to be able to proceed beyond cotyledon production. Plausibly, the GyrB2 protein is able to complement the function of GyrB1 to a limited extent during the development of these plants; although why all GK-06^{-/-} plants may not gain this advantage remains unclear.

The phenotype data obtained alone does not allow an overall conclusion regarding the role of either GyrB subunits *in vivo*. According to Klepikova *et al.*, the expression of both GyrB1 and GyrB2 is significant in the production of roots. Therefore, it was hypothesised that phenotypic differences in root analysis may help to further elucidate the *in vivo* function of these proteins.

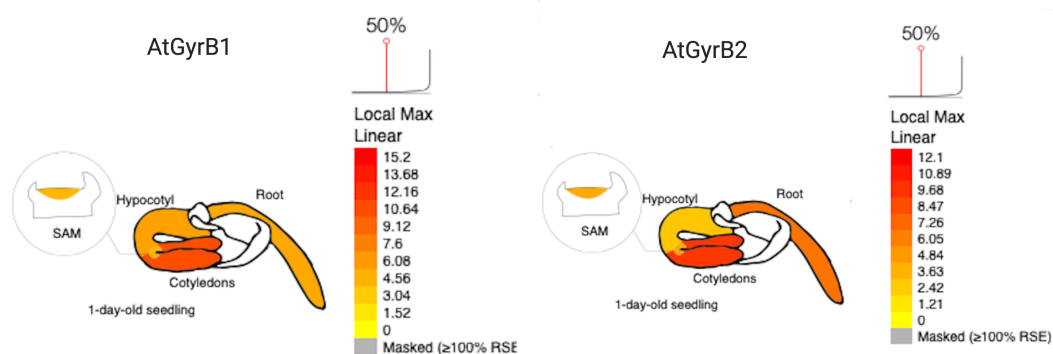


Figure 5.11: RNA-based expression profiling of *Arabidopsis* gyrase subunits.

Seedling expression profile for GyrB1 (left) and GyrB2 (right) based on total RNA extraction, with respective expression scales to the left. This image was generated using Tissue Specific Embryo Development eFP at bar.utoronto.ca/eplant by (Waese et al. 2017) using the experimental data of (Klepikova et al. 2016).

5.2.6. *In vivo* contribution of GyrB for root development

5.2.6.1. The primary root lengths of homozygous GyrB lines are similar to wild-type

Thus far, homozygous GyrB lines have been unable to provide a clear indication for the *in vivo* functions of the proteins. To augment the observations and in particular, considering the relevance of GyrB for root development implied by Klepikova *et al.*, 2016 (Figure 5.11), root analysis for homozygous lines was conducted. Homozygous seeds of each line and wild-type Columbia-0 were sterilised and plated onto half-strength MS media. Plates were stratified at 4°C for three days to synchronize germination and grown in (16-hour light/ 8-hour dark cycles) for 14 days. Roots were analysed using, SmartRoot, a semi-quantitative image analysis software (Morley and Nielsen 2016).

The primary root is formed first during development and serves as the principal anchor of the plant. The lengths of primary roots varied somewhat within each line (representative plants in Figure 5.12a). No significant difference was identified in the lengths of these roots when homozygous 67^{-/-}, 78^{-/-} and GK-06^{-/-} were compared to Columbia-0 roots (Figure 5.10b). The boxplots represent the primary root lengths of all lines, the boxes indicate inter-quartile ranges and whiskers show the minimum and maximum values. Horizontal lines within the inter-quartile ranges give median primary root lengths. Generally, the mutant lines possessed more variation in their primary root lengths than wild-type and the majority of primary roots grew to a length of ~7–8.5 cm.

5.2.6.2. GK-06^{-/-} possess altered lateral root morphology

The root branching system comprises horizontal extensions originating from the primary root, known as lateral roots. Similar to primary roots, the length of lateral roots varied within each assessed line. Typically, the lengths were inversely proportional to the depth of the root (Figure 5.10c). The Columbia-0, 67^{-/-} and 78^{-/-} lateral roots did not significantly differ from one another although the two mutant lines, 67^{-/-} and 78^{-/-} were related by a common majority lateral length of 0.6 cm and overall possessed less variation than wild-type.

The lateral root composition of GK-06^{-/-} however was significantly different to all other assessed lines, marked by the reduction in both their size and average number (Figures 5.10 a,c,d). Mutant roots of GK-06^{-/-} were only able to grow an approximate four lateral roots per primary root on average, frequently with a reduced length of 0.2 cm. Columbia-0 primary roots, under the same experimental conditions were found to generate twenty-eight lateral roots on average, most commonly of lengths of 1.1 cm.

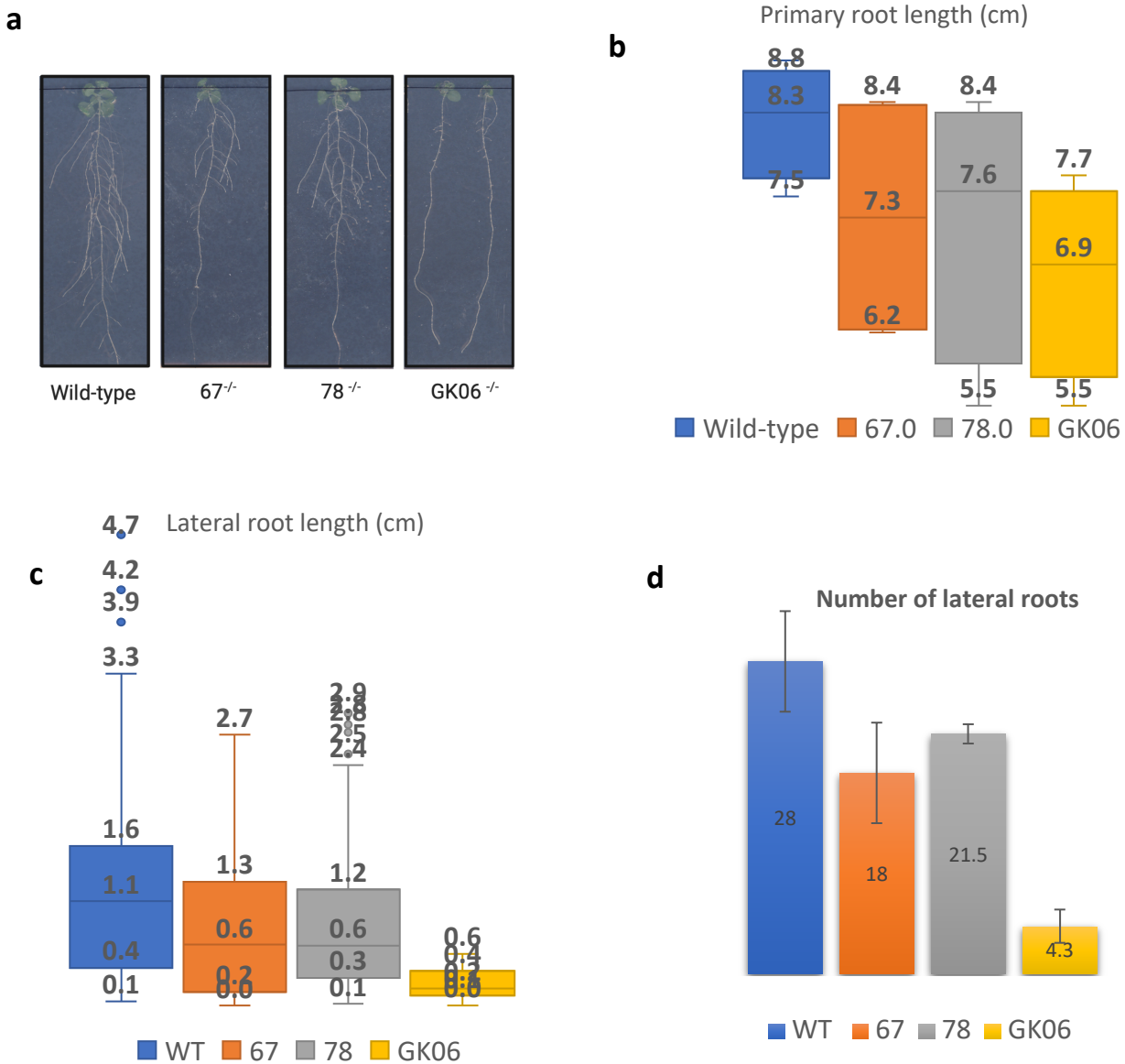


Figure 5.12: Root analysis of wild-type and homozygous lines.

(a) Representative root images of each line. (b) Box-plot for primary root lengths. The shaded areas represent the inter-quartile ranges and lines indicate median primary root lengths; the whiskers represent minimum and maximum values. (c) Box-plot representation of lateral root lengths. (d) The average number of lateral roots for each line, error bars indicate standard error mean values. Wild-type (blue), 67^{-/-} (orange), 78^{-/-} (grey) and GK-06^{-/-} (yellow).

5.2.6.3. Discussing the implications of GyrB in root development

The immobility of plants emphasises the importance of their root systems for survival. These vital organs are responsible for anchoring the plants within the vicinity of essential substrates, obtaining and transporting water and minerals and also serve as sites for the production of essential metabolites (Dubrovsky et al. 2006). The process of new root development is a continuum throughout plant growth; root architecture involves the branching of secondary lateral roots from the primary root.

The root organs possess an intricate cell composition. The outermost layer is made up of epidermis cells followed inwardly by exodermis, cortex, endodermis, pericycle and then phloem and xylem cells; all organised concentrically. The lateral roots extend horizontally from the pericycle cells of the primary root. The pericycle cells that speciate and initiate lateral roots are specifically known as founder cells. The basal meristem controls the competence of xylem-pole pericycle cells to develop into founder cells (De Smet et al. 2007). The initiation of lateral roots is tightly controlled by aspects of the cell cycle and linked to the production of hormones like auxin (Malamy and Benfey 1997). Classically, the network of lateral roots increases with an increase in leaf primordia, to maintain an appropriate balance of carbon and nitrogen fixation for the plant.

Brady *et al.* (2007) implemented microarray expression profiles during developmental time-points within *Arabidopsis* roots, in order to spatial-temporally map expression of genes for different root cell types (Brady et al. 2007). Their spatial mapping of GyrB1 and GyrB2 within the meristematic zones of primary roots for Columbia-0 *Arabidopsis* is depicted in Figure 5.13. The investigations of cell-type specific transcriptomes highlight a similar expression pattern for GyrB1 and GyrB2 proteins within the meristematic zone of the Columbia-0 roots (Brady et al. 2007) (Figure 5.13). The experimental evidence of this work concludes that the primary root lengths of all homozygous GyrB1 and GyrB2 lines did not significantly differ, suggesting a similar role for GyrB proteins to support the cellular divisions required for primary root formation. However, the GyrB1 GK-06^{-/-} plants, specifically were incompetent in lateral root formation when compared to Columbia-0, 78^{-/-}(*gyrB1*) and 67^{-/-}(*gyrB2*). Previous investigations into the precise concentric cell layers spanning the entire root, have identified elevated GyrB1 transcript levels, in comparison to GyrB2, explicitly within the pericycle cells of wild-type *Arabidopsis* (Waese et al. 2017) (Figure 5.14). The meristematic zone controls the initiation of lateral root formation, by triggering xylem-pole pericycle cells to develop into founder cells from which lateral roots arise. The instigation of founder cells, within its defined zone, correlates with zones of minimal auxin

content and response (Dubrovsky et al. 2011). The unambiguous reduction in number of lateral roots per plant for GK-06^{-/-} roots strongly implies diminished GyrB1 activity within the meristematic zone of these roots, debilitating the initiation of founder cells from pericycle cells.

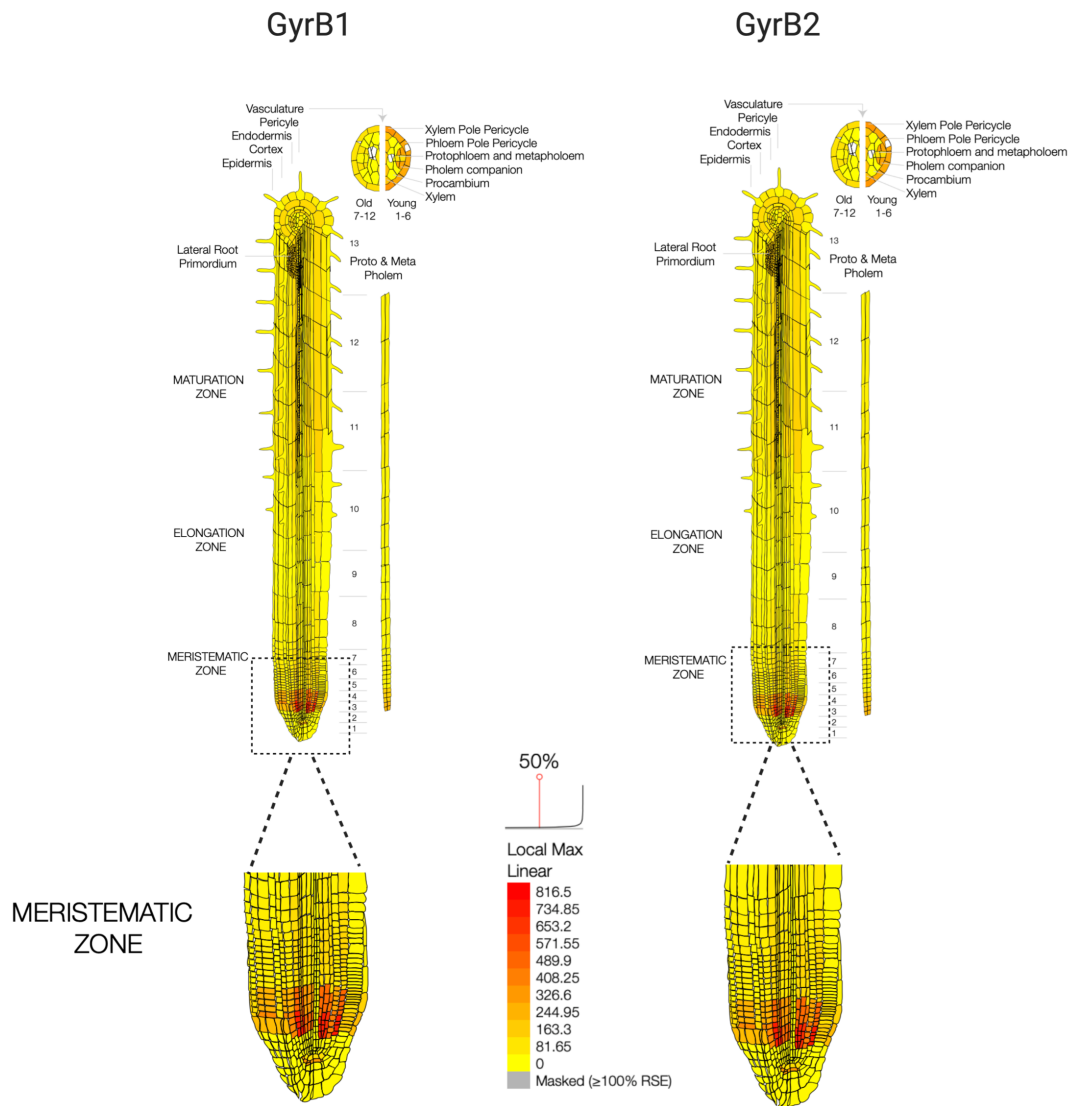


Figure 5.13: Expression profiling of GyrB1 and GyrB2 in the Columbia-0 primary roots.

Microarray expression data collected by (Brady et al. 2007) spatiotemporally mapped onto various root-cell types of the primary root. This image was generated using the Tissue and Experiment eFP viewer at eFP at bar.utoronto.ca/eplant by (Waese et al. 2017) using the experimental data of (Brady et al. 2007).

The formation of lateral roots is partially understood but a greatly complex phenomenon, involving environmental cues such as signalling of sucrose and auxin accumulation (Dimitrov and Tax 2018; Laskowski and Ten Tusscher 2017; Truernit 2001; Wind et al. 2010; Xuan et al. 2015). The photosynthetic tissues in plants contain green chloroplasts. In addition to these, heterotrophic organs contain non-green plastids, roots included (Kobayashi et al. 2012; Robertson and Laetsch 1974). Formation of plant organs involves the processes of cell proliferation and expansion; the former implicates division of cells, whereas expansion of cells does not require division but instead involves growth and differentiation (Donnelly et al. 1999; Kalve et al. 2014). Nevertheless, both developmental processes require the input of energy in the form of sugars and ATP, supplied by key organelles like mitochondria and plastids (Van Dingenen et al. 2016). The transition of cell proliferation and differentiation is tightly regulated by the cell cycle. The essential GyrB proteins investigated here are involved in numerous organellar DNA replication and metabolism processes. The *Arabidopsis* DNA gyrase function in the homeostasis of organellar R-loop processing in co-ordination with RNaseH1 proteins to maintain plastid genome integrity (Yang et al. 2017). In rice plants, DNA topoisomerase I (TOP1), a type I topoisomerase able to remove positive and negative DNA supercoils formed during replication, has been implemented to prevent the accumulation of R-loops. Interestingly, the authors found that knockdown of TOP1 resulted in altered root architecture, ultimately due to mis-regulation of auxin signalling (Shafiq et al. 2017). The molecular mechanism for the altered root architecture of GK-06^{-/-} may also be of a similar nature, given the importance of gyrase proteins in R-loop processing (Yang et al. 2017). The interruption of plastid translation results in altered lateral root stem cell formation and decreased accumulation of ribosomal RNA in roots (Nakata et al. 2018). The GyrB1 protein, undisputedly plastid targeted, may therefore cause the reduction of lateral root formation through a molecular mechanism involving the mis-regulation of R-loop processing of plastid encoded ribosomes. The results imply that *Arabidopsis* GyrB1 is crucial *in vivo* for the initiation and development of lateral roots.

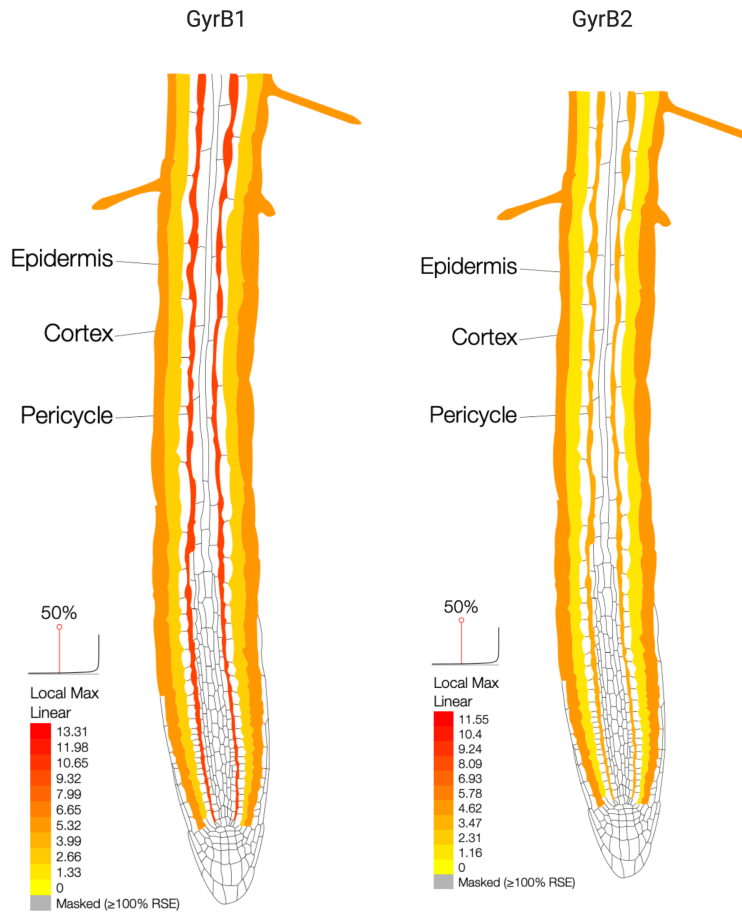


Figure 5.14: Expression profiling of GyrB1 and GyrB2 proteins within the concentric cell layers of the Columbia-0 *Arabidopsis* primary root.

Transcriptome gene analysis of wild-type *Arabidopsis*; transcript levels in epidermis, cortex and pericycle cells evaluated (Rich-Griffin et al. 2020). This image was generated using the Tissue and Experiment eFP viewer at eFP at bar.utoronto.ca/eplant by (Waese et al. 2017).

5.2.7. Probing the *in vivo* function of GyrB within chloroplasts

The *Arabidopsis* DNA gyrase is nuclear-encoded and organellar-targeted to either chloroplasts or mitochondria (Wall et al. 2004). The biological role of gyrase in these organelles remains unknown. The sequence resemblance of *A. thaliana* gyrase to the bacterial *E. coli* protein and the functional cooperation of subunits of either species, implies that the plant protein has a similar role in regulating negative supercoiling within the organellar genomes to which they are targeted. Similar to *A. thaliana*, the gyrase of *N. benthamiana* is also proposed to be encoded by a single GyrA gene and two copies of GyrB, that are organellar targeted (Cho et al. 2004). Cho *et al.*, (2004) identified the *N. benthamiana* gyrase to have a significant role in chloroplast genomic division. In light of this, a systematic approach was taken to explore the organellar role of DNA gyrase in *A. thaliana* chloroplasts, to determine potential differences in organellar size and morphology.

5.2.7.1. The mutant GyrB lines did not manifest significant differences in live chloroplasts

DNA replication is a continuous process within live cells and gyrase is implicated in its governing. The fact that plastids only originate from other plastids by binary fission confirms that the process of replication and division within these organelles is essential to the survival of the plant (Raynaud et al. 2005). Additionally, information of the health and physiological state of chloroplasts, including their ability to photosynthesise and perform carbon dioxide assimilation can be determined by monitoring their chlorophyll autofluorescence (Donaldson 2020). The premise that altered replication due to abnormal GyrB may contribute to changes in live functioning chloroplasts, such as their overall size or intensity of autofluorescence was investigated using a non-destructive technique.

Arabidopsis chloroplasts corresponding to GyrB lines of interest: 67^{-/-}, 78^{-/-}, GK-06^{-/-} and Columbia-0 were isolated from four to five-week-old plants germinated in soil. To take advantage of the abundance of chloroplasts in the rosette leaf samples, these were subjected to multiple rounds of gentle homogenisation, centrifugation and intact chloroplasts were separated by percoll density gradients as described in 2.6.9.

Live isolated chloroplasts were prepared for analysis by light microscopy (2.10.4). This involved dilution of chloroplast material with equal part glycerol and immobilisation directly onto 1% agarose beds prepared immediately prior to the application of chloroplast samples. A Zeiss Axio zoom V16 microscope attached to a monochrome camera was used for image capture. Data collection involved capture of z-stack images and

evaluation of chloroplast autofluorescence to assess individual chloroplasts and chlorophyll intensities. The image stacks were scanned to identify planes of focus and boundaries of fluorescence used to estimate chloroplast areas. Broken and damaged chloroplasts were excluded.

Table 5.6. Mean chloroplast area and autofluorescence intensities with standard deviations. Number of chloroplasts assessed: wild-type (WT): 250, 67^{-/-}: 406, 78^{-/-}: 146 and GK-06^{-/-}:296.

Line	Average chloroplast area (µm²)	Average chloroplast intensity
WT	20.4 ± 6.87	0.11 ± 0.026
67 ^{-/-}	21.4 ± 7.04	0.12 ± 0.031
78 ^{-/-}	24.1 ± 7.49	0.076 ± 0.024
GK-06 ^{-/-}	19.3 ± 7.55	0.10 ± 0.032

Chloroplasts of different plant species have been identified to have a typical diameter of ~4-6 µm and a width of ~2.5 µm (Norris 1929; Staehelin 2003). All lines sampled possessed a degree of internal fluctuation in chloroplast area, a possible reflection on the population of chloroplasts at different developmental stages. The average area per chloroplast and intensity of autofluorescence are reported in Table 5.6. The data obtained in this study endorse previous estimations of chloroplast size; the Columbia-0 chloroplasts presented an average chloroplast size of ~20 µm². The analysis of homozygous lines did not reveal a prominent change in chloroplast area. Although chloroplast area values ranged from ~19-24 µm² for lines assessed, no significant conclusions can be drawn due to the internal fluctuation within each sample (signified by the standard deviation). In addition, no significant difference was detected in the auto-fluorescence intensity of any lines from that of wild-type *Arabidopsis*, confirming the normal functioning and integrity of these live chloroplasts.

Conceivably the variation in chloroplast area for each sample could be a consequence of capturing chloroplasts at different developmental stages ranging from newly divided chloroplast to those just preceding division. The GyrB subunits investigated in this work are postulated to play a direct role in chloroplast replication and division. If the ability of mutant lines to carry out these functions is compromised this may be detected by assorting chloroplasts into size categories to assess proportions of total chloroplasts within specific area boundaries.

Intact chloroplasts with areas ranging up to 50 μm^2 were detected (Figure 5.15). The chloroplasts of 78^{-/-} possessed the most constrictive range of 10-55 μm^2 , indicating this GyrB1 line to have the largest chloroplasts and a lack of extremely small chloroplasts. These modest changes in the chloroplast sizes may in fact be representative of a potential chloroplast division defect and warrants further exploration. The remaining GyrB lines, did not display significant variation from the Columbia-0 line, under the same experimental conditions.

The assessment of live chloroplasts may have biased the evaluation towards the proportion of chloroplasts that have somehow minimised and overcome the effect of the GyrB T-DNA insertions only, therefore overlooking defective organelles. Also, the significant variability in chloroplast areas within each line could be consequential of the live chloroplasts embedding upon the agarose beds in a variety of different orientations. The organellar effect of altered GyrB proteins may actually be represented as intricate changes to the morphology, which cannot be considered by this method.

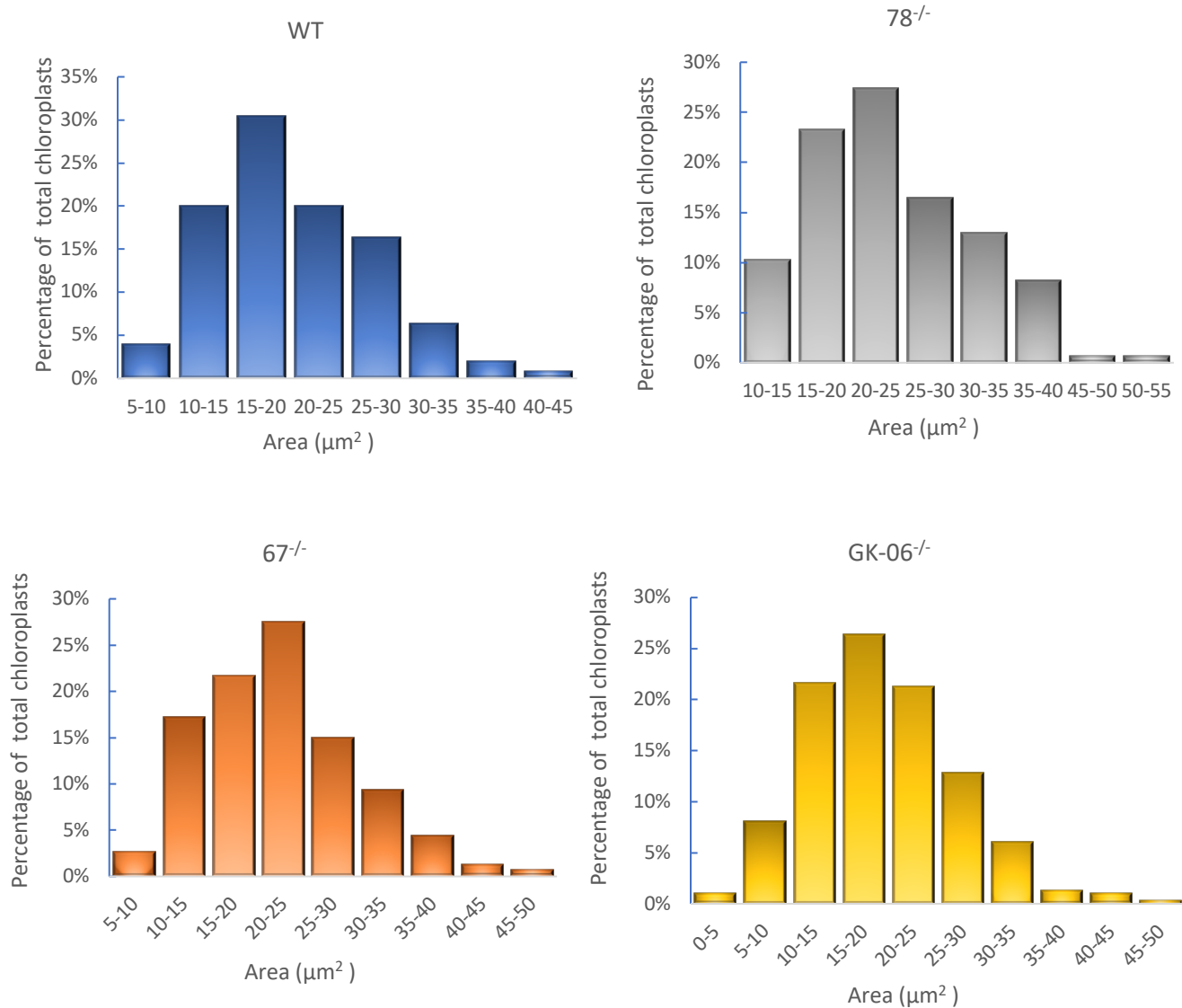


Figure 5.15: Two-dimensional determination of chloroplast area.

The percentage of total chloroplasts categorised according to their areas (μm^2) for wild-type and homozygous GyrB lines. The chloroplasts were imaged whilst live and their dimensions estimated by boundaries outlined by the chlorophyll autofluorescence (see materials and methods section 2.10.4).

5.2.8. GyrB1 mutant plants have altered thylakoid networks

The chloroplasts did not exhibit significant differences when their overall two-dimensional structures were assessed. The silencing of GyrB in *N. benthamiana* has been shown to lead to a reduction in the number of chloroplasts, structural abnormalities including altered thylakoid stacking and irregularly shaped organelles and starch grains in *N. benthamiana* (Cho et al. 2004). In order to assess potential equivalent structural abnormalities in the ultrastructures of *A. thaliana* GyrB lines, the chloroplasts were assessed by transmission electron microscopy (TEM). The structural architecture corresponding to chloroplasts of homozygous lines 78, 67 and GK-06 were assessed, samples of leaves from each homozygous line were fixed and sectioned for TEM (section 2.10.3). Two time-points of three- and six-week-old leaves were used to gauge structural differences during early and late development in the mutant lines. An *Arabidopsis* Columbia-0 line was included for comparison.

Chloroplasts possess remarkably complex structures encompassed within two separate membranes, the outer and inner membranes that create their envelopes. The inside of the chloroplast comprise granum that consist of individual thylakoid membranes stacked upon one another. Granum are surrounded by the stroma, a matrix that contains the sub-genomic DNA, ribosomes and enzymes involved in the process of photosynthesis. Inter-granum connections are made via the stroma lamellae. Gyrase are renowned for their DNA-intensive character and execute a crucial role in replication fork progression during DNA replication. Conceivably, the gyrase of the T-DNA lines being investigated may lead to aberrant replication of DNA, which in the context of the chloroplast may also amount to structural modifications.

The Columbia-0 line provided a clear example of the typical chloroplast ultrastructure expected from the leaf mesophyll cells of *Arabidopsis* (Figure 5.16). These chloroplasts were numerous and classically-shaped, with well-developed thylakoid membranes stacking upon one another and forming granum, linked to other granum close-by by lamellae. This network system is evenly distributed throughout the stroma and interrupted by the occurrence of starch granules. The chloroplasts of GyrB2 67^{-/-} largely resembled that of the control leaf, with thylakoid network structures encompassing a large proportion of the organelle. Interestingly however, these chloroplasts possessed noticeably larger starch molecules and a large proportion were witnessed just prior or post chloroplast division. Inspection of the mutant lines revealed intricate phenotypic differences when compared to the Columbia-0 line.

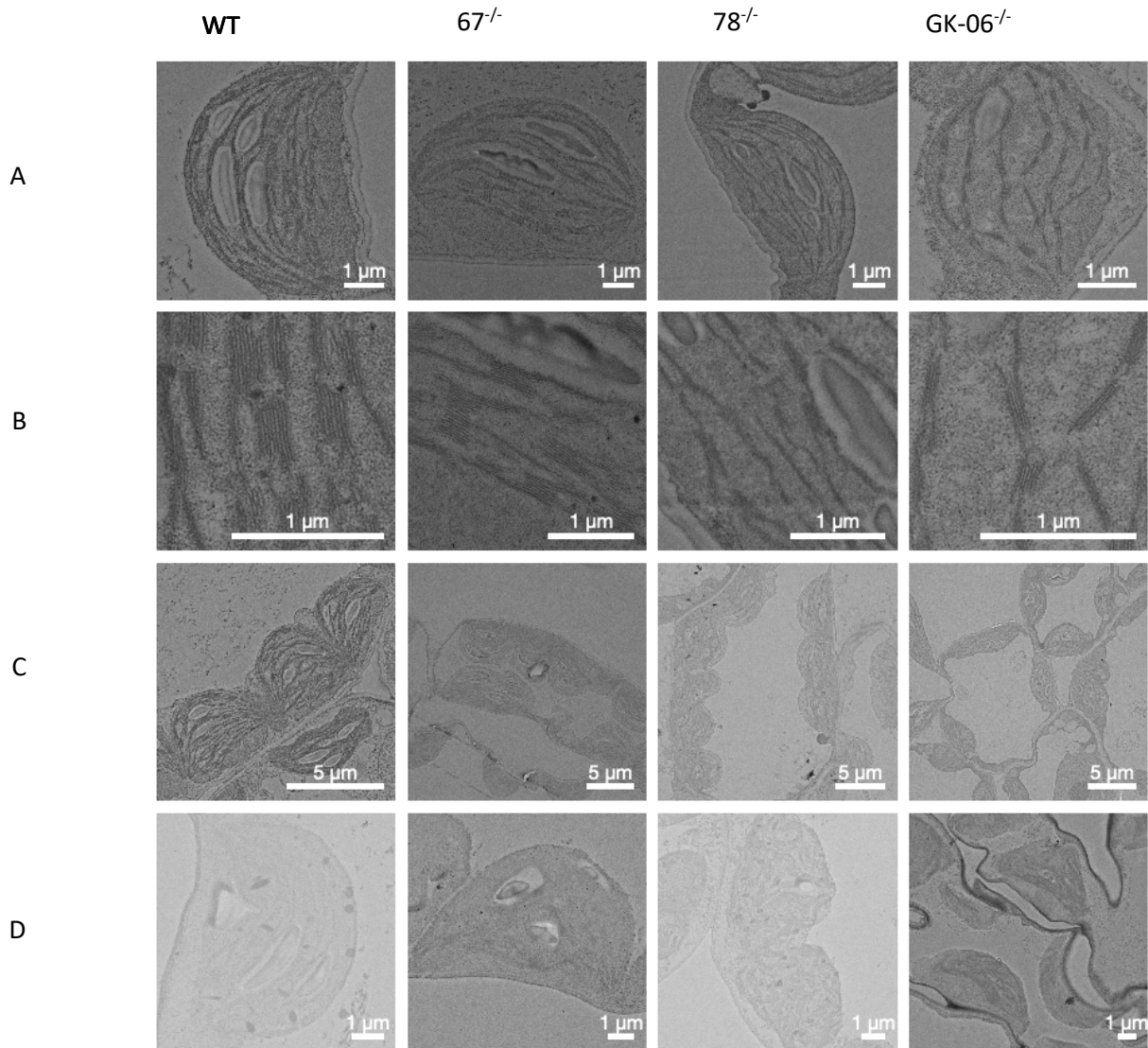


Figure 5.16: Chloroplast transmission electron microscopy images.

(a) Representative images of whole chloroplasts. (b) Intra-organellar network of granum comprising individual thylakoids stacked upon one another. (c) Low magnification image highlighting neighbouring chloroplasts and abundance. (d) Representative chloroplasts at the later time point of six-weeks of development. Columns (labelled above) represent each assessed line; images of the same nature represented by each row. Scale bars labelled in the bottom left corners.

The two GyrB1 lines assessed, 78^{-/-} and GK-06^{-/-} both possessed small differences when compared to Columbia-0. Although both lines possessed a relatively scarce thylakoid network that spanned the chloroplast, the scarcity was notably more apparent in GK-06^{-/-}. The number of thylakoid membranes per granum were visibly reduced, overall giving the appearance of a long, thin network emphasising the appearance of lamellae. Furthermore, the number of chloroplasts per cell were seemingly reduced for GK-06^{-/-} and these also appeared to be visually smaller. In order to ascertain the latter observation, the area per chloroplast for each line was determined using images from TEM. The results of this analysis are summarised by Figure 5.17; wild-type chloroplasts were found to have an average chloroplast area of 15.5 μm^2 . The chloroplasts of the GyrB1 lines yielded dissimilar results from one another; although line 78^{-/-} had a similar chloroplast size of 16.3 μm^2 to that of wild-type, the chloroplasts of GK-06^{-/-} were significantly smaller at 7.61 μm^2 . In contrast, the GyrB2 mutant (67^{-/-}) possessed chloroplasts significantly larger than wild-type; with an average area of 25.6 μm^2 .

The analysis of chloroplasts at the second time point of 6-weeks identified predominantly disintegrating chloroplasts in all lines, marked by indistinct thylakoid networks for Columbia-0 and GyrB2. The chloroplasts of GyrB1, 78^{-/-} and GK-06^{-/-} had more apparent thylakoid networks, with thylakoid networks exhibiting a large degree of swirliness, the significance of which is yet unknown (Figure 5.16d).

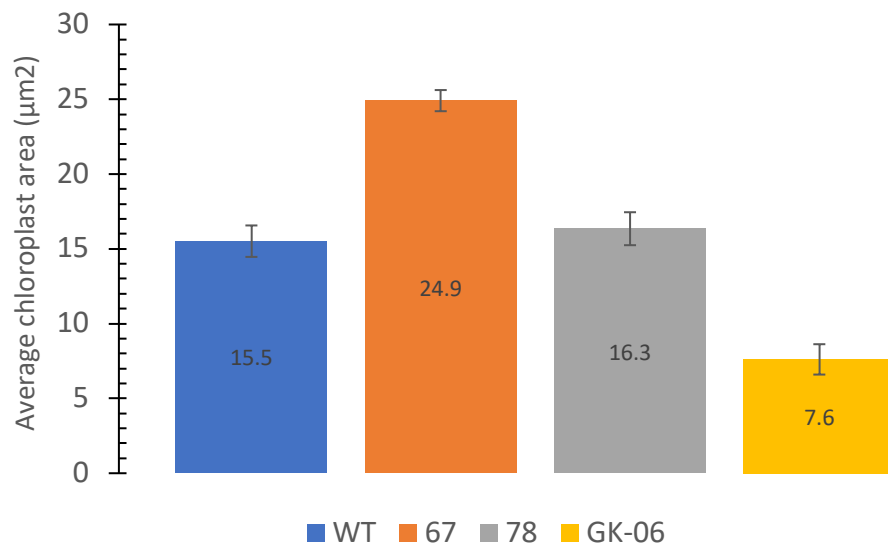


Figure 5.17: Average chloroplast area determined from TEM images.

The bar chart represents the mean area per chloroplast for each line wild-type (blue), 67^{-/-} (orange), 78^{-/-} (grey) and GK-06^{-/-} (yellow) and error bars represent standard error mean values.

5.2.8.1. The significance of ultrastructural variations in relation to the chloroplast genome

The implications of these results are of particular interest when considering the dynamics of plastid DNA organization and replication. The exposure of a unicellular haploid red alga, *Cyanidoschyzon melrolae*, to the DNA gyrase inhibitor nalidixic acid, showed that although the chloroplast nucleoids were unequally divided, the division of the whole chloroplast into equal daughter chloroplasts remained unaffected (Itoh et al. 1997). Indeed, the EM images of this study have confirmed that the chloroplasts of all GyrB lines investigated undergo normal cell division. Contrary to the initial belief that the plastid genome predominantly comprises a single circular genome that is unrestrained in the stroma of the organelle; the current opinion is the complex organisation of multiple copies of the plastid DNA with RNA and proteins, to form nucleoids, comparable to bacterial nucleoids (Sakai et al. 2004b). The complex nucleoid structures within the chloroplasts are tethered to the thylakoid membranes through thylakoid membrane-anchoring proteins (Figure 5.18) (Krupinska et al. 2013). DNA gyrase has been identified as a nucleoid associated protein (NAP) linked with the intricate DNA architecture of the chloroplast DNA that appends to the thylakoid membrane (Ono et al. 2007; Pfalz et al. 2006; Phinney and Thelen 2005). Taking into account the close association of thylakoids and nucleoids, the change of thylakoid membrane architecture identified in GyrB1 mutant lines may be a direct consequence of the altered GyrB1 activity within these organelles.

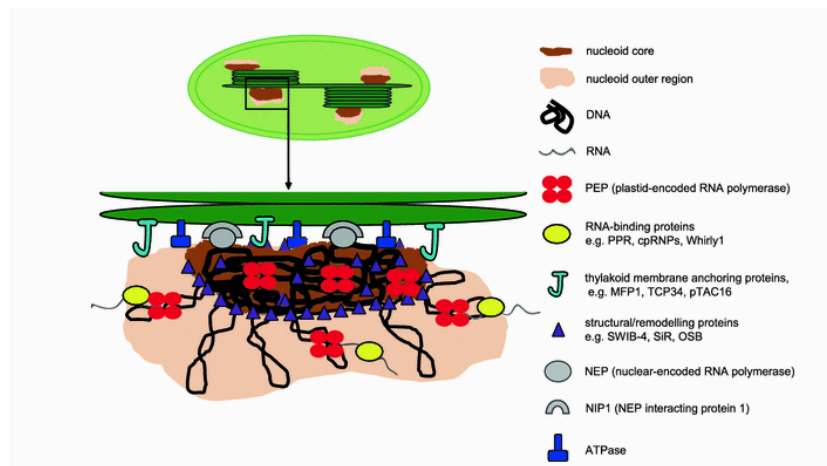


Figure 5.18: Model for intra-organellar plastid nucleoid organization.

It has been proposed that the arrangement of the plastid genome organises into a nucleoid core, comprising frequent DNA-protein interactions and high levels of transcriptional activity. The nucleoid core is surrounded by an outer region, where the genome may exist in less compact and more accessible forms. The nucleoids are thought to be attached to the thylakoid membranes of plastids via thylakoid membrane anchoring proteins. Figure adapted from (Krupinska et al. 2013) with permission.

TEM images taken during analysis of chloroplasts also revealed areas of higher electron absorption in the form of dark regions, typically round or slightly deformed to oblong in shape. These structures appeared randomly in the plant cell, often seemingly budding off from either the inner membrane of the plant or organellar membranes. The significance of these structures is not yet known, although similar observations have been made during elevated levels of cellular anthocyanins (Zhang et al. 2006).

Interestingly, anthocyanin (a variant plant pigment), has been shown to be inversely correlated with levels of chlorophyll and to increase with levels of reactive oxygen stress (ROS) within plant cells (Mattila et al. 2018; Xu et al. 2017). Anthocyanins have been implicated in the tolerance of plants to chronic unfavourable conditions; *Arabidopsis* with mutant anthocyanin production pathways display hypersensitivity to UV-B radiation (Li et al. 1993). The pigment demonstrates the ability to scavenge free radicals resulting from the accumulation of ROS as part of its protective mechanism (Philpott et al. 2004). Seemingly, the identification of potential areas of anthocyanin production is rooted from a stress signal within the mutant GyrB lines. The signal of ROS production elevates as a prerequisite to programmed cell death (Doyle et al. 2010) and specifically cause structural abnormalities in chloroplasts, usually in the form of extended chloroplasts and formation of membrane protrusions, known as stromules (Hanson 2015). The atypical GyrB subunits may constitute an enzyme that is unable to sustain the level of activity required to comprehensively replicate the organellar DNA, leading to genome instability and elevated levels of ROS; interestingly, the DNA gyrase inhibitor, ciprofloxacin has been directly implicated to lead to this response (Lepage et al. 2013).

The production of anthocyanin in *Arabidopsis*, usually serves as a clear visible indicator of stress upon the plant due to the pigment's appearance as either red, blue, purple or black, dependent on the surrounding pH. At neutral pH the pigment appears purple, acidic conditions that increase its stability cause a red colour, whilst more alkaline conditions favour a blue appearance (Khoo et al. 2017). Intriguingly, the plants of the GyrB1 line 78^{-/-} were unique in their clear phenotypic representation of increased anthocyanin production (Figure 5.20). The accumulation of anthocyanin has been linked to thylakoid membrane unstacking as part of the protective mechanism against high levels of ROS (Moustaka et al. 2018). A number of 78^{-/-} plants demonstrating signals of stress, encompassing chlorosis of leaves and a spectrum of elevated anthocyanin production were visible. The exclusive feature of line 78^{-/-} going beyond general leaf chlorosis when propagated on supplemented media, previously described for GK-06^{-/-}, and presenting colouration, indicates an immense stress response in these plants, plausibly due to a change of the GyrB1 protein.



Figure 5.20: Homozygous 78^{-/-} plants.

These mutants display a spectrum of phenotypic changes extending from chlorosis of focussed leaf areas, to total purple/black colouration of the entire plant, due to increased levels of anthocyanins.

5.2.9. Gyrase transcript levels in homozygous lines

Although all T-DNA mutant lines had been identified to be homozygous for the GyrA, GyrB1 or GyrB2 subunits by combinatorial PCR analysis (described earlier in 5.2.3), the output of these changes from expression analysis to phenotypes observed did not appear to clearly translate. A possible explanation could be that the GyrB subunits may be functionally redundant and able to complement and compensate for reduced activity of one another. Alternatively, although the lines had been confirmed as homozygous; the levels of gene expression of each individual gene may be unchanged. The expression of the gyrase subunits in select homozygous lines was evaluated by examination of the RNA transcript levels. The total RNA was extracted from GyrA line 07^{-/-}; GyrB1 lines: 78^{-/-} and GK-06^{-/-}; GyrB2 lines: 67^{-/-} and 82^{-/-} and Columbia-0 lines. Isolated RNA material was reverse-translated into cDNA. Subunit-specific gene primers were used in PCRs to gauge the levels of gyrase cDNA in each homozygous line, the constitutively expressed SAND gene was included as an internal control for comparison.

The level of GyrA transcript in 07^{-/-} or GyrB2 transcript in homozygous 67^{-/-} and 82^{-/-} did not differ from the wild-type (Figure 5.18). The GyrB1 line 78^{-/-} indicated an elevated transcript level, whilst the GK-06^{-/-} mutant line possessed a reduced level of GyrB1 transcript.

The RT-PCR results confirm that T-DNA insertional mutagenesis to achieve gene knockout has a range of effectiveness; indeed, giving the method an edge over clean gene deletions in the assessment of essential genes, such as gyrase. The efficiency of T-DNA insertional mutation is linked to various facets of the insertion, including position of the insertion along the gene of interest and nature of the insertion incorporated, i.e., the number of times the insertion has been incorporated.

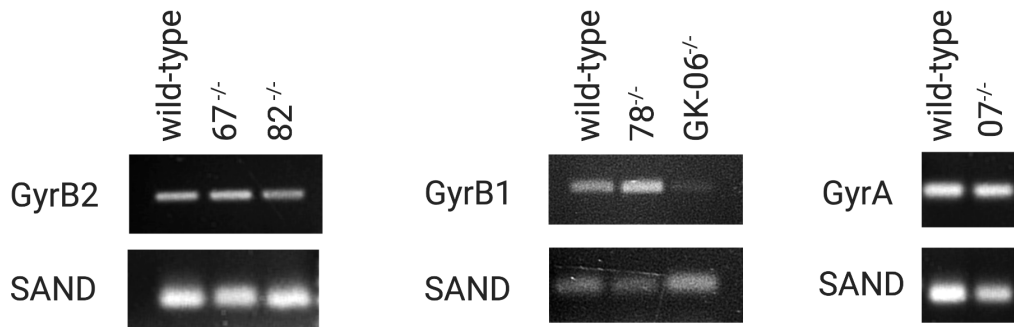


Figure 5.18: Semi-quantitative RT-PCR analysis of Gyr transcripts.

(a) Assessment of GyrB2 transcript levels in wild-type and homozygous mutants, $67^{-/-}$ and $82^{-/-}$ compared with Columbia-0. (b) Assessment of GyrB1 transcript levels in wild-type and homozygous mutants, $78^{-/-}$ and GK-06 $^{-/-}$ compared with Columbia-0. (c) Assessment of GyrA transcript levels in wild-type and the homozygous mutants $07^{-/-}$ line compared with Columbia-0. The sequences of PCR primers are given in Table 2.5, all primers bound C-terminal to T-DNA insertions. The SAND gene used as a control (bottom panel).

The importance of GyrA was unambiguously highlighted by examination of the two insertional lines. Annotated sites of insertion for both lines (GK-10 and 07) are shown in Figure 5.2b. GK-10 possessing a T-DNA insertion within the sixth intron of the GyrA subunit gave a severe phenotype, confirmed by its inability to produce a single identifiable homozygous seed; plausibly due to a defective process of embryogenesis as discussed in 5.2.5. Additionally, the rare identification of homozygous $07^{-/-}$ seeds in sterile growth conditions itself consolidates the indispensable function of GyrA; the insertion was found to be lethal in the absence of an exogenous carbon supply. Although no difference in the level of GyrA transcript occurred when wild-type plants were compared to $07^{-/-}$, the homozygous line did exhibit a difference in phenotype, marked by translucent leaves that also appeared pointed at the apex (Figure 5.3).

The conflicting results of phenotypic read-out but no detectable difference in transcript level of the GyrA gene could be consequential of either no or reduced protein production, or the production of a pool of protein that is largely unfunctional. However, the identification of homozygous 07^{-/-} seedlings suggests that a limited quantity of functional GyrA protein is possible, although the levels or retarded functionality of this protein cannot support growth of the plant beyond the rosette stage.

The insertional mutagenesis lines studied for GyrB1 included 78^{-/-} and GK-06^{-/-}. The insertion site for 78^{-/-}, within the first exon of GyrB1 is expected to cause an adjustment to the level of transcript produced; as has been previously observed to be the case in >95 % of exon insertions (Wang 2008). However this was not observed, rather the semi-quantitative analysis indicated a slight increase in the amount of GyrB1 transcript produced. No striking developmental deviations from Columbia-0 were observed during careful plate-based and soil-based phenotype analysis (section 5.2.4.1-5.2.4.2) for 78^{-/-}, suggesting that functional GyrB1 protein may be produced. Interestingly however, this line exhibited clear visual signs of increased anthocyanin production, alluding to an elevated stress response due to increased GyrB1 protein production. Taking into account the early positioning of the T-DNA insertion within the gene, it is plausible that a promoter within this inserted DNA, for example the constitutive cauliflower mosaic virus promoter, may indeed be responsible for driving downstream expression of GyrB1 protein; accounting for the increased transcript production. In contrast, the GyrB1 line GK-06^{-/-} yielded a reduced level of detectable transcript; probable given the more central location of the insertion within intron six of the gene. The insertion abolishes the production of GyrB1 transcript to a large extent. However, the small amount of detectable transcript is most likely a result of the T-DNA sequence being spliced out together with the intron, although the occurrence of T-DNA may have reduced the splicing efficiency. The reduced level of GyrB1 transcript leads to the production of functional GyrB1 protein that is able to sustain growth of the line, to an extent.

In the case of GyrB2 insertional mutagenesis, seemingly the insertion towards the end of the gene (i.e., 82^{-/-}) had a more severe effect on the development of the plant than in line 67^{-/-}. The investigation into the transcript levels for each line did not identify any difference in GyrB2 transcript production when compared to Columbia-0. The inequality of transcript level output to phenotype for each GyrB2 line is presumably down to intron vs exon insertion. The line 67^{-/-} result is explainable by efficient splicing of the intron into which T-DNA was introduced. However, the results of 82^{-/-} are not as easily explained. Despite the fact that this insertion is within an exon, viable homozygous plants propagated in a controlled growth environment are detectable for this line; suggesting that at least a

proportion of the transcript leads to the production of functional protein. Conceivably, the introduction of the T-DNA may have caused premature termination and production of a functional truncated protein, lacking the C-terminal of the GyrB2 protein yet able to sustain development of the mutant plants, to an extent, in certain conditions.

5.2.10. Genomic DNA analysis

5.2.10.1. The function of the chloroplast

Chloroplasts serve the essential function of harvesting light energy and converting it into an accessible form of carbohydrates by the process of photosynthesis. In addition, plastids also contribute towards plant development and physiology through the production of vitamins, metabolites, nucleotides, amino acids, fatty acids, phytohormones and their role in sulphur and nitrogen assimilation (Daniell et al. 2016). Several metabolites produced by chloroplasts are vital to maintain communication in different regions of the plants, the metabolic centre is able to process signals and induce a response via retrograde signalling (Bobik and Burch-Smith 2015).

5.2.10.2. The origin of chloroplasts

The original discovery of chloroplasts, as we now know them, by A.F.W. Schimper was made in 1883 and termed 'chloroplastids' (Schimper 1883). Chloroplasts originated through the process of endosymbiosis. It is believed that a free-living photosynthesizing prokaryotic cell, i.e., cyanobacteria, was engulfed by a eukaryotic cell, already harbouring a functional mitochondrion (Morley et al. 2019; Timmis et al. 2004). The endosymbiotic relationship of the cyanobacteria with the host, involved the transfer of genetic material to the host nuclear genome and synchronization of their cell divisions (Timmis et al. 2004; Zimorski et al. 2014a). The consequential impact of transfer of genetic material resulted in a considerable size reduction of the engulfed cell genome and a compensatory expansion of host cell nuclear genome.

Amongst the plant proteins encoded by the *Arabidopsis thaliana* nuclear genome, 4500 of them, equating to ~18% of the total genome, are of cyanobacterial origin (Martin et al. 2002). The organellar proteome implicates ~3000 proteins, the majority of which are nuclear-encoded (Zoschke et al. 2007). The nuclear encoded genes are translated using the cytosolic ribosome machinery; the precursor forms are targeted to the chloroplast translocons, TOC (translocon on the outer chloroplast membrane) and TIC (translocon on the inner chloroplast membrane), via N-terminal transit peptides that allow their recognition and modulate their transport through the organelles membranes

(Ling et al. 2012). Albeit a small proportion of the entire proteome, the chloroplast genome is thought to encode for 87 proteins; more than half (45) of which relate to the photosynthesis process; the remaining carry out functions related to gene expression, including 4 genes used to constitute the chloroplast RNA polymerase and 25 genes encoding components of the ribosomes, whilst 12 are yet of unknown function (Dobrogojski et al. 2020).

5.2.10.3. Structure of the chloroplast genome

Classically, the *Arabidopsis* chloroplast genome is thought to exist principally as closed circular DNA molecules (Palmer and Stein 1986; Sugiura 1995). The ~160 Kbp genome contains a pair of inverted repeats, separated by two single copy regions, the larger almost five times the size of the smaller (Sato et al. 1999). Although the plastid genomes have retained several organizational and structural features from their prokaryotic ancestors, including the formation of nucleoids; they form more intricate genomic arrangements through their multi-nucleation (Sakai et al. 2004a). A single mesophilic cell can possess 20 to 35 copies of the *A. thaliana* genome (Zoschke and Bock 2018).

The idea of chloroplasts possessing circular genomes originates from early observations made during the isolation of chloroplast DNA from peas. In these experiments, over one-third of the isolated DNA, which could account for the entire size of the chloroplast genome, was determined to be in circular form (Bendich 2004). Of the circular form, a further one-third was identified to be of supercoiled topology. Although linear DNA was observed at the time it could not account for the size of the entire chloroplast genome, the occurrence of this DNA was interpreted as a consequence of shearing of the 'circular' genome during isolation procedures and thus forming the broken circle theory (Bendich 2004). The alternative theory is the existence of plastid genomes in linear and branched forms with defined ends (Oldenburg and Bendich 2004b).

5.2.10.4. Potential role of gyrase in chloroplast genomes

Bacterial DNA gyrases are accountable for replication of the closed-circular chromosomes by compensating for the build-up of positive supercoils ahead of the replication fork, in addition to governing the compression of the genomes. Albeit the original theory of plastid genomes appearing as somewhat equivalent closed circles is now questionable, the manifestation of circular genomes, although often unaccountable for the size of the entire genome, have been identified. Other than this, the retention of

prokaryotic genome organizational features in plastids (including nucleoids) and the indication of sub-domains, both favour the possibility of the DNA featuring in topologically constrained domains such as loops; where the activity of DNA gyrase can be envisaged.

The mechanism of action of gyrase *in vivo* of *A. thaliana* chloroplasts remains elusive. Indirect evidence of functional gyrase exists through the effect of ciprofloxacin, a gyrase-specific drug, resulting in reduced biomass, etiolation, altered chloroplast morphology and a reduction in their overall number (Wall et al. 2004). Additionally, gyrase has been implicated in maintaining genome stability through its cooperation with specific chloroplast targeted RNaseH proteins to maintain R-loop homeostasis and release replication-transcription complexes in highly transcribed chloroplast DNA (Yang et al. 2017). Clearly the chloroplast genome remains a conundrum, as does the function of the essential gyrase protein *in vivo* of this organelle. Investigation of the direct role of gyrase upon the organellar DNA is therefore justified.

5.2.10.5. Attempts to probe the *in vivo* role of gyrase

Electron microscopy has traditionally been used to visualise DNA of varying topology; networks of DNA, knotted DNA and catenated DNA, subsequent to topoisomerase action have also previously been observed (Benedetti et al. 1983). Encouragingly, the chloroplast DNA from plants has also been isolated and imaged on several occasions, often identifying circular genomes; a fraction of which appear supercoiled (Kishima et al. 1986; Manning et al. 1971a). Logically, the probable outcome of harbouring abnormal gyrase activity may amount to topological changes in the genomic DNA. The DNA harvested from chloroplasts with disrupted gyrase activity will potentially be reduced in quantity and exhibit changes in topology, to include a reduction in the overall supercoiling and increased catenation of the DNA. Furthermore, the anticipation was that isolated chloroplast DNA could be subjected to recombinantly purified *Arabidopsis* gyrase and possible changes in topology of the DNA assessed. In an attempt to accomplish this, the chloroplast DNA of homozygous GyrB1 lines and wild-type was isolated. Unfortunately, however, despite several microscopy manipulations, ultimately project time-constraints did not allow for successful visualisation of isolated chloroplast DNA. This is a potential future line of work to pursue.

5.3. Discussion and Conclusions

5.3.1. *A. thaliana* GyrA

Previous investigations of GyrA using GK-10 concluded embryo-lethality; however, at the time, investigation of a second independent GK-290E11 resulted in normal growth and development of *Arabidopsis* (Wall et al. 2004). The indispensability of GyrA during *in vivo* growth and development of *Arabidopsis* has been demonstrated through the use of two independent T-DNA insertion lines here, one common (GK-10) with Wall and colleagues. The mutant line, GK-10, has indeed been confirmed to possess an embryo-lethal phenotype, demonstrated by the inability to identify a single homozygous recessive plant. Nonetheless, the embryo-lethality of GyrA was explored further by examination of heterozygous seed-bearing siliques, to identify seeds declining early in development, phenotypically distinguishable by their dark and shrivelled appearance. Albeit these seeds alone did not quantify for the expected one-quarter homozygous recessive *gyrA* seeds; detailed investigation of the embryogenesis process identified a defective transition of heart-to-torpedo-stage embryos *in vivo*. The latter observation confirms the essentiality of GyrA during early cell differentiation to maintain adequate levels of DNA replication and cell division. The essentiality of GyrA was supported through independent investigation of 07, which demonstrated lethality in the absence of an exogenous carbon source. The requirement for exogenous carbon is particularly fascinating considering that GyrA is organellar-targeted to the chloroplasts and mitochondria, both organelles essential for the supply of energy and carbon sources in the form of carbohydrates for the plant (Van Dingenen et al. 2016). The carbon dependency of 07 may be consequential of improper biogenesis or functioning of these organelles, due to GyrA deficiency. Notably, the external carbon was only temporarily able to alleviate the developmental stress experienced by homozygous plants of this line, all of which emphasised developmental strain phenotypically, which was apparent by their dwarfed size, translucent, chlorotic and pointed leaves and inability to independently sustain growth on soil. Additionally, the transcript levels of GyrA were found to be equivalent to that of Columbia-0, but the phenotypic observations suggest that at most, only a fraction of this translates to functional protein.

5.3.2. *A. thaliana* GyrB1

The GyrB1 protein has been formally investigated by Wall and co-workers. Their analysis of a single T-DNA insertion line SAIL_681G04 was concluded to be seedling lethal. The current analysis identified two viable mutant GyrB1 lines, 78 and GK-06. In-depth developmental analysis of 78 did not identify any significant difference from that of wild-type on plates or soil, unlike GK-06 that encompassed an overall slower rate of growth on plates as well as the incapability to progress beyond the point of cotyledon emergence in more than >50% of cases. The proportion of plants able to overcome this, later showed signs of developmental stress in the form of dwarfed size and rosette diameter, chlorosis and improper silique development. Interestingly, the levels of GyrB1 protein were found to affect the root architecture. Although 78 possessed wild-type like roots, GK-06 provided convincing evidence for an important *in vivo* role of GyrB1 in the initiation and extension of lateral roots. Furthermore, chloroplasts of GyrB1 revealed a scarce intracellular network emphasised by the diminished number of thylakoids constituting each granum. The level of GyrB1 transcript in GK-06 was decreased as compared to Columbia-0 accounting for the observed phenotypes; in contrast, plants of 78 showed an increased level of GyrB1 transcript, clarifying their wild-type like development. The elevated GyrB1 levels of 78 led to a reduction in chlorophyll production and increased levels of anthocyanin when propagated on supplemented media, a well-defined stress indicator linked to the production of ROS and ultimately DNA damage. Clearly, the quantity of GyrB1 needs to be precisely controlled *in vivo*.

5.3.3. *A. thaliana* GyrB2

The lack of GyrB2 protein was concluded to lead to a seedling-lethal phenotype by assessment of two insertion lines; SAIL_559H08 and SALK_002367 (Wall et al. 2004). The latter line, was reported to possess a second phenotype in 10% of cases, characterised by slow and stunted growth above and below soil and the reduced capacity to produce flowers and siliques. The reported phenotypic characteristics made this an interesting line to further investigate the *in vivo* role of GyrB2 in this study. Interestingly however, the results obtained here did not coincide with previous observations. The growth and development of 67 was followed closely and scored from the point of seed germination, yet the homozygous line did not seem to differentiate in terms of growth and development from Columbia-0 analysed in the same way. On the contrary, on average these plants grew taller and developed more siliques than Columbia-0 in the same time period. The development of both primary and lateral roots also coincided with regular *Arabidopsis*

development. Their overall chloroplast size and autofluorescence when assessed initially by estimation of parameters based on autofluorescence did not identify any differences; however, although TEM images of these chloroplasts provided evidence of normal chloroplast ultrastructure, the assessment of total area by this method identified the chloroplasts to be larger in size than wild-type. Interestingly, no significant change was observed when the total GyrB2 transcript levels were assessed and compared to wild-type. Plausibly, the effect of an intronic insertion is countered by the ability of *Arabidopsis* to carry out alternative splicing; therefore, leading ultimately to normal production of GyrB2 protein that can facilitate all the functions for DNA replication and metabolism during development. The cause for the discrepancy of the current and previous result is not entirely clear. However, given the efficiency of T-DNA incorporation, the phenotypes observed by Wall and colleagues could be an outcome of multiple T-DNA incorporation within the genome and the undetected insertion at a second loci, a phenomenon observed in >50% of insertional lines, responsible for the observed seedling lethal phenotype (Alonso et al. 2003; O'Malley and Ecker 2010; Valentine et al. 2012).

The GyrB2 protein was assessed by independent evaluation of SALK_068282; the inserted T-DNA although within an exon is C-terminal to SALK_002367. Incredibly, although observed more frequently for insertions within exons, SALK_068282 homozygous plants developed phenotypic distinctions as compared to wild-type *Arabidopsis*. Such distinctions encompassed a significantly reduced rosette diameter, reduction in the number of rosette leaves and an overall miniature size. Vitality, survival and development of the mutant and infertile plants were dependent upon supply of an exogenous carbohydrate source, in the absence of which the mutation was seedling lethal; similar to the 07 GyrA line (described in 5.2.2). These observations suggest a significant role for the GyrB2 protein during the development and growth of *Arabidopsis* chloroplasts and mitochondria, as previously discussed. Similar conditional lethal phenotypes have been observed for lines in which plastid translation or import have been disrupted (Liu et al. 2010). Considering the vital role of gyrase in DNA replication, the observed phenotype could be a result of aberrant plastid DNA replication.

5.4. Future directions

The essential nature of gyrase and that of the organs to which it is targeted, add to the difficulty of distinctly identifying the enzyme's role *in vivo*. Co-immunoprecipitation experiments to identify gyrase interactions *in vivo* of chloroplast and mitochondria would be recommended to determine the exact subunit interactions within each organelle. This would require the generation of epitope specific antibodies that can distinguish the GyrB1 and GyrB2 subunits. The generation of such a tool would be useful in determining the absolute targeting of gyrase proteins within *Arabidopsis*. Although, given the current conundrum of gyrase targeting, the result may have to be confirmed using a couple of different techniques, which could include mass-spectrometry. It is recommended that in order to study the *in vivo* role of the essential gyrase proteins *in vivo* an alternative and more reliable system for the mutation of gyrase genes is used, for example virus-induced gene silencing or RNAi mediated silencing. Although, the ultimate system may be one involving the tractable and inducible degradation of gyrase proteins, for example by a method akin to auxin-inducible degradation.

Chapter 6: Development of a novel decatenation substrate 'bis-cat' DNA

6.1. Introduction

The reactions typical of topoisomerases include the relaxation, supercoiling, knotting/unknotting and catenation/decatenation of their DNA substrates. The supercoiling reaction, a hallmark of the enzyme, is just a single example of the many fascinating reactions that DNA gyrase is able to catalyse; another interesting reaction being decatenation. This reaction involves the double-stranded cleavage of one of the catenated molecules (both strands of the DNA duplex) to form an enzyme-DNA-bridged intermediate, whilst the second intact catenated duplex is passed through the enzyme-bridged gap, unlinking and separating the two DNA molecules. Indeed, catenated DNA is biologically relevant and has been discovered in a number of diverse biological systems; the first observation being human mitochondrial DNA. Catenated DNA also exists in the form of a compact network in the mitochondria of trypanosomes, referred to as kDNA (kinetoplast DNA). The complex network of kDNA constitutes two types of DNA circles that are interlinked, maxicircles (20-40 kbp) and minicircles (~2.5 kbp). The multifaceted process of DNA replication imparts various complex topological modifications upon the DNA, in the specific case of replication termination, involving two converging replication forks, catenation (inter-linking) of the newly replicated DNA occurs, whilst positive DNA supercoils are formed in the unreplicated DNA. *In vivo* topological challenges arising due to catenation are routinely resolved by type II topoisomerases including: gyrase and topo IV (in a bacterial cell) and topo II (in higher eukaryotes). The natural process of DNA catenation is not exclusive to topoisomerase proteins but also extends to proteins involved in recombination, including resolvases.

The resolvases function under the umbrella of site-specific recombination, a process of DNA strand exchange, which in contrast to homologous recombination, requires minimal sequence similarity. The particular resolvase of interest to this work, Tn3, is encoded as part of a larger entity, the Tn3 transposon that also encodes the transposase and β -lactamase. The Tn3 resolvase protein is a serine site-specific recombinase that functions in a similar fashion to type II topoisomerases; in that, the enzyme also introduces double-stranded DNA breaks into its substrate via linking to the 5' of the phosphodiester-

backbone. Albeit, in contrast to topoisomerases, the reaction is mediated by a serine residue and the double-stranded DNA break is staggered by just two base-pairs (as opposed to the four base-pair stagger of gyrase). The precise site of action of resolvase is designated as the 'resolution site' (*res*) and encompasses a 114 bp sequence, divided into three sub-sites: site I (28 bp), site II (34 bp) and site III (25 bp) (Figure 6.1). DNA cleavage occurs at site I, whilst sites II and III act as accessory sites and may play a role in the regulation of the enzyme's activity. The Tn3 recombination reaction is initiated by the binding of Tn3 resolvase subunits to the two *res* sites to form *res*-Tn3 complexes. These complexes combine to form the synaptic complex that is composed of two intertwined *res* sites. Subsequently, double-stranded DNA cleavage occurs at each of the *res* site I sequences, after which, the DNA strands are exchanged and re-joined, leading ultimately to the formation of a two-noded catenated DNA molecule (Nollmann et al. 2005) (Figure 6.1).

The work described here was part of the NRPDTP industrial CASE partnership (iCASE) programme, in collaboration with Inspiralis Ltd (UK). Inspiralis is a small research company engaged in supporting drug discovery; they provide the research community with high-quality proteins, substrates, kits and services explicitly aimed at topoisomerase research. The current method of assaying the decatenation activity of topoisomerases *in vitro* involves the use of purified kDNA as a substrate (Nitiss et al. 2012). The inherently complex arrangement of kDNA generates a number of practical implications that can lead to difficulties in interpretation of agarose gel-based assays. One such issue is the significant size of kDNA; its large structure is prone to entrapment within the pores of an agarose gel, often rendering the substrate immobile in the wells of the gel. Additionally, the nature of the current assay does not allow for quantitative analysis of decatenation events, this is because the number of links between the maxi- and mini-circles is variable (Chen et al. 1995).

Therefore, given these issues, the objective was to develop a simpler and more suitable substrate to replace kDNA for use in decatenation assays. The development of the alternative substrate, a singly-linked DNA catenane (*bis-cat*), permits the advancement of the decatenation assay by improving its robustness and reliability. The work described in this chapter is published (Waraich et al. 2020).

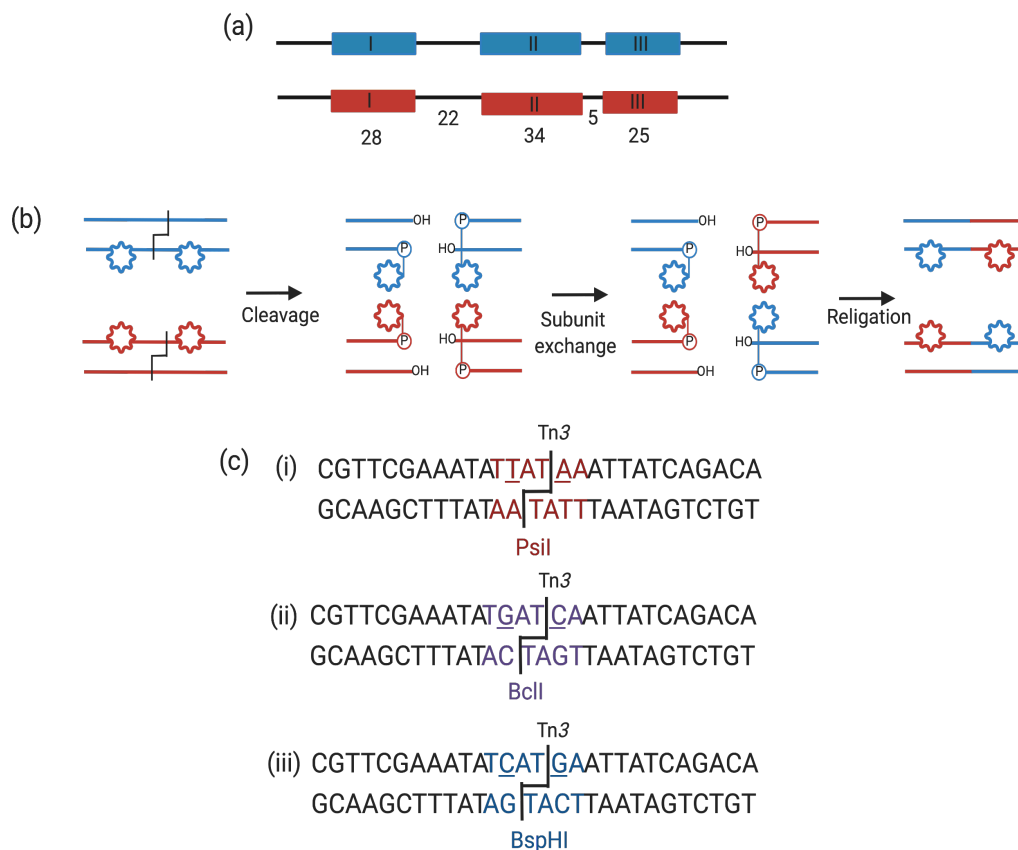


Figure 6.1: Reaction scheme for Tn3-mediated recombination. Schematic diagram of Tn3 resolvase mechanism of action.

(a) Representation of the Tn3 recombination site (res); resolvase dimers bind to each of the res sub-sites I, II and III. The numbers indicate the length of each sub-site and intermediate regions between sub-sites in bp. (b) The suggested mechanism of action of serine recombinases, focussing on res site I. Resolvase dimers (subunits depicted by polygons) are bound to each res I site (the res I sites are brought into close proximity of one another by the accessory res sites II and III to form the synaptic complex, not shown). Resolvase cleaves all four strands at res site I, each 5' end becoming covalently linked to a resolvase subunit via a phosphodiester link. Subsequently, the cleaved DNA strands are exchanged and religated in their new conformation. (c) (i) Sequence of res site I. The natural PsiI recognition sequence is highlighted in red and specific Tn3 sites of cleavage indicated by black bars. The underlined T and A bases on the top strand of the PsiI recognition sequence indicate bases which upon mutation have a minimal effect on Tn3 resolvase reaction efficiency. (ii) res site I PsiI recognition sequence changed to BclI sequence (purple). (iii) res site I PsiI recognition sequence changed to BspHI sequence (blue).

6.2. Results and Discussion

6.2.1. Expression and activity testing of Tn3 resolvase

The Tn3 resolvase protein was expressed and purified according to procedures established in the laboratory of Prof. Marshall Stark (see methods section for detailed protocol). Prof. Stark also kindly provided the resolvase expression construct (pSA1101) and an appropriate substrate DNA molecule (pMM5) that harnesses two resolvase recognition sites ('res' sites).

The activity of the purified resolvase was determined using the pMM5 plasmid as substrate in standard reaction buffer containing 50 mM Tris·HCl pH 8.2, 10 mM MgCl₂ and 0.1 mM EDTA for 60 mins at 37°C. Resolvase was thermally denatured at 70°C for 5 mins. In theory, the action of Tn3 resolvase should convert the substrate pMM5 plasmid into the desired bis-cat product (Figure 6.2a). The two entities of the bis-cat are formed by the region of pMM5 plasmid between the two res sites and are therefore sequentially distinguishable from one another. Following recombination, samples were equally divided and digested with restriction enzymes to independently target each catenated DNA molecule of the bis-cat. The reactions were treated with SDS and proteinase K to remove proteins and the DNA was analysed on agarose gels (Figure 6.2b). The activity of Tn3 resolvase was verified by the appearance of several additional DNA bands as compared to the pMM5 only control. Restriction digestion was used to confirm the presence of bis-catenated molecules. In the exemplar reaction of Figure 6.2b, digestion with NcoI or XbaI linearises unreacted substrate pMM5 and either the 2.6 kbp or 2.3 kbp catenane of the bis-cat DNA, respectively, releasing the intact partner catenane in its supercoiled form. The reaction efficiency was estimated by comparing band intensities after double-digestion, i.e., intensity of band from 4.9 kbp substrate plasmid compared to the combined intensities of the linear catenated products (2.6 kbp circle and 2.3 kbp circle). Tn3 resolvase efficiency, as judged by several independent repeats with the pMM5 plasmid, was estimated to be ~67%.

6.2.2. Manipulation of the pMM5 plasmid

The pMM5 plasmid substrate and product following recombination are sequentially and topologically indistinguishable. The pMM5 plasmid was therefore contrived to introduce sequential differences between reaction substrate and bis-cat product through introduction of a restriction enzyme sequence into the plasmid that is destroyed upon recombination with Tn3; subsequent substrate plasmid linearization with a restriction

enzyme introduces a topological difference from the supercoiled bis-cat product, which can be exploited for purification of the desired bis-cat DNA.

The pMM5 plasmid contains two *res* sites (that are termed *res^A* and *res^B*) each containing a PstI restriction site. Tn3 interacts directly with *res* sites, where it carries out double-stranded DNA cleavage, strand exchange and religation, as previously discussed (Figure 6.1). The implemented plan involved manipulation of the central PstI site (TTATAA) at *res^B* to a different unique restriction enzyme sequence, which would be abolished from the bis-cat product by resolvase biochemistry. However, sequence modifications at the site of action of Tn3 resolvase can cause drastic reductions in reaction efficiency (McIlwraith et al. 1997). The negative impact can be minimised by retaining the central AT of the PstI sequence, where the resolvase cleavage occurs, making modifications either side of this central sequence. The aim was to identify a modification that would minimise the negative effect on Tn3 resolvase efficiency, while allowing the use of restriction enzymes to distinguish recombination product from substrate.

A number of substrate plasmids were henceforth created in an effort to obtain the desired outcome. All site-directed mutagenesis reactions, involved in the creation of these substrate plasmids, were carried out using PCR amplification primed by appropriate oligonucleotides (Table 6.1) as described in methods and materials.

6.2.3. Development of pMM6

The pMM6 plasmid was constructed by mutagenesis of the PstI restriction sequence at *res^B* to a BspHI site (not unique within the plasmid), leaving a unique PstI restriction site at *res^A* (Figure 6.3). The method of small-scale resolvase recombination reaction was used to analyse the resolvase recombination efficiency with pMM6. The results indicated that the change to a BspHI site in pMM6 decreased the reaction efficiency further by ~20%. Although this decrease in efficiency is not ideal, it was not the limiting factor in pursuing the pMM6 plasmid as a suitable substrate. Unfortunately, from a commercial perspective of a small industrial research laboratory, the cost of purchasing the PstI restriction enzyme (£461 per 1000 units) was not commercially viable, particularly considering that the final bis-cat product would be marketed in direct competition with kDNA, and in order to contend, the bis-cat DNA would ideally be retailed at a similar and competitive price.

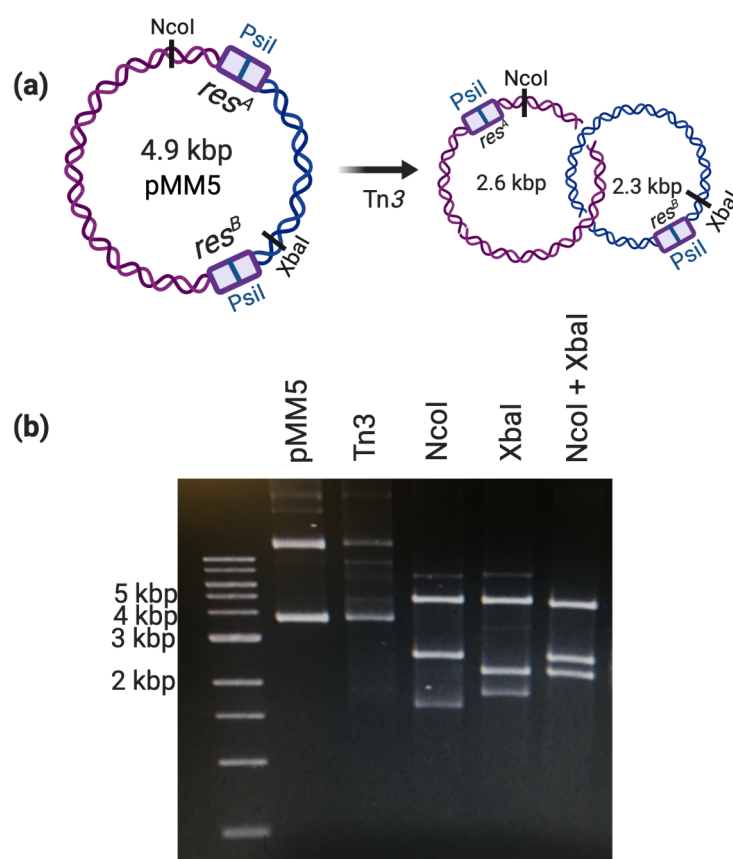


Figure 6.2: Schematic of Tn3 substrate and product; gel analysis of recombination reaction.

(a) A schematic of the substrate plasmid (pMM5) and catenated DNA product (after Tn3 reaction) with locations of restriction enzyme recognition sites labelled and size in kbps. Rectangular boxes represent *res* sites and the central blue line highlights *res* site I restriction enzyme sequence (PstI). Regions of sequence between the two *res* sites that recombine to constitute each individual entity of the bis-cat are coloured purple (2.6 kbp catenated plasmid) and blue (2.3 kbp catenated plasmid). Note: DNA molecules shown in relaxed topology for demonstrative purposes but are actually supercoiled. (b) Representative gel analysis after the resolvase reaction. pMM5: No resolvase protein, Tn3: Tn3 resolvase recombination, NcoI: resolvase reaction followed by NcoI digestion, XbaI: resolvase reaction followed by XbaI digestion, NcoI + XbaI: resolvase reaction followed by NcoI and XbaI double digestion.

Table 6.1: Plasmids created for use in Tn3 recombination reactions.

Plasmid	Res [†]	Res [′]	Unique RE [§]	FP*	RP*
pMM5	PsiI	PsiI	—		
pMM6	PsiI	BspHI	PsiI	CATGATATTTCTGAACGG ACTAGTGAGC TGTCTGATAATTGATCA	CATGAATTATCAGACATAG GAATTCGGCTTCG CGTTCGAAATATGATCAAT
pMM7	PsiI	BclI	BclI PstI	TATTTCTGAACGGTTGCA 1 AAGCGCTCATCA ‡ GCCCGAAGT	TATCAGACATAGTAAAACG 1 GGCTGATGAGCGCTTGTTT CG
pMM9	PsiI	BspHI	BspHI PstI	2 GGTAATGAGATT ATCAAAAAGGAT CTTCAC 3 GTCCCATGAGCG GATACATATTTG AATG	2 GATAATCTCATTACCAAAA TCCCTTAACGTG 3 GTATCCGCTCATGGGACAA TAACCCTG

[†]Res and Res[′] denote the restriction enzyme sequence at each site.

[§]Limited to the unique restriction enzyme sequences at *res* sites only

[‡]For pMM9, the numbers 1,2 and 3 refer to the forward and reverse primers used to remove all three natural BspHI sites to from the pMM9 plasmid.

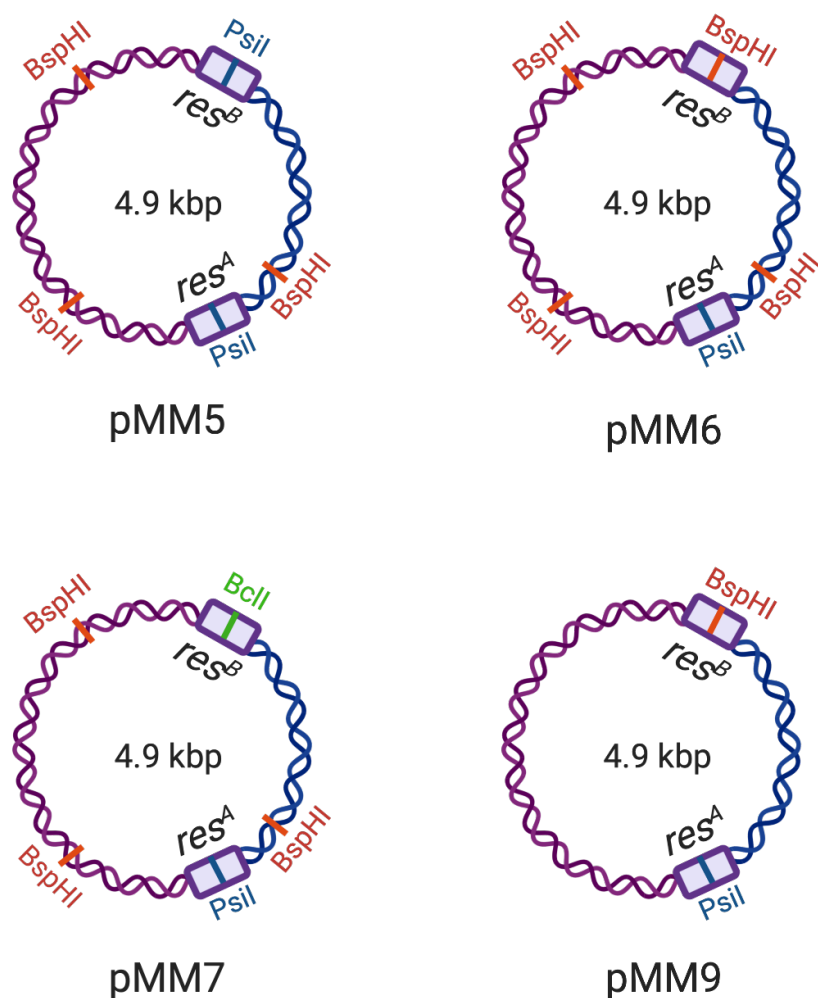


Figure 6.3: Tn3 resolvase substrate plasmids.

The *res* sites and plasmid colouring is as in Figure 2. Central lines of differing colours within the *res* site I sequences represent either natural Psil recognition sequences at *res^A* or BspHI/BclI sequences introduced through mutational efforts at *res^B*. Additional highlighted features include all BspHI recognition sequences in each plasmid (orange lines). Plasmids are labelled below each plasmid.

6.2.4. Development of pMM7

The task at hand to generate the bis-cat product by a more profitable method could potentially be achieved by inclusion of a relatively low-cost restriction enzyme to linearize unreacted substrate plasmid. This led to the generation of plasmid pMM7, with two unique restriction enzyme sequences at *res*; *res^A* site remained as PstI (TTATAA) and *res^B* was mutated to BclI (TGATCA). The compromise in the case of the cost-effective BclI enzyme (£218 - 15000 units) was the fact that its activity is blocked by DNA methylation. To circumvent this, a specially selected strain of bacteria, ER2925, that lacked the ability to methylate DNA, yet preserved a suitable genotype for the purposes of recombination reactions, was used. Remarkably, recombination through the pMM7 plasmid generated a significantly ineffective recombination reaction; the total reaction efficiency reducing to 10-20% (Figure 6.4a).

The unanticipated result warranted investigation into the possible cause of the reduced resolvase reaction efficiency through pMM7. The reduced activity may be attributable to the specific changes in sequence incorporated at *res^B* during the introduction of a BclI site; or alternatively, a consequence in the change of DNA methylation to demethylation. This investigation is not possible through the use of the pMM7 plasmid alone due to its dependence for unmethylated DNA; hence, pMM6 was also included. The pMM6 plasmid was transformed into a Dam⁺ strain and a Dam⁻ strain, the products of the recombination reactions were directly compared to one another and to the reaction of pMM7 in a Dam⁻ strain (Figure 6.4b). The difference in the efficiency of the Tn3 reaction for pMM6 was insignificant when the Dam⁺ and Dam⁻ strains were compared; implying that the methylation status of DNA does not affect the Tn3 resolvase activity. On the contrary, the Tn3 reaction efficiency decreased significantly with the pMM7 plasmid in a Dam⁻ background. These results suggest that the low reaction efficiency of the Tn3 reaction with pMM7 is most likely due to the base pair changes incorporated at the *res^B* to introduce a BclI restriction, rather than a direct consequence of DNA demethylation.

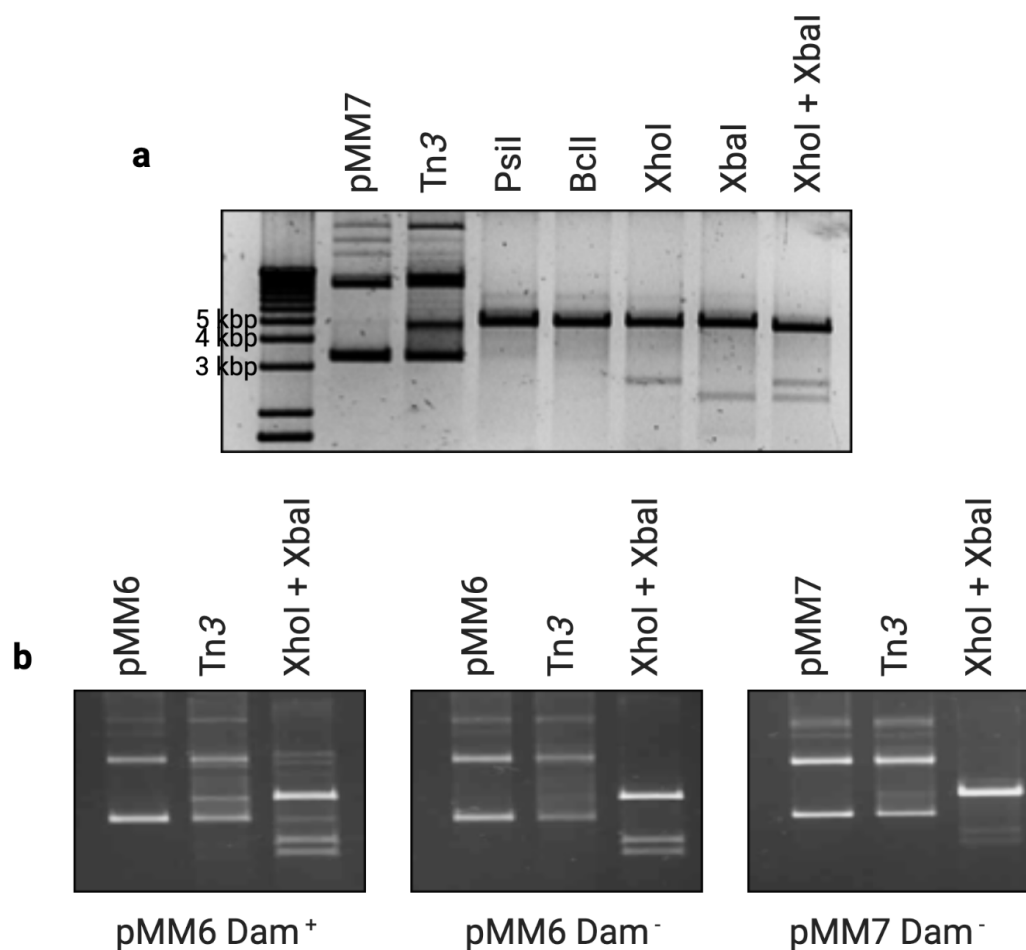


Figure 6.4: Tn3 resolvase recombination with pMM6 and pMM7.

(a) Agarose gel analysis of Tn3 resolvase-mediated recombination pMM7 (resA: PsiI, resB: BclI) as substrate. Lanes labelled as: pMM7: pMM7 plasmid only (negative control), Tn3: reaction following Tn3 resolvase addition, PsiI: PsiI restriction digestion, BclI: BclI restriction digestion, XhoI: XhoI restriction digestion (replaces NcoI digestion in previous analysis (Figure 6.2) to digest 2.6 kbp catenated DNA molecule), XbaI: XbaI restriction analysis, XhoI+XbaI: double digest with XbaI and XhoI. Double digestion was used to assess Tn3 recombination, estimated as in Figure 6.2b. (b) Gel analysis to compare the effect of methylation or sequence change at the res on the efficiency of the Tn3 resolvase recombination reaction. Lane labels as in (a). Dam +: use of LE392 cells, capable of methylating DNA; Dam -: use of ER2926 cells, unable to methylate DNA. The DNA methylation state did not affect Tn3 mediated recombination of pMM6, yet recombination efficiency significantly reduced with the use of pMM7.

6.2.5. Development of pMM9

The investigation into base-pair sequence changes at *res* and methylation status of substrate DNA confirm that Tn3 resolvase is particularly sensitive to changes to its recognition sequence and read outs often involve reduced catalysis. Additionally, the attainable changes to *res*, whilst retaining the central AT of the resolvase cleavage site and modifying bases directly adjacent, had been accomplished by the introduction of BspHI (pMM6) and BclI (pMM7); moreover, the striking result with pMM7 strongly discouraged further ill-advised manipulation of *res*.

Given the project time constraints, the infrastructure provided by pMM6 was the preferred lead. All of the BspHI recognition sequences in pMM6, apart from the that in *res^B*, were removed by site-directed mutagenesis (oligonucleotides given in Table 6.1) to create pMM9. This plasmid can be cleaved either with PstI (in *res^A*) or BspHI (in *res^B*) (Figure 6.3), and neither of these enzymes cleave the bis-cat product of recombination. Therefore, the Tn3 reaction mediated by means of the pMM9 plasmid is a necessary compromise to accomplish the task of generating the desired bis-cat substrate DNA in the constraints of an industrial environment where profitability and cost-effectiveness are crucial.

6.2.6. Generation of bis-cat DNA

The method used to generate bis-cat DNA involved Tn3 recombination with pMM9, linearisation of unreacted pMM9 by BspHI and a caesium chloride density gradient was used to separate the linearised pMM9 from the desired supercoiled bis-cat product; this is schematically summarised in Figure 6.5.

Indeed, the supercoiled DNA band extracted from the caesium chloride gradient, consisted of the bis-cat product; however, a background level of supercoiled uncatenated 2.6 kbp and 2.3 kbp plasmids were also co-purified (Figure 6.6a). The contamination of the individual supercoiled DNA plasmids may be due to the co-purification of a nuclease alongside resolvase, even though the stringent resolvase purification involved denaturation and renaturation steps. An initial investigation involved the exploitation of Mg²⁺-independent resolvase activity by use of an alternative reaction buffer, in which the 10 mM MgCl₂ of the standard reaction buffer was replaced with 5 mM spermidine. The comparison of Tn3 resolvase reactions propagated in standard and alternative recombination buffers, initially encouraged the theory of nuclease contamination, as the single uncatenated entities of the bis-cat substrate were not detectable in reactions lacking Mg²⁺ (Figure 6.6b). On the basis of this, the Tn3 recombination reaction was conducted once again, on a larger scale, using the alternative reaction buffer. The recombined DNA

was treated with proteinase K, ethanol precipitated and digested with BspHI to linearise unreacted pMM9 plasmid; followed by separation using a caesium chloride density gradient. However, the caesium chloride density band correlating to supercoiled DNA once again encompassed the 2.6 kbp and 2.3 kbp plasmids in addition to the desired bis-cat DNA product. The reappearance of the uncatenated DNA at a larger scale, remains perplexing. Unfortunately, the replacement of Mg^{2+} does not entirely rule out the possibility of nuclease action, as certain nucleases can mediate scissile phosphate attack by alternative nucleophiles to metal ions, including the use of water and the sidechains of Ser, Tyr and His (Yang 2011). Nevertheless, purification using hexa-histidine tagged resolvase would be a possible alternative purification method. This background contamination with the desired product (<20% of the total DNA), could be a consequence of downstream handling of the DNA, but seemingly persists over different resolvase preparations. It is unlikely that this is a direct result of decatenation by a co-purified topoisomerase protein, not only due to the stringent resolvase purification process, which involves denaturation with urea, but also because a topoisomerase capable of decatenating double-stranded DNA catenanes would require an energy investment from the hydrolysis of ATP, which is not present. These uncatenated supercoiled product circles could be produced by aberrant cleavage by resolvase, or failure of resolvase to religate one circle in the catenane. The appearance of the background contamination subsequent to resolvase recombination, with and without Mg^{2+} , and the appearance of both uncatenated DNA molecules in equal quantities, strongly suggests that the underlying cause is likely to be due to failure of resolvase to religate. Unfortunately, due to time limitations, it was not possible to explore the outlined possibilities in any more depth.

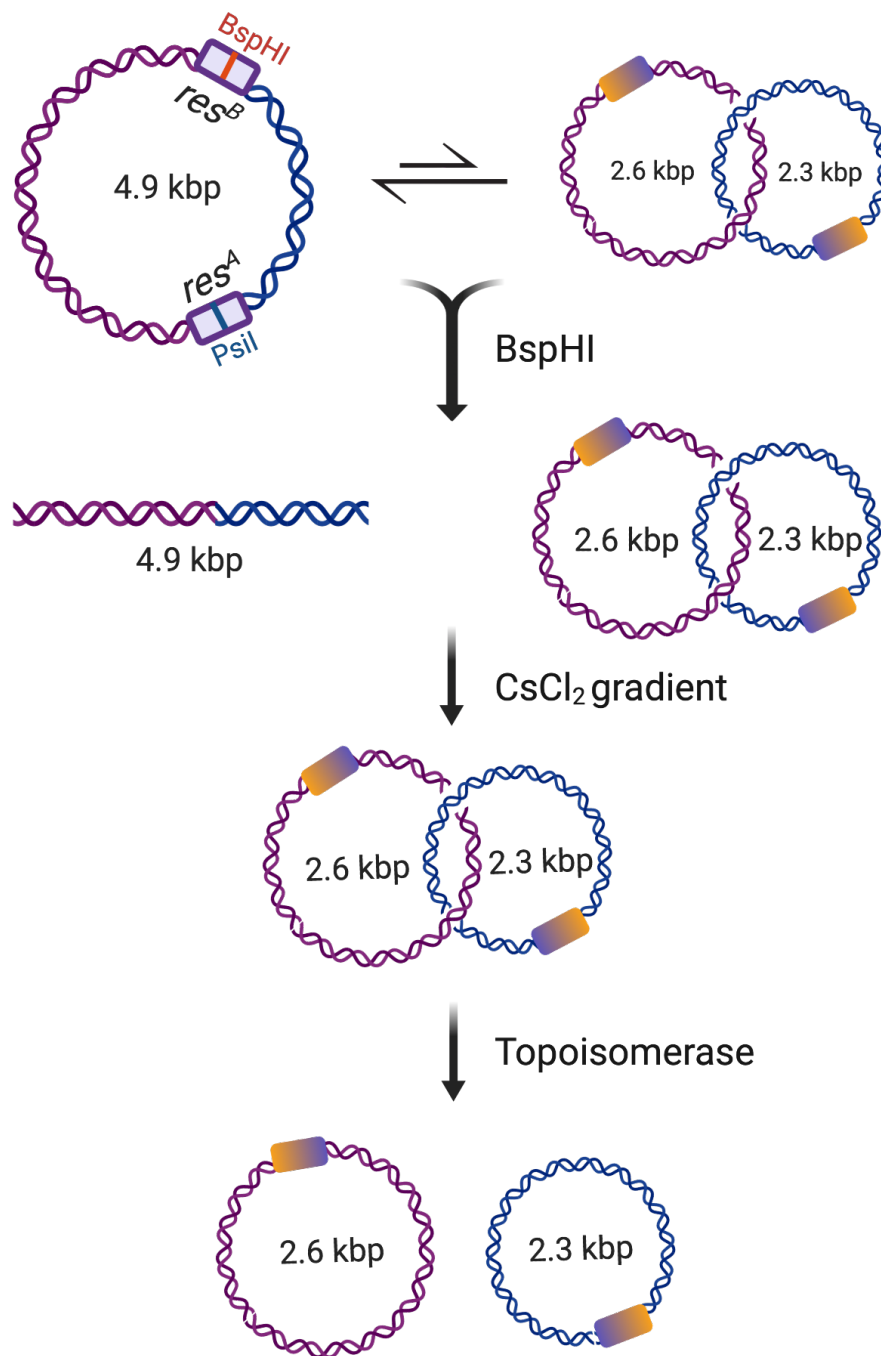


Figure 6.5: The generation of bis-cat DNA.

Tn3 recombination is mediated through the use of pMM9 (unique *res* restriction sequences: *PstI* (*res^A*) and *BspHI* (*res^B*)). The unreacted pMM9 plasmid is linearised by *BspHI* digestion, leaving the supercoiled bis-catenated DNA molecules intact. A caesium density gradient with ethidium bromide is used to separate the linear pMM9 from supercoiled bis-cat DNA. The purified bis-cat material can be used to substrate a DNA decatenation assay (in place of kDNA) to analyse the decatenation activities of various topoisomerases.

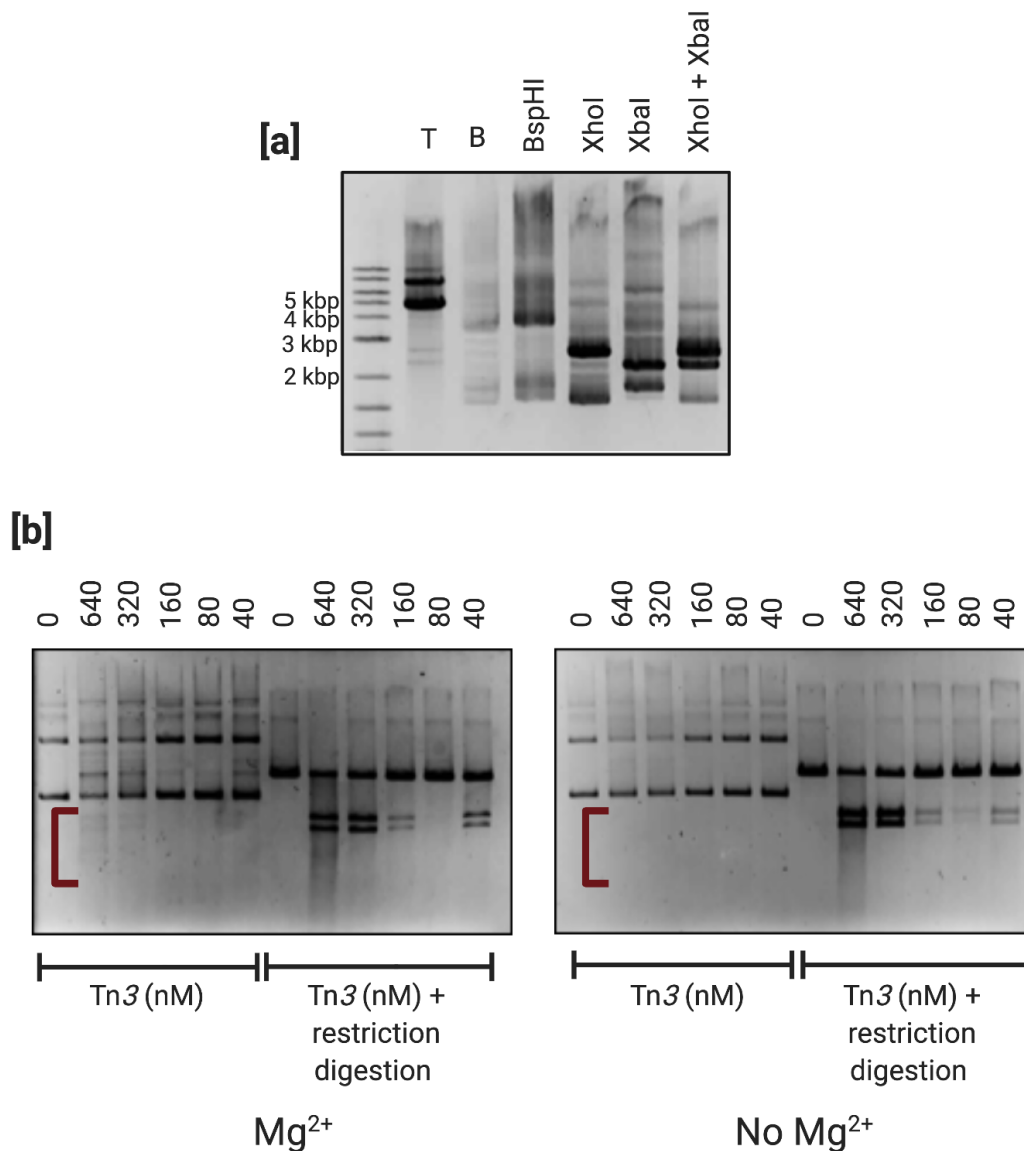


Figure 6.6: Analysis of caesium chloride gradient material.

(a) Analysis of material purified on a caesium chloride gradient (with ethidium bromide) following Tn3 recombination. T: material of caesium-chloride density band of lower density (upper band) corresponding to linear DNA material. B: material of caesium-chloride density band of higher density (lower band) corresponding to supercoiled DNA material. All restriction digestion reactions were performed on supercoiled DNA material (as in Lane B) with restriction enzymes labelled above each lane. (b) Tn3 resolvase-mediated recombination using pMM9 plasmid in the standard reaction buffer (Mg²⁺, left panel) and alternative reaction buffer (no Mg²⁺, right panel). Tn3 resolvase enzyme titrated, final enzyme concentration (nM) above each lane. Double restriction digestion carried out using XhoI and XbaI. The red brackets on each panel represent the appearance (Mg²⁺, left panel) and disappearance (No Mg²⁺, right panel) of bands corresponding to linear and supercoiled 2.6 and 2.3 kbp decatenated DNA molecules.

6.2.7. Comparison of Bis-cat and kDNA for decatenation by type II topoisomerases

The validation of purified singly-linked catenanes (bis-cat) as substrate for topoisomerase-catalysed decatenation reactions was carried out by directly comparing to kDNA. The substrates were tested using DNA topoisomerases of differing decatenation efficiencies.

6.2.7.1. Bis-cat resolves practical implications of kDNA

E. coli DNA gyrase has been shown to possess decatenation activity, albeit inefficient in comparison with other type II topoisomerases (Liu et al. 1980; Marians 1987a; Zechiedrich et al. 1997). The bis-cat DNA (purified singly-linked DNA catenanes) and kDNA were subjected to a decatenation assay with *E. coli* gyrase to directly test the efficacy of each substrate (Figure 6.7a). The mediation of the assay with kDNA highlights a significant limitation, through identification of the complex network of kDNA substrate trapped in the wells of the gel, at concentrations of *E. coli* gyrase up to 1350 pM. The issue is resolved by the bis-cat substrate that can be clearly visualised on agarose gels, prior to the addition of enzyme. Evidently, the increased sensitivity provided by the reaction on bis-cat DNA readily allows the detection of gyrase decatenation activity at lower concentrations of enzyme, resulting in two distinct bands on the agarose gel, representing the separate 2.6 kbp and 2.3 kbp supercoiled DNA molecules; the substrate is completely decatenated by 450 pM enzyme (Figure 6.7a).

6.2.7.2. Bis-cat assay: enhanced sensitivity and visualisation of multiple DNA topologies

Topoisomerase II α is a type II topoisomerase that controls and manipulates the topological state of DNA, principally during the processes of chromosome condensation, chromatid segregation, transcription and translation, by initiating transient double-stranded DNA breaks (Wang 2002b). Topoisomerase II α has a variety of activities, including the ability to relax both positively and negatively supercoiled DNA and interconvert catenated and decatenated, or knotted and unknotted DNA forms. A direct comparison of the bis-cat DNA and kDNA as substrates for topoisomerase II α -mediated decatenation revealed that the addition of topoisomerase II α leads to the decatenation of the singly-linked catenanes in a single step to release two separate circular DNA molecules of visibly distinguishable sizes: 2.6 kbp and 2.3 kbp. The reaction of topoisomerase II α with kDNA leads to the appearance of several DNA molecules of varying sizes on the

agarose gel; these are likely to be partially decatenated products. Impressively, the use of singly-linked DNA catenanes has significantly improved the sensitivity of the DNA decatenation assay by unambiguously demonstrating full decatenation with ~16-fold less enzyme than required to fully decatenate an equal amount of kDNA. In addition, the new substrate described here allows for the visual distinction between two different activities of topoisomerase II α . Under these assay conditions, at topoisomerase II α concentrations of 13-65 pM, the decatenation of the singly-linked dimers into two independent supercoiled DNA molecules is seen (Figure 6.7b). Further addition of topo II α in excess of 130 pM reveals the DNA relaxation activity of the enzyme converting the unlinked supercoiled DNA molecules into relaxed forms with a relatively lower mobility in the agarose gel; such distinction is not apparent using kDNA.

The manipulation of decatenation assay conditions for *A. thaliana* gyrase (i.e., conditions favouring supercoiling or relaxation), previously described in Chapter 4, identified enzyme-mediated decatenation activity in relaxation conditions to be more efficient than in conditions favouring supercoiling (chapter 4, Figure 4.11). The assay also allowed the novel detection of gyrase decatenation and relaxation in a single experiment.

6.2.7.3. Bis-cat mediated study of DNA decatenation

A further application of the bis-cat substrate is for inhibition assays. These are often used to test the efficacy of novel topoisomerase inhibitors. The sensitivity of the bis-cat substrate should enhance the fidelity of the information obtained by gel-based inhibition assays. Type II DNA topoisomerases, such as topoisomerase II α and gyrase, are well-known targets of anti-cancer drugs and antibiotics, respectively (Pommier 2013; Pommier et al. 2010; Tse-Dinh 2016). Ciprofloxacin is a clinically-established gyrase inhibitor that has been discussed previously; etoposide is a chemotherapy drug that functions by a method analogous to ciprofloxacin through stabilisation of the human topoisomerase II covalent cleavage-complex. The decatenation inhibition potential for etoposide and ciprofloxacin was investigated for their respective target enzymes, human topoisomerase II α and gyrase, through mediation of a decatenation assay with bis-cat DNA to replace kDNA. The approximate IC₅₀ of etoposide determined by this method, 0.3-1 μ M, can be compared with those derived from the literature (50–200 μ M IC₅₀) using kDNA as the substrate (Lassota et al. 1996; Rhee et al. 2007; Terada et al. 1993); the results suggest that the bis-cat assay is more sensitive (Figure 6.8a). In the case of ciprofloxacin inhibition of decatenation, the percentage decatenation activity was determined by taking the sum of decatenated 2.6 kbp and 2.3 kbp products over a range of ciprofloxacin concentrations,

as a fraction of the DNA gyrase decatenation activity in the absence of inhibitor; appropriate background subtractions were made to allow for pre-existing uncatenated DNA molecules in the substrate. The resultant IC₅₀ for inhibition by ciprofloxacin was calculated as 0.44 μM, which is similar to sub-micromolar values previously determined (Barnard and Maxwell 2001; Germe et al. 2018a).

6.2.7.4. Limitations of bis-cat substrate

The examples discussed in this section highlight a potential limitation of the bis-cat substrate, that is, the background level of uncatenated double-stranded DNA molecules. The background contamination is essentially the desired products of the reaction and constitutes <20% of the total DNA. The contamination could be a consequence of downstream handling of the DNA but seemingly persists over different resolvase preparations. It is unlikely that the contamination is a direct result of decatenation by a co-purified topoisomerase protein, not only due to the stringent resolvase purification process, which involves denaturation with urea, but also because a topoisomerase capable of decatenating double-stranded DNA catenanes would require an energy investment from the hydrolysis of ATP, which is not present. To investigate whether this background level was attributable to nuclease activity, we exploited the Mg²⁺-independence of Tn3 resolvase by conducting the resolvase reaction in an assay buffer lacking the divalent metal. This alteration had minimal effect on the reaction efficiency, but it did not solve the contamination problem. Nevertheless, alternative purification methods using hexa-histidine tagged resolvase should be explored. Plausibly, the uncatenated supercoiled product circles could be produced by failure of resolvase to religate one circle in the catenane.

Interestingly, in a method akin to the bis-cat substrate, surface-attached interlinked DNA minicircles have been constructed and used to sensitively and specifically detect the decatenation activity of human topoisomerase II from cell lysates (Kristoffersen et al. 2017). The assay featured a fluorometric output that was determined to be 100-fold more sensitive for human topoisomerase II decatenation when compared to kDNA.

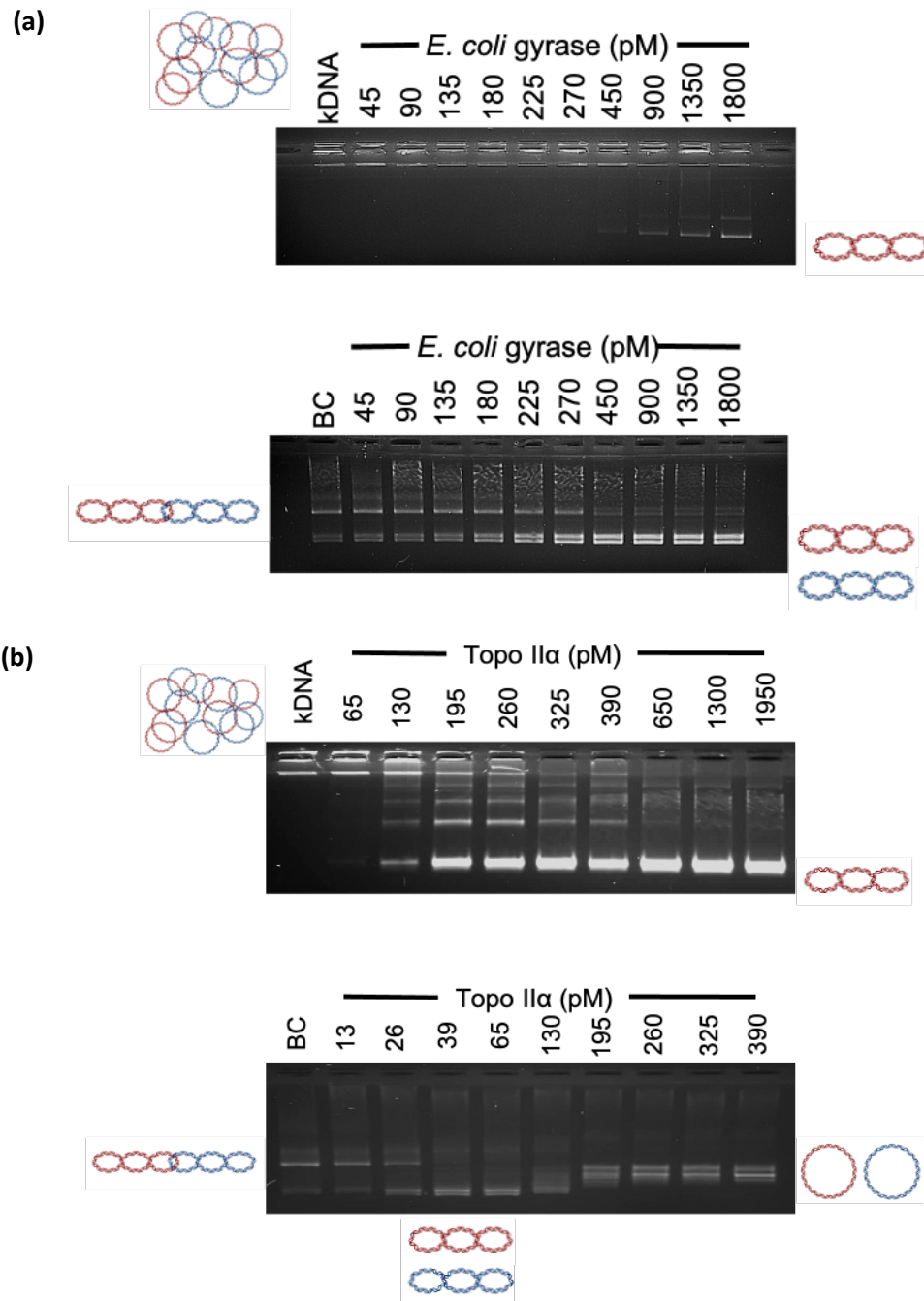


Figure 6.7: DNA decatenation mediated by kDNA and bis-cat DNA.

DNA decatenation assays to directly compare kDNA (top) and bis-cat DNA (bottom) substrates for decatenation by *E. coli* gyrase (a) and human topo II α (b). Concentration of enzyme in pM above each lane. kDNA: kDNA substrate network; BC: bis-cat DNA. Illustrations of the conversion of reaction substrate to products as illustrated from left to right of gels.

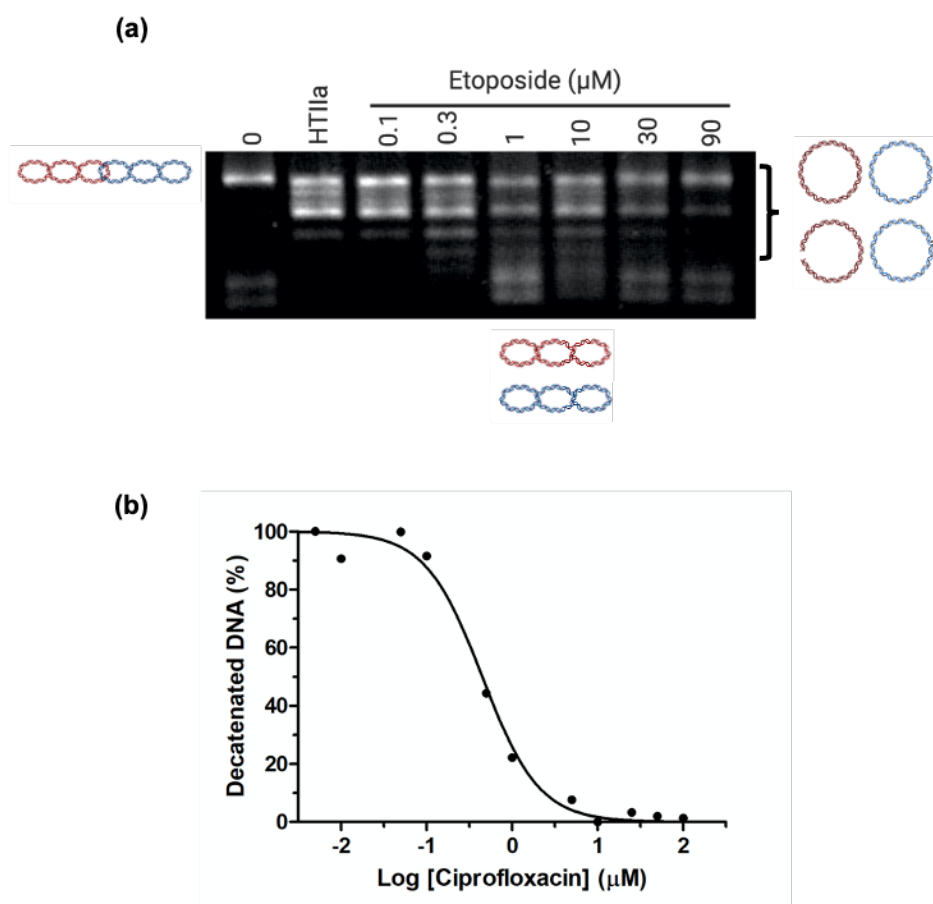


Figure 6.8: Inhibition of DNA decatenation.

The bis-cat substrate was used to mediate DNA decatenation using bis-cat as substrate for the assay. (a) Inhibition of human topoisomerase II α (HTII α) by etoposide; the IC₅₀ can be approximated to be 0.3–1 μ M by the gel-based assay; topoisomerase II α was 0.44 nM. (b) Plot of gyrase decatenation inhibition assay with at increasing levels of ciprofloxacin. The gyrase concentration was 450 pM; the calculated IC₅₀ of ciprofloxacin against *E. coli* gyrase was 0.44 μ M

6.3. Conclusions

The bis-cat substrate has been validated using well-characterised topoisomerase enzymes. This novel substrate has proved to be a superior alternative to the currently marketed kDNA substrate, by significantly enhancing the sensitivity and reliability, of gel-based decatenation assays. The potential hindrance of background decatenated DNA molecules can efficiently be accounted for by making simple background level subtractions to provide reliable results as has been demonstrated with the use of an inhibition assay. This substrate allows the novel detection of decatenation and relaxation activities of topoisomerase enzymes within a single experiment.

6.4. Future directions

The efforts to eliminate the uncatenated background DNA molecules through attempts to simplify the Tn3 resolvase purification procedure failed to show meaningful promise. The problem of background level contamination could theoretically be tackled by manipulation of the pMM9 substrate plasmid to enable the downstream purification of the singly-linked catenanes from their uncatenated counterparts; for example, the molecular mass of the substrate plasmid could be adjusted to increase its mass difference from the largest of the two decatenated circular products, in order to take advantage of downstream gel-filtration. An alternative prospect is the introduction of two different DNA triplex-binding sites into pMM9, one in each region between the two *res* site (Schluep and Cooney 1998). Purification could then proceed by the sequential passage of the singly-linked catenane mixture through two columns, each with an attached triplex DNA-forming oligonucleotide complementary to one of the triplex sites in pMM9 (Maxwell et al. 2006); thus, the catenated substrate would bind to both columns, and the uncatenated DNA molecules (only able to bind to one of the two columns) could be separated (Figure 6.9).

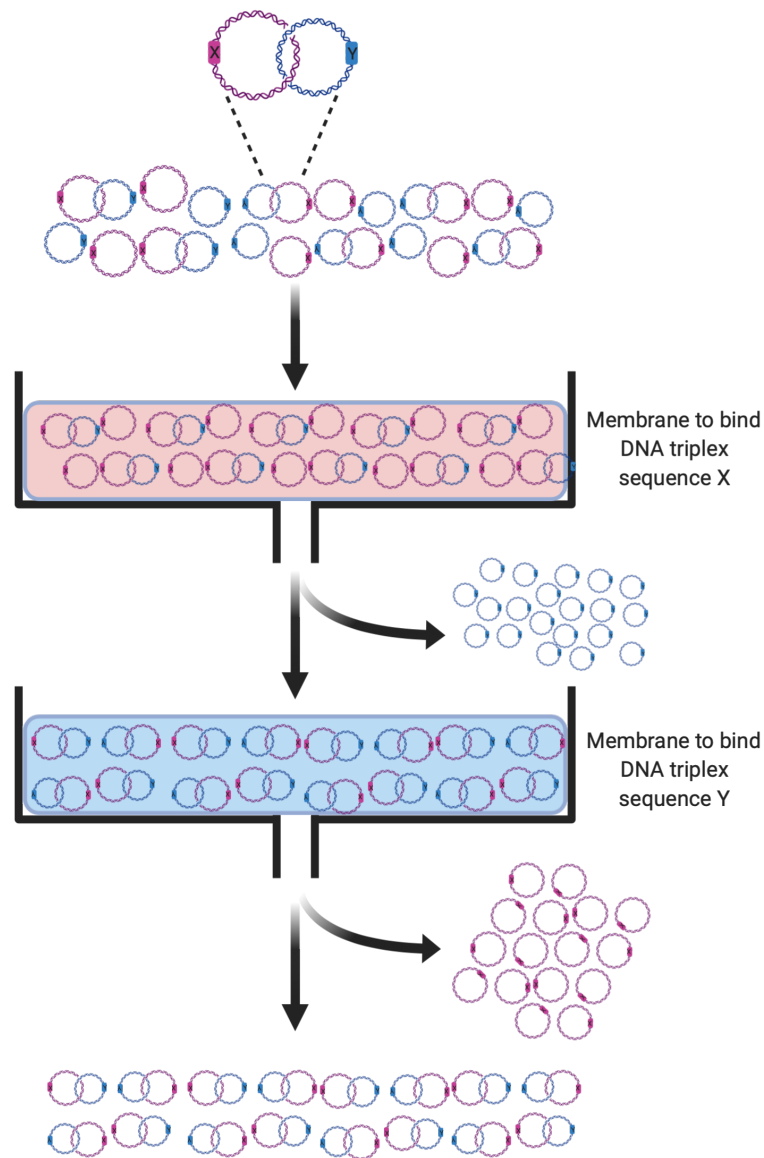


Figure 6.9: Purification of bis-cat DNA from uncatenated DNA using DNA triplex sequences. Triplex-forming sequences X (pink) and Y (blue) introduced into pMM9 would be inherited by each catenane of the bis-cat DNA, upon Tn3 resolvase recombination. Application of partially purified material extracted from the supercoiled band of a caesium chloride density gradient (possessing background level of decatenated molecules alongside bis-cat DNA) sequentially to purification columns immobilised with triplex-binding DNA oligonucleotides specific for sequences X and Y would result in purification of bis-catenated DNA.

Chapter 7: Discussion

7.1. Introduction

DNA gyrase is an essential bacterial topoisomerase. The unexpected discovery of gyrase in the genomes of eukaryotic species, including *Arabidopsis* and *Plasmodium* was made about two decades ago. Despite this, our understanding of the role of gyrase in these species is extremely limited. The aim of this work was to biochemically characterise these proteins in order to gain insight into their *in vivo* roles and potential for inhibition. The characterisation of plasmodial gyrase has not been possible due to difficulties of heterologous protein expression. However, significant efforts have been made to improve our understanding of the role of gyrase in *Arabidopsis*.

7.2. Heterologous expression of *A. thaliana* gyrase

The nuclear genome of *Arabidopsis thaliana* encodes three gyrase genes: *gyrA*, *gyrB1* and *gyrB2*. The heterologous expression of *A. thaliana* gyrase functional for supercoiling had been reported prior to the initiation of this project (Evans-Roberts et al. 2016). The functional protein was expressed in insect cells and comprised GyrA and GyrB2. The work in this thesis has extensively explored expression of *Arabidopsis thaliana* gyrase proteins through baculovirus-mediated infection of insect cells by the use of two infection and recombination systems (pOPIN and Bac-toBac) to mediate infection of three lines of *Spodoptera frugiperda* (Sf9, Sf21 and sSf9-2) at various MOIs and periods of expression. The codon-optimised sequences for expression in *S. frugiperda* used in this work did not resolve the problem of unreliable gyrase expression. However, the use of optimised sequences led to increased GyrA protein expression, particularly in the sSf9-2 cell line that is adapted for the expression of toxic proteins or those prone to degradation. Intriguingly, the separate expression of GyrA and GyrB2 prior to reconstitution of the active enzyme complex, did not generate protein active for DNA supercoiling; this was an unforeseen result. The separate expression of bacterial gyrase subunits in this way normally produces functional protein; additionally both of the *Arabidopsis* GyrA or GyrB2 subunits can form functional enzymes when complemented with the *E. coli* partner subunit (the functional association of AtGyrA and EcGyrB is a novel finding reported in Chapter 3) (Evans-Roberts et al. 2016). It is plausible that the *A. thaliana* gyrase subunits require co-expression in insect cells, possibly to facilitate proper folding of the subunits, or for reasons of stability. However, this would need further exploration. GyrB1 expression as a fusion peptide with

GyrA has been demonstrated. This was followed-up by cloning of all GyrA, GyrB1 and fusion constructs (all codon optimised) into the pOPIN suite of vectors for intended expression analysis in sSf9-2 cells. However, due to a combination of sSf9-2 cell culturing issues and interruption of work as a result of national lockdown, the intended development of this system could not be completed. The future continuation of this line of work is strongly recommended.

7.3. Where are gyrase subunits localised *in vivo*?

Wall *et al.* (2004) identified AtGyrA to be dual-targeted to chloroplasts and mitochondria, whilst GyrB1 and GyrB2 were chloroplast and mitochondrial targeted, respectively (Wall *et al.* 2004). However, errors in the online databases at the time of these experiments meant that both transit peptides used by Wall and colleagues were in fact of AtGyrB2 origin, which therefore appears also to be dual targeted to both chloroplasts and mitochondria (Evans-Roberts 2007a). Subsequent to this, Christensen *et al.* (2005) demonstrated that through inclusion of an artificial start codon and the untranslated region of AtGyrB1, the protein too appeared to be dual targeted to both organelles (Christensen *et al.* 2005). In further support, GFP localisation experiments incorporating expression of the initial 100-150 amino acids of the gyrase proteins identified GyrB1 and GyrB2 to be dual targeted, although, surprisingly, the GyrA protein was identified only in chloroplasts (Monika Murcher, personal communication, Figure 5.1). The independent investigations of T-DNA lines in the present work have been described in Chapter 5; the results of our analysis corroborate GyrA embryo-lethality (as previously observed by Wall *et al.* 2004). Interestingly, independent investigations of the chloroplast and mitochondrial proteomes by mass-spectrometry have identified GyrA, GyrB1 and GyrB2 in both organelles of *Arabidopsis* (Melonek *et al.* 2016a; Senkler *et al.* 2017; Tomizioli *et al.* 2014).

Taking all this information together, we propose that all three *Arabidopsis thaliana* gyrase subunits (AtGyrA, AtGyrB1 and AtGyrB2) are dual-targeted *in vivo* to both chloroplasts and mitochondria.

7.4. Why would *Arabidopsis* chloroplasts and mitochondria require AtGyrB1 and AtGyrB2?

Bacterial DNA gyrase serves an essential role for the replication of genomic DNA. It is expected that *A. thaliana* gyrase must, by extension, serve to function in the replication of organellar DNA in both chloroplasts and mitochondria. The functional role of *A. thaliana* gyrase (GyrA and GyrB2) has been discussed in Chapter 4. The question then remains as to why chloroplasts and mitochondria require both GyrB1 and GyrB2? Intriguingly, both subunits have been identified to interact with AtGyrA, through the yeast-two hybrid interaction of GyrA and GyrB1 (Evans-Roberts et al. 2010), and through the confirmation of an active enzyme complex of GyrA and GyrB2 (Evans-Roberts et al. 2016). *Arabidopsis* does not appear to encode the bacterial equivalent of a topoisomerase IV enzyme. The possession of two gyrase B subunits in *Arabidopsis* is seemingly a result of a gene duplication event; the two GyrB genes are >80% identical at the sequence level (Sterck et al. 2007). It is therefore possible that following gene duplication, one GyrB subunit became specific for the role of a classical gyrase protein, whilst the other GyrB subunit became adapted to more efficiently carry out the functional roles of a bacterial topoisomerase IV equivalent, i.e., by serving primarily as an efficient decatenating enzyme. How *A. thaliana* may achieve this is a fascinating prospect for future investigations; particularly considering that the fundamental differences between topoisomerase IV and gyrase have thus far been attributed to the ParC and GyrA subunit, respectively.

An alternative explanation may be that although the endosymbiotic organelles possess GyrB1 and GyrB2, the expression of the two proteins may be regulated in accordance with the stage of the cell cycle, or indeed in accordance with the cell type. This would be somewhat reminiscent of the situation of eukaryotic topoisomerase II, which has two variant forms, α and β (Capranico et al. 1992). Topoisomerase II α expression oscillates in accordance with the cell cycle and its loss affects cell proliferation (Dereuddre et al. 1997; Woessner et al. 1991). Topoisomerase II β expression does not vary in accordance with the cell cycle but increases as cells enter quiescence (Woessner et al. 1991).

A recent study assessed fluctuations in gene expression in accordance with the circadian clock of *Arabidopsis* (Romanowski et al. 2020). The expression of *Arabidopsis* gyrase from these data is given in Figure 7.1. Expression of GyrA is consistently higher than that of GyrB1 or GyrB2 (Romanowski et al. 2020), plausibly a consequence for the requirement of GyrA to partner with both GyrB subunits. The GyrB1 and GyrB2 subunits may have different affinities for GyrA that vary in accordance with the topology of the organellar DNA at any particular instance of time.

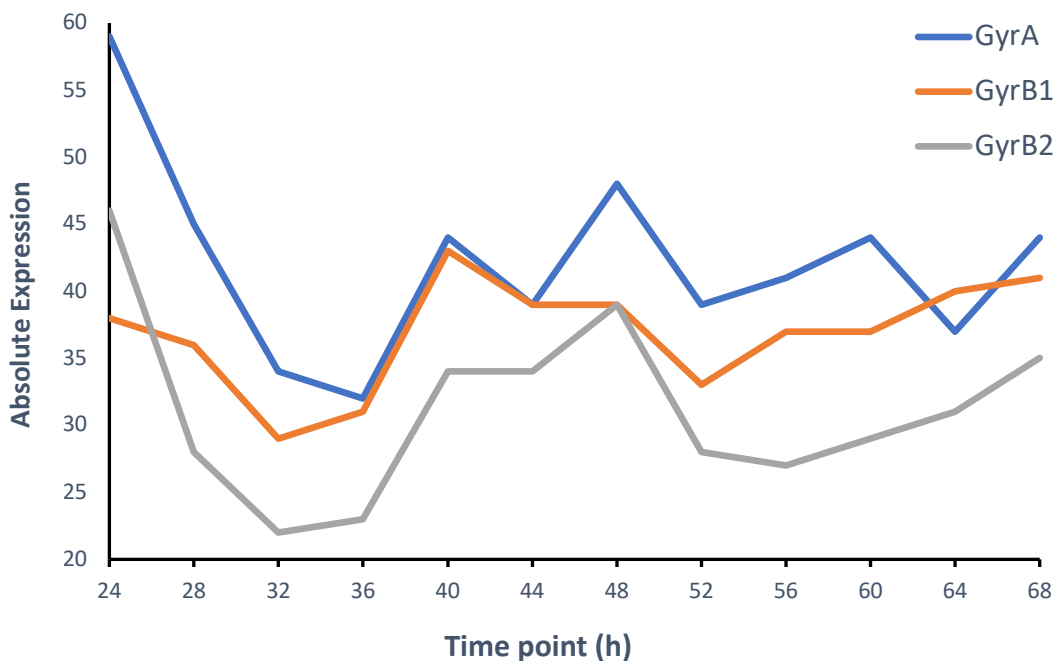


Figure 7.1: *A. thaliana* gyrase transcript levels.

RNA transcript levels relating to gyrase genes of *Arabidopsis* as determined by extraction of total RNA from 11-day old seedlings, samples collected at 4 h time intervals. Graph produced from data obtained by (Romanowski et al. 2020).

The oscillations of GyrA and GyrB2 expression synchronise somewhat better than that of GyrA and GyrB1; indeed the levels of the latter protein do not vary dramatically (Figure 7.1). Further experiments with more frequent time intervals in accordance with the cell cycle, directly, will need to be conducted before definitive conclusions can be reached.

7.5. What is the role of GyrB1 *in vivo*?

The investigations into the heterologous expression of *A. thaliana* GyrB1 in *S. frugiperda* (Chapter 3), imply that expression of the gyrase subunit is toxic; therefore the GyrB1 transcript is readily degraded. Similar conclusions of host toxicity have previously been made during heterologous expression in *E. coli* (Evans-Roberts 2007a). The *in vivo* analysis of mutant GyrB1 lines (Chapter 5) suggest that insertion of T-DNA resulting in a decrease in GyrB1 transcript, i.e., GK-06^{-/-} plants, are phenotypically distinguishable by chlorosis, dwarfed phenotypes and aberrations in silique size and development. TEM identified ultrastructural variations in the thylakoid-stacking of these chloroplasts and a reduction in their overall size. Although the overall topology and conformation of chloroplast DNA has not yet been settled, the association of the chloroplast genome with the thylakoid membranes has been proposed (Krupinska et al. 2013).

The *in vivo* observations in this work have identified AtGyrB1 to be critical for the development of lateral roots in *Arabidopsis thaliana*. What is the significance of this observation? An essential role for *A. thaliana* gyrase, through co-operation with the *Arabidopsis thaliana* chloroplast-targeted RNaseH1 protein (AtRNH1c), is to maintain chloroplast genome stability by regulating the formation of R-loops (Yang et al. 2017). Interestingly, signs of chlorosis and dwarfism have also been identified in *atrnh1c* plants; these observations are similar to those of gyrase B1 mutant plants (GK-06^{-/-}). Indeed, it may be that the interaction of AtGyrB1 and AtRNH1c is essential to manage co-transcriptional translation, particularly of highly transcribed genes (for example, the inverted repeat regions of the chloroplast genome). In support of this, patterning of lateral roots in *Arabidopsis* stem cells has previously been linked to translation in non-green plastids (Nakata et al. 2018).

In vivo work with a GyrB1 line, where the level of GyrB1 transcript is increased (78^{-/-}) demonstrated symptoms of *Arabidopsis* stress through an elevation in the production of anthocyanins. It is interesting to consider that the increased stress response within *Arabidopsis* upon GyrB1 upregulation could be interconnected with the toxicity of GyrB1 overexpression in *S. frugiperda* and *E. coli*. How may this be achieved? Interestingly, topoisomerase II β mediated DNA-cleavage at gene promoters has been demonstrated to be essential for transcriptional induction of stimulus responsive genes (Madabhushi 2018). Could gyrase (GyrA and GyrB1) induce transcription through a similar cleavage mechanism? Alternatively, perhaps the efficient relaxation of transcription-generated supercoils by gyrase (GyrA and GyrB1) absolutely requires an accessory protein, for example AtRNH1c. The AtRNH1c protein would efficiently remove R-loops, which if

allowed to persist would lead to replication fork stalling and consequent DNA strand breaks; this has been identified as a dominant cause of genome instability in *Arabidopsis* plastids (Pérez Di Giorgio et al. 2019).

In conclusion, perhaps a gyrase comprising GyrA and GyrB1 is reserved for the transcription of stimulus responsive genes, or highly expressed genes that require associated RNase activity to facilitate efficient gyrase action ahead of the replication fork. Plausibly, the 'alternative gyrase' of GyrA and GyrB2 is more suited for the unlinking of interlinked DNA during replication.

7.6. Does *A. thaliana* gyrase function as a 'dual' topoisomerase?

In vitro characterisation of *A. thaliana* GyrA/B2 gyrase has been discussed in Chapter 4. Novel relaxation and decatenation activities of *A. thaliana* gyrase have been established. Intriguingly, when compared to *E. coli* gyrase, the enzyme was shown to be more efficient for the relaxation of supercoiling and decatenation of DNA. The *A. thaliana* enzyme may also exhibit potassium glutamate (KGlu)-mediated preference of reaction catalysis. The supercoiling reaction is dependent on KGlu and enhanced at high concentrations, while the relaxation reaction is inhibited at high concentrations of KGlu, although intermediate levels facilitate the reaction. Interestingly, these observations are not unique to *A. thaliana* gyrase but appear to be similar to those of *S. aureus* gyrase (Blanche et al. 1996; Hiasa et al. 2003). The decatenation activity of *A. thaliana* gyrase was independent of the inclusion or omission of KGlu. The generation of a novel and effective singly-linked decatenation substrate formed by two supercoiled plasmids of different sizes, 'bis-cat', has been reported here (Chapter 6). The improved sensitivity and clarity of the novel bis-cat-mediated decatenation assay, allowed precise evaluation of *A. thaliana* gyrase activity. The assay provided the unique opportunity to assess and compare the decatenation activity of *A. thaliana* gyrase in conditions permitting or inhibiting supercoiling. Indeed, the decatenation activity of the enzyme was determined to be more efficient in conditions disfavoured supercoiling. Nevertheless, even in conditions favouring supercoiling, the *A. thaliana* gyrase was determined to be 9-fold more efficient for DNA decatenation than *E. coli* gyrase. This difference was increased to 35-fold for conditions favouring decatenation by *A. thaliana* gyrase.

The strong decatenation activities of the 'dual topoisomerases' of *Mycobacterium smegmatis* and *Mycobacterium tuberculosis* (both lacking a topoisomerase IV equivalent) have previously been found to be ~7-fold and 10-fold more efficient, respectively, than

that of *E. coli* gyrase (Aubry et al. 2006; Manjunatha et al. 2002). Intriguingly, through the use of kDNA as substrate, the analysis here concludes that *A. thaliana* gyrase is >20-fold more efficient than *E. coli* gyrase for decatenation. Perhaps one *in vivo* role of the GyrA/B2 *A. thaliana* gyrase is indeed to support the decatenation of organellar DNA replication intermediates within the chloroplasts and mitochondria. However, further experimental work, comparing the decatenation reaction of *A. thaliana* gyrase to classic topoisomerase IV proteins, including those from *E. coli* and *S. aureus* will be required. The protein sequences of *A. thaliana* gyrase are almost equally similar to gyrase or topo IV from *E. coli* or *S. aureus* gyrase (Table 7.2).

Table 7.2: Percentage protein sequence identities of *E. coli* and *S. aureus* gyrase and topo IV subunits to corresponding *A. thaliana* gyrase subunits. Percentage identities were determined through the NCBI protein blast feature.

<i>A. thaliana</i>	<i>E. coli</i> (%)				<i>S. aureus</i> (%)			
	ParC	ParE	GyrA	GyrB	ParC	ParE	GyrA	GyrB
GyrA	38	—	43	—	39	—	41	—
GyrB1	—	37	—	49	—	47	—	49
GyrB2	—	38	—	49	—	46	—	49

7.7. Can *A. thaliana* gyrase be exploited as a novel herbicidal target?

Bacterial DNA gyrase has been established as a successful antibacterial target. The encoding of gyrase within the eukaryotic genome of *Arabidopsis* provides the novel opportunity to exploit the enzyme for development of new herbicidal compounds. The proof of principle of *A. thaliana* gyrase inhibition has been explored in Chapter 4, by means of novel ciprofloxacin analogues that were tested for *in vitro* supercoiling inhibition activity. Indeed, several compounds with inhibition potentials of 10 μ M and lower for *A. thaliana* gyrase were identified. However, all compounds had ~2-fold selectivity in favour of *E. coli* gyrase over *A. thaliana* gyrase. Most compounds also had respectable MIC values against *E. coli*; with the notable exception of CA09 for which the *E. coli* MIC was increased >1000x when compared to ciprofloxacin, although the IC₅₀ for *Arabidopsis* was only increased <2x when compared to ciprofloxacin.

Interestingly, ciprofloxacin and other quinolones, are not specific inhibitors of gyrase, but also possess cross-reactivity to topoisomerase IV. In *E. coli*, gyrase is the main target of ciprofloxacin rather than topo IV; however, in *S. aureus* the opposite is true. An extended α -4 domain region of *S. aureus* gyrase has been identified to be at least partly responsible for a 2-fold resistance towards quinolone antibacterials; the insensitivity was mediated by KGlu (Strahilevitz et al. 2006). KGlu delivers a protective effect from the bactericidal action of quinolone inhibitors in *S. aureus* gyrase (Hiasa et al. 2003). Accordingly, it would be expected that ciprofloxacin (and by extension the novel analogues) may demonstrate increased activity against the decatenation reaction of *A. thaliana* gyrase (GyrA and GyrB2) as this activity of the enzyme does not require KGlu. Significantly, according to the results thus far, the predominant activity of *A. thaliana* (GyrA and GyrB2) is in fact decatenation, therefore suggesting that development of inhibitors of this activity may be of greater biological relevance.

The *A. thaliana* gyrase enzyme remains uncharacterised in terms of inhibition by many other classical topoisomerase inhibitors, which would be an interesting line of investigation to pursue. The exploration of classical topoisomerase inhibitors for *A. thaliana* gyrase is encouraged as a starting point in the search for novel herbicidal compounds. However, the use of antibacterials as herbicides is not recommended as this would increase the current global issue of antibiotic resistance.

7.8. Where next for *Plasmodia* gyrases?

The expression of plasmodial gyrases remains extremely limited. Expression of PfGyrB and co-operation of the subunit with EcGyrA to form an active supercoiling complex has previously been reported (Dar et al. 2007). This has been confirmed by the work reported here, through hints of supercoiling activity from PfGyrB (insect cell expressed) when complemented with EcGyrA. Unfortunately however, the expression of PfGyrA did not prove possible, despite the use of codon-optimised sequences. Perhaps the correct folding of *P. falciparum* gyrase requires co-expression of a chaperone protein; this should be investigated further. The work here initiated the novel exploration of *P. berghei* gyrase. Intriguingly, the GyrB subunit of the protein produced encouraging results for *E. coli* expression. However, due to time-constraints, this was not further investigated. Further expression and purification of this protein is recommended.

As far as our current knowledge extends, gyrase within *Plasmodia* is the sole type IIA topoisomerase enzyme (no topoisomerase IV equivalent is encoded). This is a situation likely comparable to *A. thaliana* gyrase. Therefore, the findings from the data reported in

this work strongly encourage that future activity investigations of gyrase from *Plasmodia* explore beyond the supercoiling activity and interrogate other topoisomerase activities.

7.9. Conclusions

The heterologous expression of *A. thaliana* gyrase is not a straightforward task, and expression of active GyrA/B1 enzyme has not so far been achieved. The presence of two active GyrB homologues within *Arabidopsis* remains a perplexing yet exciting idea. The possibility that plants may incorporate two 'versions' of DNA gyrase, each adapted to support replication and perhaps transcription of organellar DNA through a unique mechanism is a fascinating prospect worthy of further exploration.

Abbreviations

AcMPNV: *Autographa californica multiple nucleopolyhedrovirus*

ADP: adenosine diphosphate

Amp: ampicillin

AP: apurinic/aprimidinic

ATP: adenosine triphosphate BN: blue-native

AtGyrA: *Arabidopsis thaliana* Gyrase A

AtGyrB1: *Arabidopsis thaliana* Gyrase B1

AtGyrB2: *Arabidopsis thaliana* Gyrase B2

AtGyrB2A: *Arabidopsis thaliana* Gyrase B2 fusion with Gyrase A

bp: base pair

CaCl₂: calcium chloride

Cam: chloramphenicol

Cam^R: chloramphenicol resistant

CFU: colony forming unit

CFX: ciprofloxacin

Col-0: Colombia 0 *Arabidopsis*

CTD: C-terminal domain

DMSO: dimethyl sulfoxide

DNA: deoxyribonucleic acid

DSB: double stranded break

DTT: dithiothreitol

EB: enzyme buffer

EcGyrA: *Escherichia coli* Gyrase A

EcGyrB: *Escherichia coli* Gyrase B

EDTA: ethylenediaminetetraacetic acid EtOH: ethanol

G-segment: gate segment

GyrA: gyrase A

GyrA59: CTD truncation of GyrA

GyrB: gyrase B

h: hour/s

HCl: hydrochloric acid

kb: kilobase pairs

KCl: potassium chloride

kDNA: kinetoplast DNA

KGlu: potassium glutamate

kDa: kilo Dalton

LB: Luria-Bertani or Lysogeny Broth Media

Lk: linking number

Mb: megabase pairs

MFX: moxifloxacin

MIC: minimum inhibitory concentration

min: minute/s
NaCl: sodium chloride
NAP: Nucleoid associated protein
NFX: norfloxacin
NTD: N-terminal domain
OD₆₀₀: optical density at wavelength 600 nm
PAGE: polyacrylamide gel electrophoresis
PCR: polymerase chain reaction
PbGyrA: *Plasmodium berghei* Gyrase A
PbGyrB: *Plasmodium berghei* Gyrase B
PFU: plaque forming unit
PfGyrA: *Plasmodium falciparum* Gyrase A
PfGyrB: *Plasmodium falciparum* Gyrase B
PvGyrA: *Plasmodium vivax* Gyrase A
PvGyrB: *Plasmodium vivax* Gyrase B
QRDR: quinolone resistance-determining region
RNA: Ribonucleic acid
ROS: reactive oxygen species
s: second/s
SDM: site-directed mutagenesis
SDS: sodium dodecyl sulphate
ssDNA: single-stranded DNA
T-DNA: Transferred deoxyribonucleic acid
TEM: Transmission electron microscopy
Tet: tetracycline
topo: topoisomerase
topo I: topoisomerase I
topo II: topoisomerase II
topo III: topoisomerase III
topo IV: topoisomerase IV
topo V: topoisomerase V
topo VI: topoisomerase VI
topo VIII: topoisomerase VIII
TOPRIM: topoisomerase-primase
T-segment: transport segment
Tris.HCl: tris(hydroxymethyl)aminomethane hydrochloride
Tw: twist
v/v: volume per volume
VIGS: Virus-induced gene silencing
WHD: winged-helix domain
Wr: writhe
WT/wt: wild type

References

- Adachi, T., Mizuuchi, M., Robinson, E.A., Appella, E., O'Dea, M.H., Gellert, M., et al. 1987. DNA sequence of the *E. coli* *gyrB* gene: application of a new sequencing strategy. *Nucleic Acids Res* **15**(2): 771-784. Available from <https://www.ncbi.nlm.nih.gov/pmc/articles/PMC340466/pdf/nar00246-0387.pdf> [accessed].
- Ali, J.A., Jackson, A.P., Howells, A.J., and Maxwell, A. 1993. The 43-kilodalton N-terminal fragment of the DNA gyrase B protein hydrolyzes ATP and binds coumarin drugs. *Biochemistry* **32**(10): 2717-2724. doi:10.1021/bi00061a033.
- Alonso, J.M., Stepanova, A.N., Leisse, T.J., Kim, C.J., Chen, H., Shinn, P., et al. 2003. Genome-Wide Insertional Mutagenesis of *Arabidopsis thaliana*. *Science (New York, N.Y.)* **301**(5633): 653-657. doi:10.1126/science.1086391.
- Alt, S., Mitchenall, L.A., Maxwell, A., and Heide, L. 2011. Inhibition of DNA gyrase and DNA topoisomerase IV of *Staphylococcus aureus* and *Escherichia coli* by aminocoumarin antibiotics. *Journal of Antimicrobial Chemotherapy* **66**(9): 2061-2069. doi:10.1093/jac/dkr247.
- Anaconda. 2016. Anaconda Software Distribution. Computer Software. <https://anaconda.com>.
- Aravind, L., Leipe, D.D., and Koonin, E.V. 1998. Toprim--a conserved catalytic domain in type IA and II topoisomerases, DnaG-type primases, OLD family nucleases and RecR proteins. *Nucleic Acids Res* **26**(18): 4205-4213. Available from <https://www.ncbi.nlm.nih.gov/pmc/articles/PMC147817/pdf/264205.pdf> [accessed].
- Aravind, L., Iyer, L.M., Wellems, T.E., and Miller, L.H. 2003. Plasmodium biology: genomic gleanings. *Cell* **115**(7): 771-785. Available from http://ac.els-cdn.com/S0092867403010237/1-s2.0-S0092867403010237-main.pdf?_tid=82b9bb12-1c69-11e7-bd54-00000aacb35f&acdnat=1491662694_ddce0e742cdc94ca1a4906d4c646e570 [accessed].
- Arnold, P.H., Blake, D.G., Grindley, N.D.F., Boocock, M.R., and Stark, W.M. 1999. Mutants of Tn3 resolvase which do not require accessory binding sites for recombination activity. *The EMBO Journal* **18**(5): 1407-1414. doi:<https://doi.org/10.1093/emboj/18.5.1407>.
- Aubry, A., Fisher, L.M., Jarlier, V., and Cambau, E. 2006. First functional characterization of a singly expressed bacterial type II topoisomerase: the

enzyme from *Mycobacterium tuberculosis*. *Biochem Biophys Res Commun* **348**(1): 158-165. doi:10.1016/j.bbrc.2006.07.017.

- Backert, S., Lynn Nielsen, B., and Börner, T. 1997. The mystery of the rings: structure and replication of mitochondrial genomes from higher plants. *Trends Plant Sci.* **2**(12): 477-483. doi:10.1016/S1360-1385(97)01148-5.
- Bahl, A., Brunk, B., Crabtree, J., Fraunholz, M.J., Gajria, B., Grant, G.R., et al. 2003. PlasmoDB: the Plasmodium genome resource. A database integrating experimental and computational data. *Nucleic Acids Res* **31**(1): 212-215. doi:10.1093/nar/gkg081.
- Baker, N.M., Weigand, S., Maar-Mathias, S., and Mondragón, A. 2011. Solution structures of DNA-bound gyrase. *Nucleic Acids Res* **39**(2): 755-766. doi:10.1093/nar/gkq799.
- Baldi, M.I., Benedetti, P., Mattocchia, E., and Tocchini-Valentini, G.P. 1980. In vitro catenation and decatenation of DNA and a novel eucaryotic ATP-dependent topoisomerase. *Cell* **20**(2): 461-467.
- Baquero, F., Bouanchaud, D., Martinez-Perez, M.C., and Fernandez, C. 1978. Microcin plasmids: a group of extrachromosomal elements coding for low-molecular-weight antibiotics in *Escherichia coli*. *Journal of Bacteriology* **135**(2): 342-347. Available from <http://jb.asm.org/content/135/2/342.full.pdf> [accessed].
- Barnard, F.M., and Maxwell, A. 2001. Interaction between DNA gyrase and quinolones: effects of alanine mutations at GyrA subunit residues Ser(83) and Asp(87). *Antimicrobial Agents and Chemotherapy* **45**(7): 1994-2000. doi:10.1128/AAC.45.7.1994-2000.2001.
- Bates, A.D., and Maxwell, A. 2005. *DNA Topology* Oxford University Press.
- Bates, A.D., O’Dea, M.H., and Gellert, M. 1996. Energy coupling in *Escherichia coli* DNA gyrase: The relationship between nucleotide binding, strand passage, and DNA supercoiling. *Biochemistry* **35**(5): 1408-1416. doi:10.1021/bi952433y.
- Bates, A.D., Berger, J.M., and Maxwell, A. 2011. The ancestral role of ATP hydrolysis in type II topoisomerases: prevention of DNA double-strand breaks. *Nucleic Acids Res.* **39**(15): 6327-6339. doi:10.1093/nar/gkr258.
- Bellon, S., Parsons, J.D., Wei, Y., Hayakawa, K., Swenson, L.L., Charifson, P.S., et al. 2004. Crystal Structures of *Escherichia coli* Topoisomerase IV ParE Subunit (24 and 43 Kilodaltons): a Single Residue Dictates Differences in Novobiocin Potency against Topoisomerase IV and DNA Gyrase. *Antimicrobial Agents and Chemotherapy* **48**(5): 1856-1864. doi:10.1128/aac.48.5.1856-1864.2004.

- Belova, G.I., Prasad, R., Kozyavkin, S.A., Lake, J.A., Wilson, S.H., and Slesarev, A.I. 2001. A type IB topoisomerase with DNA repair activities. *Proceedings of the National Academy of Sciences* **98**(11): 6015-6020. doi:10.1073/pnas.111040498.
- Bendich, A.J. 2004. Circular Chloroplast Chromosomes: The Grand Illusion. *The Plant cell* **16**(7): 1661-1666. doi:10.1105/tpc.160771.
- Benedetti, P., Baldi, M.I., Mattoccia, E., and Tocchini-Valentini, G.P. 1983. Purification and characterization of *Xenopus laevis* topoisomerase II. *Embo j* **2**(8): 1303-1308.
- Berger, I., Fitzgerald, D.J., and Richmond, T.J. 2004. Baculovirus expression system for heterologous multiprotein complexes. *Nat Biotechnol* **22**(12): 1583-1587. doi:10.1038/nbt1036.
- Berger, J.M., Gamblin, S.J., Harrison, S.C., and Wang, J.C. 1996. Structure and mechanism of DNA topoisomerase II. *Nature* **379**(6562): 225-232. doi:10.1038/379225a0.
- Bergerat, A., Gadelle, D., and Forterre, P. 1994. Purification of a DNA topoisomerase II from the hyperthermophilic archaeon *Sulfolobus shibatae*. A thermostable enzyme with both bacterial and eucaryal features. *The Journal of biological chemistry* **269**(44): 27663-27669.
- Bergerat, A., de Massy, B., Gadelle, D., Varoutas, P.C., Nicolas, A., and Forterre, P. 1997. An atypical topoisomerase II from Archaea with implications for meiotic recombination. *Nature* **386**(6623): 414-417. doi:10.1038/386414a0.
- Berrow, N.S., Alderton, D., Sainsbury, S., Nettleship, J., Assenberg, R., Rahman, N., et al. 2007. A versatile ligation-independent cloning method suitable for high-throughput expression screening applications. *Nucleic Acids Res* **35**(6): e45. doi:10.1093/nar/gkm047.
- Birkholtz, L.-M., Blatch, G., Coetzer, T.L., Hoppe, H.C., Human, E., Morris, E.J., et al. 2008. Heterologous expression of plasmodial proteins for structural studies and functional annotation. *Malaria Journal* **7**(1): 197. doi:10.1186/1475-2875-7-197.
- Bjergbaek, L., Kingma, P., Nielsen, I.S., Wang, Y., Westergaard, O., Osheroff, N., et al. 2000. Communication between the ATPase and cleavage/religation domains of human topoisomerase IIalpha. *The Journal of biological chemistry* **275**(17): 13041-13048. Available from <http://www.jbc.org/content/275/17/13041.full.pdf> [accessed].
- Blackwell, J., Newbold, C., Turner, M., Vickerman, K., Roos, D.S., Crawford, M.J., et al. 2002. Mining the *Plasmodium* genome database to define organellar function: what does the apicoplast do? *Philosophical Transactions of the Royal*

- Society of London. Series B: Biological Sciences **357**(1417): 35-46. doi:doi:10.1098/rstb.2001.1047.
- Blanche, F., Cameron, B., Bernard, F.X., Maton, L., Manse, B., Ferrero, L., et al. 1996. Differential behaviors of Staphylococcus aureus and Escherichia coli type II DNA topoisomerases. Antimicrobial Agents and Chemotherapy **40**(12): 2714-2720. doi:10.1128/aac.40.12.2714.
- Bobik, K., and Burch-Smith, T.M. 2015. Chloroplast signaling within, between and beyond cells. Front Plant Sci **6**: 781. doi:10.3389/fpls.2015.00781.
- Bollimpelli, V.S., Dholaniya, P.S., and Kondapi, A.K. 2017. Topoisomerase II β and its role in different biological contexts. Archives of biochemistry and biophysics **633**: 78-84. doi:10.1016/j.abb.2017.06.021.
- Bouige, A., Darmon, A., Piton, J., Roue, M., Petrella, S., Capton, E., et al. 2013. Mycobacterium tuberculosis DNA gyrase possesses two functional GyrA-boxes. Biochem. J. **455**: 285-294. doi:10.1042/bj20130430.
- Boyes, D.C., Zayed, A.M., Ascenzi, R., McCaskill, A.J., Hoffman, N.E., Davis, K.R., et al. 2001. Growth Stage-Based Phenotypic Analysis of Arabidopsis. A Model for High Throughput Functional Genomics in Plants **13**(7): 1499-1510. doi:10.1105/tpc.010011.
- Bradski, G. 2000. The Open CV Library. Dr Dobb's Journal of Software Tools **120**: 122-125.
- Brady, S.M., Orlando, D.A., Lee, J.-Y., Wang, J.Y., Koch, J., Dinneny, J.R., et al. 2007. A High-Resolution Root Spatiotemporal Map Reveals Dominant Expression Patterns. Science (New York, N.Y.) **318**(5851): 801-806. doi:10.1126/science.1146265.
- Breuer, C., Stacey, N.J., West, C.E., Zhao, Y., Chory, J., Tsukaya, H., et al. 2007. BIN4, a novel component of the plant DNA topoisomerase VI complex, is required for endoreduplication in Arabidopsis. The Plant cell **19**(11): 3655-3668. doi:10.1105/tpc.107.054833.
- Briat, J.F., Gigot, C., Laulhere, J.P., and Mache, R. 1982. Visualization of a Spinach Plastid Transcriptionally Active DNA-Protein Complex in a Highly Condensed Structure. Plant Physiol **69**(5): 1205-1211. doi:10.1104/pp.69.5.1205.
- Broeck, A.V., Lotz, C., Ortiz, J., and Lamour, V. 2019. Cryo-EM structure of the complete E. coli DNA gyrase nucleoprotein complex. Nature Communications **10**(1): 4935. doi:10.1038/s41467-019-12914-y.
- Brown, P.O., and Cozzarelli, N.R. 1979. A sign inversion mechanism for enzymatic supercoiling of DNA. Science (New York, N.Y.) **206**(4422): 1081-1083. Available

- from <http://science.sciencemag.org/content/sci/206/4422/1081.full.pdf> [accessed].
- Brown, P.O., and Cozzarelli, N.R. 1981. Catenation and knotting of duplex DNA by type 1 topoisomerases: a mechanistic parallel with type 2 topoisomerases. *Proc Natl Acad Sci U S A* **78**(2): 843-847.
- Brown, P.O., Peebles, C.L., and Cozzarelli, N.R. 1979. A topoisomerase from *Escherichia coli* related to DNA gyrase. *Proc Natl Acad Sci U S A* **76**(12): 6110-6114. Available from <https://www.ncbi.nlm.nih.gov/pmc/articles/PMC411812/pdf/pnas00012-0094.pdf> [accessed].
- Bush, N., Evans-Roberts, K., and Maxwell, A. 2015. DNA Topoisomerases. *EcoSal Plus*. doi:doi:10.1128/ecosalplus.ESP-0010-2014.
- Cambau, E., Matrat, S., Pan, X.S., Roth Dit Bettoni, R., Corbel, C., Aubry, A., et al. 2009. Target specificity of the new fluoroquinolone besifloxacin in *Streptococcus pneumoniae*, *Staphylococcus aureus* and *Escherichia coli*. *J Antimicrob Chemother* **63**(3): 443-450. doi:10.1093/jac/dkn528.
- Capranico, G., Tinelli, S., Austin, C.A., Fisher, M.L., and Zunino, F. 1992. Different patterns of gene expression of topoisomerase II isoforms in differentiated tissues during murine development. *Biochimica et biophysica acta* **1132**(1): 43-48.
- Carucci, D.J., Gardner, M.J., Tettelin, H., Cummings, L.M., Smith, H.O., Adams, M.D., et al. 1998. The Malaria Genome Sequencing Project. *Expert Reviews in Molecular Medicine* **1**(3): 1-9. doi:10.1017/S146239949800012X.
- Casson, S., Spencer, M., Walker, K., and Lindsey, K. 2005. Laser capture microdissection for the analysis of gene expression during embryogenesis of *Arabidopsis*. *Plant J* **42**(1): 111-123. doi:10.1111/j.1365-313X.2005.02355.x.
- Chalapareddy, S., Chakrabarty, S., Bhattacharyya, M.K., and Bhattacharyya, S. 2016. Radicol-Mediated Inhibition of Topoisomerase VIB-VIA Activity of the Human Malaria Parasite *Plasmodium falciparum*. *mSphere* **1**(1). doi:10.1128/mSphere.00025-15.
- Champoux, J.J. 1981. DNA IS LINKED TO THE RAT-LIVER DNA NICKING-CLOSING ENZYME BY A PHOSPHODIESTER BOND TO TYROSINE. *J. Biol. Chem.* **256**(10): 4805-4809. Available from <Go to ISI>://WOS:A1981LR96000024 [accessed].
- Champoux, J.J., and Dulbecco, R. 1972. An activity from mammalian cells that untwists superhelical DNA--a possible swivel for DNA replication (polyoma-ethidium bromide-mouse-embryo cells-dye binding assay). *Proc Natl Acad Sci U S A*

69(1): 143-146. Available from
<https://www.ncbi.nlm.nih.gov/pmc/articles/PMC427563/>
<https://www.ncbi.nlm.nih.gov/pmc/articles/PMC427563/pdf/pnas00127-0149.pdf>
[accessed].

Changela, A., DiGate, R.J., and Mondragón, A. 2001. Crystal structure of a complex of a type IA DNA topoisomerase with a single-stranded DNA molecule. *Nature* **411**(6841): 1077-1081. doi:10.1038/35082615.

Chatterji, M., Unniraman, S., Maxwell, A., and Nagaraja, V. 2000. The additional 165 amino acids in the B protein of *Escherichia coli* DNA gyrase have an important role in DNA binding. *The Journal of biological chemistry* **275**(30): 22888-22894. doi:10.1074/jbc.M001047200.

Chavalitsheewinkoon-Petmitr, P., Worasing, R., and Wilairat, P. 2001. Partial purification of mitochondrial DNA topoisomerase II from *Plasmodium falciparum* and its sensitivity to inhibitors. *Southeast Asian J Trop Med Public Health* **32**(4): 733-738.

Cheesman, S., McAleese, S., Goman, M., Johnson, D., Horrocks, P., Ridley, R.G., et al. 1994. The gene encoding topoisomerase II from *Plasmodium falciparum*. *Nucleic Acids Res* **22**(13): 2547-2551. doi:10.1093/nar/22.13.2547.

Chen, D., Shao, Q., Yin, L., Younis, A., and Zheng, B. 2019. Polyamine Function in Plants: Metabolism, Regulation on Development, and Roles in Abiotic Stress Responses. *Frontiers in Plant Science* **9**(1945). doi:10.3389/fpls.2018.01945.

Chen, J., Rauch, C.A., White, J.H., Englund, P.T., and Cozzarelli, N.R. 1995. The topology of the kinetoplast DNA network. *Cell* **80**(1): 61-69.

Cheng, B., Zhu, C.X., Ji, C., Ahumada, A., and Tse-Dinh, Y.C. 2003. Direct interaction between *Escherichia coli* RNA polymerase and the zinc ribbon domains of DNA topoisomerase I. *The Journal of biological chemistry* **278**(33): 30705-30710. doi:10.1074/jbc.M303403200.

Cheng, C.H., Kussie, P., Pavletich, N., and Shuman, S. 1998. Conservation of structure and mechanism between eukaryotic topoisomerase I and site-specific recombinases. *Cell* **92**(6): 841-850. doi:10.1016/s0092-8674(00)81411-7.

Cheng, X., Guinn, Emily J., Buechel, E., Wong, R., Sengupta, R., Shkel, Irina A., et al. 2016. Basis of Protein Stabilization by K Glutamate: Unfavorable Interactions with Carbon, Oxygen Groups. *Biophysical journal* **111**(9): 1854-1865. doi:10.1016/j.bpj.2016.08.050.

Cho, H.S., Lee, S.S., Kim, K.D., Hwang, I., Lim, J.S., Park, Y.I., et al. 2004. DNA gyrase is involved in chloroplast nucleoid partitioning. *The Plant cell* **16**(10): 2665-2682. doi:10.1105/tpc.104.024281.

- Christensen, A.C., Lyznik, A., Mohammed, S., Elowsky, C.G., Elo, A., Yule, R., et al. 2005. Dual-Domain, Dual-Targeting Organellar Protein Presequences in *Arabidopsis* Can Use Non-AUG Start Codons. *The Plant cell* **17**(10): 2805-2816. doi:10.1105/tpc.105.035287.
- Clarke, J.L., Sodeinde, O., and Mason, P.J. 2003. A unique insertion in *Plasmodium berghei* glucose-6-phosphate dehydrogenase-6-phosphogluconolactonase: evolutionary and functional studies. *Mol Biochem Parasitol* **127**(1): 1-8. doi:10.1016/s0166-6851(02)00298-0.
- Classen, S., Olland, S., and Berger, J.M. 2003. Structure of the topoisomerase II ATPase region and its mechanism of inhibition by the chemotherapeutic agent ICRF-187. *Proc Natl Acad Sci U S A* **100**(19): 10629-10634. doi:10.1073/pnas.1832879100.
- Collin, F., Karkare, S., and Maxwell, A. 2011. Exploiting bacterial DNA gyrase as a drug target: current state and perspectives. *Appl Microbiol Biotechnol* **92**(3): 479-497. doi:10.1007/s00253-011-3557-z.
- Corbett, K.D., and Berger, J.M. 2003. Structure of the topoisomerase VI-B subunit: implications for type II topoisomerase mechanism and evolution. *Embo j* **22**(1): 151-163. doi:10.1093/emboj/cdg008.
- Corbett, K.D., Benedetti, P., and Berger, J.M. 2007. Holoenzyme assembly and ATP-mediated conformational dynamics of topoisomerase VI. *Nature structural & molecular biology* **14**(7): 611-619. doi:10.1038/nsmb1264.
- Corbett, K.D., Schoeffler, A.J., Thomsen, N.D., and Berger, J.M. 2005. The structural basis for substrate specificity in DNA topoisomerase IV. *J Mol Biol* **351**(3): 545-561. doi:10.1016/j.jmb.2005.06.029.
- Costenaro, L., Grossmann, J.G., Ebel, C., and Maxwell, A. 2007. Modular structure of the full-length DNA gyrase B subunit revealed by small-angle X-ray scattering. *Structure* **15**(3): 329-339. doi:10.1016/j.str.2007.01.013.
- Crisona, N.J., Strick, T.R., Bensimon, D., Croquette, V., and Cozzarelli, N.R. 2000. Preferential relaxation of positively supercoiled DNA by *E. coli* topoisomerase IV in single-molecule and ensemble measurements. *Genes & development* **14**(22): 2881-2892. Available from <https://www.ncbi.nlm.nih.gov/pmc/articles/PMC317058/pdf/X2.pdf> [accessed].
- Dahl, E.L., and Rosenthal, P.J. 2007. Multiple antibiotics exert delayed effects against the *Plasmodium falciparum* apicoplast. *Antimicrobial Agents and Chemotherapy* **51**(10): 3485-3490. doi:10.1128/aac.00527-07.

- Daniell, H., Lin, C.-S., Yu, M., and Chang, W.-J. 2016. Chloroplast genomes: diversity, evolution, and applications in genetic engineering. *Genome Biology* **17**(1): 134. doi:10.1186/s13059-016-1004-2.
- Dar, A., Prusty, D., Mondal, N., and Dhar, S.K. 2009. A unique 45-amino-acid region in the toprim domain of *Plasmodium falciparum* gyrase B is essential for its activity. *Eukaryot Cell* **8**(11): 1759-1769. doi:10.1128/ec.00149-09.
- Dar, M.A., Sharma, A., Mondal, N., and Dhar, S.K. 2007. Molecular cloning of apicoplast-targeted *Plasmodium falciparum* DNA gyrase genes: Unique intrinsic ATPase activity and ATP-independent dimerization of PfGyrB subunit. *Eukaryot. Cell* **6**(3): 398-412. doi:10.1128/ec.00357-06.
- Davagnino, J., Herrero, M., Furlong, D., Moreno, F., and Kolter, R. 1986. The DNA replication inhibitor microcin B17 is a forty-three-amino-acid protein containing sixty percent glycine. *Proteins* **1**(3): 230-238. doi:10.1002/prot.340010305.
- Davies, A.H. 1994. Current methods for manipulating baculoviruses. *Biotechnology (N Y)* **12**(1): 47-50. doi:10.1038/nbt0194-47.
- De Smet, I., Tetsumura, T., De Rybel, B., Frei dit Frey, N., Laplaze, L., Casimiro, I., et al. 2007. Auxin-dependent regulation of lateral root positioning in the basal meristem of *Arabidopsis*. *Development* **134**(4): 681-690. doi:10.1242/dev.02753.
- Dean, F.B., and Cozzarelli, N.R. 1985. Mechanism of strand passage by *Escherichia coli* topoisomerase-I - the role of the required nick in catenation and knotting of duplex DNA. *J. Biol. Chem.* **260**(8): 4984-4994. Available from <Go to ISI>://WOS:A1985AGT9900070
<http://www.jbc.org/content/260/8/4984.full.pdf> [accessed].
- Déclais, A.C., de La Tour, C.B., and Duguet, M. 2001. Reverse gyrases from bacteria and archaea. *Methods Enzymol* **334**: 146-162. doi:10.1016/s0076-6879(01)34464-6.
- Deibler, R.W., Rahmati, S., and Zechiedrich, E.L. 2001. Topoisomerase IV, alone, unknots DNA in *E. coli*. *Genes & development* **15**(6): 748-761. doi:10.1101/gad.872301.
- Dereuddre, S., Delaporte, C., and Jacquemin-Sablon, A. 1997. Role of Topoisomerase II β in the Resistance of 9-OH-ellipticine-resistant Chinese Hamster Fibroblasts to Topoisomerase II Inhibitors. *Cancer Research* **57**(19): 4301-4308. Available from <https://cancerres.aacrjournals.org/content/canres/57/19/4301.full.pdf> [accessed].

- Deweese, J.E., and Osheroﬀ, N. 2010. The use of divalent metal ions by type II topoisomerases. *Metallomics* **2**(7): 450-459. doi:10.1039/c003759a.
- DiGate, R.J., and Mariani, K.J. 1989. Molecular cloning and DNA sequence analysis of *Escherichia coli* topB, the gene encoding topoisomerase III. *The Journal of biological chemistry* **264**(30): 17924-17930.
- Dimitrov, I., and Tax, F.E. 2018. Lateral root growth in *Arabidopsis* is controlled by short and long distance signaling through the LRR RLKs XIP1/CEPR1 and CEPR2. *Plant Signal Behav* **13**(6): e1489667-e1489667. doi:10.1080/15592324.2018.1489667.
- DiNardo, S., Voelkel, K., and Sternglanz, R. 1984. DNA topoisomerase II mutant of *Saccharomyces cerevisiae*: topoisomerase II is required for segregation of daughter molecules at the termination of DNA replication. *Proc Natl Acad Sci U S A* **81**(9): 2616-2620. Available from <https://www.ncbi.nlm.nih.gov/pmc/articles/PMC345120/pdf/pnas00610-0023.pdf> [accessed].
- DiNardo, S., Voelkel, K.A., Sternglanz, R., Reynolds, A.E., and Wright, A. 1982. *Escherichia coli* DNA topoisomerase I mutants have compensatory mutations in DNA gyrase genes. *Cell* **31**(1): 43-51. doi:10.1016/0092-8674(82)90403-2.
- Dobrogojski, J., Adamiec, M., and Luciński, R. 2020. The chloroplast genome: a review. *Acta Physiologiae Plantarum* **42**(6): 98. doi:10.1007/s11738-020-03089-x.
- Donaldson, L. 2020. Autofluorescence in Plants. *Molecules* **25**(10). doi:10.3390/molecules25102393.
- Donnelly, P.M., Bonetta, D., Tsukaya, H., Dengler, R.E., and Dengler, N.G. 1999. Cell cycling and cell enlargement in developing leaves of *Arabidopsis*. *Dev Biol* **215**(2): 407-419. doi:10.1006/dbio.1999.9443.
- Dorman, C.J., and Dorman, M.J. 2016. DNA supercoiling is a fundamental regulatory principle in the control of bacterial gene expression. *Biophys Rev* **8**(Suppl 1): 89-100. doi:10.1007/s12551-016-0238-2.
- Dorn, A., Röhrig, S., Papp, K., Schröpfer, S., Hartung, F., Knoll, A., et al. 2018. The topoisomerase 3 α zinc-finger domain T1 of *Arabidopsis thaliana* is required for targeting the enzyme activity to Holliday junction-like DNA repair intermediates. *PLoS Genet* **14**(9): e1007674. doi:10.1371/journal.pgen.1007674.
- Doyle, S.M., Diamond, M., and McCabe, P.F. 2010. Chloroplast and reactive oxygen species involvement in apoptotic-like programmed cell death in *Arabidopsis* suspension cultures. *J Exp Bot* **61**(2): 473-482. doi:10.1093/jxb/erp320.

- Drake, F.H., Hofmann, G.A., Bartus, H.F., Mattern, M.R., Crooke, S.T., and Mirabelli, C.K. 1989. Biochemical and pharmacological properties of p170 and p180 forms of topoisomerase II. *Biochemistry* **28**(20): 8154-8160.
- Drlica, K. 1992. Control of bacterial DNA supercoiling. *Mol. Microbiol.* **6**(4): 425-433. doi:<https://doi.org/10.1111/j.1365-2958.1992.tb01486.x>.
- Drlica, K., Malik, M., Kerns, R.J., and Zhao, X. 2008. Quinolone-Mediated Bacterial Death. *Antimicrobial Agents and Chemotherapy* **52**(2): 385-392. doi:10.1128/aac.01617-06.
- Dubrovsky, J.G., Gambetta, G.A., Hernández-Barrera, A., Shishkova, S., and González, I. 2006. Lateral Root Initiation in Arabidopsis: Developmental Window, Spatial Patterning, Density and Predictability. *Annals of Botany* **97**(5): 903-915. doi:10.1093/aob/mcj604.
- Dubrovsky, J.G., Napsucialy-Mendivil, S., Duclercq, J., Cheng, Y., Shishkova, S., Ivanchenko, M.G., et al. 2011. Auxin minimum defines a developmental window for lateral root initiation. *New Phytologist* **191**(4): 970-983. doi:<https://doi.org/10.1111/j.1469-8137.2011.03757.x>.
- Duprey, A., and Groisman, E.A. 2020. DNA supercoiling differences in bacteria result from disparate DNA gyrase activation by polyamines. *PLoS Genet* **16**(10): e1009085. doi:10.1371/journal.pgen.1009085.
- Dutta, R., and Inouye, M. 2000. GHKL, an emergent ATPase/kinase superfamily. *Trends in biochemical sciences* **25**(1): 24-28. Available from http://ac.els-cdn.com/S0968000499015030/1-s2.0-S0968000499015030-main.pdf?tid=ed790078-0744-11e7-bcd2-0000aab0f6c&acdnat=1489338008_b032a86e3297e6cedc1d82402cec379d [accessed].
- Echeverria, M., Martin, M.T., Ricard, B., and Litvak, S. 1986. A DNA topoisomerase type I from wheat embryo mitochondria. *Plant molecular biology* **6**(6): 417-427. doi:10.1007/bf00027134.
- Edwards, M.J., Flatman, R.H., Mitchenall, L.A., Stevenson, C.E., Le, T.B., Clarke, T.A., et al. 2009. A crystal structure of the bifunctional antibiotic simocyclinone D8, bound to DNA gyrase. *Science (New York, N.Y.)* **326**(5958): 1415-1418. doi:10.1126/science.1179123.
- Errampalli, D., Patton, D., Castle, L., Mickelson, L., Hansen, K., Schnall, J., et al. 1991. Embryonic Lethals and T-DNA Insertional Mutagenesis in Arabidopsis. *The Plant cell* **3**(2): 149-157. doi:10.1105/tpc.3.2.149.
- Evans-Roberts, K.M. DNA gyrase of *Arabidopsis thaliana*. Biological Chemistry University of East Anglia

- Evans-Roberts, K.M. DNA Gyrase of *Arabidopsis thaliana* Biological Chemistry John Innes Centre
- Evans-Roberts, K.M., Breuer, C., Wall, M.K., Sugimoto-Shirasu, K., and Maxwell, A. 2010. *Arabidopsis thaliana* GYRB3 Does Not Encode a DNA Gyrase Subunit. *PLoS One* **5**(3): 7. doi:10.1371/journal.pone.0009899.
- Evans-Roberts, K.M., Mitchenall, L.A., Wall, M.K., Leroux, J., Mylne, J.S., and Maxwell, A. 2016. DNA Gyrase Is the Target for the Quinolone Drug Ciprofloxacin in *Arabidopsis thaliana*. *J. Biol. Chem.* **291**(7): 3136-3144. doi:10.1074/jbc.M115.689554.
- Fichera, M.E., and Roos, D.S. 1997. A plastid organelle as a drug target in apicomplexan parasites. *Nature* **390**(6658): 407-409. Available from <http://dx.doi.org/10.1038/37132>
<http://www.nature.com/nature/journal/v390/n6658/pdf/390407a0.pdf> [accessed.
- Flatman, R.H., Howells, A.J., Heide, L., Fiedler, H.P., and Maxwell, A. 2005. Simocyclinone D8, an inhibitor of DNA gyrase with a novel mode of action. *Antimicrobial Agents and Chemotherapy* **49**(3): 1093-1100. doi:10.1128/aac.49.3.1093-1100.2005.
- Fleige, T., and Soldati-Favre, D. 2008. Targeting the transcriptional and translational machinery of the endosymbiotic organelle in apicomplexans. *Current drug targets* **9**(11): 948-956.
- Forterre, P. 2002. A hot story from comparative genomics: reverse gyrase is the only hyperthermophile-specific protein. *Trends Genet* **18**(5): 236-237. doi:10.1016/s0168-9525(02)02650-1.
- Forterre, P., Gribaldo, S., Gabelle, D., and Serre, M.C. 2007. Origin and evolution of DNA topoisomerases. *Biochimie* **89**(4): 427-446. doi:10.1016/j.biochi.2006.12.009.
- Forterre, P., Mirambeau, G., Jaxel, C., Nadal, M., and Duguet, M. 1985. High positive supercoiling in vitro catalyzed by an ATP and polyethylene glycol-stimulated topoisomerase from *Sulfolobus acidocaldarius*. *Embo j* **4**(8): 2123-2128.
- Foth, B.J., Ralph, S.A., Tonkin, C.J., Struck, N.S., Fraunholz, M., Roos, D.S., et al. 2003. Dissecting apicoplast targeting in the malaria parasite *Plasmodium falciparum*. *Science (New York, N.Y.)* **299**(5607): 705-708. doi:10.1126/science.1078599.
- Franke-Fayard, B., Fonager, J., Braks, A., Khan, S.M., and Janse, C.J. 2010. Sequestration and tissue accumulation of human malaria parasites: can we learn anything from rodent models of malaria? *PLoS pathogens* **6**(9): e1001032. doi:10.1371/journal.ppat.1001032.

- Frohlich, R.F., Veigaard, C., Andersen, F.F., McClendon, A.K., Gentry, A.C., Andersen, A.H., et al. 2007. Tryptophane-205 of human topoisomerase I is essential for camptothecin inhibition of negative but not positive supercoil removal. *Nucleic Acids Res* **35**(18): 6170-6180. doi:10.1093/nar/gkm669.
- Frugier, M., Bour, T., Ayach, M., Santos, M.A., Rudinger-Thirion, J., Théobald-Dietrich, A., et al. 2010. Low Complexity Regions behave as tRNA sponges to help co-translational folding of plasmodial proteins. *FEBS Lett* **584**(2): 448-454. doi:10.1016/j.febslet.2009.11.004.
- Gadelle, D., Filee, J., Buhler, C., and Forterre, P. 2003. Phylogenomics of type II DNA topoisomerases. *BioEssays : news and reviews in molecular, cellular and developmental biology* **25**(3): 232-242. doi:10.1002/bies.10245.
- Gadelle, D., Krupovic, M., Raymann, K., Mayer, C., and Forterre, P. 2014. DNA topoisomerase VIII: a novel subfamily of type IIB topoisomerases encoded by free or integrated plasmids in Archaea and Bacteria. *Nucleic Acids Res* **42**(13): 8578-8591. doi:10.1093/nar/gku568.
- Gajiwala, K.S., and Burley, S.K. 2000. Winged helix proteins. *Current opinion in structural biology* **10**(1): 110-116. Available from http://ac.els-cdn.com/S0959440X99000573/1-s2.0-S0959440X99000573-main.pdf?tid=e6b883d2-0747-11e7-9399-00000aab0f6c&acdnat=1489339285_a463745371af45ab21a2388eee4587b8 [accessed].
- Galm, U., Schimana, J., Fiedler, H.P., Schmidt, J., Li, S.M., and Heide, L. 2002. Cloning and analysis of the simocyclinone biosynthetic gene cluster of *Streptomyces antibioticus* Tu 6040. *Archives of microbiology* **178**(2): 102-114. doi:10.1007/s00203-002-0429-z.
- Gardner, M.J., Hall, N., Fung, E., White, O., Berriman, M., Hyman, R.W., et al. 2002a. Genome sequence of the human malaria parasite *Plasmodium falciparum*. *Nature* **419**(6906): 498-511. doi:http://www.nature.com/nature/journal/v419/n6906/suppinfo/nature01097_S1.html.
- Gardner, M.J., Hall, N., Fung, E., White, O., Berriman, M., Hyman, R.W., et al. 2002b. Genome sequence of the human malaria parasite *Plasmodium falciparum*. *Nature* **419**(6906): 498-511. doi:10.1038/nature01097.
- Gellert, M., Fisher, L.M., and O'Dea, M.H. 1979. DNA gyrase: purification and catalytic properties of a fragment of gyrase B protein. *Proc Natl Acad Sci U S A* **76**(12): 6289-6293. Available from <https://www.ncbi.nlm.nih.gov/pmc/articles/PMC411849/pdf/pnas00012-0273.pdf> [accessed].

- Gellert, M., Mizuuchi, K., O'Dea, M.H., and Nash, H.A. 1976. DNA gyrase: an enzyme that introduces superhelical turns into DNA. *Proc Natl Acad Sci U S A* **73**(11): 3872-3876. Available from <https://www.ncbi.nlm.nih.gov/pmc/articles/PMC431247/pdf/pnas00041-0094.pdf> [accessed].
- Gellert, M., Mizuuchi, K., O'Dea, M.H., Itoh, T., and Tomizawa, J.I. 1977. Nalidixic acid resistance: a second genetic character involved in DNA gyrase activity. *Proc Natl Acad Sci U S A* **74**(11): 4772-4776. Available from <https://www.ncbi.nlm.nih.gov/pmc/articles/PMC432037/pdf/pnas00033-0072.pdf> [accessed].
- Gelvin, S.B. 2003. Agrobacterium-mediated plant transformation: the biology behind the "gene-jockeying" tool. *Microbiology and molecular biology reviews : MMBR* **67**(1): 16-37, table of contents. doi:10.1128/membr.67.1.16-37.2003.
- Germe, T., Voros, J., Jeannot, F., Taillier, T., Stavenger, R.A., Bacque, E., et al. 2018a. A new class of antibacterials, the imidazopyrazinones, reveal structural transitions involved in DNA gyrase poisoning and mechanisms of resistance. *Nucleic Acids Res* **46**(8): 4114-4128. doi:10.1093/nar/gky181.
- Germe, T., Vörös, J., Jeannot, F., Taillier, T., Stavenger, R.A., Bacqué, E., et al. 2018b. A new class of antibacterials, the imidazopyrazinones, reveal structural transitions involved in DNA gyrase poisoning and mechanisms of resistance. *Nucleic Acids Res.* **46**(8): 4114-4128. doi:10.1093/nar/gky181.
- Ghilarov, D., Stevenson, C.E.M., Travin, D.Y., Piskunova, J., Serebryakova, M., Maxwell, A., et al. 2019. Architecture of Microcin B17 Synthetase: An Octameric Protein Complex Converting a Ribosomally Synthesized Peptide into a DNA Gyrase Poison. *Mol. Cell.* **73**(4): 749-762.e745. doi:<https://doi.org/10.1016/j.molcel.2018.11.032>.
- Gilbert, E.J., and Maxwell, A. 1994. The 24 kDa N-terminal sub-domain of the DNA gyrase B protein binds coumarin drugs. *Mol Microbiol* **12**(3): 365-373. Available from <http://onlinelibrary.wiley.com/store/10.1111/j.1365-2958.1994.tb01026.x/asset/j.1365-2958.1994.tb01026.x.pdf?v=1&t=j0y8r46m&s=dcebd9634ead95b10f07b02d6e93e6c1805b9804> [accessed].
- Gohlke, C. 2019. *czifile* 2019.7.2.
- Gohlke, C. 2021. *tiffifile* 2021.3.5. Available from <https://pypi.org/project/tiffifile/>.
- Grelon, M., Vezon, D., Gendrot, G., and Pelletier, G. 2001. AtSPO11-1 is necessary for efficient meiotic recombination in plants. *Embo j* **20**(3): 589-600. doi:10.1093/emboj/20.3.589.

- Gubaev, A., and Klostermeier, D. 2011. DNA-induced narrowing of the gyrase N-gate coordinates T-segment capture and strand passage. *Proceedings of the National Academy of Sciences* **108**(34): 14085-14090. doi:10.1073/pnas.1102100108.
- Gubaev, A., Weidlich, D., and Klostermeier, D. 2016. DNA gyrase with a single catalytic tyrosine can catalyze DNA supercoiling by a nicking-closing mechanism. *Nucleic Acids Res.* **44**(21): 10354-10366. doi:10.1093/nar/gkw740.
- Gwatkin, R.B.L. 1995. *Baculovirus expression systems & biopesticides*, ed by M.L. Shuler et al., Wiley-Liss, 259 pp, \$85. *Molecular Reproduction and Development* **41**(4): 530-530. doi:<https://doi.org/10.1002/mrd.1080410421>.
- Haase, S., Sciocco-Cap, A., and Romanowski, V. 2015. Baculovirus insecticides in Latin America: historical overview, current status and future perspectives. *Viruses* **7**(5): 2230-2267. doi:10.3390/v7052230.
- Hamperl, S., and Cimprich, K.A. 2014. The contribution of co-transcriptional RNA:DNA hybrid structures to DNA damage and genome instability. *DNA Repair (Amst)* **19**: 84-94. doi:10.1016/j.dnarep.2014.03.023.
- Hansmann, P., Falk, H., Ronai, K., and Sitte, P. 1985. Structure, composition, and distribution of plastid nucleoids in *Narcissus pseudonarcissus*. *Planta* **164**(4): 459-472. doi:10.1007/BF00395961.
- Hanson, M.R. 2015. Reactive oxygen species signal chloroplasts to extend themselves. *Proceedings of the National Academy of Sciences* **112**(32): 9799-9800. doi:10.1073/pnas.1512645112.
- Hartung, F., and Puchta, H. 2000. Molecular characterisation of two paralogous SPO11 homologues in *Arabidopsis thaliana*. *Nucleic Acids Res* **28**(7): 1548-1554. doi:10.1093/nar/28.7.1548.
- Hartung, F., Angelis, K.J., Meister, A., Schubert, I., Melzer, M., and Puchta, H. 2002. An archaeobacterial topoisomerase homolog not present in other eukaryotes is indispensable for cell proliferation of plants. *Current biology : CB* **12**(20): 1787-1791. doi:10.1016/s0960-9822(02)01218-6.
- Heard, W., Sklenář, J., Tomé, D.F., Robatzek, S., and Jones, A.M. 2015. Identification of Regulatory and Cargo Proteins of Endosomal and Secretory Pathways in *Arabidopsis thaliana* by Proteomic Dissection. *Mol Cell Proteomics* **14**(7): 1796-1813. doi:10.1074/mcp.M115.050286.
- Hearnshaw, S.J., Chung, T.T., Stevenson, C.E., Maxwell, A., and Lawson, D.M. 2015. The role of monovalent cations in the ATPase reaction of DNA gyrase. *Acta*

Crystallogr D Biol Crystallogr **71**(Pt 4): 996-1005.
doi:10.1107/s1399004715002916.

Heazlewood, J.L., Tonti-Filippini, J.S., Gout, A.M., Day, D.A., Whelan, J., and Millar, A.H. 2004. Experimental analysis of the Arabidopsis mitochondrial proteome highlights signaling and regulatory components, provides assessment of targeting prediction programs, and indicates plant-specific mitochondrial proteins. *The Plant cell* **16**(1): 241-256. doi:10.1105/tpc.016055.

Heddle, J.G., Mittelheiser, S., Maxwell, A., and Thomson, N.H. 2004. Nucleotide binding to DNA gyrase causes loss of DNA wrap. *J Mol Biol* **337**(3): 597-610. doi:10.1016/j.jmb.2004.01.049.

Herrero, M., and Moreno, F. 1986. Microcin B17 blocks DNA replication and induces the SOS system in Escherichia coli. *Journal of general microbiology* **132**(2): 393-402. doi:10.1099/00221287-132-2-393.

Hiasa, H., Shea, M.E., Richardson, C.M., and Gwynn, M.N. 2003. Staphylococcus aureus gyrase-quinolone-DNA ternary complexes fail to arrest replication fork progression in vitro. Effects of salt on the DNA binding mode and the catalytic activity of S. aureus gyrase. *The Journal of biological chemistry* **278**(10): 8861-8868. doi:10.1074/jbc.M209207200.

Higgins, N.P., Peebles, C.L., Sugino, A., and Cozzarelli, N.R. 1978. Purification of subunits of Escherichia coli DNA gyrase and reconstitution of enzymatic activity. *Proc Natl Acad Sci U S A* **75**(4): 1773-1777. Available from <https://www.ncbi.nlm.nih.gov/pmc/articles/PMC392422/pdf/pnas00016-0171.pdf> [accessed].

Hofmann, F., Schon, M.A., and Nodine, M.D. 2019. The embryonic transcriptome of Arabidopsis thaliana. *Plant Reproduction* **32**(1): 77-91. doi:10.1007/s00497-018-00357-2.

Holmes, V.F., and Cozzarelli, N.R. 2000. Closing the ring: links between SMC proteins and chromosome partitioning, condensation, and supercoiling. *Proc Natl Acad Sci U S A* **97**(4): 1322-1324. doi:10.1073/pnas.040576797.

Holzenkämpfer, M., Walker, M., Zeeck, A., Schimana, J., and Fiedler, H.P. 2002. Simocyclinones, novel cytostatic angucyclinone antibiotics produced by Streptomyces antibioticus Tu 6040 II. Structure elucidation and biosynthesis. *The Journal of antibiotics* **55**(3): 301-307.

Hooper, C.M., Castleden, I.R., Tanz, S.K., Aryamanesh, N., and Millar, A.H. 2017. SUBA4: the interactive data analysis centre for Arabidopsis subcellular protein locations. *Nucleic Acids Res* **45**(D1): D1064-d1074. doi:10.1093/nar/gkw1041.

- Hooper, D.C., and Jacoby, G.A. 2015. Mechanisms of drug resistance: quinolone resistance. *Annals of the New York Academy of Sciences* **1354**(1): 12-31. doi:10.1111/nyas.12830.
- Horowitz, D.S., and Wang, J.C. 1987. Mapping the active site tyrosine of *Escherichia coli* DNA gyrase. *The Journal of biological chemistry* **262**(11): 5339-5344. Available from <http://www.jbc.org/content/262/11/5339.full.pdf> [accessed].
- Howe, C.J. 1992. Plastid origin of an extrachromosomal DNA molecule from *Plasmodium*, the causative agent of Malaria. *Journal of Theoretical Biology* **158**(2): 199-205. doi:[https://doi.org/10.1016/S0022-5193\(05\)80718-0](https://doi.org/10.1016/S0022-5193(05)80718-0).
- Hsieh, T., and Brutlag, D. 1980. ATP-dependent DNA topoisomerase from *D. melanogaster* reversibly catenates duplex DNA rings. *Cell* **21**(1): 115-125.
- Hu, Z.-y., Zhan, G.-m., Wang, H.-z., and Hua, W. 2012. A Simple Method for Isolating Chloroplast DNA and Mitochondria DNA from the Same Rapeseed Green Leaf Tissue. *Journal of Integrative Agriculture* **11**(7): 1212-1215. doi:[https://doi.org/10.1016/S2095-3119\(12\)60117-8](https://doi.org/10.1016/S2095-3119(12)60117-8).
- Hunter, J.D. 2007. Matplotlib: A 2D graphics environment. *Computing in science & engineering*.
- Igarashi, K., and Kashiwagi, K. 2015. Modulation of protein synthesis by polyamines. *IUBMB Life* **67**(3): 160-169. doi:<https://doi.org/10.1002/iub.1363>.
- Initiative, T.A.G. 2000. Analysis of the genome sequence of the flowering plant *Arabidopsis thaliana*. *Nature* **408**(6814): 796-815. doi:10.1038/35048692.
- Iorio, C., Vialard, J.E., McCracken, S., Lagacé, M., and Richardson, C.D. 1998. The late expression factors 8 and 9 and possibly the phosphoprotein p78/83 of *Autographa californica* multicapsid nucleopolyhedrovirus are components of the virus-induced RNA polymerase. *Intervirology* **41**(1): 35-46. doi:10.1159/000024913.
- Itoh, R., Takahashi, H., Toda, K., Kuroiwa, H., and Kuroiwa, T. 1997. DNA gyrase involvement in chloroplast-nucleoid division in *Cyanidioschyzon merolae*. *European journal of cell biology* **73**(3): 252-258.
- Kalve, S., De Vos, D., and Beemster, G.T. 2014. Leaf development: a cellular perspective. *Front Plant Sci* **5**: 362. doi:10.3389/fpls.2014.00362.
- Kampranis, S.C., and Maxwell, A. 1996. Conversion of DNA gyrase into a conventional type II topoisomerase. *Proceedings of the National Academy of Sciences* **93**(25): 14416-14421. Available from <http://www.pnas.org/content/93/25/14416.abstract> [accessed].

- Kampranis, S.C., and Maxwell, A. 1998. Conformational Changes in DNA Gyrase Revealed by Limited Proteolysis. *J. Biol. Chem.* **273**(35): 22606-22614. doi:10.1074/jbc.273.35.22606.
- Kampranis, S.C., Bates, A.D., and Maxwell, A. 1999. A model for the mechanism of strand passage by DNA gyrase. *Proc Natl Acad Sci U S A* **96**(15): 8414-8419. Available from <https://www.ncbi.nlm.nih.gov/pmc/articles/PMC17530/pdf/pq008414.pdf> [accessed].
- Karkare, S., Yousafzai, F., Mitchenall, L.A., and Maxwell, A. 2012. The role of Ca²⁺(+) in the activity of Mycobacterium tuberculosis DNA gyrase. *Nucleic Acids Res* **40**(19): 9774-9787. doi:10.1093/nar/gks704.
- Kataoka, K., Mizushima, T., Ogata, Y., Miki, T., and Sekimizu, K. 1996. Heat Shock-induced DNA Relaxation *in Vitro* by DNA Gyrase of *Escherichia coli* in the Presence of ATP *. *J. Biol. Chem.* **271**(40): 24806-24810. doi:10.1074/jbc.271.40.24806.
- Kato, J., Suzuki, H., and Ikeda, H. 1992. Purification and characterization of DNA topoisomerase IV in *Escherichia coli*. *The Journal of biological chemistry* **267**(36): 25676-25684.
- Kato, J., Nishimura, Y., Imamura, R., Niki, H., Hiraga, S., and Suzuki, H. 1990. New topoisomerase essential for chromosome segregation in *E. coli*. *Cell* **63**(2): 393-404.
- Keeney, S., Giroux, C.N., and Kleckner, N. 1997. Meiosis-specific DNA double-strand breaks are catalyzed by Spo11, a member of a widely conserved protein family. *Cell* **88**(3): 375-384. Available from http://ac.els-cdn.com/S0092867400818760/1-s2.0-S0092867400818760-main.pdf?_tid=f1a02fa2-0c10-11e7-917a-00000aacb360&acdnat=1489865437_13d9a09a777fde65775ba10ff5e0ec85 [accessed].
- Khan, T., Sankhe, K., Suvarna, V., Sherje, A., Patel, K., and Dravyakar, B. 2018. DNA gyrase inhibitors: Progress and synthesis of potent compounds as antibacterial agents. *Biomed. Pharmacother.* **103**: 923-938. doi:<https://doi.org/10.1016/j.biopha.2018.04.021>.
- Khoo, H.E., Azlan, A., Tang, S.T., and Lim, S.M. 2017. Anthocyanidins and anthocyanins: colored pigments as food, pharmaceutical ingredients, and the potential health benefits. *Food Nutr Res* **61**(1): 1361779. doi:10.1080/16546628.2017.1361779.
- Khor, V., Yowell, C., Dame, J.B., and Rowe, T.C. 2005. Expression and characterization of the ATP-binding domain of a malarial *Plasmodium vivax* gene homologous

- to the B-subunit of the bacterial topoisomerase DNA gyrase. *Mol. Biochem. Parasitol.* **140**(1): 107-117. doi:10.1016/j.molbiopara.2004.12.013.
- Kim, Y.C., Lee, J., and Koo, H.S. 2000. Functional characterization of *Caenorhabditis elegans* DNA topoisomerase III α . *Nucleic Acids Res* **28**(9): 2012-2017. doi:10.1093/nar/28.9.2012.
- Kishima, Y., Mikami, T., Harada, T., Shinozaki, K., Sugiura, M., and Kinoshita, T. 1986. Restriction fragment map of sugar beet (*Beta vulgaris* L.) chloroplast DNA. *Plant molecular biology* **7**(3): 201-205. doi:10.1007/bf00021331.
- Kitts, P.A., and Possee, R.D. 1993. A method for producing recombinant baculovirus expression vectors at high frequency. *Biotechniques* **14**(5): 810-817.
- Klepekova, A.V., Kasianov, A.S., Gerasimov, E.S., Logacheva, M.D., and Penin, A.A. 2016. A high resolution map of the *Arabidopsis thaliana* developmental transcriptome based on RNA-seq profiling. *Plant J* **88**(6): 1058-1070. doi:10.1111/tpj.13312.
- Kobayashi, K., Baba, S., Obayashi, T., Sato, M., Toyooka, K., Keränen, M., et al. 2012. Regulation of Root Greening by Light and Auxin/Cytokinin Signaling in *Arabidopsis*. *The Plant cell* **24**(3): 1081-1095. doi:10.1105/tpc.111.092254.
- Kohler, S., Delwiche, C.F., Denny, P.W., Tilney, L.G., Webster, P., Wilson, R.J., et al. 1997. A plastid of probable green algal origin in Apicomplexan parasites. *Science (New York, N.Y.)* **275**(5305): 1485-1489. Available from <http://science.sciencemag.org/content/sci/275/5305/1485.full.pdf> [accessed].
- Kolodner, R., and Tewari, K.K. 1972. Molecular size and conformation of chloroplast deoxyribonucleic acid from pea leaves. *The Journal of biological chemistry* **247**(19): 6355-6364. Available from <https://www.jbc.org/content/247/19/6355.full.pdf> [accessed].
- Koster, D.A., Croquette, V., Dekker, C., Shuman, S., and Dekker, N.H. 2005. Friction and torque govern the relaxation of DNA supercoils by eukaryotic topoisomerase IB. *Nature* **434**(7033): 671-674. doi:10.1038/nature03395.
- Kramlinger, V.M., and Hiasa, H. 2006. The "GyrA-box" Is Required for the Ability of DNA Gyrase to Wrap DNA and Catalyze the Supercoiling Reaction. *J. Biol. Chem.* **281**(6): 3738-3742. doi:10.1074/jbc.M511160200.
- Kreuzer, K.N., and Cozzarelli, N.R. 1980. Formation and resolution of DNA catenanes by DNA gyrase. *Cell* **20**(1): 245-254.
- Kristoffersen, E.L., Givskov, A., Jørgensen, L.A., Jensen, P.W., JA, W.B., Osheroff, N., et al. 2017. Interlinked DNA nano-circles for measuring topoisomerase II activity

- at the level of single decatenation events. *Nucleic Acids Res* **45**(13): 7855-7869. doi:10.1093/nar/gkx480.
- Krogh, B.O., and Shuman, S. 2002. A poxvirus-like type IB topoisomerase family in bacteria. *Proc Natl Acad Sci U S A* **99**(4): 1853-1858. doi:10.1073/pnas.032613199.
- Krupinska, K., Melonek, J., and Krause, K. 2013. New insights into plastid nucleoid structure and functionality. *Planta* **237**(3): 653-664. doi:10.1007/s00425-012-1817-5.
- Kümmel, D., Müller, J.J., Roske, Y., Henke, N., and Heinemann, U. 2006. Structure of the Bet3–Tpc6B Core of TRAPP: Two Tpc6 Paralogs Form Trimeric Complexes with Bet3 and Mum2. *J. Mol. Biol.* **361**(1): 22-32. doi:<https://doi.org/10.1016/j.jmb.2006.06.012>.
- Kümmel, D., Müller, J.J., Roske, Y., Misselwitz, R., Büssow, K., and Heinemann, U. 2005. The structure of the TRAPP subunit TPC6 suggests a model for a TRAPP subcomplex. *EMBO reports* **6**(8): 787-793. doi:10.1038/sj.embor.7400463.
- Kwan, K.Y., Greenwald, R.J., Mohanty, S., Sharpe, A.H., Shaw, A.C., and Wang, J.C. 2007. Development of autoimmunity in mice lacking DNA topoisomerase 3beta. *Proc Natl Acad Sci U S A* **104**(22): 9242-9247. doi:10.1073/pnas.0703587104.
- Lam, E., and Chua, N.-H. 1987. Chloroplast DNA gyrase and in vitro regulation of transcription by template topology and novobiocin. *Plant molecular biology* **8**(5): 415-424. doi:10.1007/BF00015819.
- Lang, B.F., and Burger, G. 2007. Purification of mitochondrial and plastid DNA. *Nat Protoc* **2**(3): 652-660. doi:10.1038/nprot.2007.58.
- Lanz, M.A., and Klostermeier, D. 2011. Guiding strand passage: DNA-induced movement of the gyrase C-terminal domains defines an early step in the supercoiling cycle. *Nucleic Acids Res* **39**(22): 9681-9694. doi:10.1093/nar/gkr680.
- Laponogov, I., Veselkov, D.A., Crevel, I.M., Pan, X.S., Fisher, L.M., and Sanderson, M.R. 2013. Structure of an 'open' clamp type II topoisomerase-DNA complex provides a mechanism for DNA capture and transport. *Nucleic Acids Res* **41**(21): 9911-9923. doi:10.1093/nar/gkt749.
- Laponogov, I., Sohi, M.K., Veselkov, D.A., Pan, X.S., Sawhney, R., Thompson, A.W., et al. 2009. Structural insight into the quinolone-DNA cleavage complex of type IIA topoisomerases. *Nature structural & molecular biology* **16**(6): 667-669. doi:10.1038/nsmb.1604.

- Laskowski, M., and Ten Tusscher, K.H. 2017. Periodic Lateral Root Priming: What Makes It Tick? *The Plant cell* **29**(3): 432-444. doi:10.1105/tpc.16.00638.
- Lassota, P., Singh, G., and Kramer, R. 1996. Mechanism of topoisomerase II inhibition by staurosporine and other protein kinase inhibitors. *The Journal of biological chemistry* **271**(42): 26418-26423. doi:10.1074/jbc.271.42.26418.
- Leirimo, S., Harrison, C., Cayley, D.S., Burgess, R.R., and Record, M.T. 1987. Replacement of potassium chloride by potassium glutamate dramatically enhances protein-DNA interactions in vitro. *Biochemistry* **26**(8): 2095-2101. doi:10.1021/bi00382a006.
- Lepage, É., Zampini, É., and Brisson, N. 2013. Plastid genome instability leads to reactive oxygen species production and plastid-to-nucleus retrograde signaling in *Arabidopsis*. *Plant Physiol* **163**(2): 867-881. doi:10.1104/pp.113.223560.
- Levine, C., Hiasa, H., and Mariani, K.J. 1998. DNA gyrase and topoisomerase IV: biochemical activities, physiological roles during chromosome replication, and drug sensitivities. *Biochimica et biophysica acta* **1400**(1-3): 29-43. Available from http://ac.els-cdn.com/S0167478198001262/1-s2.0-S0167478198001262-main.pdf?tid=731d7b8a-0c01-11e7-a444-00000aacb35d&acdnat=1489858782_5acc8cf701ec323da43dddec1759f8dd [accessed].
- Levine, N.D. 1988. Progress in taxonomy of the Apicomplexan protozoa. *The Journal of protozoology* **35**(4): 518-520. Available from <http://onlinelibrary.wiley.com/doi/10.1111/j.1550-7408.1988.tb04141.x/abstract> [accessed].
- Lewis, R.J., Singh, O.M., Smith, C.V., Skarzynski, T., Maxwell, A., Wonacott, A.J., et al. 1996. The nature of inhibition of DNA gyrase by the coumarins and the cyclothialidines revealed by X-ray crystallography. *Embo j* **15**(6): 1412-1420. Available from <https://www.ncbi.nlm.nih.gov/pmc/articles/PMC450046/pdf/emboj00006-0212.pdf> [accessed].
- Li, J., Ou-Lee, T.M., Raba, R., Amundson, R.G., and Last, R.L. 1993. *Arabidopsis* Flavonoid Mutants Are Hypersensitive to UV-B Irradiation. *The Plant cell* **5**(2): 171-179. doi:10.1105/tpc.5.2.171.
- Li, W., and Wang, J.C. 1998. Mammalian DNA topoisomerase III α is essential in early embryogenesis. *Proc Natl Acad Sci U S A* **95**(3): 1010-1013. doi:10.1073/pnas.95.3.1010.
- Lim, L., and McFadden, G.I. 2010. The evolution, metabolism and functions of the apicoplast. *Philosophical Transactions of the Royal Society B: Biological Sciences* **365**(1541): 749-763. doi:10.1098/rstb.2009.0273.

- Lima, C.D., Wang, J.C., and Mondragon, A. 1994. Three-dimensional structure of the 67K N-terminal fragment of E. coli DNA topoisomerase I. *Nature* **367**(6459): 138-146. doi:10.1038/367138a0.
- Lin, T.Y., Nagano, S., and Gardiner Heddle, J. 2015. Functional Analyses of the *Toxoplasma gondii* DNA Gyrase Holoenzyme: A Janus Topoisomerase with Supercoiling and Decatenation Abilities. *Scientific reports* **5**: 14491. doi:10.1038/srep14491.
- Ling, Q., Huang, W., Baldwin, A., and Jarvis, P. 2012. Chloroplast Biogenesis Is Regulated by Direct Action of the Ubiquitin-Proteasome System. *Science (New York, N.Y.)* **338**(6107): 655-659. doi:10.1126/science.1225053.
- Liu, D., Gong, Q., Ma, Y., Li, P., Li, J., Yang, S., et al. 2010. cpSecA, a thylakoid protein translocase subunit, is essential for photosynthetic development in *Arabidopsis*. *J Exp Bot* **61**(6): 1655-1669. doi:10.1093/jxb/erq033.
- Liu, L.F., and Wang, J.C. 1987. Supercoiling of the DNA template during transcription. *Proc Natl Acad Sci U S A* **84**(20): 7024-7027.
- Liu, L.F., Liu, C.C., and Alberts, B.M. 1980. Type II DNA topoisomerases: enzymes that can unknot a topologically knotted DNA molecule via a reversible double-strand break. *Cell* **19**(3): 697-707.
- Lo, Y.-S., Hsiao, L.-J., Cheng, N., Litvinchuk, A., and Dai, H. 2011. Characterization of the structure and DNA complexity of mung bean mitochondrial nucleoids. *Molecules and Cells* **31**(3): 217-224. doi:10.1007/s10059-011-0036-4.
- Lobet, G., Pagès, L., and Draye, X. 2011. A Novel Image-Analysis Toolbox Enabling Quantitative Analysis of Root System Architecture. *Plant Physiology* **157**(1): 29-39. doi:10.1104/pp.111.179895.
- Lundh, F. 1999. An introduction to tkinter. Available from [www pythonware com/library/tkinter/introduction/index htm](http://www.pythonware.com/library/tkinter/introduction/index.htm). 1999.
- Madabhushi, R. 2018. The Roles of DNA Topoisomerase II β in Transcription. *Int J Mol Sci* **19**(7). doi:10.3390/ijms19071917.
- Makarevitch, I., and Somers, D.A. 2005. Purification and characterization of topoisomerase IIA from *Arabidopsis thaliana*. *Plant Sci.* **168**(4): 1023-1033. doi:<https://doi.org/10.1016/j.plantsci.2004.11.019>.
- Makarevitch, I., and Somers, D.A. 2006. Association of *Arabidopsis* topoisomerase IIA cleavage sites with functional genomic elements and T-DNA loci. *The Plant Journal* **48**(5): 697-709. doi:<https://doi.org/10.1111/j.1365-313X.2006.02915.x>.

- Malamy, J.E., and Benfey, P.N. 1997. Down and out in Arabidopsis: the formation of lateral roots. *Trends Plant Sci.* **2**(10): 390-396. doi:[https://doi.org/10.1016/S1360-1385\(97\)90054-6](https://doi.org/10.1016/S1360-1385(97)90054-6).
- Malik, S.B., Ramesh, M.A., Hulstrand, A.M., and Logsdon, J.M., Jr. 2007. Protist homologs of the meiotic Spo11 gene and topoisomerase VI reveal an evolutionary history of gene duplication and lineage-specific loss. *Molecular biology and evolution* **24**(12): 2827-2841. doi:10.1093/molbev/msm217.
- Manjunatha, U.H., Dalal, M., Chatterji, M., Radha, D.R., Visweswariah, S.S., and Nagaraja, V. 2002. Functional characterisation of mycobacterial DNA gyrase: an efficient decatenase. *Nucleic Acids Res* **30**(10): 2144-2153. doi:10.1093/nar/30.10.2144.
- Manning, J.E., Wolstenholme, D.R., Ryan, R.S., Hunter, J.A., and Richards, O.C. 1971a. Circular Chloroplast DNA from *Euglena gracilis*. *Proceedings of the National Academy of Sciences* **68**(6): 1169-1173. doi:10.1073/pnas.68.6.1169.
- Manning, J.E., Wolstenholme, D.R., Ryan, R.S., Hunter, J.A., and Richards, O.C. 1971b. Circular Chloroplast DNA from *Euglena gracilis*. *Proceedings of the National Academy of Sciences* **68**(6): 1169. doi:10.1073/pnas.68.6.1169.
- Marians, K.J. 1987a. DNA gyrase-catalyzed decatenation of multiply linked DNA dimers. *J. Biol. Chem.* **21**: 10362-10368.
- Marians, K.J. 1987b. DNA gyrase-catalyzed decatenation of multiply linked DNA dimers. *The Journal of biological chemistry* **262**(21): 10362-10368. Available from <http://www.jbc.org/content/262/21/10362.full.pdf> [accessed].
- Marienfeld, J., Unseld, M., and Brennicke, A. 1999. The mitochondrial genome of *Arabidopsis* is composed of both native and immigrant information. *Trends Plant Sci.* **4**(12): 495-502. doi:10.1016/S1360-1385(99)01502-2.
- Martin, W., Rujan, T., Richly, E., Hansen, A., Cornelsen, S., Lins, T., et al. 2002. Evolutionary analysis of *Arabidopsis*, cyanobacterial, and chloroplast genomes reveals plastid phylogeny and thousands of cyanobacterial genes in the nucleus. *Proceedings of the National Academy of Sciences* **99**(19): 12246-12251. doi:10.1073/pnas.182432999.
- Martinez-Garcia, M., Schubert, V., Osman, K., Darbyshire, A., Sanchez-Moran, E., and Franklin, F.C.H. 2018. TOP2 and chromosome movement help remove interlocks between entangled chromosomes during meiosis. *Journal of Cell Biology* **217**(12): 4070-4079. doi:10.1083/jcb.201803019.

- Massé, E., and Drolet, M. 1999. Relaxation of transcription-induced negative supercoiling is an essential function of Escherichia coli DNA topoisomerase I. *The Journal of biological chemistry* **274**(23): 16654-16658. doi:10.1074/jbc.274.23.16654.
- Mattila, H., Valev, D., Havurinne, V., Khorobrykh, S., Virtanen, O., Antinluoma, M., et al. 2018. Degradation of chlorophyll and synthesis of flavonols during autumn senescence—the story told by individual leaves. *AoB PLANTS* **10**(3). doi:10.1093/aobpla/ply028.
- Maxwell, A. 1997. DNA gyrase as a drug target. *Trends in microbiology* **5**(3): 102-109. doi:10.1016/s0966-842x(96)10085-8.
- Maxwell, A., Burton, N.P., and O'Hagan, N. 2006. High-throughput assays for DNA gyrase and other topoisomerases. *Nucleic Acids Res* **34**(15): e104. Available from http://www.ncbi.nlm.nih.gov/entrez/query.fcgi?cmd=Retrieve&db=PubMed&dopt=Citation&list_uids=16936317 [accessed].
- McClendon, A.K., Rodriguez, A.C., and Osheroff, N. 2005. Human topoisomerase IIalpha rapidly relaxes positively supercoiled DNA: implications for enzyme action ahead of replication forks. *The Journal of biological chemistry* **280**(47): 39337-39345. doi:10.1074/jbc.M503320200.
- McClendon, A.K., Gentry, A.C., Dickey, J.S., Brinch, M., Bendsen, S., Andersen, A.H., et al. 2008. Bimodal recognition of DNA geometry by human topoisomerase II alpha: preferential relaxation of positively supercoiled DNA requires elements in the C-terminal domain. *Biochemistry* **47**(50): 13169-13178. doi:10.1021/bi800453h.
- McIlwraith, M.J., Boocock, M.R., and Stark, W.M. 1997. Tn3 resolvase catalyses multiple recombination events without intermediate rejoining of DNA ends. *J Mol Biol* **266**(1): 108-121. doi:10.1006/jmbi.1996.0765.
- McKinney, W., and Others. 2010. Data structures for statistical computing in python. *In* *Proceedings of the 9th Python in Science Conference*. pp. 51-56.
- Mehlin, C., Boni, E., Buckner, F.S., Engel, L., Feist, T., Gelb, M.H., et al. 2006. Heterologous expression of proteins from Plasmodium falciparum: results from 1000 genes. *Mol Biochem Parasitol* **148**(2): 144-160. doi:10.1016/j.molbiopara.2006.03.011.
- Meinke, D.W. 1995. Molecular Genetics of Plant Embryogenesis. *Annual Review of Plant Physiology and Plant Molecular Biology* **46**(1): 369-394. doi:10.1146/annurev.pp.46.060195.002101.

- Meinke, D.W. 2020. Genome-wide identification of EMBRYO-DEFECTIVE (EMB) genes required for growth and development in Arabidopsis. *New Phytol* **226**(2): 306-325. doi:10.1111/nph.16071.
- Meinke, D.W., and Sussex, I.M. 1979. Embryo-lethal mutants of Arabidopsis thaliana. A model system for genetic analysis of plant embryo development. *Dev Biol* **72**(1): 50-61. doi:10.1016/0012-1606(79)90097-6.
- Melonek, J., Oetke, S., and Krupinska, K. 2016a. Multifunctionality of plastid nucleoids as revealed by proteome analyses. *Biochimica et biophysica acta* **1864**(8): 1016-1038. doi:10.1016/j.bbapap.2016.03.009.
- Melonek, J., Oetke, S., and Krupinska, K. 2016b. Multifunctionality of plastid nucleoids as revealed by proteome analyses. *Biochimica et Biophysica Acta (BBA) - Proteins and Proteomics* **1864**(8): 1016-1038. doi:<https://doi.org/10.1016/j.bbapap.2016.03.009>.
- Mills, W.R., Reeves, M., Fowler, D.L., and Capo, S.F. 1989. DNA Synthesis in Chloroplasts: III. THE DNA GYRASE INHIBITORS NALIDIXIC ACID AND NOVOBIOCIN INHIBIT BOTH THYMIDINE INCORPORATION INTO DNA AND PHOTOSYNTHETIC OXYGEN EVOLUTION BY ISOLATED CHLOROPLASTS. *Journal of Experimental Botany* **40**(213): 425-429. Available from <http://www.jstor.org/stable/23692236> [accessed 2020/12/14/].
- Mizuuchi, K., O'Dea, M.H., and Gellert, M. 1978. DNA gyrase: subunit structure and ATPase activity of the purified enzyme. *Proc Natl Acad Sci U S A* **75**(12): 5960-5963. Available from <https://www.ncbi.nlm.nih.gov/pmc/articles/PMC393096/pdf/pnas00022-0224.pdf> [accessed].
- Mizuuchi, K., Fisher, L.M., O'Dea, M.H., and Gellert, M. 1980. DNA gyrase action involves the introduction of transient double-strand breaks into DNA. *Proc Natl Acad Sci U S A* **77**(4): 1847-1851. Available from <https://www.ncbi.nlm.nih.gov/pmc/articles/PMC348605/pdf/pnas00667-0161.pdf> [accessed].
- Mohanty, S., Town, T., Yagi, T., Scheidig, C., Kwan, K.Y., Allore, H.G., et al. 2008. Defective p53 engagement after the induction of DNA damage in cells deficient in topoisomerase 3beta. *Proc Natl Acad Sci U S A* **105**(13): 5063-5068. doi:10.1073/pnas.0801235105.
- Mondragón, A., and DiGate, R. 1999. The structure of *Escherichia coli* DNA topoisomerase III. *Structure* **7**(11): 1373-1383. doi:10.1016/S0969-2126(00)80027-1.

- Morais Cabral, J.H., Jackson, A.P., Smith, C.V., Shikotra, N., Maxwell, A., and Liddington, R.C. 1997. Crystal structure of the breakage-reunion domain of DNA gyrase. *Nature* **388**(6645): 903-906. doi:10.1038/42294.
- Morley, S.A., and Nielsen, B.L. 2016. Chloroplast DNA Copy Number Changes during Plant Development in Organelle DNA Polymerase Mutants. *Frontiers in Plant Science* **7**(57). doi:10.3389/fpls.2016.00057.
- Morley, S.A., and Nielsen, B.L. 2017. Plant mitochondrial DNA. *Front Biosci (Landmark Ed)* **22**: 1023-1032. doi:10.2741/4531.
- Morley, S.A., Ahmad, N., and Nielsen, B.L. 2019. Plant Organelle Genome Replication. *Plants (Basel)* **8**(10): 358. doi:10.3390/plants8100358.
- Morrison, A., and Cozzarelli, N.R. 1979. Site-specific cleavage of DNA by *E. coli* DNA gyrase. *Cell* **17**(1): 175-184.
- Moustaka, J., Panteris, E., Adamakis, I.-D.S., Tanou, G., Giannakoula, A., Eleftheriou, E.P., et al. 2018. High anthocyanin accumulation in poinsettia leaves is accompanied by thylakoid membrane unstacking, acting as a photoprotective mechanism, to prevent ROS formation. *Environmental and Experimental Botany* **154**: 44-55. doi:<https://doi.org/10.1016/j.envexpbot.2018.01.006>.
- Mudeppa, D.G., Kumar, S., Kokkonda, S., White, J., and Rathod, P.K. 2015. Topoisomerase II from Human Malaria Parasites: EXPRESSION, PURIFICATION, AND SELECTIVE INHIBITION. *The Journal of biological chemistry* **290**(33): 20313-20324. doi:10.1074/jbc.M115.639039.
- Mudgil, Y., Singh, B.N., Upadhyaya, K.C., Sopory, S.K., and Reddy, M.K. 2002. Cloning and characterization of a cell cycle-regulated gene encoding topoisomerase I from *Nicotiana tabacum* that is inducible by light, low temperature and abscisic acid. *Molecular genetics and genomics : MGG* **267**(3): 380-390. doi:10.1007/s00438-002-0669-2.
- Muralidharan, V., and Goldberg, D.E. 2013. Asparagine repeats in *Plasmodium falciparum* proteins: good for nothing? *PLoS pathogens* **9**(8): e1003488. doi:10.1371/journal.ppat.1003488.
- Nagano, S., Lin, T.Y., Edula, J.R., and Heddle, J.G. 2014. Unique features of apicoplast DNA gyrases from *Toxoplasma gondii* and *Plasmodium falciparum*. *BMC Bioinformatics* **15**(1). doi:10.1186/s12859-014-0416-9.
- Nagano, S., Seki, E., Lin, T.Y., Shirouzu, M., Yokoyama, S., and Heddle, J.G. 2015. Investigating the Roles of the C-Terminal Domain of *Plasmodium falciparum* GyrA. *PLoS One* **10**(11). doi:10.1371/journal.pone.0142313.

- Nakata, M.T., Sato, M., Wakazaki, M., Sato, N., Kojima, K., Sekine, A., et al. 2018. Plastid translation is essential for lateral root stem cell patterning in *Arabidopsis thaliana*. *Biol Open* **7**(2): bio028175. doi:10.1242/bio.028175.
- Negruk, V.I., Eisner, G.I., Redichkina, T.D., Dumanskaya, N.N., Cherny, D.I., Alexandrov, A.A., et al. 1986. Diversity of *Vicia faba* circular mtDNA in whole plants and suspension cultures. *Theoretical and Applied Genetics* **72**(4): 541-547. doi:10.1007/BF00289538.
- Neuman, K.C., Charvin, G., Bensimon, D., and Croquette, V. 2009. Mechanisms of chiral discrimination by topoisomerase IV. *Proceedings of the National Academy of Sciences* **106**(17): 6986-6991. doi:10.1073/pnas.0900574106.
- Newbold, C.I. 1999. Antigenic variation in *Plasmodium falciparum*: mechanisms and consequences. *Curr Opin Microbiol* **2**(4): 420-425. doi:10.1016/s1369-5274(99)80074-5.
- Nichols, M.D., DeAngelis, K., Keck, J.L., and Berger, J.M. 1999. Structure and function of an archaeal topoisomerase VI subunit with homology to the meiotic recombination factor Spo11. *Embo j* **18**(21): 6177-6188. doi:10.1093/emboj/18.21.6177.
- Nitiss, J.L., Soans, E., Rogojina, A., Seth, A., and Mishina, M. 2012. Topoisomerase assays. *Current protocols in pharmacology / editorial board, S.J. Enna* **Chapter 3**: Unit 3 3. doi:10.1002/0471141755.ph0303s57.
- Noble, C.G., and Maxwell, A. 2002. The role of GyrB in the DNA cleavage-religation reaction of DNA gyrase: a proposed two metal-ion mechanism. *J Mol Biol* **318**(2): 361-371. doi:10.1016/s0022-2836(02)00049-9.
- Nollmann, M., Byron, O., and Stark, W.M. 2005. Behavior of Tn3 resolvase in solution and its interaction with res. *Biophysical journal* **89**(3): 1920-1931. doi:10.1529/biophysj.104.058164.
- Norris, F.W. 1929. Die methodik der fermente. By C. Oppenheimer and L. Pincussen. Part IV. Pp. 945–1264 Part V. Pp. xxx + 1265–1578. Leipzig: G. Thieme. 1928. 28 rm. each part. *Journal of the Society of Chemical Industry* **48**(18): 448-449. doi:<https://doi.org/10.1002/jctb.5000481812>.
- O'Malley, R.C., and Ecker, J.R. 2010. Linking genotype to phenotype using the *Arabidopsis* unimutant collection. *The Plant Journal* **61**(6): 928-940. doi:<https://doi.org/10.1111/j.1365-313X.2010.04119.x>.
- Oborník, M., Janouskovec, J., Chrudimský, T., and Lukes, J. 2009. Evolution of the apicoplast and its hosts: from heterotrophy to autotrophy and back again. *International journal for parasitology* **39**(1): 1-12. doi:10.1016/j.ijpara.2008.07.010.

- Oda, K., Yamato, K., Ohta, E., Nakamura, Y., Takemura, M., Nozato, N., et al. 1992. Gene organization deduced from the complete sequence of liverwort *Marchantia polymorpha* mitochondrial DNA: A primitive form of plant mitochondrial genome. *J. Mol. Biol.* **223**(1): 1-7. doi:[https://doi.org/10.1016/0022-2836\(92\)90708-R](https://doi.org/10.1016/0022-2836(92)90708-R).
- Oldenburg, D.J., and Bendich, A.J. 2004a. Most chloroplast DNA of maize seedlings in linear molecules with defined ends and branched forms. *J Mol Biol* **335**(4): 953-970. doi:10.1016/j.jmb.2003.11.020.
- Oldenburg, D.J., and Bendich, A.J. 2004b. Most Chloroplast DNA of Maize Seedlings in Linear Molecules with Defined Ends and Branched Forms. *J. Mol. Biol.* **335**(4): 953-970. doi:<https://doi.org/10.1016/j.jmb.2003.11.020>.
- Oliphant, T.E. 2006. A guide to NumPy Trelgol Publishing USA.
- Olorunniji, F.J., He, J., Wenwieser, S.V.C.T., Boocock, M.R., and Stark, W.M. 2008. Synapsis and catalysis by activated Tn3 resolvase mutants. *Nucleic Acids Res.* **36**(22): 7181-7191. doi:10.1093/nar/gkn885.
- Ono, Y., Sakai, A., Takechi, K., Takio, S., Takusagawa, M., and Takano, H. 2007. NtPoll-like1 and NtPoll-like2, Bacterial DNA Polymerase I Homologs Isolated from BY-2 Cultured Tobacco Cells, Encode DNA Polymerases Engaged in DNA Replication in Both Plastids and Mitochondria. *Plant and Cell Physiology* **48**(12): 1679-1692. doi:10.1093/pcp/pcm140.
- Orphanides, G., and Maxwell, A. 1994. Evidence for a conformational change in the DNA gyrase-DNA complex from hydroxyl radical footprinting. *Nucleic Acids Res* **22**(9): 1567-1575. Available from <https://www.ncbi.nlm.nih.gov/pmc/articles/PMC308031/pdf/nar00033-0065.pdf> [accessed].
- Palmer, J.D., and Stein, D.B. 1986. Conservation of chloroplast genome structure among vascular plants. *Current genetics* **10**(11): 823-833. doi:10.1007/BF00418529.
- Papillon, J., Menetret, J.F., Batisse, C., Helye, R., Schultz, P., Potier, N., et al. 2013. Structural insight into negative DNA supercoiling by DNA gyrase, a bacterial type 2A DNA topoisomerase. *Nucleic Acids Res* **41**(16): 7815-7827. doi:10.1093/nar/gkt560.
- Paterson, M., and Kennedy, J.F. 1998. Protein Engineering - Principles and Practice; J.L. Cleland & C.S. Craik. *Bioseparation* **7**(6): 347-347. doi:10.1023/A:1008086215812.

- Pelosse, M., Crocker, H., Gorda, B., Lemaire, P., Rauch, J., and Berger, I. 2017. MultiBac: from protein complex structures to synthetic viral nanosystems. *BMC Biology* **15**(1): 99. doi:10.1186/s12915-017-0447-6.
- Peng, H., and Marians, K.J. 1993. Escherichia coli topoisomerase IV. Purification, characterization, subunit structure, and subunit interactions. *The Journal of biological chemistry* **268**(32): 24481-24490.
- Pérez Di Giorgio, J.A., Lepage, É., Tremblay-Belzile, S., Truche, S., Loubert-Hudon, A., and Brisson, N. 2019. Transcription is a major driving force for plastid genome instability in Arabidopsis. *PLoS One* **14**(4): e0214552. doi:10.1371/journal.pone.0214552.
- Perez-Cheeks, B.A., Lee, C., Hayama, R., and Marians, K.J. 2012. A role for topoisomerase III in Escherichia coli chromosome segregation. *Mol. Microbiol.* **86**(4): 1007-1022. doi:<https://doi.org/10.1111/mmi.12039>.
- Peyret, H., Brown, J.K.M., and Lomonosoff, G.P. 2019. Improving plant transient expression through the rational design of synthetic 5' and 3' untranslated regions. *Plant Methods* **15**(1): 108. doi:10.1186/s13007-019-0494-9.
- Pfalz, J., Liere, K., Kandlbinder, A., Dietz, K.-J., and Oelmüller, R. 2006. pTAC2, -6, and -12 Are Components of the Transcriptionally Active Plastid Chromosome That Are Required for Plastid Gene Expression. *The Plant cell* **18**(1): 176-197. doi:10.1105/tpc.105.036392.
- Pham, D.Q., Hice, R.H., Sivasubramanian, N., and Federici, B.A. 1993. The 1629-bp open reading frame of the Autographa californica multinucleocapsid nuclear polyhedrosis virus encodes a virion structural protein. *Gene* **137**(2): 275-280. doi:10.1016/0378-1119(93)90020-4.
- Philpott, M., Gould, K.S., Lim, C., and Ferguson, L.R. 2004. In situ and in vitro antioxidant activity of sweetpotato anthocyanins. *J Agric Food Chem* **52**(6): 1511-1513. doi:10.1021/jf034593j.
- Phinney, B.S., and Thelen, J.J. 2005. Proteomic Characterization of A Triton-Insoluble Fraction from Chloroplasts Defines A Novel Group of Proteins Associated with Macromolecular Structures. *Journal of Proteome Research* **4**(2): 497-506. doi:10.1021/pr049791k.
- Pierrat, O.A., and Maxwell, A. 2003. The Action of the Bacterial Toxin Microcin B17: INSIGHT INTO THE CLEAVAGE-RELIGATION REACTION OF DNA GYRASE. *J. Biol. Chem.* **278**(37): 35016-35023. doi:10.1074/jbc.M304516200.
- Plank, J.L., Chu, S.H., Pohlhaus, J.R., Wilson-Sali, T., and Hsieh, T.S. 2005. Drosophila melanogaster topoisomerase IIIalpha preferentially relaxes a positively or negatively supercoiled bubble substrate and is essential during development.

The Journal of biological chemistry **280**(5): 3564-3573.
doi:10.1074/jbc.M411337200.

Pommier, Y. 2013. Drugging topoisomerases: lessons and challenges. *ACS chemical biology* **8**(1): 82-95. doi:10.1021/cb300648v.

Pommier, Y., Leo, E., Zhang, H., and Marchand, C. 2010. DNA topoisomerases and their poisoning by anticancer and antibacterial drugs. *Chem Biol* **17**(5): 421-433. doi:10.1016/j.chembiol.2010.04.012.

Raghu Ram, E.V.S., Kumar, A., Biswas, S., Kumar, A., Chaubey, S., Siddiqi, M.I., et al. 2007. Nuclear gyrB encodes a functional subunit of the Plasmodium falciparum gyrase that is involved in apicoplast DNA replication. *Mol. Biochem. Parasitol.* **154**(1): 30-39. doi:<https://doi.org/10.1016/j.molbiopara.2007.04.001>.

Rajan, R., Taneja, B., and Mondragón, A. 2010. Structures of minimal catalytic fragments of topoisomerase V reveals conformational changes relevant for DNA binding. *Structure* **18**(7): 829-838. doi:10.1016/j.str.2010.03.006.

Rajan, R., Prasad, R., Taneja, B., Wilson, S.H., and Mondragón, A. 2013. Identification of one of the apurinic/apyrimidinic lyase active sites of topoisomerase V by structural and functional studies. *Nucleic Acids Res* **41**(1): 657-666. doi:10.1093/nar/gks1017.

Ralph, S.A., van Dooren, G.G., Waller, R.F., Crawford, M.J., Fraunholz, M.J., Foth, B.J., et al. 2004. Tropical infectious diseases: metabolic maps and functions of the Plasmodium falciparum apicoplast. *Nature reviews. Microbiology* **2**(3): 203-216. doi:10.1038/nrmicro843.

Rawdon, E.J., Dorier, J., Racko, D., Millett, K.C., and Stasiak, A. 2016. How topoisomerase IV can efficiently unknot and decatenate negatively supercoiled DNA molecules without causing their torsional relaxation. *Nucleic Acids Res* **44**(10): 4528-4538. doi:10.1093/nar/gkw311.

Raynaud, C., Perennes, C., Reuzeau, C., Catrice, O., Brown, S., and Bergounioux, C. 2005. Cell and plastid division are coordinated through the prereplication factor AtCDT1. *Proc. Natl. Acad. Sci. U. S. A.* **102**(23): 8216-8221. doi:10.1073/pnas.0502564102.

Reddy, M.K., Nair, S., and Tewari, K.K. 1998. Cloning, expression and characterization of a gene which encodes a topoisomerase I with positive supercoiling activity in pea. *Plant molecular biology* **37**(5): 773-784. doi:10.1023/A:1006086311875.

Reddy, M.K., Nair, S., Tewari, K.K., Mudgil, Y., Yadav, B.S., and Sopory, S.K. 1999. Cloning and characterization of a cDNA encoding topoisomerase II in pea and

analysis of its expression in relation to cell proliferation. *Plant molecular biology* **41**(1): 125-137. doi:10.1023/A:1006352820788.

Reddy, M.K., Achary, V.M.M., Singh, B.N., Manna, M., Sheri, V., Panditi, V., et al. 2018. Molecular characterization of pea DNA gyrase-A reveals dual localization of protein in plastid and mitochondria. *Journal of Plant Biochemistry and Biotechnology*. doi:10.1007/s13562-018-0478-2.

Redinbo, M.R., Stewart, L., Kuhn, P., Champoux, J.J., and Hol, W.G.J. 1998. Crystal structures of human topoisomerase I in covalent and noncovalent complexes with DNA. *Science (New York, N.Y.)* **279**(5356): 1504-1513. doi:10.1126/science.279.5356.1504.

Reece, R.J., and Maxwell, A. 1989. Tryptic fragments of the *Escherichia-coli* DNA gyrase A-protein. *J. Biol. Chem.* **264**(33): 19648-19653. Available from <Go to ISI>://WOS:A1989AZ87200027
<http://www.jbc.org/content/264/33/19648.full.pdf> [accessed].

Reece, R.J., and Maxwell, A. 1991. The C-terminal domain of the *Escherichia coli* DNA gyrase A subunit is a DNA-binding protein. *Nucleic Acids Res* **19**(7): 1399-1405. Available from
<https://www.ncbi.nlm.nih.gov/pmc/articles/PMC333892/pdf/nar00243-0050.pdf> [accessed].

Reeder, J.C., and Brown, G.V. 1996. Antigenic variation and immune evasion in *Plasmodium falciparum* malaria. *Immunol Cell Biol* **74**(6): 546-554. doi:10.1038/icb.1996.88.

Rhee, H.-K., Park, H.J., Lee, S.K., Lee, C.-O., and Choo, H.-Y.P. 2007. Synthesis, cytotoxicity, and DNA topoisomerase II inhibitory activity of benzofuroquinolinediones. *Bioorganic & Medicinal Chemistry* **15**(4): 1651-1658. doi:<https://doi.org/10.1016/j.bmc.2006.12.012>.

Rich-Griffin, C., Eichmann, R., Reitz, M.U., Hermann, S., Woolley-Allen, K., Brown, P.E., et al. 2020. Regulation of Cell Type-Specific Immunity Networks in Arabidopsis Roots. *The Plant cell* **32**(9): 2742-2762. doi:10.1105/tpc.20.00154.

Richter, S.N., Frasson, I., Palumbo, M., Sissi, C., and Palu, G. 2010. Simocyclinone D8 turns on against Gram-negative bacteria in a clinical setting. *Bioorganic & medicinal chemistry letters* **20**(3): 1202-1204. doi:10.1016/j.bmcl.2009.11.135.

Riou, J.F., Gabillot, M., Philippe, M., Schrevel, J., and Riou, G. 1986. Purification and characterization of *Plasmodium berghei* DNA topoisomerases I and II: drug action, inhibition of decatenation and relaxation, and stimulation of DNA cleavage. *Biochemistry* **25**(7): 1471-1479. doi:10.1021/bi00355a001.

- Robertson, D., and Laetsch, W.M. 1974. Structure and Function of Developing Barley Plastids. *Plant Physiology* **54**(2): 148-159. doi:10.1104/pp.54.2.148.
- Roca, J., and Wang, J.C. 1992. The capture of a DNA double helix by an ATP-dependent protein clamp: a key step in DNA transport by type II DNA topoisomerases. *Cell* **71**(5): 833-840.
- Rodríguez, A.C. 2003. Investigating the role of the latch in the positive supercoiling mechanism of reverse gyrase. *Biochemistry* **42**(20): 5993-6004. doi:10.1021/bi034188l.
- Rodríguez, A.C., and Stock, D. 2002. Crystal structure of reverse gyrase: insights into the positive supercoiling of DNA. *Embo j* **21**(3): 418-426. doi:10.1093/emboj/21.3.418.
- Romanowski, A., Schlaen, R.G., Perez-Santangelo, S., Mancini, E., and Yanovsky, M.J. 2020. Global transcriptome analysis reveals circadian control of splicing events in *Arabidopsis thaliana*. *The Plant Journal* **103**(2): 889-902. doi:<https://doi.org/10.1111/tpj.14776>.
- Sakai, A., Takano, H., and Kuroiwa, T. 2004a. Organelle nuclei in higher plants: structure, composition, function, and evolution. *Int Rev Cytol* **238**: 59-118. doi:10.1016/s0074-7696(04)38002-2.
- Sakai, A., Takano, H., and Kuroiwa, T. 2004b. Organelle Nuclei in Higher Plants: Structure, Composition, Function, and Evolution. *In* *International Review of Cytology*. Academic Press. pp. 59-118.
- Sakamoto, T., and Kimura, S. 2018. Plant Temperature Sensors. *Sensors (Basel)* **18**(12). doi:10.3390/s18124365.
- Sander, M., and Hsieh, T. 1983. Double strand DNA cleavage by type II DNA topoisomerase from *Drosophila melanogaster*. *The Journal of biological chemistry* **258**(13): 8421-8428. Available from <http://www.jbc.org/content/258/13/8421.full.pdf> [accessed].
- Sandri, M.I., Hochhauser, D., Ayton, P., Camplejohn, R.C., Whitehouse, R., Turley, H., et al. 1996. Differential expression of the topoisomerase II alpha and beta genes in human breast cancers. *British journal of cancer* **73**(12): 1518-1524. Available from <https://www.ncbi.nlm.nih.gov/pmc/articles/PMC2074549/pdf/brjncancer00040-0068.pdf> [accessed].
- Sato, S. 2011. The apicomplexan plastid and its evolution. *Cell Mol Life Sci* **68**(8): 1285-1296. doi:10.1007/s00018-011-0646-1.

- Sato, S., Nakamura, Y., Kaneko, T., Asamizu, E., and Tabata, S. 1999. Complete structure of the chloroplast genome of *Arabidopsis thaliana*. *DNA Res* **6**(5): 283-290. doi:10.1093/dnares/6.5.283.
- Scharff, L.B., and Koop, H.U. 2006. Linear molecules of tobacco ptDNA end at known replication origins and additional loci. *Plant molecular biology* **62**(4-5): 611-621. doi:10.1007/s11103-006-9042-x.
- Schimana, J., Fiedler, H.P., Groth, I., Sussmuth, R., Beil, W., Walker, M., et al. 2000. Simocyclinones, novel cytostatic angucyclinone antibiotics produced by *Streptomyces antibioticus* Tu 6040. I. Taxonomy, fermentation, isolation and biological activities. *The Journal of antibiotics* **53**(8): 779-787.
- Schimper, A.F.W. 1883. Über die Entwicklung der Chlorophyllkörner und Farbkörper. *Bot Zeit* **41**: 105-112. Available from <https://ci.nii.ac.jp/naid/10016772673/en/> [accessed].
- Schluep, T., and Cooney, C.L. 1998. Purification of plasmids by triplex affinity interaction. *Nucleic Acids Res.* **26**(19): 4524-4528. doi:10.1093/nar/26.19.4524.
- Schmidt, B.H., Osheroff, N., and Berger, J.M. 2012. Structure of a topoisomerase II-DNA-nucleotide complex reveals a new control mechanism for ATPase activity. *Nature structural & molecular biology* **19**(11): 1147-1154. doi:10.1038/nsmb.2388.
- Schmidt, S.B., Eisenhut, M., and Schneider, A. 2020. Chloroplast Transition Metal Regulation for Efficient Photosynthesis. *Trends Plant Sci.* **25**(8): 817-828. doi:10.1016/j.tplants.2020.03.003.
- Schoeffler, A.J., and Berger, J.M. 2008. DNA topoisomerases: harnessing and constraining energy to govern chromosome topology. *Quarterly reviews of biophysics* **41**(1): 41-101. doi:10.1017/s003358350800468x.
- Senkler, J., Senkler, M., Eubel, H., Hildebrandt, T., Lengwenus, C., Schertl, P., et al. 2017. The mitochondrial complexome of *Arabidopsis thaliana*. *Plant J* **89**(6): 1079-1092. doi:10.1111/tpj.13448.
- Shafiq, S., Chen, C., Yang, J., Cheng, L., Ma, F., Widemann, E., et al. 2017. DNA Topoisomerase 1 Prevents R-loop Accumulation to Modulate Auxin-Regulated Root Development in Rice. *Molecular Plant* **10**(6): 821-833. doi:<https://doi.org/10.1016/j.molp.2017.04.001>.
- Shaver, J.M., Oldenburg, D.J., and Bendich, A.J. 2008. The structure of chloroplast DNA molecules and the effects of light on the amount of chloroplast DNA during development in *Medicago truncatula*. *Plant Physiol* **146**(3): 1064-1074. doi:10.1104/pp.107.112946.

- Sheahan, M.B., McCurdy, D.W., and Rose, R.J. 2005. Mitochondria as a connected population: ensuring continuity of the mitochondrial genome during plant cell dedifferentiation through massive mitochondrial fusion. *The Plant Journal* **44**(5): 744-755. doi:<https://doi.org/10.1111/j.1365-3113.2005.02561.x>.
- Shibata, T., Nakasu, S., Yasui, K., and Kikuchi, A. 1987. Intrinsic DNA-dependent ATPase activity of reverse gyrase. *The Journal of biological chemistry* **262**(22): 10419-10421.
- Siedlecki, J., Zimmermann, W., and Weissbach, A. 1983. Characterization of a prokaryotic topoisomerase I activity in chloroplast extracts from spinach. *Nucleic Acids Res* **11**(5): 1523-1536. Available from <https://www.ncbi.nlm.nih.gov/pmc/articles/PMC325812/pdf/nar00350-0311.pdf> [accessed].
- Singh, B.N., Sopory, S.K., and Reddy, M.K. 2004. Plant DNA topoisomerases: Structure, function, and cellular roles in plant development. *Critical Reviews in Plant Sciences* **23**(3): 251-269. doi:10.1080/07352680490452816.
- Singh, B.N., Mudgil, Y., Sopory, S.K., and Reddy, M.K. 2003. Molecular characterization of a nuclear topoisomerase II from *Nicotiana tabacum* that functionally complements a temperature-sensitive topoisomerase II yeast mutant. *Plant molecular biology* **52**(5): 1063-1076. doi:10.1023/a:1025427700337.
- Singh, D., Kumar, A., Raghu Ram, E.V., and Habib, S. 2005. Multiple replication origins within the inverted repeat region of the *Plasmodium falciparum* apicoplast genome are differentially activated. *Mol Biochem Parasitol* **139**(1): 99-106. doi:10.1016/j.molbiopara.2004.09.011.
- Sissi, C., and Palumbo, M. 2009. Effects of magnesium and related divalent metal ions in topoisomerase structure and function. *Nucleic Acids Res.* **37**(3): 702-711. doi:10.1093/nar/gkp024.
- Sissi, C., Marangon, E., Chemello, A., Noble, C.G., Maxwell, A., and Palumbo, M. 2005. The Effects of Metal Ions on the Structure and Stability of the DNA Gyrase B Protein. *J. Mol. Biol.* **353**(5): 1152-1160. doi:<https://doi.org/10.1016/j.jmb.2005.09.043>.
- Skourti-Stathaki, K., and Proudfoot, N.J. 2014. A double-edged sword: R loops as threats to genome integrity and powerful regulators of gene expression. *Genes & development* **28**(13): 1384-1396. doi:10.1101/gad.242990.114.
- Slesarev, A.I., Stetter, K.O., Lake, J.A., Gellert, M., Krah, R., and Kozyavkin, S.A. 1993. DNA topoisomerase V is a relative of eukaryotic topoisomerase I from a hyperthermophilic prokaryote. *Nature* **364**(6439): 735-737. doi:10.1038/364735a0.

- Smith, G.E., Summers, M.D., and Fraser, M.J. 1983. Production of human beta interferon in insect cells infected with a baculovirus expression vector. *Mol Cell Biol* **3**(12): 2156-2165. doi:10.1128/mcb.3.12.2156.
- Stack, C.M., Lowther, J., Cunningham, E., Donnelly, S., Gardiner, D.L., Trenholme, K.R., et al. 2007. Characterization of the Plasmodium falciparum M17 leucyl aminopeptidase. A protease involved in amino acid regulation with potential for antimalarial drug development. *The Journal of biological chemistry* **282**(3): 2069-2080. doi:10.1074/jbc.M609251200.
- Staehelein, L.A. 2003. Chloroplast structure: from chlorophyll granules to supra-molecular architecture of thylakoid membranes. *Photosynth Res* **76**(1-3): 185-196. doi:10.1023/a:1024994525586.
- Sterck, L., Rombauts, S., Vandepoele, K., Rouzé, P., and Van de Peer, Y. 2007. How many genes are there in plants (... and why are they there)? Current opinion in plant biology **10**: 199-203. doi:10.1016/j.pbi.2007.01.004.
- Stewart, L., Redinbo, M.R., Qiu, X., Hol, W.G., and Champoux, J.J. 1998a. A model for the mechanism of human topoisomerase I. *Science (New York, N.Y.)* **279**(5356): 1534-1541. Available from <http://science.sciencemag.org/content/sci/279/5356/1534.full.pdf> [accessed.
- Stewart, L., Redinbo, M.R., Qiu, X., Hol, W.G.J., and Champoux, J.J. 1998b. A Model for the Mechanism of Human Topoisomerase I. *Science (New York, N.Y.)* **279**(5356): 1534-1541. doi:10.1126/science.279.5356.1534.
- Stockum, A., Lloyd, R.G., and Rudolph, C.J. 2012. On the viability of Escherichia coli cells lacking DNA topoisomerase I. *BMC Microbiol* **12**: 26. doi:10.1186/1471-2180-12-26.
- Strahilevitz, J., Robicsek, A., and Hooper, D.C. 2006. Role of the Extended $\alpha 4$ Domain of *Staphylococcus aureus* Gyrase A Protein in Determining Low Sensitivity to Quinolones. *Antimicrobial Agents and Chemotherapy* **50**(2): 600-606. doi:10.1128/aac.50.2.600-606.2006.
- Sugimoto-Shirasu, K., Stacey, N.J., Corsar, J., Roberts, K., and McCann, M.C. 2002. DNA topoisomerase VI is essential for endoreduplication in Arabidopsis. *Current biology : CB* **12**(20): 1782-1786. doi:10.1016/s0960-9822(02)01198-3.
- Sugimoto-Shirasu, K., Roberts, G.R., Stacey, N.J., McCann, M.C., Maxwell, A., and Roberts, K. 2005. RHL1 is an essential component of the plant DNA topoisomerase VI complex and is required for ploidy-dependent cell growth. *Proc Natl Acad Sci U S A* **102**(51): 18736-18741. doi:10.1073/pnas.0505883102.

- Sugino, A., and Cozzarelli, N.R. 1980. The intrinsic ATPase of DNA gyrase. *The Journal of biological chemistry* **255**(13): 6299-6306. Available from <http://www.jbc.org/content/255/13/6299.full.pdf> [accessed].
- Sugino, A., Higgins, N.P., and Cozzarelli, N.R. 1980. DNA gyrase subunit stoichiometry and the covalent attachment of subunit A to DNA during DNA cleavage. *Nucleic Acids Res* **8**(17): 3865-3874. Available from <https://www.ncbi.nlm.nih.gov/pmc/articles/PMC324200/pdf/nar00434-0127.pdf> [accessed].
- Sugino, A., Peebles, C.L., Kreuzer, K.N., and Cozzarelli, N.R. 1977. Mechanism of action of nalidixic acid: purification of *Escherichia coli* nalA gene product and its relationship to DNA gyrase and a novel nicking-closing enzyme. *Proc Natl Acad Sci U S A* **74**(11): 4767-4771. Available from <https://www.ncbi.nlm.nih.gov/pmc/articles/PMC432036/pdf/pnas00033-0067.pdf> [accessed].
- Sugino, A., Higgins, N.P., Brown, P.O., Peebles, C.L., and Cozzarelli, N.R. 1978. Energy coupling in DNA gyrase and the mechanism of action of novobiocin. *Proc Natl Acad Sci U S A* **75**(10): 4838-4842.
- Sugiura, M. 1995. The chloroplast genome. *Essays Biochem* **30**: 49-57.
- Sun, Q.Y., Ding, L.W., Lomonosoff, G.P., Sun, Y.B., Luo, M., Li, C.Q., et al. 2011. Improved expression and purification of recombinant human serum albumin from transgenic tobacco suspension culture. *J Biotechnol* **155**(2): 164-172. doi:10.1016/j.jbiotec.2011.06.033.
- Taanman, J.-W. 1999. The mitochondrial genome: structure, transcription, translation and replication. *Biochimica et Biophysica Acta (BBA) - Bioenergetics* **1410**(2): 103-123. doi:[https://doi.org/10.1016/S0005-2728\(98\)00161-3](https://doi.org/10.1016/S0005-2728(98)00161-3).
- Takahashi, T., Matsuhara, S., Abe, M., and Komeda, Y. 2002. Disruption of a DNA topoisomerase I gene affects morphogenesis in *Arabidopsis*. *The Plant cell* **14**(9): 2085-2093. doi:10.1105/tpc.001925.
- Takahashi, T.S., Da Cunha, V., Krupovic, M., Mayer, C., Forterre, P., and Gadelle, D. 2019. Expanding the type IIB DNA topoisomerase family: identification of new topoisomerase and topoisomerase-like proteins in mobile genetic elements. *NAR Genomics and Bioinformatics* **2**(1). doi:10.1093/nargab/lqz021.
- Tan, Y.F., O'Toole, N., Taylor, N.L., and Millar, A.H. 2010. Divalent metal ions in plant mitochondria and their role in interactions with proteins and oxidative stress-induced damage to respiratory function. *Plant Physiol* **152**(2): 747-761. doi:10.1104/pp.109.147942.

- Taneja, B., Patel, A., Slesarev, A., and Mondragón, A. 2006. Structure of the N-terminal fragment of topoisomerase V reveals a new family of topoisomerases. *Embo j* **25**(2): 398-408. doi:10.1038/sj.emboj.7600922.
- Tang Girdwood, S.C., Nenortas, E., and Shapiro, T.A. 2015. Targeting the gyrase of *Plasmodium falciparum* with topoisomerase poisons. *Biochem Pharmacol* **95**(4): 227-237. doi:10.1016/j.bcp.2015.03.018.
- Terada, T., Fujimoto, K., Nomura, M., Yamashita, J., Wierzba, K., Yamazaki, R., et al. 1993. Antitumor agents. 3. Synthesis and biological activity of 4.beta.-alkyl derivatives containing hydroxy, amino, and amido groups of 4'-O-demethyl-4-desoxypodophyllotoxin as antitumor agents. *Journal of Medicinal Chemistry* **36**(12): 1689-1699. doi:10.1021/jm00064a002.
- Terekhova, K., Marko, J.F., and Mondragón, A. 2013. Studies of bacterial topoisomerases I and III at the single-molecule level. *Biochem Soc Trans* **41**(2): 571-575. doi:10.1042/bst20120297.
- Teuscher, F., Lowther, J., Skinner-Adams, T.S., Spielmann, T., Dixon, M.W., Stack, C.M., et al. 2007. The M18 aspartyl aminopeptidase of the human malaria parasite *Plasmodium falciparum*. *The Journal of biological chemistry* **282**(42): 30817-30826. doi:10.1074/jbc.M704938200.
- The Arabidopsis Genome, I. 2000. Analysis of the genome sequence of the flowering plant *Arabidopsis thaliana*. *Nature* **408**(6814): 796-815. doi:10.1038/35048692.
- Timmis, J.N., Ayliffe, M.A., Huang, C.Y., and Martin, W. 2004. Endosymbiotic gene transfer: organelle genomes forge eukaryotic chromosomes. *Nature Reviews Genetics* **5**(2): 123-135. doi:10.1038/nrg1271.
- Tomizioli, M., Lazar, C., Brugière, S., Burger, T., Salvi, D., Gatto, L., et al. 2014. Deciphering thylakoid sub-compartments using a mass spectrometry-based approach. *Mol Cell Proteomics* **13**(8): 2147-2167. doi:10.1074/mcp.M114.040923.
- Tosh, K., and Kilbey, B. 1995. The gene encoding topoisomerase I from the human malaria parasite *Plasmodium falciparum*. *Gene* **163**(1): 151-154. doi:10.1016/0378-1119(95)00376-h.
- Tosh, K., Cheesman, S., Horrocks, P., and Kilbey, B. 1999. *Plasmodium falciparum*: stage-related expression of topoisomerase I. *Exp Parasitol* **91**(2): 126-132. doi:10.1006/expr.1998.4362.
- Trefzer, A., Pelzer, S., Schimana, J., Stockert, S., Bihlmaier, C., Fiedler, H.P., et al. 2002. Biosynthetic gene cluster of simocyclinone, a natural multihybrid antibiotic. *Antimicrobial Agents and Chemotherapy* **46**(5): 1174-1182. Available from

<https://www.ncbi.nlm.nih.gov/pmc/articles/PMC127163/pdf/0755.pdf>

[accessed.

- Tretter, E.M., and Berger, J.M. 2012. Mechanisms for defining supercoiling set point of DNA gyrase orthologs: I. A nonconserved acidic C-terminal tail modulates *Escherichia coli* gyrase activity. *The Journal of biological chemistry* **287**(22): 18636-18644. doi:10.1074/jbc.M112.345678.
- Truernit, E. 2001. Plant physiology: The importance of sucrose transporters. *Current biology : CB* **11**(5): R169-171. doi:10.1016/s0960-9822(01)00085-9.
- Tse-Dinh, Y.C. 1991. Zinc (II) coordination in *Escherichia coli* DNA topoisomerase I is required for cleavable complex formation with DNA. *The Journal of biological chemistry* **266**(22): 14317-14320.
- Tse-Dinh, Y.C. 2016. Targeting bacterial topoisomerases: how to counter mechanisms of resistance. *Future Med Chem* **8**(10): 1085-1100. doi:10.4155/fmc-2016-0042.
- Tzfira, T., and Citovsky, V. 2006. *Agrobacterium*-mediated genetic transformation of plants: biology and biotechnology. *Curr Opin Biotechnol* **17**(2): 147-154. doi:10.1016/j.copbio.2006.01.009.
- Valentine, M.E., Wolyniak, M.J., and Rutter, M.T. 2012. Extensive Phenotypic Variation among Allelic T-DNA Inserts in *Arabidopsis thaliana*. *PLoS One* **7**(9): e44981. doi:10.1371/journal.pone.0044981.
- Van Beek, N., and Davis, D.C. 2016. Baculovirus Insecticide Production in Insect Larvae. *Methods Mol Biol* **1350**: 393-405. doi:10.1007/978-1-4939-3043-2_20.
- Van der Walt, S., Schönberger, J.L., Nunez-Iglesias, J., Boulogne, F., Warner, J.D., Yager, N., et al. 2014. scikit-image: image processing in Python. *PeerJ* **2**: e453. doi:10.7717/peerj.453.
- Van Dingenen, J., Blomme, J., Gonzalez, N., and Inzé, D. 2016. Plants grow with a little help from their organelle friends. *Journal of Experimental Botany* **67**(22): 6267-6281. doi:10.1093/jxb/erw399.
- van Oers, M.M., Pijlman, G.P., and Vlak, J.M. 2015. Thirty years of baculovirus–insect cell protein expression: from dark horse to mainstream technology. *Journal of General Virology* **96**(1): 6-23. doi:<https://doi.org/10.1099/vir.0.067108-0>.
- Vedadi, M., Lew, J., Artz, J., Amani, M., Zhao, Y., Dong, A., et al. 2007. Genome-scale protein expression and structural biology of *Plasmodium falciparum* and related Apicomplexan organisms. *Mol Biochem Parasitol* **151**(1): 100-110. doi:10.1016/j.molbiopara.2006.10.011.

- Vialard, J.E., and Richardson, C.D. 1993. The 1,629-nucleotide open reading frame located downstream of the *Autographa californica* nuclear polyhedrosis virus polyhedrin gene encodes a nucleocapsid-associated phosphoprotein. *J Virol* **67**(10): 5859-5866. doi:10.1128/jvi.67.10.5859-5866.1993.
- Victor, M.E., Bengtsson, A., Andersen, G., Bengtsson, D., Lusingu, J.P., Vestergaard, L.S., et al. 2010. Insect cells are superior to *Escherichia coli* in producing malaria proteins inducing IgG targeting PfEMP1 on infected erythrocytes. *Malaria Journal* **9**(1): 325. doi:10.1186/1475-2875-9-325.
- Vitlin Gruber, A., Nisemblat, S., Zizelski, G., Parnas, A., Dzikowski, R., Azem, A., et al. 2013. *P. falciparum* cpn20 is a bona fide co-chaperonin that can replace GroES in *E. coli*. *PLoS One* **8**(1): e53909. doi:10.1371/journal.pone.0053909.
- Vizan, J.L., Hernandez-Chico, C., del Castillo, I., and Moreno, F. 1991. The peptide antibiotic microcin B17 induces double-strand cleavage of DNA mediated by *E. coli* DNA gyrase. *Embo j* **10**(2): 467-476. Available from <https://www.ncbi.nlm.nih.gov/pmc/articles/PMC452668/pdf/emboj00100-0222.pdf> [accessed].
- Vos, S.M., Tretter, E.M., Schmidt, B.H., and Berger, J.M. 2011. All tangled up: how cells direct, manage and exploit topoisomerase function. *Nature Reviews Molecular Cell Biology* **12**(12): 827-841. doi:10.1038/nrm3228.
- Waese, J., Fan, J., Pasha, A., Yu, H., Fucile, G., Shi, R., et al. 2017. ePlant: Visualizing and Exploring Multiple Levels of Data for Hypothesis Generation in Plant Biology. *The Plant cell* **29**(8): 1806-1821. doi:10.1105/tpc.17.00073.
- Wall, M.K., Mitchenall, L.A., and Maxwell, A. 2004. *Arabidopsis thaliana* DNA gyrase is targeted to chloroplasts and mitochondria. *Proc. Natl. Acad. Sci. U. S. A.* **101**(20): 7821-7826. doi:10.1073/pnas.0400836101.
- Wallace, M.D., Waraich, N.F., Debowski, A.W., Corral, M.G., Maxwell, A., Mylne, J.S., et al. 2018. Developing ciprofloxacin analogues against plant DNA gyrase: a novel herbicide mode of action. *Chemical communications (Cambridge, England)* **54**(15): 1869-1872. doi:10.1039/c7cc09518j.
- Waller, R.F., and McFadden, G.I. 2005. The apicoplast: a review of the derived plastid of apicomplexan parasites. *Curr Issues Mol Biol* **7**(1): 57-79.
- Wang, H., Di Gate, R.J., and Seeman, N.C. 1996. An RNA topoisomerase. *Proc Natl Acad Sci U S A* **93**(18): 9477-9482. doi:10.1073/pnas.93.18.9477.
- Wang, J.C. 1971. INTERACTION BETWEEN DNA AND AN *ESCHERICHIA-COLI* PROTEIN OMEGA. *J. Mol. Biol.* **55**(3): 523-&. doi:10.1016/0022-2836(71)90334-2.

- Wang, J.C. 1998. Moving one DNA double helix through another by a type II DNA topoisomerase: the story of a simple molecular machine. *Quarterly reviews of biophysics* **31**(2): 107-144.
- Wang, J.C. 2002a. Cellular roles of DNA topoisomerases: a molecular perspective. *Nat Rev Mol Cell Biol* **3**(6): 430-440. Available from <http://dx.doi.org/10.1038/nrm831> [accessed].
- Wang, J.C. 2002b. Cellular roles of DNA topoisomerases: a molecular perspective. *Nat Rev Mol Cell Biol* **3**(6): 430-440. doi:10.1038/nrm831 nrm831 [pii].
- Wang, Y. 2008. How effective is T-DNA insertional mutagenesis in Arabidopsis? *Journal of Biochemical Technology* **1**: 11-20.
- Waraich, N.F., Jain, S., Colloms, S.D., Stark, William M., Burton, N.P., and Maxwell, A. 2020. A novel decatenation assay for DNA topoisomerases using a singly-linked catenated substrate. *BioTechniques* **69**(5): 356-362. doi:10.2144/btn-2020-0059.
- Waskom, M. 2017. Seaborn. Available from <https://github.com/mwaskom/seaborn/tree/v0.8.1>.
- Watson, J.D., and Crick, F.H. 1953a. Molecular structure of nucleic acids; a structure for deoxyribose nucleic acid. *Nature* **171**(4356): 737-738.
- Watson, J.D., and Crick, F.H.C. 1953b. Genetical implications of the structure of deoxyribonucleic acid. *Nature* **171**(4361): 964-967. doi:10.1038/171964b0.
- Weissig, V., Vetro-Widenhouse, T.S., and Rowe, T.C. 1997. Topoisomerase II inhibitors induce cleavage of nuclear and 35-kb plastid DNAs in the malarial parasite *Plasmodium falciparum*. *DNA and cell biology* **16**(12): 1483-1492. doi:10.1089/dna.1997.16.1483.
- Wigley, D.B., Davies, G.J., Dodson, E.J., Maxwell, A., and Dodson, G. 1991. Crystal structure of an N-terminal fragment of the DNA gyrase B protein. *Nature* **351**(6328): 624-629. doi:10.1038/351624a0.
- Williams, N.L., and Maxwell, A. 1999. Probing the two-gate mechanism of DNA gyrase using cysteine cross-linking. *Biochemistry* **38**(41): 13502-13511. Available from <http://pubs.acs.org/doi/pdfplus/10.1021/bi9912488> [accessed].
- Williams, N.L., Howells, A.J., and Maxwell, A. 2001. Locking the ATP-operated clamp of DNA gyrase: probing the mechanism of strand passage. *J Mol Biol* **306**(5): 969-984. doi:10.1006/jmbi.2001.4468.

- Williamson, D.H., Preiser, P.R., and Wilson, R.J. 1996. Organelle DNAs: The bit players in malaria parasite DNA replication. *Parasitology today (Personal ed.)* **12**(9): 357-362.
- Williamson, D.H., Denny, P.W., Moore, P.W., Sato, S., McCready, S., and Wilson, R.J.M. 2001. The in vivo conformation of the plastid DNA of *Toxoplasma gondii*: implications for replication. Edited by N.-H. Chua. *J. Mol. Biol.* **306**(2): 159-168. doi:<https://doi.org/10.1006/jmbi.2000.4385>.
- Williamson, D.H., Preiser, P.R., Moore, P.W., McCready, S., Strath, M., and Wilson, R.J. 2002. The plastid DNA of the malaria parasite *Plasmodium falciparum* is replicated by two mechanisms. *Mol Microbiol* **45**(2): 533-542. doi:10.1046/j.1365-2958.2002.03033.x.
- Wilson, R.J., and Williamson, D.H. 1997. Extrachromosomal DNA in the Apicomplexa. *Microbiology and molecular biology reviews* : MMBR **61**(1): 1-16. Available from <http://mmbbr.asm.org/content/61/1/1.full.pdf> [accessed].
- Wilson, R.J., Denny, P.W., Preiser, P.R., Rangachari, K., Roberts, K., Roy, A., et al. 1996. Complete gene map of the plastid-like DNA of the malaria parasite *Plasmodium falciparum*. *J Mol Biol* **261**(2): 155-172.
- Wind, J., Smeekens, S., and Hanson, J. 2010. Sucrose: metabolite and signaling molecule. *Phytochemistry* **71**(14-15): 1610-1614. doi:10.1016/j.phytochem.2010.07.007.
- Woessner, R.D., Mattern, M.R., Mirabelli, C.K., Johnson, R.K., and Drake, F.H. 1991. Proliferation- and cell cycle-dependent differences in expression of the 170 kilodalton and 180 kilodalton forms of topoisomerase II in NIH-3T3 cells. *Cell Growth Differ* **2**(4): 209-214.
- Wohlkonig, A., Chan, P.F., Fosberry, A.P., Homes, P., Huang, J., Kranz, M., et al. 2010. Structural basis of quinolone inhibition of type IIA topoisomerases and target-mediated resistance. *Nature structural & molecular biology* **17**(9): 1152-1153. doi:10.1038/nsmb.1892.
- World Health, O. 2019. World malaria report 2019. World Health Organization, Geneva.
- Xie, S., and Lam, E. 1994a. Characterization of a DNA Topoisomerase II cDNA from *Arabidopsis thaliana*. *Plant Physiology* **106**(4): 1701-1702. doi:10.1104/pp.106.4.1701.
- Xie, S., and Lam, E. 1994b. Abundance of nuclear DNA topoisomerase II is correlated with proliferation in *Arabidopsis thaliana*. *Nucleic Acids Res* **22**(25): 5729-5736. doi:10.1093/nar/22.25.5729.

- Xu, Z., Mahmood, K., and Rothstein, S.J. 2017. ROS Induces Anthocyanin Production Via Late Biosynthetic Genes and Anthocyanin Deficiency Confers the Hypersensitivity to ROS-Generating Stresses in Arabidopsis. *Plant and Cell Physiology* **58**(8): 1364-1377. doi:10.1093/pcp/pcx073.
- Xuan, W., Audenaert, D., Parizot, B., Möller, B.K., Njo, M.F., De Rybel, B., et al. 2015. Root Cap-Derived Auxin Pre-patterns the Longitudinal Axis of the Arabidopsis Root. *Current biology* : CB **25**(10): 1381-1388. doi:10.1016/j.cub.2015.03.046.
- Yang, W. 2011. Nucleases: diversity of structure, function and mechanism. *Quarterly reviews of biophysics* **44**(1): 1-93. doi:10.1017/s0033583510000181.
- Yang, Z., Hou, Q., Cheng, L., Xu, W., Hong, Y., Li, S., et al. 2017. RNase H1 Cooperates with DNA Gyrase to Restrict R-Loops and Maintain Genome Integrity in Arabidopsis Chloroplasts. *The Plant cell* **29**(10): 2478-2497. doi:10.1105/tpc.17.00305.
- Yaseen, M., Ahmad, T., Sablok, G., Standardi, A., and Hafiz, I.A. 2013. Review: role of carbon sources for in vitro plant growth and development. *Molecular Biology Reports* **40**(4): 2837-2849. doi:10.1007/s11033-012-2299-z.
- Yoshida, H., Bogaki, M., Nakamura, M., and Nakamura, S. 1990. Quinolone resistance-determining region in the DNA gyrase *gyrA* gene of Escherichia coli. *Antimicrobial Agents and Chemotherapy* **34**(6): 1271-1272. Available from <http://aac.asm.org/content/34/6/1271.full.pdf> [accessed].
- Yu, X., Davenport, J.W., Urtishak, K.A., Carillo, M.L., Gosai, S.J., Kolaris, C.P., et al. 2017. Genome-wide TOP2A DNA cleavage is biased toward translocated and highly transcribed loci. *Genome Res* **27**(7): 1238-1249. doi:10.1101/gr.211615.116.
- Zechiedrich, E.L., and Cozzarelli, N.R. 1995. Roles of topoisomerase IV and DNA gyrase in DNA unlinking during replication in Escherichia coli. *Genes & development* **9**(22): 2859-2869. doi:10.1101/gad.9.22.2859.
- Zechiedrich, E.L., Khodursky, A.B., and Cozzarelli, N.R. 1997. Topoisomerase IV, not gyrase, decatenates products of site-specific recombination in Escherichia coli. *Genes & development* **11**(19): 2580-2592. Available from <https://www.ncbi.nlm.nih.gov/pubmed/9334322> [accessed].
- Zhang, H., Wang, L., Deroles, S., Bennett, R., and Davies, K. 2006. New insight into the structures and formation of anthocyanic vacuolar inclusions in flower petals. *BMC Plant Biology* **6**(1): 29. doi:10.1186/1471-2229-6-29.
- Zhao, Y., Chapman, D.A., and Jones, I.M. 2003. Improving baculovirus recombination. *Nucleic Acids Res* **31**(2): E6-6. doi:10.1093/nar/gng006.

- Zhu, C.X., Qi, H.Y., and Tse-Dinh, Y.C. 1995. Mutation in Cys662 of Escherichia coli DNA topoisomerase I confers temperature sensitivity and change in DNA cleavage selectivity. *J Mol Biol* **250**(5): 609-616. doi:10.1006/jmbi.1995.0402.
- Zimorski, V., Ku, C., Martin, W.F., and Gould, S.B. 2014a. Endosymbiotic theory for organelle origins. *Current Opinion in Microbiology* **22**: 38-48. doi:<https://doi.org/10.1016/j.mib.2014.09.008>.
- Zimorski, V., Ku, C., Martin, W.F., and Gould, S.B. 2014b. Endosymbiotic theory for organelle origins. *Curr Opin Microbiol* **22**: 38-48. doi:10.1016/j.mib.2014.09.008.
- Zoschke, R., and Bock, R. 2018. Chloroplast Translation: Structural and Functional Organization, Operational Control, and Regulation. *The Plant cell* **30**(4): 745-770. doi:10.1105/tpc.18.00016.
- Zoschke, R., Liere, K., and Börner, T. 2007. From seedling to mature plant: Arabidopsis plastidial genome copy number, RNA accumulation and transcription are differentially regulated during leaf development. *The Plant Journal* **50**(4): 710-722. doi:<https://doi.org/10.1111/j.1365-313X.2007.03084.x>.
- Zuegge, J., Ralph, S., Schmuker, M., McFadden, G.I., and Schneider, G. 2001. Deciphering apicoplast targeting signals--feature extraction from nuclear-encoded precursors of Plasmodium falciparum apicoplast proteins. *Gene* **280**(1-2): 19-26. Available from http://ac.els-cdn.com/S0378111901007764/1-s2.0-S0378111901007764-main.pdf?_tid=35f0f57c-1bc7-11e7-a93d-00000aab0f02&acdnat=1491592987_51a179e4d850914e4a075979e997b766 [accessed].



Cite this: *Chem. Commun.*, 2018, 54, 1869

Received 12th December 2017,
Accepted 24th January 2018

DOI: 10.1039/c7cc09518j

rsc.li/chemcomm

Developing ciprofloxacin analogues against plant DNA gyrase: a novel herbicide mode of action†

Michael D. Wallace,^a Nidda F. Waraich,^b Aleksandra W. Debowski,^{ib,ac}
Maxime G. Corral,^{ad} Anthony Maxwell,^{ib,b} Joshua S. Mylne,^{ib,*ad} and
Keith A. Stubbs^{ib,*a}

Ciprofloxacin has been shown to exhibit potent herbicidal activity through action against plant DNA gyrase, presenting a novel mode of action. Analogues of ciprofloxacin have been prepared with increased herbicidal activity and diminished antibacterial activity, compared to ciprofloxacin, as demonstrated using model systems.

The rapid emergence of herbicide resistance is reducing the efficacy of herbicides, the most important tool in the control of weeds.^{1,2} Currently, 254 weed species have been reported to have resistance to one or more herbicide chemistries (www.weedscience.org). More importantly 41 species are reported to have developed resistance to glyphosate, which is considered the most important herbicide in global weed control.³ Therefore, there is a desperate need for the introduction of herbicides with novel modes of action, something which has not been achieved in over 20 years.⁴

DNA topoisomerases are enzymes that control the unwinding of DNA during DNA replication, and are classified based on whether the enzymatic reaction they catalyse proceed *via* a transient single- (type I) or double-stranded break (type II) in DNA.⁵ DNA gyrase is an essential type II topoisomerase, first found in the bacterium *Escherichia coli*,⁶ and has been demonstrated to have the unique ability to relax positively supercoiled DNA by introducing negative supercoils using ATP hydrolysis or relaxing negative supercoils independently of ATP.⁵ As DNA gyrase is absent in humans it is an appealing antibacterial target with fluoroquinolones developed as a successful class of antibiotics.⁷ Recently, DNA gyrase and its activity has been characterized in plants^{8–10} and shown to be essential for proper

growth.⁹ Interestingly the fluoroquinolone ciprofloxacin **1** (Fig. 1A) has herbicidal activity⁹ (Fig. 1B) and it has been shown that the mode of action of **1** is through inhibition of DNA gyrase.¹¹ This presents a potential new herbicidal mode of action.

Despite **1** having the benefits of high potency towards plant DNA gyrase,^{9,11} it lacks selectivity relative to bacterial DNA gyrases, hindering its potential as a herbicide. Here in an effort to increase selectivity towards a herbicidal mode of action we present a synthesis for preparing analogues of **1** where the fluoroquinolone scaffold is retained, but is elaborated at the N-1 and C-7 positions with various chemical moieties varying in size, shape and hydrophobicity (Fig. 1A). Using the model plant *Arabidopsis thaliana*, (a widely used model plant in plant biology as its genome is known and sequenced, and since it is small, it can be grown under laboratory conditions¹²), as well as bacterial strains and *in vitro* assays, against both plant and bacterial DNA gyrase, we evaluated these molecules for potency and selectivity.

To realise a synthetic pathway for preparing analogues bearing the fluoroquinolone core we felt that the ester **2** would serve as a useful intermediate. Starting with the aniline **3**, application and adaptation of the known synthetic procedures of Koga *et al.*¹³ (Fig. 2A) gave the desired fluoroquinolone substructure **2**. With this compound in hand, attention focussed on modifying the N-1 position. Recently an interactive database containing physicochemical data of 334 commercial

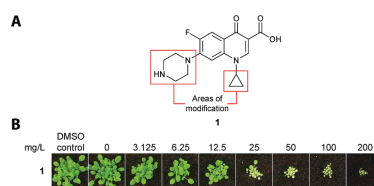


Fig. 1 (A) Ciprofloxacin with sites of modification highlighted. (B) Post-emergent herbicidal activity of ciprofloxacin **1**.

^a School of Molecular Sciences, University of Western Australia, Crawley, WA 6009, Australia. E-mail: keith.stubbs@uwa.edu.au, joshua.mylne@uwa.edu.au

^b Department of Biological Chemistry, John Innes Centre, Norwich Research Park, Norwich, NR4 7UH, UK

^c School of Biomedical Sciences, University of Western Australia, Nedlands, WA 6009, Australia

^d ARC Centre of Excellence in Plant Energy Biology, University of Western Australia, Crawley, WA 6009, Australia

† Electronic supplementary information (ESI) available. See DOI: 10.1039/c7cc09518j

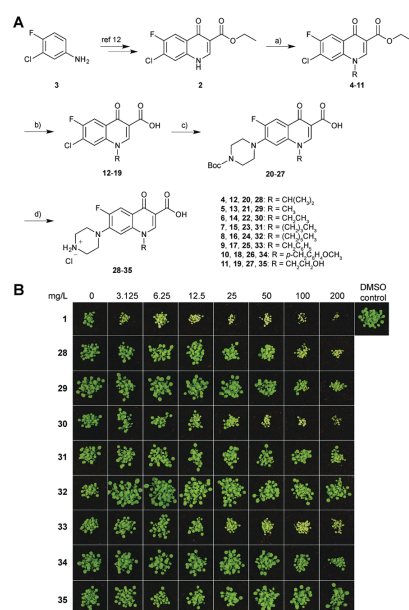


Fig. 2 (A) (a) R-X (X = I, Br or Cl), K_2CO_3 , DMF; (b) 2 M aq. NaOH, EtOH; (c) i. piperazine, DMSO; ii. Boc_2O , 1 M aq. NaOH, THF; (d) 3 M aq. HCl, EtOH. (B) Representative screening assay of ciprofloxacin **1** and analogues **28–35** with modification at N-1. *A. thaliana* Col-0 was grown on soil and treated with the relevant compound after three and six days of growth, with 2% DMSO as a control. Images were taken at day 16.

herbicides was prepared¹⁴ and has been employed for herbicide discovery^{15–17} and so we used this database to choose a simple set of analogues that varied in size, shape and hydrophobicity, but retained favourable physicochemical properties for herbicides (Fig. S1, ESI[†]). The synthesis of the esters **4–11** was achieved via alkylation of the N-1 position with the relevant alkyl halide in good yields (73–93%), except for the *i*-propyl derivative **5**, where a low yield of 17% was obtained, which was consistent with the alkylation reaction involving **2** being unfavourable toward secondary alkyl halides.¹⁸ Subsequent base-mediated hydrolysis of the esters **4–11** gave the acids **12–19** in good yields. Nucleophilic aromatic substitution of the chlorides **12–19** with piperazine using a modified procedure¹⁸ followed by the Boc-protection of the resultant amine using a modified procedure by Dhaneshwar *et al.*,¹⁹ in a one-pot reaction, produced the Boc-protected fluoroquinolones **20–27**. Removal of the Boc-protecting group from **20–27** furnished the desired compounds **28–35** with acceptable overall yields.

The compounds **28–35** were evaluated for their post-emergent herbicidal activity against *A. thaliana* (Fig. 2B). Overall, all the modified compounds showed a loss in activity compared to ciprofloxacin **1**. The ethyl derivative **30** and benzyl derivative **33**

retained modest activity and the *i*-propyl derivative **28** also retained some activity, compared to **1**. The smaller methyl group of **29** and the longer alkyl groups of **31** and **32** as well as the introduction of H-bond acceptors as in **34** and **35** resulted in a loss of activity.

Consequently, attention turned to analogues with modification at the C-7 position. As ciprofloxacin **1** and **30** (norfloxacin-HCl) were the best compounds in the first round of herbicidal assays we decided to retain the cyclopropyl and ethyl groups at the N-1 position for the second round of analogues. Eighteen analogues were selected using the same methodology as for the preparation of **28–35**, specifically via use of the interactive database (ESI,† Fig. S1).¹⁴ Treatment of the chloride **36** or **14** with the appropriate amine using S_NAr reaction conditions as described by Grohe *et al.*¹⁸ gave the desired compounds **37–43** and **44–50** respectively in good yields (Table 1). In addition, the (2-aminoethyl)amino analogues **51** and **52** were prepared via a similar methodology with **36** and **14**, respectively but using an intermediate Boc-protected moiety to aid purification (ESI,† Scheme S1). Furthermore, the *N*-methyl derivative of ciprofloxacin **1**, namely **53**, was prepared via an Eschweiler–Clarke methylation of **1** (ESI,† Scheme S2) and **54**, was obtained commercially.

Assays against *A. thaliana* with **37–54** found that substitution of the secondary amine to a methylene **37** or oxygen atom **38** retained herbicidal activity, with an increase in potency for **38** (Fig. 3). A change in ring size as for **39**, **40**, **46** and **47** resulted in a reduction of activity compared to the parent compounds **1** and **30** respectively. The open chained moieties **41–43** and **48–50** had differing activity, with the smaller dimethyl moieties **41** and **48** being the most potent and with **41** being similar to **1**.

Table 1 Synthesis of compounds based on ciprofloxacin **1** and **30** with modification at C-7

Fluoroquinolone-Cl + HNR ₂		DMSO → Fluoroquinolone-NR ₂			
		Fluoroquinolone-Cl			
		36	14		
Entry	Amine	Product	Yield (%)	Product	Yield (%)
1		37	61	44	37
2		38	85	45	59
3		39	58	46	40
4		40	58	47	43
5		41	41	48	44
6		42	32	49	35
7		43	32	50	28

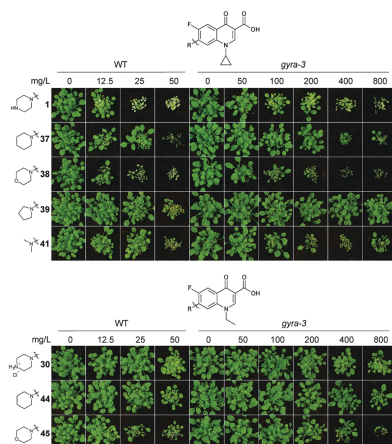


Fig. 4 Representative testing assay of analogues which showed herbicidal activity ($IC_{50} < 25 \text{ mg L}^{-1}$), against wild-type (WT) and *gyra-3* mutant *A. thaliana*. Testing was conducted as described in Fig. 2B and images were taken at day 20 of growth.

encoded ATGYRA, to confirm these compounds were on target, affecting only the DNA gyrase protein *in vivo* (Fig. 4). The results are highly suggestive that DNA gyrase is the sole target as the mutants demonstrate an increased resistance to not only ciprofloxacin **1**, but also to the analogues. To further confirm that these compounds act in a similar manner to ciprofloxacin **1**, DNA cleavage assays were conducted. Fluoroquinolones, such as **1**, inhibit DNA gyrase by stabilising the covalent complex that forms between the enzyme and DNA⁶ and such complexes can be detected as a linear band in agarose gel electrophoresis. The most herbicidal compounds were assayed (ESI,† Fig. S2B) and found to be able to stabilise the gyrase cleavage complex with both *E. coli* and *A. thaliana* gyrase, similar to ciprofloxacin **1**, suggesting that they all act by a similar mechanism.

In conclusion, herbicide resistance is a growing concern and there is a pressing need for new modes of action. Previous research has shown that DNA gyrase presents a potential new target for herbicide development. We have demonstrated here using a known chemical inhibitor scaffold of DNA gyrase, fluoroquinolones, that tuning of molecules for selectivity towards a herbicidal rather than an antibiotic mode of action is possible at the organism level. However, the *gyra-3* mutant highlights that, as for all herbicidal targets, resistance can be selected for, so practices that delay the evolution of resistance will also need to be considered.²¹ Overall this work presents a platform for further research into this enzyme, both at the chemical, biological and structural level, as a possible new mode of action for herbicide development.

The authors wish to thank Melissa Andrade and Marina Silich-Carrara for providing bacterial strains from the UWA Microbiology Culture Collection. The authors also thank the Centre for Microscopy, Characterisation and Analysis at The University of Western Australia, which is supported by University, State and Federal Government funding. KAS and JSM also thank the Australian Research Council for funding (FT100100291 and FT120100013 respectively). MDW thanks the University of Western Australia for a UWA Alumni SWANS Rural Scholarship and a Research Training Program Scholarship. MGC is supported by a University Postgraduate Award for International Students and a Scholarship for International Research by the University of Western Australia. AWD thanks the National Health and Medical Research Council for funding (APP1073250). AM is supported by the Biotechnology and Biological Sciences Research Council UK (BB/P012523/1) and the John Innes Foundation. NFW is supported by a CASE studentship from the BBSRC and Inspiralis. This work was also funded in part by a Bayer AG division Crop Science Grants4Targets grant 2016-01-55 to JSM, KAS and AM.

Conflicts of interest

There are no conflicts to declare.

Notes and references

- S. B. Powles and Q. Yu, *Annu. Rev. Plant Biol.*, 2010, **61**, 317.
- L. P. Gianessi, *Pest Manage. Sci.*, 2013, **69**, 1099.
- S. O. Duke and S. B. Powles, *Pest Manage. Sci.*, 2008, **64**, 319.
- S. O. Duke, *Pest Manage. Sci.*, 2012, **68**, 505.
- N. G. Bush, K. Evans-Roberts and A. Maxwell, *EcoSal Plus*, 2015, **6**, DOI: 10.1128/ecosalplus.ESP-0010-2014.
- M. Gellert, K. Mizuuchi, M. H. O'Dea and H. A. Nash, *Proc. Natl. Acad. Sci. U. S. A.*, 1976, **73**, 3872.
- G. A. Jacoby and D. C. Hooper, in *Antibiotic Discovery and Development*, ed. T. J. Dougherty and M. J. Pucci, Springer US, Boston, MA, 2012, pp. 119.
- H. S. Cho, S. S. Lee, K. D. Kim, I. Hwang, J. Lim, Y. Park and H. Pai, *Plant Cell*, 2004, **16**, 2665.
- M. K. Wall, L. A. Mitchenall and A. Maxwell, *Proc. Natl. Acad. Sci. U. S. A.*, 2004, **101**, 7821.
- C. V. Morgante, R. A. O. Rodrigues, P. A. S. Marbach, C. M. Borgonovi, D. S. Moura and M. C. Silva-Filho, *Mol. Genet. Genomics*, 2009, **281**, 525.
- K. M. Evans-Roberts, L. A. Mitchenall, M. K. Wall, J. Leroux, J. S. Mylne and A. Maxwell, *J. Biol. Chem.*, 2016, **291**, 3136.
- M. Koornneef and D. Meinke, *Plant J.*, 2010, **61**, 909.
- H. Koga, A. Itoh, S. Murayama, S. Suzue and T. Irikura, *J. Med. Chem.*, 1980, **23**, 1358.
- M. N. Gandy, M. G. Corral, J. S. Mylne and K. A. Stubbs, *Org. Biomol. Chem.*, 2015, **13**, 5586.
- M. Corral, J. Leroux, K. A. Stubbs and J. S. Mylne, *Sci. Rep.*, 2017, **7**, 45871.
- S. Funar-Timofei, A. Borota and L. Crisan, *Mol. Diversity*, 2017, **21**, 437.
- M. G. Corral, J. Leroux, S. Tresch, T. Newton, K. A. Stubbs and J. S. Mylne, *Angew. Chem., Int. Ed.*, 2017, **56**, 9881.
- K. Grohe and H. Heitzer, *Liebigs Ann. Chem.*, 1987, **29**.
- S. Dhaneshwar, K. Tewari, S. Joshi, D. Godbole and P. Ghosh, *Chem. Phys. Lipids*, 2011, **164**, 307.
- J. P. Hughes, S. Rees, S. B. Kalindjian and K. L. Philpott, *Br. J. Pharmacol.*, 2011, **162**, 1239.
- J. A. Evans, P. J. Tranel, A. G. Hager, B. Schutte, C. Wu, L. A. Chatham and A. S. Davis, *Pest Manage. Sci.*, 2015, **72**, 74.

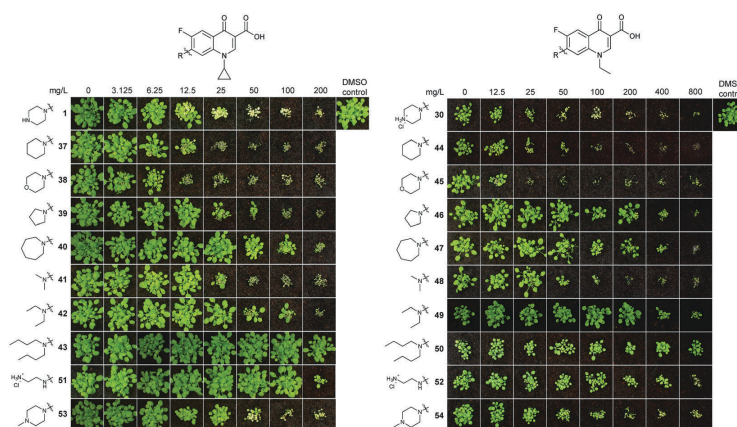


Fig. 3 Representative screening assay of analogues of ciprofloxacin **1** and **30**, which have been modified at C-7. The screening was conducted as described in Fig. 2B and images were taken at day 20 of growth.

Compounds **51** and **52** bearing a single linear chain had very little herbicidal activity. Finally, compound **53** retained herbicidal activity compared to **1** and **54** retained modest herbicidal activity compared to **1**.

To assess if there was any selectivity gained between plants and bacteria, either due to a difference in the compounds ability to penetrate the organism or its affinity for plant and bacterial gyrase, antibiotic susceptibility tests (MIC) against *Escherichia coli* (Table 2), *Pseudomonas aeruginosa* and *Staphylococcus aureus* (ESI,† Table S2) were conducted, as well as DNA gyrase supercoiling assays against recombinant *A. thaliana* and *E. coli* DNA gyrase (Table 2 and ESI,† Fig. S2A, Table S1).

Specifically for *E. coli*, the synthesised analogues all had MIC values greater than ciprofloxacin **1**, except for **53**. Not surprisingly the selectivity of the known antibiotics **30** and **54** remained poor along with the parent compound **1**, towards a herbicidal mode of

action. On the other hand some compounds saw a considerable improvement in selectivity towards a herbicidal mode of action. Analogues **37** and **38**, which have similar herbicidal activities compared to **1**, showed a significant increase in MIC against *E. coli* and *P. aeruginosa*, and modest changes against *S. aureus* (See ESI,† Table S2). Of note is **44** which, despite having a slight reduction in herbicidal potency compared to ciprofloxacin **1**, has >600-fold increase in selectivity toward a herbicidal mode of action based on testing against the organismal models. Evaluation of the potency of all the compounds against the recombinant DNA gyrases of *A. thaliana* and *E. coli* in supercoiling assays also produced interesting results. Overall the potency of the prepared analogues was less to that observed for ciprofloxacin **1** with respect to both enzymes, however like **1** each of the compounds were more active against recombinant *E. coli* gyrase compared to *A. thaliana* gyrase. From these results it is clear that the overall differences in potency observed against organismal models is not manifested at the level of enzyme inhibition, but rather the availability of the compound through plant and/or bacterial uptake. This result is important in terms of potential future development of the scaffolds for use as herbicides for not only ciprofloxacin-based analogues, but fluoroquinolones in general. Typically compounds are first evaluated against recombinantly expressed enzymes for potency and selectivity (where needed) and only then progressed to more complex systems.²⁰ Our data suggest evaluation should be conducted at the level of the plant/bacterium to evaluate potency and selectivity as compounds may be excluded if a protein-first evaluation is used.

Analogues that demonstrated reasonable herbicidal activity namely **30**, **37–39**, **41**, **44** and **45**, were assayed against a ciprofloxacin resistant *A. thaliana* mutant (*gyra-3*),¹¹ which has a point mutation that causes an amino acid substitution in its

Table 2 Overview of compounds displaying herbicidal potency against *A. thaliana* with an IC₅₀ value less than 25 mg L⁻¹. Minimum inhibitory concentrations (MICs) against *E. coli*. IC₅₀ values of compounds against recombinant *A. thaliana* and *E. coli* gyrase in supercoiling assays. Errors represent standard error of the mean

	IC ₅₀ ^a		Selectivity ^b	DNA gyrase IC ₅₀ ^c	
	<i>A. thaliana</i>	<i>E. coli</i>		<i>A. thaliana</i>	<i>E. coli</i>
1	10.2 ± 0.4	0.0078	7 × 10 ⁻⁴	0.68 ± 0.06	0.56 ± 0.07
30	19.3 ± 2.8	0.0625	3 × 10 ⁻³	3.15 ± 0.15	1.35 ± 0.25
37	6.1 ± 1.0	1	0.16	4.70 ± 0.70	1.90 ± 0.50
38	4.0 ± 0.3	0.25	0.06	5.85 ± 0.65	0.77 ± 0.095
39	21.4 ± 2.6	2	0.09	2.80 ± 0.60	0.25 ± 0.04
41	24.0 ± 3.2	0.5	0.02	8.13 ± 1.76	1.90 ± 0.40
44	17.8 ± 1.6	8	0.45	26.9 ± 3.3	2.65 ± 0.05
45	12.0 ± 1.0	1	0.08	28.4 ± 3.6	2.45 ± 0.45

^a mg L⁻¹. ^b Selectivity towards a herbicidal mode of action (defined as MIC/IC₅₀). ^c μM.

A novel decatenation assay for DNA topoisomerases using a singly-linked catenated substrate

Nidda F Waraich¹, Shruti Jain^{4,2}, Sean D Colloms³, William Marshall Stark³, Nicolas P Burton² & Anthony Maxwell¹

¹Department of Biological Chemistry, John Innes Centre, Norwich Research Park, Norwich, NR4 7UH, UK; ²Inspiralis Ltd, Innovation Centre, Norwich Research Park, Colney Lane, Norwich, NR4 7GJ, UK; ³Institute of Molecular Cell & Systems Biology, University of Glasgow, Bower Building, Glasgow G12 8QQ, UK; ⁴Lonza Biologics, 228 Bath Road, Slough SL1 4DX, UK; *Author for correspondence: tony.maxwell@jic.ac.uk

BioTechniques 69: 357–362 (November 2020) 10.2144/btn-2020-0059

First draft submitted: 28 April 2020; Accepted for publication: 13 August 2020; Published online: 1 October 2020

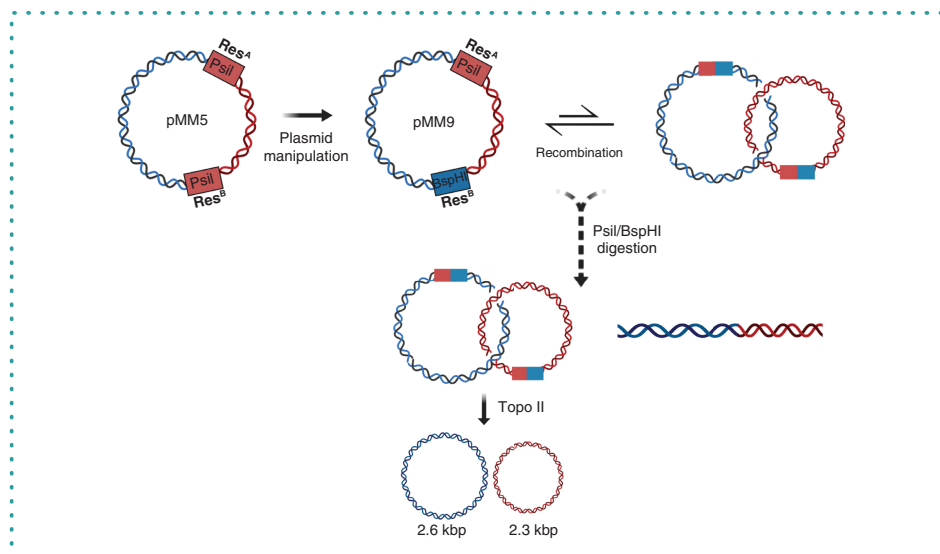
ABSTRACT

Decatenation is a crucial *in vivo* reaction of DNA topoisomerases in DNA replication and is frequently used in *in vitro* drug screening. Usually this reaction is monitored using kinetoplast DNA as a substrate, although this assay has several limitations. Here we have engineered a substrate for Tn3 resolvase that generates a singly-linked catenane that can readily be purified from the DNA substrate after restriction enzyme digestion and centrifugation. We show that this catenated substrate can be used with high sensitivity in topoisomerase assays and drug-inhibition assays.

METHOD SUMMARY

We engineered a plasmid such that reaction with Tn3 resolvase generates a singly-linked catenane product. Restriction enzyme digestion and caesium chloride density gradient centrifugation enable the purification of the catenane product substantially free from starting plasmid. This product may be utilized in topoisomerase enzyme assays.

GRAPHICAL ABSTRACT



Reports

KEYWORDS:

antibiotics • anticancer drugs • decatenation • gyrase • topoisomerase

DNA topoisomerases are enzymes that modulate DNA topology [1–3]. These essential enzymes catalyze the interconversion between different topological forms of DNA and are categorized, on evolutionary and mechanistic grounds, into two types: I and II. The two types are distinguished by the number of phosphotyrosyl linkages established in the covalent DNA–protein complex. Type I enzymes form a single linkage, leading to transient single-stranded DNA breaks, whereas type II topoisomerases form transient double-stranded breaks via two phosphotyrosyl linkages. The reactions characteristic of topoisomerases include the relaxation, supercoiling, knotting/un knotting and catenation/decatenation of their DNA substrates.

Topoisomerases are biologically essential enzymes involved in several critical cellular processes including DNA replication [2,4]. The process of replication imposes various topological modifications upon the DNA at different stages. At replication termination, as two replication forks converge, catenation (interlinking) of the daughter chromosomes can result [5] and are removed by the action of type II topoisomerases passing one daughter through a double-stranded break in the other. Naturally occurring DNA catenanes were first observed in mitochondrial DNA isolated from HeLa cell lines [6] and have since been identified to be the predominant method of organizing DNA in the mitochondria of trypanosomes; this mitochondrial DNA is commonly referred to as kinetoplast DNA (kDNA) [7]. Analysis of the kDNA network reveals two types of DNA circles that are interlinked to form an intricate network of maxicircles (20–40 kbp) and mini-circles (~2.5 kbp) [8].

The most common method for assaying the decatenation activity of topoisomerases *in vitro* involves the use of purified kDNA as a substrate [9]. The assay monitors the production of mini-circles released from the kDNA. The inherently complex arrangement of kDNA has several practical implications that can lead to difficulties in interpretation of agarose gel-based assays. One such issue is the significant size of kDNA; its large structure barely enters the pores of an agarose gel, and it is normally retained in the wells. Additionally, the nature of the current assay does not allow for quantitative analysis of decatenation events; this is because the number of links between the maxi- and mini-circles that must be removed to release the circles is variable [10].

Given these issues, we aimed to develop a simpler and more suitable substrate to replace kDNA in decatenation assays. The development of our alternative substrate, a singly-linked DNA catenane, improves the sensitivity and reliability of the assay. The method involves the use of a site-specific recombinase protein, Tn3 resolvase, which is encoded by the Tn3 transposon, together with β -lactamase and Tn3 transposase genes [11]. Tn3 resolvase is a DNA site-specific serine recombinase, responsible for the resolution of cointegrate intermediates during the replicative transposition pathway. The specific site of action of resolvase, the 'resolution site' (*res*), encompasses a 114-bp sequence, divided into three subsites: site I (28 bp), site II (34 bp) and site III (25 bp) (Figure 1). DNA cleavage and rejoining reactions occur at site I, whereas sites II and III act as accessory sites and play a role in the regulation of the enzyme's activity. The Tn3 recombination reaction is initiated by the binding of Tn3 resolvase subunits to the two *res* sites to form *res*–resolvase complexes. These complexes combine to form the synaptic complex that is composed of two intertwined *res* sites. Subsequently, double-stranded DNA cleavage occurs at each of the *res* site I sequences, followed by strand exchange and rejoining to re-form two intact *res* sites. When the substrate is a circular DNA molecule containing two directly repeated *res* sites, this process leads to the formation of singly-linked catenanes as products [12].

We have harnessed the Tn3 resolvase reaction to generate a singly-linked catenated product ('bis-cat') comprising two DNA circles of different sizes that can be used in DNA topoisomerase assays, building on recently published work [13]. We modified the Tn3 *res* sites so that restriction sites present before recombination are destroyed during the reaction, allowing easy purification of the bis-cat product.

Materials & methods

Tn3 resolvase overexpression & purification

Overexpression of Tn3 resolvase was achieved by transforming the expression vector pSA1101 [14] into BL21 (DE3) pLysS competent cells. The *Escherichia coli* culture was grown to late log phase, induced with 0.1 mM of IPTG and grown for a further 3 h. Resolvase purification was carried out as described previously [15].

Plasmids & DNA

Plasmid pMM6 was modified from pMM5 [16] by site-directed mutagenesis at *res* site I. This was achieved using the In-Fusion HD[®] cloning kit following the manufacturer's guidelines and using the oligonucleotides in Table 1. The conversion of pMM6 into pMM9 involved the removal of three natural BspHI restriction enzyme sites from the pMM6 plasmid, again by site-directed mutagenesis using the In-Fusion HD[®] cloning kit; primer sequences are given in Table 1. The resultant plasmid, pMM9, was transformed into ER2925 cells (a *dam* methylation-deficient background). Supercoiled pBR322 and kDNA were obtained from Inspiralis Ltd. (Norwich, UK).

Tn3 resolvase-mediated *in vitro* recombination

The optimum concentration of resolvase determined for an efficient recombination reaction was 20 μ M per 1 μ M of substrate DNA. Resolvase was diluted in resolvase dilution buffer (20 mM of Tris-HCl [pH 7.5], 1 mM DTT, 0.1 mM EDTA, 1 M NaCl, 50% v/v glycerol) as required. Standard recombination reactions were performed in 50 mM of Tris-HCl (pH 8.2), 10 mM of MgCl₂ and 0.1 mM of EDTA.

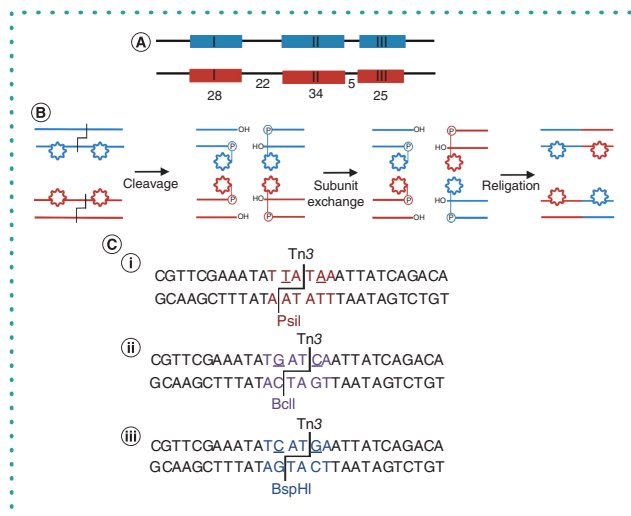


Figure 1. Reaction scheme for Tn3-mediated recombination. (A) Representation of the Tn3 recombination site (*res*); resolvase dimers bind to each of the *res* subsites I, II and III. The numbers indicate the length of each subsite and intermediate regions between subsites in bp. (B) The suggested mechanism of action of serine recombinases, focusing on *res* site I. Resolvase dimers (subunits depicted by polygons) are bound to each *res* I site (the *res* I sites are brought into close proximity with one another by the accessory *res* sites II and III to form the synaptic complex, not shown). Resolvase cleaves all four strands at *res* site I, each 5' end becoming covalently linked to a resolvase subunit via a phosphodiester link. Subsequently, the cleaved DNA strands are exchanged and religated in their new configuration. (C) (i) Sequence of *res* site I. The natural Psil recognition sequence is highlighted in red, and specific Tn3 sites of cleavage are indicated by black bars. The underlined T and A bases on the top strand of the Psil recognition sequence indicate nucleotide mutation of which have a minimal effect on Tn3 resolvase reaction efficiency. (ii) *res* site I Psil recognition sequence changed to BclI sequence (purple). (iii) *res* site I Psil recognition sequence changed to BspHI sequence (blue).

Table 1. Plasmids created for use in the Tn3 recombination reactions.

Plasmid	<i>res</i> ^{A†}	<i>res</i> ^B	Unique RE	Forward primer	Reverse primer
pMM5	Psil	Psil	–		
pMM6	Psil	BspHI	Psil	CATGATATTCGAACGGACTAGTGAGC	CATGAATTATCAGACATAGGAATTCGGCTTCG
pMM7	Psil	BclI	BclI Psil	TGCTGTGATAATTGATCATATTCGAACGGTTGCA	CGTTCGAAATATGATCAATTATCAGACATAGTAAAACG
pMM9	Psil	BspHI	BspHI Psil	1 [‡] AAGCGCTCATGCCCGAAGT	1 GGCTGATGAGCGCTGTTTCG
				2 GGTAAATGAGATTATCAAAAAGGATCTTCAC	2 GATAATCTCATTACCAAAATCCCTTAACGTG
				3 GTCCCATGAGCGGATACATATTTGAATG	3 GTATCCGCTCATGGGCAATAACCCCTG

[†]*Res*^A and *Res*^B denote the restriction enzyme sequence at each site.

[‡]For pMM9, the numbers 1, 2 and 3 refer to the forward and reverse primers used to remove all three natural BspHI sites to from the pMM9 plasmid.

Recombination reactions were carried out at 37°C for 1 h, after which the reaction was stopped by incubation at 70°C for 5 min. Recombination reactions were treated with proteinase K (50 µg/ml, 60 min, 50°C) and ethanol precipitated. Approximately 1 mg of Tn3 resolvase-treated DNA was subjected to BspHI (200 units, NEB) linearization in a final volume of 20 ml for 1 h at 37°C, followed by heat inactivation at 80°C for 20 min. The sample was prepared for separation by caesium chloride density gradient by the addition of 1.019 g of CsCl and 0.11 ml of 10 mg/ml of ethidium bromide solution, per gram of heat-treated solution. Separation was performed using a WX Ultra 1000 centrifuge and a TV860 rotor at 45,000 rpm, at 18°C overnight. The denser supercoiled DNA bands were extracted from the gradient using wide-gauge needles, and ethidium bromide was removed by several washes with water-saturated butanol. The extracted material was then ethanol-precipitated and analyzed on agarose gels.

Reports

Topoisomerase assays

DNA topoisomerase enzymes were supplied by Inspiralis Ltd, and assays were carried out following the manufacturer's protocols. Human topo II α decatenation assays were carried out in the following assay buffer: 50 mM of Tris-HCl (pH 7.5), 125 mM of NaCl, 10 mM of MgCl₂, 5 mM of DTT, 1 mM of ATP and 100 μ g of ml⁻¹ albumin. *E. coli* DNA gyrase assay buffer was 35 mM of Tris-HCl (pH 7.5), 24 mM of KCl, 4 mM of MgCl₂, 2 mM of DTT, 1.8 mM of spermidine, 1 mM of ATP and 100 μ g ml⁻¹ of BSA. Assays were conducted in a volume of 30 μ l at 37°C for 30 min with either 200 ng of kDNA (Inspiralis Ltd) or 200 ng of singly-linked catenated substrate; inhibition assays incorporated ciprofloxacin (0–100 μ M). Reactions were stopped by addition of 30 μ l of STEB (40% w/v sucrose, 100 mM of Tris-HCl pH 8, 10 mM of EDTA and 0.5 mg ml⁻¹ of bromophenol blue) and 30 μ l of chloroform/isoamyl alcohol (v/v, 24:1), vortexed, centrifuged and the upper aqueous phase analyzed on a 1% (w/v) TAE agarose gel at 85 V for 90 min. Gels were run without intercalator and were post-stained with ethidium bromide before visualization under UV illumination. Gel bands were quantified using GeneTools. Reactions in the presence of inhibitors (etoposide and ciprofloxacin) were carried out as previously with the addition of varying concentrations of inhibitor (Figure 2); in the case of etoposide, reactions were carried at in 1% DMSO with human topo II α (0.44 nM).

Results & discussion

Construction & purification of singly linked catenated DNA

The decatenation activity of enzymes has conventionally been determined by agarose gel-based assays using kDNA as a substrate. The inherently complex structure of kDNA leads to difficulties in detecting both the substrate and products of the reaction. Here we describe the construction of an alternative substrate, a singly-linked DNA catenane, to replace the use of kDNA in decatenation assays.

Tn3 resolvase can convert a circular substrate DNA molecule containing two directly repeated *res* sites into a pair of singly-linked catenated DNA rings. However, as a result of imperfect recombination efficiency, the challenge of separating the reaction product from the substrate arises. Substrate and product are identical in terms of DNA sequence and size. Recombination by Tn3 resolvase involves double-stranded DNA cleavage and strand exchange precisely at *res* site I (Figure 1). We therefore considered modifications of site I that would not be inherited by the product singly-linked catenanes, thus allowing the differentiation of the reaction substrate from the products. Site I comprises a 28-bp sequence containing a natural PstI restriction enzyme site (TTATAA) at its center; Tn3 resolvase cleaves each strand symmetrically after the T of the AT in the PstI site. Therefore, in a plasmid containing two *res* sites, if the PstI restriction site in one *res* site is changed to a different restriction site (e.g., BclI TGATCA), the product *res* sites will lack both sites. It is thus possible, in theory, to design a substrate containing a restriction site that will be missing in the catenane product. However, sequence modifications at the site of action of Tn3 resolvase can cause drastic reductions in reaction efficiency [16]. The negative impact can be minimized by retaining the central AT of the PstI sequence, where the resolvase cleavage occurs, making modifications on either side of this sequence. We aimed to identify a modification that would minimize the negative effect on Tn3 resolvase efficiency while allowing us to use restriction enzymes to distinguish recombination product from substrate.

The starting substrate, plasmid pMM5, contains two *res* sites (that we term *res*^A and *res*^B) each containing a PstI restriction site. This plasmid was modified to introduce recognition sites for either BspHI (TCATGA) or BclI (TGATCA) into *res*^B. The resulting plasmids were named pMM6 (*res*^A contains a PstI site [unique in the plasmid], and *res*^B contains a BspHI site [not unique]) and pMM7 (*res*^A contains a PstI site, and *res*^B contains a BclI site [both unique]) (Table 1). Both pMM6 and pMM7 can be cleaved by restriction enzymes that will not cleave the catenated recombination product; pMM6 can be cleaved with PstI, whereas pMM7 can be cleaved with either PstI or BclI. However, the efficiency of Tn3 resolvase-mediated recombination of pMM7 was approximately fourfold lower than for pMM6 (results not shown). BspHI cannot be used for pMM6 because it cleaves elsewhere in the plasmid, and using PstI with pMM6 would be too expensive, due to the high cost of the PstI enzyme. Therefore, to generate a more economical method, all of the BspHI recognition sequences in pMM6, apart from the one in *res*^B, were removed by site-directed mutagenesis, creating pMM9. This plasmid can be cleaved either with PstI (in *res*^A) or BspHI (in *res*^B), and neither of these enzymes cleave the catenated product of recombination.

Singly-linked catenane substrates for topoisomerases were produced by treating pMM9 with Tn3 resolvase. Any unreacted circular pMM9 was cleaved with BspHI, and the supercoiled catenane was purified away from the linearized substrate by ethidium bromide–CsCl density centrifugation as described in the materials and methods section. The resulting singly-linked catenanes purified by this method included a background contamination of uncatenated DNA molecules.

Decatenation reactions with type II topoisomerases

The validation of purified singly-linked catenanes as substrates for topoisomerase-catalyzed decatenation reactions was carried out by analyzing the decatenation activity of enzymes using the new substrate in direct comparison with kDNA. The substrates were tested using two DNA topoisomerases, possessing differing decatenation efficiencies.

Topo II α is a type II topoisomerase that controls and manipulates the topological state of DNA, principally during the processes of chromosome condensation, chromatid segregation, transcription and translation, by initiating transient double-stranded DNA breaks [4]. Topo II α has a variety of activities, including the ability to relax both positively and negatively supercoiled DNA and interconvert catenated and decatenated, or knotted and unknotted, DNA forms.

A direct comparison of the singly-linked catenanes and kDNA as substrates for topo II α -mediated decatenation revealed that the former substrate produced a more discernible and sensitive decatenation assay when compared with kDNA (Figure 2). The singly-linked

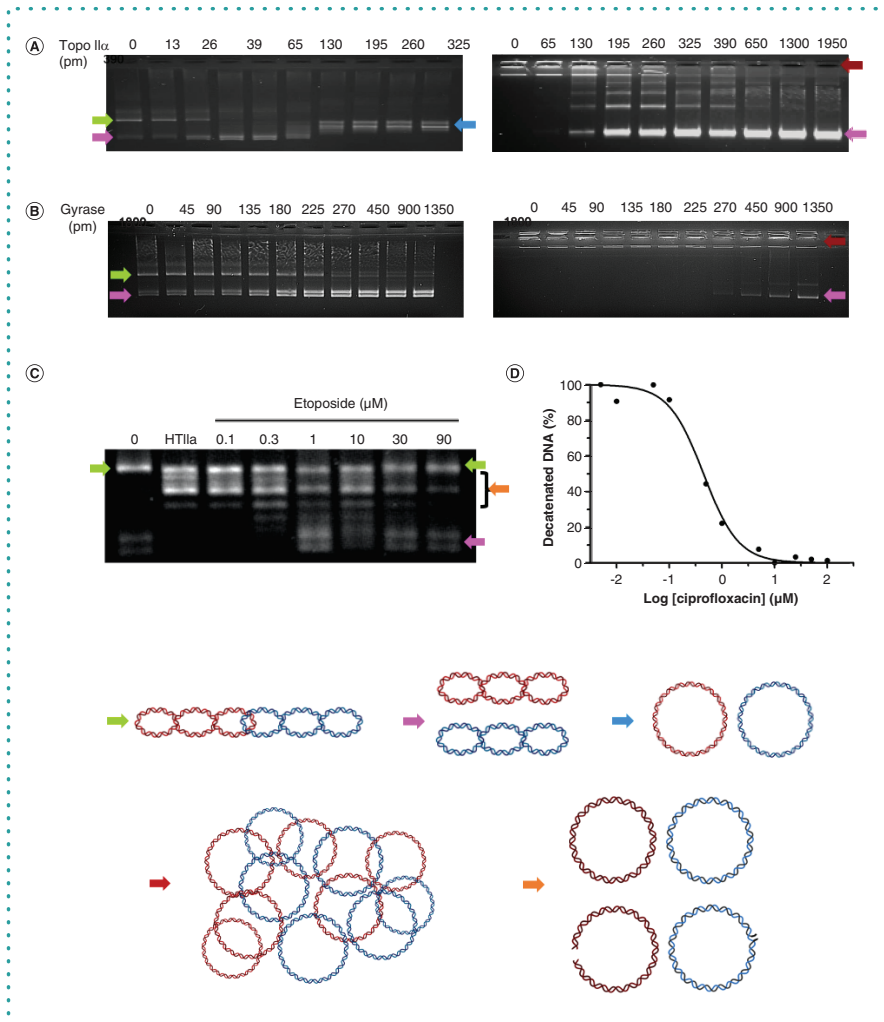


Figure 2. Topoisomerase-mediated decatenation assays. (A) Topo II α decatenation reaction to compare the use of singly-linked catenanes (bis-cat; left panel) and kinetoplast DNA (kDNA; right panel) as substrates. In addition, 200 ng of singly linked substrate (green arrow) is completely decatenated by 39 pM of topo II α into supercoiled decatenated DNA molecules (pink arrow); further addition of topo II α relaxes the supercoiled decatenated DNA molecules (pink arrow) into their relaxed form (blue arrow). An equal amount of kDNA is completely decatenated by 650 pM of topo II α , almost no decatenation of kDNA is detected at 65 pM of topo II α , and a large proportion of the substrate can be seen immobile in the wells of the agarose gel (red arrow). (B) *Escherichia coli* gyrase-mediated decatenation of singly-linked catenanes (left panel) and kDNA (right panel). The singly linked catenanes are decatenated by 450 pM of gyrase, whereas even at a concentration of 1800 pM of gyrase, it is difficult to ascertain whether kDNA substrate still remains in the wells of the agarose gel. Notably, the singly-linked catenated substrate only (lane 1) also has a background level of supercoiled uncatenated DNA molecules. (C) Inhibition of human topo II α (HTIla) by etoposide; the IC₅₀ can be approximated to be 0.3–1 μM ; topo II α was 0.44 nM. (D) Inhibition of *E. coli* gyrase by ciprofloxacin. Plot of gyrase decatenation inhibition assay with singly-linked substrate at increasing levels of ciprofloxacin. The gyrase concentration was 450 pM; the calculated IC₅₀ of ciprofloxacin against *E. coli* gyrase was 0.44 μM .

Reports

catenanes can be clearly visualized on agarose gels, prior to the addition of enzyme, at which point the kDNA is trapped in the wells of the gel. The addition of topo II α leads to the decatenation of the singly-linked catenanes in a single step to release two separate circular DNA molecules of visibly distinguishable sizes: 2.6 and 2.3 kbp. In contrast, the reaction of topo II α with kDNA leads to the appearance of several DNA molecules of varying sizes on the agarose gel; these are likely to be partially decatenated products. Impressively, the use of singly linked DNA catenanes has significantly improved the sensitivity of the DNA decatenation assay by unambiguously demonstrating full decatenation with ~16-fold less enzyme than required to fully decatenate an equal amount of kDNA. In addition, the new substrate described here allows for the visual distinction between two different activities of topo II α . Under these assay conditions, at topo II α concentrations of 13–65 pM, the decatenation of the singly-linked dimers into two independent supercoiled DNA molecules is seen. Further addition of topo II α in excess of 130 pM reveals the DNA relaxation activity of the enzyme, converting the unlinked supercoiled DNA molecules into relaxed forms with a relatively lower mobility in the agarose gel. This illustrates how the bis-cat assay can be used to simultaneously monitor decatenation and relaxation, showing, in this case, that topo II α is a preferential decatenase; such distinction is not apparent using kDNA. (Note that the gels in Figure 2 are run in the absence of ethidium bromide; in the presence of this intercalator, the relaxed and supercoiled band would run together, allowing easier quantitation of the decatenation reaction.)

E. coli DNA gyrase, a type II topoisomerase, is distinguished by its unique ability to negatively supercoil DNA in an ATP-dependent reaction [17]. The enzyme has also been shown to possess decatenation activity, albeit inefficient in comparison with other type II topoisomerases [18–20]. The singly-linked DNA catenanes and kDNA were subjected to the relatively modest decatenation activity of gyrase to test the effectiveness of each substrate. Evidently, the increased sensitivity provided by the reaction on singly linked DNA catenanes readily allows the detection of gyrase decatenation activity at lower concentrations of enzyme, resulting in two distinct bands on the agarose gel, representing the separate 2.6 and 2.3 kbp supercoiled DNA molecules (Figure 2). The singly-linked DNA catenane shows promise for both the reassessment of previously identified topoisomerases and characterization of novel decatenation activities. No relaxation is seen here, as under these conditions (presence of ATP), gyrase maintains the negative supercoiling of the DNA.

A further application of the singly-linked catenated substrate is for inhibition assays, which are often used to test the efficacy of novel topoisomerase inhibitors. We envisage that the sensitivity of our substrate will enhance the fidelity of the information obtained by gel-based assays. Type II DNA topoisomerases, such as topo II α and gyrase, are well-known targets of anticancer drugs and antibiotics, respectively [21–23]. We show in Figure 2 an example of this application using topo II α and etoposide, a well-known anticancer drug targeted to topo II. The approximate IC₅₀ from this assay (0.3–1 μ M) can be compared with those derived from the literature (50–200 μ M IC₅₀) using kDNA as the substrate [24–26], suggesting that the bis-cat assay is more sensitive. Ciprofloxacin, a clinically established gyrase inhibitor, was tested in an exemplar gyrase decatenation inhibition assay using the singly-linked DNA catenanes to assess its half-maximal inhibitory concentration (IC₅₀) (Figure 2). The percentage of decatenation activity was determined by taking the sum of decatenated 2.6 and 2.3 kbp products over a range of ciprofloxacin concentrations, as a fraction of the DNA gyrase decatenation activity in the absence of inhibitor; appropriate background subtractions were made to allow for pre-existing uncatenated DNA molecules in the substrate. The resultant IC₅₀ for inhibition by ciprofloxacin was calculated as 0.44 μ M, which is similar to values determined previously [27,28].

These examples highlight a potential limitation of the singly-linked substrate – that is, the background level of uncatenated double-stranded DNA molecules. This background contamination with the desired product (<20% of the total DNA) could be a consequence of downstream handling of the DNA but seemingly persists over different resolvase preparations. It is unlikely that the contamination is a direct result of decatenation by a co-purified topoisomerase protein, not only due to the stringent resolvase purification process, which involves denaturation with urea, but also because a topoisomerase capable of decatenating double-stranded DNA catenanes would require an energy investment from the hydrolysis of ATP, which is not present. To investigate whether this background level was attributable to nuclease activity, we exploited the Mg²⁺-independence of Tn3 resolvase by conducting the resolvase reaction in an assay buffer lacking the divalent metal. This alteration had minimal effect on the reaction efficiency, but it did not solve the contamination problem; nevertheless, alternative purification methods using hexa-histidine tagged resolvase would be possible. These uncatenated supercoiled product circles could be produced by failure of resolvase to religate one circle in the catenane.

The problem of background-level contamination could theoretically be tackled by manipulation of the pMM9 substrate plasmid to enable the downstream purification of the singly-linked catenanes from their uncatenated counterparts. For example, the molecular mass of the substrate plasmid could be adjusted to increase its mass difference from the largest of the two decatenated circular products to take advantage of downstream gel filtration. An alternative prospect is the introduction of two different DNA triplex-binding sites into pMM9, one in each region between the two *res* sites [29]. Purification could then proceed by the sequential passage of the singly-linked catenane mixture through two columns, each with an attached triplex DNA-forming oligonucleotide complementary to one of the triplex sites in pMM9 [30]. Thus, the catenated substrate would bind to both columns, and the uncatenated DNA molecules (only able to bind to one of the two columns) could be separated.

In conclusion, the singly-linked catenated substrate has been validated using well-characterized topoisomerases. This novel substrate has proved to be a superior alternative to the currently marketed kDNA substrate by significantly enhancing the sensitivity and reliability of gel-based decatenation assays. The potential hindrance of background uncatenated DNA molecules can efficiently be accounted for by making simple background-level subtractions to provide reliable results, as has been demonstrated with the use of an inhibition assay.

Future perspective

The singly-linked catenated substrate (bis-cat) described here proved to be an effective means of characterizing decatenation activities. We envisage that with the focus of future efforts upon the improvement of Tn3 resolvase-mediated reaction efficiency and downstream purification to remove background uncatenated circles, this would lead to an ideal assay. The additional advantage of the high sensitivity and simplicity provided by the substrate highlights it as a desirable candidate for automated high-throughput assays that may be implemented to test the potency of novel topoisomerase inhibitors on a larger scale.

Author contributions

Experimental work involving the production and optimization of the singly-linked catenated substrate was carried out by NF Waraich. S Jain carried out topoisomerase assays. The study was designed and supervised by A Maxwell and NP Burton, with provision of valuable guidance and materials from WM Stark and SD Colloms. NF Waraich and A Maxwell wrote the manuscript, with input from NP Burton, WM Stark and SD Colloms.

Acknowledgments

We thank Andy Bates of the University of Liverpool for helpful comments on the manuscript.

Financial & competing interests disclosure

Work in A Maxwell's laboratory was supported by the Biotechnology and Biosciences Research Council (UK) Institute Strategic Programme Grant BB/P012523/1, and the Wellcome Trust (Investigator Award 110072/Z/15/Z). NF Waraich was funded by a BBSRC-CASE studentship (BB/M011216/1) supported by Inspiralis Ltd. SD Colloms was funded by a Leverhulme Trust grant (RP2013-K-017). The authors have no other relevant affiliations or financial involvement with any organization or entity with a financial interest in or financial conflict with the subject matter or materials discussed in the manuscript apart from those disclosed.

No writing assistance was utilized in the production of this manuscript.

Open access

This work is licensed under the Creative Commons Attribution 4.0 License. To view a copy of this license, visit <http://creativecommons.org/licenses/by/4.0/>

References

1. Bates AD, Maxwell A. *DNA Topology*. Oxford University Press, Oxford, UK (2005).
2. Vos SM, Tretter EM, Schmidt BH, Berger JM. All tangled up: how cells direct, manage and exploit topoisomerase function. *Nat. Rev. Mol. Cell Biol.* 12(12), 827–841 (2011).
3. Chen SH, Chan NL, Hsieh TS. New mechanistic and functional insights into DNA topoisomerases. *Annu. Rev. Biochem.* 82(1), 139–170 (2013).
4. Wang JC. Cellular roles of DNA topoisomerases: a molecular perspective. *Nat. Rev. Mol. Cell Biol.* 3(6), 430–440 (2002).
5. Zechiedrich EL, Cozzarelli NR. Roles of topoisomerase IV and DNA gyrase in DNA unlinking during replication in *Escherichia coli*. *Genes Dev.* 9(22), 2859–2869 (1995).
6. Hudson B, Vinograd J. Catenated circular DNA molecules in HeLa cell mitochondria. *Nature* 216(5116), 647–652 (1967).
7. Englund PT, Hajduk SL, Marini JC. The molecular biology of trypanosomes. *Annu. Rev. Biochem.* 51, 695–726 (1982).
8. Lukes J, Guilbride DL, Votykka J, Zikova A, Benne R, Englund PT. Kinetoplast DNA network: evolution of an improbable structure. *Eukaryot. Cell* 1(4), 495–502 (2002).
9. Nitiss JL, Soans E, Rogojina A, Seth A, Mishina M. Topoisomerase assays. *Curr. Protocols Pharmacol.* 57(1), 3.3.1–3.3.27 (2012).
10. Chen J, Rauch CA, White JH, Englund PT, Cozzarelli NR. The topology of the kinetoplast DNA network. *Cell* 80(1), 61–69 (1995).
11. Stark WM, Boocock MR, Sherratt DJ. Site-specific recombination by Tn3 resolvase. *Trends Genet.* 5(9), 304–309 (1989).
12. Nollmann M, Byron O, Stark WM. Behavior of Tn3 resolvase in solution and its interaction with res. *Biophys. J.* 89(3), 1920–1931 (2005).
13. Nielsen CF, Huttner D, Bizard AH et al. PIC1 promotes sister chromatid disjunction and co-operates with topoisomerase II in mitosis. *Nature Comm.* 6(8962), (2015).
14. Arnold PH, Blake DG, Grindley ND, Boocock MR, Stark WM. Mutants of Tn3 resolvase which do not require accessory binding sites for recombination activity. *EMBO J.* 18(5), 1407–1414 (1999).
15. Olorunniji FJ, He J, Wenwieser SV, Boocock MR, Stark WM. Synapsis and catalysis by activated Tn3 resolvase mutants. *Nucleic Acids Res.* 36(22), 7181–7191 (2008).
16. McIlwraith MJ, Boocock MR, Stark WM. Tn3 resolvase catalyses multiple recombination events without intermediate rejoining of DNA ends. *J. Mol. Biol.* 266(1), 108–121 (1997).
17. Gellert M, Mizuchi K, O'dea MH, Nash HA. DNA gyrase: an enzyme that introduces superhelical turns into DNA. *Proc. Natl Acad. Sci. USA* 73(11), 3872–3876 (1976).
18. Zechiedrich EL, Khodursky AB, Cozzarelli NR. Topoisomerase IV, not gyrase, decatenates products of site-specific recombination in *Escherichia coli*. *Genes Dev.* 11(19), 2580–2592 (1997).
19. Marians KJ. DNA gyrase-catalyzed decatenation of multiply linked DNA dimers. *J. Biol. Chem.* 262(21), 10362–10368 (1987).
20. Liu LF, Liu CC, Alberts BM. Type II DNA topoisomerases: enzymes that can unknot a topologically knotted DNA molecule via a reversible double-strand break. *Cell* 19(3), 697–707 (1980).
21. Tse-Dinh YC. Targeting bacterial topoisomerases: how to counter mechanisms of resistance. *Future Med. Chem.* 8(10), 1085–1100 (2016).
22. Pommier Y. Drugging topoisomerases: lessons and challenges. *ACS Chem. Biol.* 8(1), 82–95 (2013).
23. Pommier Y, Leo E, Zhang H, Marchand C. DNA topoisomerases and their poisoning by anticancer and antibacterial drugs. *Chem. Biol.* 17(5), 421–433 (2010).
24. Lassota P, Singh G, Kramer R. Mechanism of topoisomerase II inhibition by staurosporine and other protein kinase inhibitors. *J. Biol. Chem.* 271(42), 26418–26423 (1996).
25. Rhee H-K, Park H-J, Lee SK, Lee C-O, Choo H-Y. Synthesis, cytotoxicity, and DNA topoisomerase II inhibitory activity of benzofuroquinolinediones. *Bioorg. Med. Chem.* 15(4), 1651–1658 (2007).
26. Terada T, Fujimoto K, Nomura M et al. Antitumor agents. 3. Synthesis and biological activity of 4 beta-alkyl derivatives containing hydroxy, amino, and amido groups of 4'-O-demethyl-4-desoxy podophyllotoxin as antitumor agents. *J. Med. Chem.* 36(12), 1689–1699 (1993).
27. Barnard FM, Maxwell A. Interaction between DNA gyrase and quinolones: effects of alanine mutations at GyrA subunit residues Ser(83) and Asp(87). *Antimicrob. Agents Chemother.* 45(7), 1994–2000 (2001).
28. Germe T, Voros J, Jeannot F et al. A new class of antibacterials, the imidazopyrazinones, reveal structural transitions involved in DNA gyrase poisoning and mechanisms of resistance. *Nucleic Acids Res.* 46(8), 4114–4128 (2018).
29. Schlupe T, Cooney CL. Purification of plasmids by triplex affinity interaction. *Nucleic Acids Res.* 26(19), 4524–4528 (1998).
30. Maxwell A, Burton NP, O'Hagan N. High-throughput assays for DNA gyrase and other topoisomerases. *Nucleic Acids Res.* 34(15), e104 (2006).

DNA in a twist? How topoisomerases solve topological problems in DNA

Natassja G. Bush, Monica Agarwal, Sara R. Henderson, Nidda F. Waraich and Anthony Maxwell (John Innes Centre, UK)

DNA topoisomerases have been described as 'the magicians of the DNA world', somehow allowing DNA strands to pass through each other. These ingenious enzymes are both essential and potentially dangerous, as any interruption in their DNA breakage-reunion reactions can lead to chromosome breaks and cell death. This has led to their development as important targets for antibacterial and anti-cancer chemotherapy.

DNA topology and the importance of topoisomerases

Watson and Crick, upon proposing the double-helical structure of DNA, noted that the two strands of the helix would have to untwist in order to separate. They also suggested that this untwisting and separating of the two strands would lead to entanglements. While the structure of the DNA double helix is ideally suited to its function – the opening of the helix permitting access to the bases that encode the genetic information – it does indeed lead to topological problems. This process of helix unwinding, which occurs in DNA replication and transcription, leads to DNA supercoiling, where the DNA helix is coiled about its own axis (Figure 1). The DNA topoisomerases have evolved to deal with problems of over-winding (and under-winding) of the DNA helix, as well as to take care of DNA catenanes (interlinked DNA molecules) that can occur at the termination of replication and knots in DNA that can arise during recombination events (Figure 1). These different forms of DNA: supercoiled, relaxed, catenated and knotted, represent topological isomers of double-stranded circular DNA, i.e. they have the same molecular mass, but differ in the path taken by the DNA strands.

DNA topology, literally how the two complementary single strands of DNA are intertwined, is an important topic in itself and is

often the domain of mathematicians. However, for the purpose of discussing topoisomerases, a broad understanding is all that is necessary (see Box 1). In general terms, positive supercoiling (over-winding of DNA) is bad, with some exceptions, and moderate negative supercoiling (under-winding of DNA) is good; knots are generally bad and catenanes normally should be removed (Figure 1). Resolving these unwanted species is the job performed by topoisomerases, which, remarkably, carry out these reactions by transiently cleaving one or both strands of DNA (see below). DNA breakage is a danger to cell viability and the cleavage-religation process must be carefully controlled. Interruption of this process can lead to broken DNA and cell death, which is why these enzymes have been exploited as targets for both antibacterial chemotherapy and anti-cancer agents. As topoisomerases occur in all organisms (prokaryotes, eukaryotes and archaea) it is the differences between them that need to be established and exploited to develop successful clinical agents.

Mechanistic aspects of type II topoisomerases

DNA topoisomerases are divided into two types, I and II, depending on whether their reactions proceed via transient single- or double-stranded DNA breaks. They are further divided into subtypes: IA, IB, IC, IIA, IIB; these subtypes differ both

mechanistically and structurally (Figure 2). Type I enzymes are less relevant to this article, as they are not strictly molecular machines and do not use ATP. The exception is the type IA topoisomerase reverse gyrase that uses ATP to introduce positive supercoils into DNA. Despite this, the type I topoisomerases are still of considerable interest as drug targets (see below) and because the subtypes show fundamental mechanistic differences.

The type IB and C enzymes relax supercoiled DNA using a 'swivel' mechanism by making transient single-stranded breaks involving a covalent bond to the 3'-phosphate end of the DNA, and allowing the DNA to swivel within the enzyme in a controlled rotation. The type IA enzymes work by a strand-passage mechanism making transient covalent bonds to the 5'-phosphate end of DNA at the break site. The type IA enzymes also relax supercoiled DNA, with reverse gyrase being the only type IA enzyme capable of introducing supercoils. It consists of two domains, a helicase domain, which binds and hydrolyses ATP, and a topoisomerase domain, which cleaves the DNA. The helicase domain transiently unwinds the double-stranded DNA in an ATP-dependent reaction increasing the linking number (Lk) (see Box 1). The topoisomerase domain carries out strand passage by cleaving one strand of the DNA helix and passing the other strand through the cleaved strand before resealing. This strand-passage event results in positive supercoiling. Reverse gyrase has only been found in thermophilic archaea and eubacteria. These organisms are thought to have positively supercoiled genomes, which, in this case, is beneficial as positively supercoiled DNA is thought to be more resistant to the harmful effects of high temperature.

Type II topoisomerases use the free energy provided by ATP hydrolysis to carry out their reactions in which one segment of double-stranded DNA is cleaved and another segment is passed through the break. The two subtypes, type IIA and type IIB, are similar mechanistically but differ structurally (Figure 2). The type II topoisomerases are either homodimers (e.g. human topoisomerase (topo) IIA) or heterotetramers (e.g. prokaryotic topo IV). Although the quaternary structures may differ, all type IIA enzymes share similar domains (Figure 2). The biggest structural difference between the two subtypes is that the type IIB topoisomerases lack the bottom protein interface or 'exit gate', which has mechanistic implications as there is no post-strand-passage cavity (Figures 2 & 3). This post-strand-passage cavity has been suggested to have a 'proofreading' role, potentially allowing backtracking of the transported segment.

DNA topology

If a linear double-stranded DNA molecule is closed into a circle with both strands sealed, then the two strands are 'linked' together a number of times, corresponding to the number of double-helical turns in the original linear molecule. This number, the linking number (Lk), must be an integer and its value will depend on the number of base pairs in the DNA (N) and the helical repeat (h), generally taken to be ~10.5 in B-form DNA:

$$Lk = N/h$$

Strictly, the linking number of this most 'relaxed' circular molecule will be the closest integer to N/h – the ends may need to be twisted slightly to join up. The exact non-integer value of N/h is called Lk^* , representing the imaginary undistorted circular molecule. If the ends of the original linear molecule had been rotated a number of turns either in the same direction as the helical twist of the double helix, or in the opposite direction, before joining, this changes the linking number, and the circular DNA is said to be 'supercoiled', and has a linking difference, ΔLk , where:

$$\Delta Lk = Lk - Lk^*$$

ΔLk can be positive (corresponding to positive supercoiling) or negative (corresponding to negative supercoiling). The distinction between Lk^* and the true integer value of Lk for the relaxed molecule is largely insignificant for molecules of plasmid size or above.

Lk can be broken down into two parameters: Tw, the twist of the DNA, i.e. how many times the two strands coil around the helix axis (the number of double-helical turns), and Wr, writhe, the coiling of the helix axis in space:

$$Lk = Tw + Wr$$

Tw and Wr can be interconverted and do not have to be integers. The term DNA supercoiling, the higher order coiling of the DNA, is really describing the writhe, but the overall distortion of the molecule is really represented by the linking difference (ΔLk), and the density of supercoiling (σ), or specific linking difference, is defined as:

$$\sigma = \Delta Lk / Lk^*$$

For a fuller description of supercoiling, knots and catenanes see Bates, A.D. and Maxwell, A. (2005) DNA Topology, Oxford University Press, Oxford.

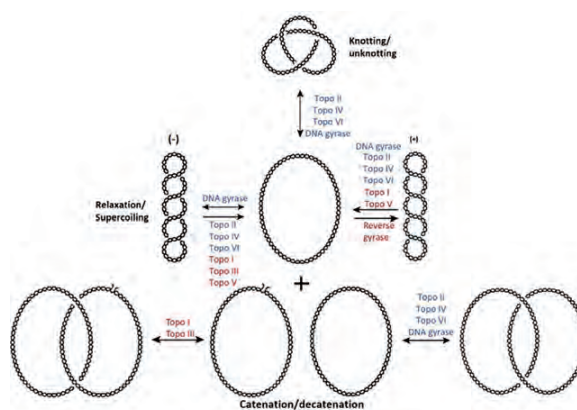


Figure 1. Various DNA topological reactions catalysed by DNA topoisomerases. Type I topoisomerases are indicated in red and the type II topoisomerases are indicated in blue. Arrows represent the direction of the reaction. For illustrative purposes, in the catenation/decatenation reactions, the non-nicked substrates are drawn as relaxed; however, it is more likely that these are supercoiled in this reaction. Figure has been adapted from Bush et al. (2015).

Movement and Motors

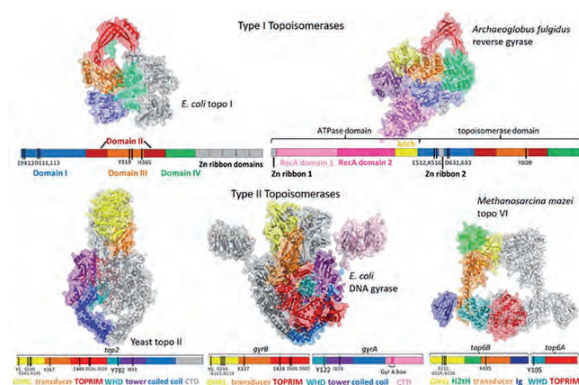


Figure 2. Domain diagrams and structures of type I and type II DNA topoisomerases. Type I topoisomerases: *E. coli* topo I (left-hand side; PDB: 4RUL) and *Archaeogloblobus fulgidus* reverse gyrase (right-hand side; PDB: 1GKU) coloured by their various domains indicated in the domain diagrams below. Blue is Domain I, red – Domain II, orange – Domain III, green – Domain IV, grey shows the Zn-binding domains. The pink (light and dark) on the *A. fulgidus* reverse gyrase indicates the two RecA domains and the yellow shows the latch domain. Type II topoisomerases: yeast (*Saccharomyces cerevisiae*) topo II (left-hand side) – truncated structure (lacking the CTD) showing amino acids 1-1177 (PDB: 4GFH), *E. coli* DNA gyrase (middle) – assembled from a number of truncated structures (PDB: 1E11, 3NUH and 3L6V) and *Methanosarcina mazei* topo VI (right-hand side, PDB: 2Q2E) all with their respective domain diagrams below. Yellow shows the GHKL domain which binds ATP, orange indicates the transducer domain, red the TOPRIM domain which binds the Mg²⁺ ion cofactor, teal is the winged-helix domain (WHD), which contains the catalytic tyrosine, purple is the tower domain and blue shows the coiled coil domain. The grey on the yeast topo II domain diagram (missing in the structure) shows the C-terminal domain (CTD), which is structurally and functionally different to the *E. coli* DNA gyrase CTD (light pink). The *M. mazei* structure has two additional domains in the helix-2-turn-helix (H2tH in green) and the Ig domain (in dark blue).

All type II topoisomerases use strand passage to relax DNA or resolve knots and catenanes, but only DNA gyrase can introduce supercoils into DNA. Strand passage occurs by a two-gate mechanism in which one segment of DNA (the T or transported segment) is passed through a transient break in another (the G or gate segment) (Figure 3). Supercoiling via gyrase works by a slightly different mechanism in which DNA is wrapped around the C-terminal domains of GyrA, presenting the T segment to the G segment such that strand passage, driven by the binding and hydrolysis of ATP, occurs in the correct direction (Figure 3).

Although we have an understanding of the mechanism of strand passage, the role of ATP hydrolysis is less clear. With gyrase it seems obvious that the free energy is utilized to drive negative supercoiling. However, this is not the case for the other type II topoisomerases,

which catalyze reactions that, in general, do not require energy. One proposal is that binding and hydrolysis of ATP is used to stabilize or destabilize protein interfaces within type II topoisomerases allowing efficient strand passage while reducing the risk of accumulating potentially toxic double-stranded breaks.

Type II topoisomerases as drug targets

A major reason for the continued interest in DNA topoisomerases over the last 40 years or so has been their utility as drug targets both for antibacterial and anti-cancer chemotherapy. The quinolone class of antibiotics, of which ciprofloxacin is the best known, are the only clinically successful bacterial topoisomerase inhibitors. They have a dual-targeting mechanism of action whereby they can inhibit both type II bacterial topoisomerases (gyrase and topo IV). Their mode of action is well-studied and involves stabilizing a cleavage complex with bound DNA. This can be bacteriostatic (i.e. prevents replication, most likely a result of stalling of the replication fork due to the presence of a gyrase-DNA complex), or bactericidal (i.e. kills the bacteria) due to induction and processing of double-stranded breaks in DNA. As with most antibiotics there is significant resistance, and it is imperative that new agents to replace quinolones are found.

Aside from quinolones, there are several other small molecules and toxins that inhibit gyrase and, in some cases, also topo IV. These include novobiocin and simocyclinone, and the proteinaceous toxins microcin B17 and CcdB (Figure 4). Novobiocin is an aminocoumarin compound produced by *Streptomyces* species. These are extremely potent inhibitors of gyrase (and topo IV) that act by competitively inhibiting the ATPase reaction. Despite having little similarity to ATP, aminocoumarins bind at the ATPase active site (Figure 4). In contrast, simocyclinones, which also contain an aminocoumarin moiety, do not inhibit the ATPase reaction, but instead bind to two pockets in GyrA preventing the enzyme's interaction with DNA (Figure 4). There are issues with both the aminocoumarins and simocyclinones in terms of toxicity and solubility that currently preclude their use in clinical medicine.

Recently, a new novel class of gyrase-specific compounds with a distinct mode of action was discovered: the thiophenes. These compounds bind allosterically in a pocket away from the quinolone-binding site, resulting in a conformation that promotes cleavage complexes. These compounds have not been optimized for clinical use, and it is yet to be determined if this will be feasible.

Although bacterial type I topoisomerases (e.g. topo I) are potential targets for antibacterial chemotherapy, there are currently no clinical agents that target these compounds; this remains an active area of research.

Human topoisomerases (topo I and II) have been successfully exploited in anti-cancer chemotherapy; examples include camptothecin, etoposide and amsacrine. Like quinolones, these drugs stabilize cleavage complexes with DNA. In addition to these topo II poisons, there are other compounds that act via different modes of action, including inhibiting ATP hydrolysis.

Topo VI, a type IIB topoisomerase, is not currently a drug target, as archaea are not generally regarded as pathogens. However, its occurrence in plants and *Plasmodium* parasites (see below) raises the possibility of targeting topo VI for the development of herbicides and antimalarial drugs. A few inhibitors of archaeal topo VI have been reported.

Finding new topoisomerases in unexpected places

DNA topoisomerases have been found in all organisms, but there is considerable variation in the number and types of topoisomerases. For example, *Mycobacterium tuberculosis* has two topoisomerases, topo I (type IA) and gyrase (type IIA). In contrast, *Escherichia coli* has four topoisomerases with an additional enzyme in each class, topo III (type IA) and topo IV (type IIA). DNA gyrase in *M. tuberculosis* possesses enhanced decatenation ability, an activity normally attributed to topo IV. In recent years, gyrase and topo VI have been found in eukaryotes including *Arabidopsis thaliana* (a model plant species) and *Plasmodium falciparum* (a causative agent of malaria).

The genes for eukaryotic gyrases are nuclear-encoded but the proteins are organelle-targeted in both *A. thaliana* and *P. falciparum*. The enzyme is targeted to both the chloroplast and mitochondria in *A. thaliana*, and to the apicoplast, a relict plastid, in *P. falciparum*. The requirement for gyrase in eukaryotes may at first seem unnecessary given the ability of these organisms to negatively supercoil DNA through the action of DNA wrapping around histones. However, in accordance with the bacterial origins of these organelles, they appear to have retained prokaryotic aspects of organellar DNA replication and organization.

In *A. thaliana* there are two genes for GyrB; it is currently not clear what the roles of the two B subunits are. *A. thaliana* gyrase is sensitive to quinolone drugs, like its prokaryotic counterpart,

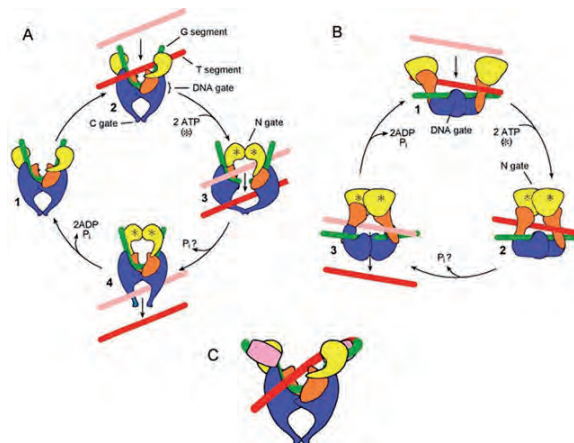


Figure 3. Mechanism of type II topoisomerases. The DNA T-segment (coloured pink to red) is transported through the enzyme-stabilized double-stranded break in the DNA G-segment (green). (A) is the core strand-passage mechanism of type IIA topoisomerases. (B) shows the type IIB topoisomerase mechanism, note the lack of the post-strand-passage cavity. (C) shows the wrapping of the DNA around DNA gyrase C-terminal domains (light pink). For all panels the domains are approximately coloured by domain: yellow is the GHKL domain, orange shows the TOPRIM domain and blue indicates the cleavage-religation domain; adapted from Bates et al. 2011.

and it has been shown that plants can be killed by these compounds, raising the possibility of developing herbicides based on quinolones.

Relatively little is known about *P. falciparum* gyrase. This is possibly due to the difficulties of heterologous protein expression attributable to the AT-rich genome of the malarial parasite. *P. falciparum* gyrase B has successfully been characterized, but the A subunit has proved more difficult, with only truncated fragments producing soluble protein. The initial indication of the presence of gyrase in *P. falciparum* came from the sensitivity of the apicoplast to ciprofloxacin. Given the drastic health impacts of malaria, developing this enzyme as a drug target is viewed with importance.

Topo VI (type IIB) is a DNA-relaxing enzyme originally found in archaea. In plants it is required for endoreduplication, a polyploidization process responsible for the enlargement of plant cells, which determines plant size. Topo VI is related to type IIA topoisomerases in terms of structure/function, but differs in the strand-passage mechanism (Figures 2 & 3). It is a heterotetramer composed of two subunits, A and B. Subunit A is a homologue of the Spo11

Downloaded from http://portlandpress.com/biochemj/article-pdf/410/2/26/6851741/bio040020026.pdf by UK user on 28 March 2021

